JAEA-Technology
2011-035

JAEA-Technology

Technical Design Report of Spallation Neutron Source Facility in J-PARC

Neutron Source Section
Materials and Life Science Division

J-PARC Center

February 2012

Japan Atomic Energy Agency
日本原子力研究開発機構

独立行政法人日本原子力研究開発機構　研究技術情報部　研究技術情報課
〒319-1195　茨城県那珂郡東海村白方白根 2 番地 4
電話 029-282-6387, Fax 029-282-5920, E-mail:ird-support@jaea.go.jp

Intellectual Resources Section, Intellectual Resources Department,
Japan Atomic Energy Agency
2-4 Shirakata Shirane, Tokai-mura, Naka-gun, Ibaraki-ken 319-1195 Japan
Tel +81-29-282-6387, Fax +81-29-282-5920, E-mail:ird-support@jaea.go.jp

JAEA-Technology 2011-035

Technical Design Report of Spallation Neutron Source Facility in J-PARC

Neutron Source Section
Materials and Life Science Division

J-PARC Center
Japan Atomic Energy Agency
Tokai-mura, Naka-gun, Ibaraki-ken

(Received December 12,2011)

One of the experimental facilities in Japan Proton Accelerator Research Complex (J-PARC) is the Materials and Life Science Experimental Facility (MLF), where high-intensity neutron beams are used as powerful probes for basic research on materials and life science, as well as research and development in industrial engineering. Neutrons are generated with nuclear spallation reaction by bombarding a mercury target with high-intensity proton beams. The neutrons are slowed down with supercritical hydrogen moderators and then extracted as beams to each experimental apparatus. The principal design of the spallation neutron source is compiled in this comprehensive report.

Keywords : J-PARC, Materials and Life Science Experimental Facility, Spallation Neutron Source, Mercury Target, Supercritical Hydrogen Moderators, Remote Handling

---

(Ed.) Shinichi SAKAMOTO

JAEA-Technology 2011-035

J-PARC 核破砕中性子源施設の設計

日本原子力研究開発機構 J-PARC センター
物質・生命科学ディビジョン中性子源セクション

（2011 年 12 月 12 日受理）

大強度陽子加速器施設 J-PARC の実験施設のひとつである物質・生命科学実験施設 MLF では、強力なプローブである中性子ビームを用いて物質科学、生命科学での基礎研究の推進、さらには産業分野での技術開発が期待される。大強度の陽子ビームを水銀標的に照射し、核破砕反応により大量の中性子を発生させる。その中性子は超臨界水素により減速され、最適のエネルギーのビームとして各実験装置へ供給される。実験施設の中枢というべき核破砕中性子源の基本的な技術設計を集大成した。

J-PARC センター：〒319-1195 茨城県那珂郡東海村白方白根 2-4
（編）坂元眞一

Contents

目次

List of Authors

1. Introduction to Materials and Life Science Experimental Facility (MLF)
   Shinichi SAKAMOTO
2. Neutron Source Facility
   - 2.1 Outline of Neutron Source Facility — Masatoshi FUTAKAWA
   - 2.2 Mercury Target System — Katsuhiro HAGA, Hiroyuki KOGAWA, Takashi WAKUI, Masatoshi FUTAKAWA
   - 2.3 Moderator and Reflector — Makoto TESHIGAWARA, Tetsuya KAI, Masahide HARADA, Hiroyuki KOGAWA, Tomokazu ASO, Hideki TATSUMOTO
   - 2.4 Cryogenic Hydrogen Circulation System — Tomokazu ASO, Shoichi HASEGAWA, Kiichi OHTSU, Hideki TATSUMOTO, Toshiaki UEHARA, Takashi KATO
   - 2.5 Fundamental Components for Neutron Source Station — Hiroshi TAKADA, Fujio MAEKAWA, Shiro HONMURA, Yoshimi KASUGAI, Hiroyuki KOGAWA, Takuji TERAOKU, Katsuhiko YOSHIDA
   - 2.6 Neutron Beam Line Components in Neutron Source Station — Hiroshi TAKADA, Kenichi OIKAWA, Kenji SAKAI, Yoshihiro HOSHINO, Tetsuya KAI, Hironori OHASHI, Daisuke SHIGAKI, Katsuhiko YOSHIDA
   - 2.7 Remote Handling Facility — Hidetaka KINOSHITA, Makoto TESHIGAWARA
   - 2.8 Proton Beam Transport Line — Shinichi SAKAMOTO, Shin-ichiro MEIGO, Tetsuya KAI, Yoshimi KASUGAI, Motoki OOI, Chikara KONNO, Masahide HARADA, Hiroshi FUJIMORI*, Takehiro ONO, Hidenori OHTAKE, Shigenori AZUMA, Kiyomi IKEZAKI, Kenji SHINOMIYA
   - 2.9 Handling and Storage of Activated Components — Hidetaka KINOSHITA
   - 2.10 Utility — Hidetaka KINOSHITA, Masakazu SEKI, Masanori KAMINAGA

---

* High Energy Accelerator Research Organization (KEK)

* High Energy Accelerator Research Organization (KEK)

Preface

The conceptual design of the spallation neutron source in the Japan Proton Accelerator Research Complex (J-PARC) was systematized in early stage of the construction project. Since then the construction team had been devoting their effort to develop the design into thousands of blueprints for fabrication. The scenarios of the facility maintenance and the commissioning strategy had been also discussed in the course of the construction. The essence of the final design on the spallation neutron source is collected in this report.

1. Introduction to Materials and Life Science Experimental Facility (MLF)

1.1 Outline of J-PARC

The Japan Proton Accelerator Research Complex[1-1)] (J-PARC) is one of the leading power frontiers in the proton accelerators (Fig. 1.1). J-PARC is a multi-purpose research facility complex, consisting of three accelerators[1-2)] and four experiment facilities. The linear accelerator (Linac) accelerates H^- particles up to 400 MeV, which are then injected to the rapid-cycling synchrotron (RCS). Those particles are converted to H^+ particles with a charge stripping foil and accelerated to 3 GeV. The maximal current of the output beam is 333 μA, which provides 1-MW beam power for the Materials and Life Science Experimental Facility (MLF). The 3-GeV beam is also injected to a larger synchrotron (MR) and accelerated up to 50 GeV. The beam current is 15 μA, which provides 750-kW beam power for the Hadron Hall of the Nuclear and Particle Physics Facility (HD) and the Neutrino Facility (NU). The Layout of the J-PARC accelerators and the experiment facilities is shown in Photo. 1.1.

The high-intensity proton beams are transported into experiment facilities, where targets are bombarded and various kinds of secondary particles, such as neutrons and K mesons, are produced. Those secondary particles are selected, collected, decelerated or let to decay into other particles for experiments in the wide range of research fields in basic science, such as particle physics, nuclear physics, materials science, chemistry and biology. J-PARC also expects a lot of users from applied sciences and industries for practical researches.

The J-PARC started construction in 2001 in the south site of the Nuclear Science Research Institute, Japan Atomic Energy Agency (JAEA). The beam commissioning was initiated with Linac in 2006, and succeeded with RCS, MR and the experiment facilities in turn. The first phase of J-PARC construction project was completed in 2009. The research facility for accelerator-driven nuclear transmutation is to be built in the second phase of the project.

1.2 Outline of Materials and Life Science Experimental Facility (MLF)

The Materials and Life Science Experimental Facility (MLF) was built[1-3, -4)] to become one of the leading research laboratories in the world, providing powerful probes and excellent experiment environment. Neutron beams and muon beams of good quality and unique characteristics are generated with high-intensity proton beams from the 3-GeV RCS accelerator.

A “Slow” neutron beam is the best probe for looking into the atomic structure of materials. The materials are irradiated with neutrons and some of them are scatted by colliding with the atoms. Those neutrons provide clue to the structure. The beam intensity had not been necessarily high and research fields had been rather limited. The J-PARC Spallation Neutron Source substantially overcomes this weak point and brings out new excitements on materials and life sciences with high-intensity and high-quality neutron beams.

The neutron beams in J-PARC are pulsed, since it is generated by irradiating mercury target with pulsed proton beam from the accelerator. The instantaneous beam intensity is tremendously high, contrary to continuous neutron beams from nuclear reactors. This advantage surely broadens horizons in the dynamics of materials.

Muon is the lepton of the second generation and has either positive charge or negative charge. Positively charged muon behaves like 200 times heavier positron in materials and works as an excellent probe to study the magnetic properties of the material. Negatively charged muon, on the other hand, behaves like lighter proton in materials and is used as a unique probe to study the atomic properties of the materials.

The facility was designed to provide diverse users with excellent research environment as well as power beams, laying emphasis on the following conditions,

- stable beam supply,
- users' safety in terms of radiation and other hazards, and
- user-friendly research environment and accessibility.

The construction of the MLF building was started in December 2003 and the devices of the neutron source and the muon source were being installed in parallel. The building was completed in April 2007 (Photo. 1.2) and the first proton beam was finally delivered to MLF on 30 May 2008.

1.3 Structure of Materials and Life Science Experimental Facility (MLF)

The Materials and Life Science Experimental Facility (MLF) consists of six parts, 1) 3-GeV proton beam transport line, 2) neutron source, 3) muon target, 4) neutron spectrometers, 5) muon spectrometers and 6) conventional facilities. They are organically combined and operated to achieve high performance and surmount difficulties in dealing with 1-MW proton beam.

The proton beam transport line connects the 3-GeV RCS and the Materials and Life Science Experimental Facility (MLF) and extends over 300 m. The final goal of the proton beam is the neutron production target at the center of the MLF building. The muon production target is placed in the proton beam line 33-m upstream of the neutron target.

The proton beam bombards the neutron production target and plenty of neutrons are produced by nuclear spallation reactions. The neutrons are cooled down and extracted radially as a beam to neutron spectrometers in experimental halls. The neutron beams are guided into the neutron spectrometers for experiments.

Several percent of the proton beam is dissipated at the muon production target before reaching the neutron production target. Muons and pions are generated in the target and transported to the muon spectrometers in the experimental halls.

Conventional facilities, such as coolant and drain facilities, air conditioning facilities and electric power supply facilities, are sustaining the beam productions and the research activities in MLF all the time. They were specially designed for handing high-intensity proton beams steadily and highly-activated components soundly.

References

1-1) The Joint Project Team of JAERI and KEK: “The Joint Project for High Intensity Proton Accelerators”, JAERI-Tech 99-056, 1999.

1-2) High-intensity Proton Accelerator Project Team: “Accelerator Technical Design Report for High-intensity Proton Accelerator Facility Project, J-PARC”, JAERI-Tech 2003-004/KEK Report 2002-13, 2003.

1-3) Materials & Life Science Experimental Facility Construction Team: “High-intensity Proton Accelerator Project (J-PARC) Technical Design Report Materials & Life Science Experimental Facility” JAERI-Tech 2004-001/KEK Report 2004-03, 2004, in Japanese.

1-4) S. Sakamoto et. al.: “Design Report on the 3-GeV Proton Beam Transport Facility (3NBT) of High Intensity Proton Accelerator Facility Project (J-PARC)”, JAERI-Tech 2004-020, 2004, in Japanese.

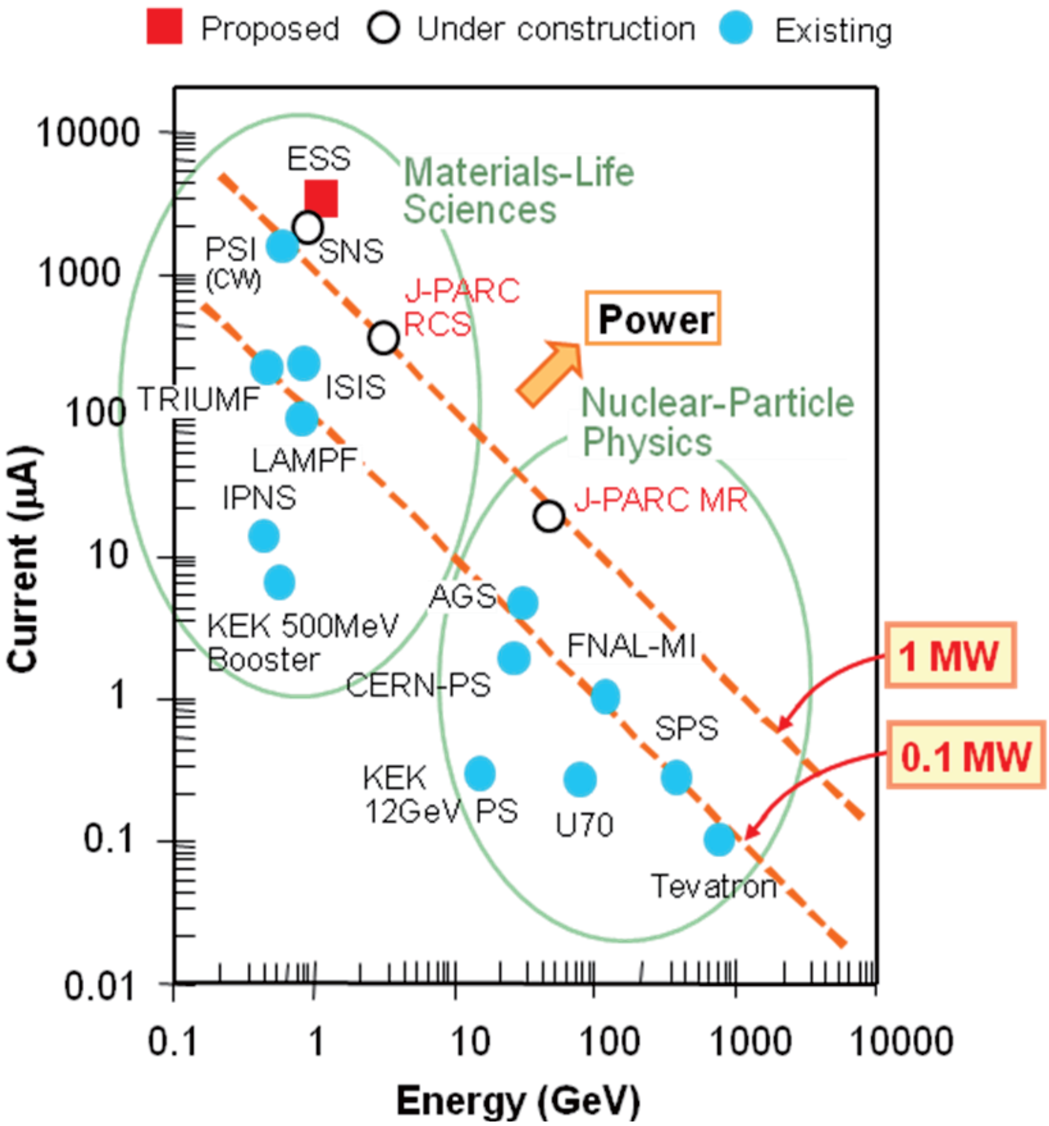

Fig. 1.1: Beam powers of proton accelerators in the world (compiled in 2001).

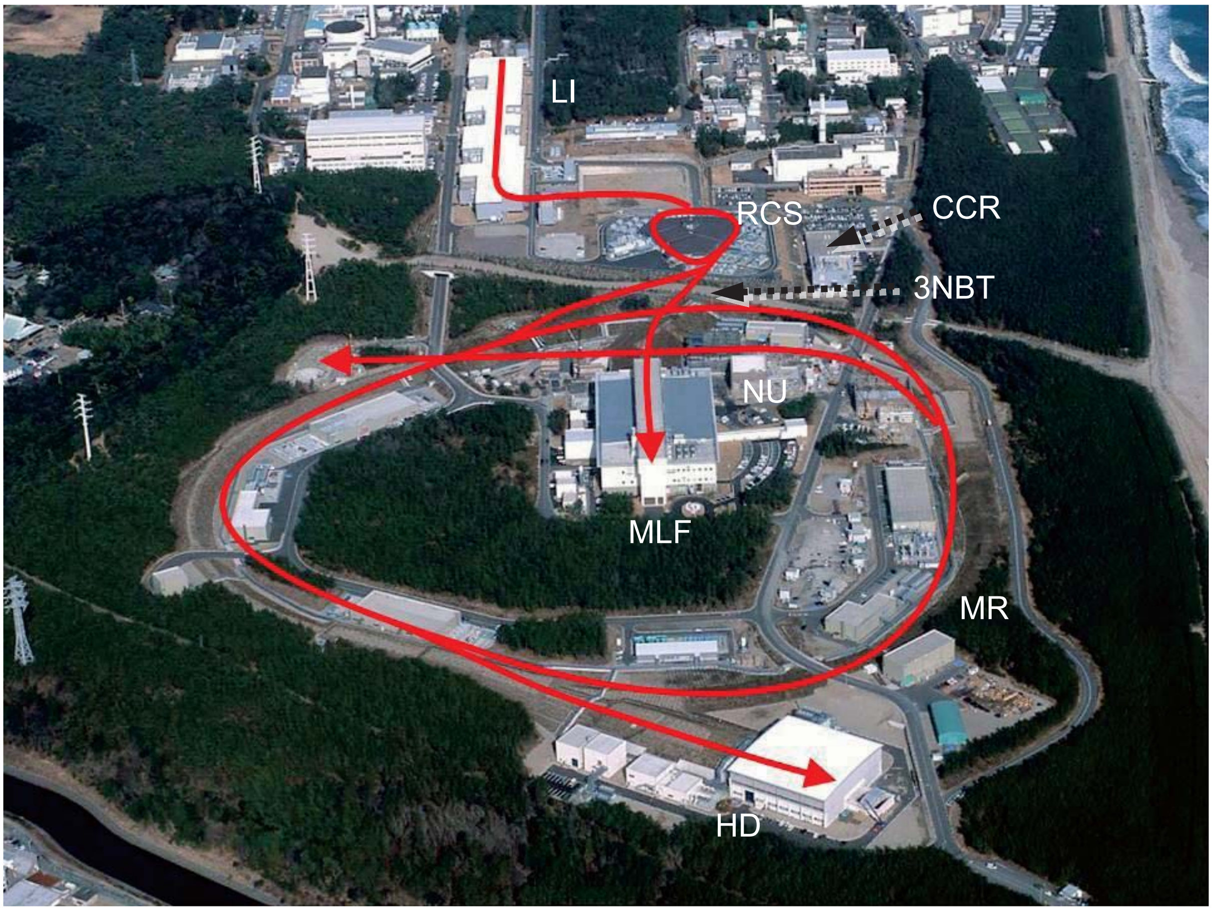

Photo. 1.1: Layout of J-PARC accelerators and experiment facilities (photographed in January 2008, CCR: Central Control Room, HD: Hadron Facility, LI:Linac, MLF: Materials and Life Science Experimental Facility, MR: 50-GeV Synchrotron, NU: Neutrino Facility, RCS: 3-GeV Rapid- Cycling Synchrotron, 3NBT: Beam Transport form RCS to MLF)

Photo. 1.2: The Materials and Life Science Experimental Facility building and the 3NBT building (photographed in January 2008)

2. Neutron Source Facility

2.1 Outline of Neutron Source Facility

The Materials and Life Science Experimental Facility (MLF) consists of 1-MW pulsed spallation neutron and muon sources for various experiments in terms of materials and life sciences. Fig. 2.1.1 shows a drawing of the MLF building and photos of main components installed in it. The dimension of the facility building is 146 m in length, 70 m in width and 30 m in height. The total amount of floor space is 19,440 m^2, including two experimental halls. Fig. 2.1.2 shows a cutaway view of the experimental halls. The MLF receives a 3-GeV, 333-μA, 25-Hz pulsed proton beam through a proton beam line. About 10% of the proton beam is spent at a muon production target and collimators, which are located just after the muon production target, and the rest of the beam is injected into a mercury target. Total 23 neutron beam lines are to be installed in the experimental halls.

Fig. 2.1.3 shows a cutaway view of the target station and the irradiation components handling room. The mercury target and the mercury circulation loop are installed on a target trolley. The mercury target vessel and mercury circulation components such as a mercury pump will be replaced or repaired by remote handling devices such as an in-cell crane and a power manipulator in the irradiated components handling room that is located opposite to the proton beam line. The mercury circulation loop supplies mercury to the target vessel at the maximum flow rate of 41 m^3/h. A reflector-moderator assembly is fixed on the bottom of a reflector plug and set in a helium vessel. Neutrons generated in the target are degraded in energy to appropriate value by three cryogenic hydrogen moderators, and then the neutrons are supplied to the user instruments through neutron beam lines, as shown in Fig. 2.1.2. The reflector–moderator assembly is removed vertically from the target station with the reflector plug by a 130-tons crane that is located above the target station and is transferred into the irradiated components handling room for their maintenance by remote handling. Used components such as the target vessel, moderator and mercury circulation components are stored in the irradiated components storage room in the basement.

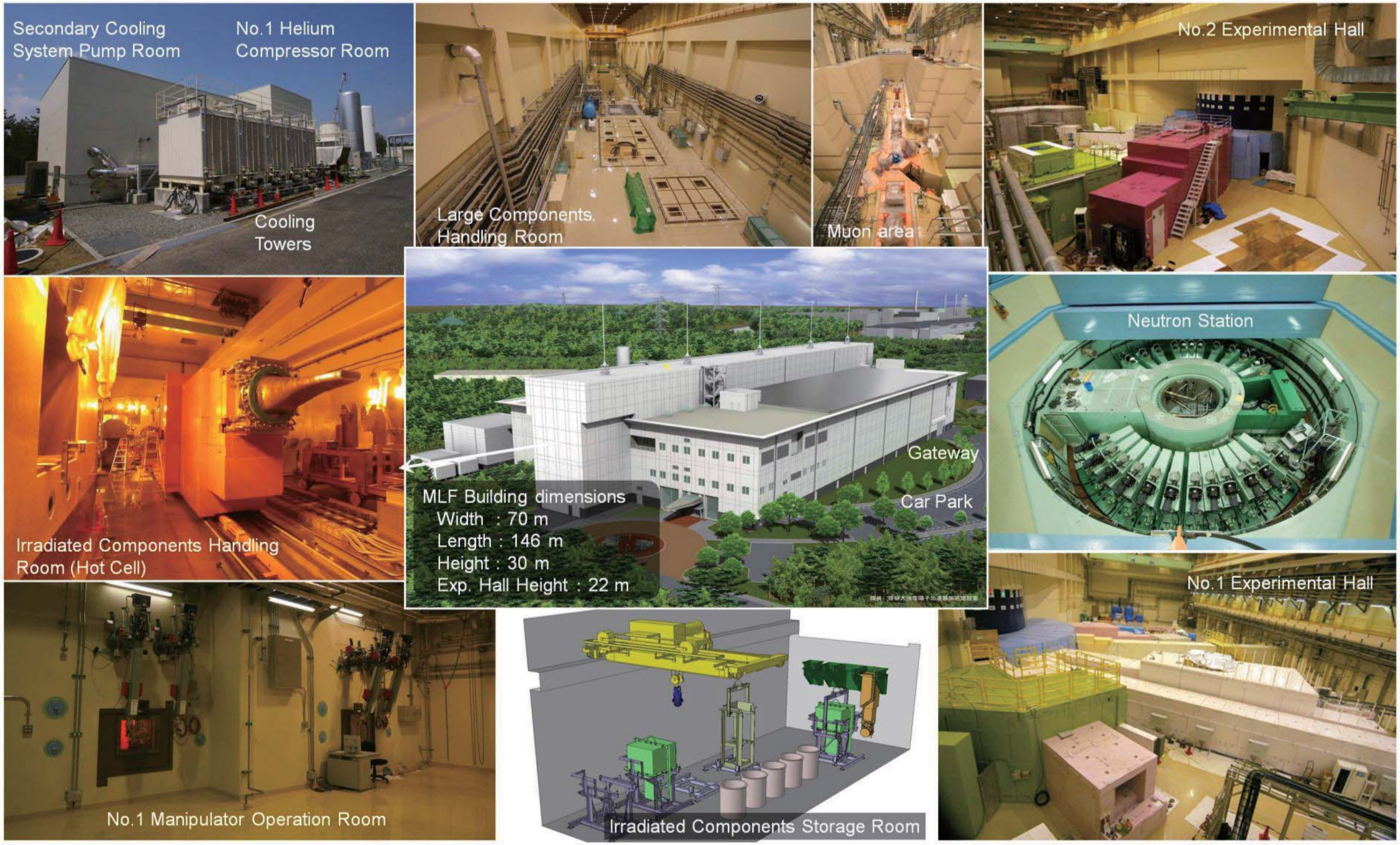

Fig. 2.1.1: The Materials and Life Science Experimental Facility, MLF. A drawing of the MLF building and pictures of main components installed in it.

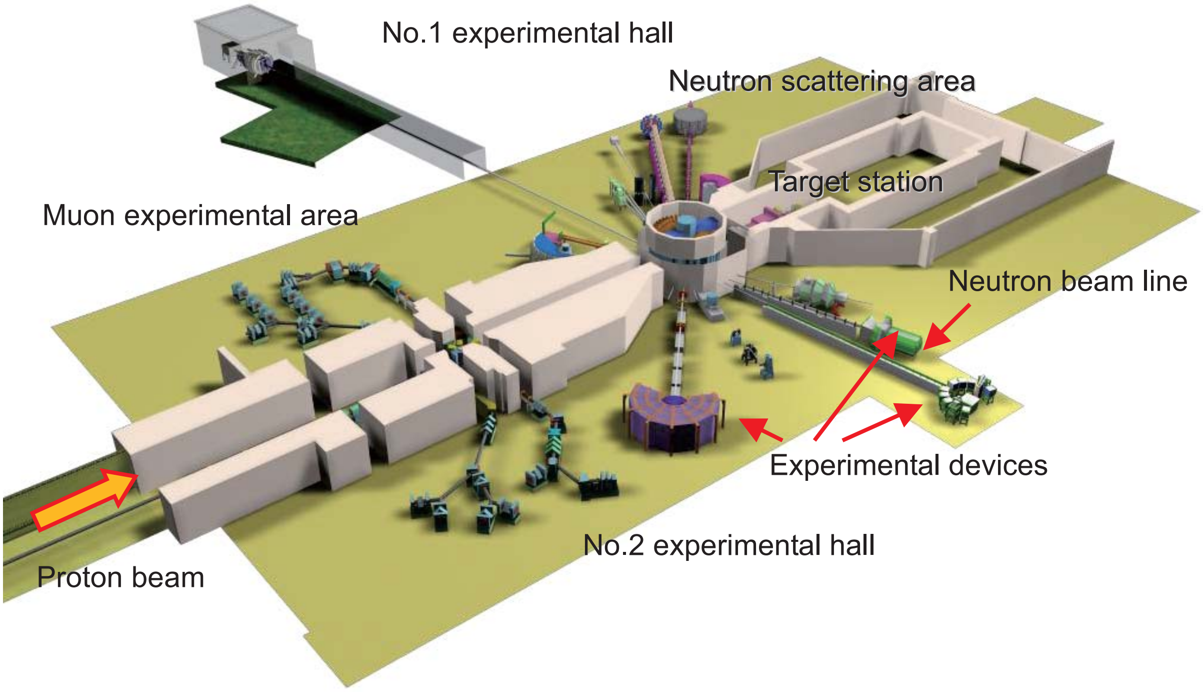

Fig. 2.1.2: A cutaway view of experimental halls

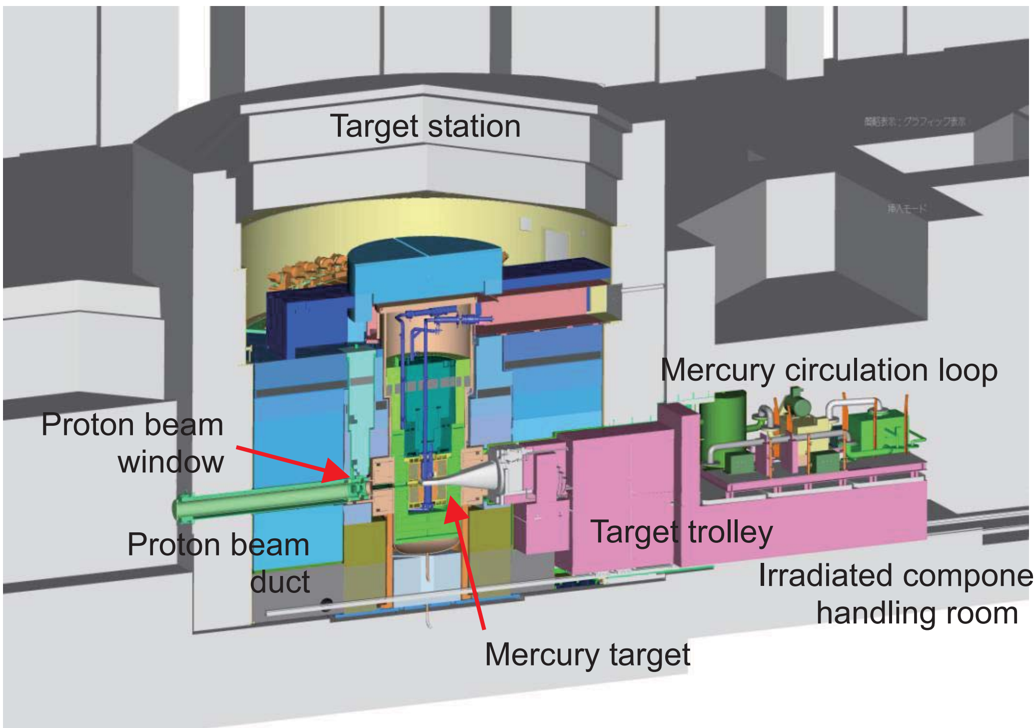

Fig. 2.1.3: A cutaway view of the target station and the target system in the irradiation components handling room

2.2 Mercury Target System

2.2.1 Overview

Fig. 2.2.1 shows the bird's eye view of the mercury target vessel and the mercury circulation system mounted on the target trolley. The target vessel is installed at the front end of the target trolley and two mercury pipes, the inner diameter of 148 mm, penetrate the radiation shield blocks to connect the mercury circulation system to the target vessel. Once the target system operation starts, mercury, the target vessel and the surrounding components are highly irradiated, so that all the replacement and maintenance operations have to be done with remote handling. The target vessel can be attached to and detached from the mercury pipes using the remote handling pipe connector developed for this system. The mercury circulation system has the ability to circulate the mercury at the rated flow rate of 41 m^3/h and main components are designed so that they can be replaced also by remote handling. Mercury circulation system components such as a mercury pump, a heat exchanger, a flow meter and a surge tank are installed on the target trolley. The mercury target system is 12.2 m in length, 2.6 m in width, 4 m in height and 300 t in weight including the mercury target, the mercury circulation system components, the target trolley and the mercury itself. Loaded mercury will be used during the MLF lifetime of more than 30 years without replacement.

Fig. 2.2.2 shows the target trolley inserted into the target station core which consists of a helium vessel, a neutron reflector and bulk shielding blocks. The target trolley carries the heavy components of the target vessel and the mercury circulation system into the core of the target station, and fixes the target vessel at the right position during the on-beam operation, and also withdraws to the maintenance room of hot cell during the system maintenance period. Once the target trolley is withdrawn into the maintenance room, the component exchange or repairing work is carried out by the remote-handling using a power manipulator and some master-slave manipulators. Because the components are packed in the target station core with least spatial gap in order to maximize the neutronic performance, the target vessel must be positioned very accurately on the proton beam axis, where the gap between the neutron reflector housing and the target vessel is only 8 mm.

2.2.2 Mercury Target

(1) Overall description

The mercury target vessel is designed as multi-walled vessels in order to ensure the system safety by avoiding the mercury leakage into the helium vessel in case of the mercury vessel failure. Fig. 2.2.3 shows the schematic drawing of the mercury target structure. The double-walled safety hull covers the single-walled mercury vessel, so that it can play roles of 1) prevention of the mercury leakage to the outside and 2) support of the mercury vessel though the reinforcement ribs. Helium gas is filled between the mercury vessel and the safety hull. The mercury vessel and the safety hull are cooled by mercury flow and the heavy water flow between double walls, respectively. The forefront wall of the mercury target vessel is called as the beam window, since it is directly irradiated by proton beam. The size of the mercury target vessel is shown in Table 2.2.1. The condition of proton beam and criteria for designing the mercury target vessel are shown in Tables 2.2.2 - 2.2.4. It was confirmed that these design conditions were fulfilled using numerical analyses.

(2) Design of mercury vessel

Fig. 2.2.4 shows the schematic drawing of the mercury vessel without the safety hull. A cross-flow type (CFT) mercury vessel is adopted from the viewpoint of good thermal-hydraulic performance in JSNS, in which mercury flows across the proton beam path. In CFT mercury vessel, mercury flow was optimized to be distributed corresponding to the heat density by flow vanes and to suppress the re-circulation flow in the mercury vessel. Hence, the high heat density in mercury can be removed effectively by low flow velocity to distribute appropriate flow rate to a region near the beam window where the peak heat density is generated. The flow vanes (10 mm) also have a function as the reinforcements to enhance the mechanical strength of the mercury vessel. In order to reduce the bulk heating by the energy loss of incident protons and proton induced nuclear reaction at the beam window, the wall thickness of the beam window (2.5 mm) is thinner than that of the side walls (10 mm). Type 316LN austenitic stainless steel is selected as the material for the mercury vessel considering its high corrosion resistance against mercury. The specifications of the mercury vessel are summarized in Table 2.2.5.

In order to connect with the mercury vessel and the mercury pipe on the target trolley by remote handling, the mercury pipe connector is applied. Fig. 2.2.5 and Table 2.2.6 show the schematic drawing and specifications of the mercury pipe connector. Both flanges of two mercury flow lines can be connected simultaneously by turning a driving shaft with the power manipulator. Bellows between the mercury vessel and the mercury pipe connector can adjust the distance between flanges. By connecting the flanges, double knife edges indent the iron plate seal and this system has a good seal performance (Helium leak rate < 1×10^{-6} $MPam^3/s$). In order to use the flange of the mercury pipe set on the target trolley for long time, the knife edges are composed of harder Stellite alloy than iron plate seal. The tray with three mercury leak detectors is put under the mercury pipe connector so that it can catch the mercury spilt from mercury pipe connection flange. If the amount of mercury leaks is too large to overflows from the tray, the spilt mercury tanks in the target trolley can storage it.

Five thermo-couples and three optical fiber strain gauges are set on the upper surface of the mercury vessel to observe the temperature and strain of the mercury vessel, respectively. The optical fiber strain gauges were used at just the on-beam commissioning with the low beam power.

(3) Safety hull

The specifications of the safety hull are shown in Table 2.2.7. The safety hull is connected the mercury vessel with bolts. The holes for these bolts are filled up by the welding to keep airtight. The container wall shown in Fig. 2.2.3 divides the space between the mercury vessel and the safety hull into two spaces, the front and rear spaces. If the beam window of the mercury vessel fails, the mercury leaking from the mercury vessel is contained only in the front space. Two mercury leak detectors are set on front surface of the container wall and the mercury leak monitoring system can detect the mercury leakage. The minimum detection of the mercury leakage is about 120 cm^3.

In order to investigate the vibration behavior of the mercury target vessel due to the impact of the pulsed proton beam injections, the Laser Doppler vibration system was adopted and a self reflecting mirror was fixed on the upper surface of the safety hull with silver brazing.

The helium vessel seal mechanism shown in Fig. 2.2.6 is set on the target flange to keep airtightness of the helium vessel flange. The helium vessel seal mechanism has a double bellows structure. The metal seal with a gold coating is pressed against the helium vessel flange by supplying the helium gas between bellows. The design pressure of the helium gas is 0.95 MPa and the line load becomes higher than 60 kgf/cm. The specifications of the helium vessel seal mechanism are shown in Table 2.2.8.

2.2.3 Target Trolley

(1) Overall description

The target trolley is the carriage of main components of the mercury target system. It consists of two parts; the shielding trolley and the mercury system trolley. The shielding trolley consists of a carriage base, radiation shield blocks and many piping penetrating the radiation shield. The mercury system trolley consists of iron blocks that surround two mercury drain tanks and two spilt mercury tanks in it, and a trolley driving mechanism. Radiation shield blocks on the shielding trolley are for shielding the radiation generated by mercury spallation reactions during on-beam operation, while the iron blocks on the mercury system trolley are for shielding X-ray from irradiated mercury in the drain tanks during off-beam maintenance operation. The primary specifications of the target trolley are shown in Table 2.2.9. The general design conditions of the target trolley are shown in Table 2.2.10.

(2) Design of the shielding trolley

Radiation shield blocks consist of iron (or stainless steal) blocks and normal concrete blocks, which are shown as hatched area and dotted area respectively in Fig. 2.2.7. The combination of the radiation shield blocks was decided by neutronic analyses, so that the radiation dose rate would be less than the design criterion of 0.125 μSv/h on the border of the public area. The radiation shield block at the forehead of the target trolley, which is called the water cooling block, is made of stainless steal and is cooled by water to cool down the radiation heating of approximately 2 kW.

In case of heavy mercury leakage accident in the water cooling block, where the mercury leak from the pipe connection flange of the target vessel is the most presumable, the spilt mercury would be guided to the spilt mercury tanks through the spilt mercury pipe, and the mercury leak coming through the pipe can be detected by a mercury senser mounted on the pipe. There are many pipes and senser cables installed through the radiation shield blocks with rectangular bending at 4 different positions in order to reduce streaming effect. Fig. 2.2.8 shows the isometric drawing of the pipes. It can be seen that the mercury pipe is bent two times vertically and also two times horizontally, and it is designed such that all the mercury is drained out of the mercury circulation system to the drain tanks. The specifications of the shielding trolley are shown in Table 2.2.11.

(3) Design of the mercury system trolley

Fig. 2.2.9 shows the inner structure of the mercury system trolley. The mercury drain tanks and the spilt mercury tanks are mounted in the mercury system trolley. In order to minimize the height of the tanks and to use the space in the mercury system trolley effectively, the drain tank and the spilt mercury tank consists of two tanks respectively. The gas phase and the liquid phase of each two tanks are connected together with pipes and they works as one component units. The total capacity of the drain tank is 1.8 m^3 and that of the spilt mercury tank is 0.7 m^3. All of the mercury drain pipes have the inclination of more than 1/100. The specifications of the mercury system trolley, the mercury drain tank and the spilt mercury tank are shown in Tables 2.2.12, 2.2.13 and 2.2.14, respectively.

Mercury loaded into the drain tanks is pressurized by helium gas and filled into the mercury circulation system. Also mercury is drained to the mercury drain tanks during the maintenance period. In case of a mercury leakage accident, mercury would be collected on a spilt mercury pan spread beneath the mercury circulation system, shown in Fig. 2.2.10, and led to the spilt mercury tanks. Mercury leak detector is also mounted on the spilt mercury pan to detect the leakage. Though the mercury initially loaded is supposed to be used until the end of the facility lifetime, the mercury transfer line to the dump tank on the basement floor is prepared for mercury exchange just in case.

As shown in Photo. 2.2.1, all the pipes and cables, except the mercury pipes, on the target trolley are laid along a cableveyer, using flexible pipes, to connectors or plugs on the hot cell wall, and the target trolley can move free from connection or disconnection operation of pipes and cables, which might be necessary when rigid pipes are used. Rack & pinion system was chosen as the driving mechanism of the target trolley to ensure the positioning accuracy of the target trolley. The maximum moving velocity of the target trolley is 20 mm/s, and the minimum velocity is 4 mm/s. Rotation speed and number of rotation of the driving motor can be converted to trolley speed and trolley position respectively because there is no slip between rack and pinion. In addition to the position detection by the motor rotation, an ITV (Industrial Television) camera was mounted on the side surface, making it possible to visualize a position scale laid on the hot cell floor along the linear roller way rail. The specifications of the trolley driving mechanism and the ITV camera are shown in Tables 2.2.15 and 2.2.16.

(4) Load on the linear roller way

A linear roller way (Fig. 2.2.11) was adopted to ensure high accuracy and reproducibility of the target vessel positioning. One linear roller way can sustain the static burden of 74.3 tons, which sums up to the total sustainable burden of 1,188 tons, 4 times heavier than the trolley itself. Although the linear roller ways are set up such that they can be replaced in case of their trouble, the replacement operation will need a long period of system shutdown. In order to reduce the possibility of the linear roller way trouble, we gave them the enough design margins.

2.2.4 Mercury Circulation System

(1) Overall description

Mercury circulation system provides mercury to the mercury target and removes the generated heat in the mercury target due to the spallation reaction. Fig. 2.2.1 shows layout of components of the mercury circulation system on the target trolley with the mercury target. Fig. 2.2.12 shows a phase and instrument diagram and conceptual design view of mercury circulation system. Main components of the system are a mercury circulation pump, a heat exchanger, and a surge tank. These components are connected with pipes of 165 mm in outer diameter and 11 mm in thickness to make closed loop for mercury to prevent leak of mercury vapor and other gas which are radioactive due to spallation reaction.

The surge tank absorbs volume change due to the temperature change in the mercury target to control pressure change in mercury. The heat exchanger removes a heat generated in the mercury target and the mercury circulation pump. And the mercury circulation pump circulates mercury and provides mercury into the mercury target.

The mercury circulation system is set on the target trolley which mentioned in subsection 2.2.3. Drain tanks are set into the target trolley to drain mercury from the mercury target and mercury circulation system when the mercury target and the components are exchanged or some deficiencies occur. Spilt mercury storage tanks are also available into the target trolley to store the spilt mercury on the target trolley in exchange of the components. Mercury in the spilt mercury storage tanks can move to the drain tanks and it in the drain tanks can move to a dump tank which is set on the underground of the MLF and stores mercury spilt on the floor of the hot cell.

Design conditions are shown in Table 2.2.17.

(2) Design guideline and specification of components

(2.1) Mercury inventory

Mercury inventory in the mercury circulation system is shown in Table 2.2.18. The volume of the drain tanks is 1.8 m^3 and the volume of the spilt mercury storage tanks is 0.7 m^3.

(2.2) Surge tank

Table 2.2.19 shows a specification of the surge tank.

Pressurized helium gas is used for a cover gas in the surge tank to prevent the cavitation at an inlet of the pump. The pressure is 0.1 MPaG.

Since most of the impurity compositions in mercury are lighter than mercury, they can be separated in the surge tank. To separate more impurities, the inlet and outlet pipes to the surge tank are set on the upper and bottom part of the tank so that the holdup time in the surge tank can be long as possible. Furthermore, the inlet pipe has bent inside of the tank to make a swirl of mercury in the tank.

The surge tank is surrounded with steel shielding to decrease a radiation from remained mercury after drainage of mercury so that the radiation damage can be reduced on the maintenance tools such as a power manipulator, cameras etc.

(2.3) Mercury circulation pump

Two types of the mercury circulation pumps have been prepared. A permanent magnet rotating type induction pump (PM pump) is used as a main pump. A mechanical gear pump is a backup for the PM pump. The gear pump is surrounded by the steel shielding. However the PM pump is not surrounded by the shielding because mercury would not be remained in the PM pump after drainage as well as pipes.

At first, the gear pump was developed for the mercury circulation pump. Mechanical seals are required for mercury leak between the pump casing and drive shaft. However, it does not seem that these seals can keep the function for long time. The leaked mercury from the mechanical seals of the gear pump can be stored into the spilt mercury storage tank with surveillance by three stage leak detector. That is, the mercury circulation system will be operated in allowance of mercury leak to the spilt mercury storage tanks from the mechanical seals. As for the PM pump, since there are no seal parts, the system can be operated in low possibility of mercury leak. However, the large motor is required to obtain sufficient flow rate on account of the low efficiency of the PM pump. Almost motor power is changed to the Joule heating in the PM pump, which should be removed by a heat exchanger in the mercury circulation system. Therefore, the PM pump was developed to reduce the Joule heating and to increase the flow rate of the mercury[2.2-1)]. Tables 2.2.20 and 2.2.21 show specifications of the gear pump and the PM pump, respectively. Fig. 2.2.13 shows a photograph and schematic drawing of the PM pump.

(2.4) Heat exchanger

Table 2.2.22 shows a specification of the heat exchanger.

The heat exchanger is a double walled type to prevent the mercury leak into secondary cooling water if the mercury wall is broken.

The double walled type heat exchanger has a helium layer between the heat transfer walls of mercury and cooling water. If the mercury wall is broken, mercury would spill into the helium layer. A mercury leak detector is set in the helium layer to detect spilt mercury into helium layer.

The heat exchanger is designed to remove the heat generated in the mercury target with 10% margin. This margin will be used for the heat removal generated in the PM pump.

The heat exchanger is surrounded by shielding.

(2.5) Pipes

The pipes are connecting between (a) the surge tank and the pump, (b) pump and the heat exchanger, and (c) the heat exchanger and inlet of the target vessel. These pipes can disconnect from the system before the exchange of the components such as the pump, the heat exchanger and the surge tank. These pipes have bellows to absorb a small size error of new components.

Mercury flow velocity in pipes is limited up to 1 m/s to reduce erosion of the pipes. Pipes of 150A-Sch.80 (JIS) made of Type 316L stainless steel are used as the main pipes. The size of the main pipes is 165.1 mm in outer diameter and 11 mm in wall thickness. The flow velocity of mercury in main pipes is 0.86 m/s (< 1 m/s) at maximum flow rate of system Q=50 m^3/h.

Three pipes can be disconnected from the system by remote handling tools. These pipes have a three layer-walled bellow at one end of the pipes to adjust the position between the components and pipes when the maintenance is carried out by remote handling.

Mercury drain lines are connected to the lower points of the parts and the pipes of the mercury loop. Other ends of the drain lines are connected to the drain tank. Pneumatic valves are set on the drain lines between the mercury circulation system and the drain tanks.

A vent line with pneumatic valve is set between the target outlet and surge tank to avoid the remaining of gas in the target part.

(2.6) Pneumatic valves

Pneumatic valves are set on the side of the mercury system trolley. The pneumatic valves are connected to all the drain lines that come out from the lower points of the mercury loop. Supply of air pressure to operate the pneumatic valve is controlled by solenoid valves set in a shielding box on the target trolley. The pneumatic valves are also opened and closed by the power manipulator providing against the air-supply stop. The pneumatic valves keep close if the air pressure is lost by the fail of the air supply system or the solenoid valves to prevent increase of temperature on the target vessel and mercury circulation system due to the loss of mercury while the beam operation.

(2.7) Pressure sensor

Detector and distributor of pressure sensor are separated and connected with capillary tube. Detector and capillary tube are made of type 316 stainless steel. The inside is filled with silicone oil to transfer the pressure to the distributor. The lifetime of detector and capillary tube is estimated to be 40 years.

The distributors of the pressure sensors are shielded against radiation damage by the shielding box. Three distributors are enclosed in one box. Three pressure sensors or two pressure sensors and one pair of differential pressure sensors must be exchanged simultaneously even if one sensor is in out of order.

Electric cables with polyimide shielding are used for the signal transfer lines to prevent the radiation damage of the cables. As for all the other cables in the hot cell such as the thermometer, power cable for the pump, the polyimide shielding is applied to them.

(2.8) Flow meter

A Venturi type flow meter is set on the pipe connecting between the heat exchanger and the inlet of the target vessel.

A differential pressure sensor set on the venturi to detect the flow velocity of mercury is the same type with the pressure sensor mentioned above. That is, the detectors and distributor are separated and they are connected with capillary tube.

(2.9) Level meter

Mercury level in the surge tank is measured to monitor whether mercury leak occurs or not and to use for confirmation of the end of filling mercury into and drain of mercury from the system.

A level meter consists of two pressure sensors set on top and bottom of the surge tank, which measure the pressure of the cover gas and the sum of the static pressure of the head of mercury in the surge tank and the cover gas pressure, respectively. Therefore, difference between the bottom and top sensors indicates the static pressure of the head of mercury. Mercury level is calculated from the difference of pressures.

(2.10) Thermometer

A couple of thermometers are mounted both at the outlet of the mercury target and at the outlet of the heat exchanger.

(2.11) Mercury leak detector

Mercury leak detectors are set on the catch pan, the catch pan for the valves and the helium layer of the heat exchanger. These detectors monitor conductivity between the electrode of the detector and earth (catch pan, wall of the helium layer of the heat exchanger). If mercury spills, circuit short occurs between the electrode and earth.

(2.12) Safety

Mercury circulation system is set on the catch pan which is installed between the system and top of the target trolley. The catch pan has a drain line connected to the spilt mercury storage tanks and mercury detectors are set in the drain line. If mercury spills from the system, the spilt mercury is stored in the catch pan at first and it is detected by the detector and then the spilt mercury is stored into the spilt mercury storage tank.

(3) Operation modes

(3.1) Normal operation

The proton beam can be injected to the mercury target after mercury is filled up and flowed with the related flow rate in mercury circulation system. A pump to flow mercury can be operated remotely at a control room. A driving motor of the pump is controlled by inverter. Rotation speed of the motor can be controlled at a local control panel.

The mercury circulation system has interlock against high temperature of mercury, low flow rate of mercury, high pressure in the loop, low level of mercury in the surge tank and mercury loop from the components.

(3.2) Component maintenance

Mercury should be drained for maintenance such as exchanges of the target vessel and components of the mercury circulation loop. The mercury drain follows to the evacuation of cover gas in the surge tank to prevent diffusion of the high radio-activated cover gas to the drain. The drain lines with the pneumatic valves are set on between all low points of the mercury circulation loop and the drain tank. All components are designed to be exchanged by remote handling.

(3.3) Preparation for normal operation

After the maintenance, the mercury circulation loop is filled with mercury for the normal operation. To reduce the gas accumulation in the loop after filling up mercury, the mercury circulation loop is evacuated at first after the leak check. And then, mercury is filled up by pressurizing the drain tank. The pneumatic valves are automatically closed when the mercury level of the surge tank attains to set level. After that, the cover gas is supplied to the surge tank. And the drain tank is evacuated to be able to drain mercury for the emergency in the normal operation.

Reference

2.2-1) H. Kogawa et al.: “Development on mercury pump for JSNS”, Nuclear Instruments and Methods in Physics Research, A 600, 2009, pp. 97-99.

Table 2.2.1: Primary specifications of the mercury target

1	Total length	2.3 m
2	Diameter of target flange	1.2 m
3	Total weight	1.5 tons

Table 2.2.2: Conditions of proton beam

1	Proton beam : Energy	3 GeV
2	Proton beam : Electric current	0.333 μA
3	Proton beam : Power	1 MW
4	Proton beam : Frequency	25 Hz

Table 2.2.3: Criteria of structural strength

1	Structure strength	JIS Pressure Vessel Code
2	Displacement of beam window center (mercury filling up)	< 1 mm
3	Displacement of beam window center (Seismic acceleration force: 0.25G)	< ±1 mm
4	Deformation (mercury and helium gas filling up)	< ±1 mm
5	Resonance frequency	> 25 Hz

Table 2.2.4: Criteria of thermal hydraulics

1	Velocity of flowing mercury at inlet	< 1 m/s
2	Maximum temperature of mercury	< 300ºC
3	Maximum temperature of mercury vessel	< 200ºC
4	Pressure drop of mercury in mercury vessel	< 50 kPa
5	Velocity of flowing heavy water at inlet	< 3 m/s
6	Maximum temperature of heavy water	< 110ºC
7	Maximum temperature of safety hull	< 150ºC
8	Pressure drop of heavy water in safety hull	< 0.1 MPa

Table 2.2.5: Specifications of the mercury vessel

1	Type	Cross flow type mercury vessel
2	Dimension	2100 mm (length) × 540 mm (width) × 190 mm (thickness)
3	Slope for draining	> 1/100
4	Weight	425 kg
5	Design temperature	200ºC
6	Design pressure	0.5 MPaG
7	Target fluid	Mercury (0.5 MPaG)
8	Atmosphere	Helium gas (0.5 MPaG)
9	Mercury pipe	150A
10	Material	Type 316LN Austenitic stainless steel
11	Accessories	K type thermo-couple with sheath Beam damp Mercury pipe connector

Table 2.2.6: Specifications of the mercury pipe connector

1	Type	Link mechanism type pipe connector
2	Dimensions	370 mm (length) × 680 mm (width) × 750 mm (height)
3	Weight	150 kg
4	Design temperature	150ºC
5	Design pressure	0.5 MPaG
6	Atmosphere	Inner part : Mercury (0.5 MPaG) Outer part : Helium gas (0.5 MPaG)
7	Seal performance of flange and connector	$< 1\times10^{-6}$ Pa・m^3/s
8	Deformation of the bellow	> 10 mm
9	Material	Type 316LN Austenitic stainless steel
10	Accessories	Metal seal

Table 2.2.7: Specifications of the safety hull

1	Type	Double-walled vessel
2	Dimensions	2300 mm (length) × 1200 mm (diameter of flange)
3	Weight	925 kg
4	Design temperature	150ºC
5	Design pressure	0.5 MPaG
6	Coolant	Heavy water (0.5 MPaG)
7	Atmosphere	Inner part : Helium gas (0.5 MPaG) Helium vessel : Helium gas (0.003 MPaG)
8	Seal performance of target flange	< 1×10^{-6} Pa·m^3/s
9	Material	SUS316LN
10	Accessories	Metal seal Mercury leak detector Cable and pipe connector Optical fiber strain gauge Helium vessel seal mechanism

Table 2.2.8: Specifications of the helium vessel seal mechanism

1	Type	Helium pressurized below type seal mechanism
2	Dimensions	1030 mm / 820 mm (external / internal diameter) × 95 mm (thickness)
3	Weight	150 kg
4	Design temperature	150ºC
5	Atmosphere	Inner part : Helium gas (0.95 MPaG) Helium vessel : Helium gas (0.5 MPaG) Hot cell : Air (atmospheric pressure)
6	Line load	> 60 kgf/cm
7	Seal performance of flange and connector	< 1×10^{-2} Pa·m^3/s
8	Deformation of the below	> 10 mm
9	Material	SUS316LN
10	Accessories	Metal seal with gold coating

Table 2.2.9: Primary specifications of the target trolley

1	Total length	12.2 m
2	Trolley width	2.6 m
3	Maximum height	4 m
4	Total weight	300 tons (including the mercury target, the mercury circulation system components, the target trolley and the mercury itself)
5	Total mercury inventory	1.5 m^3
6	Maximum moving distance	23 m
7	Number of slide units to sustain the trolley	16
8	Travelling speed	high : 20 mm/s, low : 4 mm/s

Table 2.2.10: General design conditions of the target trolley

1	Lifetime of the system	30 years (Necessary maintenance will be carried out.)
2	Seismic acceleration force	0.25G (horizontal), 0.25G (vertical)
3	Positioning accuracy of the target vessel	±1 mm
4	Dimension tolerance of the total size	±3 mm
5	Rust prevention	Not necessary for stainless steel Painting with radiation resistant paint for steel surface

Table 2.2.11: Specifications of the shielding trolley

1	Dimensions	5000 mm (length) × 2600 mm (width) × 4000 mm (height*) * Datum of the height is bottom level of the linear roller way rail.
2	Weight	approximately 150 tons
3	Operation temperature	Max. 100ºC (water cooled block of the forefront) Max. 60ºC (other places)
4	Atmosphere	Air (atmospheric pressure)
5	Material	Carbon steel (density > 7.6 g/cm^3) Normal concrete (density > 2.2 g/cm^3) Stainless steel 316LN for water cooled block

Table 2.2.12: Specifications of the mercury system trolley

1	Dimensions	6200 mm (length) × 2600 mm (width*) × 1650 mm (height**) * It does not include the mercury catch pan on the trolley side. ** Datum of the height is bottom level of the linear roller way rail.
2	Weight	approximately 100 tons
3	Operation temperature	Max. 100ºC (water cooled block of the forefront) Max. 60ºC (other places)
4	Atmosphere	Air (atmospheric pressure)
5	Material	Carbon steel (density > 7.6 g/cm^3) Normal concrete (density > 2.2 g/cm^3) Stainless steel 316LN for water cooled block

Table 2.2.13: Specifications of the mercury drain tank

1	Dimensions	3736 mm (length) × 560 mm (inner diameter) × 8 mm (wall thickness) for 1 tank
2	Total capacity	1.8 m^3 (0.9 m^3 × 2)
3	Design pressure	0.99 MPa
4	Design temperature	100ºC
5	Material	Stainless steel 316LN
6	Sensors	Thermocouple (well type) : 1 Mercury level sensor : 1

Table 2.2.14: Specifications of the spilt mercury tank

1	Dimensions	1534 mm (length) × 560 mm (inner diameter) × 8 mm (wall thickness) for 1 tank
2	Total capacity	0.7 m^3 (0.35 m^3 × 2)
3	Design pressure	0.99 MPa
4	Design temperature	100ºC
5	Material	Stainless steel 316LN
6	Sensors	Thermocouple (well type) : 1 Mercury level sensor : 1

Table 2.2.15: Specifications of the trolley driving mechanism

1	Dimensions	1000 mm (length) × 1740 mm (width) × 931 mm (height*) * Datum of the height is bottom level of the linear roller way rail.
2	Weight	approximately 2.6 tons
3	Type	Rack & Pinion
4	Motor power	2.2 kW, 6 P, 960 rpm
	Rotational speed of motor	High : 480 rpm (travelling speed : 20 mm/s) Low : 40 rpm (travelling speed : 4 mm/s)
5	Reduction gear ratio	1/388
6	Pinion gear	Module:16, Number of teeth:19
7	Positioning accuracy	±1 mm
8	Material	Carbon steel Density of shielding plate > 7.6 g/cm^3

Table 2.2.16: Specifications of the ITV camera

1	Picture resolution	600 TV line
2	S/N ratio	> 40 dB
3	Zoom	× 2 (analog zoom)
4	View angle	34 degree
5	Focusing distance	50 mm ~ infinity
6	Lighting	Halogen light (20 W × 2)
7	Radiation resistance	Gamma ray dose rate : 3×10^3 Gy/h Accumulative dose rate : 7×10^5 Gy
8	Operation temperature	10 ~ 50ºC
9	Material	Stainless steel

Table 2.2.17: design conditions of mercury circulation system

Operational pressure :	0.1 MPaG (at helium gas part in the surge tank)
Maximum temperature of mercury :	90ºC
Related flow rate of mercury :	41 m^3/h
Capacity of heat exchanger :	600 kW 500 kW (heat generated in the mercury target) 100 kW (heat generated in the pump)
Main material of components :	Type 316L austenitic stainless steel

Table 2.2.18: Mercury inventory in mercury system

Pipes :	0.8 m^3
Heat exchanger :	0.17 m^3
Circulation pump :	0.005 m^3
Mercury target :	0.08 m^3
Surge tank :	0.5 m^3
Drain tank :	0.1 m^3
Total :	1.5 m^3

Table 2.2.19: Specification of surge tank

Surge tank	
Type	Vertically setting cylindrical tank
Inner diameter	ϕ 900 mm
Height	1,300 mm (Curved end covers on top and bottom)
Thickness	12 mm
Material	316L stainless steel
Design pressure	0.9 MPaG
Weight	900 kg
Shielding	
Outer diameter	ϕ 1,154 m
Height	1,760 mm
Thickness	95 mm
Material	Steel (SS400)
Weight	4,900 kg
Total weight	5,800 kg

Table 2.2.20: Specification of Gear pump

Pump	
Type	Belt driven gear pump
Size	450 mm (L) × 1100 (D) × 500 (H) mm
Material	(Casing) SCS14 (Gear shaft) SUS630 (Gear) SUS440C
Gear shape	V shaped gear to reduce cavitation
Seal of gear shaft	Double sealed mechanical seal (Material) METECO15E/RCCL
Weight	560 kg
Motor	
Power	30 kW
Poles	6 Poles
Voltage	400 V
Weight	360 kg
Shielding	
Size	840 (L) × 1,630 (D) × 1,000 (H) mm
Thickness	80 mm
Material	Steel (SS400)
Weight	3,480 kg
Total weight	4,400 kg

Table 2.2.21: Specification of PM pump

Pump	
Type	Permanent magnet rotating type induction pump
Size	800 (L) × 1075 (D) × 2035 (H, including motor) mm
Magnet	16 poles Sm-Co type (Magnetic field strength at magnet surface) 0.55 T
Mercury duct size	(Center diameter) ϕ 379 mm × 340 (H) mm
Thickness of duct	(Inner) 3 mm, (Outer) 5mm
Material of duct	SUS316
Motor	
Power	90 kW
Poles	6 Poles
Voltage	400 V
Size	ϕ 575 mm × 900 (H) mm
Weight	850 kg
Total weight	2,000 kg

Table 2.2.22: Specification of heat exchanger

Heat exchanger		
Type	All welded double wall type heat exchanger	
Size	905 × 400 × 795 (H) mm	
Material	SUS316L	
Heat removal capacity	600 kW	
	Primary	Secondary
Fluid	Mercury	Light water
Flow rate	50 m^3/h	25 m^3/h
Inlet temp.	74ºC	35ºC
Outlet temp.	50ºC	55ºC
Cross sectional area of channel	1.94 mm^2	1.89 mm^2
Weight	620 kg	
Shielding		
Size	1,290 × 775 × 920 (H) mm	
Thickness	90 mm	
Material	Steel (SS400)	
Weight	2,500 kg	
Total weight	3,120 kg	

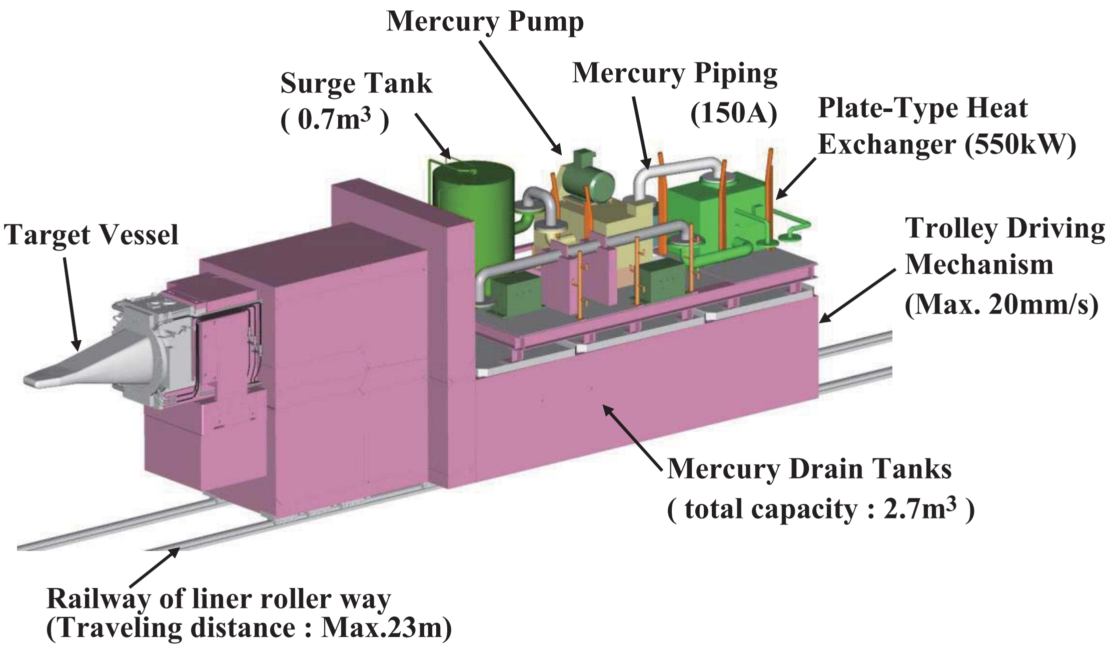

Fig. 2.2.1: Layout of devices in the target system on the target trolley

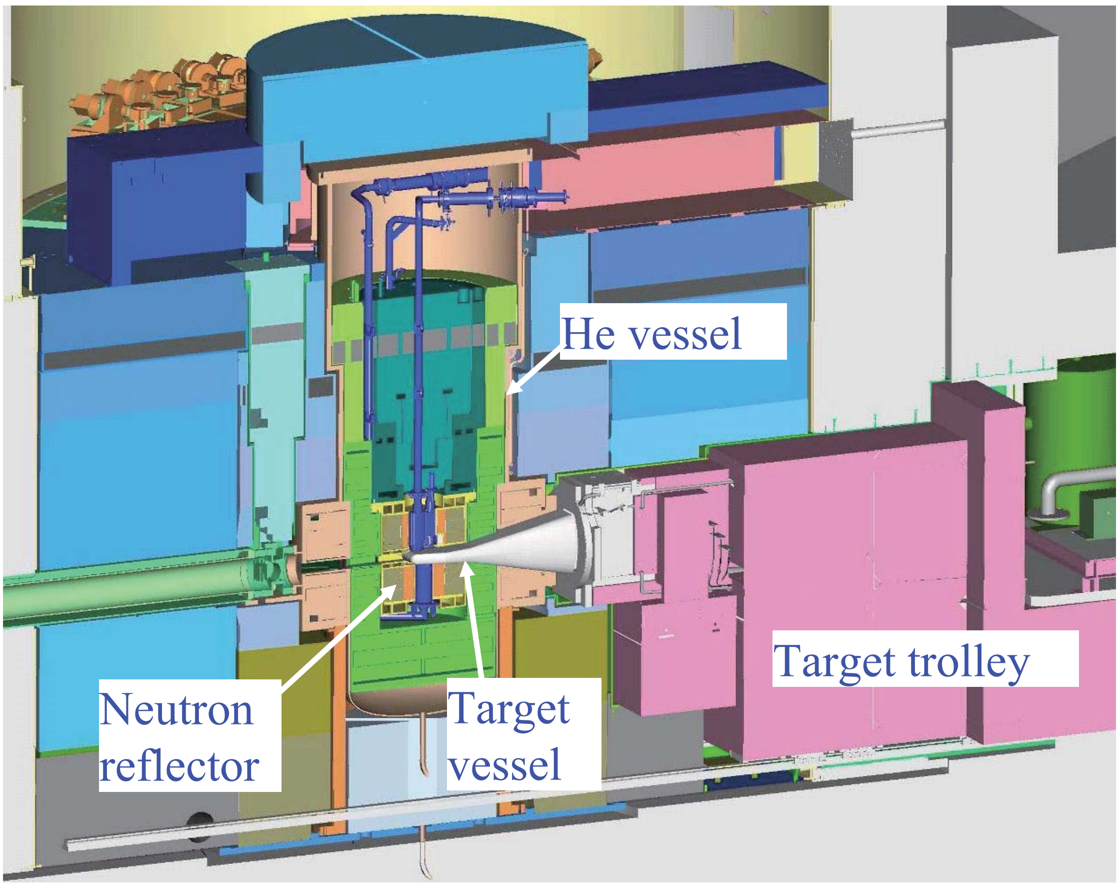

Fig..2.2.2: Cross section of the target system core

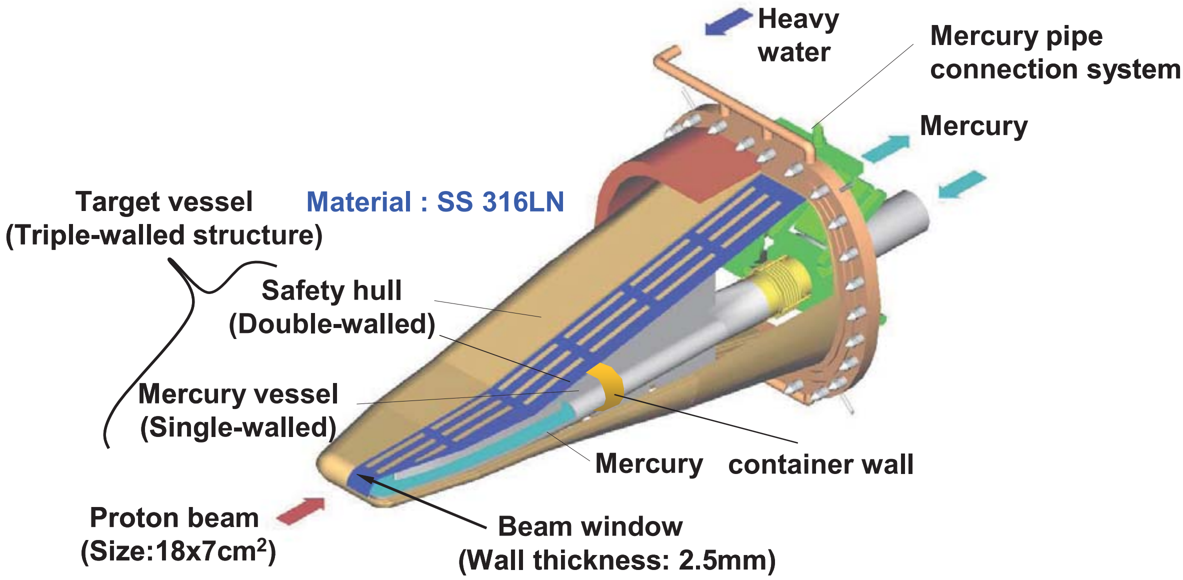

Fig. 2.2.3: Schematic drawing of mercury target structure

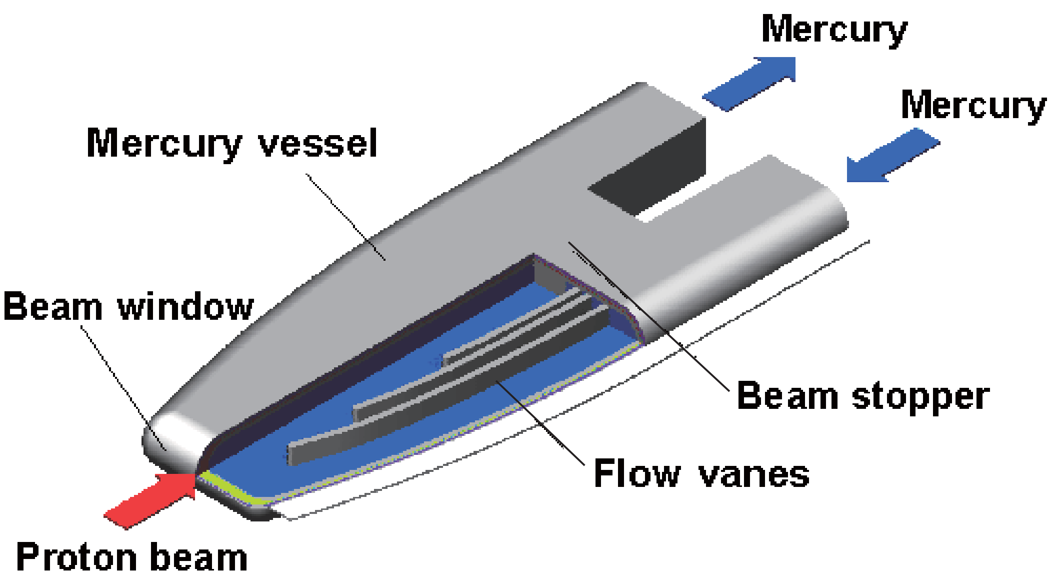

Fig. 2.2.4: Schematic drawing of mercury target structure without the safety hull

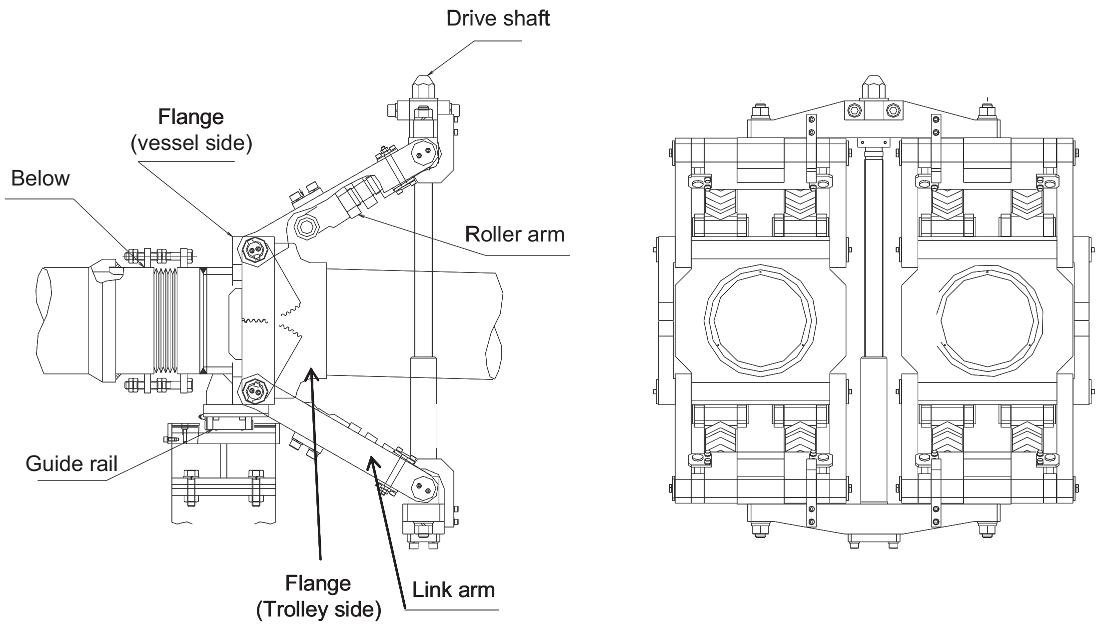

Fig. 2.2.5: Structure of mercury pipe connector

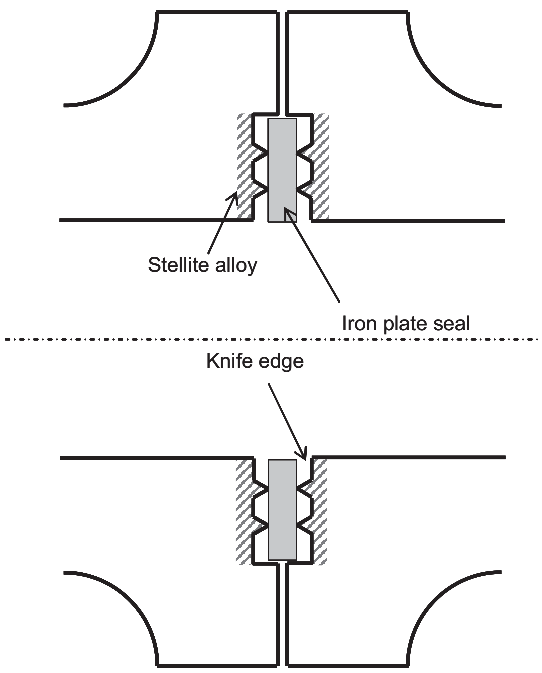

Fig. 2.2.6: Schematic drawing of mercury pipe flange

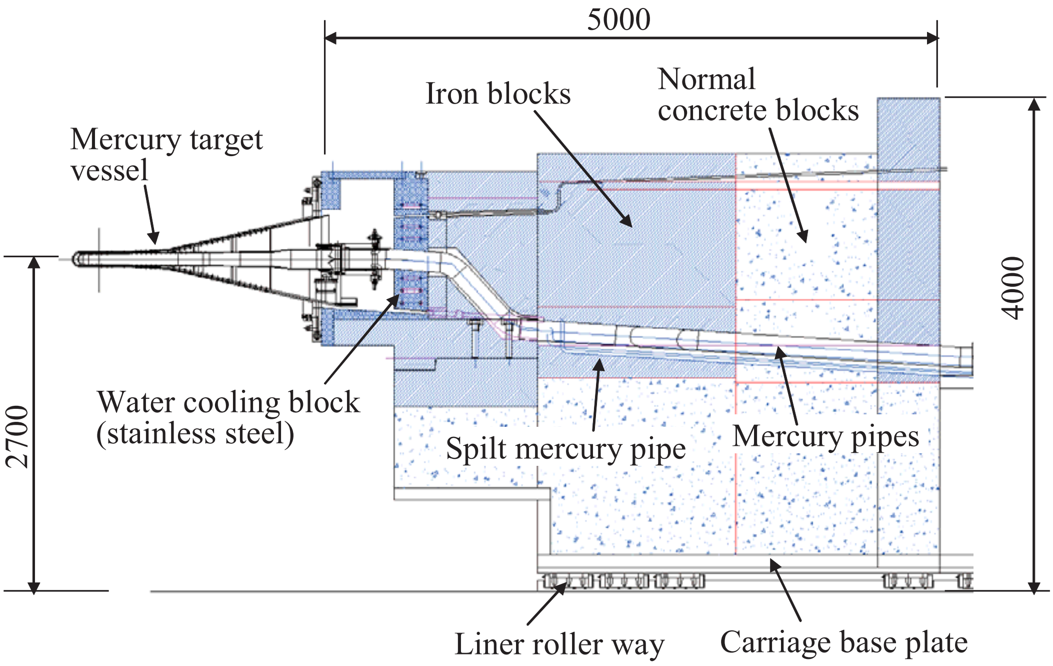

Fig. 2.2.7: Shielding trolley structure

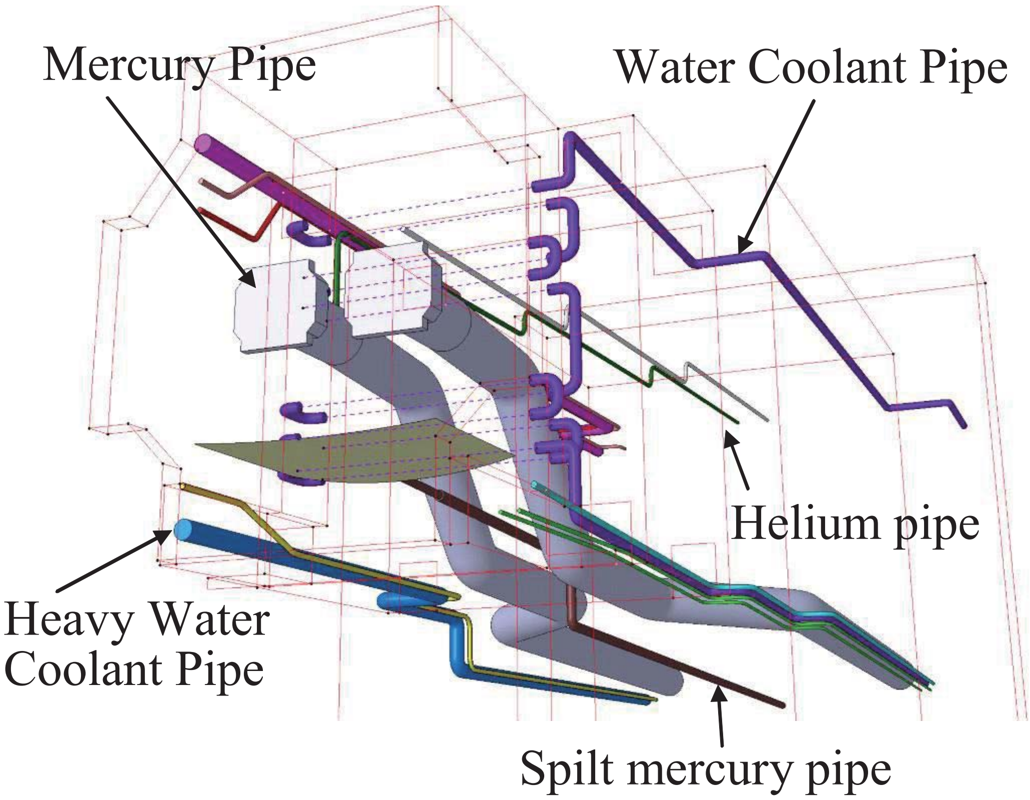

Fig. 2.2.8: Piping route through the shielding trolley

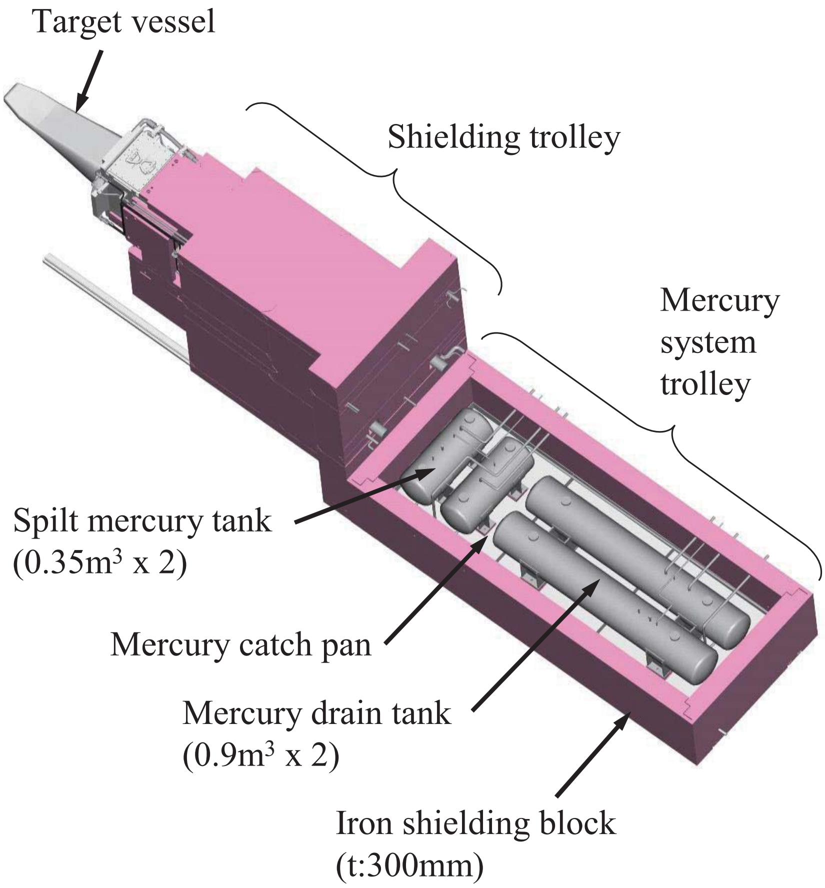

Fig. 2.2.9: Inner structure of the mercury system trolley

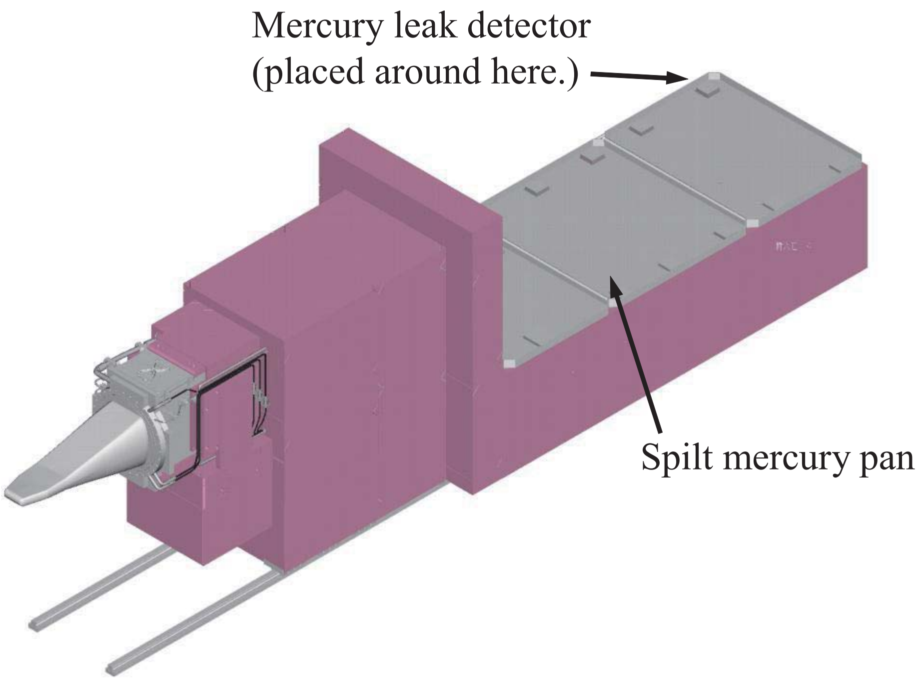

Fig. 2.2.10: Spilt mercury pan on the target trolley

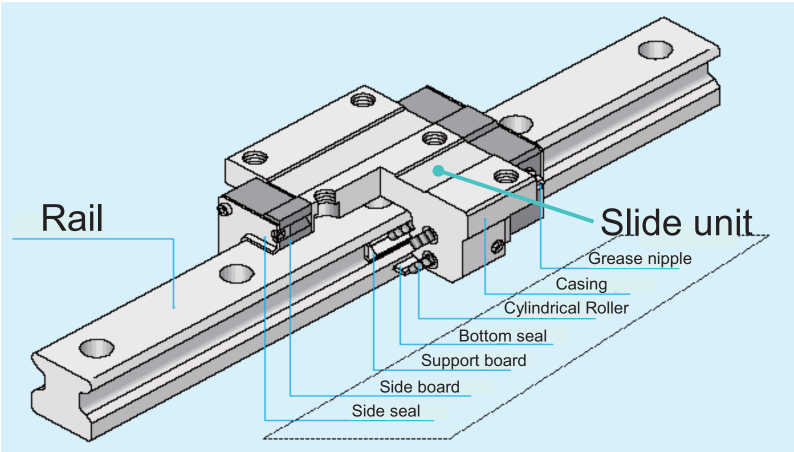

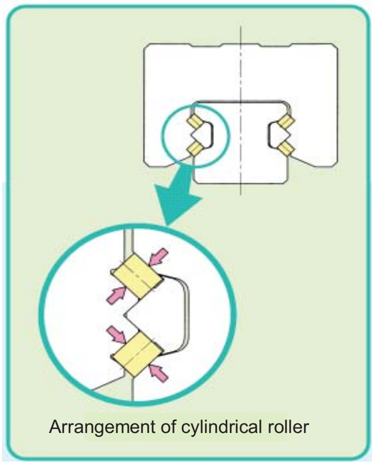

Weight: Slide unit 32kg, Rail 37kg/m (catalogue of NIPPON THOMPSON CO.,LTD)

Fig. 2.2.11: Structure of the linear roller way

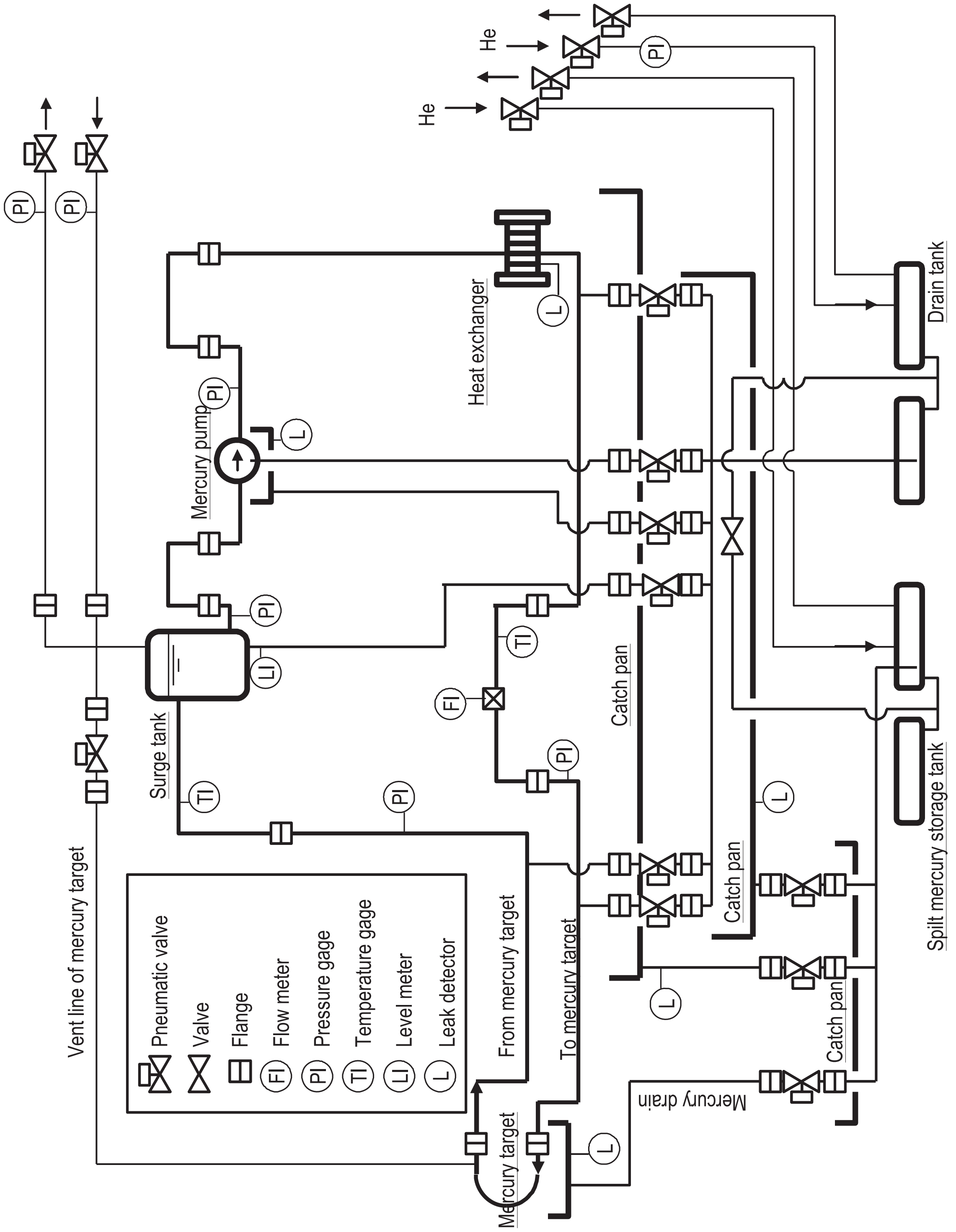

Fig. 2.2.12: Phase and instruments diagram of mercury system

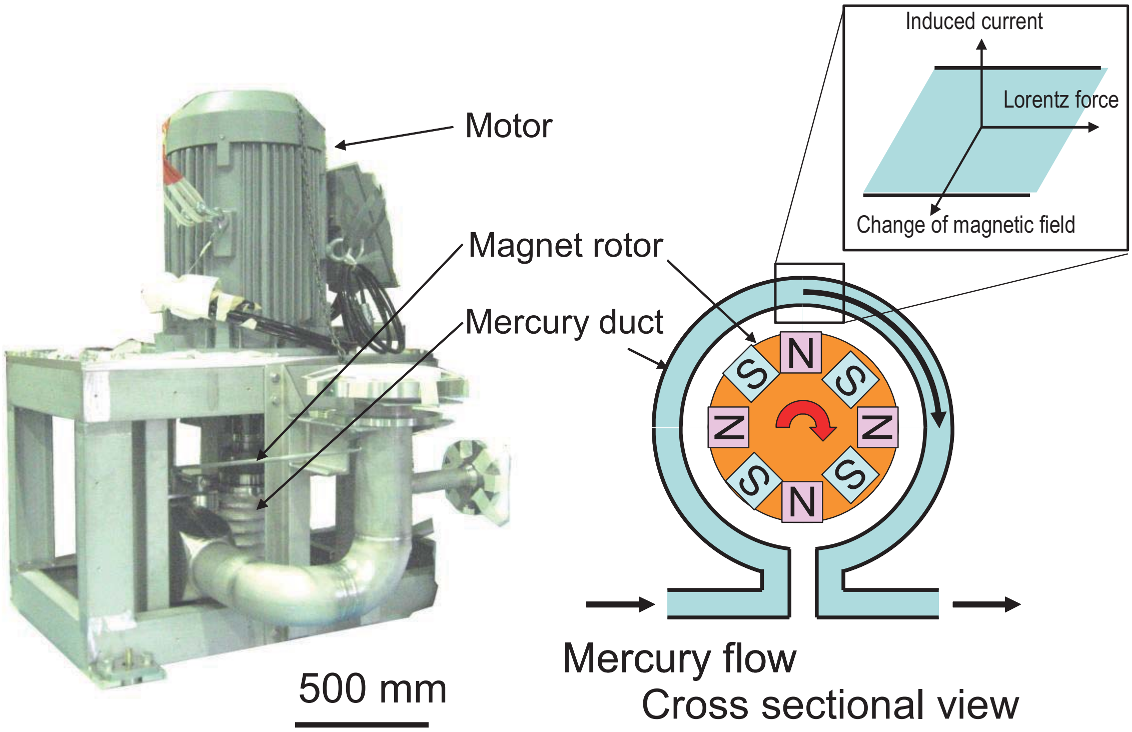

Fig. 2.2.13: Photo and schematic drawing of the PM pump

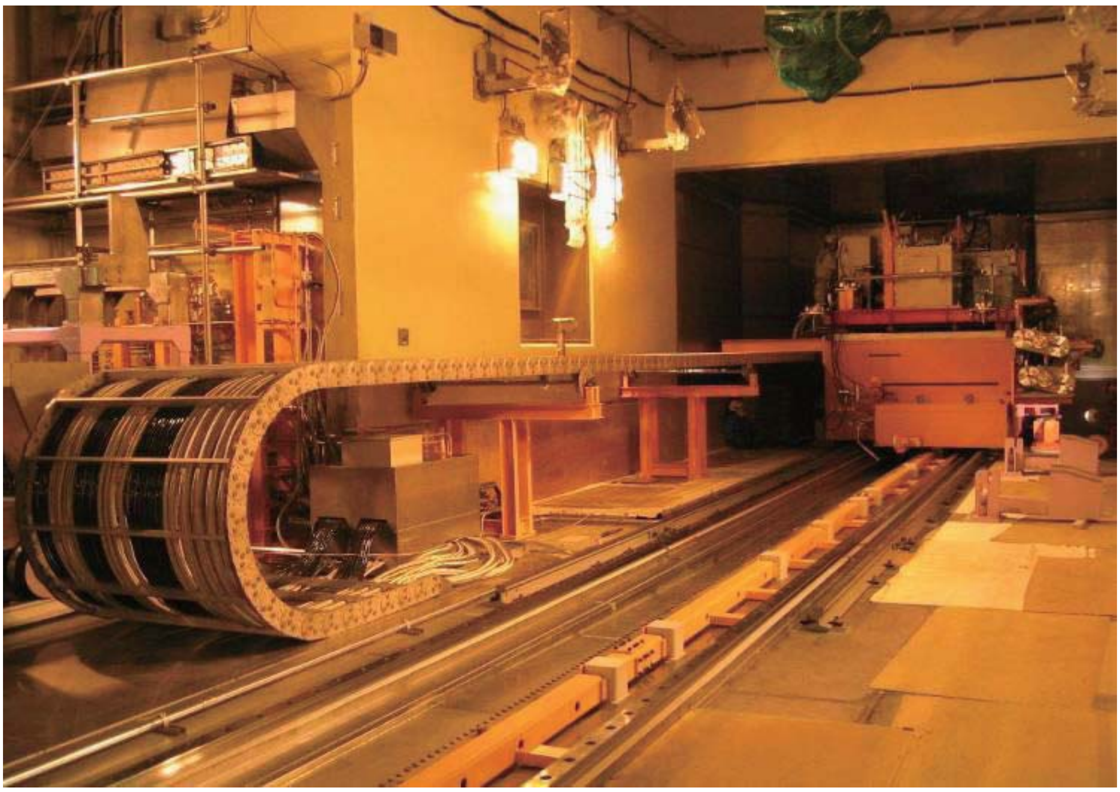

Photo. 2.2.1: Cableveyer of the target trolley

2.3 Moderator and Reflector

2.3.1 Overview of Moderator and Reflector

2.3.1.1 Concept of target-moderator-reflector

In spallation neutron source energetic neutrons are produced when a target is irradiated with proton beams. They are slowed down to appropriate energy in moderators and are extracted to neutron instruments. It is very important to settle a target-moderator-reflector concept for the optimal performance of the neutron source. In our neutron source design basic conditions[2.3-1)] are as follows.

(a) proton beam: horizontal injection

(b) moderator: 3 kinds of moderators; coupled, decoupled and poisoned moderators

(c) moderator arrangement: wing geometry (moderators are placed on and under the target for maximal neutron production)

(d) thermal loads with 1-MW incident proton beam

target:	530 kW
reflector:	198 kW
moderator:	24 kW
reflector plug:	11 kW
water cooled shield plug:	94 kW

(e) access to the components for maintenance and replacement

target: extracted horizontally from the other side of proton beam injection (full remote control)

moderator-reflector: lifted up vertically from the top of the vessel (partial remote control)

(f) vessel: filled with helium (He) gas , slightly higher than the atmospheric pressure

The wing geometry in the horizontal proton beam injection was adopted for the moderator arrangement. It is common to major pulsed neutron sources, former KENS (KEK), ISIS (RAL) and SNS (ORNL). Three moderators are so arranged that two decoupled moderators (decoupled and poisoned) are on the target and a coupled moderator under the target, as shown in Fig. 2.3.1. This arrangement was chosen for the moderator maintenance and neutron instruments. One of the reasons why the coupled moderator is placed under the target is as follows. The high energy neutrons from the target can be reduced for a vertically inclined neutron beam line when a moderator is placed under the target. A neutron reflectometer with horizontal sample geometry is built at the neutron beam line from the coupled moderator and high S/N ratio is required by its users.

In order to obtain the maximal neutron fluxes from the moderators, we performed the neutronic calculation[2.3-2, 3)] taking account of proton beam energy and its profile. It was found that the maximum neutron production was obtained when the cross section of proton beam was 13×5 cm^2 at the energy of 3 GeV. In this calculation, we also considered a matching efficiency, such as a flat target shape to fit the proton beam cross section and closer position of the target-moderator to the combination of target-moderator-reflector material. The clearance between the target and the moderators is 8mm (target side: 5 mm, moderator side: 3 mm), which was determined by the constraint on fabrication. The center of neutron source is the maximum neutron intensity from the moderator, which corresponds to 15.5 cm downstream from the proton incident surface of Hg target as shown in Fig. 2.3.2. The moderators are arranged at the center position.

The moderators are arranged as shown in Fig. 2.3.3 under the condition as follows

a) Coupled moderator: the moderator center in the horizontal face is the center of neutron source. Both neutron beam extraction (95.8° for coupled mod.)
b) Decoupled and poisoned moderators: The center of two moderators is the center of neutron source. Each both neutron beam extraction (42.2° and 27° for decoupled and poisoned mod. respectively)

The target container, the moderators and the reflector are integrated into the helium vessel, reflector, etc. as shown in Fig. 2.3.4. They are expected to be irradiated highly and can be replaced independently by a full remote controlled machine. Only the target container is extracted and inserted horizontally from the helium vessel for replacement because it has much shorter lifetime than other components and has to be often replaced. The other components, the moderators and the reflector, do not necessarily have to be replaced at the same time. The target container, which is attached to the target trolley, is pulled in the opposite direction of the proton beam injection into the hot cell. The target container is replaced by the remote handling machine and tools, such as a target container exchange track, a power manipulator and master slave manipulators. On the other hand, the moderator-reflector assembly is pulled vertically into a transfer cask once and then transferred to the same hot cell. The pipes of the moderators and the reflector are detached by hand on the top of the helium vessel in advance. The dose rate for radiation workers there is expected to be ~100 μSv/hr, which does not include the radiation from beryllium-7 (^{7}Be) in the shielding design[2.3-4, 5, 6].

The reflector plug is separated into two parts, an inner plug and an outer plug, as shown in Fig. 2.3.5, which enables us to replace each moderator independently. The reflector is connected to the outer plug. The coupled moderator is attached along the outer walls of the outer plug and the reflector. The decoupled moderator and the poisoned moderator are fixed to the inner plug. The inner plug with two moderators is inserted into the outer plug from the top side. The inner plug and the outer plug are selectively griped by the gripper inside the transfer cask. The moderator-reflector assembly, the combination of the moderators and the reflector fitted into the plugs, is installed in the helium vessel by using a rough guide and alignment pins. This structure enables us to replace a used component selectively and independently, which may reduce radioactive waste. The 20 cm thick concrete layer is installed between SS316 and iron layers to reduce the total weight of the moderator-reflector assembly and the radiation dose on the top of the helium vessel as well. The total weight of the moderator-reflector assembly is approximately 35 tons.

2.3.1.2 Moderator design

(1) Structure of moderator

The configuration of moderators[2.3-7)] is shown in Table 2.3.1. Three kinds of moderators, coupled, decoupled and poisoned moderators, are adopted to obtain the highest neutronic performance. The shape and size of each moderator were optimized for 100% para-hydrogen[2.3-8, 9, 10)]. The hydrogen (20K, 1.5 MPa) is supplied to the moderators from the hydrogen circulation system, which has a ortho- to para-hydrogen converter. It is circulated though three moderators in parallel to reduce the temperature difference between the start and the end of the hydrogen circulation for better neutronic performance. The moderators consist of a moderator head and a hydrogen transfer line, as shown in Fig. 2.3.6.

The moderator is made of multiple aluminum containers and hydrogen, vacuum, helium and cooling water are contained from inside to outside, as shown in Figs. 2.3.7 to 2.3.9. Beryllium (Be) is also installed in the moderator head not to reduce the neutron intensity from the moderator due to the lack of the reflector material. Aluminum alloy A6061-T6 was adopted to fabricate the moderator chamber with an allowable stress of 60 MPa in its design. The thinner the wall of the moderator chamber is, especially the neutron beam extraction window, the higher the neutron transmission is. The wall of the most inner hydrogen chamber is estimated to be 4 mm thick in the coupled moderator and 5 mm thick in the decoupled and poisoned moderators as shown in Figs. 2.3.10 and 2.3.11. The welding position in the moderator hydrogen chamber was also optimized, since the allowable stress was lowered by welding. The optimal welding position is also shown in Figs. 2.3.10 and 2.3.11.

In the moderator design study, especially for the coupled moderator, it was found that a unique large cylindrical shape (ϕ14 cm × 10^{H} cm) gave a large angular coverage with 100% para-hydrogen, as shown in Figs 2.3.7 and 2.3.11. The neutron extraction viewed surface is 10 × 10 cm^2. 100% para-hydrogen gives higher neutron luminosity on the brink of the viewed surface than in its center with the optimized H_2O premoderator.

The decoupled and poisoned moderators look like a canteen ($13^{W} \times 12^{H} \times 6.2^{T}$ cm^3), as shown in Fig. 2.3.11, which was also optimized for 100% para-hydrogen. These moderators contain a decoupler to shorten the tail of neutron beam pulse. The decoupler is inserted in the container between He layer and coolant layer, except the neutron beam extraction window, as shown in Fig. 2.3.8. The neutron beam users in JSNS required at least a decoupling energy of 1 eV. Boron carbide (B_4C) has been used to satisfy the requirement for the decoupling energy. It is however difficult to use one in a MW class neutron source, because swelling may occur with local nuclear heat and helium generation from $^{10}B(n, \alpha)^{7}Li$ reaction. Silver-indium-cadmium (AIC) alloy was newly proposed[2.3-11)] to overcome this difficulty. The AIC achieves is higher decouling energy by combining materials of different nuclear resonances. The AIC has been already utilized as control rods in pressurized water reactors (PWR) and its composition is different from that of the decoupler in JSNS. The composition and the thickness of the AIC decoupler were optimized for JSNS. The optimal thickness is 3 mm, which is determined by the burn-up and the irradiation damage (lifetime) of the structural material (aluminum alloy). The lifetime of aluminum (Al) alloy is estimated to be 6 years in the case of 1-MW, 5000-hours operation per year, which corresponds to roughly 20 dpa. The constituent-atoms are lost by burn-up and the neutronic performance, such as pulse tail is affected. The AIC decoupler of 3-mm thickness has to be bonded firmly to the structural moderator material, Al alloy, to remove heat. The technique was developed to bond AIC and Al alloy with Hot Isostatic Pressing (HIPing) process[2.3-12, 13)] for the material of the decoupled and the poisoned moderators. We also succeeded in fabricating the actual moderator containers with the AIC decopuler and their fabrication precision is better than 0.1 mm with HIPing process (Fig. 2.3.12) and the machining process, such as 3 dimensional NC machining as shown in Fig. 2.3.13. The HIPing condition is shown in Fig. 2.3.12.

In the poisoned moderator, a cadmium (Cd) poison plate of 1.3-mm thickness is asymmetrically installed at 2.5 cm from the neutron extraction window to obtain even narrower pulse width [2.3-14)]. The thickness of Cd poison sheet was also considered to be burned up for 6 years. It was found that the moderator chamber of an arch shape gave higher neutronic performance, i.e. narrower pulse width and higher peak intensity, than that of a canteen shape, as the neutron extraction opening angle got larger. There were some difficulties in fabricating the moderator chamber of an arch shape because of its complicated shape. The moderator chamber of a canteen shape with a small opening extraction angle of about 14° was finally adopted for the poisoned moderator. Thorough inspections are important during its fabrication process. The loss of the Cd poison sheet might be missed in welding process as shown in Fig. 2.3.14, unless we took an X-ray transmission measurement.

(2) Hydrogen transfer line

The hydrogen transfer line, which connects the moderator head and the coupler on the top of the helium vessel, has the structure shown in Fig. 2.3.6. A multi-ply coaxial pipe is converted to parallel pipes in the hydrogen transfer line to detach the coupler on the top of the helium vessel. The design requirements for the hydrogen transfer line are as follows.

- At least two bends are necessary to reduce neutron duct streaming and keep low activation on the top of the helium vessel. It is important for radiation workers to minimize the exposure to radiation during maintenance work.
- The bends are positioned asymmetrically to absorb the thermal shrinkage at 20K, as shown in Fig. 2.3.15.
- The transfer line is fixed only at one position between the room part and the cold part. As shown in Fig. 2.3.16, the optimal position is 200 mm higher than the center of the moderator chamber and the movement of the moderator chambers is less than 0.8 mm due to the shrinkage at 20 K.
- Commercially available pipe sizes are adopted for fabrication design.
- A multi-ply coaxial pipe is converted to parallel pipes. As shown in Fig. 2.3.17, the structure of the conversion part is so complicated that it is very difficult to make it with aluminum pipes. The conversion part is fabricated with stainless steel (SS316L) pipes and connected to aluminum pipes with friction welding method.
- Superinsulation (~25 μm thick aluminized polyimide film) is fitted to reduce the thermal load of

the cryogenic refrigerator. The superinsulation covers only the upper part from the couplers to the coaxial-parallel conversion position, since the radiation dose is very high around the lower part, as shown in Fig. 2.3.18. The radiation resistance test of this type of superinsulation was estimated to be less than 100 MGy by gamma-ray irradiation test[2.3-15)]. The radiation dose is estimated to be ~30 MGy/6years at the coaxial-parallel conversion position.

(3) Coupler

The structure of the coupler for the coupled moderator is shown in Photo. 2.3.1. The coupler is used to attach and detach the hydrogen transfer line on the top of the helium vessel for the maintenance of the moderators and the reflectors. The structures of the poisoned and decoupled moderators are the same as that of the coupled moderator. The design requirements of the couplers are as follows.

- Commercial 3/4-inch VCR connectors are used for the hydrogen transfer line.
- The vacuum and helium layers are made simultaneously by a flange with double O-ring seal. When the hydrogen transfer line is detached, the flange moves at least 100 mm with double welded bellows, which make the vacuum and helium layers.
- The flange is connected by hand as shown in Photo. 2.3.1.
- The flange is made as small as possible.

2.3.1.3 Reflector design

The configuration of the reflector is shown in Table 2.3.2. Beryllium and pure iron are adopted as reflector materials. A beryllium cylinder (50 cm in diameter × 100 cm in height) is surrounded with iron blocks (100 cm in diameter × 100 cm in height) and they are stored in an aluminum alloy container. The reflector has several openings, a moderator insertion hole, an incident proton beam hole, neutron beam holes. The reasons why beryllium and pure iron are chosen as reflector materials are as follows.

Selection of beryllium

- The property of slowing down neutrons is excellent, which is desirable for good neutronic performance.
- The thermal conductivity is high (one order of magnitude higher than that of stainless steel), which is good for heat removal.

Selection of pure iron

- The thermal conductivity is high, ~5 times higher than that of austenitic stainless steel.
- It has good shielding property for high energy neutrons.
- Less radioactivity is produced than austenitic stainless steel, since nickel is not contained.

^{60}Co produced in stainless steel makes a radiation shield thicker, which causes a heavier transfer cask. Pure iron, on the other hand, occurs the electric corrosion with the aluminum container. The surface of pure iron was coated with ~100 μm thick aluminum by thermal spray. The reflector is divided into three parts, top, middle and bottom, as shown in Fig 2.3.19 for effective cooling with coolant. The water circulates from the inlet below the bottom part though the entire reflector blocks to the outlet above the top part. The plenum structure is therefore installed at the inlet and the outlet of cooling water to rectify the water flow properly. Heavy water (D_2O) is preferable as cooling water for better neutronics performance. 3-mm gaps are kept among the blocks and the container for water channels in the reflector. AIC liners of 3-mm thickness are installed around the neutron beam openings of the decoupled moderator and the poisoned moderator. The AIC liners are bonded to the aluminum alloy container by HIPing.

2.3.1.4 Reflector plug

As shown in Fig. 2.3.20, the reflector plug consists of outer and inner plugs. These separated plugs enable us to replace a moderator independently. Stainless steel, normal concrete and iron are piled up in the plugs from the bottom. Stainless steel (SS316L) is adopted to make the water channel inside for heat removal. The plenum structure is also fitted at the inlet and the outlet of cooling water to rectify the water flow properly. The normal concrete of 20-cm thickness is adopted to reduce the weight of the reflector plug and the radiation dose at the top of the helium vessel as well. The concrete is stored in an iron container. The design dose rate is 100 μS/h at the top of the helium vessel, where the dose rate from ^{7}Be is not included. The Stainless steel, the concrete and the iron are connected with stud bolts. Commercially available NW-series quick couplers are used to attach the water pipes on the top of the helium vessel.

2.3.1.5 Installation accuracy of moderator-reflector assembly

Dowel pins are adopted to install each component of the moderator-reflector assembly with the accuracy within ±0.5 mm. The total installation accuracy of the moderator-reflector assembly could be better than ±3 mm against the ideal position, including the deformation in the fabrication process such as welding.

2.3.1.6 Hands-on maintenance at top of helium vessel

The water pipes and the hydrogen transfer line have to be disconnected by hand on the top of the helium vessel when the moderator or the reflector is replaced after beam operation starts. Hanging tools for transfer cask are also installed by hand. It is important to make these works simpler and takes less time for reducing the radiation dose of personnel even below the design dose rate of 100 μSv/h. The design requirements for the top of the helium vessel are as follows:

- enough work space for personnel
- pipe arrangement for easy access in order
- clear marking on pipes

Photo. 2.3.2 shows the arrangement of the water pipes and the hydrogen transfer line. A series of pipe disconnection work was carried out (Photo. 2.3.3) and the validity of the design was examined in terms of the accessibility of the water pipes and the time elapse. It was found that it took less than half hour to detach one water pipe.

2.3.2 Neutronics Design of Coupled Moderator

(1) Outline

The coupled hydrogen (H_2) moderator of J-PARC aims at providing intense pulsed cold neutrons with the highest possible time-integrated and pulse-peak intensities with reasonable pulse widths and decay times. The proposed JSNS instrument suite[2.3-16)] requires a large number of neutron beam lines which view a coupled moderator (11 beam lines out of the total 23 ones), resulting in a wide angular coverage of neutron extraction. As a result of extensive studies[2.3-17, 18)], we adopted the cylindrical moderator with 140 mm in diameter and 100 mm in height using 100% para-hydrogen. Table 2.3.3 shows main parameters of the coupled hydrogen moderator. In this section, results of neutronic studies on the coupled hydrogen moderator are shown.

(2) Para-hydrogen concentration and moderator thickness

In a hydrogen moderator the ortho- to para-hydrogen ratio plays an important role to determine the neutronic performance, especially in the energy range below about 50 meV. Fig. 2.3.21 shows calculated scattering cross-sections for ortho- and para-hydrogen compared with experimental data, reproduced from reference 2.3-19. The sharp drop in the para-hydrogen curve below 50 meV is due to spin coherence and the second drop below 5 meV is due to intermolecular interference. The main energy transfer mechanism for neutrons (neutron energy loss) at low energies is the para to ortho spin-flip transition. The neutron energy loss in the transition is 14.7 meV.

Fig. 2.3.22 shows time-integrated neutron intensity below 15 meV as a function of moderator thickness for various para-hydrogen concentrations. For the 50 mm thick moderator the 75% para-hydrogen one gives the maximum time-integrated neutron intensity. The optimal thickness which gives the maximum neutron intensity increases with para-hydrogen concentration. The maximum attainable time-integrated neutron intensity also increases with para-hydrogen concentration. For the 100% para-hydrogen moderator, the time-integrated neutron intensity is almost saturating above 220 mm in thickness. This moderator thickness (220 mm) is too thick in comparison with existing hydrogen moderators in the world. From the engineering and safety points of view, a smaller hydrogen inventory is essentially important. On the other hand, from the time-integrated neutron intensity points of view the thicker the better: At least, more than 140 mm is required for a 100% para-hydrogen moderator to surpass moderators of other para-hydrogen concentrations.

Another important objective of a coupled moderator is to provide the highest possible pulse peak-intensity in addition to the highest possible time integrated intensity. Commonly, the optimum parameters are not same for the time-integrated intensity and for the pulse peak intensity. Fig. 2.3.23 shows the pulse peak intensities and the pulse widths as a function of moderator thickness. The maximum values of the pulse peak intensities at 2 and 10 meV are attained by 100% para-hydrogen moderator of 120 and 100 mm in thickness, respectively. Meanwhile, the pulse widths at 2 and 10 meV increase monotonously with thickness and increase almost linearly especially for 100% para-hydrogen. The results mean that, although being saturating, the continuous increase in the time-integrated intensity of a 100% para-hydrogen moderator is mainly due to the linear increase in pulse width. In other words, the increase in the pulse width with moderator thickness is larger than the increase in the time-integrated intensity, exhibiting maxima in the pulse peak intensity. A higher value of the pulse peak intensity at 2 and 10 meV is obtainable with a higher para-hydrogen concentration for a thicker moderator beyond 100 mm. On the contrary, the pulse peak intensity at 50 meV continuously decreases with increasing moderator thickness. The higher values of the pulse peak intensity at lower energies (2 and 10 meV) are only obtainable at a penalty in that at higher energies (>30 meV).

(3) Intensity spatial distribution on moderator viewed surface

It turned out from the above results that a thick (about 140 mm) 100% para-hydrogen is essential for a coupled hydrogen moderator, although the optimal hydrogen thickness should be discussed. In order to study the effect of moderator height on the neutronic performance, calculations were performed on the time integrated intensity and the pulse peak intensities as a function of moderator height and thickness for a fixed value of the moderator width at 120 mm. The dimensions of the viewed surface is fixed at 100 × 100 mm^2, and located at the moderator center. The results are shown in Fig. 2.3.24, which clearly shows that the coupled hydrogen moderator of 100 mm in height gives the highest intensities in both the time-integrated and the pulse peak intensities. Commonly, for a fixed viewed surface (for example, 100 × 100 mm^2) a moderator having larger lateral dimensions (for example, 140^H mm×120^W mm) gives higher intensity than that having smaller ones (for example, 100^H mm × 120^W mm).

In order to understand this peculiar result, the spatial distribution of cold neutrons on the viewed surface of a coupled moderator has been studied. Fig. 2.3.25 shows a calculated two-dimensional spatial distribution of the time integrated intensity on the coupled hydrogen moderator, $140^T \times 100^H \times 120^W$ mm^3, of 100% para-hydrogen. The moderator had two viewed surfaces at opposite sides; the remaining four surfaces were covered by a light water premoderator. The calculated result was rather surprising as follows; the fringe part of the viewed surface is brighter by a factor of two compared with the central part.

(4) Cylindrical moderator

A cylindrical coupled hydrogen moderator was proposed to provide cold neutrons in wide beam coverage. Fig. 2.3.26 compares pulse shapes at beam extraction angle, θ=0º and 25º from the cylindrical ($140^{\Phi} \times 100^{H}$ mm^3) and the rectangular ($140^T \times 100^H \times 120^W$ mm^3) moderators at 2, 10 and 50 meV. It is clear that the pulse shape deterioration with beam extraction angle is much smaller in the cylindrical moderator. Fig. 2.3.27 shows pulse peak intensities and pulse widths as a function of the beam extraction angle for cylindrical and rectangular moderators. At 2 and 10 meV, the cylindrical moderator gives a higher pulse peak intensity with a narrower pulse width than the rectangular one over the entire range of θ, while at 50 meV the pulse peak intensity and pulse width exhibit a crossover at about θ =15º. The θ-averaged values are almost even between the moderators. Note that the θ dependence is much more rapid in the rectangular moderator as shown in Fig. 2.3.26. These comparisons demonstrated that the cylindrical moderator provides higher pulse peak intensity with narrower pulse widths than the rectangular moderator does. In the J-PARC spallation neutron source we decided to adopt the cylindrical coupled hydrogen moderator.

2.3.3 Neutronics Design of Decoupled Moderators

(1) Introduction

A decoupled moderator is surrounded with a neutron absorber called “decoupler” to eliminate slow (time-delay) neutrons. The decoupled moderator aims at providing sharp pulse with a finite penalty of neutron intensity. For providing neutrons with much narrower pulse width, neutron absorber called “poison” is inserted into the moderator. In JSNS, a poisoned decoupled moderator (PM) and an unpoisoned decoupled moderator (DM) are arrayed side by side upside of the mercury target. Both of front and rear surfaces of those moderators are used for the neutron extraction, resulting six neutron beam lines were designed at each decoupled moderator, respectively.

The design parameters for manufacturing DM and PM were optimized by neutronics calculations. The code system combining nucleon meson transport code NMTC/JAM [2.3-20] with low energy neutron transport code MCNP-4C [2.3-21] were used at early stage, and they were replaced with the upgraded version PHITS[2.3-22]. The cross section libraries of JENDL-3.2[2.3-23], JENDL Fusion File[2.3-24] and an evaluated library of mercury[2.3-25] were used for the transport calculation of neutrons with energies lower than 20 MeV. At cold neutron region, the kernel for liquid hydrogen processed from END/B-VI Release3[2.3-19] was employed. Fig. 2.3.28 shows an example of three-dimensional calculation model of the target-moderator-reflector region of the neutron source.

(2) Design parameters

a) Moderator materials

In low power neutron sources, solid or liquid methane has been used as a moderator material for a cold neutron source due to its high hydrogen density. However, in a MW class spallation neutron source, only hydrogen must be used considering the radiation damage[2.3-26, 27]. In our neutron source, hydrogen, which had lower hydrogen density than methane or light water was chosen. Though substitute moderators of hydrogen, such a changeable methane moderator or methane hydride moderator, are being studied, these are not reached for practical use. Fig. 2.3.29 shows pulse peak intensities (I_{pk}), pulse widths in full width at half maximum (FWHM, or $\Delta t_{1/2}$) and pulse widths at 1/100 ($\Delta t_{1/100}$) of a liquid hydrogen moderator and a solid methane moderator. No decoupler case, Cadmium decoupler case and AIC decoupler case are taken into account. The methane moderator provides sharper pulses than the hydrogen moderator in the energy region above about 8 meV. The reason is that the methane moderator has a higher hydrogen density than the hydrogen moderator. However, in the energy region below 8 meV, the hydrogen moderator has sharper pulses than the liquid moderator due to the effect of para-hydrogen as discussed in the next subsection.

b) Para-hydrogen and ortho-hydrogen

As described in the subsection 2.3.2(2), para-hydrogen decelerates neutrons quickly to cold region via the para to ortho spin-flip transition and the cold neutrons easily leak from the para-hydrogen environment. This characteristic is very suitable for the decoupled moderator providing sharp pulse. Fig. 2.3.30 shows that a better pulse characteristic is obtained for higher the para- to ortho-hydrogen ratio in the decoupled moderator. Since the para-hydrogen changes to ortho-hydrogen naturally, it is required to keep the para-hydrogen ratio from the beginning to the end of operation period.

The para- to ortho-hydrogen conversion under radiation environment has not been characterized yet. That caused by the neutron scattering would be very low and negligible. It is reported[2.3-28)] that chemical reactions under operation accelerate the para- to ortho-hydrogen conversion. On the other hand, it is pointed out[2.3-29)] that the conversion is small due to energy balance (heat balance).

An ortho-para converter using catalyst is installed into hydrogen circulation loop to keep the para-hydrogen concentration at almost 100%. And, we are planning to measure para- to ortho-hydrogen conversion during the beam operation period. It is noted that 99.8% para-hydrogen concentration was employed in our neutronics design study. More detailed study of the para-hydrogen moderator is reported in ref. 2.3-30).

c) Hydrogen temperature

Hydrogen temperature in the moderator is one of important factors to achieve good pulse characteristics. Temperature change causes little wave length shift at the Maxwellian peak but affects density largely as shown in Fig. 2.3.31. The pulse shape at 15K, 20K and 25K was calculated in which the density change of hydrogen was taken into account. Figs. 2.3.32 and 2.3.33 show pulse shape of neutrons with energies of 5 and 50 meV in DM and PM, respectively. For easy comparison, Fig. 2.3.34 shows time-integrated intensity (I_{int}), I_{pk} and $\Delta t_{1/2}$ as a function of neutron energy (E_n), which were normalized to the values at 20 K. The variations of those ratios against the hydrogen temperature are summarized in Table 2.3.4. The results suggest that higher hydrogen density provides sharper pulse. Therefore the hydrogen density (hydrogen temperature) should be kept during the operation not to deteriorate the pulse characteristics.

d) Moderator size and moderator shape

Moderator size is one of the elementary parameters. In the neutronics design study, the decoupled moderator was modeled as a canteen shape with corner-cubes of R=21cm on neutron extraction surfaces and R=20 cm on the other surfaces. A neutron beam line having 10 × 10 cm^2 cross section is extracted from the center of the neutron extraction surfaces. Fig. 2.3.35 shows I_{pk}, $\Delta t_{1/2}$ and Figure Of Merit (FOM) as a function of moderator thickness for five cases of moderator sizes in DM. The moderator with 12 cm in height and 14 cm in width provides the highest neutron intensity without deteriorating the pulse width. As the moderator thickness increases, the neutron intensity increases with broadening the pulse width. It is best choice that the moderator thickness is 6 cm. However, the size of DM was determined as $13 \times 12 \times 6.2$ cm^3 considering that smaller volume is better in view of heat removal, and the same dimension was adopted for PM.

e) Relative position of DM and PM to target

Two decoupled moderators are arrayed upward the mercury target while the coupled moderator (CM) is placed downward separately. Fig. 2.3.36 compares I_{pk} and $\Delta t_{1/2}$ for single decoupled moderator with the case that two decoupled moderators are arrayed with 15 and 30 degrees of opening angles. I_{pk} for the two decoupled moderator case is 30% lower at maximum than the single moderator case due to deficit of the reflector and the shift from the optimal position with respect to the mercury target.

Therefore, DM and PM are placed as near as possible. PM is set upstream and DM is downstream to the proton beam advancing direction, where the center of mass between DM and PM is located on the center of the reflector to obtain maximum neutron intensity. According to the neutronic calculation, DM provides a bit higher intensity than PM. The decoupler between DM and PM plays role of suppressing cross talk of the cold neutrons from these moderators.

f) Reflector material and cooling water in reflector

It is known that a Lead (Pb) reflector, which is no slowing-down type, provides higher neutron intensity with longer pulse tail than a Beryllium (Be) reflector, which is slowing-down type. On the other hand, Mercury (Hg) and Iron (Fe) reflectors, which are no slowing-down type with $1/v$ neutron absorber, provide shorter pulse tail with a bit penalty of neutron intensity than the Pb reflector[2.3-31)]. However, Be reflector has been used at ISIS (160-kW Spallation Neutron Source in U.K.) for a long time considering its higher heat conductivity and good feasibility in manufacturing. Therefore, we also adopted Be as the reflector material.

Fig. 2.3.37 shows neutron intensity for the cylindrical Pb and Be reflectors with radius from 20 to 110 cm in which the moderator is located at the center. For the Be case, Fe reflector surrounds the Be region. The optimized reflector radius of the Be reflector is about 20 cm. For the small radius case, heat density in the Fe region increases too high to be removed. In consequence, the radius of the Be reflector radius was determined as 30 cm.

Figs. 2.3.38 to 2.3.40 show the pulse shapes and time- and energy-integrated intensity with changing the amount of the light water (H_2O) and heavy water (D_2O) coolants in the Be reflector. The neutron intensity decreases with a bit deterioration in pulse tail for both H_2O and D_2O. The result in Fig. 2.3.40 indicates that D_2O causes lower penalty of neutron intensity than H_2O. If the volume fraction of the D_2O coolant is kept below 10%, intensity penalty is only below 5% in comparison with the case without coolant.

g) Premoderator

A premoderator composed of high hydrogen density material makes neutrons pre-slow-downing and increases the neutrons transported to the moderator. The premoderator is commonly located outside the moderator. H_2O are generally used due to easiness in handling. It should be noted that the effect of the premoderator depends upon the reflector material. It is effective in combination with no slowing-down type reflector such as Pb and Hg, but not for the slowing-down type reflector such as Be due to too much deceleration of neutron[2.3-31)]. As shown in Tables 2.3.5 and 2.3.6, the change of the premoderator thickness around the Be reflector bears little gain of the neutron intensity. The difference of the neutron intensity between the H_2O and the D_2O premoderator is also small as shown in Tables 2.3.5 and 2.3.6. Therefore, only cooling of the moderator vessels, decouplers and liners are considered as a usage of the premoderator. H_2O was chosen as the premoderator material in DM considering the compatibility of the H_2O premoderator for CM. The neutronics calculation requires that the gap of the H_2O premoderator is limited below 0.5 cm in view of penalty of the neutron intensity. However, the gap size was determined based on the result of the thermal hydraulics analysis.

h) Extraction angle

A pulse width is broadened at a large extraction angle because emitted neutrons have delayed flight time with vast emitted positions at an extracted surface. Fig. 2.3.41 shows pulse shapes of DM and PM at the extraction angle of 0°, 7.5° and 17.5° at E_n = 5 meV and 50 meV. At the maximum extraction angle of 17.5° in DM and that of 7.5° in PM, there are 10% reduction of the peak intensity and 10% increase of the pulse width compared with the result at 0°.

Although a concave type PM (Fig. 2.3.42) has a merit to reduce the influence of the extracted angle on the pulse width, it has a demerit such as the difficulty in manufacturing and the increase of nuclear heat due to volume increase. Fig. 2.3.43 compares the extraction angle dependence on the pulse shapes of DM and PM between the canteen and the concave type. The concave type PM provides smaller pulse width than the canteen type. As a matter of fact, since the number of neutron instrument requesting DM and/or PM was less, the case viewing DM or PM with large extraction angle is rare. Then, the concave type was eliminated.

i) Decoupling energy and decoupler material

Decoupling energy (E_d) is one of the most important parameters for PM and DM. A decoupled moderator with higher E_d provides a shorter pulse tail with a finite intensity penalty. As shown in Fig. 2.3.44, as E_d increases, pulse tail is improved with decreasing neutron intensity. The pulse tail becomes a background for neutron scattering experiments. With consideration of neutron user's requests, reliability, and so on, we determined E_d as 1 eV.

In theory, a Boron (B) decoupler can realize E_d = 1 eV by controlling the amount of ^{10}B. As a matter of fact, however, it is quite difficult to realize the control because swelling under high radiation environment and the composition change through burn-up of ^{10}B by the $^{10}B(n,\alpha)$ reaction take place at 1 MW operation. The candidate material is limited to that the (n,γ) reaction is domain in thermal and resonance regions. To satisfy this condition, we focused the materials combined by thermal neutron absorber and neutron absorbers with resonance absorption. Finally, we proposed Silver-Indium-Cadmium

(Ag-In-Cd, AIC) alloy which has been used for control rods in the Pressured Water Reactor[2.3-11)]. Pulse characteristics obtained with the B_4C (controlled to be E_d=1 eV), the Cd and the AIC decouplers are shown in Fig. 2.3.45. The Cd decoupler provides longer pulse tails due to lower E_d. On the other hand, the AIC decoupler provides short pulse tail similar to the result of the B_4C decoupler. Therefore, we adopted the AIC decoupler in views of the irradiation effect, the material property and the manufacturing feasibility[2.3-12, 13)] as well as the neutronics performance. We reported in the following subsection about study of material property and manufacturing feasibility for the decoupler in detail.

j) Poison material and poison shape

Candidates for the poison material were Cd, Gd and B_4C. For the B_4C case, nuclear heat is high and there is not any merit in the pulse characteristics. On the other hand, Cd and Gd provide better pulse characteristics than B_4C. Comparing the Cd poison with the Gd poison, the pulse width at several hundreds of meV is narrower due to the high cut-off energy of Cd. (see Fig. 2.3.46). Based on this neutronic performance, the Cd poison was adopted[2.3-14)]. Material property and mechanical property will be mentioned in the following subsection.

As shown in Figs. 2.3.47 and 2.3.48, the pulse width is proportional to the position of the poison material. In other words, the pulse width can be controlled by the poison position. In our design, the poison position was set 2.5 cm from the moderator extraction surface on the basis of neutron user's requests. Detailed studies for poisoned moderator are reported in ref. 2.3-14.

k) Epi-thermal neutron pulse

Epi-thermal neutron is also available although the design is not optimized. Considering that the proton beam delivered to MLF has dual bunch structure, we studied the usage of the epi-thermal neutrons as reported in ref 2.3-32). Fig. 2.3.49 shows I_{pk}, $\Delta t_{1/2}$ and FOM for the proton beam structures of the delta function, single bunch and dual bunch, respectively. The H_2O moderator case is depicted as a reference. The proton beam structure is dominant to the pulse characteristics of neutrons above 10 eV. This suggests that the users wishing to conduct experiments using epi-thermal neutrons are requested to pay attention to the pulse characteristics provided by the dual bunch proton beam.

l) Conclusion

We could obtain necessary parameters for a design and a manufacture of two decoupled moderators, DM and PM in the JSNS. Based on these parameters, we have completed to manufacture the first DM and PM. Next step, we will measure neutronic data, such as neutron intensities, pulse shape (width and tail), and so on, in order to confirm that our design is optimal.

The following item is necessary for more accuracy calculation.

・Considering scattering kernels such as an Aluminum alloy

In this evaluation, scattering kernels for Hydrogen and Beryllium were considered. However, other material, such as an aluminum alloy used in neutron beam windows, should be considered (for example, to represent the Bragg cut-off of the aluminum alloy).

・Considering (γ,n) reaction

In several tens of MeV, it is estimated that this reaction is 10% of photon reaction cross sections. However, even if this reaction is taken into account, this effect might be negligible for neutronic performances.

2.3.4 Structural Strength Design of Moderator Vessels

(1) Introduction

Cold moderator vessels are made of aluminum alloy from the viewpoint of a suppression of neutron absorption. Wall thickness of the moderator vessels should be thin as possible, while keeping the structural integrity of the vessels against the design pressure of 2.0 MPaG.

The conceptual configurations of the moderators were decided first by the neutronic analyses[2.3-8,9)], and then were designed in detail based on the thermal-hydraulic analyses[2.3-33)] and the mechanical strength analyses. Dimensions of the moderator vessels, especially hydrogen vessels, are as follows:

(a) Decoupled moderator (flat type) : 130 mmW × 120 mmH × 62 mmD

(b) Coupled moderator (cylindrical type) : ϕ140 mm × 111 mmH.

These moderator vessels are made of forged aluminum alloy (A6061-T6) from the viewpoint of low neutron absorption rate and enough mechanical performance against radiation damage[2.3-34)].

(2) Allowable stress

In Japan, the High Pressure Gas Safety Law covers components dealing with high pressure gas and liquefied gas. This law recommends the design by formulas with safety margin of 4 to decide minimum wall thickness of the vessels. Then, the wall thickness necessary for the weakest region is applied to the whole region. For example, in a flat head of vessel where the edge is the weakest region, the wall thickness at the edge is applied to all the area of the flat head, so that the center of the flat head has unnecessary thickness. To rationalize the wall thickness of the moderator vessels, the design by analyses and a pressurized test are favorable, which are permitted in the law. However, it is very difficult to complete the design by analyses in a limited period available for the moderator design. On the other hand, the pressurized test is normally permitted in the law for the component for which it is difficult to adopt the design by formulas, such as bellows. The test is carried out under the pressure of 4 times as high as the design pressure in order to investigate whether the vessel fails or not, that is, to confirm whether the safety margin of 4 is ensured or not.

To ensure the safety margin of 4, the allowable stress should be set to decide the wall thickness of the moderator vessel. Mechanical properties of the aluminum alloy A6061-T6 are shown in Table 2.3.7.

The basic stress intensity limit, S, was decided as follows,

S = Min{1/4 $\sigma_{u\,R.T.}$, 2/3 $\sigma_{y\,R.T.}$, 1/4 $\sigma_{u\,D.T.}$, 2/3 $\sigma_{y\,D.T.}$ }=66 MPa

where $\sigma_{u\,R.T.}$ is the minimum tensile strength at room temperature, $\sigma_{y\,R.T.}$ the minimum yield strength or 0.2% proof strength at room temperature, $\sigma_{u\,D.T.}$ the minimum tensile strength at the design temperature and $\sigma_{y\,D.T.}$ the minimum yield strength or 0.2% proof strength at the design temperature. The basic stress intensity limit, S, indicates the allowable stress for a membrane stress. Generated stresses are usually the combination of the membrane stress and the bending stress. Under the combined stress condition, the mechanical strength criteria described in ASME sec.III and sec.VIII codes etc. shows high allowable stress; the allowable stress for the combined stress condition is 1.5 times as high as the basic stress intensity limit. Accordingly, the structural integrity is secured unless plastic deformation occurs in the all cross section.

The allowable stress under the combined stress condition is defined in the following way. Fig. 2.3.50 shows the schematic of the stress and strain distributions along the thickness direction assuming elastic-perfectly plastic model when the strain on the surface reaches the failure strain, ε_F, under the condition that the axial force, F, and the bending moment, M, are simultaneously applied on a beam whose cross section is rectangle with height of h and width of b. The stress exceeds the yield or 0.2% proof strength from the surface of the beam due to the bending moment.

Equilibrium equation for the axial force is expressed by

$$F = \int_A \sigma(z) dA = Eb\left[-\int_{-h/2}^{-(z1+zm)} \varepsilon_y dz + \int_{-(z1+zm)}^{z1-zm} \varepsilon(z) dz + \int_{z1-zm}^{h/2} \varepsilon_y dz \right] = 2Ebz_m \varepsilon_y \tag{2.3.1}$$

where E is the Young's modulus of the material, z_1 half-length of elastic region, z_m distance between the center of the cross section and a natural axis and ε_y the strain when the material reaches the yield or 0.2% proof strength. Then the membrane stress, P_m is expressed by

$$P_m = \frac{F}{bh} = \frac{2Ez_m \varepsilon_y}{h} . \tag{2.3.2}$$

Equilibrium equation for the bending moment is expressed by

$$\begin{aligned} M &= \int_A \sigma(z) z dA = Eb\left[-\int_{-h/2}^{-(z1+zm)} \varepsilon_y z dz + \int_{-(z1+zm)}^{z1-zm} \varepsilon(z) z dz + \int_{z1-zm}^{h/2} \varepsilon_y z dz \right] \\ &= Eb\varepsilon_y \left(\frac{h^2}{4} - \frac{z_1^2}{3} - z_m^2 \right) \end{aligned} . \tag{2.3.3}$$

Then, the bending stress on the surface is expressed by

$$P_b = \frac{6M}{bh^2} = E\varepsilon_y \left[1.5 - 2(z_1/h)^2 - 6(z_m/h)^2 \right] . \tag{2.3.4}$$

Also, the combined stress are expressed by

$$P_m + P_b = E\varepsilon_y \left[2z_m/h + \left\{1.5 - 2(z_1/h)^2 - 6(z_m/h)^2\right\}\right], \tag{2.3.5}$$

then,

$$\varepsilon_y/\varepsilon_F = z_1/(h/2 + z_m),$$

so that,

$$\begin{aligned} P_m + P_b &= E\varepsilon_y \\ &\times\left[1.5 - 0.5(\varepsilon_y/\varepsilon_F)^2 + \left\{2 - 2(\varepsilon_y/\varepsilon_F)^2\right\}z_m/h - \left\{2(\varepsilon_y/\varepsilon_F)^2 + 6\right\}(z_m/h)^2\right], \end{aligned} \tag{2.3.6}$$

and from Eq. (2.3.2),

$$z_m/h = P_m/2E\varepsilon_y ,$$

then, the combined stress is expressed by the function of the membrane stress as follows:

$$\begin{aligned} (P_m + P_b)/E\varepsilon_y &= 1.5 - 0.5(\varepsilon_y/\varepsilon_F)^2 \\ &+ \left\{1 - (\varepsilon_y/\varepsilon_F)^2\right\}(P_m/E\varepsilon_y) - \left\{0.5(\varepsilon_y/\varepsilon_F)^2 + 1.5\right\}(P_m/E\varepsilon_y)^2. \end{aligned} \tag{2.3.7}$$

The allowable stress is written as follows:

$$\begin{aligned} (P_m + P_b)/E\varepsilon_y &< 1.5 - 0.5(\varepsilon_y/\varepsilon_F)^2 \\ &+ \left\{1 - (\varepsilon_y/\varepsilon_F)^2\right\}(P_m/E\varepsilon_y) - \left\{0.5(\varepsilon_y/\varepsilon_F)^2 + 1.5\right\}(P_m/E\varepsilon_y)^2, \end{aligned} \tag{2.3.8}$$

Fig. 2.3.51 shows a failure curve expressed by Eq. (2.3.7), that is, the relationship between the combined stress, P_m+P_b, and the membrane stress, $P_{m.}$ This relation assumes the failure strain of 5%, which is much lower than the failure strain of 11% of A6061-T6 at room temperature. In Fig. 2.3.51, allowable stresses available for the pressurized test and for the design pressure condition are also shown. To judge the structural integrity easily, the allowable stress under the combined stress condition available for the pressurized test was divided into two regions within the failure curve. The allowable stress under the design pressure condition is obtained from 1/4 of the allowable stress available for the pressurized test to ensure the safety factor of 4. Consequently, the allowable stress under the combined stress condition is 66 MPa in the case where the membrane stress is over 40.8 MPa, and 91 MPa where the membrane stress is below 40.8 MPa.

(3) Mechanical strength performance

The analyses were carried out using ABAQUS/Standard. The analytical models were 1/4 of the moderator vessels from the viewpoint of the symmetry.

1) Decoupled moderator vessel

Fig. 2.3.52 shows the analytical model of the decoupled moderator. The wall thickness and curvature radius are 5 mm and 210 mm, respectively, which were decided on the basis of preliminary analyses. For the side, top and bottom surface, the wall thickness and the curvature radius are 4 mm and 200 mm, respectively. Since it has been predicted that the bending stress becomes very high on the corners of the inner surface, the corner radius was set at 20 mm. The number of elements in the analytical model was about 50,000.

Fig. 2.3.53 shows the analytical result of stress intensity distribution under the design pressure condition (P = 2.1 MPa-abs). The absolute pressure is used as the design pressure because the moderator is insulated thermally by vacuum condition. The membrane stress, which is indicated by the stress at the center of the thickness, was lower than 40.8 MPa except the neutron extraction surface and the bottom surface and the combined stress (the membrane stress and the bending stress) was less than 91 MPa at the bottom surface. The membrane stress of the neutron extraction surface and bottom surface exceeded the boundary of 40.8 MPa. At the bottom surface, the combined stress was less than 66 MPa. Hence, the structural integrity of the decoupled moderators is secured except the neutron extraction surface. However, since the allowable stress has margin as shown in Fig. 2.3.51, the neutron extraction surface would not fail under the design pressure condition. On the other hand, the maximum displacement of 0.23 mm was generated near the center of the neutron extraction surface, which is lower than the allowable displacement of 1mm. The allowable displacement of the moderator vessel surrounded by the vacuum vessel was defined so as not to contact the vacuum vessel.

Then, the elastic plastic analyses were carried out under the pressurized test condition (P = 8.1 MPa-abs) assuming the elastic-perfectly plastic model for the stress-strain relation of A6061-T6. In the elastic-perfectly plastic model, stiffness of the material become zero after yielding, so the analytical results show higher strain than that obtained under the practical pressurized test. Since the elongation of A6061-T6 is 11% at room temperature as shown in Table 2.3.7, the moderator vessel would not fail if the generated strain is much less than 11%. Fig. 2.3.54 shows the analytical result of strain distribution obtained under the pressurized test condition. The maximum strain of 0.6% was generated at the neutron extraction surface, which is much lower than 11%. Therefore, the moderator vessel would withstand the high pressure in the pressurized test and keep its structural integrity except the welding line, because the mechanical strength of the welding region usually becomes lower than the ordinary allowable stress.

2) Welding Line of Decoupled Moderator Vessel

The moderator vessel is to be fabricated by welding. Then, a couple of vessel parts are formed out of aluminum blocks by a precise shaving processing. The location of the welding line should be apart from the target to decrease radiation damage as possible. Also, the welding line should be located on the minimum stress region, because A6061-T6 is heat-treated material and welding heat reduces the mechanical strength. A proposed region of the welding line is shown in Fig. 2.3.55, which was supposed on the basis of the analytical result of the stress intensity distribution under the design pressure condition. As seen in the figure, one welding line locates horizontally so as to form the vessel with two vessel parts, upper and bottom parts. We will minimize the deformation due to the welding heat effect.

The basic stress intensity limit decreases down to 42 MPa at the welding line. Then, the allowable stress of the combined stresses is 42 MPa when the membrane stress is over 28 MPa and it is 63 MPa when the membrane stress is below 28 MPa. As seen in Fig. 2.3.55, the combined stress exceeds the limit of 42 MPa under the present wall thickness. The wall thickness of the vessel should be made thicker especially on the welding line. So, the thickness of the side wall was changed from 4mm to 6mm, and the curvature radius of the outer surface of upper part on the neutron extraction surface was changed from 215 mm to 400 mm. So that, the thickness of the neutron extraction surface gradually increases with the distance from the target. The lower part of the neutron extraction surface was kept original dimensions so as to maintain low thermal stress and low heat flux because the lower part has relatively high heat density.

Fig. 2.3.56 shows the analytical model and the schematic of the neutron extraction surface including the welding line, respectively. The wall thickness at the welding line under planning was changed from 5.3 mm to 7.9 mm, which is 50 mm away from the center of the vessel (the border of a neutron viewed surface). Fig. 2.3.57 shows the analytical result of stress distribution in the welding line under the design pressure condition. The membrane stress was kept less than 28 MPa and the combined stress was also kept less than 63 MPa.

3) Coupled Moderator Vessel

Fig. 2.3.58 shows the analytical model of the coupled moderator. The wall thickness and curvature radius were decided from preliminary analyses. The wall thickness of the neutron extraction surface which is the cylindrical shape is 4 mm. At the top and bottom surface, the wall thickness and the curvature radius are 6 mm and 220 mm, respectively. The corner radius was set at 20 mm in order to reduce the bending stress. The number of elements in the analytical model was about 50,000.

Fig. 2.3.59 shows the analytical result of the stress intensity distribution under the design pressure condition (P = 2.1 MPa-abs). The membrane stress was below the limit of 40.8 MPa and the combined stress was below the limit 91 MPa except the neutron extraction surface. Although the membrane stress of the neutron extraction surface was over the limit of 40.8 MPa, the combined stress was below the limit of 66 MPa of the stress limit. Hence, the structural integrity of the coupled moderator would be secured under the design pressure condition. Then, the maximum displacement of 0.32 mm was generated near the center of the neutron extraction surface, which is less than the allowable displacement of 1 mm. The welding line can be located horizontally on 25 mm away from the center of the moderator vessel (near the outlet), where the generated membrane and the generated combined stresses were less than the limits of 28 MPa and 63 MPa, respectively.

(4) Summary

The rational wall thickness of the moderator vessels made of aluminum alloy A6061-T6 was estimated under the criteria of the high pressure gas safety law (Japan's law). To keep low combined stress, especially at the welding line, the welding line was decided to locate at 50 mm and 25 mm away from the center of the decoupled and coupled moderators (near the outlet), respectively. For the decoupled moderator (flat type), the wall thickness at the welding line was increased from 5.3 mm to 7.9 mm in the neutron extraction surface and from 4mm to 6mm in the side wall.

Based on these results, we have decided the concept of the multiple vessels surrounding the moderator vessels such as vacuum and helium vessels [2.3-35].

2.3.5 Thermal-hydraulic Design of Moderators

(1) Introduction

The spallation neutron source aims to realize the highest neutronic performance in the world. The neutronic performance both in intensity and resolution is affected directly by the moderators using supercritical hydrogen of 1.5 MPa and 20 K[2.3-36, 37]. Presently two types of moderator vessels, the cylindrical and flat types (coupled and decoupled moderator) shown in Fig. 2.3.60, are being designed[2.3-38, 30]. These are to be operated under supercritical hydrogen circulation condition while keeping away from boiling and hot spots in the hydrogen, since excessive change of hydrogen density in the moderator affects the neutronic performance such as neutron intensity. The hydrogen and the moderator vessel are heated by radiation. Especially, the bottom wall of the moderator vessel near the target has high heat density[2.3-37]. So, the impinging jet flow has been applied to cool down the bottom wall of the moderator vessels, and to suppress the local temperature rise of hydrogen (hot spot) within 3K by using jet-induced flows under low flow rate condition as possible. Three-dimensional thermal-hydraulic analyses and flow visualization experiments using simulated moderator vessels were carried out to prove the feasibility of the thermal-hydraulic design of the moderators[2.3-38]. And then, we had designed the moderator from the viewpoint of the thermal hydraulic design using by the analysis code STAR-CD that was verified through the experiments[2.3-39].

(2) Analytical models

Three-dimensional hydraulic analyses were carried out with the computational fluid dynamics code, STAR-CD, under hydrogen flowing conditions. The analytical models are shown in Fig. 2.3.61. Fig. 2.3.61(a) is the coupled moderator of cylindrical shape, and a distance to the bottom of the vessel from the inlet pipe nozzle is 10 mm. The analytical mesh is made by prism mesh as nearby the wall (0.3 mm height, 5 layers) and tetra mesh as others, are the total number of 1.7×10^6 (fluid part; 1.07×10^6, solid part; 0.63×10^6). The vessel wall of structure material that is an aluminum alloy was modeled in order to consider the nuclear heat density.

Fig. 2.3.61(b) is the decoupled moderator of flat shape, and a distance to the bottom of the vessel from the inlet pipe nozzle is 10 mm. The analytical mesh is made by prism mesh as nearby the wall (0.3 mm height, 5 layers) and tetra mesh as others like a case of the coupled moderator, are the total number of 1.3×10^6 (fluid part; 0.79×10^6, solid part; 0.51×10^6).

(3) Analytical conditions

The STAR-CD code has many analytical options for turbulence models, boundary conditions, solution algorithms. The standard k-ε model was used as the turbulence model, and the standard law-of-the-wall boundary condition was applied to the boundary condition. In the analyses, a steady state solution algorithm of the SIMPLE (Semi-Implicit Method for Pressure-Linked Equations) was used. In the temperature field analysis, a zero-degree equation model was used, and the turbulent Prandtl number was 0.996 calculated by the experimental equation of Kasagi et al.[2.3-40)].

As shown in Fig. 2.3.62, the hydrogen and an aluminum alloy of the vessel material have heat densities due to nuclear heating, about 1 W/cc and 2.5 W/cc at maximum, respectively[2.3-28)]. As the inlet hydrogen conditions, the flow velocity is 2.56 m/s for the coupled moderator and 1.44 m/s for the decoupled moderator, and inlet temperature is 18 K. Outside of the moderator vessel is assumed to be an insulated condition as a boundary condition.

Physical properties of hydrogen and aluminum alloy are shown in Table 2.3.8.

(4) Analytical results and discussion

1) Cylindrical type (coupled) moderator

Fig. 2.3.63 shows the velocity vector distribution adjacent to inner wall of the vessel and Fig. 2.3.64 shows the temperature distribution on inner wall surface of the vessel. In Fig. 2.3.63, it is observed that the jetted hydrogen from an inlet pipe flows along the vessel wall. The heat density of the moderator vessel is higher than one of hydrogen as mentioned above. The heat quantity increases in the upper and lower part of the vessel corner, because the vessel is thick at the corner part. In Fig. 2.3.64, as for the upper part, the temperature rise is suppressed even if the corner part of vessel, because the wall is cooled by the impinging jet flow. However, the flow velocity is slow at the lower part of the vessel and the maximal temperature of the wall would be 22.2 K at the corner part.

Fig. 2.3.65 shows the velocity vector distribution in cross section from a view point of the neutron extraction face and Fig. 2.3.66 shows the temperature distribution in cross section. As seen in Fig. 2.3.65, the recirculation flow and the stagnant region are observed in the vessel. The hydrogen temperature was raised in the recirculation flow. The temperature of the center of the recirculation flow was, however, 20.8 K as shown in Fig. 2.3.66. Therefore, the temperature rise in most of vessel region is suppressed within 3 K which was the neutron user requirement. It was confirmed that the design of the coupled moderator vessel was appropriate.

2) Flat type (decoupled) moderator

Fig. 2.3.67 shows the velocity vector distribution adjacent to inner wall of the vessel and Fig.

2.3.68 shows the temperature distribution on inner wall surface of the vessel. In Fig. 2.3.67, because it is a flat type vessel differing from the coupled moderator, the flow pattern is complex and stagnant flow region occurs. The heat quantity also increases in this upper and lower part of the vessel corner, because the vessel is thick at the corner part. The maximum temperature is 25.1 K in the upper part of the vessel corner, which is higher than the case of the coupled moderator.

Figs. 2.3.69 and 2.3.70 show the velocity vector distribution and the temperature distribution in cross section from a view point of the neutron extraction face, respectively. Figs. 2.3.71 and 2.3.72 also show the velocity vector distribution and the temperature distribution in cross section from a side face, respectively. From Figs. 2.3.69 and 2.3.71, situations of the flow are very complex in the vessel. The maximum temperature of hydrogen is 21.0 K in stagnant region around the inlet pipe. Because the flow velocity around vessel wall near the neutron extraction face is very low that is shown in Fig. 2.3.72, there is an area where hydrogen temperature is over 21 K. However, this hot layer around the vessel wall and hot spots in the stagnant region were so thin, and it would not affect the neutronic performance. Therefore, the temperature rise in most of vessel region is suppressed within 3 K which was the neutron user requirement and it was confirmed that the design of the decoupled moderator vessel was appropriate.

3) Summary

Three-dimensional thermal-hydraulic analyses were also carried out under the supercritical hydrogen condition of 20 K for the two type moderator vessels. As a result, the local temperature rise in the almost hydrogen bulk flow could be suppressed within 3 K which was required to obtain better neutronic performance.

References

2.3-1) N. Watanabe et al.: “A Target-moderator-reflector concept of the JAERI 5MW pulsed spallation neutron source,” JAERI-Tech 98-011, 1998.

2.3-2) M. Teshigawara et al.: “Neutronic studies of bare targets for JAERI 5MW pulsed spallation neutron source,” JAERI Research 99-010, 1999.

2.3-3) M. Teshigawara et al.: “Proton Energy Dependence of Slow Neutron Intensity,” Proc. Int. Collaboration on Advanced Neutron CANS-XV, Tsukuba, Japan, 6-9 Nov. 2000, JAERI-Conf 2001-002 & KEK Proc. 2000-22, 2001, pp. 835-847.

2.3-4) F. Maekawa et al.: “Study of Bulk Shielding for a Spallation Neutron Source Facility in the High-Intensity Proton Accelerator Project,” JAERI-Tech 2002-035, 2002, in Japanese.

2.3-5) F. Maekawa et al.: “Shielding Design Study for the JAERI/KEK Spallation Neutron Source,” Proc. Int. Collaboration on Advanced Neutron Sources ICANS-XV, Tsukuba, Japan, 6-9 Nov. 2000, JAERI-Conf 2001-002 & KEK Proc. 2000-22, 2001, pp. 907-916.

2.3-6) M. Tamura et al.: “3-Dimensional Shielding Design for a Spallation Neutron Source Facility in the High-Intensity Proton Accelerator Project,” Proc. Int. Collaboration on Advanced Neutron

Sources ICANS-XVI, Dusseldorf-Neuss, Germany, 12-15 May 2003, 2003, pp. 1077-1086.
2.3-7) M. Teshigawara et al.: "Development of Cd poisoned moderator," Proc. Int. Collaboration on Advanced Neutron Sources ICANS-XVI, Dusseldorf-Neuss, Germany, 12-15 May 2003, 2003, pp. 689-695.
2.3-8) T. Kai et al.: "Neutronic Study on Coupled Hydrogen Moderator for Japanese Spallation Neutron Source," Proc. Int. Collaboration on Advanced Neutron Sources ICANS-XVI, Dusseldorf-Neuss, Germany, 12-15 May 2003, 2003, pp. 657-666.
2.3-9) M. Harada et al.: "Optimization of poisoned and unpoisoned decoupled moderators in JSNS," Proc. Int. Collaboration on Advanced Neutron Sources ICANS-XVI, Dusseldorf-Neuss, Germany, 12-15 May 2003, 2003, pp. 697-706.
2.3-10) N. Watanabe et al.: J. Neutron Research, Vol. 11, no. 1-2, 2003, pp. 13-23.
2.3-11) M. Harada et al.: "Silver-Indium-Cadmium decoupler and liner," Proc. Int. Collaboration on Advanced Neutron Sources ICANS-XVI, Dusseldorf-Neuss, Germany, 12-15 May 2003, 2003, pp. 677-687.
2.3-12) M. Teshigawara et al.: "Cladding technique for development of Ag–In–Cd decoupler," J. Nucl. Mat., 343, 2005, pp. 154-162.
2.3-13) M. Teshigawara et al.: "Development of aluminum (Al5083)-clad ternary Ag-In-Cd alloy for JSNS decoupled moderator," J. Nucl. Mat., 356, 2006, pp. 300-307.
2.3-14) M. Harada et al.: "Neutronics of a poisoned para-hydrogen moderator for a pulsed spallation neutron source," Nucl Instr. and Meth. Phys. Res., A 574, 2007, pp. 407-419.
2.3-15) M. Teshigawara et al.: "Gas Yield and Mechanical Property of Super Insulator (Polyimide and Polyester) after Gamma Ray Irradiation", TEIONKOUGAKU, vol. 41, no.3, 2006, pp. 99-104, in Japanese.
2.3-16) M. Arai, et al.: "Strategy and performance of instrument suite for JSNS, J-PARC." Proc. Int. Collaboration on Advanced Neutron Sources ICANS-XVI, Dusseldorf-Neuss, Germany, 12-15 May 2003, 2003, pp. 157-175.
2.3-17) T. Kai, M. Harada, M. Teshigawara, N. Watanabe, Y. Ikeda: "Coupled Hydrogen Moderator Optimization with Ortho/Para Hydrogen Ratio", Nucl Instr. and Meth. Phys. Res., A 523, 2004, pp. 398-414.
2.3-18) T. Kai, M. Harada, M. Teshigawara, N. Watanabe, Y. Kiyanagi, Y. Ikeda: "Neutronic performance of rectangular and cylindrical coupled hydrogen moderators in wide-angle beam extraction of low-energy neutrons", ibid A 550, 2005, pp. 342-345.
2.3-19) R. E. MacFarlane: "Cold-moderator Scattering Kernel Methods," LA-UR-98-655, Los Alamos National Laboratory, 1998.
2.3-20) K. Niita et al.: "High-energy particle transport code NMTC/JAM," Nuclear Instruments Methods in Phys. Res., B 184, 2001, pp. 406-420.
2.3-21) J. F. Briesmeister (Ed.): "MCNP^{TM} - A General Monte Carlo N-Particle Transport Code, Version 4C," LA-13709-M, Los Alamos National Laboratory, 2000.

2.3-22) H. Iwase, K. Niita and T. Nakamura: “Development of a general purpose particle and heavy ion transport Monte Carlo Code,” J. Nucl. Sci. Technol. 39,, 2002, pp. 1142-1151.

2.3-23) T. Nakagawa et al.: “Japanese Evaluated Nuclear Data Library version 3 revision-2: JENDL-3.2,” J. Nucl. Sci. Technol., 32, 1995, pp. 1259-1271.

2.3-24) S. Chiba et al.: “JENDL fusion file 99,” J. Nucl. Sci. Technol., 39, 2002, pp. 187-194.

2.3-25) K. Shibata et al.: “Evaluation of neutron nuclear data for mercury,” J. Nucl. Sci. Technol., 34, 1997, pp. 1171-1177.

2.3-26) J. M. Carpenter, U. Walter: “Analysis of the burping behavior of the cold solid methane moderator at IPNS,” Proc. Int. Collaboration on Advanced Neutron Sources ICANS-IX, Villigen, Switzerland, 22-26 Sep. 1986, 1986, pp. 279-304.

2.3-27) T. A. Broome, J. R. Hogston M. Holding, W. S. Howells: “The ISIS methane moderator,” Proc. Int. Collaboration on Advanced Neutron Sources ICANS-XII, Abingdon, UK, 24-28 May 1993, 1993, pp. T-156 - T-163.

2.3-28) E. B. Iverson et al.: private communication, 2001.

2.3-29) I. Ushijima et al.: private communication, 2003.

2.3-30) M. Harada et al.: “Neutronic studies on decoupled hydrogen moderator for a short-pulse spallation source,” Nucl. Instruments Methods in Phys. Res., A 539, 2005, pp. 345-362.

2.3-31) M. Harada et al.: “Neutronic Optimization of Premoderator and Reflector for Decoupled Hydrogen Moderator in 1 MW Spallation Neutron Source,” J. Nucl. Sci. Technol., 39, 2002, pp. 827-837.

2.3-32) M. Harada et al.: “Pulse characteristics of epithermal neutrons from a spallation source,” Nucl Instr. and Meth. Phys. Res., A 597, 2008, pp. 242-256.

2.3-33) T. Aso, et al.: “Thermal-Hydraulic Design of J-PARC Cold Moderators,” Proc. Int. Collaboration on Advanced Neutron Sources ICANS-XVI, Dusseldorf-Neuss, Germany, 12-15 May 2003, 2003, pp. 935-944.

2.3-34) K. Farrell, “Materials Selection For The HFIR Cold Neutron Source”, ORNL/TM-99-208, 2001.

2.3-35) M. Teshigawara, et al.: “Development status of moderator-reflector system in JSNS,” Proc. Int. Collaboration on Advanced Neutron Sources ICANS-XVI, Dusseldorf-Neuss, Germany, 12-15 May 2003, 2003, pp. 601-611.

2.3-36) N. Watanabe: “Outline of Spallation Neutron Source Engineering”, JAERI-Review 2000-031, 2000, in Japanese.

2.3-37) M. Teshigawara et al.: “Neutronic Characteristics of Coupled Moderator Proposed in Integrated Model”, JAERI-Research 2001- 022, 2001, in Japanese.

2.3-38) T. Aso, et al.: “Thermal-Hydraulic Experiments and Analysis on Cold Moderator,” Proc. Int. Collaboration on Advanced Neutron Sources ICANS-XV, Tsukuba, Japan, 6-9 Nov. 2000, JAERI-Conf 2001-002 & KEK Proc. 2000-22, 2001, pp. 893-903.

2.3-39) T. Aso et al.: ,Proc. of the 30th Symposium on Visualization, 2001, pp. 127-130.

2.3-40) M. Hohara et al.: Numerical fluid dynamics, 1993, 267.

Table 2.3.1: Main configuration of moderators

Moderator	coupled	decoupled	poisoned
Quantity	1	1	1
Beam extraction	both sides	both sides	both sides
Angular coverage	50.8°/45.0°	24.4°/17.8°	13.4°/13.6°
Main moderator	H_2, 20K, 15 atm	←	←
Shape	cylindrical	canteen	←
Size	ϕ14cm×10^H cm	$13^W\times12^H\times6.2^T$ cm^3	←
Premoderator	H_2O (1cm^t)	Non	←
Decoupler	-	Ag-In-Cd	←
Decoupling energy		1 eV	←
Poison	-	-	Cd (1.3 mm^t)
Viewed surface	10×10 cm^2	10×10 cm^2	10×10 cm^2
Center of viewed surface	center of moderator height	←	←
Heat deposition (W/MW)	1100 in H_2 485 in moderator vessel	534 in H_2 422 in moderator vessel	498 in H_2 522 in moderator vessel 116 in poison

Table 2.3.2: Configuration of reflector

Inner (main) material	beryllium	ϕ50 cm × 100 cm^H
Outer material	pure iron (coated by aluminum)	~ϕ100 cm × 100 cm^H
Container	aluminum alloy (A5083)	t2.5 cm at maximum
Liner	Ag-In-Cd liner	beam holes for decoupled and poisoned moderators
Coolant	D_2O, 3-mm cooling channel	

Table 2.3.3: Main parameters for coupled moderator

Moderator	
Material:	liquid or super critical hydrogen (100% para) at 20 K
Shape:	cylindrical
Dimension:	140 mm in diameter, 100 mm in height
Premoderator (PM)	
Material:	light water (H_2O) at ambient temperature
Shape:	cylindrical (covering main moderator except viewed surfaces)
Dimension:	20 mm (near-target), 10 mm (side, far-target)
Neutron Beam Line	
Center height:	−163 mm from proton beam center
Viewed surface:	100 mm × 100 mm
Extraction angle:	±22.5°(forward), ±25.4°(backward)
Reflector	
Material:	beryllium (inner) stainless steel or iron coated with aluminum (outer)
Shape:	530 mm in max. diameter, 1,000 mm in max. height (inner) 1,000 mm in max. diameter, 1,000 mm in max. height (outer)
Coolant:	Heavy water (D_2O)

Table 2.3.4: Temperature dependence of ratio of peak intensities, FWHM and time integrated intensities

	Time-integrated intensity		Peak intensity		FWHM	
	0-20meV	50meV-1eV	0-20meV	50meV-1eV	0-20meV	50meV-1eV
	%/5K	%/5K	%/5K	%/5K	%/5K	%/5K
DM	-12	-2	-12	-8	0	5
PM	-13	-2	-15	-8	0	5
CM	-2	2	3	2	2	5
	%/K	%/K	%/K	%/K	%/K	%/K
DM	-2.4	-0.4	-2.4	-1.6	0.0	1.0
PM	-2.6	-0.4	-3.0	-1.6	0.0	1.0
CM	-0.4	0.4	0.6	0.4	0.4	1.0

Table 2.3.5: Premoderator material and thickness dependence of energy-integrated intensity ratio (E_n=5~100 meV) for DM. "Near" means a premoderator near target and "Side" means a side premoderator (not near or far target)

No.	H_2O Premoderator thickness (mm)		D_2O Premoderator thickness (mm)		Sum_ratio
	Near	Side	Near	Side	
1	0	0			1.0270
2	5	0			1.0130
3	5	5			1.0126
4	5	10			1.0176
5	10	0			1.0009
6	15	0			0.9882
7	20	0			0.9852
8			0	0	1.0000
9			5	0	1.0019
10			5	5	0.9709
11			5	10	0.9412
12			10	0	0.9914
13			15	0	0.9745
14			20	0	0.9737

Table 2.3.6: Premoderator material and thickness dependence of energy-integrated intensity ratio (E_n=5~100 meV) for PM. "Near" means a premoderator near target and "Side" means a side premoderator (not near or far target)

No.	H_2O Premoderator thickness (mm)		D_2O Premoderator thickness (mm)		Sum Ratio
	Near	Side	Near	Side	
1	0				1.0258
2	5	0			1.0151
3		5			1.0163
4		10			1.0228
5	10				1.0193
6	15				0.9827
7	20				0.9864
8			0		1.0000
9			5	0	1.0039
10				5	0.9861
11				10	0.9646
12			10		1.0084
13			15		0.9851
14			20		0.9761

Table 2.3.7: Material properties of aluminum alloy A6061-T6

Temperature (K)	Min. Tensile strength (MPa)	Min. 0.2% proof strength (MPa)	Elongation (%)	Young's modulus (GPa)	Poisson's ratio
R. T.	265	245	11	68.5	0.35
20 (78)	(415)	(325)	22	68.6	0.35

Table 2.3.8: Physical properties of liquid hydrogen and aluminum alloy

	Hydrogen (20K)	Aluminum alloy (300K)
Density, ρ (kg/m^3)	72.74	2,700
Viscosity, η (μPa·s)	14.0	—
Specific heat, Cp (J/(kg·K))	8,977	896
Thermal conductivity, λ (W/(m·K))	0.103	180

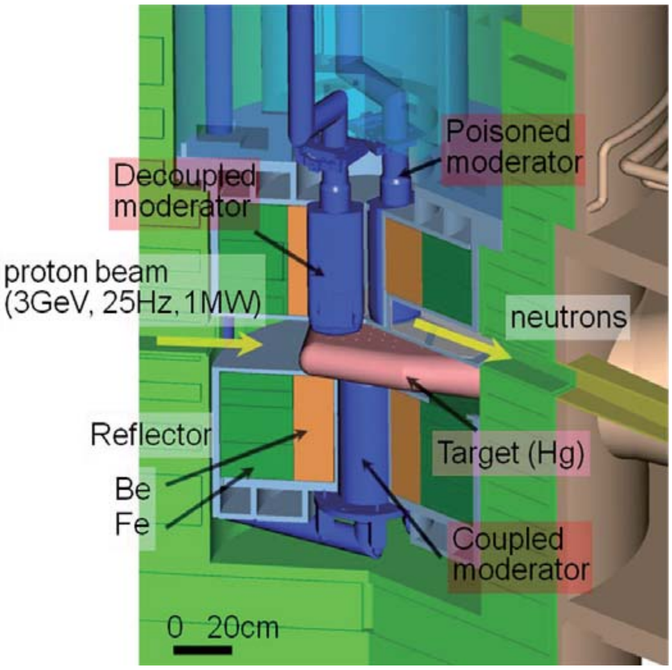

Fig. 2.3.1: Cross sectional view of target-moderator-reflector assembly

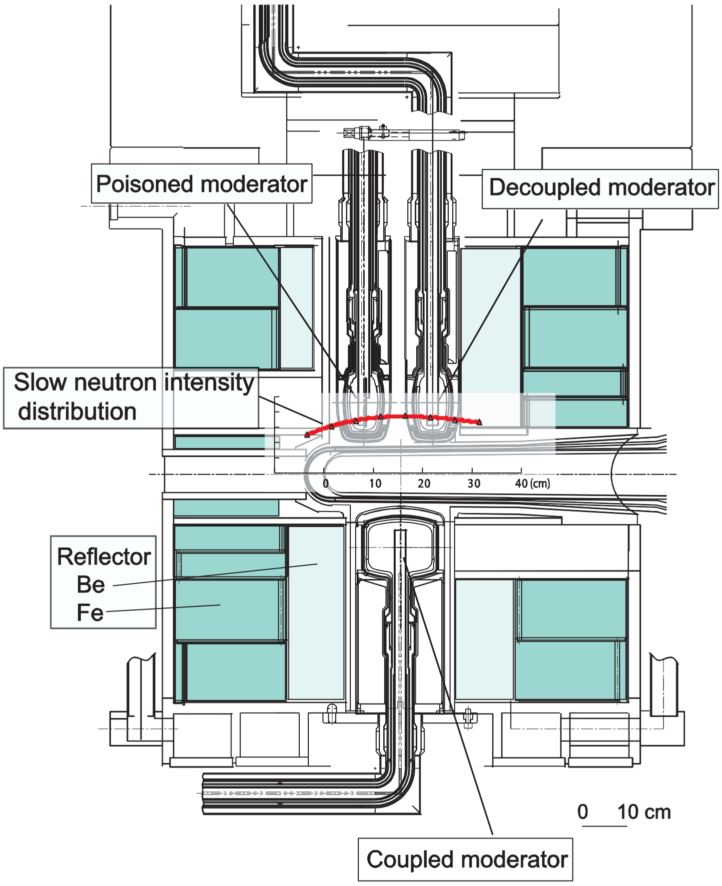

Fig. 2.3.2: Intensity distribution of slow neutrons from moderator along the proton beam axis. The arrangement of moderators is also shown as a reference.

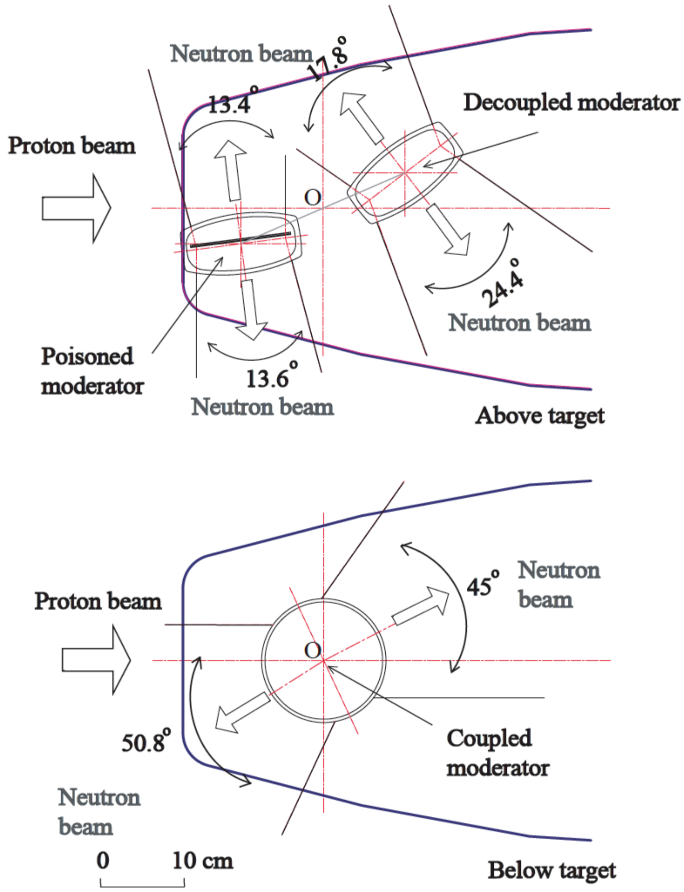

Fig. 2.3.3: Moderators layout

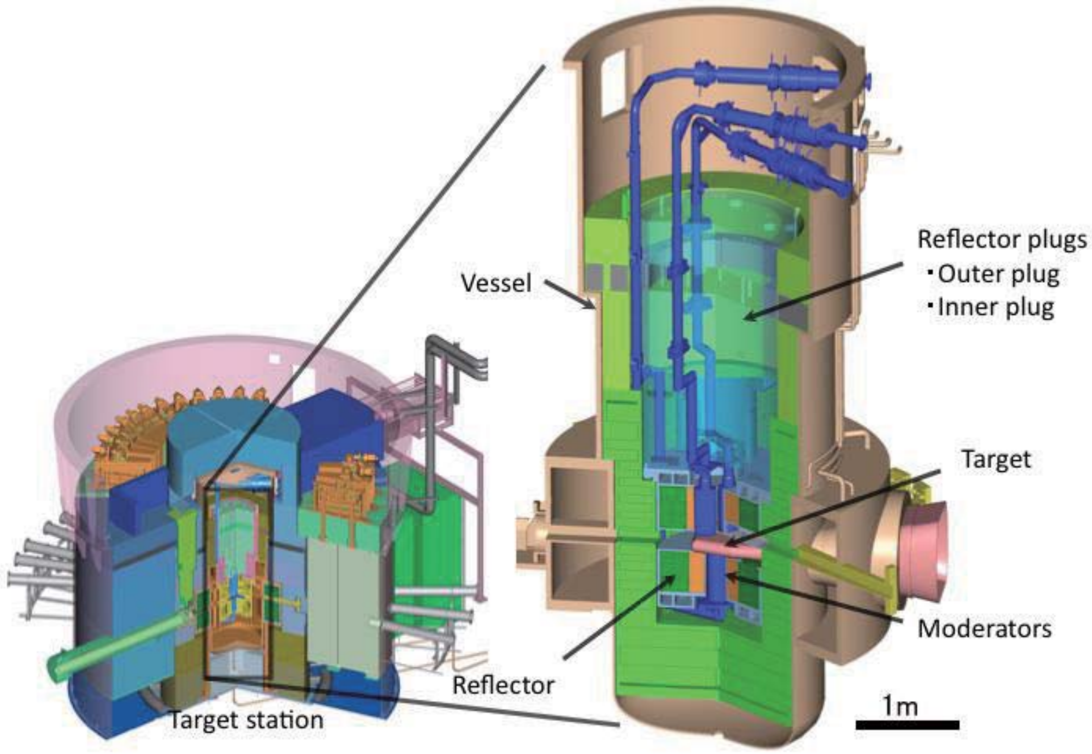

Fig. 2.3.4: In-vessel components

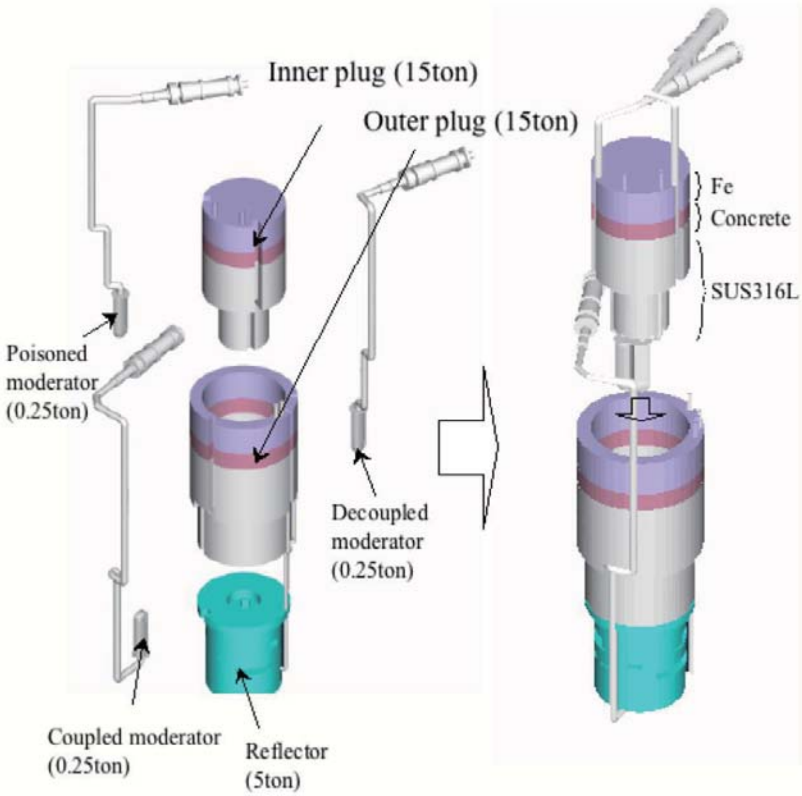

Fig. 2.3.5: Structure of moderator, reflector nad reflector plug

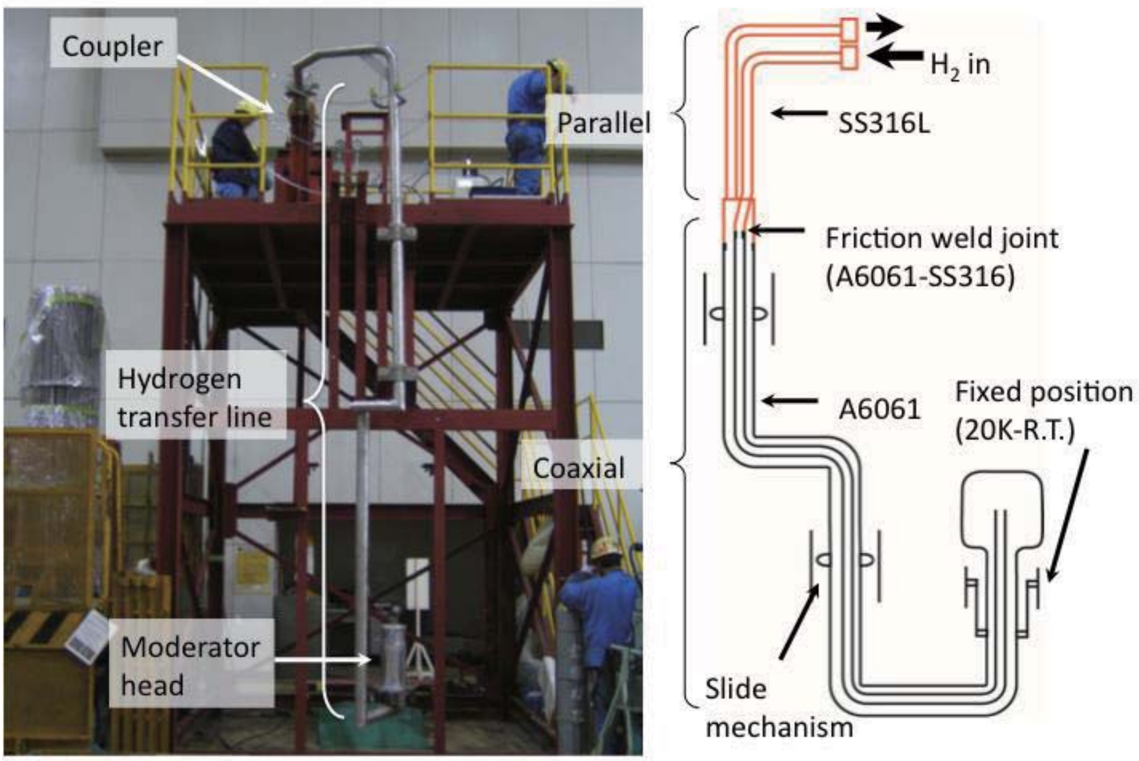

Picture of coupled moderator   Inside structure of hydrogen transfer line

Fig. 2.3.6: Picture of coupled moderator and inside structure of moderator

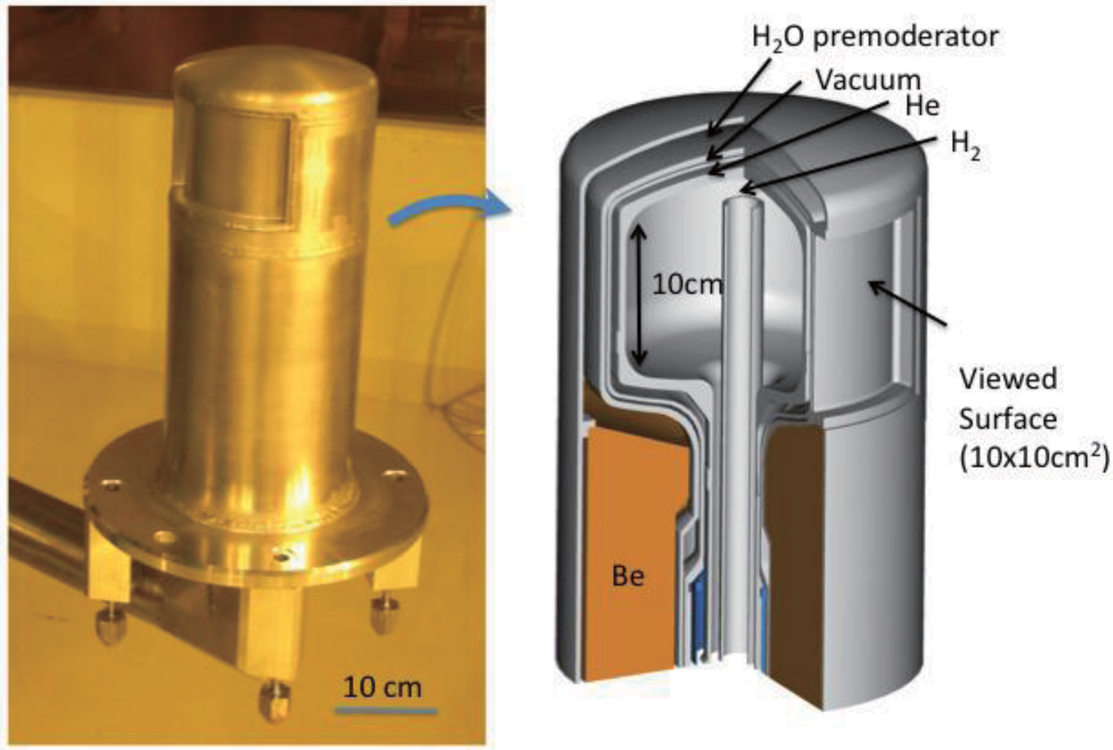

Fig. 2.3.7: Structure of coupled moderator

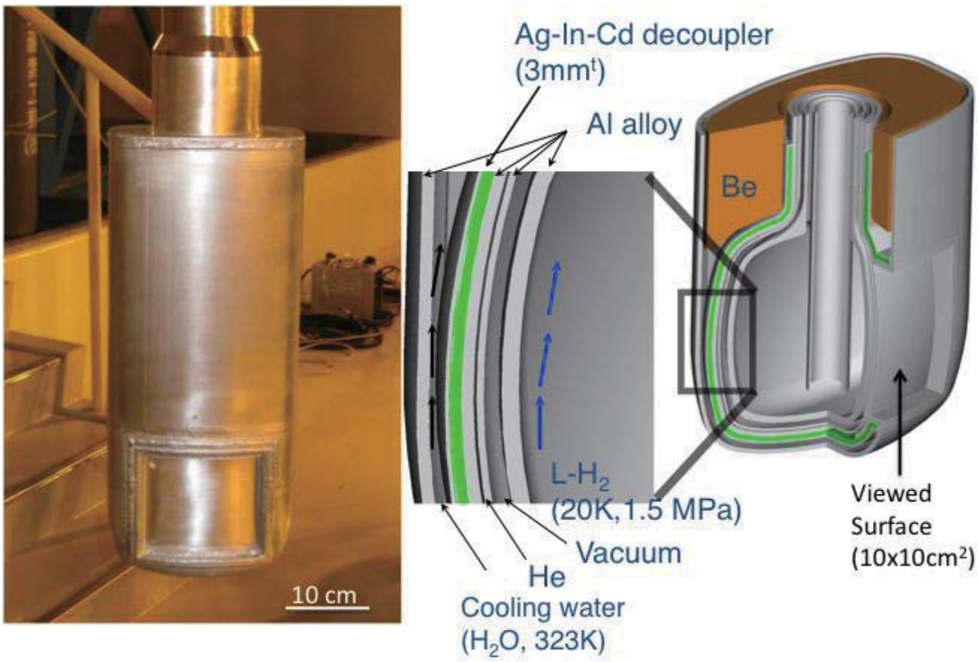

Fig. 2.3.8: Structure of decoupled moderator

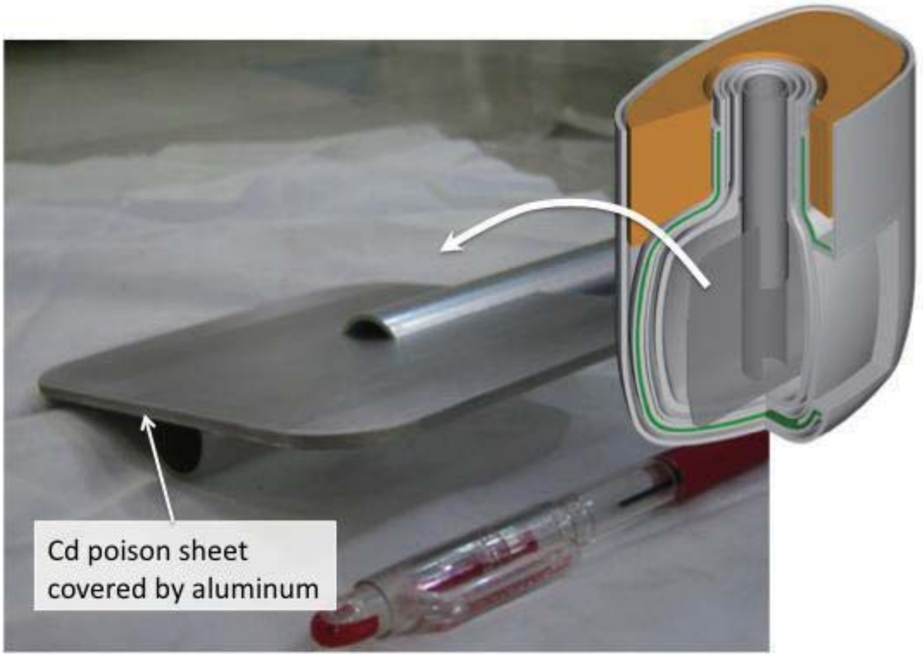

Fig. 2.3.9: Structure of poisoned moderator. It is the same as that of decoupled moderator except for cadmium (Cd) poison sheet. The Cd poison sheet is asymmetrically installed in moderator hydrogen chamber.

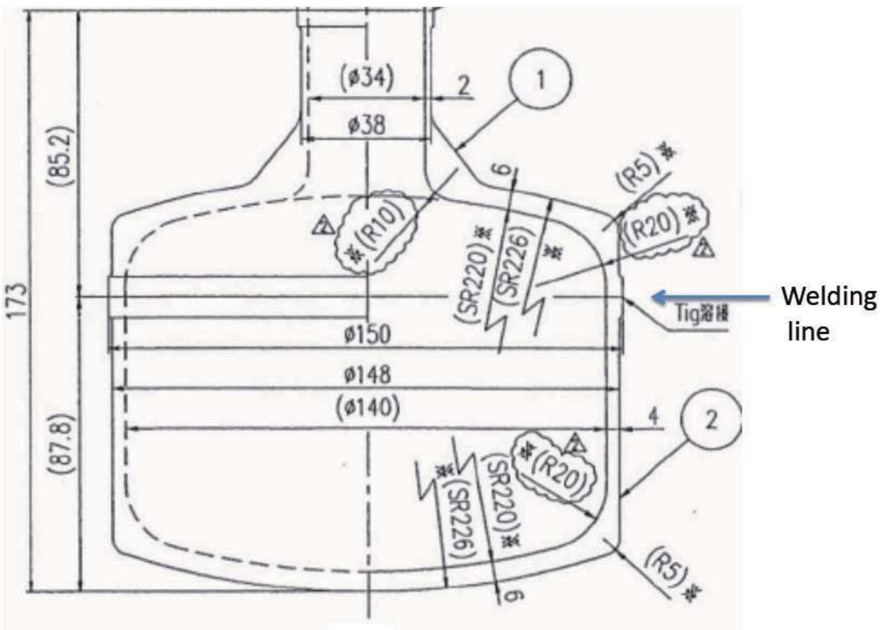

Fig. 2.3.10: Drawing of coupled moderator hydrogen chamber

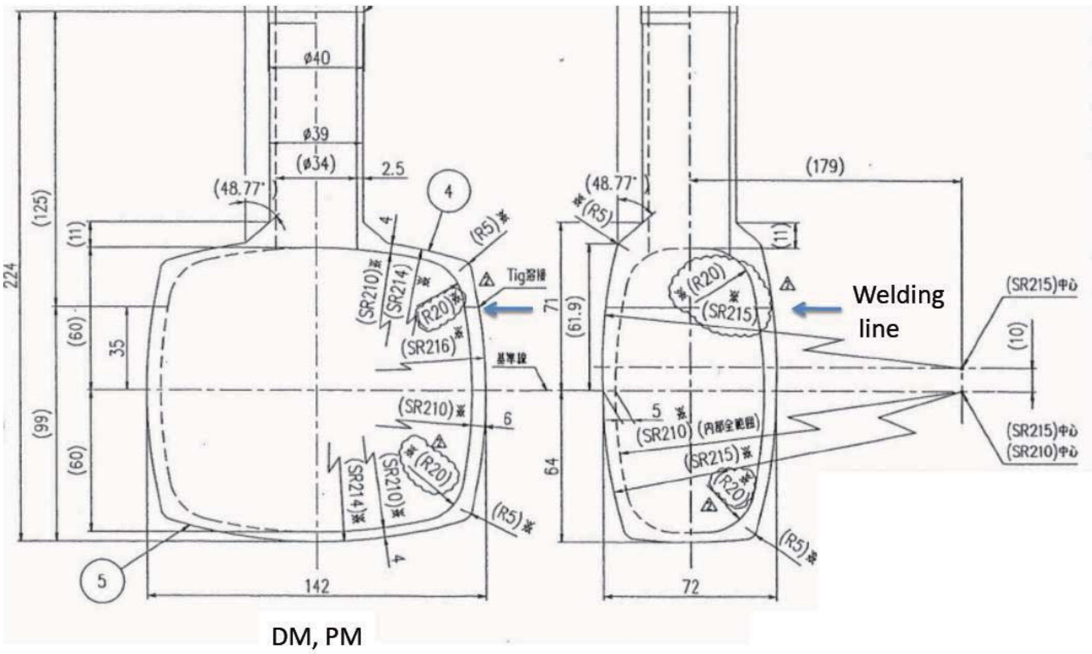

Fig. 2.3.11: Drawing of decoupled moderator hydrogen chamber. It is the same as poisoned moderator.

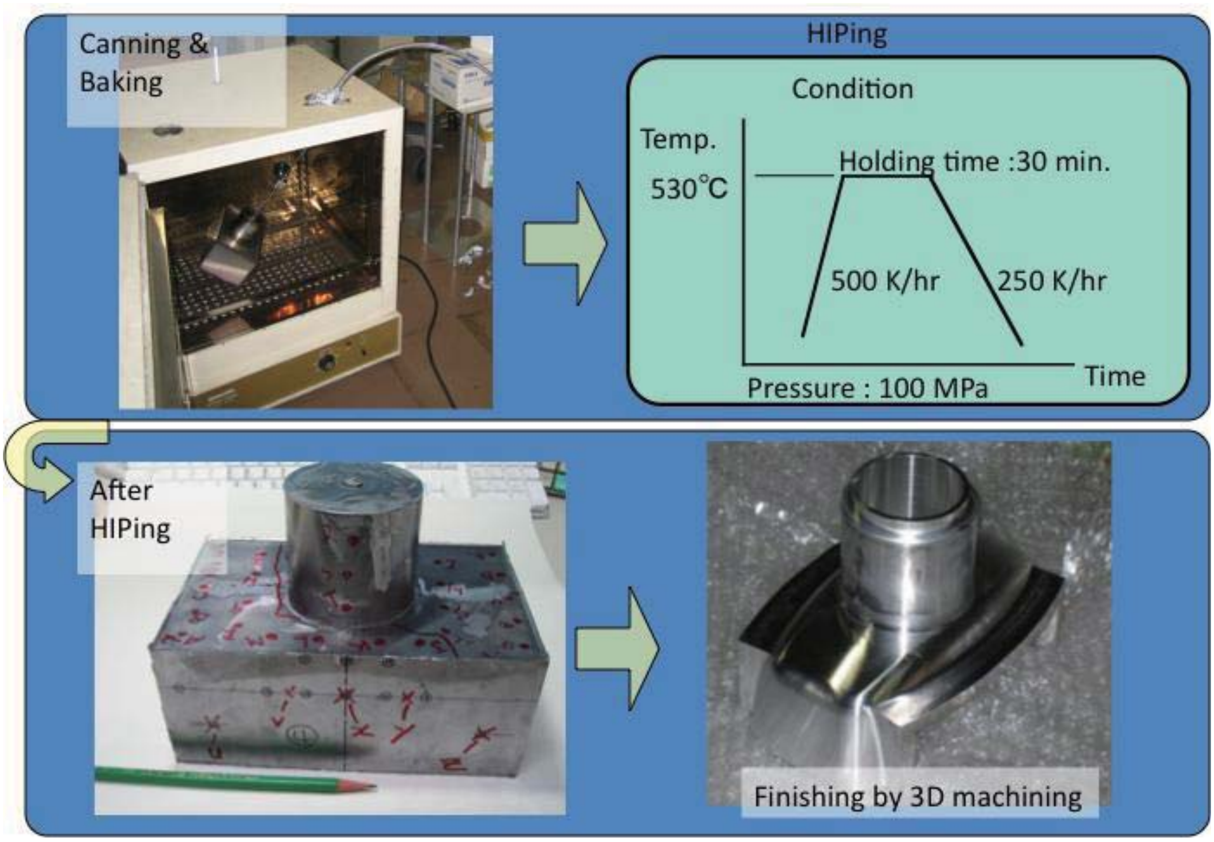

Fig. 2.3.12: HIPing process to fabricate bonding material of AIC and Al alloy.

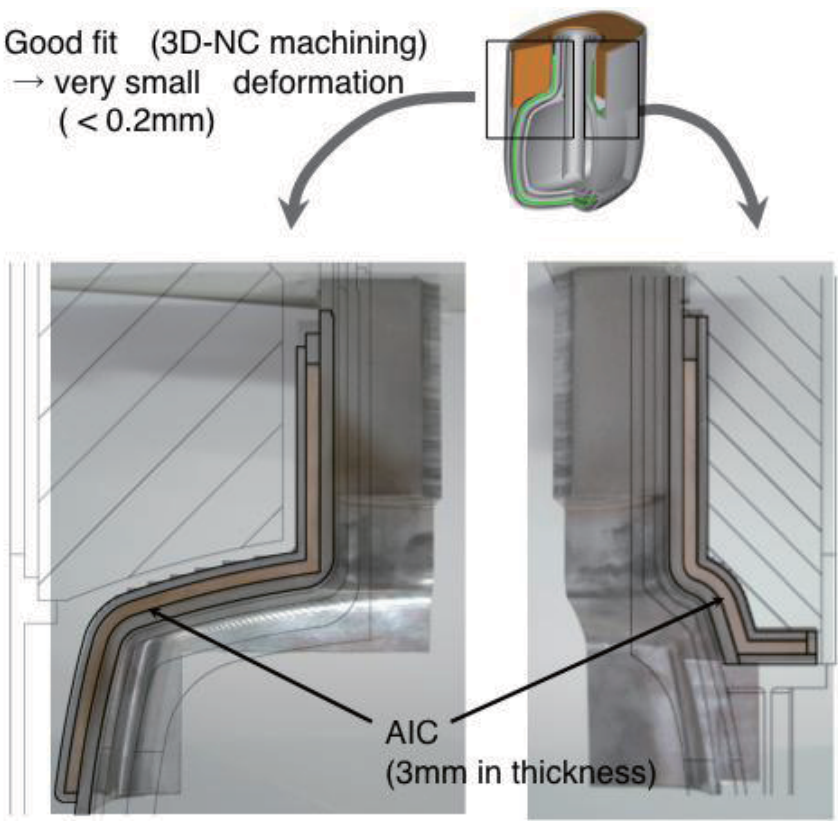

Fig. 2.3.13: Cross section of AIC decoupler. After fabrication process (HIPing and 3-D NC machining to fabricate the moderator container that includes AIC decoupler), it was cut to observe the bonding situation between AIC and Al alloy and performance of the fabrication process.

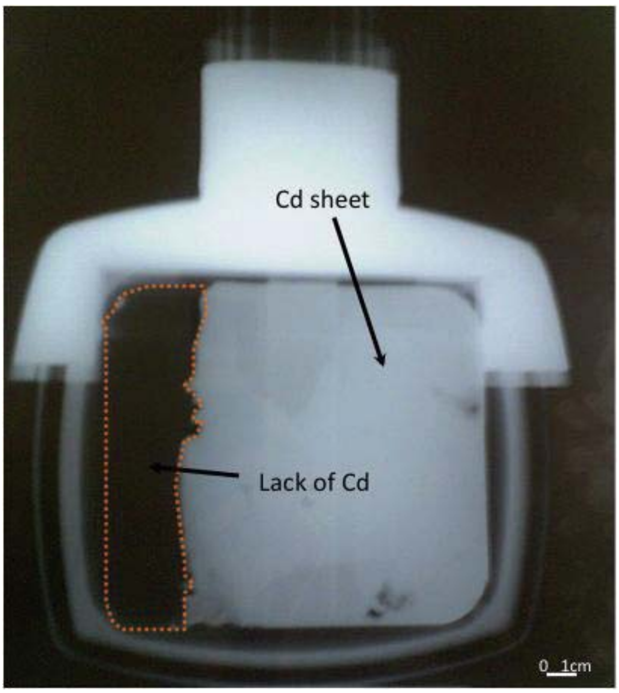

Fig. 2.3.14: X-ray transmission of Cd poison moderator in fabrication process.

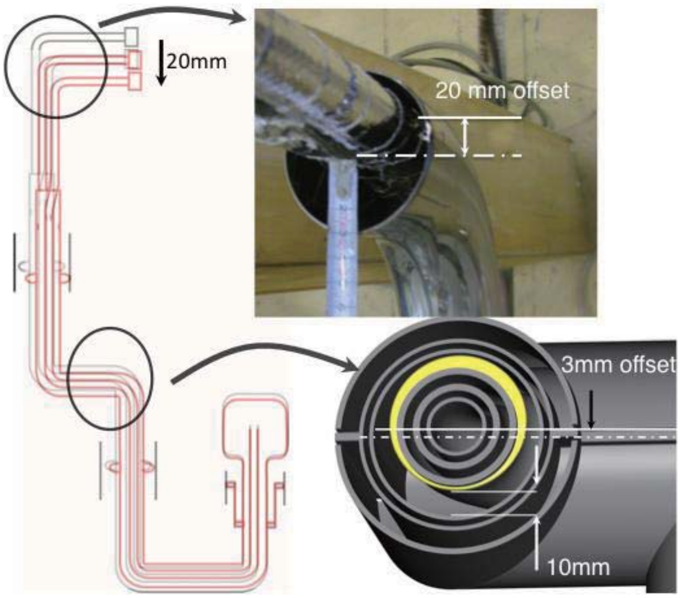

Fig. 2.3.15: Asymmetrical pipe arrangement at bent position for thermal shrinkage.

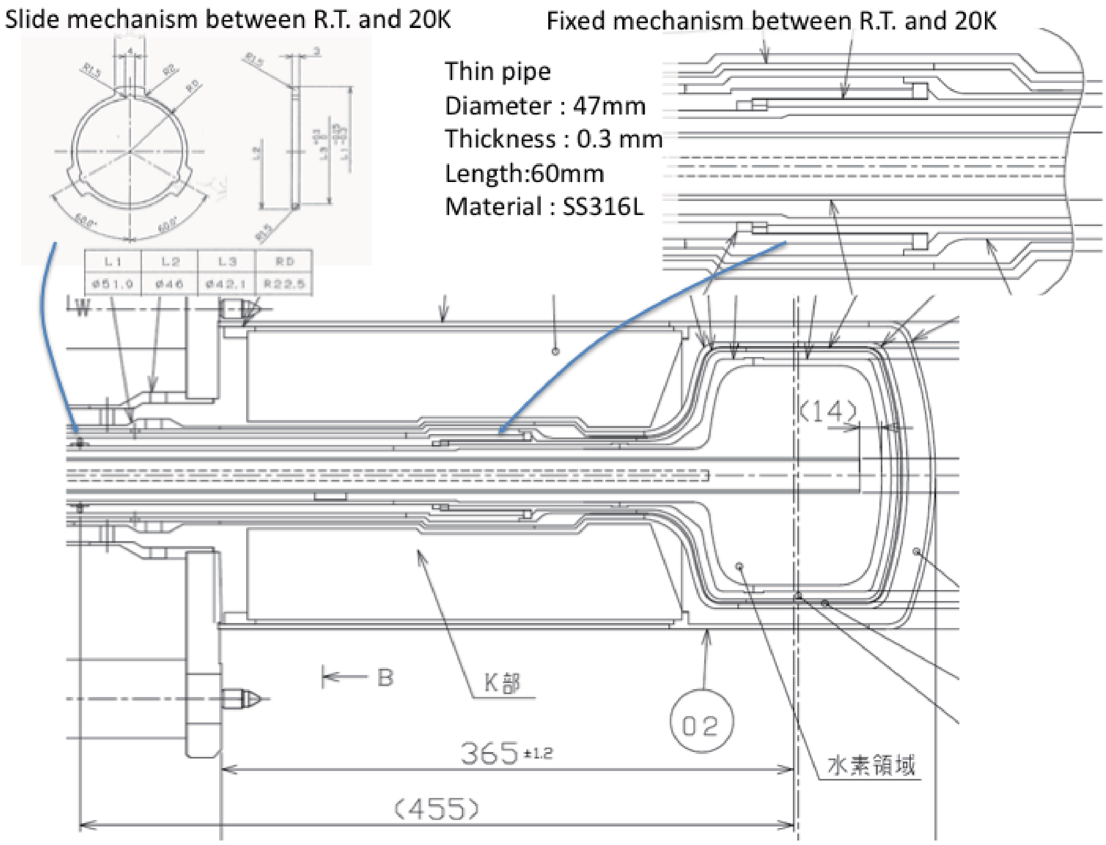

Fig. 2.3.16: Fix mechanism to minimize the movement of moderator hydrogen chamber at cold (20K) temperature. This figure shows the drawing of the coupled moderator and the fix mechanism is the same for the decoupled moderator and the poisoned moderator.

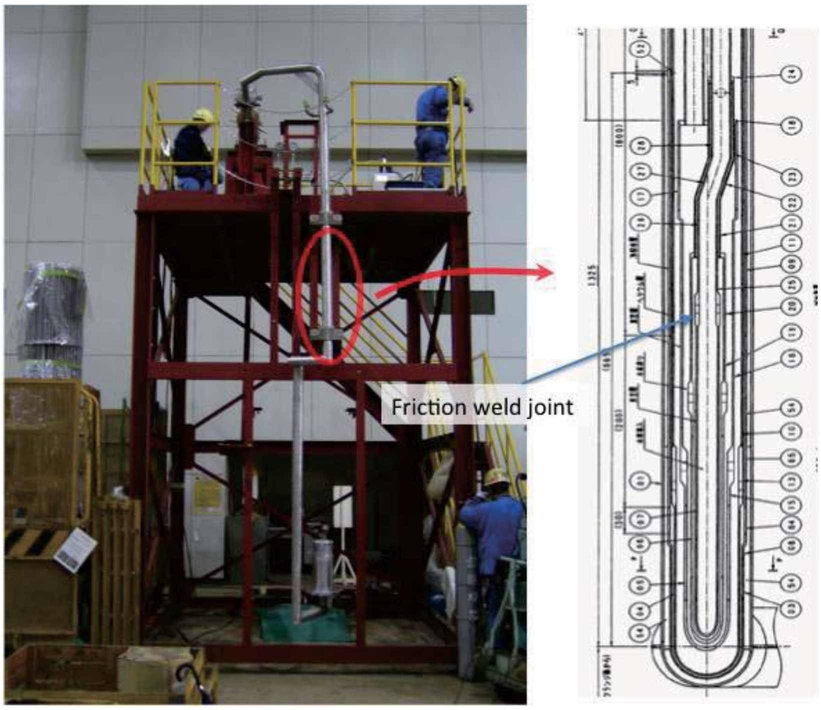

Fig. 2.3.17: Conversion section from multi-ply coaxial pipe to parallel pipes

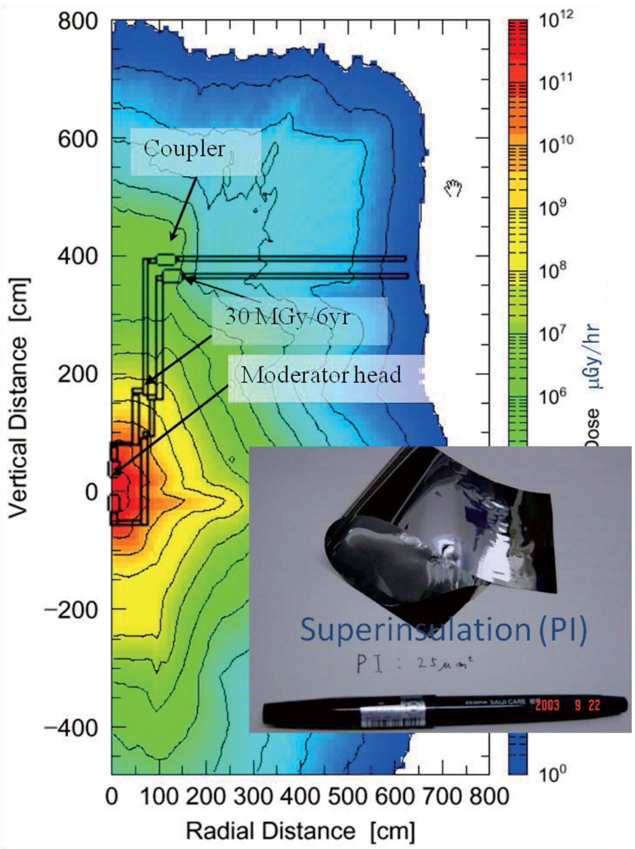

Fig. 2.3.18: Radiation dose distribution of neutrons around moderators. The part of the hydrogen transfer line where the accumulated radiation dose is below of 30 MGy is wraped with polyimide-based superinsulation to reduce the thermal load to the hydrogen transfer line.

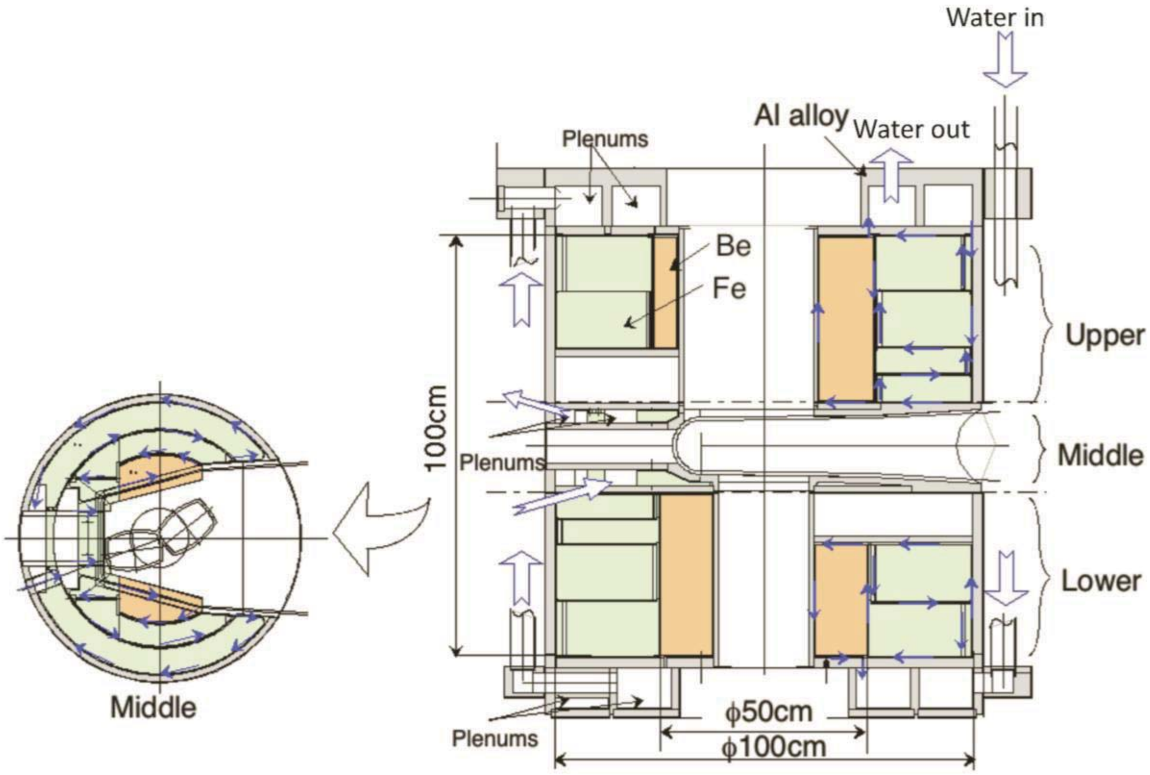

Fig 2.3.19: Conception of water flow in reflector

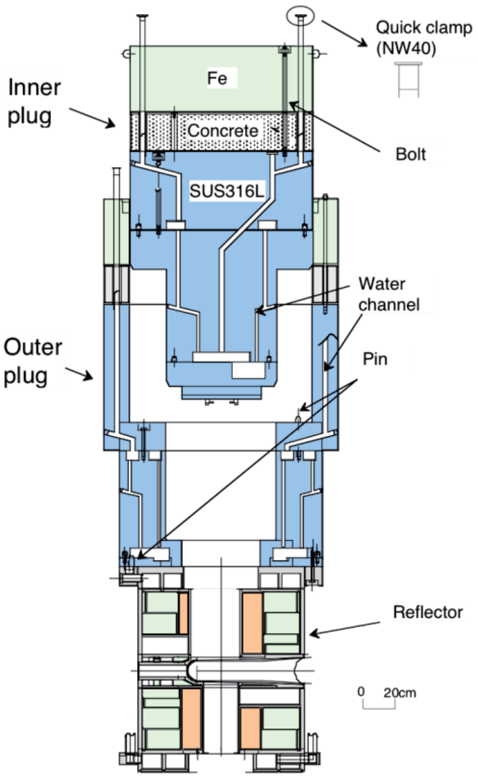

Fig. 2.3.20: Cross-sectional view of reflector and reflector plug (inner and outer plugs)

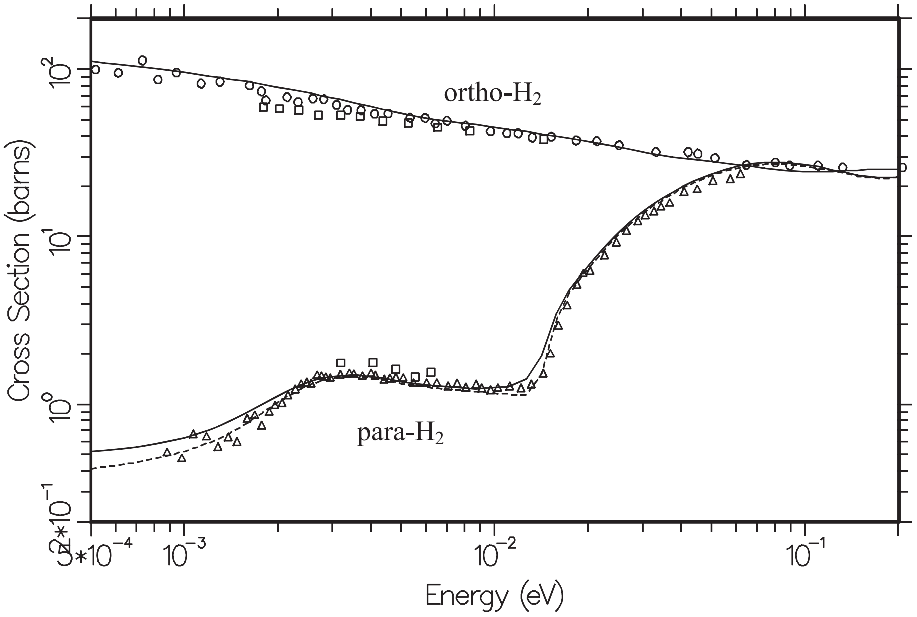

Fig.2.3.21: Calculated values of scattering cross-sections for liquid ortho-hydrogen and liquid para-hydrogen are compared with experimental data, reproduced from reference 2.3-6. Solid curves are at 20K and dashed curve is at 14K.

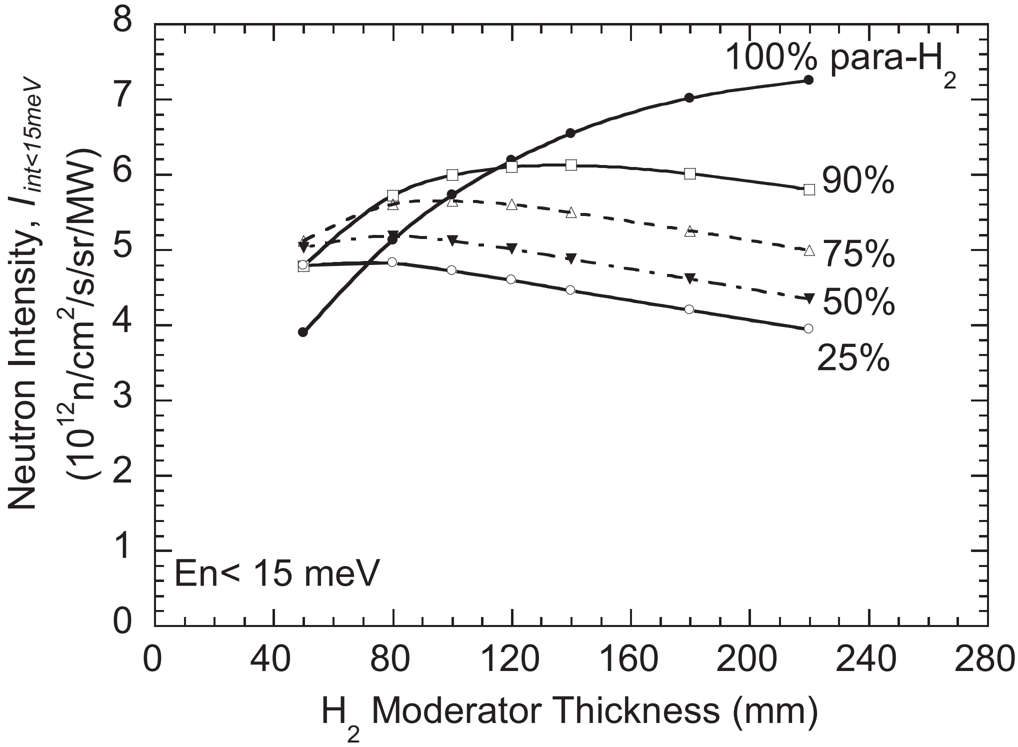

Fig. 2.3.22: Cold neutron intensities below 15 meV as a function of para-hydrogen concentration and moderator thickness.

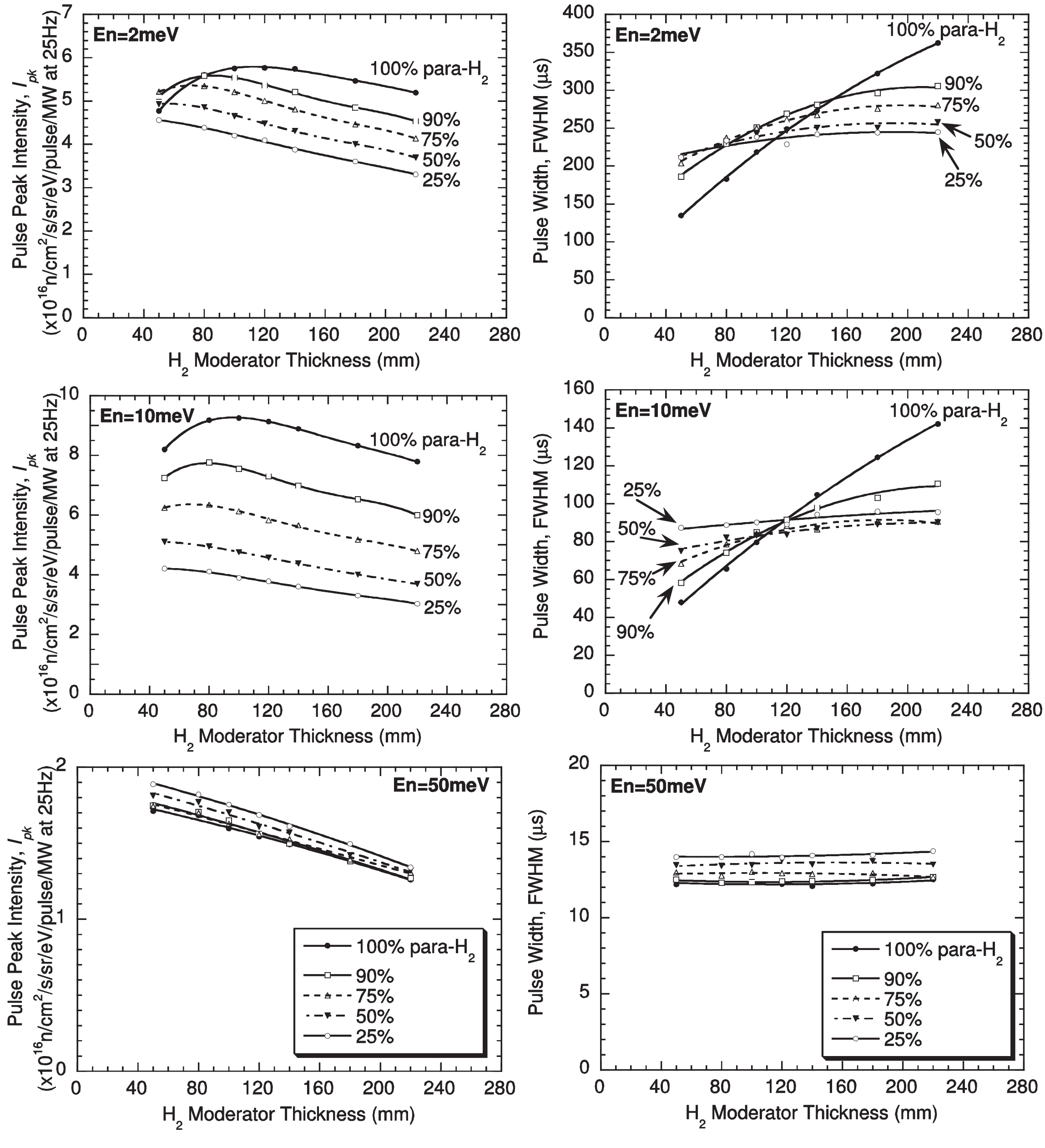

Fig. 2.3.23: Pulse peak intensities and widths (at FWHM) of 2, 10 and 50 meV neutrons as a function of para-hydrogen concentration and moderator thickness. 'E_n' means neutron energy.

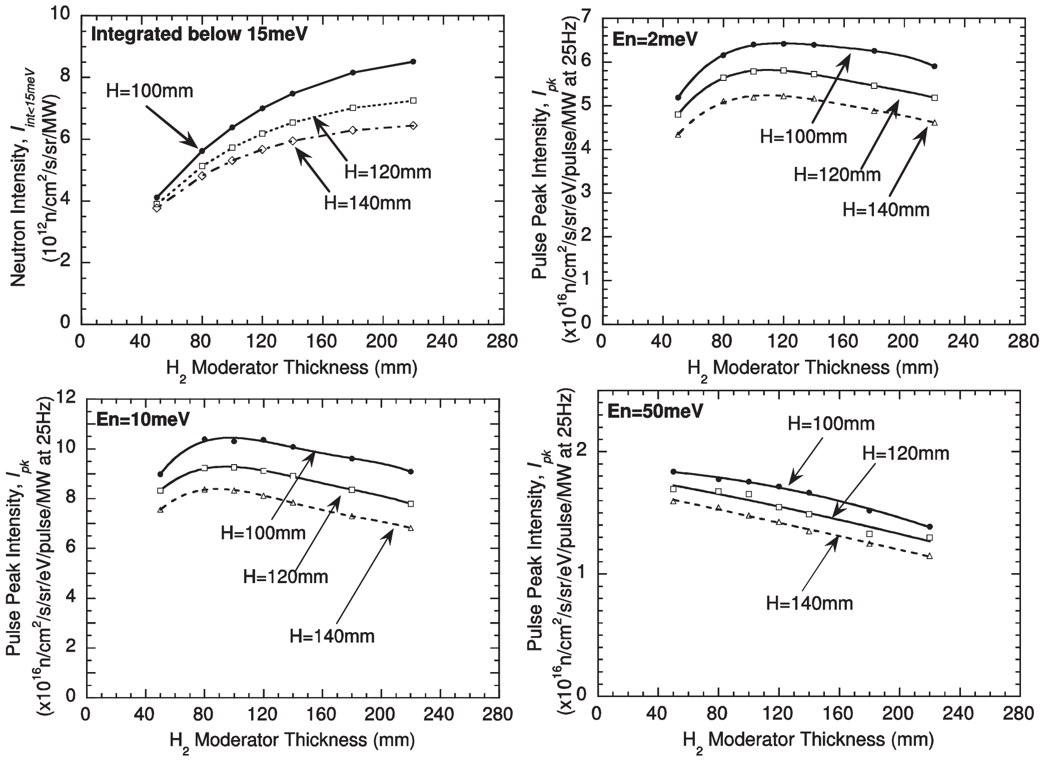

Fig. 2.3.24: Integrated cold neutron intensity ($I_{int<15meV}$), and pulse peak intensity (I_{pk}) at 2, 10 and 50 meV as a function of hydrogen moderator height(H) and thickness.

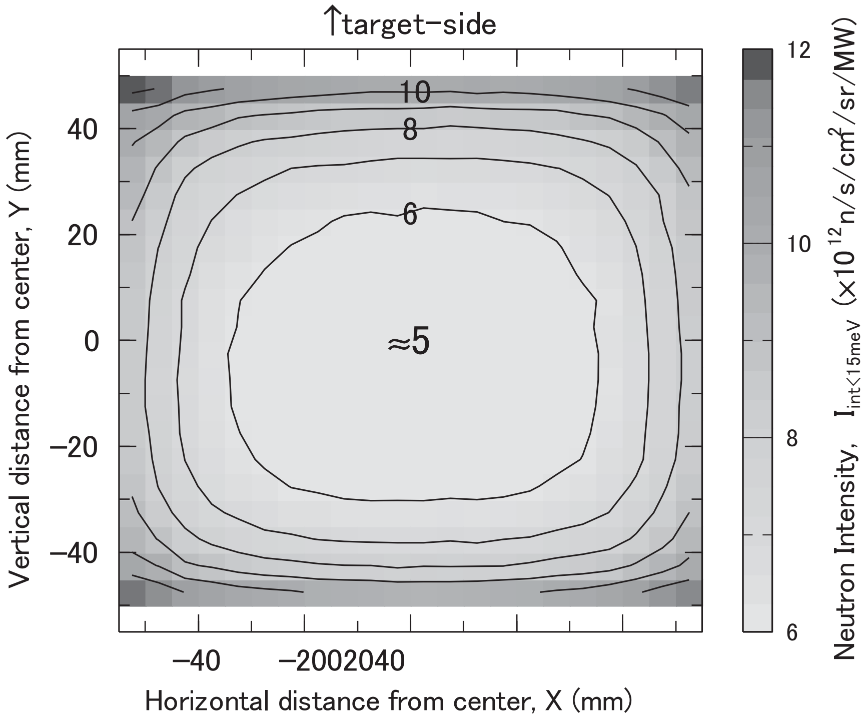

Fig. 2.3.25: Spatial distribution of the time integrated neutron intensity on viewed surface (100 × 100 mm^2) of 100% para-hydrogen moderator ($140^T\times100^H\times120^W$ mm^3) with premoderator in Be reflector. Center of viewed surface is defined as X=Y=0.

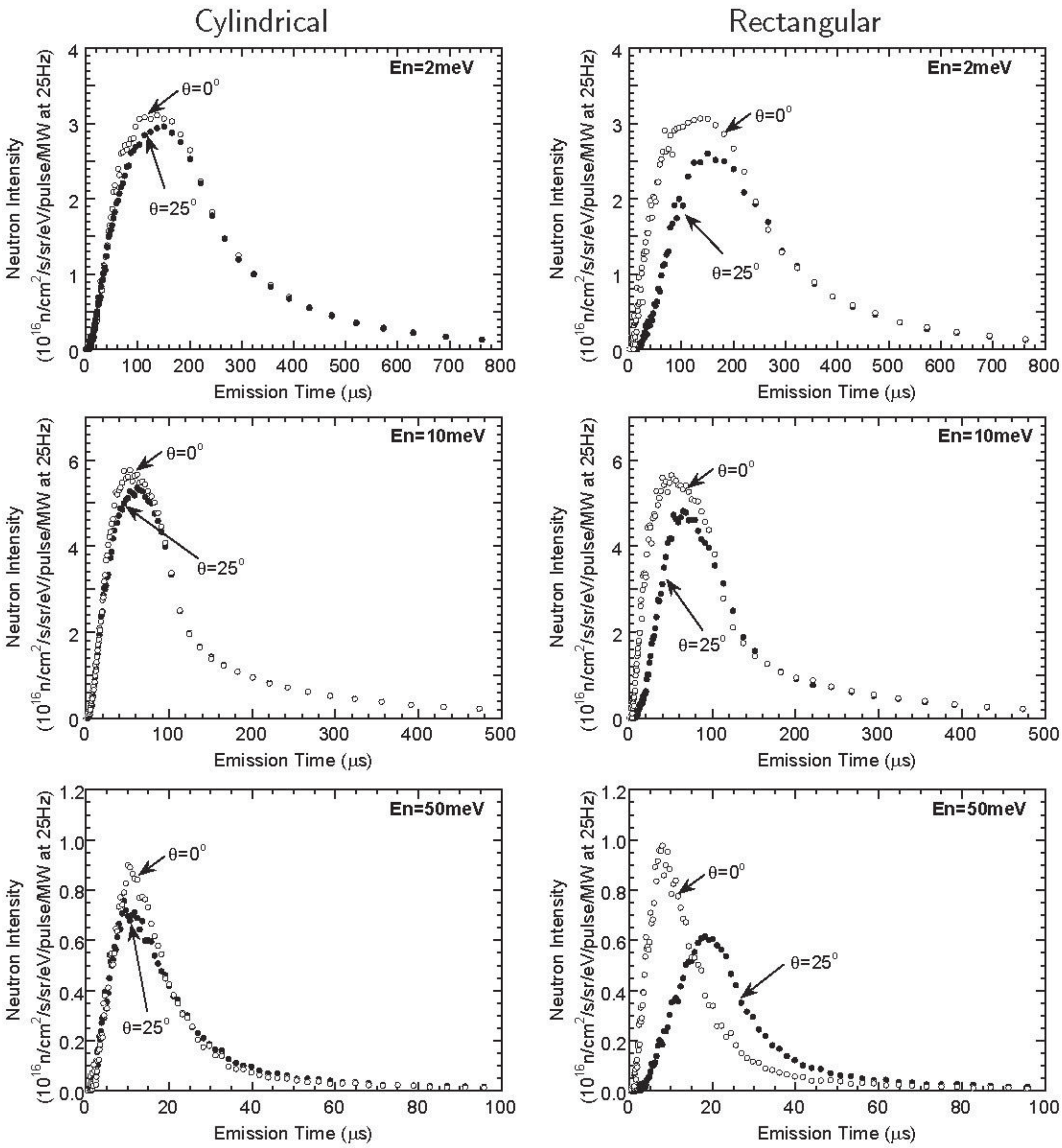

Fig. 2.3.26: Pulse shapes of 2, 10, and 50 meV neutrons at θ = 0º and 25º for cylindrical (left) and rectangular (right) moderators.

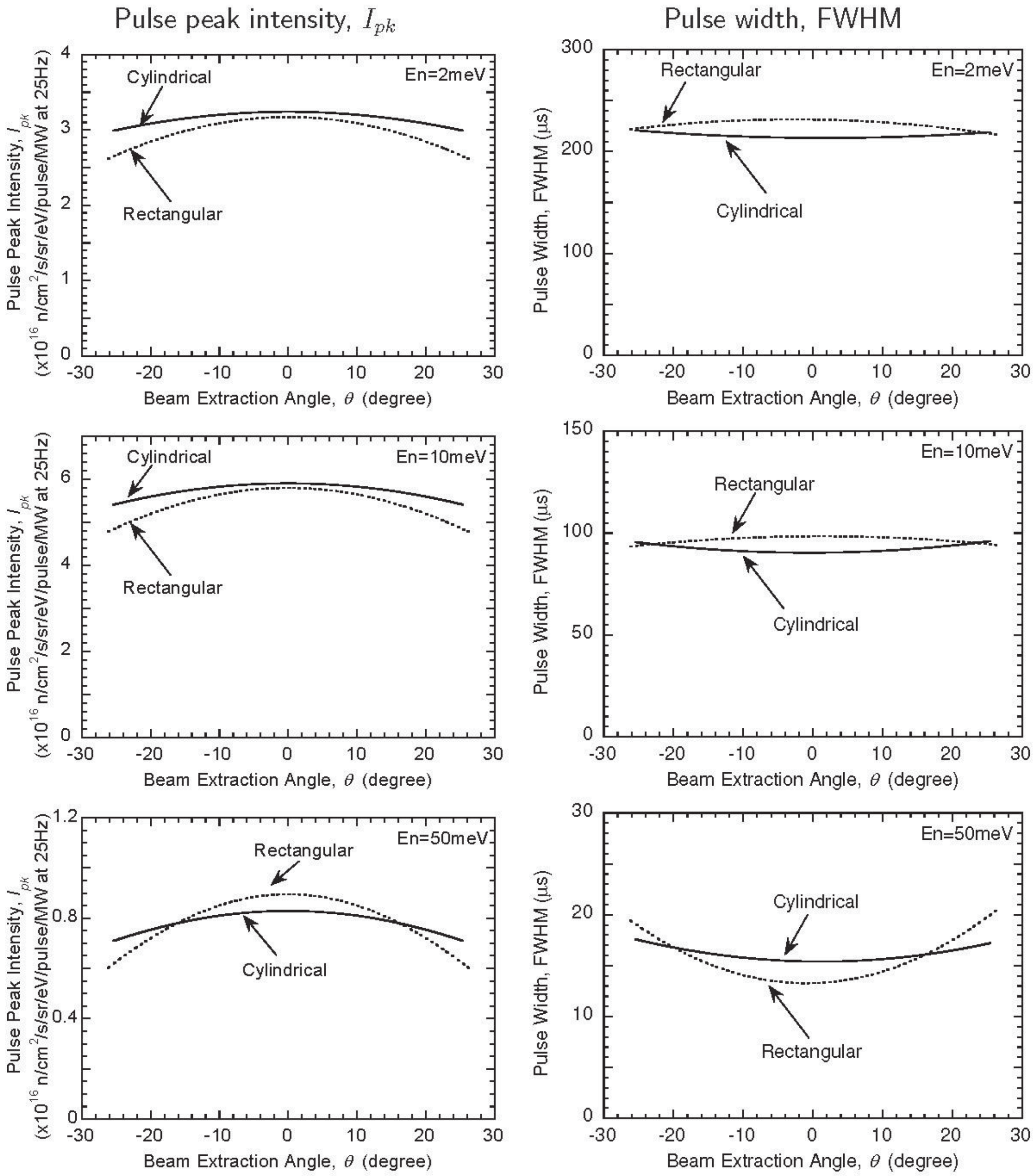

Fig. 2.3.27: Pulse peak intensities (I_{pk}) and pulse widths (FWHM) at 2, 10, and 50 meV for rectangular and cylindrical moderators as a function of θ.

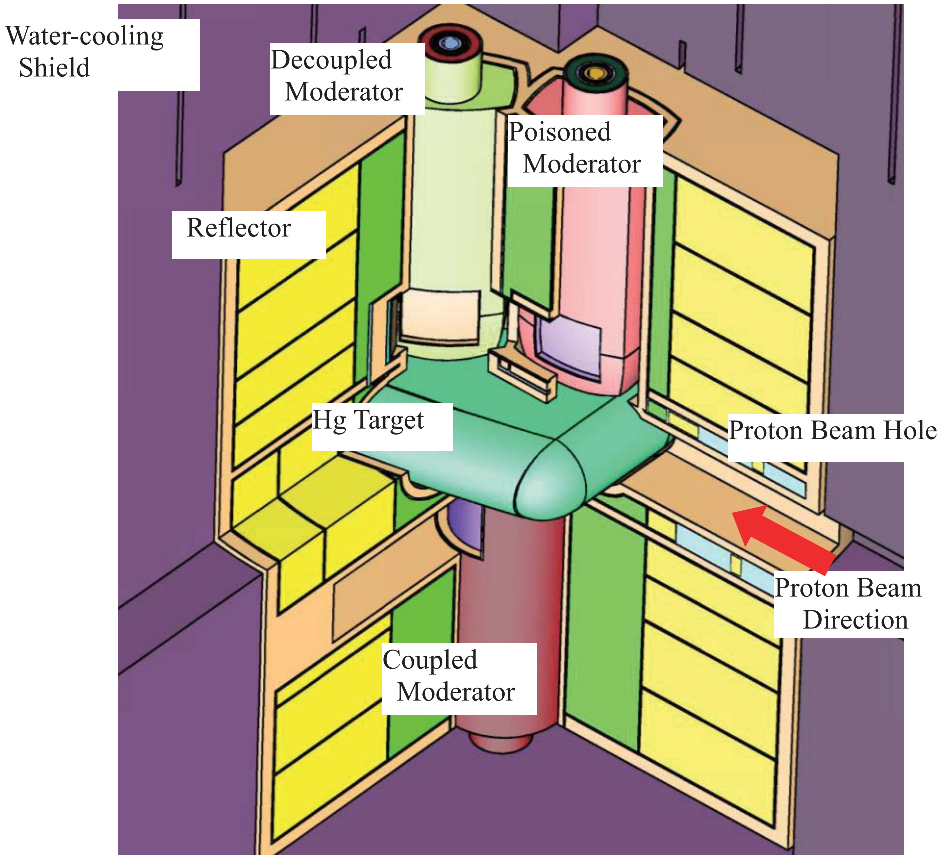

Fig. 2.3.28: Schematical 3D-view of target-moderator-reflector assembly

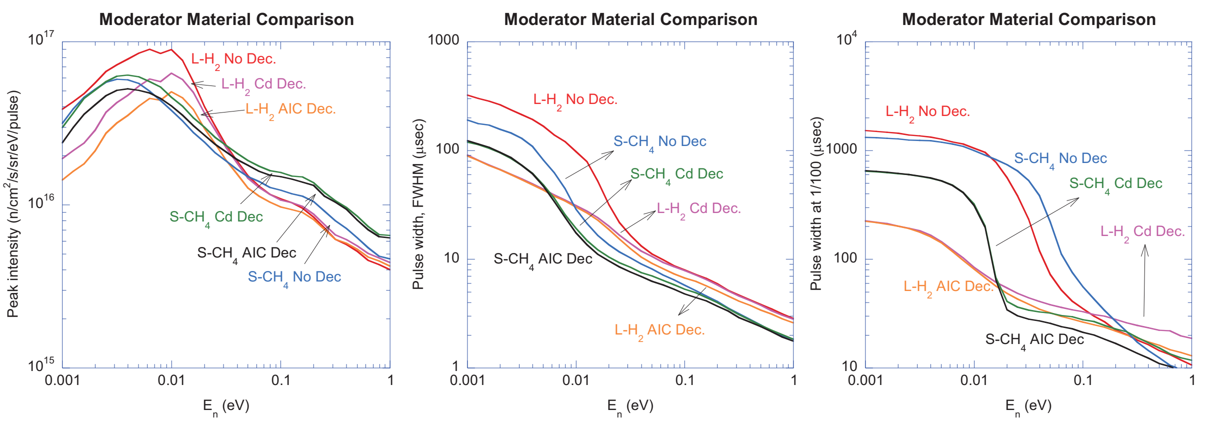

Fig. 2.3.29: Pulse peak intensities, pulse widths at half maximum and pulse widths at hundredth maximum of liquid hydrogen moderator and solid hydrogen moderator. No decoupler case, Cadmium decoupler case and AIC decoupler case are taken into account.

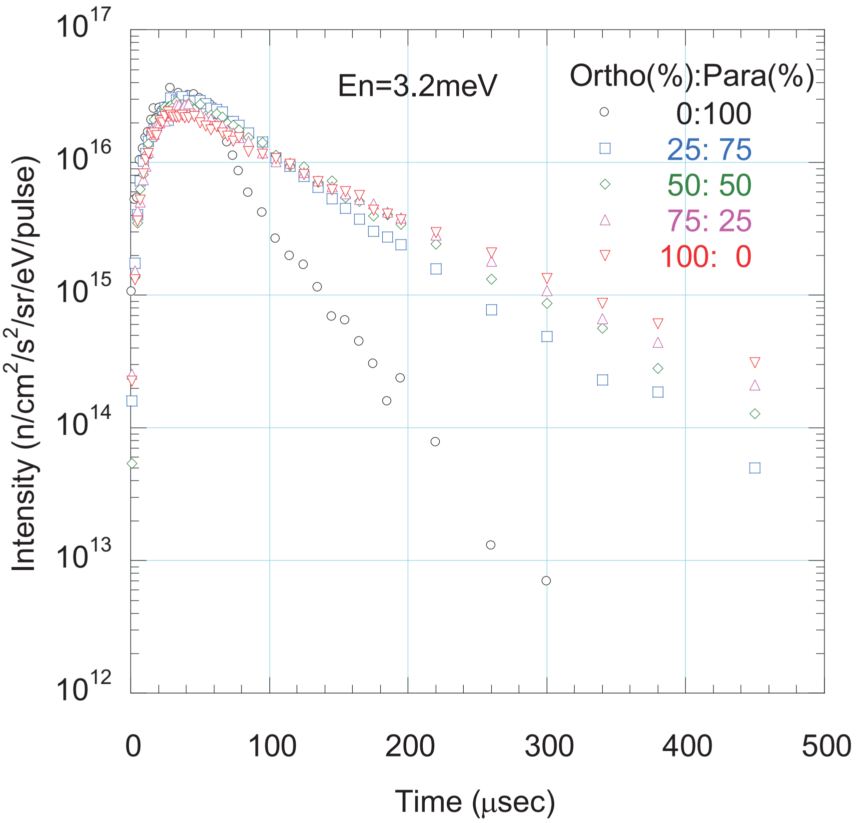

Fig. 2.3.30: Para-hydrogen ratio dependence of pulse structures (E_n = 3.2meV)

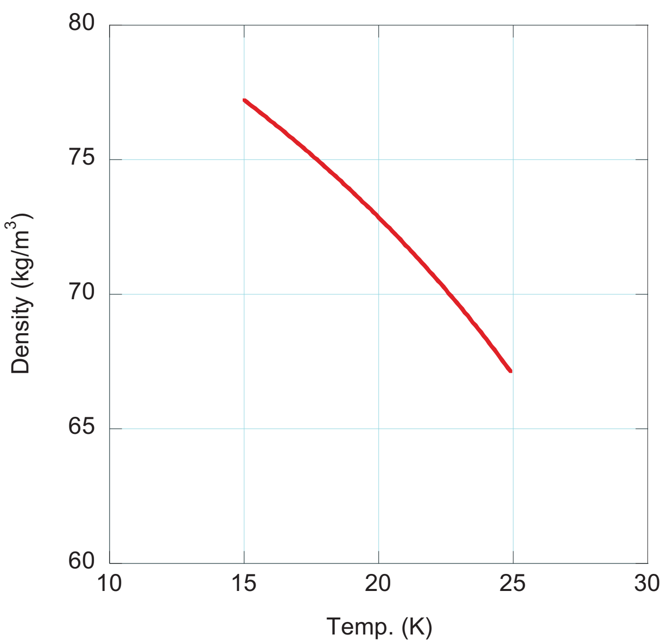

Fig. 2.3.31: Temperature dependence of liquid hydrogen density at 1.5 MPa of pressure.

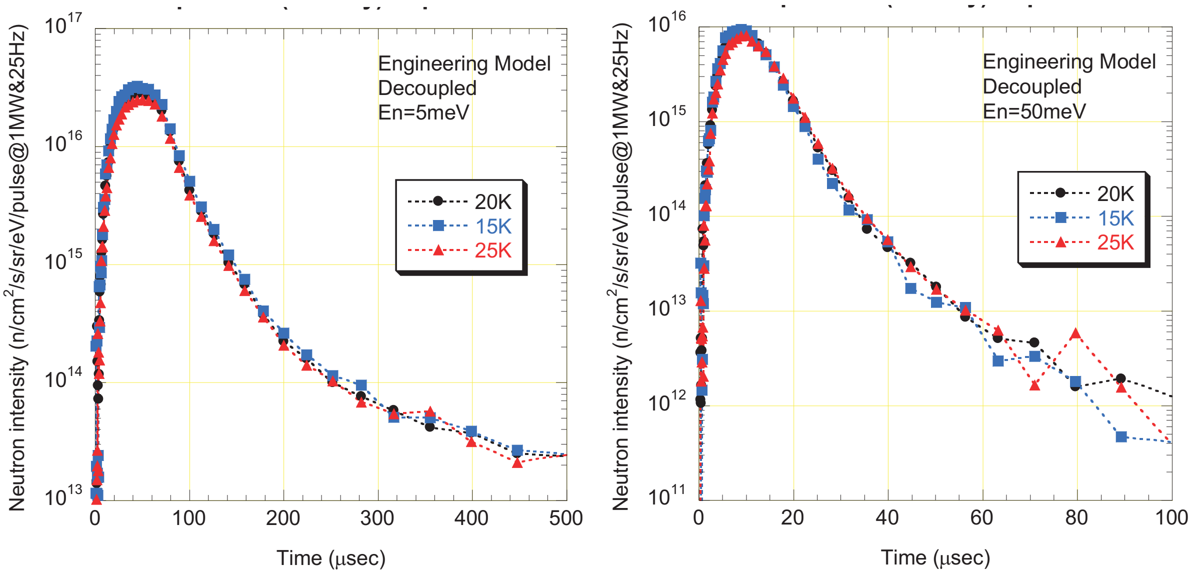

Fig. 2.3.32: Density dependence of pulse structures of the decoupled moderator

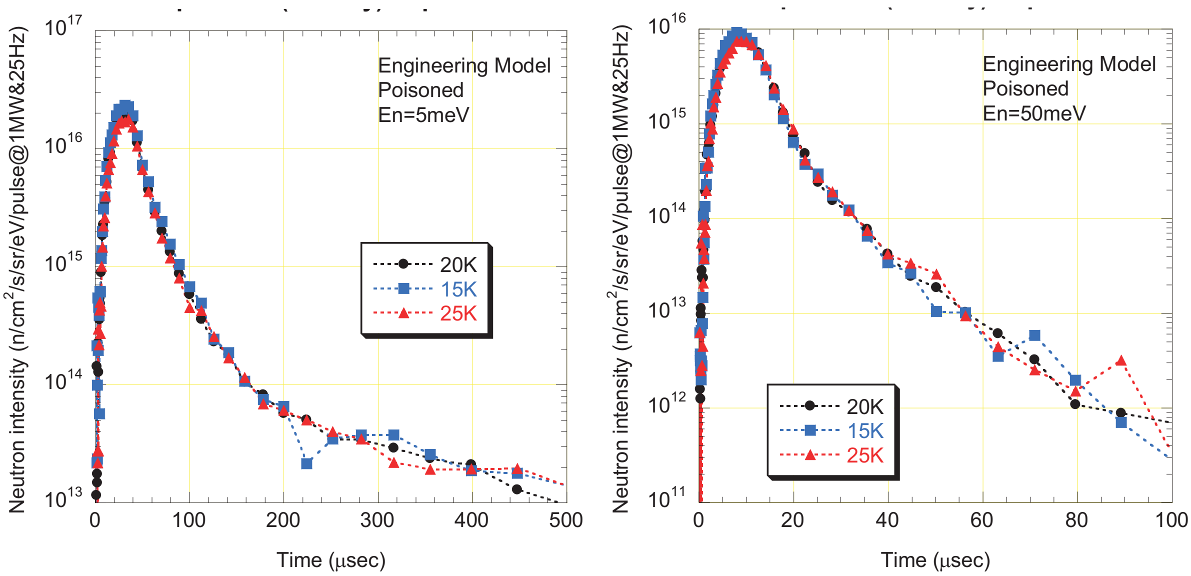

Fig. 2.3.33: Density dependence of pulse structures of the poisoned moderator

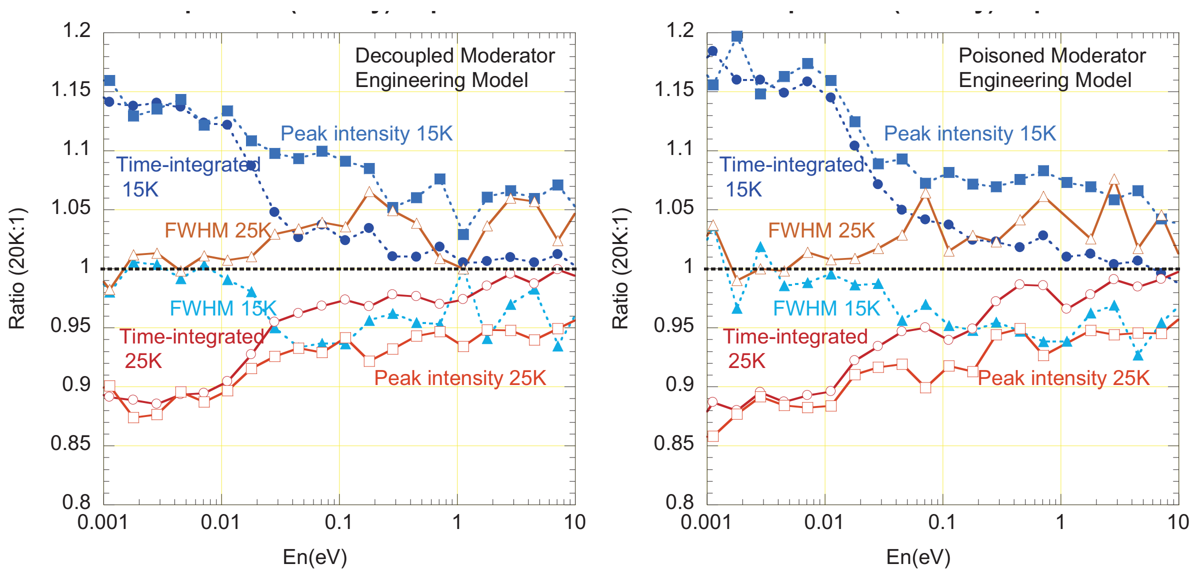

Fig. 2.3.34: Temperature dependence of peak intensities, FWHM and time-integrated intensities of the decoupled moderators

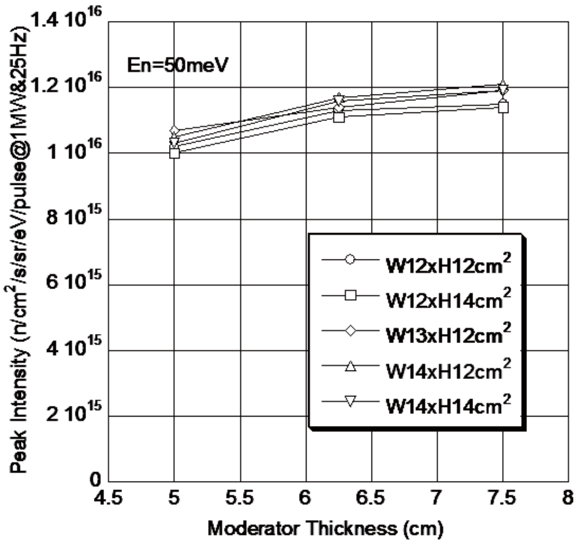

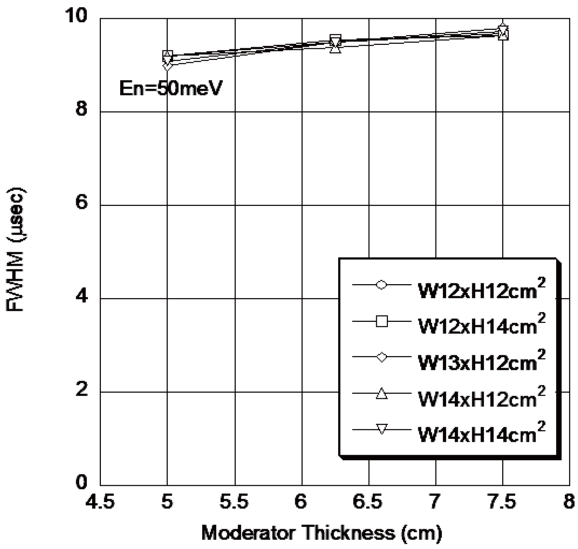

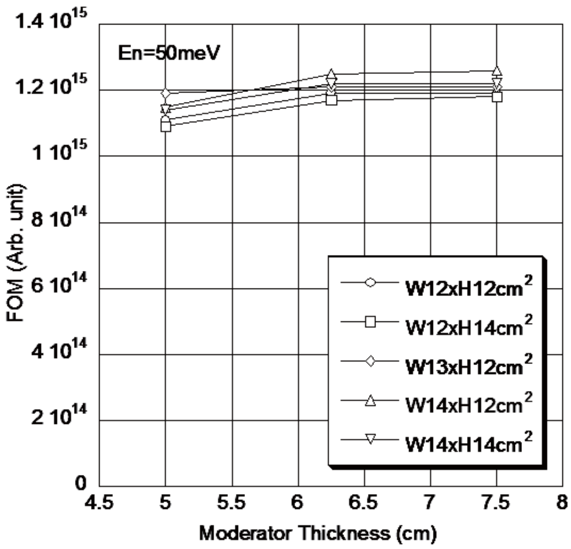

Fig. 2.3.35: Moderator size dependence of peak intensity, full with of half maximum and Figure Of Merit (E_n = 3.2 meV)

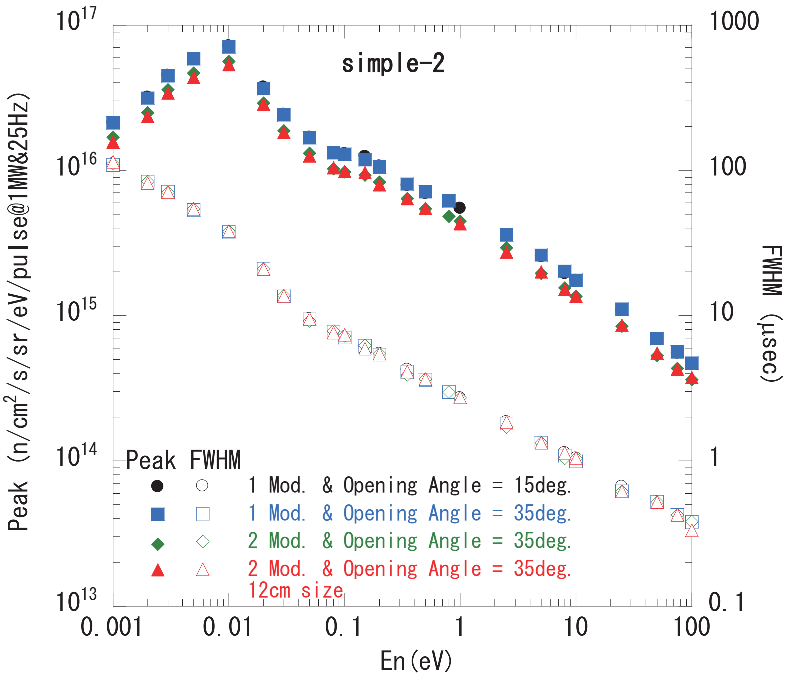

Fig. 2.3.36: Peak intensities and pulse widths (one moderator case and two moderators case)

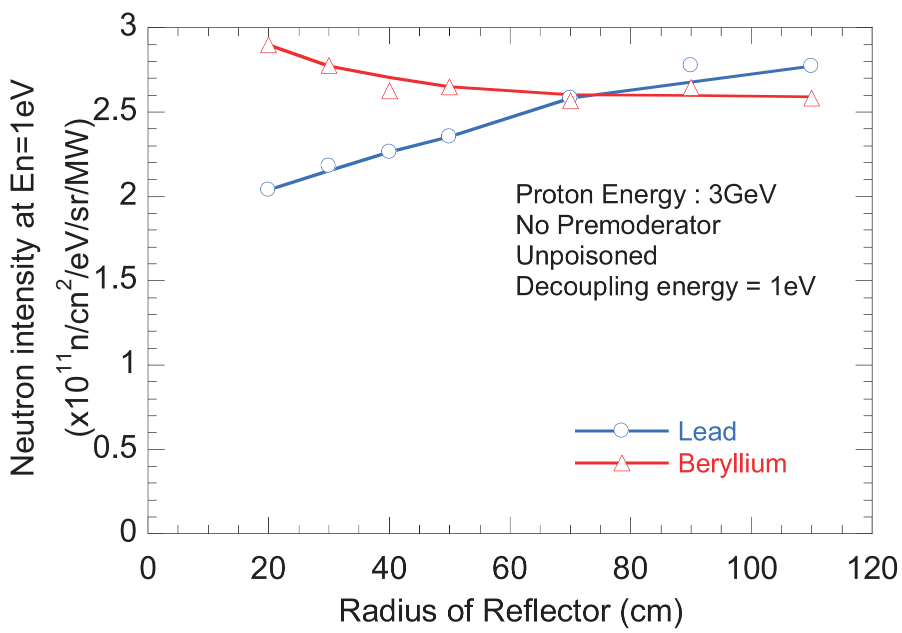

Fig. 2.3.37: Reflector size dependence on the neutron intensity at $E_n = 1$ eV (beryllium reflector and lead reflector)

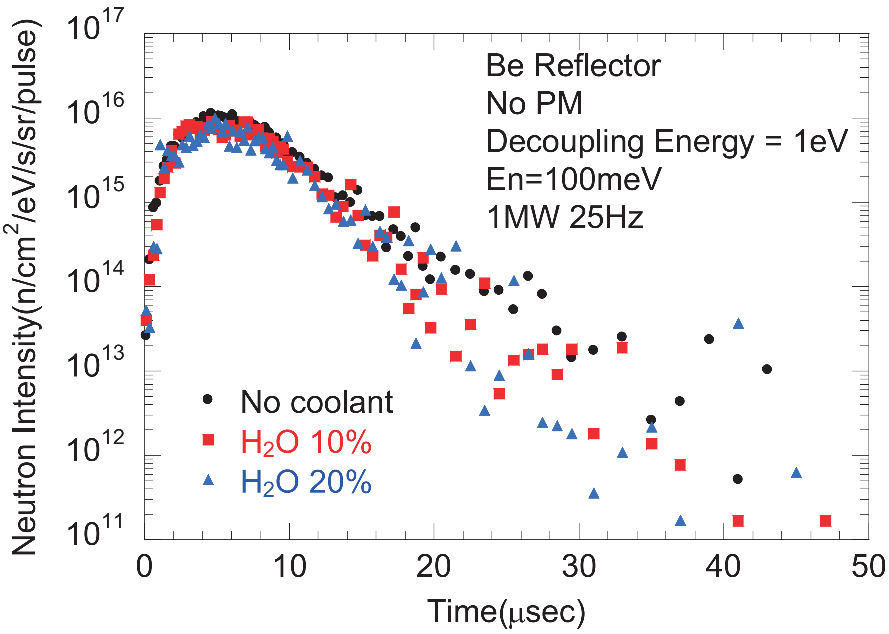

Fig. 2.3.38: H_2O coolant ratio dependence of pulse shape at E_n = 100 meV in case of beryllium reflector

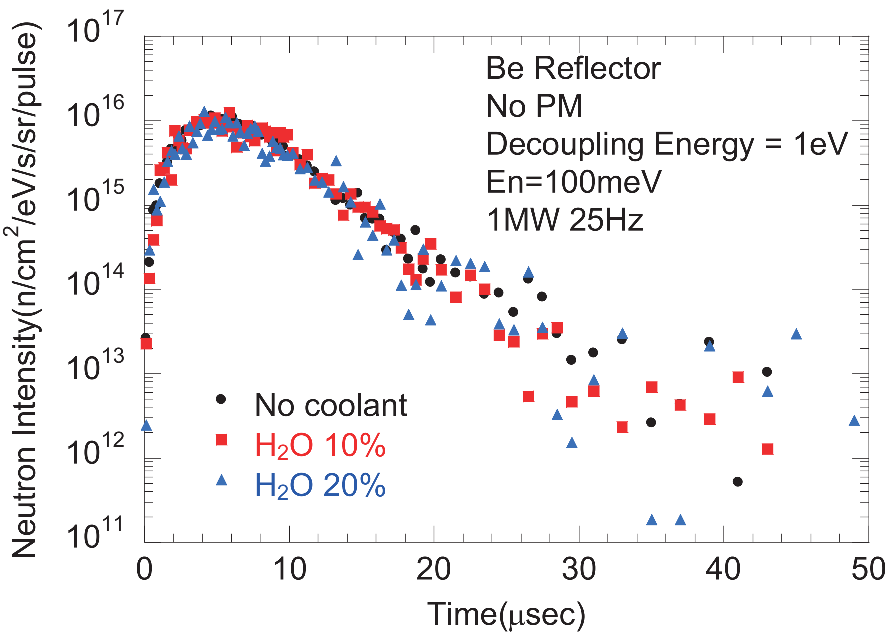

Fig. 2.3.39: D_2O coolant ratio dependence of pulse shape at E_n =100 meV in case of beryllium reflector

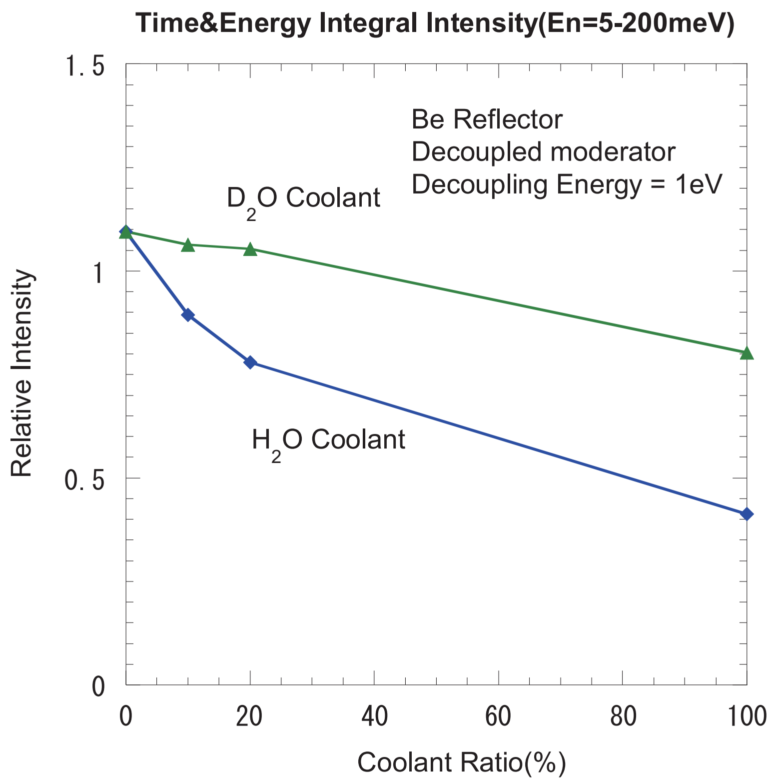

Fig. 2.3.40: H_2O and D_2O coolant ratio dependence of time- and energy-integrated intensities (E_n = 5-200 meV) in case of beryllium reflector

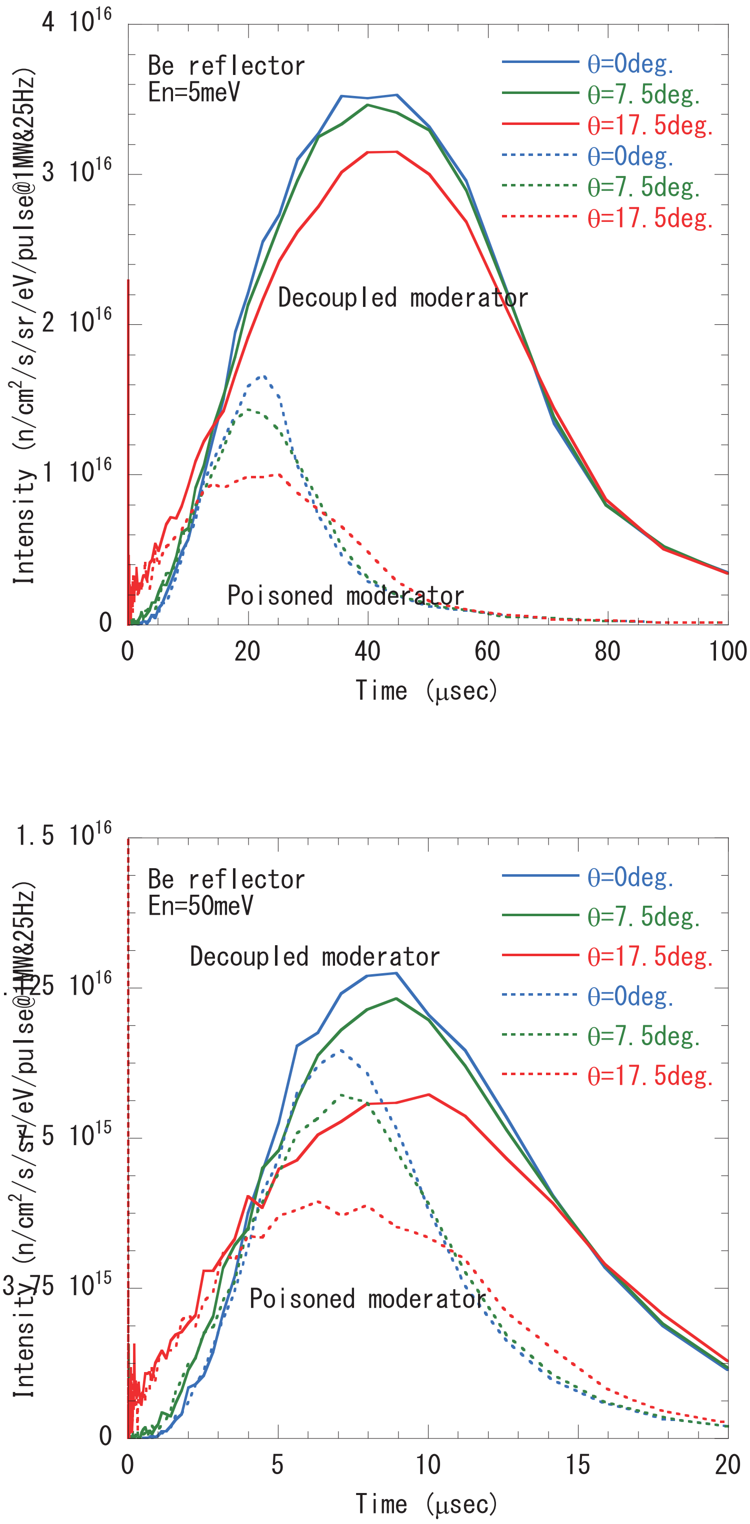

Fig. 2.3.41: Pulse shape of DM and PM at the extraction angle of 0°, 7.5° and 15° at E_n = 5 meV (top) and 50 meV (bottom)

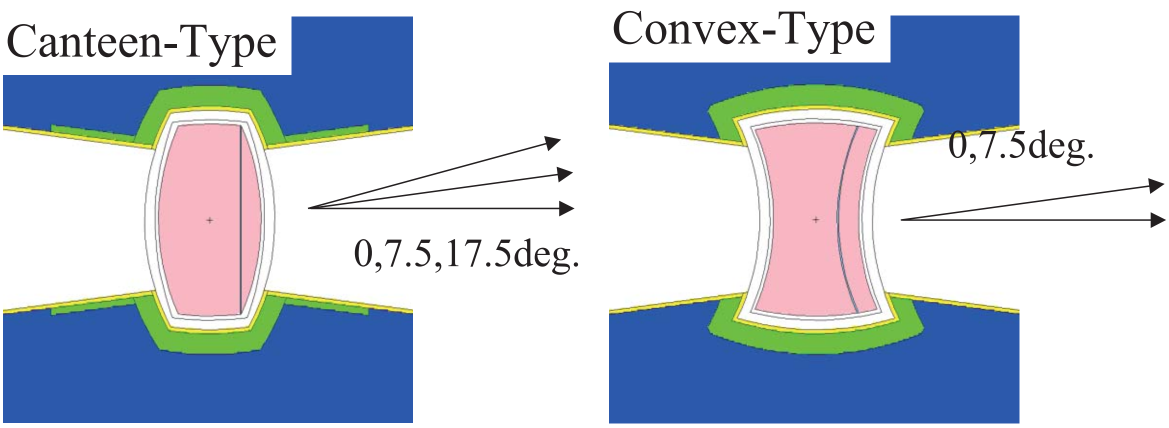

Fig. 2.3.42: Calculation models of the canteen-type moderator and the convex-type one

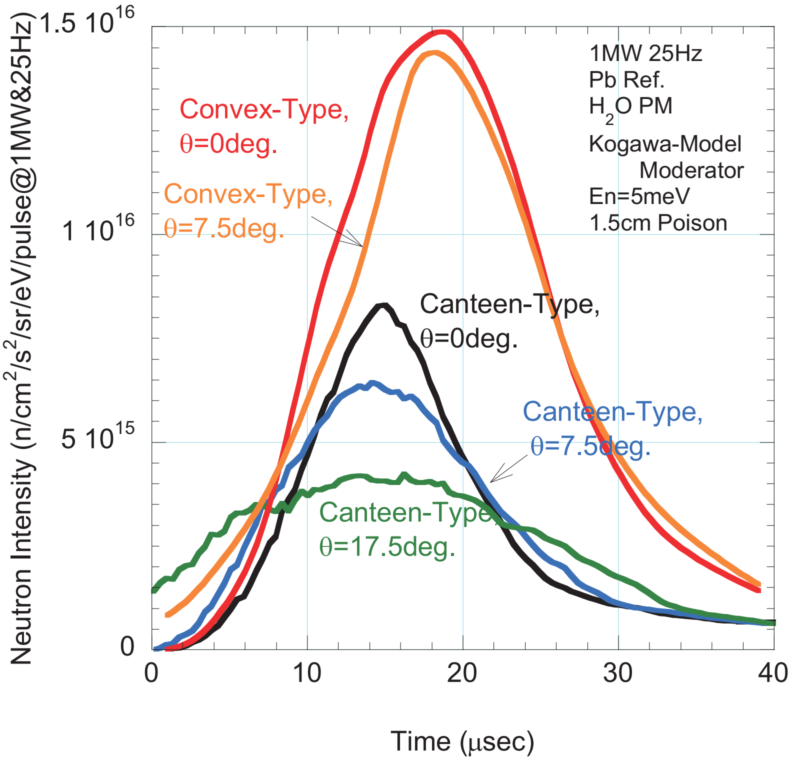

Fig. 2.3.43: Extraction angle dependence of pulse shape of PM with canteen type and concave type

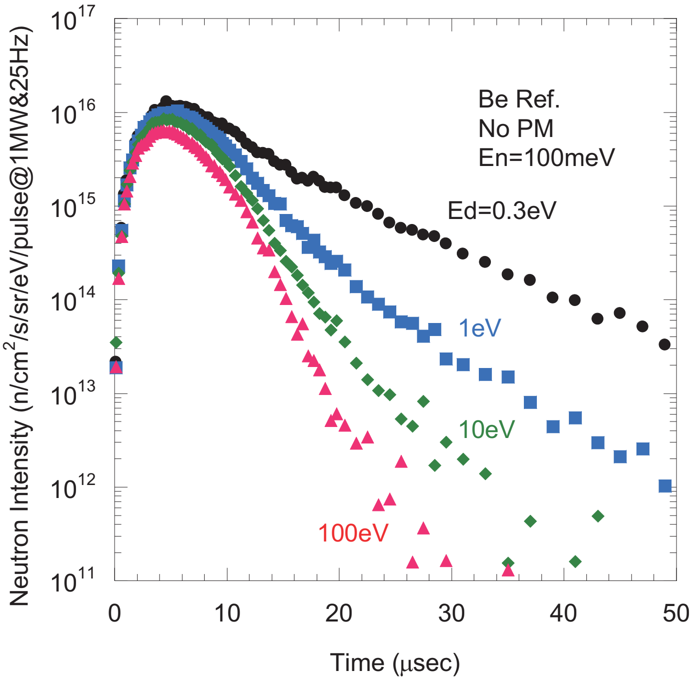

Fig. 2.3.44: Decoupling energy dependence of pulse structure at E_n = 100 meV

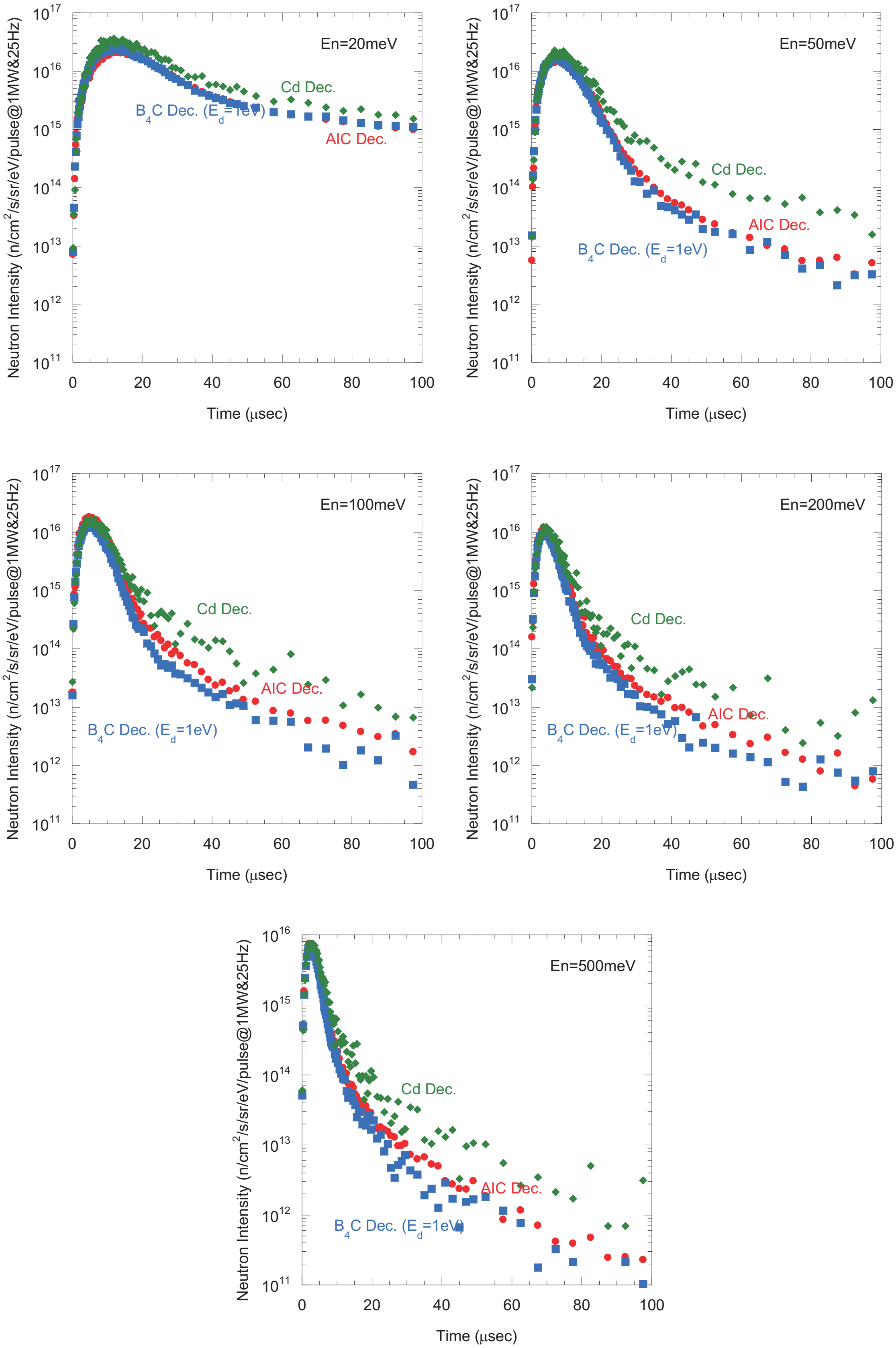

Fig. 2.3.45: Decoupler material (B_4C, Cd and AIC) dependence of pulse structure at several neutron energies

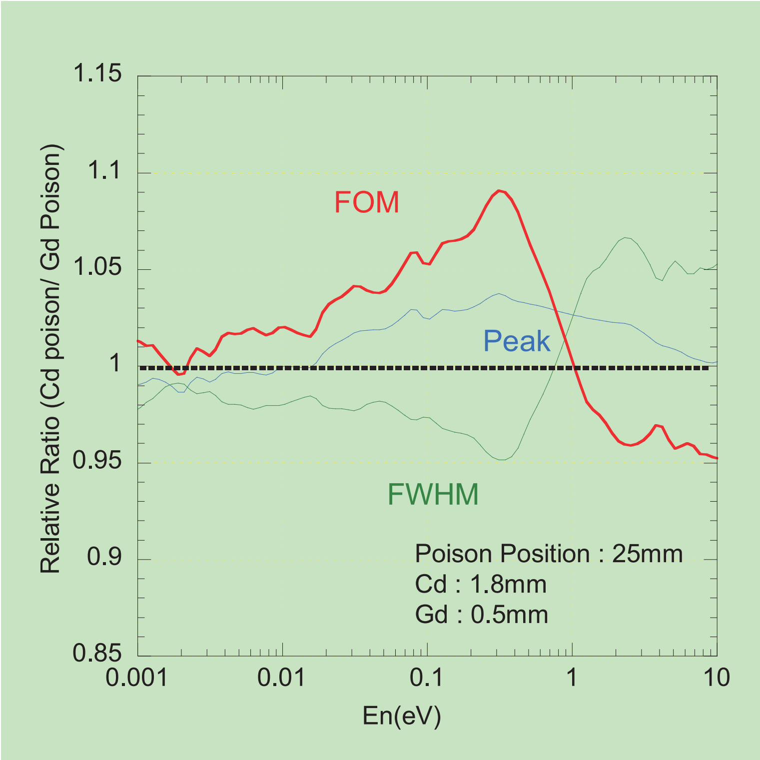

Fig. 2.3.46: Poison material dependence (Cd poison and Gd poison) of peak intensities, pulse widths and FOM (Figure Of Merit)

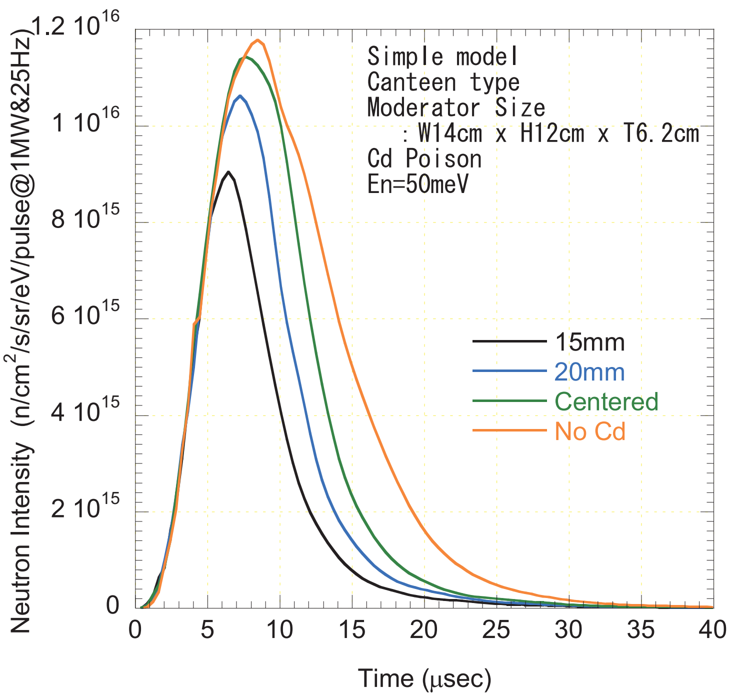

Fig. 2.3.47: Poison position dependence of pulse structure at $E_n = 50$ meV

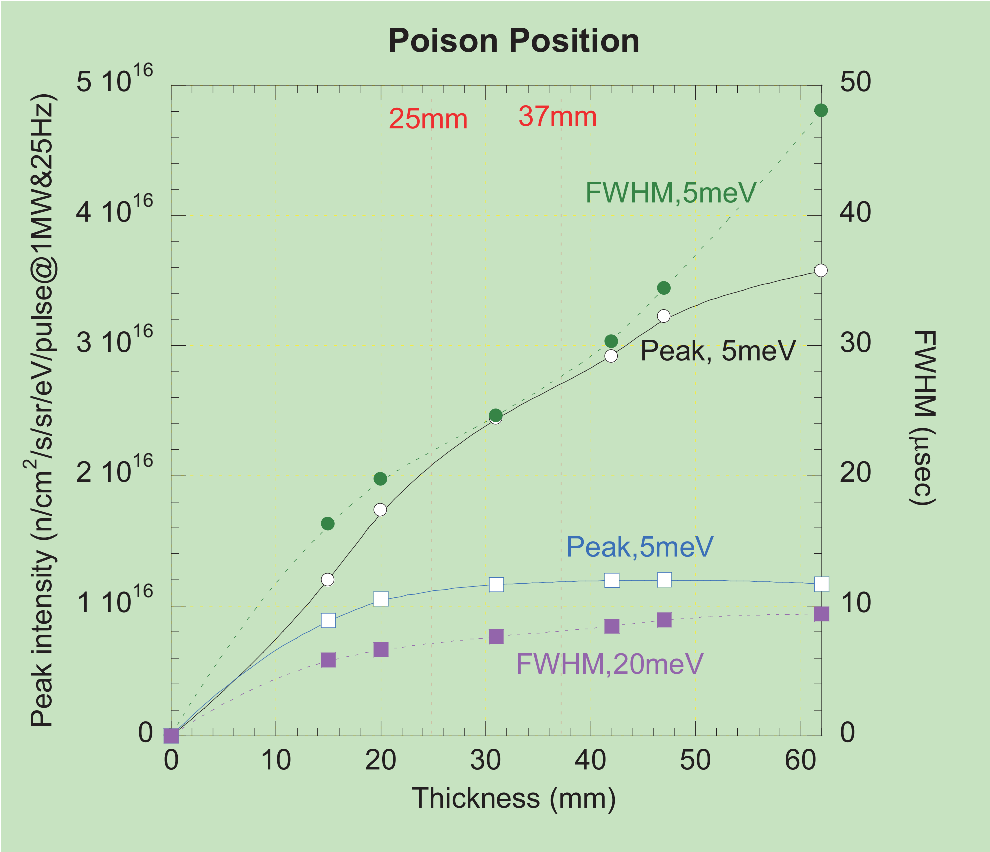

Fig. 2.3.48: Poison position dependence of peak intensities and pulse widths at E_n = 5 and 20 meV

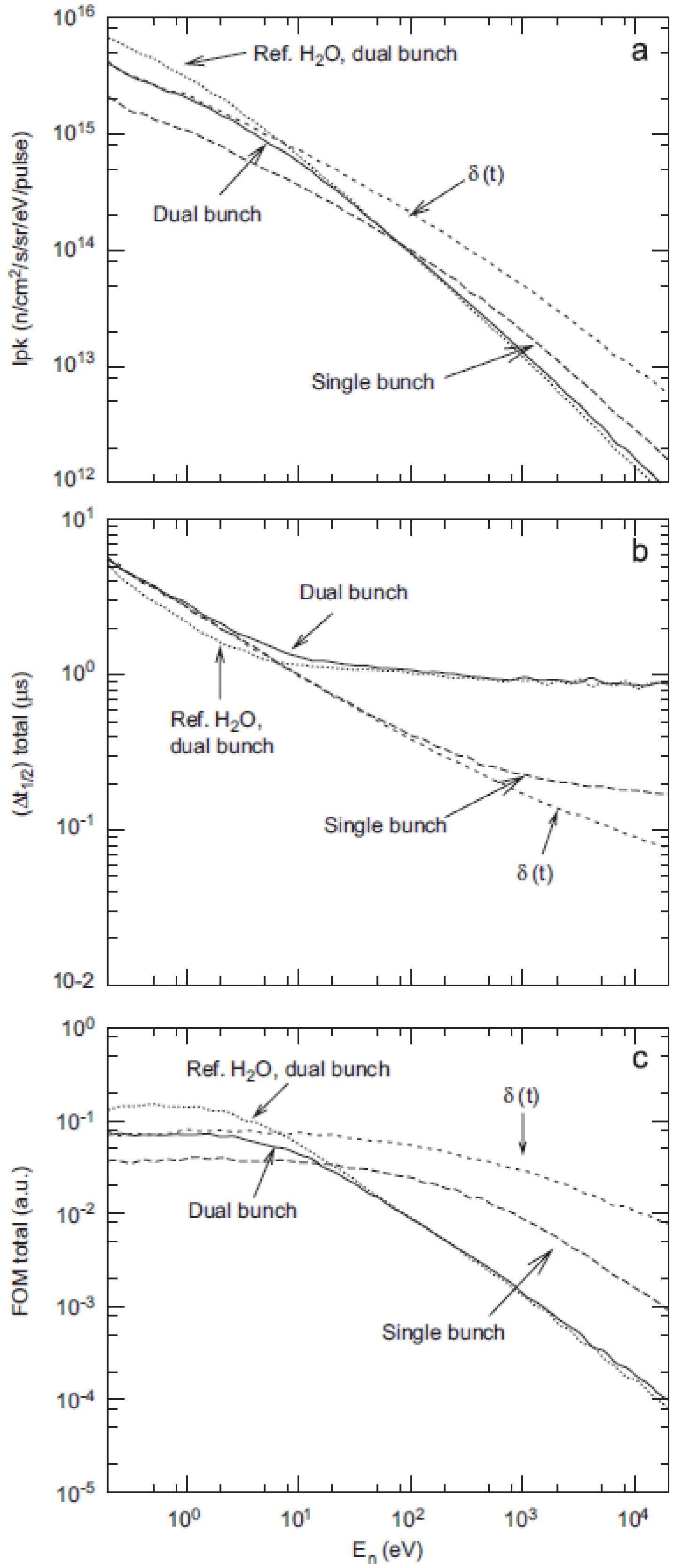

Fig. 2.3.49: Peak intensity (a), pulse width in full width at half maximum (b) and Figure of Merit (c) in cases of delta function $\delta(t)$, single bunch and dual bunch in proton beam structure

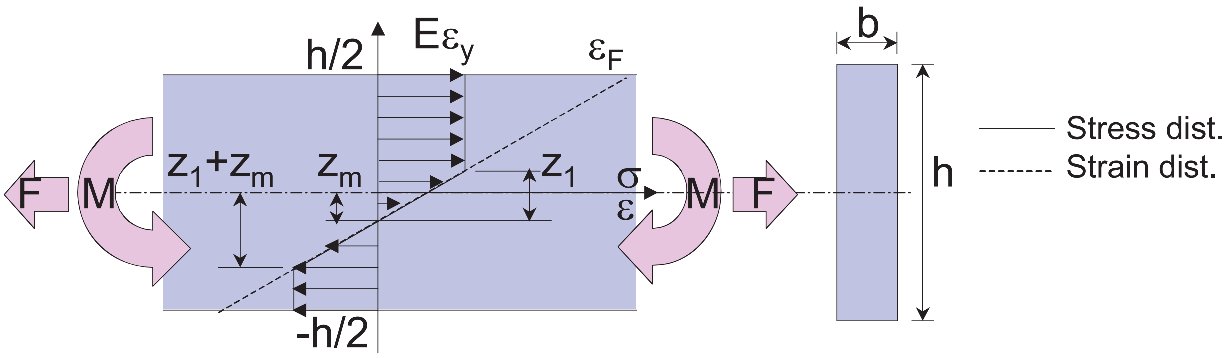

Fig. 2.3.50: Stress and strain distribution in beam

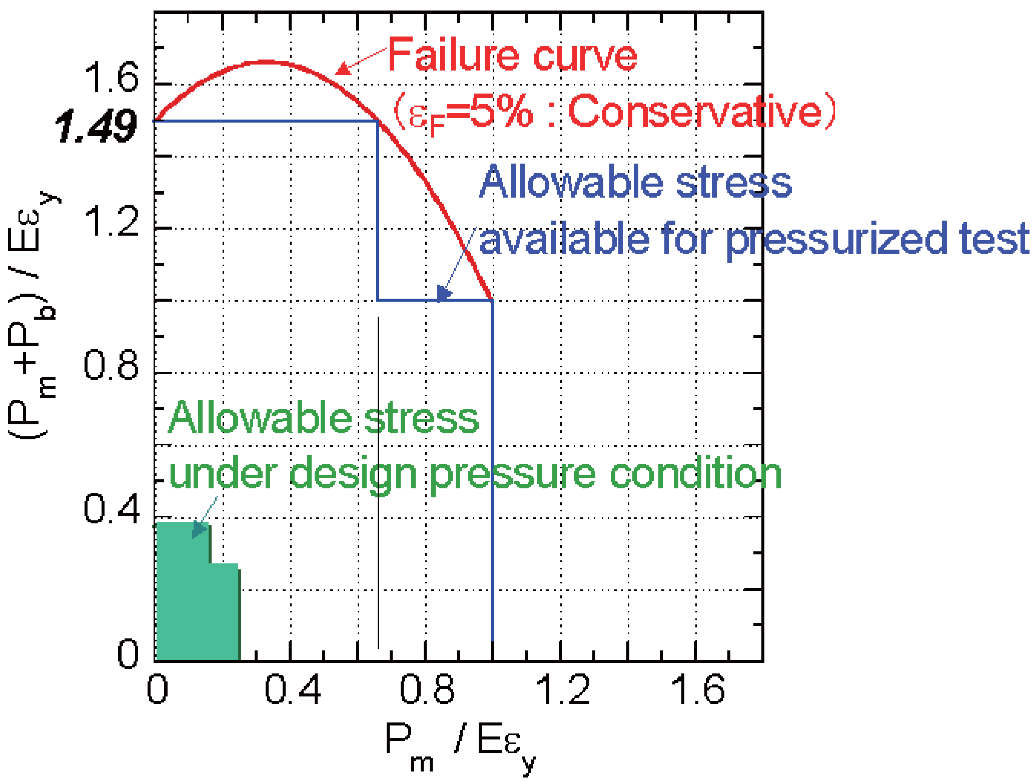

Fig. 2.3.51: Allowable stress for combined stress

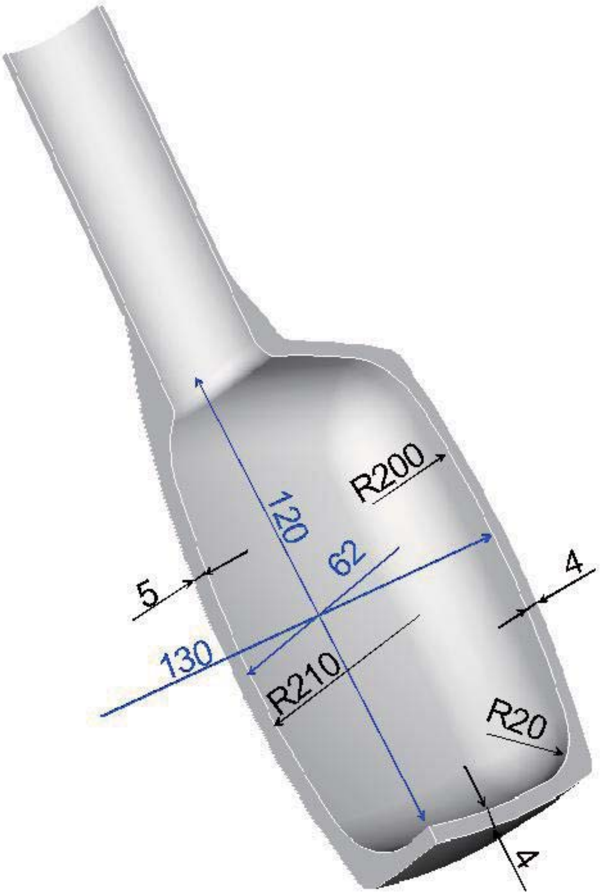

Fig. 2.3.52: Decoupled moderator vessel

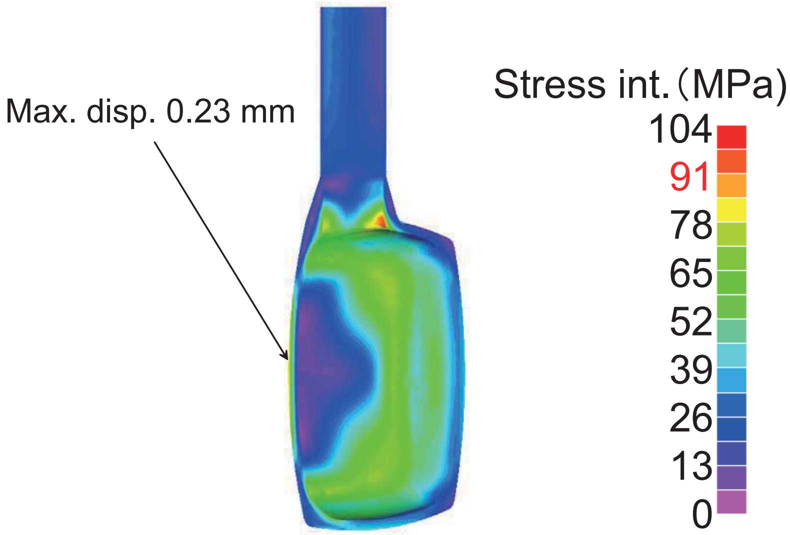

Fig. 2.3.53: Analytical result of stress distribution on decoupled moderator vessel under design pressure condition

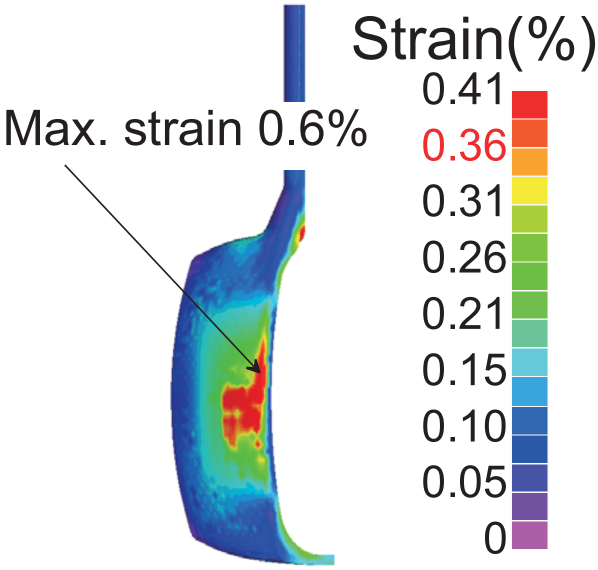

Fig. 2.3.54: Strain distribution on the decoupled moderator vessels under pressurized test condition

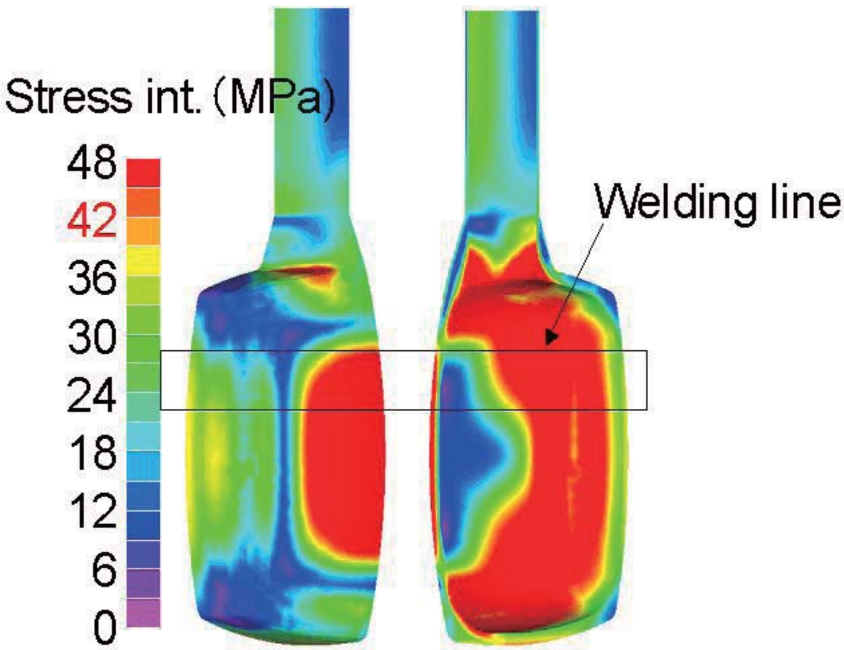

Fig. 2.3.55: Desirable location of welding line on decoupled moderator vessel under the design pressure condition

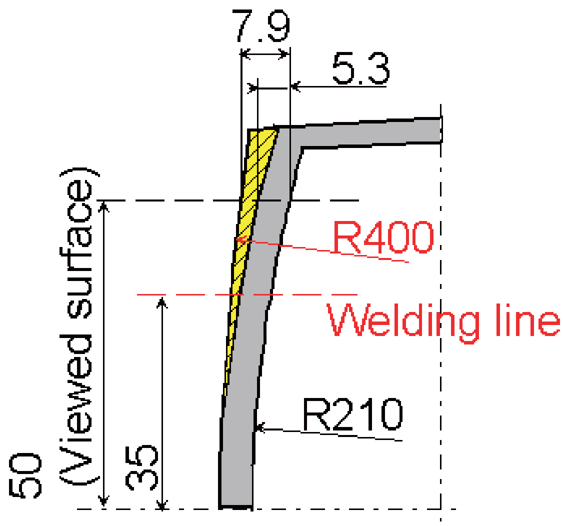

(a) Analytical model (b) Schematic of the neutron extraction surface

Fig. 2.3.56: Decoupled moderator considering the welding

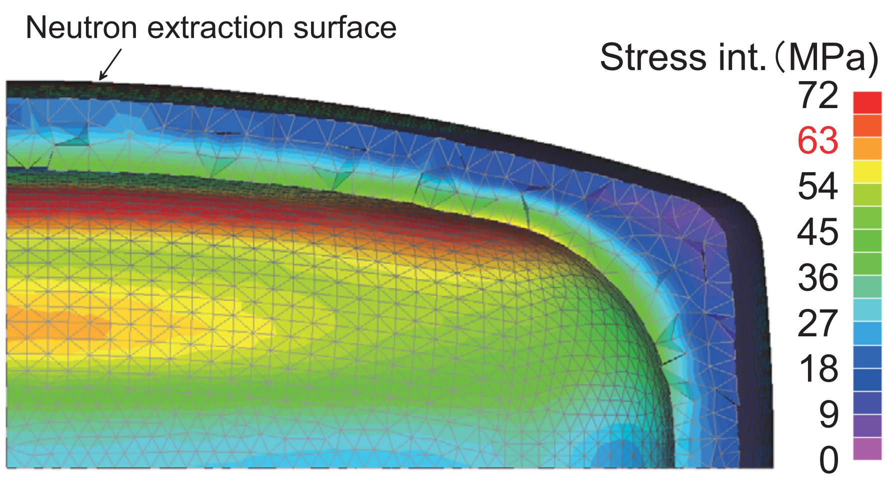

Fig. 2.3.57: Stress distribution on the welding line of the decoupled moderator

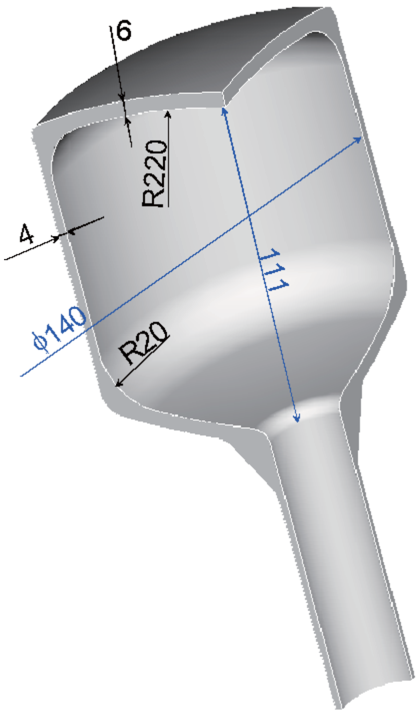

Fig. 2.3.58: Coupled moderator vessel

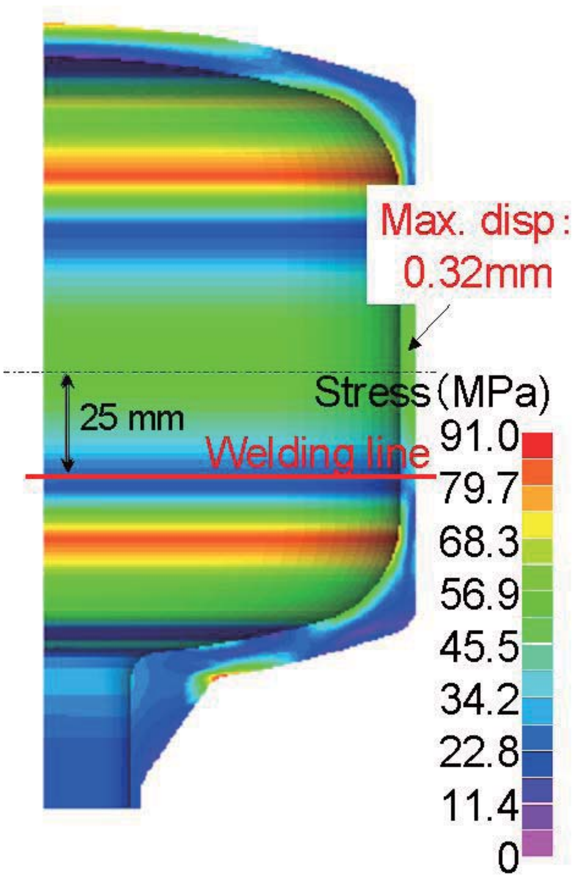

Fig. 2.3.59: Stress distribution on the coupled moderator vessel under the design pressure condition

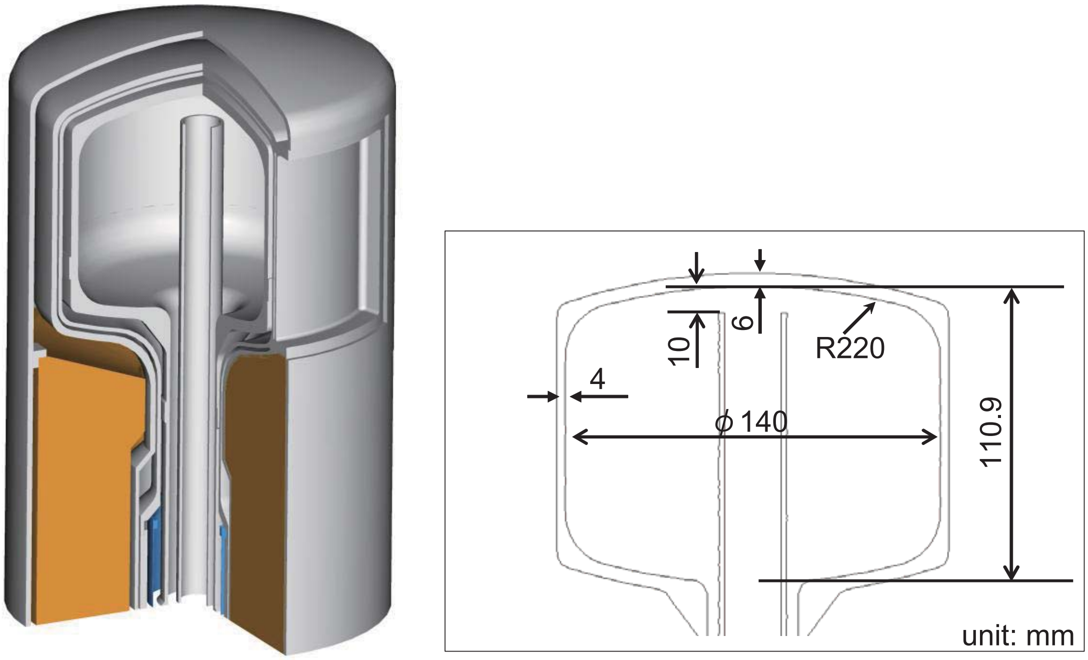

(a) Cylindrical type (coupled) moderator

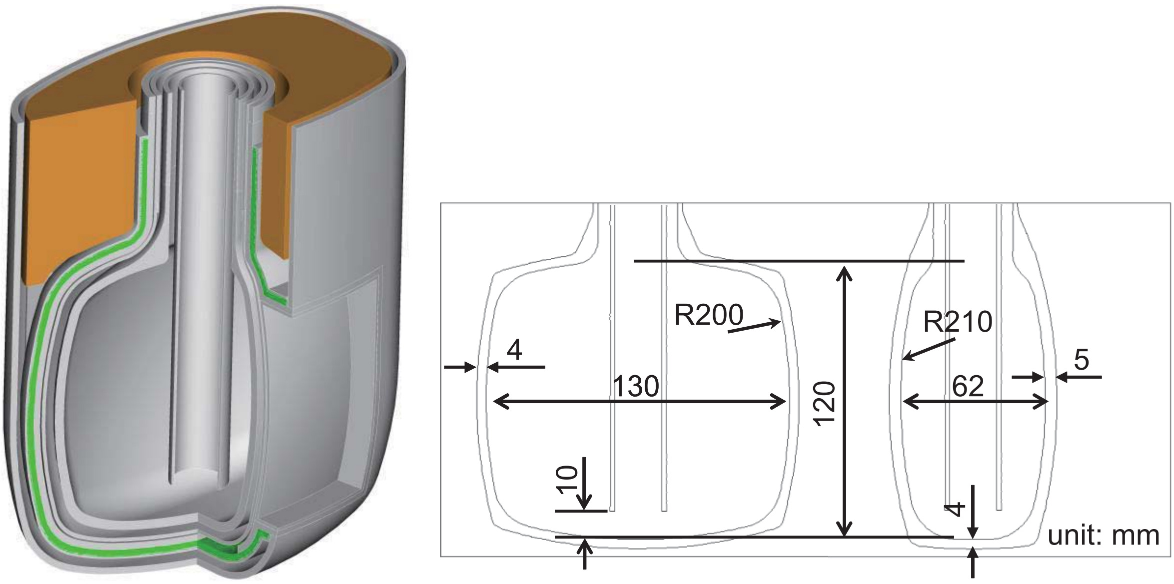

(b) Flat type (decoupled) moderator

Fig. 2.3.60: Moderator constructions for the JSNS

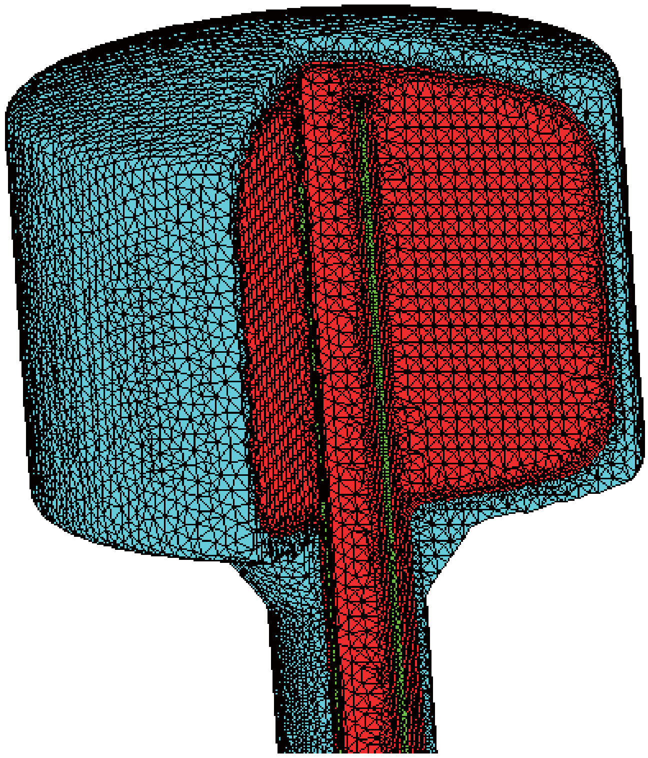

(a) Cylindrical type (coupled) moderator

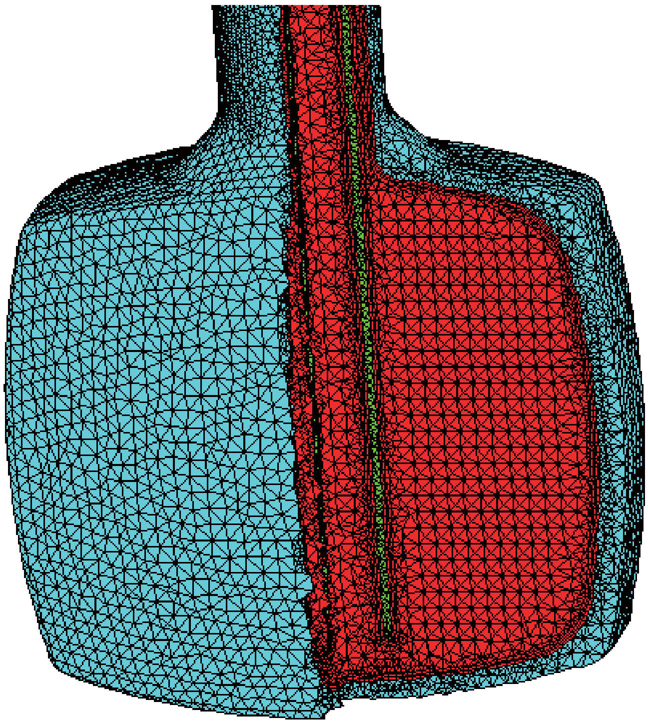

(b) Flat type (decoupled) moderator

Fig. 2.3.61: Cutaway view of analytical grids

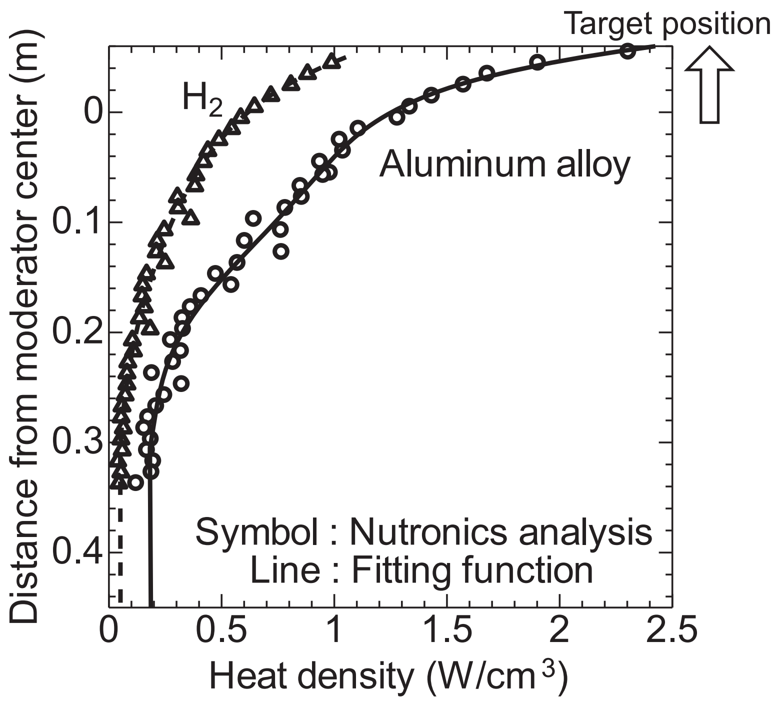

(a) Cylindrical type (coupled) moderator

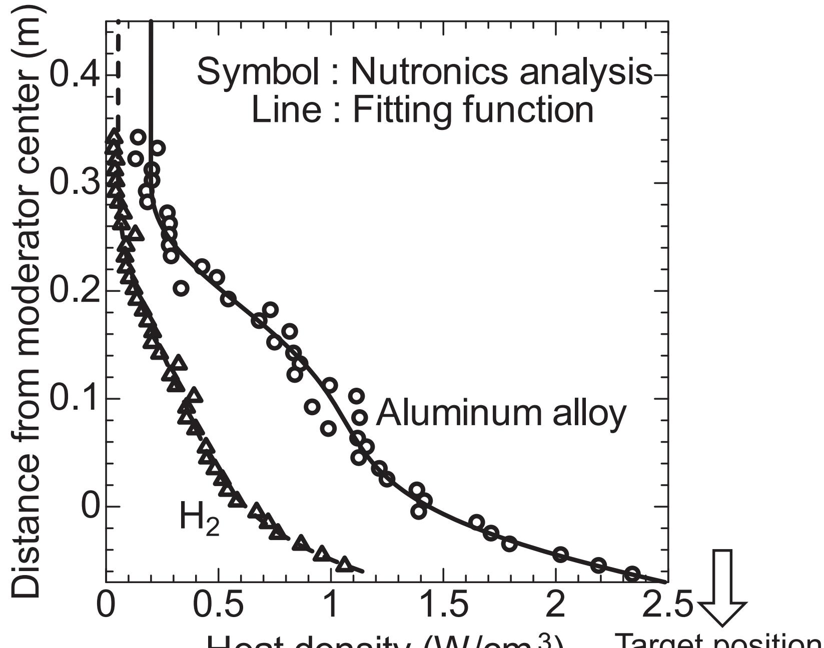

(b) Flat type (decoupled) moderator

Fig. 2.3.62: Heat density distribution

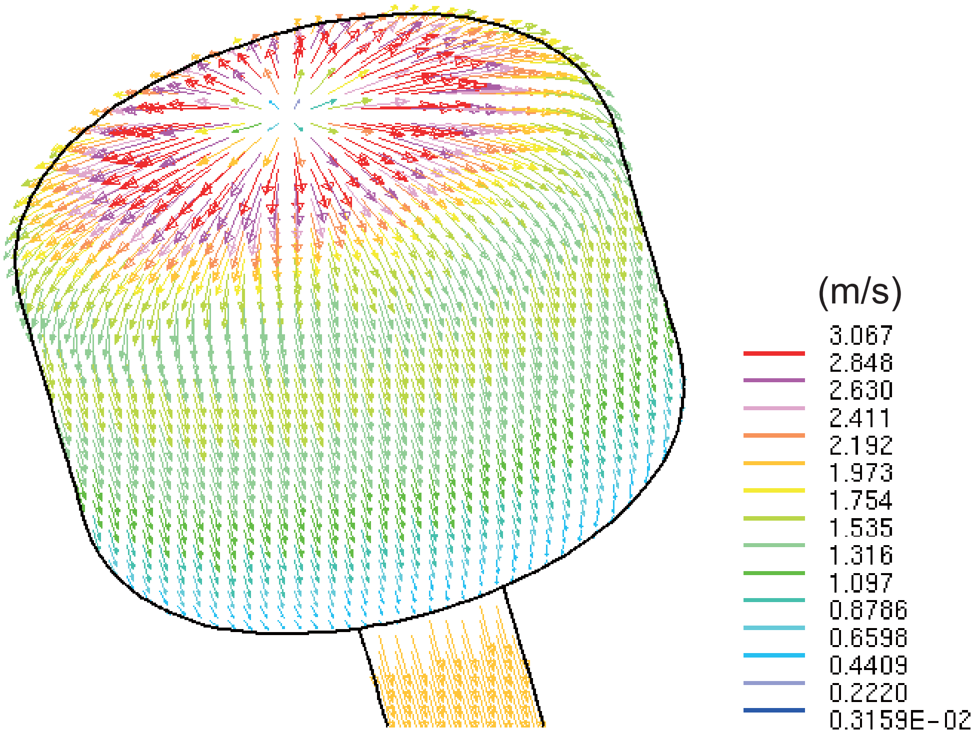

Fig. 2.3.63: Velocity vector distribution adjacent to inner wall (coupled moderator)

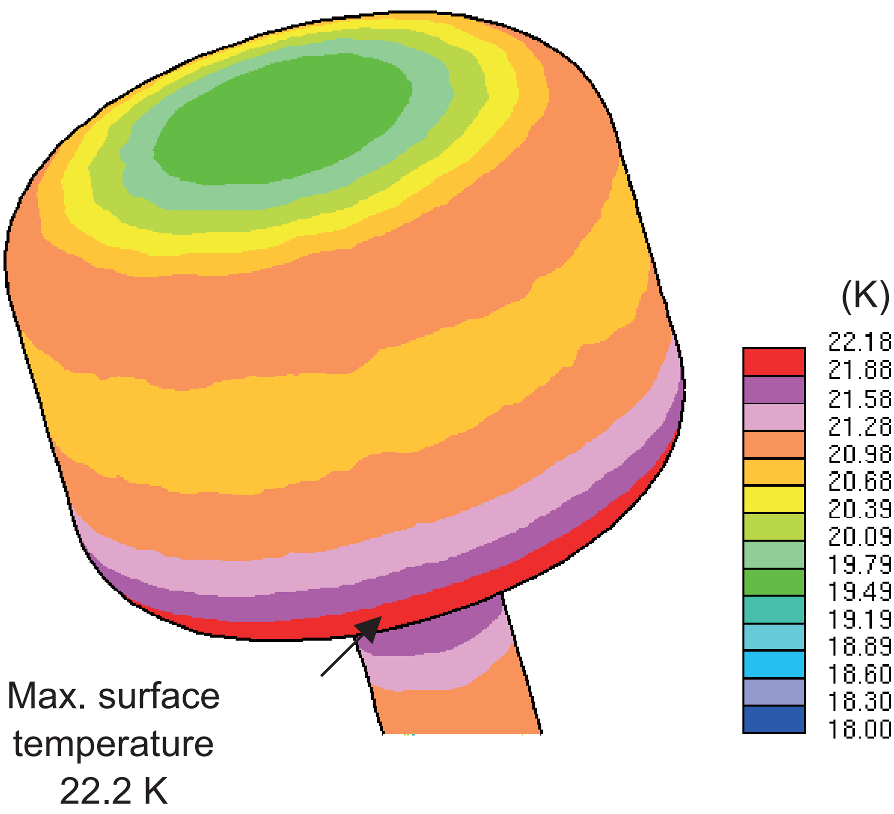

Fig. 2.3.64: Temperature distribution on inner wall surface (coupled moderator)

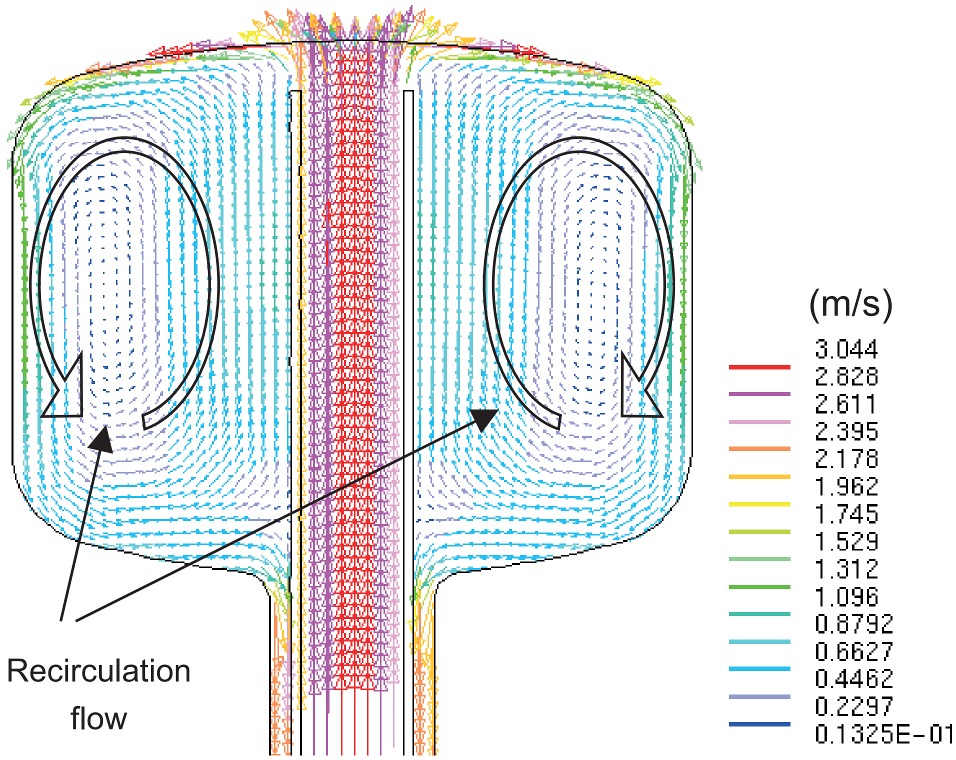

Fig. 2.3.65: Velocity vector distribution in cross section (coupled moderator)

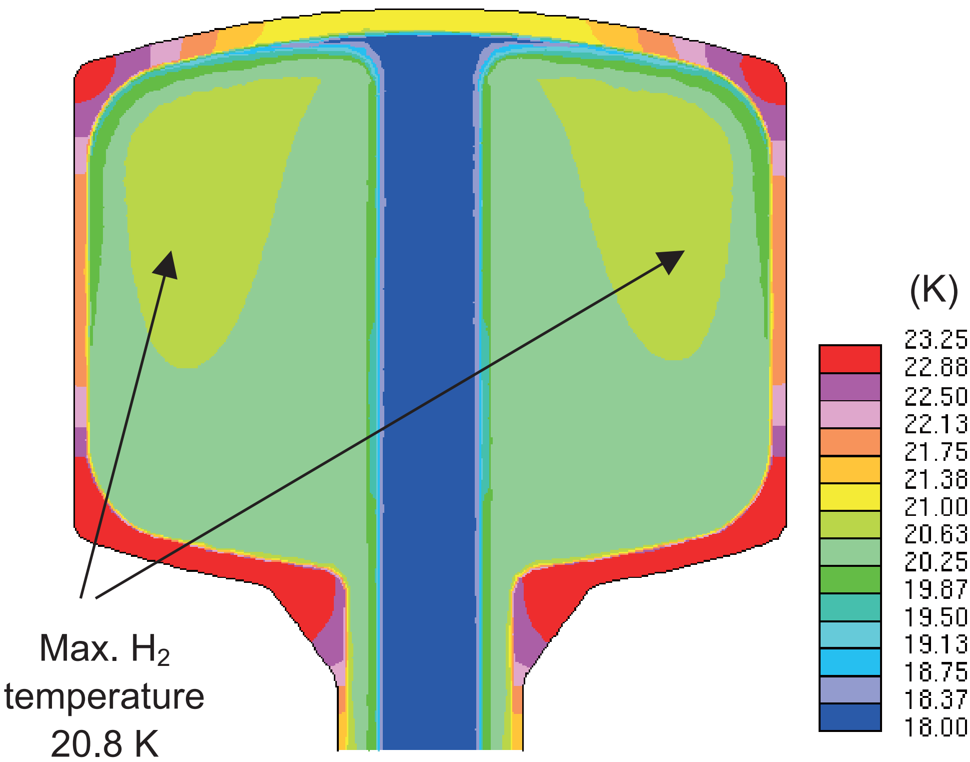

Fig. 2.3.66: Temperature distribution in cross section (coupled moderator)

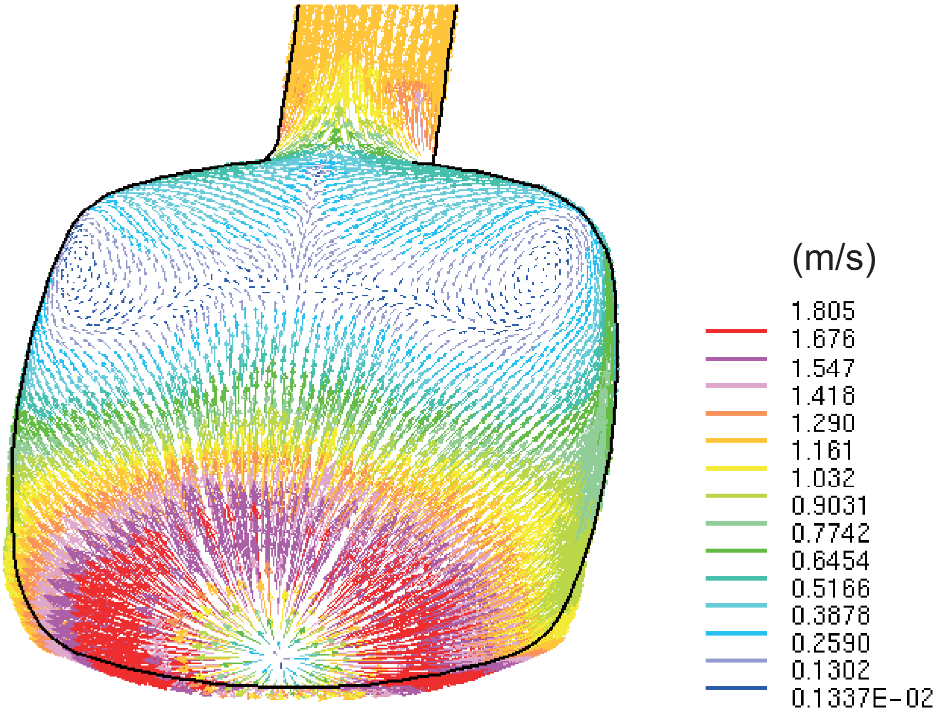

Fig. 2.3.67: Velocity vector distribution adjacent to inner wall (decoupled moderator)

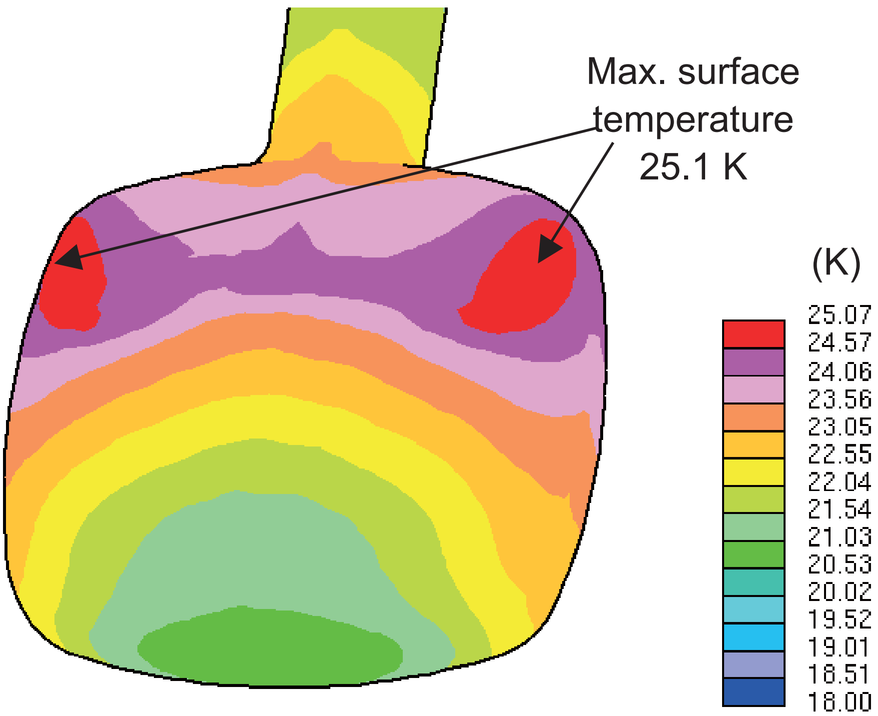

Fig. 2.3.68: Temperature distribution on inner wall surface (decoupled moderator)

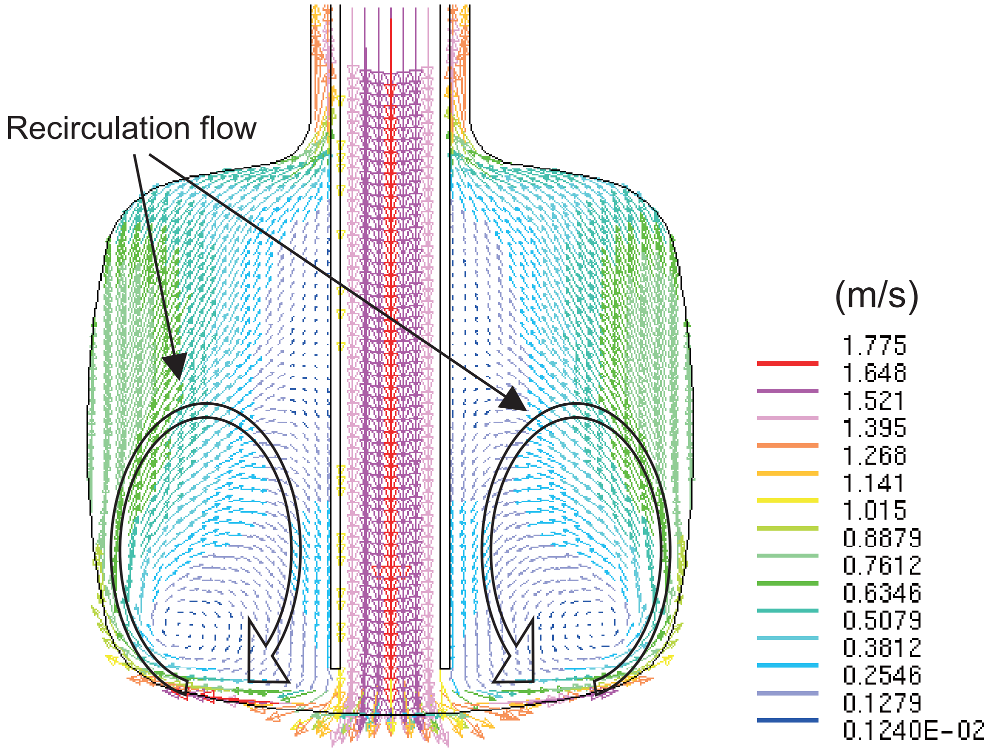

Fig.2.3.69: Velocity vector distribution in cross section (decoupled moderator)

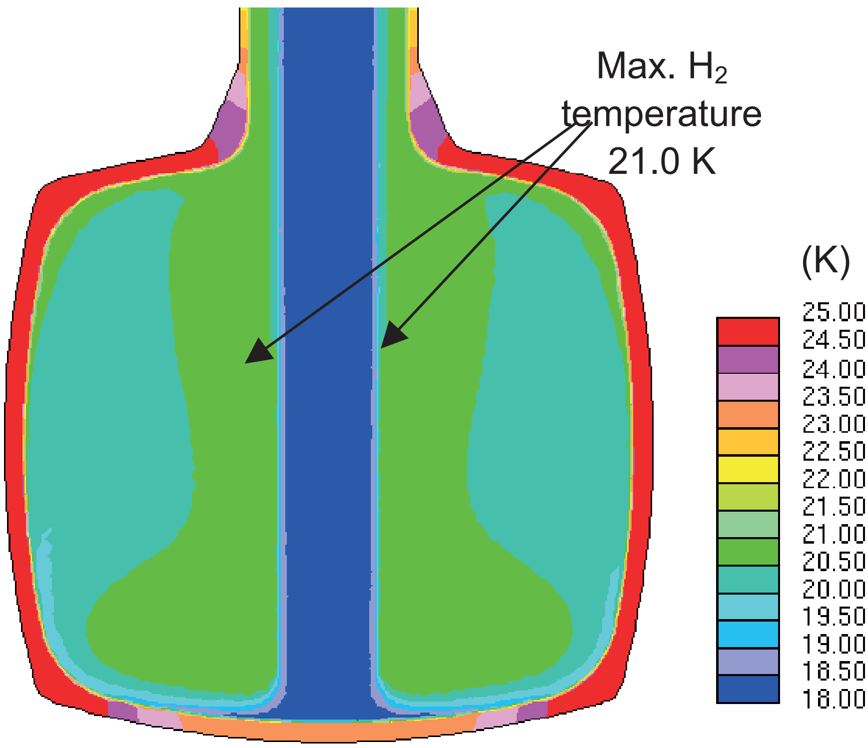

Fig. 2.3.70: Temperature distribution in cross section (decoupled moderator)

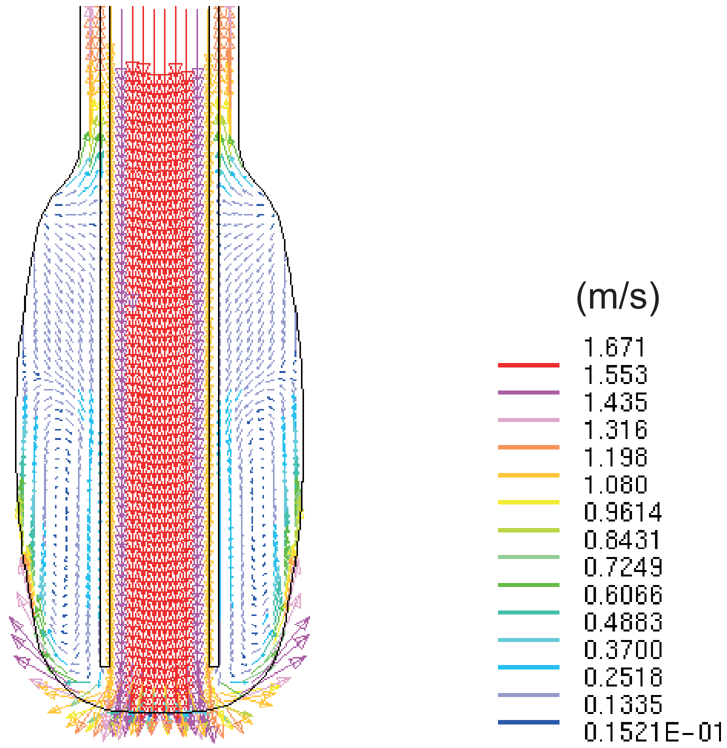

Fig. 2.3.71: Velocity vector distribution in cross section (decoupled moderator)

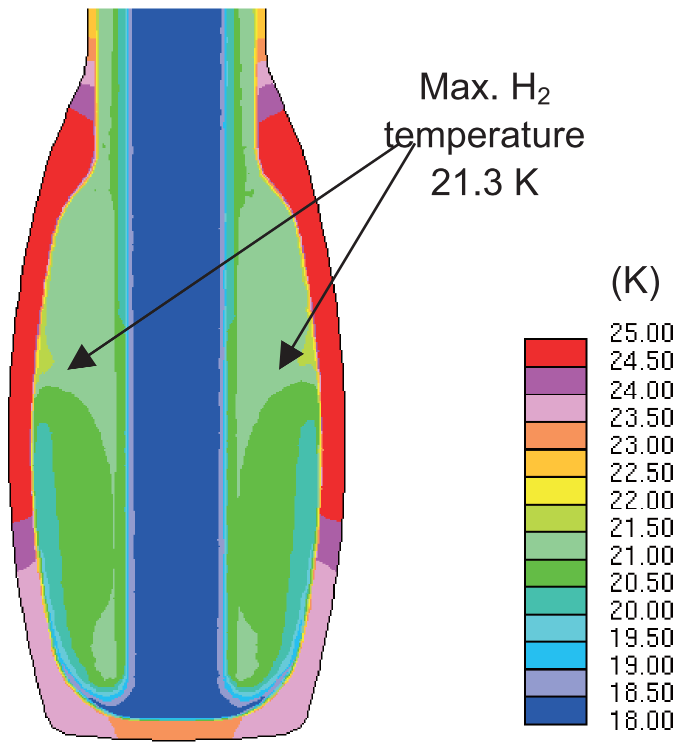

Fig. 2.3.72: Temperature distribution in cross section (decoupled moderator)

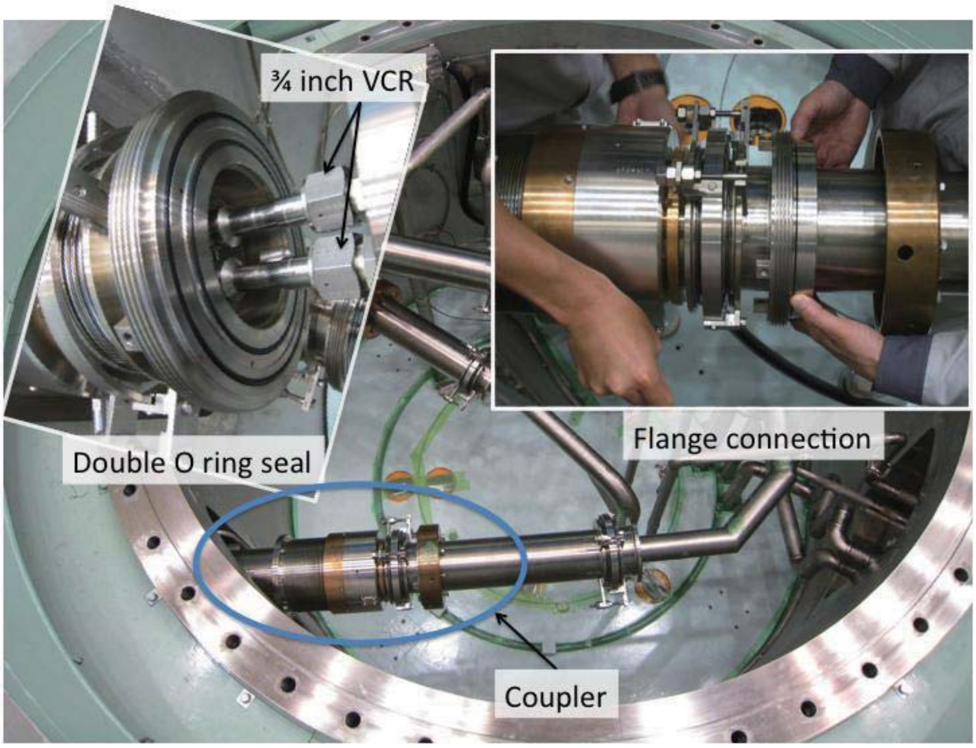

Photo. 2.3.1: Structure of coupler for coupled moderator

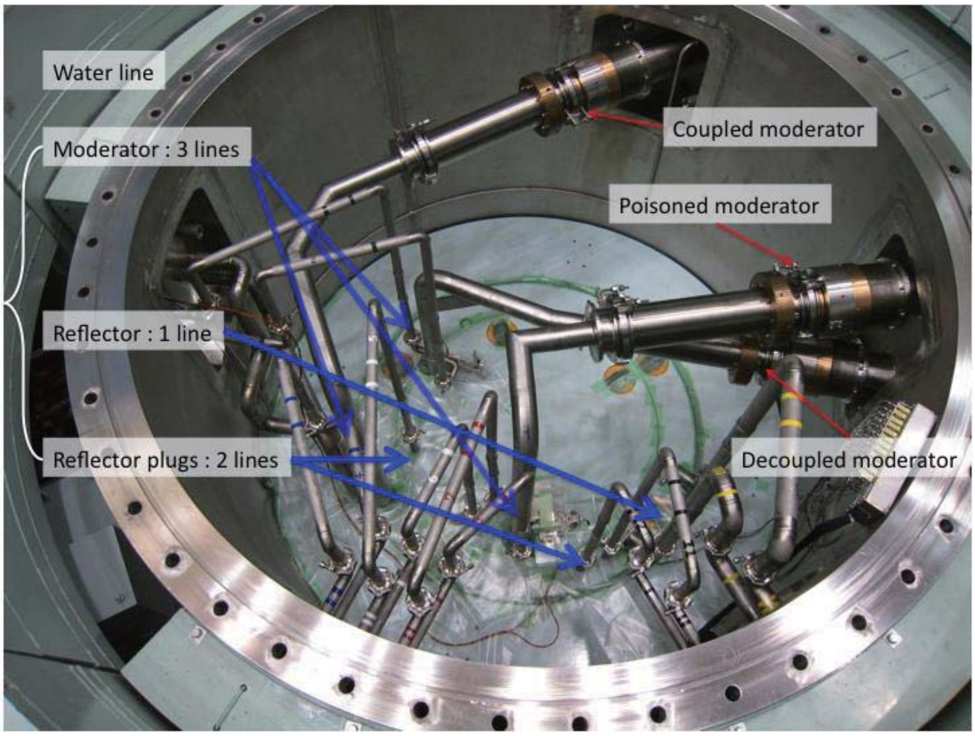

Photo. 2.3.2: Arrangement of water pipes and hydrogen transfer line at the top of helium vessel

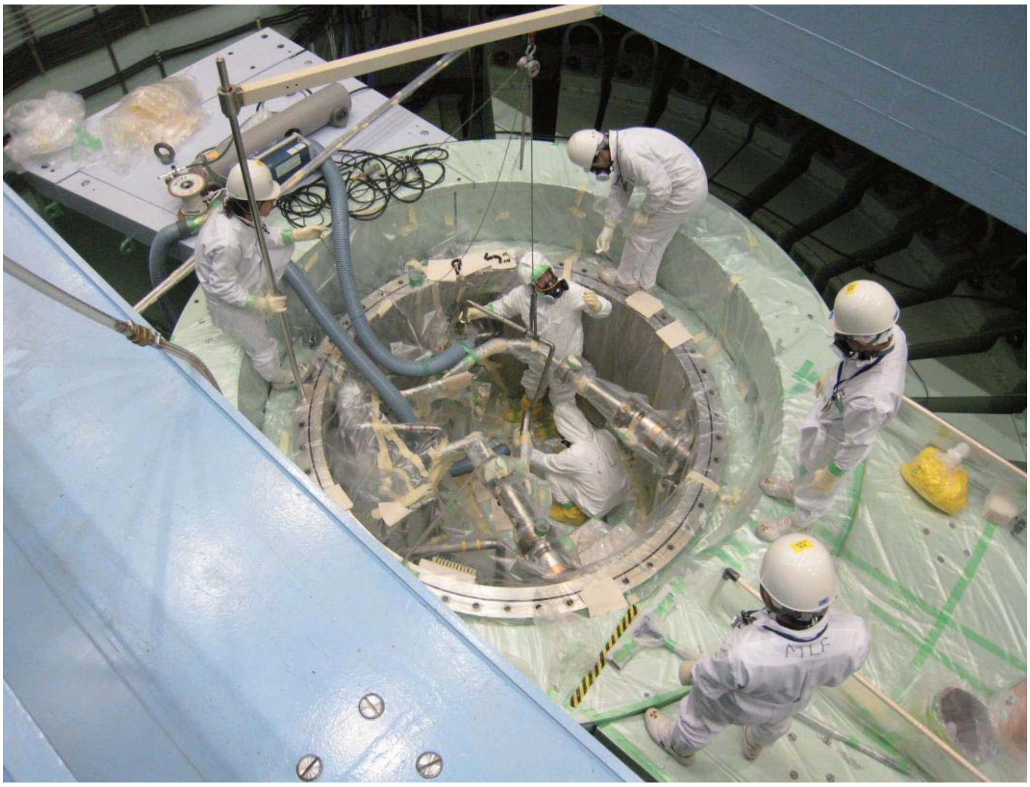

Photo. 2.3.3: Test work to disconnect pipes for design confirmation

2.4 Cryogenic Hydrogen Circulation System

2.4.1 Outline

The JSNS is aiming to produce the highest intensity of the pulsed cold neutron and to provide the highest qualified pulse structure. Accordingly, cryogenic hydrogen with the temperature of around 20 K and the pressure of 0.5 to 1.5 MPa is selected as the moderator. In order to achieve the aims mentioned above, three types of moderator are prepared. One is a coupled moderator that supplies the highest cold neutron intensity but a relatively long pulse structure. The second is a decoupled moderator that provides high intensity with a sort pulse. And the third is a poisoned moderator that allows a very sharp pulse but a relatively low intensity.

A cryogenic system in JSNS has a role to provide the moderator system with cryogenic hydrogen continuously when the proton beam is turned on. Estimation of nuclear heating at the moderators expects to be several kW. Correspondingly, the cryogenic system should have a kW-power system that will be the largest cryogenic system compared to the conventional one used for the cold neutron source. A forced-flow circulation cooling is also required to maintain the temperature of the moderators at 20-K regime and to attain the small temperature difference through the moderator inlet and the outlet. Though such a forced-flow hydrogen cooling system was already experienced at the ISIS and the LANSCE, circulation mass flow in the JSNS is going to be the largest one as well as the system in the SNS. Therefore, a world largest cryogenic hydrogen circulation system appears.

2.4.2 Basic Design

2.4.2.1 System configuration and layout in the MLF

(1) System configuration

1) Design requirements

In order to satisfy the aims of the JSNS, the following requirements are applied to the cryogenic system design.

a) Cryogenic hydrogen with the temperature of around 20 K and the pressure of 0.5 to 1.5 MPa is selected as the neutron moderator.
b) Hydrogen moderator should have para-hydrogen concentration of more than 99%.
c) The average temperature through each moderator should be kept in less than 20 K and the temperature difference through each moderator should be also maintained within 3 K at the rated proton beam power of 1 MW.

Heat loads of the moderators are composed of the absorbed neutron kinetic energy and the nuclear heating of the moderator material, summing up to be 1 kW for each decoupled moderator and 1.75 kW for the coupled moderator, totally being 3.75 kW, as shown in Table 2.4.1. A feature of the heat load at the moderator is a high heat density of approximately 1 W/cm^3. Therefore, a large mass flow rate and an effective heat transfer configuration are required for the moderator. A further consideration is that the heat load has a pulse configuration and suddenly shuts down or starts up due to turning the beam on and off. These phenomena have the potential to induce rapid changes of pressure and temperature in the hydrogen loop, especially, since cryogenic hydrogen behaves like an incompressive fluid and a slight density change produces a large pressure change. Accordingly, the cryogenic system requires a pressure control system.

2) System configuration

The cryogenic system in JSNS has been designed to have the following system configuration to achieve the requirements mentioned above. This system consists of a hydrogen circulation system to cool high-energy neutrons at the moderators and a helium refrigerator system to cool hydrogen in the hydrogen circulation system. A schematic configuration of the systems is shown in Fig. 2.4.1 and the detail of the flow diagram is shown in Fig. 2.4.2

Sizing of the main components has been evaluated through the process flow design with the resulting preliminary specifications indicated in Table 2.4.2. Total heat load is evaluated around 5.1 kW, including 3.75 kW from the moderators plus another 1.36 kW from heat losses in transfer tubes, valves and other components.

(a) Helium refrigerator system

The system produces the refrigeration power at around 20 K by using the helium Brayton cycle. The helium-refrigerator’s refrigeration power at 17 K is specified to be around 6 kW that has a margin of 17% for the estimated total heat load. A helium compressor system used in the helium refrigerator is estimated to have a mass flow rate of 0.285 kg/s with the suction pressure of 0.31 MPa(A) and the outlet pressure of 1.7 MPa(A), respectively. The motor rating of the compressor is evaluated to be around 690 kW. The hydrogen circulation system is cooled through the heat exchanger. An expansion turbine is located after the He-H_2 heat exchanger, which prevents hydrogen leak into the refrigerator to keep hydrogen pressure such as 1.6 MPa in the helium part to be higher than that of the hydrogen part (less than 1.5 MPa). A heater of the helium cold-box installed before the heat exchanger is to keep the hydrogen outlet temperature of the He-H_2 heat exchanger constantly.

(b) Hydrogen circulation system

This system functions to circulate the cryogenic hydrogen through the all moderators and to absorb the heat of the moderators and the circulation system. The absorbed heat is transferred to the helium refrigerator through the heat exchanger. The system is made up of a helium-hydrogen heat exchanger, two of hydrogen circulators (pumps), an ortho-para hydrogen converter, an accumulator and a heater.

The hydrogen pump is designed to circulate the mass flow rate of 0.162 kg/s with the pump head of 0.12 MPa at the rated condition where the inlet temperature and pressure are 19.6 K and 1.5 MPa, respectively. The hydrogen pump is an essential component to realize a reliable operation in the stability. Therefore, two pumps of the same specification are utilized in the design, which are arranged in parallel and operated simultaneously. The loads to the pumps are assumed equal. This configuration allows us to continue a stable operation without stopping so that one pump is switched to operate with a 100% load when another is failed.

The ortho-para hydrogen converter has a volume of about 35 liters of the iron-hydroxide catalyst, suitable for the flow rate up to 0.162 kg/s with a conversion efficiency of 80%. It is installed to maintain the para-hydrogen concentration of more than 99% at the inlet of the moderators for the neutronic performance.

The hydrogen circulation system makes up a closed loop filled with cryogenic hydrogen, and the average density in the loop is almost constant. Namely, the pressure change in the loop is expected to follow the behavior at the constant density. In our case, the heating of around 3.75 kW is suddenly applied to and removed from the loop through the moderators in response to the proton beam being turned on and off, which causes a severe pressure change. Therefore, the accumulator as a passive volume control and the heater as an active control for thermal compensation are designed to reduce the pressure changes. This is called a hybrid pressure control system.

(c) Cryogenic hydrogen transfer lines

The transfer lines function to supply the cryogenic hydrogen to the moderators and to return the heated hydrogen to the hydrogen circulation system. These lines are also fully covered with the helium-gas blanket. Each moderator has a separate transfer line which is merged in the hydrogen circulation system. A parallel flow configuration is adopted for the moderators cooling. This configuration increases hydrogen inventory and the potential of inducing unstable flow distribution. But it has merits to reduce the total heat load of the system, to unify the inlet temperature of each moderator, and to provide a low pumping head for the hydrogen circulators. A bypass line is, then, used to avoid the unstable flow distribution.

(d) Other components

Other components are a gas hydrogen supply line, a hydrogen vent system and a vacuum pump unit. The hydrogen gas supply line provides hydrogen gas to the hydrogen circulation system through a buffer tank and a gas analyzer that monitors moisture and oxygen concentrations during filling. The hydrogen vent line is one of the most important parts of the safety operation, and will function to rapidly vent the hydrogen in the system to the air in the case of any off-normal conditions. Inert gas, such as helium or nitrogen, always purges the inside of the vent line to avoid air ingress to the vent line. One of our safety concepts is to minimize the stored hydrogen gas in the system. Therefore, a hydrogen-gas recovery tank is not installed. Two vacuum pump units for thermal insulation are installed for the moderators and the hydrogen circulation unit. Additionally, hydrogen and helium detectors are installed in the evacuation lines to monitor leaks of hydrogen and helium.

(2) Layout of the system components

Layout of the cryogenic hydrogen circulation system is shown in Fig. 2.4.3. Three moderators are connected to a hydrogen circulation unit with hydrogen transfer lines. The hydrogen transfer lines that correspond with the part between the moderators and connection couplers will be replaced every 6 years due to the radiation. The hydrogen circulation unit is composed of cryogenic hydrogen circulation pumps, a hydrogen pressure control system, an ortho-para hydrogen converter and a hydrogen-helium heat exchanger. A cryogenic helium system, which has a refrigeration power of 6 kW at 17 K, supplies the 17-K helium to the hydrogen-helium heat exchanger to cool the hydrogen. These systems are installed in the Materials and Life Science Experimental Facility (MLF) building. Several gas supply systems such as a helium compressor system, a liquid nitrogen tank, and gaseous holders are located at the outside of the building.

The first floor ground plan of the MLF building is shown in Fig. 2.4.4. The No.1 helium compressor room to install the compressor unit of the helium refrigerator system, the cylinders storage space to put hydrogen and helium cylinders units, the cooling tower, a helium buffer tank, a liquid nitrogen tank and an evaporator is installed in the southwest of the MLF building. The No.1 helium compressor room is 11 m in length, 9 m in width and 9 m in height. The floor toughness is about 5 t/m^2. The crane capacity is 7 t and the crane height is 5 m from bottom of hook. The door size of the room is 4 m × 4 m. The cylinders storage space has a roof and is 7 m in length, 13 m in width and 5 m in height. The cooling tower, a helium buffer tank, a liquid nitrogen tank and so on are installed around the No.1 helium compressor room and the cylinders storage space. Several gas pipes and cables go through the MLF building wall, the T0 chopper cooling system room, the off-gas prosess room and the piping space from this area. Then, these pipes stand up to the second floor. The penetration hole size through the wall is 1.3 m in length and 1.1 m in width, 5 m in height from ground level.

The second floor of the MLF building is shown in Fig. 2.4.5. The cable rack and many pipes of hydrogen, helium and nitrogen standing up from the first floor, pass the piping space in the second floor, and stand up inside piping space to go to the third floor. There is cryogenic hydrogen components room around the center of the MLF building, which is 6-12 m in length, 6 m in width and 4 m in height and its ceiling is made by a grating plate to lead to the large components handling room of the third floor. The hydrogen circulation unit is installed in this room, and it supplys hydrogen from here to the moderator vessels by hydrogen transfer lines.

A cross section around the cryogenic hydrogen components room is shown in Fig. 2.4.6. It shows the vertical positions of the hydrogen circulation unit, the reflector exchanging plug, the target trolly and so on. The hydrogen transfer lines pass a cooling system distribution room from the cryogenic hydrogen room and they go through the wall. Then, they pass a piping gutter and are connected with mechanical couplers on the reflector exchanging plug. They lay piping vertically from couplers to the moderator vessels.

The third floor of the MLF building is shown in Fig. 2.4.7. The cable rack and many pipes from the second floor are connected to a cold box for the helium refrigerator system and to the hydrogen circulation unit in the cryogenic hydrogen components room under the grating plate. The hydrogen vent line to release hydrogen gas when the system operation stops or the emergency release goes along the wall of the large components handling room stands up to under the 130-t crane and goes out of the MLF building through a sleave of the wall. Fig. 2.4.8 shows the roof of the MLF building. After the vent line goes through the large components handling room, it is connected to the stuck directly.

2.4.2.2 Process Flow Diagram (PFD)

(1) Design conditions

The hydrogen circulation system should provide high flow supercritical hydrogen to three moderators (CM, DM, PM), in which the cryogenic hydrogen cools the spallation neutron to get the pulsed cold neutron with the highest intensity and the highest qualified pulse structure. Then the nuclear heating in the moderators is estimated to be 3.75 kW. It is necessary for the design of the cryogenic hydrogen system to satisfy the following conditions in order to obtain the cold neutron.

a) The average temperature through the moderator is kept within 20 K.
b) The temperature difference between the inlet and the outlet of the moderator is kept within 3K.
c) The moderator should have para-hydrogen concentration of more than 99.0%
d) Operational pressure to get sub-cooled hydrogen is from 0.6 MPa to 1.5 MPa.

In this section, the process flow of the cryogenic hydrogen system is calculated by solving mass and heat balance at each section of components; the moderators, the pumps, the accumulator, the ortho-para hydrogen converter, the heat exchanger and so on, in order to determine the sizing and the specification.

(2) Basic equations

1) Heat balance equation

$$\sum_i (\dot{m}_{1i} * h_{1i}) + Q = \sum_j (\dot{m}_{2j} * h_{2j}) \tag{2.4.1}$$

where $\dot{m}$ is mass flow rate (kg/s), h is enthalpy (J/kg), and Q is heat leak (W). The subscripts 1 and 2 denote inlet, and outlet condition, respectively.

Enthalpy of hydrogen with para-hydrogen concentration of x_p is expressed by using that of ortho- and para-hydrogen.

$$h\,(P,T,x_p)=h_p * x_p + h_o * (1-x_p) \tag{2.4.2}$$

where P is pressure (MPa), T is temperature (K), and x_p is para-hydrogen concentration. The subscripts p and o denote para-hydrogen and ortho-hydrogen.

2) Conservation equation in ortho-para converter

The energy balance in the ortho-para converter is as follows.

$$\dot{m}_1 * h_1(P_1, T_1, x_{p1}) + Q_{HL} = \dot{m}_1 * h_2(P_2, T_2, x_{p2}) \tag{2.4.3}$$

In this equation, the influence of the heat loss, Q_{HL}, in the converter is considered. If the adiabatic condition is kept, the enthalpy of cryogenic hydrogen through the converter is kept constant.

Since the reaction in the catalyst is exothermic, the temperature at the outlet increases and then the system reaches the equilibrium condition of higher concentration of para-hydrogen. In this report the conversion efficiency of the catalyst is given by using para-hydrogen concentration in equilibrium at outlet temperature, x_{pe}.

$$\eta_p = \frac{x_{p2} - x_{pf}}{x_{pe-}x_{pf}} \tag{2.4.4}$$

where x_{p2} and x_{pf} are para-hydrogen concentrations at the outlet and the inlet, respectively.

3) Power of hydrogen circulation pump

The input power of the pump is described as follows.

$$Q_w = \frac{V \times h}{\eta} \tag{2.4.5}$$

where Q_w is the input power of the pump (W), V is volumetric flow rate (ℓ/s), h is pump head (kPa) and η is adiabatic efficiency of pump.

(3) Numerical procedure

The temperature and pressure at the outlet of heat exchanger is set as initial condition. The enthalpy at the outlet of each component is calculated by using Eq. (2.4.1) and the heat leak. The pressure distribution is calculated by the pressure drop of each component. Finally, the values of the enthalpy and the pressure are converted into the temperature. In the ortho-para hydrogen converter, the temperature and the para-hydrogen concentration is calculated by means of iteration. The heat load of the circulation pump is estimated by using Eq. (2.4.5).

Heat and mass balance calculation is performed under the following assumption and design conditions mentioned above in order to determine the process flow of the cryogenic system.

(4) Numerical conditions

1) Re-conversion rate into ortho-hydrogen through moderators.

There are not any obvious data that can estimate the re-conversion rate from para-hydrogen to ortho-hydrogen through the moderator by neutron and gamma ray. However, we tentatively assumed that a half of nuclear heating in the moderator might be used for reaction heat to ortho-hydrogen, which corresponds to the conversion rate of around 2% from the para-hydrogen concentration of from 99% to 97%. This will be an overestimation but it is adopted for the calculation as considering a margin.

2) Ortho-para hydrogen conversion efficiency

To reduce the inventory of hydrogen in the converter, the conversion efficiency of ortho- to para-hydrogen is estimated to be 80%.

3) Heat load of hydrogen pump

An adiabatic efficiency of the hydrogen pump is assumed to be 52%. Total heat load of the pump is estimated to be the sum of the motor input power and the heat leaks of 10 W to the pump by heat conduction.

4) Temperature difference through the moderator within 3 K

In the assessment, re-conversion effect of ortho-hydrogen is eliminated to avoid accounting excessive hydrogen temperature decrease caused by re-conversion into ortho-hydrogen. Namely this assessment uses constant concentration of para-hydrogen.

5) Bypass flow rate in the parallel flow configuration for the moderators cooling.

To stabilize the flow distribution in the parallel flow configuration for the moderators cooling, a bypass line is installed and 10% of the total flow is distributed.

(5) Numerical results

We calculated a cooling process for a parallel and series cooling system as shown in Fig. 2.4.9. The numerical results for the system pressure of 1.5 MPa are shown in.Tables 2.4.3 and 2.4.4. Table 2.4.5 compares the results for parallel cooling with those for the series cooling. The pumping head required for the series cooling becomes larger. It is, therefore, difficult to use the centrifugal pump in the series cooling system. The refrigeration power required for the series cooling becomes larger due to the heat load of the pump. It is estimated that the refrigeration power of 24% increases. Therefore, the parallel cooling is adopted in this hydrogen circulation system.

On the other hand, the results for subcooled hydrogen at the pressure of 0.6 MPa are shown in Fig. 2.4.10 and Table 2.4.6. The pressure drops in each component are almost equal to those at the pressure of 1.5 MPa. The results of PFD calculation for 0.6 MPa are almost identical to those for 1.5 MPa. Therefore, it is found that the hydrogen circulation system can be operated in pressure ranging from 0.6 MPa to 1.5 MPa.

2.4.2.3 Pressure drop through the hydrogen circulation system

(1) Introduction

It was important to estimate the pressure drop of the hydrogen circulation system, to design for the hydrogen circulation pump, the control valves, and the other equipments in this system. In this chapter, the pressure drop of the hydrogen circulation system is calculated.

(2) Conditions

a) The calculations of the pressure drop were estimated separately into the pipes, the inserts of the pipe, and the equipments in this system. The inserts of the pipe were elbows, glove valves, manifolds, and so on. The equipments in this system were the heater, the accumulator, the ortho-pata hydrogen converter, and the helium-hydrogen heat exchanger.
b) The pressure drops were calculated by two methods, one by the Fanning's equation and the other by a loss factor.
c) The pressure drops of the equipments in this system were assumed to be the fixed values. It shows in Table 2.4.7.
d) The total flow rate of this system was assumed to be 162.2 g/s. The flow rate for the coupled moderator was assumed to be 68.0 g/s. The flow rate for the decoupled moderator was assumed to be 38.2 g/s. The flow rate for the poisoned moderator was assumed to be 39.8 g/s. The flow rate of

the by-pass line for the moderators was assumed to be 16.2 g/s.

e) In the plan, the moderator supply temperature was assumed to be 18 K, the moderator return temperature was assumed to be 21 K, and the equivalent temperature was assumed to be 19.5K of the mean value.

f) The equivalent pressure was assumed to be 1.4 MPa.

g) The physical property values were para-hydrogen.

h) The pressure drops were calculated as one hydrogen circulation pump.

i) The *Cv* value of the valves for the moderator supply line was assumed to be 17.05, and the *Cv* value of the valve for the moderator by-pass line was 10.32.

j) These valves were adjusted so that the pump head of the hydrogen circulation pump might become 0.1 MPa.

(3) Estimation methods

The pipe types were a circular pipe, a multiple concentric pipe, and a corrugated pipe. The pipe shapes were an elbow, a glove valve, a vent and manifolds. It was shown below that the calculation types of the Reynolds numbers, the friction factors with each pipe type and the pressure drops with pipe of shapes.

1) Reynolds numbers

a) Circular pipe, Corrugated pipe (quintet pipe)

$$\mathrm{Re} = \frac{D_h \cdot v \cdot \rho}{\mu} \tag{2.4.6}$$

where Re is Reynolds number, D_h is equivalent diameter (m), v is velocity (m/s), ρ is density (kg/m^3), μ is viscosity (Pa·s).

b) Multiple concentric pipe

$$\mathrm{Re} = \frac{2 \cdot Q \cdot \rho}{\pi \cdot \mu \cdot (d_1 + d_2)/2} \tag{2.4.7}$$

where Q is volume flow rate (m^3/s), ρ is density (kg/m^3), π is circle ratio, μ is viscosity (Pa-s), d_1 is outer diameter (m), d_2 is inner diameter (m).

2) Friction factors

The values of the friction factor considered to the pipe types. They were calculated as turbulent flow, because the Reynolds number is more than 3000.

a) Circular pipe（Blasius's equation）

$$\lambda = 0.3164 \cdot \mathrm{Re}^{-1/4} \cdot \alpha \tag{2.4.8}$$

where λ is friction factor, Re is Reynolds number, α is 1.25. α was the coefficient considered to the smooth surface roughness of a stainless pipe about 22 μm, and the friction factor of Reynolds number of about 100,000.

b) Multiple concentric pipe

$$\lambda = 0.3051 \cdot \mathrm{Re}^{-1/4} \cdot c$$
$$c = 0.1056 + 0.02 \cdot \log_{10}\left(\frac{d_2}{d_1} - 0.0015\right) \tag{2.4.9}$$

where Re is Reynolds number, d_1 is outer diameter (m), d_2 is inner diameter (m).

c) Corrugated pipe (quintet pipe)

The values of friction factor of the corrugated pipe were 0.11, and this value was a recommendation of the manufacturer.

$$\lambda = 0.11 \tag{2.4.10}$$

3) Pressure drops

a) Fanning's equation

$$\Delta P = \lambda \cdot \left(\frac{\rho \cdot v^2}{2}\right) \cdot \left(\frac{l_e}{D_h}\right) \tag{2.4.11}$$

where ΔP is pressure drop (Pa), λ is friction factor, ρ is density (kg/m^3), v is velocity (m/s), l_e is pipe length (m), D_h is equivalent diameter (m).

b) Loss factor for pipe

The values of loss factor were considered to the pipe of shapes.

$$\Delta P = \zeta \cdot \left(\frac{\rho \cdot v^2}{2}\right) \tag{2.4.12}$$

where ζ is lass factor, ρ is density (kg/m^3), v is velocity (m/s).

(4) Result of calculation

The pressure drops of the hydrogen circulation system were calculated in the normal operation at a low temperature. It was the condition at 1.4 MPa, 19.5 K. Table 2.4.8 shows the calculation results of pressure drops in this system. Fig. 2.4.11 shows the reference of the calculated pressure drops in this system. As a result of the calculation, the pressure drops didn't have a big change from that of basic design value estimated with the PFD. And, the pressure drop in this system was no problem, because the total of the calculated pressure drops was less than 0.1 MPa.

2.4.2.4 Heat load

It is important to estimate the heat loads applied to the hydrogen circulation system in order to determine a refrigeration power of the helium refrigerator. The nuclear heating generated in the three moderators, which estimated to be 3.75 kW for a proton beam power of 1 MW, is very large. All cryogenic hydrogen pipes are insulated by the vacuum layer and are laped with the multilayer insulation with 20 layers. All compornets of the hydrogen circulation system such as the pumps, the heat exchanger, the ortho-para hydrogen converter, the accumulator, and the heater are installed into the safety box. For the hydrogen transfer line, the multilayer insulation with 20 layers is installed except for around moderators. This is because the moderator is exposed to very high radiation field. However, the heat load in the moderators is estimated by using the conventional correlation of the thermal radiation and the thermal conduction.

(1) Nuclear heating in moderators

For a proton beam power of 1 MW, the nuclear heating in each moderator is shown in Table 2.4.9.

.

(2) Cryogenic hydrogen pipe

1) Heat load applied to the cryogenic hydrogen pipe with multilayer insulation

The cryogenic hydrogen pipes have the multilayer insulation (MLI) with 20 layers except for moderator. The multilayer insulation is made of polyimide, whose surface is coated by Aluminum with the thickness of 50 nm. The thickness of the multilayer insulation is 12.5 μm. Carren[2.4-1)] experimentally measured the effect of a number of the MLI layers. He treated the heat transfer through the MLI as the equivalent thermal conduction problem, and then the following empirical equation was derived.

$$\lambda_{SI} = \left\{ 3.65 \times 10^{-7} N^2 \left(\frac{T_h + T_c}{2} \right) + 1.1 \times 10^{-13} \frac{\left(T_h^{\ 2} + T_c^{\ 2} \right)\left(T_h + T_c \right)}{N} \right\} \tag{2.4.13}$$

where λ is the equivalent thermal conductivity (W/m·K), N is the layer density of MLI (layer/m), T is the temperature (K). The subscripts of h and c indicate high temperature wall and low temperature wall, respectively. The layer density is decided to be 5700 layer/m.

Effects of not only the thermal conduction through the MLI but also the thermal radiation are included in Eq. (2.4.13). By modifying Eq. (2.4.13), the correlation has been derived based on various experimental data as follows.

$$\lambda_{SI} = 8.5 \left\{ 3.65 \times 10^{-7} N^2 \left(\frac{T_h + T_c}{2} \right) + 1.1 \times 10^{-13} \frac{\left(T_h^{\ 2} + T_c^{\ 2} \right)\left(T_h + T_c \right)}{N} \right\} \tag{2.4.14}$$

When N = 20 layers, T_h = 300 K, and T_c = 20 K, the equivalent thermal conductivity is calculated to be 2.087×10^{-4} W/m·K. The heat leakage in the cryogenic pipes except for moderators was estimated by the following equation for a cylinder.

$$Q = \frac{2\pi \lambda_{SI} l}{\ln\left(d_h / d_c \right)} \left(T_h - T_c \right) \tag{2.4.15}$$

where Q is the heat load (W), l is the length of the pipe, d_h is the outside diameter of the pipe with MLI, and d_c is the outside diameter of the pipe.

2) Heat load applied to the cryogenic hydrogen pipe with no multilayer (moderator region)

Around moderators, the MLI receives the influence of the radiation damage. Therefore, we cannot use the MLI in the moderator region. The heat load into the cryogenic hydrogen is mainly dominated by the thermal radiation.

$$Q = \sigma\left(T_h^{\ 4} - T_c^{\ 4}\right)A_c \frac{1}{\dfrac{1}{\varepsilon_h} + \dfrac{A_h}{A_c}\left(\dfrac{1}{\varepsilon_c} - 1\right)} \tag{2.4.16}$$

where σ is the Stefan-Boltzman constant (5.6697×10^{-8} W/m^2·K^4), ε is the emissivity, and A is the surface area. The subscripts of h and c indicate high temperature wall and low temperature wall, respectively.

The results of the heat load into the pipe are shown in Table 2.4.10.

(3) Components in safety box

1) Hydrogen heater

The hydrogen heater vessel is 0.1652 m in outer diameter and 1.68 m in length. The vessel has the MLI with 20 layers, and the thickness is 0.01 m. The heat leakage was estimated to be 3.49 W by using λ_{eff} (= 1.35×10^{-4} W/m·K) and Eq. (2.4.15).

$$Q_{heater} = 2.082\times10^{-4} \times \frac{(2\pi\times1.68)}{\ln\left(\dfrac{0.1652+2\times0.01}{0.1652}\right)}(300-20) = 5.38(\mathrm{W}) \tag{2.4.17}$$

Suppose that the heater vessel is supported by four cylindrical bars made of stainless steal, which 0.03 m in diameter and 0.5 m in length. The heat leakage can be described the thermal conduction for one-dimensional. It is calculated to be 17.26 W for four supports.

$$Q_{\sup} = \frac{\lambda_{SS} A}{L}\left(T_h - T_c\right) \tag{2.4.18}$$

where λ_{ss} (= 10.9 W/m·K) is thermal conductivity of stainless steal, L is the length of the support bar, and A is the cross-section of the bar.

The total heat load in the heater is 22.64 W.

2) Accumulator

The accumulator vessel is 0.36 m in outer diameter and 0.68 m in length. It has the MLI with 20 layers, and then the thickness is 0.01 m. The heat leakage was estimated to be 4.64 W by using λ_{eff} (= 2.082×10^{-4} W/m·K) and Eq. (2.4.15). The heat load from the top and bottom of the vessel was estimated to be 1.19 W.

$$Q_{acc,bt} = 2.082\times10^{-4} \times \frac{(300-20)}{0.01}\left(\pi(0.36/2)^2\right)\times 2 = 1.19(\mathrm{W}) \tag{2.4.19}$$

Suppose that the heater vessel is supported by four cylindrical bars made of stainless steal, which 0.03 m in diameter and 0.5 m in length. The heat load from the support can be obtained from Eq. (2.4.18). It is calculated to be 17.26 W for four supports.

The total heat load applied to the accumulator is 23.09 W.

3) Hydrogen pump

For the hydrogen pump, we consider two kinds of the heat loads. One is the pump power, Q_{pump}. The other is the heat load from the vessel wall, Q_{vessel}. The pump power, Q_{pump} (W) can be expressed as follows.

$$Q_{pump} = \frac{\dot{V}H}{\eta} \tag{2.4.20}$$

where V is the flow rate (ℓ/s), H is the pump head (kPa), and η is the efficiency. The efficiency η is determined to be 0.5.

The flow rate is 2.22 ℓ/s, which corresponds to the mass flow rate of 0.162 kg/s at the temperature of 20 K and the pressure of 1.5 MPa. The pressure drop in the hydrogen circulation system was estimated to be 77 kPa and the pump power is calculated to be 311 W. On the other hand, the heat load from the vessel, Q_{vessel}, is set to be 10 W. The total heat load from the pump Q is 321 W.

4) Ortho-para hydrogen converter

The vessel of the ortho-para hydrogen converter is 0.2594 m in outer diameter and 0.66 m in length. The vessel has MLI with 20 layers, whose thickness is 0.01 m. the heat load from the top and bottom of the vessel was also estimated, as well as the accumulator case. The heat load from the side of the vessel is calculated to be 3.25 W, and that from the bottom and the top of the vessel is 0.62 W. Suppose that the heater vessel is supported by four cylindrical bars made of stainless steal, which 0.03 m in diameter and 0.5 m in length. The heat load from the supports is 17.26 W. The total heat load in the orhto-para hydrogen converter is estimated to be 21.13 W.

5) Heat Exchanger

The heat exchanger is 0.1 m in width, 0.14 m in length and 1.0 m in height. The surface are is 0.508 m^2. The heat exchanger has MLI with 20 layers, whose thickness is 0.01 m. The heat leakage can be estimated by Fourier’s law for one -dimensional. It is calculated to be 3.18 W.

$$Q_{HX} = \lambda_{SI} \frac{A}{t}(T_h - T_c) = 2.082 \times 10^{-4} \times \frac{0.508}{0.01}(300-20) = 3.18\,(\mathrm{W}) \tag{2.4.21}$$

where t is the thickness of MLI layer.

Suppose that the heater vessel is supported by four cylindrical bars made of stainless steal, which 0.03 m in diameter and 0.5 m in length. The heat load from the supports is 17.26 W. The total heat load in the heat exchanger is estimated to be 20.44 W.

6) Valve

Four valves with the size of 32A and three valves with the size of 25A are installed into the hydrogen circulation system. It is described in the Cryogenic Handbook[2.4-2)] that the heat load from the valve of 32A size and 25A size with 0.5 m extension length are 3.5 W and 3.0 W, respectively. The total heat leak is calculated to be 23.0 W. The results are shown in Table 2.4.11.

7) Pipes such as measurement for the pressure, hydrogen discharge, hydrogen gas supply and so on.

The pipes except for the main loop have a temperature distribution between an ambient temperature and 20 K. The heat load through the pipes is estimated by using thermal conduction equation.

$$Q = \lambda_{ss} \times \frac{\pi / 4 \times \left(d_{out}^{\ 2} - d_{in}^{\ 2}\right)}{L}\left(T_h - T_c\right) \tag{2.4.22}$$

where λ_{ss} (= 10.9 W/m· K) is thermal conductivity of stainless steal, L is the length of the pipe (set to be 2 m), d_{out} is the outer diameter, and d_{in} is the inner diameter. The results are shown in Table 2.4.12.

(4) Moderator

1) Spacer in the parallel piping

The parallel piping is supported by spacers at interval of 2 m. The total number of the spacer needs to be 10 per one moderator. The spacers made of Teflon are 5 mm in thickness. It is touched to the vacuum piping wall at two points, and then the connecting is set to be 3 mm×5 mm. The minimum length between the hydrogen piping and the vacuum wall is regarded as the conduction length (= 20 mm). The heat load from the spacer is obtained from the thermal conductivity of 0.245 W/m· K and the Fourier's law. It is estimated to be 0.1 W per one support.

2) Spacer in the coupler

There are three spacers in the coupler. The spacers made of stainless steal are 5 mm in thickness. The heat load is estimated to be 4.58 W per one support.

3) Spacer around the moderator vessel

Around moderator vessel, the moderator is supported by a spacer. The spacer made of stainless steal is 0.04 m in outer diameter, 0.05 m in length, and 0.005 m in thickness. It is assumed that the temperature at the outer wall of the vacuum layer would increase up to 373 K, because of the effect of the nuclear heating. The heat load from the spacer is estimated to be 4.77 W for one moderator.

The results of 1), 2) and 3) are shown in Table 2.4.13.

4) Thermal radiation in each Moderator

The heat load caused by the thermal radiation can be calculated by Eq. (2.4.16) and summarized in Table 2.4.14.

The heat load in the cryogenic hydrogen circulation system is summarized in Table 2.4.15.

2.4.2.5 Hydrogen inventory in the hydrogen circulation system

(1) Introduction

Volume of the hydrogen circulation system was calculated. The volume was separated to the hydrogen circulation unit, the hydrogen transfer tube for CM, the hydrogen transfer tube for DM, and the hydrogen transfer tube for PM. They were totaled separately. The hydrogen circulation unit was totaled separately into the pipes and the equipment, because it was composed of the pipes and the equipment.

Fig. 2.4.12 shows flow diagram of the hydrogen circulation system. The inventory at the normal operation of the hydrogen circulation system was estimated.

(2) Conditions

a) The condition at the normal operation of the hydrogen circulation system was at 1.4 MPa, 19.5 K.
b) The dimension of the equipment and the pipes used an actual design.
c) The volumes of the accumulator, the heater, the ortho-para hydrogen converter, the helium-hydrogen heat exchanger, the moderators, and the hydrogen circulation pump were a fixed value.
d) The valves, the orifices, the filters were treated as pipe.

(3) Calculation of result

Table 2.4.16 shows the calculation result of volume and inventory in hydrogen circulation system. And the breakdown of the volume is shown from Tables 2.4.17 to 2.4.21.

2.4.3 Design of Main Components

2.4.3.1 Helium refrigeration system

The required refrigeration power has been designed to be 5.1 kW based on the heat loss calculation mentioned in Section 2.4.2.4. The nuclear heating through the moderators is estimated to be 73.8 kW for a proton beam power of 1 MW, the heat loss in the hydrogen circulation system is 1.2 kW, and the heat loss in the helium refrigeration system, which is mainly applied at the transfer line between the helium refrigeration system and the hydrogen circulation system, is 100 W. Therefore, we should design the helium refrigeration system with the refrigeration power of 6 kW at 17 K, which has a margin of 17% for the estimated total heat load.

From the viewpoint of the refrigeration power, economic efficiency and convenient system control, we have designed the helium refrigeration system that has adopted Brayton cycle with a turbine expander and a liquid nitrogen precooling. The supply pressure to the hydrogen circulation system should be determined to be 1.6 MPaG, which is larger than the design pressure of 1.5 MPaG in the hydrogen circulation system. This is because the hydrogen leak into the helium refrigeration system should be avoided even if the helium-hydrogen heat exchanger would be broken. The supply temperature is determined to be 17 K. In order to satisfy the above design conditions, we have conducted the process design of the helium refrigeration system. The design results are shown in Fig. 2.4.13.

In the process calculation, the turbine expander efficiency is 0.75 independent of the temperature and the pressure. The required circulation flow rate is determined to be 0.274 kg/s and the flow rate of the liquid nitrogen is determined to be 0.0229 kg/s. Based on the result of the process design, we have designed the helium refrigeration system, as shown in Fig. 2.4.14. An oil lubricated screw compressor has a capacity to compress the helium gas with the mass flow rate of 290 g/s from 0.3 to 1.66 MPa. The compressor has the rated shaft power of 690 kW. The high pressure stream enters the cold box with the mass flow rate of 274 g/s and is cooled down to approximately 80 K through the plate-fin heat exchanger of HX1 and HX2 by liquid nitrogen and the counter flow of low pressure stream. In design, the liquid nitrogen consumption is estimated to be approximately 80 K through the plate-fin heat exchanger of HX1 and HX2 by liquid nitrogen and the counter flow of low pressure stream. The feed gas passed through HX1 and HX2 is routed to the 80 K adsorber, in which nitrogen trace impurities in the feed gas are removed. The high pressure stream purified by the 80 K adsorber is cooled down to 15.5 K through the third heat exchanger, HX3, by the low pressure turbine outlet stream. The high pressure cold stream heated up to 17 K is controlled by the helium heater with the capacity of 8 kW, and then it is provided to the hydrogen circulation system. The turbine is located after the H_2-He heat exchanger to keep the helium pressure higher than the hydrogen pressure such as 1.5 MPa, and to prevent hydrogen leak into the refrigeration system. The helium stream out of the H_2-He heat exchanger is expanded and cooled to 0.3 MPa and 12.7 K by the turbine. The low pressure stream is passed through HX3 and HX1 and is warmed up to ambient temperature, and finally comes back to the compressor suction.

2.4.3.2 Hydrogen circulation system

(1) Hydrogen circulation pump

1) Outline

The cryogenic hydrogen circulation system adopts a centrifugal-type pump that can circulate the cryogenic hydrogen (20 K, 0.5 to 1.5 MPa) with the mass flow up to 162 g/s through the three moderators. This forced flow circulation can remove the nuclear heating from the moderators and can keep the temperature difference through the moderators within 3 K that is a requirement from neutron users.

The hydrogen pump was designed to circulate at the mass flow rate of 162 g/s with the pump head of 0.12 MPa under the rated condition. Since the hydrogen pump was required for high reliability, two pumps were installed into the cryogenic hydrogen system, and will be operated simultaneously with its capacity of 50%. Even if one pump would be stopped due to its failure, the cryogenic hydrogen system can continue by the other pump with its capacity of 100% without stopping. We developed the hydrogen pump based on the large-scale supercritical helium pump that was applicable to use for a fusion experimental reactor such as International Thermonuclear Experimental Reactor (ITER).

2) Design conditions

The design conditions and specifications of the hydrogen circulation pump are shown in Table 2.4.22.

3) Design method and result for centrifugal pump

From the design conditions of Table 2.4.22, the fundamental design parameters that are a revolution, an impeller circumference velocity and an impeller diameter, are caluculated by using the database of a supercritical helium pump and the similar law of a centrifugal pump. The design value of the pump is decided from optimized design parameters considering possibility of the manufacturing and the operation.

In the database of the supercritical helium pump, the three basic design values are shown in Table 2.4.23. There are three types of the parameter set that is the revolution, the impeller velocity and the impeller diameter.

Based on these data, the design parameters are calculated by the similar law using the following equations.

(a) A similar law regarding the specific velocity

$$N_s = N \frac{Q_s^{1/2}}{H_{ad}^{3/4}} \tag{2.4.23}$$

Here, N is a revolution of the impeller (rpm), Q_s is a flow rate of the suction volume (m^3/min), and H_{ad} is a insulation head (m).

(b) A similar law regarding the pressure function, φ (-)

$$\varphi = \frac{H_{ad} \cdot g}{u^2} \tag{2.4.24}$$

Here, u is an impeller circumference velocity (m/s), and g is a gravity accelation (m/s^2).

(c) A similar law regarding the flow rate function, ϕ (-)

$$\phi = \frac{Q_s}{A_s u} = \frac{\dfrac{60\dot{m}}{\rho_s}}{\dfrac{\pi^2}{4} N D^3} \tag{2.4.25}$$

Here, A_s is a suction cross section to the impeller (m^2), $\dot{m}$ is a mass flow rate (kg/s), ρ_s is a suction density of the fluid and D is a diameter of the impeller.

The insulation head, H_{ad}, and the flow rate of the suction volume, Q_s, are given by the following equations.

$$H_{ad} = \frac{\Delta h}{g} = \frac{(h_{out} - h_{in})}{g} = \frac{(\Delta P / \rho_s)}{g} \tag{2.4.26}$$

$$Q_s = \frac{60\dot{m}}{\rho_s} \tag{2.4.27}$$

Here, Δh is a difference in inlet and outlet enthalpy at the pump, h_{out} is an outlet enthalpy, h_{in} is an inlet enthalpy (kJ/kg) and ΔP is a pump head (Pa).

ρ_s and ΔP are given by the design conditions, and H_{ad} is obtained to substitute them for Eq. (2.4.26). Q_s is geven from Eq. (2.4.27) using by the design flow rate and density. From the database of parameters in Table 2.4.24, a design revolution, an impeller circumference velocity and an impeller diameter is obtained from Eqs. (2.4.23), (2.4.24) and (2.4.25). The impeller diameter is also obtained by the following eqation easily.

$$D = \frac{60u}{\pi N} \tag{2.4.28}$$

The calculated results of the design parameters are shown in Table 2.4.24. We decided the parameter as type-2 from the viewpoint of manufacturing and operation. The design result is shown in Table 2.4.25.

4) Non-dimensional characteristics curve and estimation of operating characteristics

A non-dimensional characteristics curve of the designed pump is shown in Fig. 2.4.15. This is an achievement curve as the type-2 pump. From this curve, the operating characteristics were estimated under the rated condition of 19 K, 1.4 MPa at inlet in the pump, and also room temperature.

(a) Estimation for the rated condition

Fig. 2.4.16 shows a result of the relationships between the mass flow rate and the pressure head for the several revolutions (25,000, 30,000, 35,000, 40,000 rpm) at 1.4 MPa and 19 K of the inlet pump condition. The rated operating point would be able to be achieved the design point with the revolution of about 27000 rpm from this figure., The designed pump would have therefore satisfactory performance at the rated condition.

(b) Estimation for the ambient condition

In this cryogenic system, the pumps operate from the ambient temperature at the first time in the hydrogen circulation system filled with hydrogen gas of 1.5 MPa. And then, the turbine in the helium refrigeration system is operated at the rated revolution from ambient temperature and cool-down of the system is started. Therefore it is necessary to circulate hydrogen gas in the hydrogen loop at the ambient condition.

Fig. 2.4.17 shows a result of the relationships between the mass flow rate and the pressure head for the revolutions of 35,000 and 50,000 rpm at 1.0 MPa and 300 K of the inlet pump condition. From this figure, hydrogen flow rate of 5 g/s would be able to be achieved with 50,000 rpm at the pressure head of 0.0037 MPa, which is more than the pressure drop of 0.0031 MPa as the case of piping of 50 m in length and 0.025 m in diameter.

5) Latest specification and off-beam commissioning results

(a) Latest specification

The latest specification of the pump is decided from re-estmation by the vender taken the possibility of manufacturing, etc. into account. The pump specificasion is shown in Table 2.4.26.

(b) Off-beam commissioning results for helium circulation

The cryogenic hydrogen system commissioning was started from January 2008. For the first time, we carried out a cryogenic test on the whole system, in which helium gas was used instead of hydrogen. The cryogenic hydrogen system could be cooled down to 18 K within 30 hours, and be kept to be the rated condition for 36 hours without any problems. We confirmed the soundness of each component such as circulation pumps and operation control system.

The performance of the hydrogen circulation pump was measured during the rated operation. The temperature at the inlet of the pump was 20.7 K, which was maintained by the hydrogen heater. The inlet pressure was around 1.56 MPa. The pump heads and the mass flow rates were measured for various pump revolutions. The pump head was changed by controlling the supply valves to the moderators and the bypass valve. The performance result of the hydrogen pump is shown in Fig. 2.4.18. For comparison, the design curve of the pump is also shown in the figure. The experimental results are almost in agreement with the design curve where the pressure coefficients are more than about 0.35, including the rated points. Where the pressure coefficients are less than 0.35, the experimental results are lower than the design curve. As one of the reasons, the precision of the pressure gages is low where the pump head is small, because the pump head was measured by the pressure gages with 2 MPa range. And another reason is that the pump is for hydrogen circulation not but for helium. Therefore, it is necessary to confirm that the performance test is carried out using by actual hydrogen at the next step.

(c) Off-beam commissioning for hydrogen circulation and results of the improved pump

The off-beam commissioning for hydrogen circulation was carried out in April 2008. We reached the Day-1 that was the first beam acceptance in the spallation target and the first neutron generation on May 30. However, when the pump performance test was carried out with changing the revolution and pump head, the pump flange, installing the pump into the safety box, had got cold to less than −20°C. We thought it is because the superclitical hydoegen was raised to the part of ambient temperature area in the pump with the pump head changing. Therefore, the hydrogen pump was improved by changing seal performance and the volume of the ambient temperature area. At last, the pump performance test was carried out with the improved pumps in September 2008.

The performance result of the improved hydrogen pump is shown in Fig. 2.4.19. The experimental results are lower than the design curve for the pump. In other words, the experimental results for hydrogen circulation are lower than one in the case of helium. This is probably because the hydrogen pump was designed based on the supercritical helium pump with the experimental database. Since we didn’t have the database of hydrogen, we will build it up through the on-beam or off-beam operation if the schedule allows us. On the other hand, where the pressure coefficients are low, the experimental results are lower than the design curve that was also found in Fig. 2.4.18. It seems due to the precision of the pressure gages as mentioned above. We are installing the defference pressure gage for the hydrogen pump in order to measure more precisely now.

(2) Accumulator

1) Design conditions

(a) Type of accumulator

The vertical variable capacity type tank which uses the bellows is adopted. Helium is used as a gas for pressure adjustment.

(b) Design conditions for accumulator

An accumulator works to absorb the pressure fluctuation from changing heat load of the proton beam. The accumulator forms the hybrid pressure control system combining with a heater which is installed inside the hydrogen loop. The installation area of heater and moderator differ, approximately 10-m distance exists. From the fact that hydrogen capacity is approximately 65 ℓ in this section, time lag occurs. The accumulator is necessary to have a performance to absorb this time delay. The accumulator adjusts pressure by changing the capacity of the liquid hydrogen. The mechanism of capacity change is passive according to the pressure fluctuation of hydrogen side. The capacity change of helium gas is absorbed by its buffer tank.

2) Estimation of variable volume

Largest heat load fluctuation occurs when proton beams turn on and off. In this case the capacity volume should be estimated to absorb the pressure fluctuation of hydrogen between the moderator and the heater. From the inventory caluculation in subsection 2.4.2.5, 64.54 ℓ of hydrogen exists between three systems of the moderator and the heater.

With the beam injection, enthalpy after the beam injection is

$$h' = \frac{Q}{\dot{m}} + h \tag{2.4.29}$$

Here an enthalpy before the beam injection is h, hydrogen flow is $\dot{m}$ (kg/S) and beam heat is Q (W). A hydrogen density of incident ρ (kg/m^3) and density after the injection ρ' (kg/m^3) are represented as a function of P and h.

$$\begin{aligned} \rho &= \rho(P,h) \\ \rho' &= \rho(P,h') \end{aligned} \tag{2.4.30}$$

P is pressure of hydrogen, does not change before and after beam injection. But hydrogen mass is invariant, it is necessary to absorb this density change by the volume fluctuation dV.

$$M = \rho \cdot V = \rho' \cdot (V + dV) \tag{2.4.31}$$

When the status of the hydrogen before beam injection is 1.5 MPa and 18 K, hydrogen density is 74.92 kg/m^3. In the moderator section, the heat load from beam is 3.75 kW when the maximum 1 MW proton beam is injected. After injection, hydrogen density is changed to be 72.15 kg/m^3, then 2.32 ℓ volume capacity is needed. The design values of accumulator are listed in Table 2.4.27. In this design the capacity volume fluctuation of 3.5 ℓ is possible.

(3) Hydrogen heater

A hydrogen heater is one of the pressure control system in the cryogenic hydrogen system. The hydrogen heater plays a role in compensating the nuclear heating of 3.8 kW for a proton beam power of 1 MW generated at the moderators when the proton beam is turned off. Furthermore, the accumulator temperature should be maintained constant by the heater. A high power and high responsive heater that can be used in the supercritical hydrogen should be required for such a pressure control of the cryogenic hydrogen system in JSNS. We have developed a new type heater, which should be designed to be compact and kept stable flow condition.

The design conditions are as follows,

a) Circulation flow rate is 0.162 kg/s,
b) Inlet temperature of the heater is below 20 K,
c) Required heater power is above 5 kW,
d) Heat flux on the heated surface is below 5,000 W/m^3,
e) Pressure drop through the heater is below 2 kPa.

It is difficult to apply a large heat input by a heater to the cryogenic fluids such as helium, hydrogen, nitrogen and so on. This is because the cryogenic fluids have smaller specific heat and thermal conductivity and smaller subcooling. For non-cryogenic fluids, a shell-and-tube type heater has been generally used as a heater for high heat load. The fluid mainly flows along buffles that are alternately arranged in the shell-and-tube heater, and a stagnation flow region locally exists between the baffles. The inhomogeneous flow distribution would bring about the local heat transfer deterioration. Therefore, the shell-and-tube heater should be designed to take the local heat transfer deterioration into consideration. Accordingly, the required heater size should become quite large in order to reduce the heat flux on the heated surface. In JSNS, we should develop a compact and high-responsive heater that can apply a high heat load uniformly to the supercritical hydrogen.

The developed new type heater is shown in Fig. 2.4.20. The sheathed heater that can directly apply high heat load to fluid is adopted as a heater element, and can be expected to be high response performance. Ten sheathed heaters with the diameter of 12 mm and the length of 2,720 mm are arranged as shown in Fig. 2.4.20. The average heat flux on the heated surface should be maintained below the allowable heat flux of 5×10^3 W/m^2. Both ends of the sheathed heater have an electrode and is welded to a flange in order to avoid direct contact of the electrode with hydrogen as an explosion protection countermeasure. A baffle plate has twenty holes with the diameter of 16 mm, which is slightly larger than that of the sheathed heater, and is arranged along the length direction of the sheathed heater at a certain interval. The heater vessel has an inner diameter of 133 mm, a thickness of 3.4 mm and a total length of 1600 mm. The inner diameter of inflow and outflow piping is 38.7 mm, which corresponds to main piping size of the cryogenic hydrogen system. In order to support the baffles, threaded rods are arranged around periphery of the baffles. A pipe with the same length of the desirable distance is inserted into the threaded rod in order to maintain the distance between the baffles. At the lowest baffle, the rods are fastened by a nut. At the lowest baffle, the sheathed heaters are fixed in order to eliminate fluid vibration and maintain clearances between the sheathed heaters and the baffle.

The sheathed heater has non-heated region above the outlet piping in order to avoid warmed supercritical hydrogen below around the flange. The heater vessel, the baffles and the sheathed heater are made of the same material; stainless steal in order to avoid contacting between them by the thermal shrinkage. The heater vessel and the flange with the sheathed heaters are sealed by an O-ring made of pure aluminum for ease in the maintenance.

When supercritical hydrogen passes through the holes on the baffle, the mainstream and the thermal boundary layer that develops along the heated surface would be agitated by the throttle effect, and the flow velocity would also increase locally. Therefore, it is considered that the heat transfer characteristics would be improved by the throttle effect. The supercritical hydrogen would be able to be heated uniformly, although the temperature distribution exists along the length direction of the sheathed heaters. We can select the sheathed heaters with the high heat flux on the heated surface. We have confirmed that the developed heater shown in Fig. 2.4.20 satisfies the design conditions mentioned above by a CFD analysis. Accordingly, we succeeded to develop the new type compact heater.

(4) Ortho-para hydrogen convertor

The process flow diagram (PFD) of the cryogenic hydrogen circulation system is calculated in section 2.4.2.2. The design conditions for ortho-para hydrogen converter obtained from the results are summarized as follows,

- Mass flow rate of hydrogen: 162.2 g/s,
- Inlet pressure: 1.5 MPa,
- Inlet / outlet temperature: 19.9 / 21.3 K,
- Conversion efficiency of ortho- into para-hydrogen: 0.8,
- Inlet / outlet concentration of para-hydrogen: 97.20% / 99.2%,
- Allowable pressure drop: 0.01 MPa,
- Design pressure: 2.0 MPa.

To design the minimum volume for catalyst is significant in viewpoint of less hydrogen hazard, besides less heat capacity for cool-down or warm-up. In this section, the volume of catalyst for the ortho–para hydrogen converter is considered under the conditions.

1) The conversion data of catalyst

The IONEX-type O-P manufactured by IONEX corporation, which the main component is $Fe(OH)_3$, is used as a catalyst to convert ortho-hydrogen into para-hydrogen. The para-hydrogen with the concentration of 25% and 51.5% are fed under the conditions of 0.204 MPa and 19.7 K. The space velocity is defined as the volume flow rate per minute at standard temperature and pressure (STP) per unit volume of catalyst.

2) Estimation of the space velocity (SV value) for the converter

The rate of the reaction can be expressed by using the rate constant, k, under the assumption that the reaction of the ortho-para conversion is first-order.

$$-\frac{dXo}{dt} = kXo - k'(1 - Xo) \tag{2.4.32}$$

where k is rate constant for the reaction of the conversion from ortho-hydrogen into para-hydrogen, k' is that for the reversed reaction of the conversion from para-hydrogen into ortho-hydrogen, and *Xo* is the concentration of the ortho-hydrogen. In equilibrium condition , the value of *Xo* is equal to that of *Xoe*, and $\frac{dXo}{dt} = 0$. Therefore, the rate constant of the conversion into the ortho-hydrogen *k'*, can be described as the following equation.

$$k' = \frac{k * Xoe}{1 - Xoe} \tag{2.4.33}$$

Substituting Eq. (2.4.33) for Eq. (2.4.32) and rearranging, the rate of the reaction can be expressed as follows.

$$-\frac{dXo}{dt} = \frac{k}{1 - Xoe}(Xo - Xoe) \tag{2.4.34}$$

Rearranging Eq. (2.4.34) by using $Xo = Xof$ for *t*=0, the value of SV (space velocity) can be calculated.

$$SV = \frac{1 - Xoe}{t} = -k / \ln\frac{Xo - Xoe}{Xof - Xoe} = -k / \ln(1 - \frac{Xp - Xpf}{Xpe - Xpf}) \tag{2.4.35}$$

where X_p and X_{pf} denote the concentration of para-hydrogen at outlet and inlet, respectively. X_{pe} is that of para-hydrogen in equilibrium at the outlet temperature.

Here, the efficiency of the conversion can be defined as follows.

$$\eta_p = \frac{Xp - Xpf}{Xpe - Xpf} \tag{2.4.36}$$

Substituting Eq. (2.4.36) into Eq. (2.4.35) and rearranging, the space velocity can be summarized as follows.

$$SV = -k / \ln(1 - \eta_p) \tag{2.4.37}$$

The concentration of para-hydrogen in equilibrium at t=19.7 K is 0.9984. With increase in the value of SV, the concentration of para-hydrogen at outlet decreases, that is, the efficiency of the conversion becomes worse.

The efficiency, η_P, and the rate constant, *k*, are given. The rate constant, *k*, increases as the inlet temperature rises. For X_{pf}=0.25, the rate constant is almost kept constant for η<0.8. With further increase in η, that is, X_p, the values of *k* rapidly decrease. For the case, it is considered that the reaction of the conversion cannot be regarded as first-order, and it takes long time to obtain the para-hydrogen with high purity. In subsection 2.4.2.2, we determined the process diagram flow of the hydrogen circulation system under the assumption that 99% para-hydrogen decreased to 97% due to nuclear heating in the moderator. However, the investigations that treated the conversion of high purity para-hydrogen to ortho-hydrogen have not been reported so far. Hence, the value of *SV* in this system is estimated by means of the rate constant for X_{pf}=0.515 and η=0.8, and then is determined to be 2100.

$$SV = -k / \ln(1 - \eta p) = -3500 / \ln(1 - 0.8) = 2174 \rightarrow 2100 \tag{2.4.38}$$

3) Dimensions of the catalyst column

The hydrogen circulation system has the mass flow rate of 162.2 g/s (=1.081×10^5 Nℓ/min). Therefore, the volume of the catalyst required for the system is to be 29.2 ℓ by means of the value of SV mentioned above.

Considering distribution size of the catalyst particle from 30 to 50 meshes, the filling volume of 60 L is required with 20% margin. The diameter of the vessel is designed such that the allowable pressure drop in the catalyst layer is within 0.01 MPa. The pressure drop in the catalyst vessel is expressed as follows.

$$\Delta P = \frac{f * l * \bar{u}_2 * \rho * a_v}{g_c * \varepsilon_d^{\ 3}} \tag{2.4.39}$$

where f is friction factor, l is length of the catalyst layer, u is velocity through the vessel, g_c is gravitational acceleration, a_v is ratio of surface to volume, ε_d is void rate, d_p is particle diameter of the catalyst, ϕ is shape factor of particle, ρ is density of hydrogen, and μ is viscosity. The values of a_v, f, and R_e are calculated by the following equations.

$$a_v = \frac{6\,(1-\varepsilon_d)}{\phi * d_p} \tag{2.4.40}$$

$$R_e = \frac{\bar{u} * \rho}{a_v * \mu} \tag{2.4.41}$$

$$f = \frac{5}{R_e} + \frac{0.4}{R_e^{\ 0.1}} \qquad (R_e > 2) \tag{2.4.42}$$

The diameter and height of the catalyst layer are determined to be 259.4 mm and 660 mm, respectively.

(5) Helium-hydrogen heat exchanger

1) Design conditions

(a) Type of heat exchanger

Plate-fin type of heat exchanger made of Aluminum alloy is adopted in order to reduce the inventory of hydrogen.

(b) Design conditions for heat exchanger

The helium inlet/outlet temperature of heat exchanger is estimated on the assumption that the heat loss of each helium transfer line between the helium refrigerator and the hydrogen circulation system is 35 W. The design conditions of the heat exchanger are shown in Table 2.4.28.

2) Required heat transfer area of the heat exchanger

The heat transfer area is calculated as follows. The cross section area of cooling channel A_f, and the equivalent diameter De are

$$A_f = \frac{X*Y*W*n}{P} \tag{2.4.43}$$

$$D_e = \frac{2X*Y}{X+Y} \tag{2.4.44}$$

$$X = P - t$$
$$Y = H - t$$

where P is fin pitch, H is fin height, t is fin thickness, W is effective width of fin, and n is the number of fin layer.

The heat transfer coefficient, h, is described by using the following form.

$$h = j_T(\mathrm{Re})*C_p*G*\mathrm{Pr}^{-2/3} \tag{2.4.45}$$

where $j_T(\mathrm{Re})$ is Colburn's j factor, Re is Reynolds number, G is mass flow velocity, C_p is specific heat, and Pr is Prandtl number.

The heat transfer area per length S is expressed as follows.

$$S = S_1 + \eta S_2 + \eta' S_3 \tag{2.4.46}$$

where

First heat transfer area $$S_1 = \frac{(2n_1 - n_3)*W}{P} \tag{2.4.47}$$

Second heat transfer area $$S_2 = \frac{2Y*W*n_2}{P} \tag{2.4.48}$$

Third heat transfer area $$S_3 = \frac{2Y*W*n_3}{P} \tag{2.4.49}$$

n_1 is number of layers including plate section, n_2 is number of layers including fin section, n_3 is number of layers including end fin section, η is efficiency of fin and η' is efficiency of end fin.

Net thermal rating unit length $A*U$ is obtained from Eqs. (2.4.45) and (2.4.46)

$$A*U = \sum(h*S)_h * \sum(h*S)_c \;/\; (\sum(h*S)_h + \sum(h*S)_c) \tag{2.4.50}$$

where the subscripts, h and c, denote the path with higher temperature, and that with lower temperature, respectively.

The length required for the heat exchange is described as follows.

$$l = \frac{Q}{A*U*\Delta T_{lm}} \tag{2.4.51}$$

Table 2.4.29 shows the calculation results of the heat transfer area, the fin shape, and the number of the fin layer for plate-fin heat exchanger. As a result, the heat exchanger size of 200×120×700 mm^3 is preferable.

(6) Hydrogen transfer line

1) Outline

The transfer lines function to supply the cryogenic hydrogen to the three moderators and to return the heated hydrogen to the hydrogen circulation system. As mentioned above, a parallel flow configuration is adopted for the moderators cooling. The transfer line from the circulation unit to the moderator vessels is separated into three parts as shown in Fig. 2.4.21: coaxial-pipe structure part from the hydrogen circulation unit to the hekium vessek (part i), parallel-pipe structure part (part ii) and coaxial-pipe structure part to the moderators (part iii). A detail of the moderator section after terminal box, which consists of the moderator vessels, part iii of the transfer line, coupler and part ii of the transfer line, is reported in subsection 2.3.1.2.

2) Specifications

The specifications of the hydrogen transfer line are shown in Table 2.4.30. The coaxial-pipe structure means a multiplex tube that is hydrogen supply, vacuum layer, hydrogen return, vacuum layer again and helium blanket layer, as shown in Fig. 2.4.22. The material of the transfer line is SUS316L.

3) Installing

Fig. 2.4.23 is the overview of installation works of the hydrogen transfer line in the MLF building. The transfer line is mainly helically corrugated and longitudinally welded stainless steel tubes, so that is able to be flexible. They were manufactured in the factory, and were installed in MLF in the autumn of 2006. The main installation process is shown in the following subsections and Fig. 2.4.24.

(a) Lead-in the tubes

The transfer lines were carried into the MLF building by using the 130 tons crane, and led in the cooling system distribution room through the cryogenic H_2 components room from the large components handling room. Then, the lines were led in the shutter drive mechanism room and were put temporarily after bending process using the bend machine. (Fig. 2.4.24(i) and (ii))

(b) Setting up supports

Some supports of the transfer lines were set up in adequate position, and the lines were fixed. (Fig. 2.4.24 (iii))

(c) Connecting with the safety box

They were connected with the safety box that was installed in the cryogenic hydrogen components room. (Fig. 2.4.24 (iv))

(d) Disposal of the penetration

At last, the shielding block and material, whose shielding ability is equal to the thickness of the wall, were filled up as disposal of the penetrations. (Fig. 2.4.24 (v))

- Lead-wool between the cryogenic H_2 components room and the cooling system distribution room: more than 1,299 kg
- Polyethylene block between the cooling system distribution room and the shutter drive

mechanism room: more than 0.5 m in length

4) Situation at the cryogenic system operation

After the cryogenic hydrogen system was completed, the operation test was carried out under supercritical hydrogen condition of 20 K and 1.5 MPa. At that time, it was observed that the rigid part of the transfer line connecting the safety box was covered by frost (Photo. 2.4.1). Especially, the transfer line of the coupled and poisoned decouple moderator was done.

Photo. 2.4.2 shows X-ray radiograph for the transfer line of the coupled moderator. From this photograph, the hydrogen return layer is shift upward and the outer vacuum layer is very narrow. Therefore, it is considered that the vacuum insulation performance was reduced at the narrow gap in the pipe and frost was formed. A heat loss to the fluid for this point was evaluated as about 30 W from surface temperature of this pipe of −3°C at the room temperature of 17°C. Total heat loss for a transfer line was about 110 W. Because the design value of the heat loss for a line is 100 W, this does not influence on the vacuum insulation performance. We installed the cover around that point of the pipe to prevent frost.

2.4.3.3 Control system

(1) Control unit

Components in unit for the hydrogen system exist in many areas of MLF. For example, the hydrogen cryogenic hydrogen cycle unit is set in Cryogenic H_2 components room, the helium refrigeration in Large components handling room, the helium compressor in No.1 He compressor unit room outside of the MLF building. Therefore, the local panels for each instrument and each device have been installed in the room. Each unit can be controlled basically by local panel. On the other hand, the central control panels of cryogenic hydrogen system are installed in the MLF central control room. The operator can control all units and devices basically with remote in the MLF central control room. Table 2.4.31 shows the local and control panels of cryogenic hydrogen system.

A concept of Hydrogen circulation system control unit is shown in Fig. 2.4.25. VME (VERSAmodule Eurocard bus) is a main control unit for all components of hydrogen cryogenic system to order the local control panel, to acquire the data, to order the open/close of valve basically. VME unit inside of cryogenic central panel has a stored program for control flow, automatic sequence.

An operator can access VME unit through two applications of FAPP, plant operation software, and LabVIEW, data logging software, running on PCs. Fig. 2.4.26 shows an image of desktop view of FAPP. FAPP software indicates the control unit, valve and all components. LabVIEW software is adapted for data logging.

VME unit is set in the MLF central control room. Similarly, the three PCs for operators of cryogenic hydrogen system are set in the central control room. Two PCs are for operation, one of them sets process values of system controlling and monitoring. The other PC, where FAPP and LabVIEW are installed, is set up in the Large Components Handling Room to control the system. An operator can check the status of cryogenic hydrogen system locally.

In addition, a PLC unit exists in the central control panel. The PLC unit transfers data from the MLF central control panel and send data from VME of cryogenic hydrogen system. One role of this PLC is to exchange data and information thorough MELSEC/NET-connected. The other role of PLC unit is to generate a MPS (Machine Protection System) interlock signal. The digital and analog signals for source of MPS are input directly to the PLC unit. PLC has logic program and generates the MPS signal.

VME, PLC and all PCs are connected with Ethernet for mutual exchange of data and information. The Ethernet network is set for hydrogen system independently of the other networks.

(2) Operation mode of the cryogenic hydrogen system

The cryogenic hydrogen system can be automatically operated by using automatic operation modes, which are cool-down mode, steady-sate mode, beam injection mode, standby mode, normal warm-up mode, and emergency discharge mode. Fig. 2.4.27 shows a schematic of an automatic operation mode of the cryogenic hydrogen system.

1) Cool-down mode

The hydrogen circulation system is cooled by the helium refrigeration system. The hydrogen is cooled down only with the turbine from room temperature to 45 K, slightly higher than the critical temperature of hydrogen. The turbine expansion ratio was controlled by operating the turbine inlet valve. It was necessary to avoid exceeding the allowable temperature difference of 50 K through the warm to the cold end of the hydrogen-helium heat exchanger during the cool-down process. Therefore, the cooling rate of the refrigerator was controlled to maintain within the allowable heat exchanger temperature difference by the helium heater and the mixing valve that behaved to supply a warm high-pressure stream before entering the cold box to the turbine outlet stream.

On the other hand, the hydrogen pumps were operated at 52,000 rpm, which was larger than a rated speed of 42,000 rpm, to generate a few-g/s helium flow despite very low density around ambient temperature. The hydrogen gas was supplied to the hydrogen circulation system through a hydrogen buffer tank with the volume of 1 m^3, in which the pressure was maintained to be 1.65 MPa. The pressure in the hydrogen circulation system is always maintained to be 1.5 MPa during the cool-down process. On the other hand, the helium pressure in the bellows of the accumulator is maintained to be 1.6 MPa larger than that in the hydrogen circulation system, and the bellows is always fixed at fully extended location, which corresponded to the level of 90.5 mm. As the temperature decreases down to 100 K, the supply temperature to the hydrogen circulation system is maintained to be 45 K for an hour. The larger refrigeration power is required for hydrogen condensation below 34 K. Therefore, the liquid nitrogen is used as a precooling material and the hydrogen pump revolution is reduced to the rated value of 42,000 rpm. The supply temperature is directly controlled by the heater. When the temperature at the accumulator reaches 23.8 K, helium gas supply into the bellow of the accumulator is stopped. With decrease in the temperature, the bellow is automatically contracted to the normal position. On the other hand, the hydrogen heater control is started when the accumulator temperature reaches 21 K. The accumulator temperature is always maintained to be 21 K by PID control of the hydrogen heater. When the supply hydrogen temperature becomes below 18 K, the automatic sequence of the cool-down mode is finished. Then, the operation mode of the cryogenic hydrogen system makes the transition from the cool-down mode to the steady-state mode.

2) Steady-state mode

After the cool-down mode is finished, the operation mode automatically changes to the steady-state mode. In the steady-state mode, the cryogenic hydrogen system is mainly operated at the rated condition. The operation sould be shifted to the beam injection mode, the standby mode and the warm-up through the steady-state mode.

3) Beam injection mode

Supercritical hydrogen around 20 K behaves as incompressible fluid. Slight temperature rise caused by turning the proton beam on and off brings about severe pressure change. Therefore, we should design the pressure control system, which consists of the hydrogen heater and the accumulator. In the steady-state mode, the accumulator temperature is maintained to be 21 K by the hydrogen heater whose power corresponds to 4.0 kW for the flow rate of 0.162 kg/s. And the bellows of the accumulator is located from 40 mm to 60 mm, which corresponds to around the normal position of it. Before the proton beam is injected to the MLF, the cryogenic hydrogen system should be moved to the beam injection mode. After the beam injection, the supercritical hydrogen warmed by the nuclear heating generated in the moderator travels to the hydrogen heater. When the temperature rise of 0.2 K appears at the inlet of the hydrogen heater, the hydrogen heater power of 4.0 kW is decreased down to 250 W. The decrease in the heater power corresponds to the nuclear heating at the moderators for a proton beam power of 1 MW. Although the difference between the predicted decrease in the heater and the real nuclear heating exists, the temperature at the accumulator should be automatically maintained to be 21 K by the PID control of the hydrogen heater.

When the proton beam is turned off, the temperature at the moderator decreases down to the supply temperature of 18 K. Therefore, after a few seconds, the temperature at the inlet of the hydrogen heater also decreases down to around 18.5 K, which is slightly larger than the supply temperature because of the heat inleak through the moderators and the transfer lines. After that, the hydrogen heater power is reset to the value that is before the proton beam is turned on. After that, the temperature at the accumulator should be automatically maintained to be 21 K by the PID control of the hydrogen heater. The operation mode is automatically changed to the steady-state mode.

4) Standby mode

In J-PARC, the accelerator will be operated with a period of 4 weeks; operation for three weeks and maintenance for a week. We need 7 days for the preparation, 2 days for the cool-down operation, and 2 days for the warm-up operation. Therefore, the cryogenic hydrogen system should be maintained around

20 K during the accelerator maintenance period. For the accelerator maintenance, the helium refrigeration system is operated without the liquid nitrogen in order to reduce the consumption of the liquid nitrogen. This operation mode is standby mode.

5) Warm-up mode

The cryogenic hydrogen system has no recovery tank because the hydrogen inventory should be minimized from the viewpoint of safety reasons. Therefore, when the cryogenic hydrogen system is stopped, the hydrogen should be warmed up and discharged to the atmosphere. The operation mode is the warm-up mode. When the warm-up mode sequence is worked, the turbine, the supply of the liquid nitrogen and the heater in the cold box are stopped, and the hydrogen heater in the hydrogen circulation system is turned off. In the helium refrigeration system, the helium gas feeds through the turbine bypass valve, instead of the turbine. The hydrogen, which is circulated by the hydrogen pumps at the rated revolution, is warmed up through the helium-hydrogen heat exchanger. The hydrogen is discharged through the control valve, maintaining the hydrogen pressure at 1.5 MPa. With increase in the accumulator temperature, the bellows of the accumulator expands to the lower limit location and the pressure in the bellows also increases to 1.68 MPa. The pressure is controlled to be maintained at 1.68 MPa, by the supply valve into the bellows.

When the hydrogen temperature reaches 270 K, the hydrogen with the pressure of 1.5 MPa and the pressure is reduced to atmospheric pressure. Finally, the hydrogen in the hydrogen circulation system is replaced by helium gas, inert gas.

6) Emergency discharge mode

When off normal events such as an earthquake and a disaster happen, the cryogenic hydrogen system should discharge hydrogen to atmosphere as quickly as possible. In such a case, we use an “emergency discharge mode”. In the emergency discharge mode, the turbine, the supply of liquid nitrogen, the hydrogen heater, and the hydrogen pump are stopped, although the compressor is running. Helium gas, which has a boiling point lower than hydrogen, is injected into the vacuum layer of the hydrogen circulation system until the vacuum pressure reaches 6 kPa. The temperature of the cryogenic hydrogen increases by increase of the heat inleak. Most of the cryogenic hydrogen is discharged within 10 minutes. After that, the hydrogen in the hydrogen circulation system is replaced by helium gas.

(3) Interlock system

Interlock system for the occurrence of failures should be established to stop the cryogenic hydrogen system securely. The interlock system is divided into the following categories by the post-processing methods. When all interlock systems work, we will stop the turbine. Therefore, it is difficult to maintain the cryogenic hydrogen system at the rated condition and then we should warm up the system.

1) Interlock 1 : Turbine failure and hydrogen heater failure

When the turbine failure and the hydrogen heater failure occur, the turbine and the hydrogen heater should be stopped. If it is impossible to restart the turbine and the heater, the cryogenic hydrogen system should be warmed up and discharge hydrogen to atmosphere by using the normal warm-up mode.

2) Interlock 2 : Hydrogen pump failure and blanket pressure failure

When the hydrogen pump failure and the blanket pressure failure occur, the hydrogen pump, the hydrogen heater, and the turbine will be stopped. Especially, the pressure rise in the blanket indicates that the hydrogen leak to the blanket layer would occur. And, when the blanket pressure is decreased down to atmospheric pressure, it is impossible to have hydrogen in the cryogenic hydrogen system. We should stop the hydrogen leak by discharging hydrogen quickly and the helium refrigeration system will be warmed up. The hydrogen circulation system will be warmed up by purged gas and inserting helium gas into the vacuum layer.

3) Interlock 3 : Hydrogen pressure rise

When the relief valves and the rupture disks installed in the hydrogen circulation system function, the hydrogen pump, the hydrogen heater and the turbine will be stopped. If the soundness of the hydrogen circulation system is confirmed, the hydrogen circulation system is warmed up by using the normal warm-up mode or the emergency discharging mode.

4) Interlock 4 : Occurrence of hydrogen leak

When hydrogen leaks to atmosphere, we should stop the hydrogen leak by discharging hydrogen quickly. After the hydrogen concentration becomes lower than the explosive lower limit of 4%, the hydrogen circulation system should be warmed up by the emergency discharge mode and the helium refrigeration system will be independently warmed up.

5) Interlock 5 : Vacuum failure

When the pressure in the vacuum layer increases, all the components are stopped except the compressor. The heat flow into the cryogenic hydrogen rapidly increases and the relief valve or the rupture disk will function. Accordingly, hydrogen is automatically discharged without exceeding the design pressure of the hydrogen circulation system as well as the emergency discharge mode.

6) Interlock 6 : Compressor failure.

Immediately after the compressor failure occurs, the turbine also stops. Since it is impossible to maintain the cryogenic hydrogen system at the rated condition, we should warm up the cryogenic hydrogen system. The hydrogen circulation system is warmed up by using the emergency discharge mode. The helium refrigeration system is naturally warmed up by stopping the vacuum pump.

2.4.4 Design for System Operation

(1) Fluctuation and control at the time of proton beam on/off

The hydrogen circulation system forms a closed loop filled with cryogenic hydrogen, and the density in the loop is almost constant. Namely, the pressure change in the loop is expected to follow the behavior at the constant density. Referring to the phase diagram of para-hydrogen at fluid regime as shown in Fig. 2.4.28, it can be found that even the temperature change of a few kelivins might raise the pressure by factor 10 or so along the constant density line. In the case of 1-MW proton beam injection in JSNS, the hydrogen temperature in the moderators will rise from 17 K up to 20 K in the cryogenic hydrogen circulation condition, which brings about severe pressure change. Therefore, the control of the cryogenic fluid in the closed loop should pay more attention to such pressure change. The nuclear heating raises the hydrogen temperature in the moderators and the heated hydrogen circulates by flow velocity from the moderators to the heat exchanger. Then the heated hydrogen should expand and reduce its density, which occupies in a part of the closed loop. The loop pressure, therefore, increases significantly. In order to mitigate the pressure change by beam on/off, JSNS adapts the hybrid pressure control system that consists of the heater and accumulator. The best control techniques were estimated by the analysis when proton beam is turned on and off, as follows.

1) Analysis model

The calculation model and flow are shown in Fig. 2.4.29 for beam shut-off case. In the hydrogen loop, the points of heat input and output are a moderator, a heater and a heat exchanger. The heat inputs from other parts, a pump, a ortho-para converter and pipes.are ignored. The volume is therefore divided to three parts for this calculation. M_1, M_2 and M_3 indicate the masses at the corresponding area in the hydrogen loop. Q_2 and Q_3 are the heat loads of moderators and heater, respectively. The characters of ρ and V are the density and the volume. When the pressure behavior analysis is done in this study, the following assumptions are used for the calculation. In the initial condition, the fluid density and the pressure are constant. When the heat load is changed, the heated part appeares in the moderator and moves downstream with the flow velocity. The boundary between the heated part and non-heated part exists, which means a diffusion of boundary is neglected.

This boundary moves by the flow velocity, too. The flow velocity of 0.162 kg/sec and the output temperature of helium–hydrogen heat exchanger are constant. The nuclear heating is set to be 3.75 kW for 1-MW proton beam. The initial condition and volumes are listed in Table 2.4.32. When the heat load fluctuation occurs such as proton beam shut-off, a safety range of operational pressure is as follows. In the hydrogen loop of JSNS, the hydrogen is maintained at supercritical pressure state. This is due to the policy to prevent hydrogen phase shift. The operational pressure of hydrogen is necessary to be maintained higher than the critical pressure, which is 1.29 MPa. On the other hand, it should not exceed the setting pressure 1.7 MPa of release valve that is installed in the system. If the hydrogen pressure goes over 1.7 MPa, hydrogen discharge startes. This situation is regarded as an unstable situation because the hydrogen circulating system of JSNS cannot form the closed loop any longer. In this analysis the stability range of pressure is set from 1.4 to 1.6 MPa, since the safety margin of about 0.1 MPa is taken in the condition mentioned above.

The procedure of analysis is explained, taking an example of proton beam shut-off. In numerical analysis, physical properties were calculated by GASPAK library, Cryodata Inc, in each time step such as 0.01 sec. As for the heater control, there is time delay to start, to stop or to transfer heat to hydrogen. It was handled as dead time of 1.0 sec in this analysis. Calculation was carried out roughly in three stages. The first stage was the initial state, which corresponded to the left-end of the plot in Fig. 2.4.30. In the first stage, the total mass was calculated for each volume using initial conditions and heat load. The total mass of system is constant because of the closed loop system. It is 18.1 kg.

$$Mt = M_1 + M_2 + M_3 = \rho_1 V_1 + \rho_2 V_2 + \rho_2 V_3 \tag{2.4.52}$$

Here, ρ_2 is a function of pressure and enthalpy, h_2

$$\rho_2 = \rho(P_1, h_2)\, ,\quad h_2 = (Q_2 / \dot{m}) + h_1 \tag{2.4.53}$$

h_1 is enthalpy of V_1. In the second stage, the mass of local volume generated by heat load change was estimated as the same way in the first stage. The hydrogen pressure was searched so that the total mass would be conserved. This process was repeated until the hydrogen loop reaches the third stage. The third stage is final and the hydrogen pressure is recovered to stable pressure. The most severe heat fluctuation for the cryogenic hydrogen system will take place when 1-MW proton beam is turend on or of. These two cases should be analyzed.

2) Pressure control method

Fig. 2.4.30 indicates an effect of hybrid pressure control system. In this figure, 1-MW proton beam is injected at 0 second. The dashed dotted curve is hydrogen pressure without control system. The dashed curve means the pressure controlled with the heater alone and the dotted curve means the pressure controlled with the heater only with accumulator. The solid line shows the result of the hybrid control system.

Without pressure control, hydrogen pressure reaches to 3.7 MPa. By control only with heater, hydrogen pressure exceeds 2.1 MPa. It is not sufficient at all. However, this is the result when the output heater is set to be equal to the heat load of proton beam. The reason for this setting is described in the following subsection. The difference between hybrid control and accumulator only is quite small. Namely the effect of heater in hybrid pressure control system looks small. The heater compensates the whole heat balance in this system and the effect on the pressure is small. However, the heater is effective to control the cryogenic hydrogen system, because the heat load of the hydrogen system is maintained uniformly with the heater. Therefore it is not necessary to control the helium refrigerator and the cryogenic hydrogen system can be kept very stable.

The policy of the heater control is an important point relating to the stability of the hydrogen system. If the power of heater is larger than nuclear heating, the hydrogen pressure can be maintained constantly. However, the cooling power of helium refrigerator has to be changed. Accodingly we adopted the accumulator for passive pressure control so that we may control only the hydrogen loop. The cooling power of helium refrigerator is set from the total heat loads of the cryogenic system first and the refrigerator is operated so that the temperatue of the hydrogen-helium heat exchanger inlet would be constant.

There is another issue about the heater control, an input timing of the heater. As already mentioned, the position of the heater is different from those of the moderators. There is time delay when the local fluctuation in the moderators travels to the heater. During this fluctuation, the heater should be controlled so that the pressure is kept constant. Therefore it is necessary to estimate the timing of heater control in order to keep the hydrogen system stable.

Fig. 2.4.31 indicates the result when 1-MW proton beams are injected. The Solid curve and the chained curve are the cases that the heater power is set to be 3.75 kW (= heat load by 1-MW proton beam). The timings to turn off the heater are different in these cases. In the case of the solid curve, the power of heater is turned off 30 seconds after the beam injection. For this 30-second period, the volume V_2 is warmed up by proton beams. Therefore, there is no change in heat load. In the case of the chained curve, the power of heater is turned off at the same timing with the beam injection. It takes 90 seconds till the heat travel to the whole V_2 and V_3 and the pressure gets stable. Comparing these two control cases, the former is more profitable, because the hydrogen pressure can be stabilized much quicker after beam injection.

The dashed curve in Fig. 2.4.31 is the result when the heat load of proton beams in the whole hydrogen system is compensated with the heater. The power of heater is 4.8 kW. Although the hydrogen pressure finally recovers to the initial value, the fluctuation of the hydrogen pressure is not small as compared with the former two cases. The refrigerating capacity has to be also controlled depending on the heater output in this case.

Fig. 2.4.32 shows the result when 1-MW proton beams are shut off. In this situation, the timing of heater power to turn on is the same as the beam shut-off but the heater power is different. The pressure drops in the same way but the pressure recovery behavior is different. From the viewpoint of the stability in the pressure sequence, the solid line is better.

In order to keep the hydrogen system stable, it is desirable that the fluctuation duration is shorter when the fluctuation of pressure is the same. Therefore the power of heater is set equal to the heat load of beams and the control is started when the local fluctuation in the moderators reaches the heater.

In the system of JSNS, the heater supplies only the amount of the thermal load fluctuation of the proton beams and the refrigerating capacity is not changed. When the thermal load of the whole hydrogen system fluctuates, the accumulator can mitigate the pressure change with the hybrid pressure control mechanism. Therefore the heater power can be set equal to the heat load of the beams.

3) Summary

In the case that the proton beam is turned on or off, the hydrogen pressure can be maintained within the allowable operation range with the hybrid pressure control system, combining the heater and accumulator. For the hydrogen pressure control, the heater power is set equal to the heat load fluctuation of the proton beams. There are many cases left, which are not simulated as a change of proton beams in this work. The hybrid pressure control system is however effective for 1-MW proton beam, which is the maximal heat load for JSNS hydrogen system.

(2) Study of cool-down operation process

We develop a one-dimensional simulation code of the cryogenic hydrogen system to study its cool-down process. The simulation model is shown in Fig. 2.4.33. Although the transfer lines to the moderators are parallel configuration, we consider them as a single loop for the sake of shorthand. The initial total hydrogen inventory is 223 ℓ. The bellows of the accumulator is fully expanded. The hydrogen circulation system is made of stainless steel except the moderators, which are made of aluminum alloy. The total weight of the stainless steel is estimated to be 1500.0 kg, and the weight of aluminum alloy is 22.85 kg. The hydrogen circulation system is divided into 855 grids, which correspond to 0.117 ℓ per grid.

The numerical procedure is as follows.

a) The heat transfer coefficient between piping and hydrogen are calculated by using Dittus-Boelter correlation.
b) Pressure drop in piping is estimated by Brasius equation.
c) Correlation of the pressure drops in the components, the hydrogen heater, the accumulator, the ortho-para converter and the heat exchanger, was derived by using the results of CFD analysis. The pressure drops were calculated by the correlation.
d) Circulation flow rate by the pump was estimated by the pressure drop in the hydrogen loop and the predicted pump properties.
e) Time step is set to be 0.01 sec.

The cool-down process analyses were performed by using the temperature differences in the heat exchanger as follows,

- Temperature difference is 40 K from 300 K to 40 K
- Temperature difference is 4 K from 40 K to 35 K
- Temperature difference is 1 K from 35 K to 32 K
- Temperature difference is 3 K below 32 K

The simulation result is shown in Fig. 2.4.34. When the hydrogen circulation system is cooled in the above conditions, the hydrogen is cooled down to 40 K within 13 hours. It takes 5 hours to pass through its critical temperature. Around its critical temperature, the specific heat of hydrogen has maximum. Therefore, the condensation of supercritical hydrogen requires large refrigeration power from the helium refrigerator. As show in Fig. 2.4.34(b), it is confirmed that the cooling power required from the hydrogen circulation system is lower than the refrigeration power in the condition of the temperature differences. We found that the above temperature control at the heat exchanger enabled the hydrogen circulation system to cool down the hydrogen to the rated condition within 21 hours.

2.4.5 Safety Design

2.4.5.1 Safety design concept

(1) Safety features of system

First of all, this system is a high-pressure gas facility with hydrogen and helium. The system includes a helium cryogenic system, which is the typical high-pressure gas facility. Many helium cryogenic systems have ever been constructed in Japan and a lot of experiences their safety operations have been compiled. A room temperature hydrogen gas facility is nowaday a common technology.

Secondly, the system uses hydrogen at cryogenic temperature. Hydrogen is also combustible even in the cryogenic temperature. A typical instance to use cryogenic hydrogen is a rocket engine test facility. Japan has ever constructed five hydrogen liquefaction facilities and two of them are running now. Liquid hydrogen liquefied there is mainly used for rocket fuel. Recently, the developments of hydrogen-fueled car consume a lot of liquid hydrogen. Therefore, the experiences of cryogenic hydrogen safety treatment and technology have been accumulated.

Lastly, the most unique characteristic of the system is to circulate cryogenic hydrogen through the moderators in high neutron irradiation environment. Such instances are found in the JRR-3 cold neutron source at JAEA in Japan, the ISIS cold neutron source at RAL in UK, the LANSCE cold neutron source at LANL and the SNS at ORNL in USA. However, the neutron beam power in JSNS is six or seven time higher than the others. Especially, the circulation flow rate of the system is the largest in the world. Accordingly, the hazard potentials of the system are much larger than the conventional cold neutron sources.

(2) Safety policy

Since conventional technology is used for the most parts of the system, the law and the safety standards can be directly applied to the system without any problems. The design and fabrication complied with the law and the standards secure a basic safety of the system. Indeed, the system is subject to the Japanese high-pressure gas safety law.

On the other hand, the special feature of the system is to circulate a large amount of cryogenic hydrogen into the highly neutron-irradiated area. Then, the hazard potential in such condition should be evaluated and the unique measures should be implemented if necessary. A fail-safe design should be also required to maintain safety for off-normal conditions and failures of the system.

Accordingly, the basic safety policy for the system is to perform the safety design subject to the law and the safety standards, to carry out the fail-safe design and to adopt the safety structure against any cases of hazard.

2.4.5.2 Safety design conditions - hazard potential

(1) Hydrogen gas explosion

The explosion range of hydrogen concentration in air is quite wide, from 4.1% to 75%. Especially, the air mixture with the hydrogen concentration range from 18.3% to 59% generates detonation. Ignition energy of hydrogen is also very small and just 0.6 mJ in air. Then, it can be said that hydrogen might explode easily by a tiny bit of energy. The total combustion energy of the system due to the hydrogen inventory is calculated to be around 3 GJ, assuming stoichiometric combustion reaction in air. Accordingly, the system should provide an explosion-proof structure for hydrogen.

(2) Explosion due to pressure rise by cryogenic hydrogen vaporization

Cooling and thermal insulation maintain a cryogenic fluid in the cryogenic state. Loss of cooling or thermal insulation brings about considerable vapor of cryogenic fluid and then the volume would expand significantly. For instance, the volume of the saturated liquid hydrogen at 1 bar expands by around 800 times at room temperature at 1 bar. Assuming that the cryogenic fluid becomes stuck in the piping and that losses of cooling and thermal insulation simultaneously occur, the piping will easily explode by pressure rise. Therefore, the piping line with valves at the both ends must be equipped with a pressure release mechanism such as a pressure relief valve or a rupture disk. Their blowing diameter sizes should be designed to keep the pressure within the design value of piping for the pressure-rise hazard.

(3) Activation and radiation damage by neutron irradiation

Hydrogen circulates through the highly neutron-irradiated area and then the hydrogen and the contaminations in the hydrogen will be simultaneously irradiated. The materials of the moderators and their hydrogen piping lines are also irradiated. Therefore, it requires that the activation intensities of the circulating hydrogen and its contaminations are evaluated, as well as the radiation damages and lifetimes of the materials.

2.4.5.3 Required unique safety measures

(1) Reduction of hydrogen inventory

In order to reduce hazard potentials of the system, the best way is to reduce the hydrogen inventory in the system. This policy is the first priority in our safety design. Therefore the system is designed to separate into two stages such as a refrigeration stage by helium and a circulation stage by hydrogen as shown in Fig. 2.4.35. The helium cryogenic system only refrigerates hydrogen through the heat exchanger in the hydrogen circulation unit and the refrigerated hydrogen is circulated through the moderators by cryogenic hydrogen pumps. Heat received at the moderators is carried to the heat exchanger and then it is transferred to the helium refrigerator. Hydrogen is only used in the circulation stage, permitting a considerable reduction of hydrogen inventory. A hydrogen gas tank is also removed in the system to reduce the hydrogen inventory, which imposes us to fill up hydrogen gas at every start of operation by using a hydrogen gas container that is temporally prepared at the outside of the building. On the contrary, hydrogen is discharged to the air at every stop of operation. This seems to be wasteful, but the stop and start operations are performed every half year and the cost of hydrogen gas is fortunately not significant. And exchanging hydrogen gas at every half year will have an effect to clean up a small amount of radioactive contaminations. In consequence, the hydrogen inventory in the system is determined to be 226 litters that coincide with the maximum hydrogen weight of 16.5 kg.

(2) Use of a blanket structure with inert gases

Oxygen will condense on the surface of the cryogenic hydrogen piping when occurring air leak in a conventional vacuum-insulated piping. On the contrary, the hydrogen leak will take place from the hydrogen piping and it will mix with such condensed air in the irradiation circumstance. These situations rise up a high hydrogen explosion potential. Consequently, a blanket structure, which forms an inert gas layer to wraps the vacuum-insulated hydrogen piping as indicated in Fig. 2.4.36, is adopted for the hydrogen piping system. This structure can prevent the hydrogen leak from mixing with air.

A blanket with helium gas, called as helium–gas blanket, is equipped at the vacuum insulated cryogenic hydrogen piping. That allows blocking the air leak into the vacuum insulation of the piping when the blanket piping breaks. And even the case that the air penetrates to the vacuum insulation area through the blanket and then the helium gas in the blanket also penetrates with the air, the air leak will be immediately found if a helium leak detector is installed in the vacuum-insulation piping system. On the contrary, when hydrogen leak takes place, the leaked hydortgen will be very difficult to mix with air through the double walls such as the vacuum-piping wall and the blanket-piping wall. Preparation of vacuum gages and a mass analyzer in the piping system provides sensitive hydrogen leak detection.

The blanket for room-temperature hydrogen piping uses nitrogen gas as a blanket gas because nitrogen has a good electric insulation compared to helium. The blanket with nitrogen gas, called as nitrogen-gas blanket, forms a hydrogen explosion-proof structure as well as the helium blanket and monitoring the blanket-gas pressure change can check the leak of air or hydrogen.

(3) Blanket piping area

The areas of adopting the blanket piping system are shown in Fig. 2.4.37. The areas are determined to consider the following criteria.

Helium blanket area: the piping where cryogenic hydrogen flows continuously or temporarily.

Nitrogen blanket area: the piping where room-temperature hydrogen flows.

(4) Pressure release system

Mentioned in 2.4.5.2(2), relief valves and rupture disks will be prepared in the system to prevent a pressure-rise explosion when the cryogenic fluid piping are plugged. Their blowing diameters are also designed not to surpass their design pressure. On the other hand, hydrogen gas in the system cannot be released in the building. A hydrogen gas release system is prepared, allowing directly releasing hydrogen to the air as shown in Fig. 2.4.38. There are two pressure stages of manifolds, which are connected to the high pressure output and the low pressure output of the relief valves and the rupture disks, and a main release piping line that leads the gas to the outside of the building.

To ensure safety for releasing hydrogen gas, the following measures are taken.

1) Prevention of air ingress to the release piping

Nitrogen gas continuously flows in the release piping line, avoiding air ingress into the piping line. The cryogenic hydrogen is occasionally released in the manifolds and then nitrogen might be iced. Therefore, helium gas is selected for a filled-up gas in the manifolds.

2) Dilution of hydrogen-gas release

In Fig. 2.4.38, the release piping line is connected to the stack of the MLF building where a large amount of ventilating air such as 1.6×10^5 Nm^3/h blows. Accordingly, hydrogen gas will be controlled to release with its concentration of less than 4% by diluting it with the blowing air in the stack. Allowable hydrogen releasing is calculated to be 6.52×10^3 Nm^3/h, which is large enough to release hydrogen in the short time.

In case of electric power failure, the air-ventilation system will only operate partially by using back-up electricity. Ventilating air is reduced to be 6.52×10^3 Nm^3/h and the hydrogen release is limited to less than 634 Nm^3/h. Such hydrogen releasing will be automatically controlled in the release valve system.

3) Source of ignition

The released hydrogen is mixed with the ventilating air in the stack and there is a possibility of the hydrogen concentration of higher than 4% in its mixing process. As the ventilating air passes through an air-cleaning filter, dusts that might cause an ignition are removed. There are no electric equipments in the stack. Therefore, hydrogen explosion will not occur in the stack. Even if the ignition is occurred, fire will stop at the flame arrestor that is installed in the release piping. Then, the fire will not be propagated to the hydrogen circulation system.

(5) Activation by neutron irradiation

1) Activation of hydrogen

Cold source operation time in a year is planned to be 5000 hours and the source will be stopped every 2500-hours operation, corresponding every half year, to exchange a target vessel. In that time, the cryogenic system is also stopped and all hydrogen in the system is renewed.

Considering hydrogen activation, it can be estimated to calculate the tritium production in hydrogen through the 2500-hours operation with the proton beam power of 1 MW. It is found that the produced tritium should correspond to the radioactivity of 0.8×10^7 Bq. Since the amount of the radioactivity is discharged into the air through the stack taking more than an hour, an average radioactivity in the released air is diluted to be 4.9×10^{-5} Bq/cm^3 due to the ventilating air of 1.6×10^5 Nm^3/h in the stack. This is smaller by less than one hundredth than the legal allowable value of 5.0×10^{-3} Bq/cm^3.

2) Activation of contaminations in hydrogen

Since four nines hydrogen will be used in the system, contamination in the hydrogen is calculated to be 100 ppm. All the contamination is here assumed to be air.

Hydrogen is cooled down to around 20 K and air components of the contamination are freezed and condensed in the heat exchanger. Only helium as the contamination is circulated through the moderators. Therefore, activation of the contamination is provided to evaluate the tritium production from the helium through the neutron irradiation. Note that all about helium with the atomic number of three, so called “helium-3”, should transform to the tritium.

Helium concentration in air is around 5 ppm and helium-3 is 1.4 ppm in helium, respectively. Remember that the air in the hydrogen should be 100 ppm, and then the helium-3 concentration in the hydrogen is estimated to be 7×10^{-16} that is very small. On the other hand, the ratio between the nuclear reaction cross-section to transform deuterium into tritium and that to transform helium-3 into tritium is evaluated to be around 1×10^{7}. Multiplying the helium-3 concentration by the above ratio, which is 7×10^{-9}, provides a comparison of the hydrogen activation intensity with the contamination activation intensity. Accordingly, radioactivity of the contamination in the hydrogen is so smaller by around eight orders than that of the hydrogen, which is certainly negligible.

(6) Selection materials and evaluation of lifetime

1) Moderator materials

Neutron irradiation intensity at the moderator position is evaluated to be 3 dpa par year at the maximum. Consequently, a radio-proof material is required as the moderator material. The 6061-T6 aluminum alloy is selected due to one of the radio-proof materials and we evaluated a lifetime of this alloy to use the following neutron irradiation test data. After irradiated by thermal neutron with the level of around 4×10^{27} n/m^3, the fracture toughness of the alloy was reduced to be 25% compared with that of unirradiated case[2.4-3)]. These tests were performed by the HFIR in ORNL. Converting this irradiation level to a dpa unit, it results in the value of 19 dpa[2.4-4)]. Therefore, the lifetime is defined to be 6.3 years and then we determine that the moderators should be replaced every six years.

2) Piping materials

The alloy piping is also used in high irradiation area around the moderators. But a stainless steel piping displaces the aluminum alloy piping at the irradiation intensity of 0.03 dpa per year that is smaller by one hundredth than that of the moderator position.

According to the irradiation data for the 316L stainless steel, which are supplied by LLNL and LANSCE, embrittlement becomes prominent at the intensity of 3 dpa[2.4-5)]. Then, this value is defined to be the maximum allowable irradiation intensity and the lifetime is calculated to be 100 years. Therefore, the use of the stainless steel at that position will not cause any problems. Practically such piping line will be removed with the moderators every six years. Irradiation intensity at the parts that are not removed is less than 0.003 dpa per year.

3) Effect of radiation on insulation in moderator and hydrogen transfer line

Cryogenic hydrogen piping lines use layered multi-layer insulators, called as MLI, in their thermal insulation vacuum layer to reduce thermal radiation heat load. However, it is known that the MLI would discharge several gases under an irradiation environment. Such gases from the MLI will slightly degrade the vacuum or will be absorbed and frozen at the outer surface of the cryogenic hydrogen piping. The gases also include oxygen and nitrogen as a part of air components. It is reported that the frozen oxygen will transform ozone and ozonous free radical in irradiation environment. And the free radical is known to explode easily. Therefore, we should evaluate amounts of the discharged gases in our cryogenic hydrogen piping lines with the irradiated condition.

On the other hand, an allowable value of ozone in a nuclear reactor is determined to be less than 25 mg in U.S.ACE.[2.4-6] Then, we will define this value as our allowance value of oxygen in the discharge gases.

Amount of the discharge gases from the MLI was measured by using gamma-ray irradiation test facility at the JAEA-Takasaki establishment.[2.4-7] In the tests, two types of MLI were tested such as the Polyimide base and the Polyester base. Fig. 2.4.39 shows the specifications and the installed area of MLI. MLI of Polyimide base is used in hydrogen transfer line that is irradiated up to 1 MGy. On the other hand, MLI of Polyester base is used for the transfer line that is irradiated by less than 0.1 MGy. Table 2.4.33 shows the results of the irradiation test, where the outgases that include oxygen are indicated. Table 2.4.34 shows the maximum radiation dose at each kind of MLI. These correspond to the value after 2500 hours continuous operation.

From the measurement and calculation results above the total amount of oxygen from MLI in transfer line is estimated as shown in Table 2.4.35.

Assuming that the whole oxygen will be changed to ozone, the ozone is 8.64 mg in total, which is less than the guideline. Therefore, the possibility of an explosion by outgases from MLI under radiation is negligibly small

2.4.5.4 Fail safe design for off-normal events

Preliminary scenarios for the measures of off-normal events are summarized in Figs. 2.4.40 to 2.4.43, respectively, which are categorized by the causes of the off-normal events.

(1) Off-normal events caused by proton beam

First of all, proton beam incidence and beam off operations are performed in millisecond order in the accelerator system and the beam power instantaneously rises up to the rated value of 1 MW, which provides the hydrogen moderator system with a large pulsed heat-load such as 3.75 kW and which induces a large pressure disturbance in the cryogenic hydrogen loop. According to the estimation of the phenomenon, the pressure rise is calculated to be more than 2.0 MPa after the beam incidence in the target[2.4-8]. Therefore, the cryogenic hydrogen system should require a pressure control system that can mitigate the pressure change when beam incidence or beam off occurs. However, the phenomenon is not an off-normal event but a design-based event. The cryogenic hydrogen system, of course, prepares the pressure control system that is composed of a heater system and a volume change mechanism. The heater system behaves to compensate the heat load of the proton beam and the volume change mechanism operates to absorb a partial density change by changing the hydrogen volume such as a bellow mechanism. The control system will control the pressure change at not only beam incidence and beam off but also a fluctuation of the beam power, an emergency beam off and an expected beam incident. If the pressure control system is failed, so to say, an off-normal event occurs, pressure alarm system will work and the interlock will be on. Then, the following sequences will be driven.

① The beam is compelled to stop by MPS.
② The cryogenic system is automatically stopped.
③ The hydrogen in the system is automatically discharged to air.

(2) Off-normal events caused by the composed equipment failure

Although the system is composed of a lot of components, a hydrogen circulation pump is one of the most important parts to continue a stable operation. Therefore, a redundant pump is prepared and two-pump system is adopted in the system. Considering that the start of the redundant pump, which is warm near room temperature due to no cooling flow, should disturb the cryogenic system, the following operation method is adopted; two pumps are simultaneously running with each capacity of 50% and one pump is switched to operate with 100% capacity when another one is failed.

Valve malfunction, the pressure control system failure, the helium cryogenic system failure and malfunction of the instruments are considerable as the failures in the system except the pumps. And a blockage in pipe by solidification of impurities due to the cryogenic system is also taken account. Anyhow, the degree of influence by these failures depends on the level and the location of failure. In case of a minor failure, it will be repaired during operation. But when the operator judges to stop the system, the system will be manually stopped. On the other hand, in the case that the off-normal condition will be detected and then the interlock system will be initiated, the following sequences will be performed.

a) The beam is compelled to stop by MPS.
b) The cryogenic system is automatically stopped.
c) The hydrogen in the system is automatically discharged to air.

(3) Leak from piping and components

The piping and components will be fully inspected through their manufacturing and installation process. However, we should take measures even for the case that a leak occurres. Consequently, we prepare a sensible leak detection system by using the helium gas blanket system. A helium leak detector and a mass spectrometer continually monitor the leak of helium and hydrogen from the piping and the components through their vacuum insulation layer. Sensitivity of leak is expected to be less than 10^{-4} $Pa{\cdot}m^3/s$. Accordingly, the leak at an early stage will be found and measures will be taken easily, preventing a large accident. In the case that a large leak will suddenly occur and the vacuum pressure in the piping vacuum layer will rise up rapidly, the interlock system will be initiated and the following sequences will be performed.

a) The beam is compelled to stop by MPS.
b) The cryogenic system is automatically stopped.
c) The hydrogen in the system is automatically discharged to air.

(4) Disaster

In case of power outage, the interlock is initiated and the same sequences that are mentioned above are carried out. The instrumentation system will kept working for 20 min by an uninterruptible power supply system and 90% of the hydrogen in the system will be discharged during this time. Furthermore, the valves are also designed to be controlled to release the cryogenic hydrogen to air safely in case of power outage.

Fires and earthquakes will induce automatically power outage and then the interlock will be also initiated.

2.4.5.5 Safety analysis for hydrogen leakage event

A hydrogen leak occurring at the moderator piping is anticipated to be the most dangerous leak event. Therefore, we simulate such events by computer calculation and estimate the temporal pressure rise, discharge hydrogen amounts, and so on. The calculations were performed at the following two assumptions, one is the case of the slow leak and the other is the rapid leak, respectively.

a) Slow leak (case 1)

- A small hydrogen leak will occur, which increases the vacuum pressure slowly.

And then

- Automatic relief valve, which can control the hydrogen loop pressure, is operated.
- Helium is injected into an insulation vacuum to enhance the hydrogen discharge in the moderators' section.

b) Rapid leak (case 2)

Assuming a crack occurred onto the moderators' piping,

- The hydrogen leak into the vacuum is too fast to operate the automatic relief valve.
- Safety relief valve or rupture disk functions instead of the automatic relief valve.

(1) Analysis for hydrogen discharge in case of slow leakage

In case of failures that need to stop the hydrogen system, it is necessary for the hydrogen to discharge as soon as possible. As an emergency discharge, we consider supplying helium gas into an insulation vacuum in order to break the thermal insulation vacuum slightly, which enhances the heat conduction and the hydrogen discharge and then the hydrogen discharge time should be reduced.

Above method applies to the slow leak analysis and the analysis confines to the moderators' piping. That is, a hydrogen circulation unit is still running by using a moderator bypass line but it does not supply hydrogen to the moderators. Therefore, the hydrogen volume is limited to be 91.5 ℓ in the calculation. (Total hydrogen volume in the system is 250 ℓ, for example.) Typical calculation results are shown in the Fig 2.4.44. We design a pressure rise through the discharge piping line below 0.1 MPa. Accordingly, a pressure of helium gas injection is selected to be less than 0.044 MPa. Fig. 2.4.45 shows the results with the helium gas injection pressure of 0.04 MPa. The maximum hydrogen discharge appeares to be 0.047 kg/s after around 150 sec. The concentration of hydrogen in the stack is kept below 4%. After 5 min, around 90% hydrogen in the moderator piping lines is discharged. These results satisfy the present design. It is found that the helium injection pressure of 0.04 MPa is suitable for safety release of hydrogen in the case of emergency.

(2) The pressure rise analysis for rapid hydrogen leakage to the vacuum layer[2.4-9)]

Fig. 2.4.46 shows pressure and temperature profiles for a small crack (0.2 mm^2). As soon as hydrogen leaks into the vacuum space, hydrogen pressure rapidly increases to 2.1 MPa. The cryogenic hydrogen is vented through the safety valve. In the vacuum layer, the pressure gradually increases to 0.2 MPa due to the slow leak. The rupture disk for the vacuum layer works after the safety valve works, and then the hydrogen is discharged. Once the rupture disk works, the hydrogen continued to be released until the pressure decreases to around atmospheric pressure. The pressure of helium blanket decreases down to 0.08 MPa. This is because the helium gas is cooled by the hydrogen. The temperature decreases to 250 K after 1000 sec. In this case, most of the cryogenic hydrogen is discharged from the safety valve. The hydrogen pressure and the pressure in the vacuum layer are maintained below the design pressures, respectively.

Fig. 2.4.47 shows pressure and temperature profiles for the crack size of 10.0 mm^2. With increase in the crack size, the hydrogen leak ratio to the vacuum layer also increases. The pressure rise in the hydrogen layer is slower. It takes 50 s to reach the working pressure of the safety valve. The working time of the safety valve is shorter. On the other hand, the pressure rise in the vacuum layer becomes faster. The rupture disk works within 1 sec. The release rate from the rupture disk becomes larger. In the vacuum layer, the secondary peak of the pressure appears when the hydrogen temperature goes through the critical temperature. This is due to a large density change in pseudo-critical state.

Fig. 2.4.48 shows pressure and temperature profiles for the maximum crack size of 27.5 mm^2. After such a large crack generates, the hydrogen pressure rapidly decreases to around 0.1 MPa. The hydrogen pressure rises when the hydrogen temperature approaches around the critical temperature. However, the pressure is below 2.1 MPa. The pressure in the vacuum layer immediately reaches the working pressure of the rupture disk at 0.2 MPa. In such a large crack case, the hydrogen is discharged not from the safety valve but from the rupture disk for the vacuum layer. The pressure in the vacuum layer is maintained to be below the design value of 0.2 MPa. It is concluded that the rupture disk with the diameter of 37.1 mm can discharge the hydrogen safely.

Fig. 2.4.49 indicates effect of the crack size on the maximum pressure in each layer. When the crack size is smaller than 10 mm^2, the pressure of the hydrogen reaches 2.1 MPa. The hydrogen is mainly discharged from the safety valve. The safety valve with the diameter of 16.6 mm can discharge the hydrogen without exceeding the design pressure. With increase in the crack size, the release rate from the rupture disk increases. For a crack size larger than 10 mm^2, the hydrogen pressure does not increase up to 2.1 MPa. Therefore, it is found that all the hydrogen is released from the rupture disk. With a further increase in the crack size, the pressures of the first and secondary peaks also increase. The pressure exceeds 0.2 MPa for the crack size larger than 35 mm^2. However, it is found from the analysis that the cryogenic hydrogen system is kept within the design pressures for cracks with the maximum size postulated in this analysis. The required sizes for relief devices were determined, the safety valve is ϕ42.7 mm and the rupture disk is ϕ37.1 mm, respectively.

Fig. 2.4.50 shows averaged mass flow rate of the released hydrogen for various crack sizes. For small crack size, the hydrogen is released below 0.1 kg/s after the safety valve works. When the rupture disk works, the flow rate rises temporarily. After that, the hydrogen continued to be discharged from the safety valve and the rupture disk. When the hydrogen temperature rises up to around the critical temperature, the release rate rapidly increases. With increase in the crack size, the maximum flow rate becomes larger.

The hydrogen vent line is connected to the stack, where an air flow of 1.69×10^5 Nm^3/h is released to the atmosphere, diluting the hydrogen. To keep the hydrogen concentration in the stack below the lower explosive limit of 4%, it is necessary to maintain the hydrogen release flow rate below 170 g/s. As shown in Fig. 2.4.50, the release flow rates are kept below 170 g/s for the crack sizes postulated here, although this is momentarily exceeded for the maximum crack size when the rupture disk works. It is found that the relief devices mentioned above can discharge the hydrogen safely even if such an off-normal event occurs.

References

2.4-1) R.W.Vance and H.Weinstock: Applications of cryogenic technology, Tinnon-Brown Inc., Los Angeles, 1968, pp. 45-80.

2.4-2) Superconductivity and Cryogenic Handbook, Cryogenic Association of Japan, 1993, p. 383, in Japanese.

2.4-3) J.R.Weeks et al.: Amer. Soc. for Testing and Materials, 1993, p. 1168.

2.4-4) K. Farrell: ORNL/TM-99-208, 2001.

2.4-5) S.A.Moloy et al.: Journal of Nuclear Materials, 318, 2003, pp. 283-291.

2.4-6) J.D.Gault et al.: “Ozone Formation by the Radiolysis of Liquid Nitrogen: Calculation and Measurement,” Nuclear Safety, Vol.14, no. 5, 1973, pp. 446-451.

2.4-7) M.Teshigawara et al.: Proceedings of the 69th Meeting on Cryogenics and Superconductivity, 2003, p. 88, in Japanese.

2.4-8) T.Kato et al.: “Cryogenic System Design for Cryogenic Hydrogen Moderator of the Spallation Neutron Source in J-PARC.” Proc. Int. Collaboration on Advanced Neutron Sources ICANS-XVI, Dusseldorf-Neuss, Germany, 12-15 May 2003, 2003, pp. 645-654.

2.4-9) H.Tatsumoto et al.: “Pressure Rise Analysis when a Hydrogen Pipe is Broken in the Cryogenic Hydrogen System of the Japanese Spallation Neutron Source”, CEC 2005, Vol.51, 2005, pp. 753-760.

Table 2.4.1: Estimated nuclear heating power of each moderator at the rated proton beam power

	Coupled moderator	Decoupled moderator	Poisoned moderator	Total
Volume (L)	1.54	0.97	0.97	3.84
Nuclear heating in hydrogen (W)	946	467	442	1855
Nuclear heating in vessel (W)	793	519	584	1896
Total heating in the moderator (W)	1739	986	1026	3751

Table 2.4.2: Specification for the main components in the cryogenic system

Helium refrigerator system	
Cold box	Helium compressor system
Type: Helium Brayton cycle Refrigeration capacity: 6,000 W at 17 K Supply pressure: 1.6 MPa Liquid nitrogen consumption: 103 ℓ/h	Type: Oil injection screw compressor Suction / Discharge pressure: 0.31 / 1.7 MPa Mass flow rate: 0.285 kg/s Motor ratings: 690 kW

Hydrogen circulation system	
Hydrogen circulation pump	Ortho-para hydrogen convertor
Type: Centrifugal pump Inlet temperature: 19 K (available for 300 to 17 K) Inlet pressure: 1.5 MPa (available for 0.5 to 1.8 MPa) Mass flow rate: 0.162 kg/s Pressure head: 0.12 MPa (0.162 kg/s) Revolution: 30,000 to 57,000 Adiabatic pump efficiency: more than 60%	Catalyst: Iron hydroxide ($Fe(OH)_3$) Conversion efficiency: 80% SV value for catalyzer: 3700 min^{-1} Mass flow rate: 0.162 kg/s Inlet / Outlet temperature: 19.8 / 21.2 K Inlet / Outlet ortho-para concentration: 97.2% / 99.0% Catalyst filling volume: 35 ℓ

Table 2.4.3: PFD Data of Hydrogen Loop in case of Parallel Cooling for 1.5-MPa Operation

No	m [g/s]	P (MPa)	ΔP (MPa)	Q_{HL} (W)	i (J/g)	xp (%)	T (K)
①	162.20	1.470	0.0241	36.0	-257.0	99.01	17.80
②	162.20	1.468	0.0018	11.3	-256.9	99.01	17.81
③	68.00	1.454	0.0139	4.4	-256.9	99.01	17.84
④	68.00	1.442	0.0120	3.0	-256.8	99.01	17.86
⑤	68.00	1.431	0.0116	72.5	-255.8	99.01	18.01
⑥	68.00	1.431		1744.7	-230.1	99.01	20.93
⑥’	68.00	1.431			-230.1	97.00	19.40
⑦	68.00	1.418	0.0127	135.1	-228.1	97.00	19.64
⑧	38.20	1.455	0.0127	4.4	-256.8	99.01	17.84
⑨	38.20	1.426		3.0	-256.7	99.01	17.89
⑩	38.20	1.422	0.0038	66.6	-255.0	99.01	18.11
⑪	38.20	1.422		990.1	-229.1	99.01	21.05
⑪’	38.20	1.422			-229.1	97.00	19.53
⑫	38.20	1.418	0.0041	120.7	-225.9	97.00	19.89
⑬	39.80	1.455	0.0128	4.4	-256.8	99.01	17.84
⑭	39.80	1.426		3.0	-256.7	99.01	17.89
⑮	39.80	1.422	0.0040	63.6	-255.1	99.01	18.09
⑯	39.80	1.422		1030.1	-229.3	99.01	21.03
⑯’	39.80	1.422			-229.3	97.00	19.51
⑰	39.80	1.418	0.0044	116.2	-226.3	97.00	19.84
⑱	146.00	1.418			-227.1	97.00	19.76
21	16.20	1.468	0.0003	3.3	-256.7	99.01	17.84
22	16.20	1.418		3.0	-256.5	99.01	17.93
23	162.20	1.418	0.0003	3.3	-230.0	97.20	19.60
24	162.20	1.417	0.0009	20.2	-229.9	97.20	19.61
25	162.20	1.416	0.0013	62.6	-229.5	97.20	19.66
26	162.20	1.415	0.0008	24.9	-229.3	97.20	19.68
27	162.20	1.520		460.3	-226.5	97.20	19.88
28	162.20	1.519	0.0019	27.3	-226.3	97.20	19.90
29	162.20	1.494	0.0241	20.2	-226.2	99.01	21.27
30	162.20	1.494	0.0003	6.2	-226.2	99.01	21.28
total			0.1058	5040.4			

Table 2.4.4: PFD Data of Hydrogen Loop in case of Series Cooling for 1.5 MPa Operation

No	P (MPa)	ΔP (MPa)	Q_{HL} (W)	i (J/g)	xp (%)	T (K)
①	1.630	0.052	74.9	-273.2	98.99	15.40
②	1.578		1030.1	-272.5	98.99	15.58
③	1.578	0.061	182.8	-263.2	98.99	16.86
④	1.517		990.1	-261.6	98.99	17.16
⑤	1.517	0.062	193.2	-252.6	98.99	18.29
⑥	1.455		1744.7	-250.9	98.99	18.57
⑦	1.455	0.039	242.8	-235.1	98.99	20.37
	1.455			-235.1	97.00	18.78
⑧	1.416		10.0	-233.0	97.00	19.09
⑨	1.416	0.004	27.3	-232.9	97.00	19.10
⑩	1.412	0.024	20.2	-232.6	97.00	19.13
⑪	1.388	0.001	6.2	-232.4	98.99	20.73
⑫	1.387	0.024	34.0	-232.4	98.99	20.73
total		0.267	4556.3			

Table 2.4.5: Comparison of Hydrogen Cooling Flow Pattern for Moderators

Cooling Flow Pattern		Parallel	Series
Hydrogen Circulating Flow Rate		162.2 g/s (2.25 ℓ/s)	110.8 g/s (1.48 ℓ/s)
Total Pressure Drop In Hydrogen Loop		0.106 MPa	0.267 MPa
Delivery Pressure of Hydrogen Pump		1.52 MPa	1.68 MPa
Heat Input of Hydrogen Pump		460 W	782 W
Total Heat Load in Hydrogen Loop		5,040 W	5,328 W
Helium Refrigerator Capacity		5,110 W at 17 K	5,400 W at 14.6 K
(Equivalent Refrigeration Capacity)		5,110 W at 17 K	6,340 W at 17 K
Inlet / Outlet*1 Temp. of Moderator	PM	18.09 K / 21.03 K	15.58 K / 16.86 K
	DM	18.11 K / 21.05 K	17.16 K / 18.29 K
	CM	18.01 K / 20.93 K	18.57 K / 21.20 K
Para-Hydrogen Concentration		99.01%	98.99%

*1) In case without re-conversion of para- into ortho-hydrogen

Table 2.4.6: PFD Data of Hydrogen Loop in case of 0.6 MPa Operation

No	m (g/s)	P (MPa)	ΔP (MPa)	Q_{HL} (W)	i (J/g)	xp (%)	T (K)	T_{av} (K)	ρ [kg/m^3]	vol (m^3)	M (kg)
①	162.20	0.648	0.0241	36.0	-265.8	99.03	17.80	19.49	74.01	5.00E-02	3.700
②	162.20	0.646	0.0018	11.3	-265.7	99.03	17.81	17.80	74.11	1.35E-02	0.999
③	68.00	0.632	0.0139	4.4	-265.7	99.03	17.84	17.82	74.07	1.44E-03	0.107
④	68.00	0.620	0.0120	3.0	-265.6	99.03	17.86	17.85	74.04	0.00E+00	0.000
⑤	68.00	0.609	0.0116	72.5	-264.6	99.03	18.00	17.93	73.89	9.70E-03	0.717
⑥	68.00	0.609		1744.7	-238.9	99.03	20.85	19.43	70.83	1.54E-03	0.109
⑥’	68.00	0.609			-238.9	97.00	19.34	20.09	72.50		
⑦	68.00	0.596	0.0127	135.1	-236.9	97.00	19.57	20.21	72.25	1.01E-02	0.728
⑧	38.20	0.633	0.0127	4.4	-265.6	99.03	17.84	18.71	74.03	1.44E-03	0.107
⑨	38.20	0.604		3.0	-265.5	99.03	17.89	17.86	73.99	0.00E+00	0.000
⑩	38.20	0.600	0.0038	66.6	-263.8	99.03	18.11	18.00	73.77	8.84E-03	0.652
⑪	38.20	0.600		990.1	-237.9	99.03	20.96	19.53	70.67	9.70E-04	0.069
⑪’	38.20	0.600			-237.9	97.00	19.46	20.21	72.37		
⑫	38.20	0.596	0.0041	120.7	-234.7	97.00	19.81	20.39	71.99	9.20E-03	0.662
⑬	39.80	0.633	0.0128	4.4	-265.6	99.03	17.84	18.83	74.02	1.44E-03	0.107
⑭	39.80	0.604		3.0	-265.5	99.03	17.89	17.86	73.99	0.00E+00	0.000
⑮	39.80	0.600	0.0040	63.6	-263.9	99.03	18.09	17.99	73.79	8.56E-03	0.632
⑯	39.80	0.600		1030.1	-238.1	99.03	20.94	19.51	70.70	9.70E-04	0.069
⑯’	39.80	0.600			-238.1	97.00	19.44	20.19	72.39		
⑰	39.80	0.596	0.0044	116.2	-235.1	97.00	19.76	20.35	72.04	8.92E-03	0.643
⑱	146.00	0.596			-235.9	97.00	19.69	19.73	72.12	0.00E+00	0.000
21	16.20	0.646	0.0003	3.3	-265.5	99.03	17.84	18.76	74.03	1.85E-03	0.137
22	16.20	0.596		3.0	-265.3	99.03	17.92	17.88	73.95	0.00E+00	0.000
23	162.20	0.596	0.0003	3.3	-238.8	97.20	19.52	18.72	72.30	1.85E-03	0.134
24	162.20	0.595	0.0009	20.2	-238.7	97.20	19.53	19.53	72.28	1.35E-02	0.974
25	162.20	0.594	0.0013	62.6	-238.3	97.20	19.58	19.56	72.23	5.00E-02	3.612
26	162.20	0.593	0.0008	24.9	-238.1	97.20	19.60	19.59	72.21	1.57E-02	1.135
27	162.20	0.698		465.8	-235.3	97.20	19.79	19.69	72.14	1.00E-03	0.072
28	162.20	0.697	0.0019	27.3	-235.1	97.20	19.81	19.80	72.10	1.12E-02	0.810
29	162.20	0.672	0.0241	20.2	-235.0	99.03	21.18	20.50	70.58	1.08E-01	7.623
30	162.20	0.672	0.0003	6.2	-234.9	99.03	21.19	21.18	70.50	6.74E-03	0.475
total			0.1058	5045.9						0.3364	24.270

Table 2.4.7: Pressure drop of the equipments in hydrogen circulation system

Item	Pressure drop (kPa)
Heat exchanger	4.000
Orifice	5.000
Accumulator	0.360
Heater	0.580
Valve	*
Ortho-para hydrogen converter	9.900
Filter	5.000

* The pressure drop depends on the opening ratio of a valve.

Table 2.4.8: Pressure drop in the hydrogen circulation system

<table>
<tr><th>No</th><th>item</th><th>Pipes
(kPa)</th><th>Equipments
(kPa)</th><th>Total
(kPa)</th></tr>
<tr><td>(1)</td><td>Pipe1</td><td>1.973</td><td>5.000</td><td>6.973</td></tr>
<tr><td>(2)</td><td>Ortho-para hydrogen converter</td><td></td><td>9.900</td><td>9.900</td></tr>
<tr><td>(3)</td><td>Pipe2</td><td>0.462</td><td></td><td>0.462</td></tr>
<tr><td>(4)</td><td>Heat exchanger</td><td></td><td>4.000</td><td>4.000</td></tr>
<tr><td>(5)</td><td>Pipe3</td><td>0.757</td><td></td><td>0.757</td></tr>
<tr><td>(6)-1</td><td>Coupled moderator line for supply</td><td>26.726</td><td>27.459</td><td rowspan="7">68.285</td></tr>
<tr><td>(6)-2</td><td>Coupled moderator line for return</td><td>14.100</td><td></td></tr>
<tr><td>(7)-1</td><td>Poisoned moderator line for supply</td><td>8.288</td><td>55.381</td></tr>
<tr><td>(7)-2</td><td>Poisoned moderator line for return</td><td>4.616</td><td></td></tr>
<tr><td>(8)-1</td><td>Decoupled moderator line for supply</td><td>7.824</td><td>56.092</td></tr>
<tr><td>(8)-2</td><td>Decoupled moderator line for return</td><td>4.369</td><td></td></tr>
<tr><td>(9)</td><td>Bypass line</td><td>1.455</td><td>66.830</td></tr>
<tr><td>(10)</td><td>Pipe4</td><td>2.149</td><td></td><td>1.576</td></tr>
<tr><td>(11)</td><td>Heater</td><td></td><td>0.580</td><td>0.580</td></tr>
<tr><td>(12)</td><td>Pipe5</td><td></td><td></td><td>0.573</td></tr>
<tr><td>(13)</td><td>Accumulator</td><td></td><td>0.360</td><td>0.360</td></tr>
<tr><td>(14)</td><td>Pipe6</td><td>1.533</td><td>5.000</td><td>6.533</td></tr>
</table>

Table 2.4.9: Nuclear heating in each moderator

	Coupled Moderator (W)	Decoupled Moderator (W)	Poisoned Moderator(W)
Hydrogen	946	467	442
Al vessel	793	519	447
Cd poison	0	0	137
Total	1739	986	1026

Table 2.4.10: Heat load results for pipe

No.	from	to	Length (m)	O.D. of pipe (m)	I.D. of vacuum layer (m)	MLI density (layer/m)	T_{high} (K)	T_{low} (K)	Q (W)
Hydrogen Circulation unit : 45.1 W									
1	Pump	O/P converter	5.50	4.27E-02	-	5700	300	20	1.33E+01
2	O/P converter	Heat Exchanger	3.30	4.27E-02	-	5700	300	20	7.96E+00
3	Heat Exchanger	Manifold	4.30	4.27E-02	-	5700	300	20	1.04E+01
4	Manifold	Heater & Accumulator	2.80	4.27E-02	-	5700	300	20	6.76E+00
5	Heater & Accumulator	Pump	2.80	4.27E-02	-	5700	300	20	6.76E+00
Coupled Moderator : 60.7 W									
21	Manifold	Terminal box	12.00	2.50E-02	3.00E-02	5700	20	20	0.00E+00
22	Terminal box	Coupler	2.59	1.90E-02	9.56E-02	5700	300	20	5.89E-01
23	Coupler		0.83	1.90E-02	1.08E-01	0	300	20	1.54E+00
24	Coupler	para -> coaxial	3.85	1.90E-02	6.60E-02	0	300	20	6.76E+00
25	para -> coaxial	CM vessel	3.73	2.20E-02	2.70E-01	0	20	20	0.00E+00
26	CM vessel	para -> coaxial	3.73	4.40E-02	5.30E-02	0	300	20	1.21E+01
27	para -> coaxial	Coupler	3.85	1.90E-02	6.60E-02	0	300	20	6.76E+00
28	Coupler		0.83	1.90E-02	1.08E-01	0	300	20	1.54E+00
29	Coupler	Terminal box	2.59	1.90E-02	9.56E-02	5700	300	20	5.89E-01
30	Terminal box	Manifold	12.00	5.20E-02	6.00E-02	5700	300	20	3.08E+01
Poisoned Moderator : 53.2 W									
41	Manifold	Terminal box	12.00	2.50E-02	3.00E-02	5700	20	20	0.00E+00
42	Terminal box	Coupler	2.05	1.90E-02	9.56E-02	5700	300	20	4.66E-01
43	Coupler		0.23	1.90E-02	1.08E-01	0	300	20	4.25E-01
44	Coupler	para -> coaxial	3.58	1.90E-02	6.60E-01	0	300	20	7.14E+00
45	para -> coaxial	PM vessel	1.95	2.20E-02	2.70E-02	0	20	20	0.00E+00
46	PM vessel	para -> coaxial	1.95	4.40E-02	5.30E-02	0	300	20	6.32E+00
47	para -> coaxial	Coupler	3.58	1.90E-02	6.60E-01	0	300	20	7.14E+00
48	Coupler		0.23	1.90E-02	1.08E-01	0	300	20	4.25E-01
49	Coupler	Terminal box	2.05	1.90E-02	9.56E-02	5700	300	20	4.66E-01
50	Terminal box	Manifold	12.00	5.20E-02	6.00E-02	5700	300	20	3.08E+01
Decoupled Moderator : 53.8 W									
61	Manifold	Terminal box	12.00	2.50E-02	3.00E-02	5700	20	20	0.00E+00
62	Terminal box	Coupler	1.87	1.90E-02	9.56E-02	5700	300	20	4.25E-01
63	Coupler		0.23	1.90E-02	1.08E-01	0	300	20	4.28E-01
64	Coupler	para -> coaxial	3.67	1.90E-02	6.60E-01	0	300	20	7.33E+00
65	para -> coaxial	DM vessel	2.06	2.20E-02	2.70E-02	0	20	20	0.00E+00
66	DM vessel	para -> coaxial	2.06	4.40E-02	5.30E-02	0	300	20	6.67E+00
67	para -> coaxial	Coupler	3.67	1.90E-02	6.60E-01	0	300	20	7.33E+00
68	Coupler		0.23	1.90E-02	1.08E-01	0	300	20	4.28E-01
69	Coupler	Terminal box	1.87	1.90E-02	9.56E-02	5700	300	20	4.25E-01
70	Terminal box	Manifold	12.00	5.20E-02	6.00E-02	5700	300	20	3.08E+01
Total heat load from pipes : 212.8 W									

Table 2.4.11: Heat load of various size valves

	Extension length (m)	Q (W)
25A	0.5	9.0
32A	0.5	14.0

Table 2.4.12: Heat load from pipes except for main loop

		length (m)	size	Q (W)
Relief line	for circulation unit	2	25A	0.31
	for moderators	2	25A	0.31
	for pump	2	25A	0.31
Measurement line	for O/P concentration	2	25A	0.31
	for impurity	2	25A	0.31

Table 2.4.13: Heat load from the spacer

	Parallel tube	Coupler	Moderator
Material	Teflon	SS	SS
Numbers	10×3	3×3	1×3
Heat leakage per one spacer (W)	0.1	4.58	4.77
Total heat leak (W)	3.0	41.22	14.31

Table 2.4.14: Thermal radiation heat transfer in each moderator

	Surface area (moderator) (m^2)	Surface area (vacuum layer) (m^2)	Temperature (moderator) (K)	Temperature (vacuum layer) (K)	Q (W)
Coupled Moderator	0.0872	0.1005	20	373	1.48
Decoupled Moderator	0.0622	0.0753	20	373	1.02
Poisoned Moderator	0.0622	0.0753	20	373	1.02

Table 2.4.15: Heat load in the cryogenic hydrogen circulation system

Component		Heat load (W)
Nuclear heating	CM	1739
	DM	986
	PM	1026
Radiation	CM	1.48
	DM	1.02
	PM	1.02
Pipe	in safety box	45.1
	in moderators	167.7
	other than main pipe	1.55
Heater for pressure control		22.64
Accumulator		23.09
Pump		321
Ortho-para converter		21.13
Heat exchanger		20.44
Valves		23.0
Spacer	parallel tube	3.0
	coupler	41.22
	moderator	14.31
Total		4458.7

Table 2.4.16: Calculation results of volume and inventory in the hydrogen circulation system

<table>
<tr><th colspan="2">Item</th><th colspan="2">Volume (L)</th><th colspan="2">Inventory (kg)</th></tr>
<tr><td rowspan="2">Hydrogen circulation unit</td><td>Pipes</td><td>42.2</td><td rowspan="2">150.2</td><td>3.09</td><td rowspan="2">10.99</td></tr>
<tr><td>Equipment</td><td>108.0</td><td>7.90</td></tr>
<tr><td colspan="2">The hydrogen transfer tube for CM</td><td colspan="2">26.9</td><td colspan="2">1.97</td></tr>
<tr><td colspan="2">The hydrogen transfer tube for DM</td><td colspan="2">24.3</td><td colspan="2">1.78</td></tr>
<tr><td colspan="2">The hydrogen transfer tube for PM</td><td colspan="2">24.2</td><td colspan="2">1.77</td></tr>
<tr><td colspan="2">Total</td><td colspan="2">225.6</td><td colspan="2">16.51</td></tr>
</table>

Table 2.4.17: Volumes of the pipes in the hydrogen circulation unit

No.	From	To	ID (mm)	OD (mm)	L (m)	V (ℓ)
1	Hydrogen circulation Pump	Ortho-para hydrogen converter	38.7	42.7	5.5	6.5
2	Ortho-para hydrogen converter	Helium- hydrogen heat exchanger	38.7	42.7	3.3	3.9
3	Helium- hydrogen heat exchanger	Manifold of inlet	38.7	42.7	3.0	3.5
6	Manifold of inlet		30.0	34.0	15.0	10.5
7	Manifold of outlet	Heater	38.7		6.1	7.2
8	Heater	Accumulator	38.7		4.3	5.1
9	Accumulator	Hydrogen circulation Pump	38.7		4.7	5.5
Total						42.2

Table 2.4.18: Volumes of equipment in the hydrogen circulation unit

Item	Volume (ℓ)
Heater	27.8
Accumulator	44.2
Ortho-para Hydrogen converter	32.1
Helium-hydrogen heat exchanger	3.4
Hydrogen circulation pump	0.5
Total	108.0

Table 2.4.19: Volumes of hydrogen transfer tubes for CM

No.	From	To	ID (mm)	OD (mm)	L (m)	V (ℓ)
1	Manifold of inlet	Terminal box	23.0		12.0	5.0
2	Hydrogen transfer tube for CM		―			8.9
4	Terminal box	Manifold of outlet	32.0	49.0	12.0	13.0
Total						26.9

Table 2.4.20: Volumes of hydrogen transfer tubes for DM

No.	From	To	ID (mm)	OD (mm)	L (m)	V (ℓ)
1	Manifold of inlet	Terminal box	23.0		12.0	5.0
2	Hydrogen transfer tube for DM		－			6.3
4	Terminal box	Manifold of outlet	32.0	49.0	12.0	13.0
Total						24.3

Table 2.4.21: Volumes of hydrogen transfer tubes for PM

No.	From	To	ID (mm)	OD (mm)	L (m)	V (L)
1	Manifold of inlet	Terminal box	23.0		12.0	5.0
2	Hydrogen transfer tube for PM		－			6.2
4	Terminal box	Manifold of outlet	32.0	49.0	12.0	13.0
Total						24.2

Table 2.4.22: Design condition of the cryogenic hydrogen circulation pump

Design items	Condition	Note
Circulation fluid	Sub-cooled liquid to supercritical	
Inlet temperature	19 K	Available for 300～17 K
Inlet pressure	1.4 MPa	Available for 0.1～1.9 MPa
Mass flow	0.18 kg/s	
Pump head	0.12 MPa	
Design pressure	2.0 MPa.(G)	

Table 2.4.23: Three basic design databases on the supercritical helium pump

	Specific velocity	Pressure coefficient	Flow coefficient
Type-1	345	0.4	0.44
Type-2	285	0.4	0.44
Type-3	860	0.2	0.12

Table 2.4.24: Cryogenic hydrogen pump design result for each type

	Revolution (rpm)	Impeller velocity (m/s)	Impeller diameter (m)
Type-1	41,700	63.8	0.029
Type-2	34,400	63.8	0.035
Type-3	103,900	90.2	0.017
Experience	20,000<*N*<80,000	*u*<100	*D*>0.02

Table 2.4.25: Cryogenic hydrogen pump design result

Design revolution	Maximum revolution	Design impeller speed	Design impeller dia.
35,000 rpm	50,000 rpm	64 m/s (Max. 92 m/s)	0.035 m

Table 2.4.26: Latest specifications of the hydrogen pump

Mass flow rate	0.162 kg/s
Pump head	0.12 MPa
Adiabatic efficiency	more than 50%
Operation pressure	0.1～1.8 MPa
Operation temperature	300～17 K
Driving	Induction motor with inverter
Bearing	Foil type self acting gas bearing
Revolution	57,000 rpm max

Table 2.4.27: Design data of accumulator

		Inner Bellow	Outer Bellow
Type		Welding double walls	Molding double walls
Fluid	Inner	He	He
	Outer	Hydrogen	Vacuum
Temrerature (K)		17 ~ 312	17 ~ 312
Pressure (MPa)	Inner	−0.103 ~ 2.0	−0.103 ~ 2.0
	Outer	−0.103 ~ 2.0	−0.103 ~ 2.0
Maximum differential pressure (MPa)	Inner	2.1013 (in: 2.0, out: −0.1013)	2.1013 (in: 2.0, out: −0.1013)
	Outer	−2.1013 (in: −0.1013, out: 2.0)	−0.4013 (in: −0.1013, out: 0.3)
Operation Pressure (MPa)	Inner	1.5	1.5
	Outer	1.5	−0.1003
Operation temperature (K)		17	17
Variable volume (ℓ)		3.5	−
Diameter (mm)	Inner	217	59
	Outer	257	80
Stroke (mm)		80	80
Material		Inconel 718	SUS316L
Designe life time		10^6 strokes	10^6 strokes

Table 2.4.28: Design condition of heat exchanger

Fluid	Helium	Hydrogen
Flow Rate	307.1 [g/s]	162.2 [g/s]
Warm end Temp. / Pressure	1.57 [MPa] / 20.12 [K]	0.67 [MPa] / 21.19 [K]
Cold end Temp. / Pressure	1.59 [MPa] / 16.97 [K]	0.65 [MPa] / 17.8 [K]
Exchanged Heat	5930 [W]	
ΔT_{LM}	0.945 [K]	
Net Thermal Rating $A*U$	6275 [W / K]	
Allowable Pressure Drop	0.02 [MPa]	0.02 [MPa]

Table 2.4.29: Design data of heat exchanger

Fluid	Helium	Hydrogen
Density ρ [g/cm^3]	4.11×10^{-2}	7.24×10^{-2}
Viscosity μ [g/cm·s]	4.03×10^{-5}	1.54×10^{-4}
Specific Heat C_p [J/g·K]	6.103	8.935
Prandtl number P_r	0.796	1.385
Fin Height H [cm]	0.508	0.508
Fin Thickness t [cm]	0.0203	0.0203
Fin Pitch P [cm]	0.1155	0.1155
Number of Plate Layers n_1	9	8
Number of Fin Layers n_2	9	8
Number of End Fin Layers n_3	2	0
Effective Width W [cm]	17.0	
Af [cm^2]	61.48	54.65
De [cm]	0.159	0.159
G [g/s·cm^2]	4.99	2.97
Re	1.972×10^4	3.068×10^4
j-factor j_T	5.8×10^{-3}	1.15×10^{-2}
h [W/cm^2·K]	0.208	0.246
S_1 [cm^2/cm]	224.1	224.1
S_2 [cm^2/cm]	1149	1293
S_3 [cm^2/cm]	287.1	0
Fin η	0.587	0.562
End Fin η'	0.319	-
S [cm^2/cm]	990.1	950.8
$h*S$ [W/K·cm]	205.9	233.9
$A*U$ [W/K·cm]	109.5	
Length L' [cm]	57.3	
Thermal Design Margin [%]	22	
Effective Length L [cm]	70	

Table 2.4.30: Specifications of hydrogen transfer lines

Item	Unit	Layer					
		Supply H_2	Vacuum	Return H_2	Vacuum	Helium	Light water
Pressure	MPa	2.1	0.2	2.1	0.2	0.2	0.4
Temperature	K	15	15	15	15	313	313
Length	m	30	30	30	30	30	10
Inner/Outer Diameter1*1)	mm	–/21	25/30	34/46	52/64	70/75	–/–
Inner/Outer Diameter2*2)	mm	–/19	22/32	27/39	44/61	65/72.1	76.3/84.9
Heat loss*3)	W	100					
Pressure drop*4)	MPa	0.024					

*1) hydrogen transfer line

*2) moderator's line

*3) design value of heat loss at one line

*4) design value of pressure drop at one line

Table 2.4.31: List of control panels of hydrogen system

panel name	control unit	setting room
hydrogen control central panel	total control	MLF central control room
relay terminal panel	electric relay	Large components handling room
gas analysis panel	gas analysis	Large components handling room
vacuum control panel	vacuum unit	Large components handling room
hydrogen pump panel	hydrogen pump	Large components handling room
hydrogen heater panel	hydrogen heater	Large components handling room
cold box panel	He refrigerator	Large components handling room
gas leak detector panel	hydrogen leak detector	Large components handling room
local control panel	electric power supply	Cryogenic H_2 components room
temperature convert panel	temperature sensor	Cryogenic H_2 components room
He compressor panel	He compressor	No.1 He compressor unit room
reactor start panel	high voltage supply for compressor	No.1 He compressor unit room
cold water panel	cold water unit	side of cold water unit

Table 2.4.32: Hydrogen initial value

Pressure (MPa)	1.5
Temperature (K)	17
V_1 (ℓ)	41.2
V_2 (ℓ)	58.9
V_3 (ℓ)	133.2

Table 2.4.33: Measurement of amounts of discharged gases from Polyimide and Polyester under irradiation

MLI	H_2O	CO	O_2	CO_2
Polyimide	2.0×10^{-7}	1.0×10^{-7}	2.5×10^{-9}	5.0×10^{-8}
Polyester	3.7×10^{-8}	2.0×10^{-6}	3.9×10^{-9}	8.7×10^{-6}

(unit : mol/MGy/g-MLI)

Table 2.4.34: The doses of the neutron and gamma-ray in Polyimide area and Polyester area

MLI area	Polyimide area	Polyester area
Neutron dose (Gy)	1.0×10^{6}	2.5×10^{3}
γ -ray dose (Gy)	2.5×10^{4}	2.5×10^{4}
Total of radiation dose (Gy)	1.03×10^{6}	2.75×10^{4}

Table 2.4.35: Calculation results of amounts of oxygen in discharged gases

MLI area	Polyimide area	Polyester area
Radiation dose (Gy)	1.03×10^{6}	2.75×10^{4}
Amount of oxygen in discharged gases (g/MGy/g-MLI)	6.48×10^{-6}	3.11×10^{-4}
Surface area of MLI (m^2)	32.12	32.83
Weight for unit area (g/m^2)	18.375	16.8
Weight of MLI (g)	590.18	551.52
Subtotal of oxygen (mg)	3.92	4.72
Total oxygen (mg)	8.64	

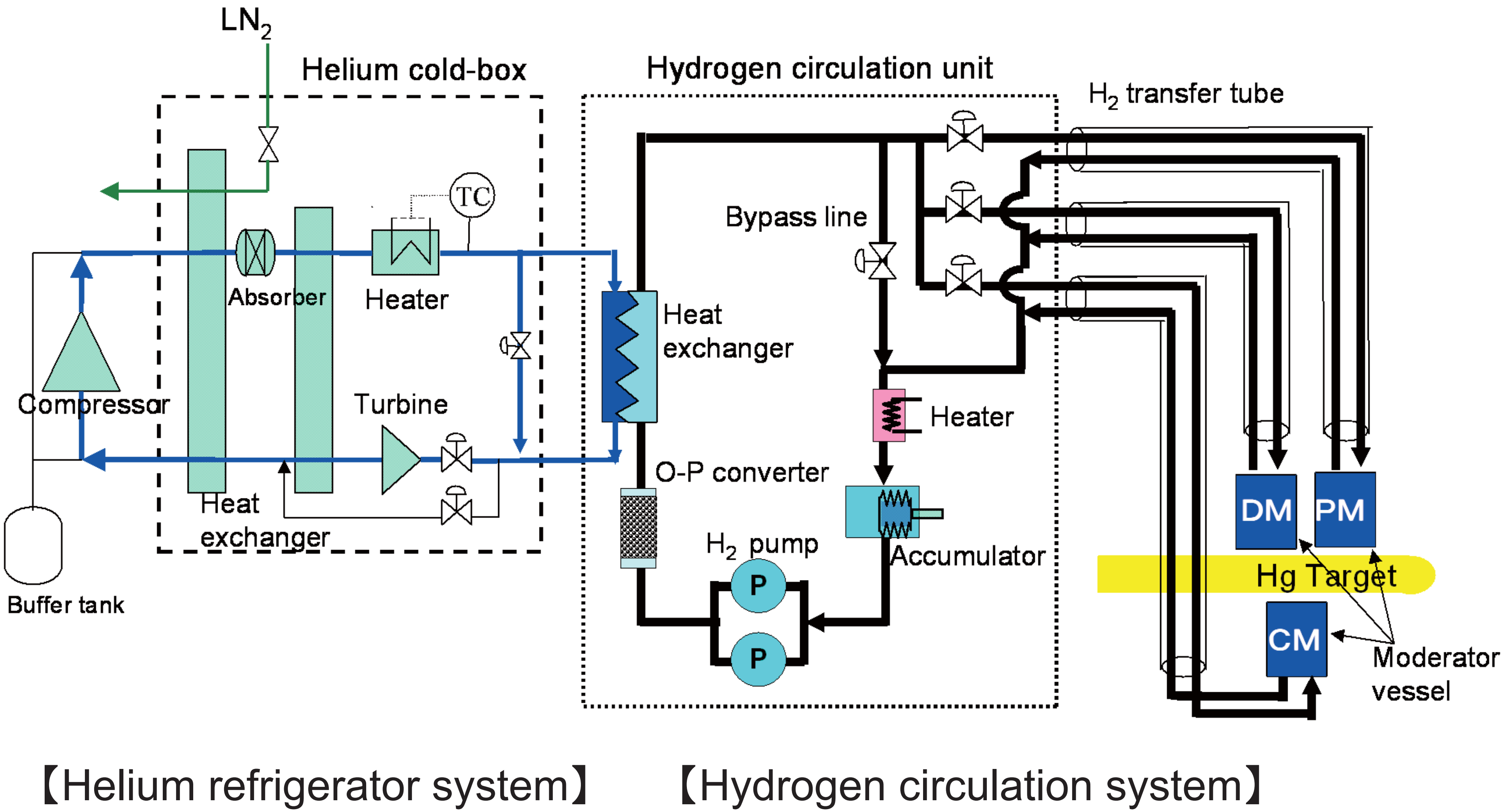

Fig.2.4.1: Schematic configuration of the cryogenic system in JSNS

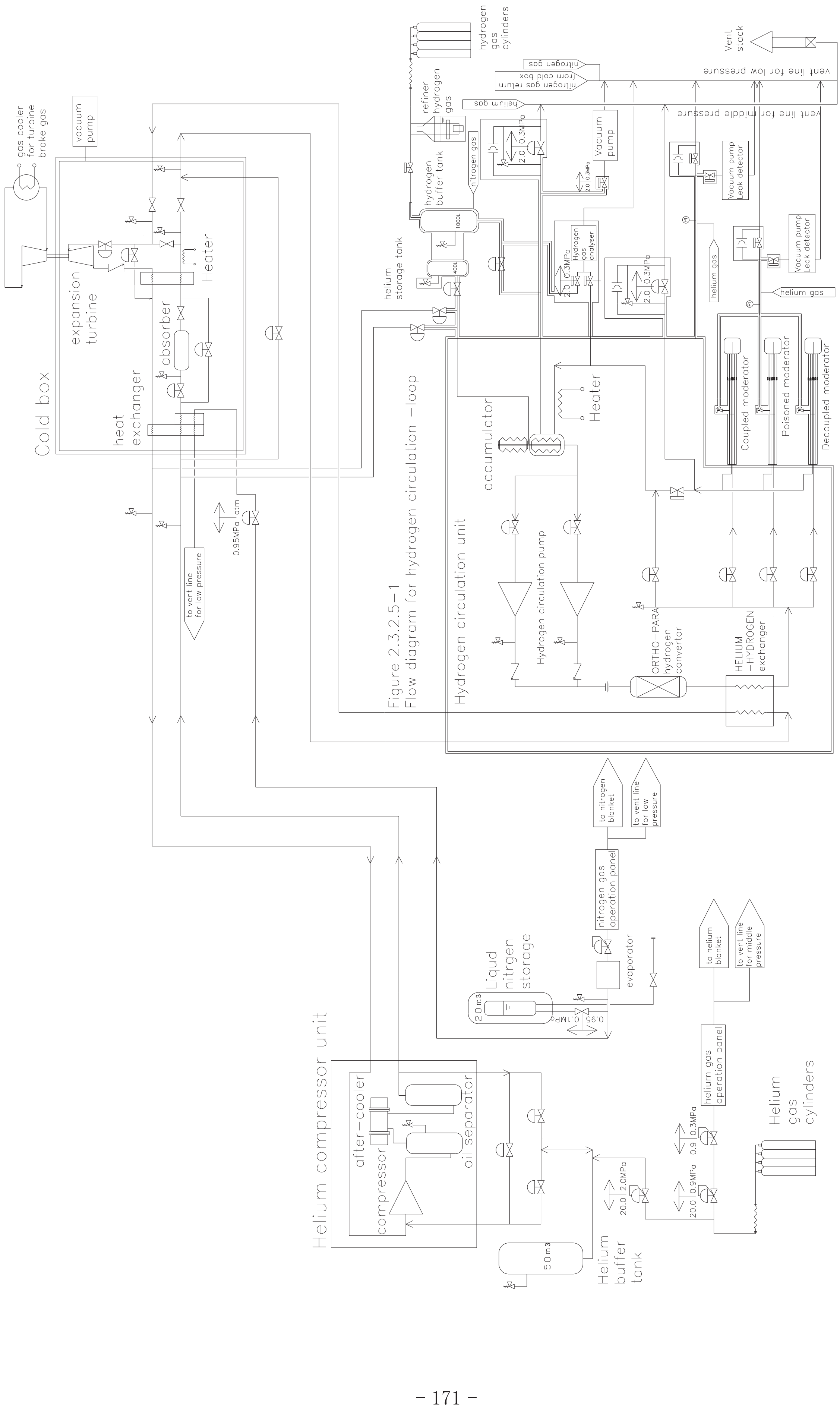

Fig. 2.4.2: Detailed flow diagram of the cryogenic system

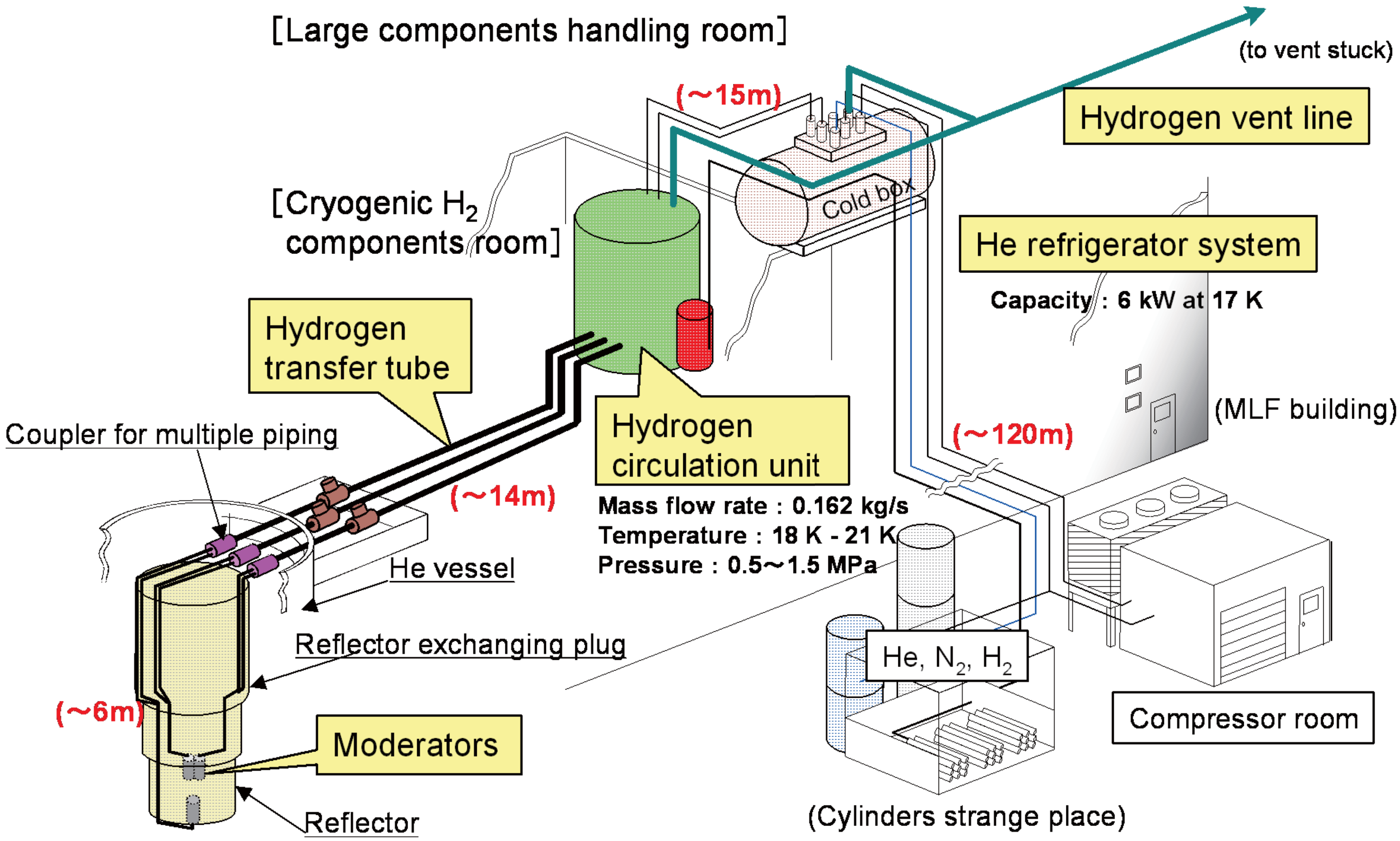

Fig. 2.4.3: Layout of the cryogenic system at MLF building

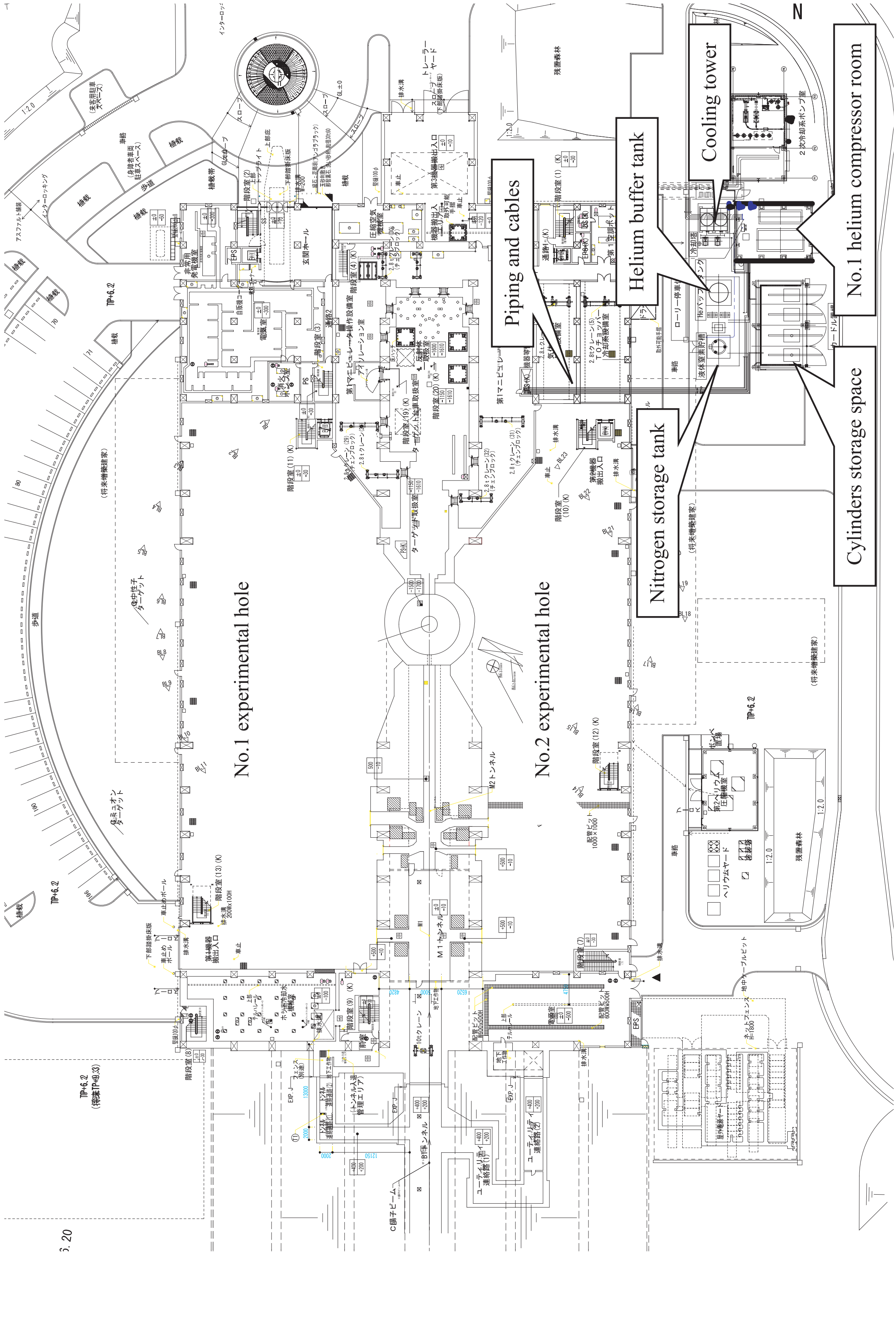

Fig. 2.4.4: Materials and Life Science Experimental Facility building (1st floor)

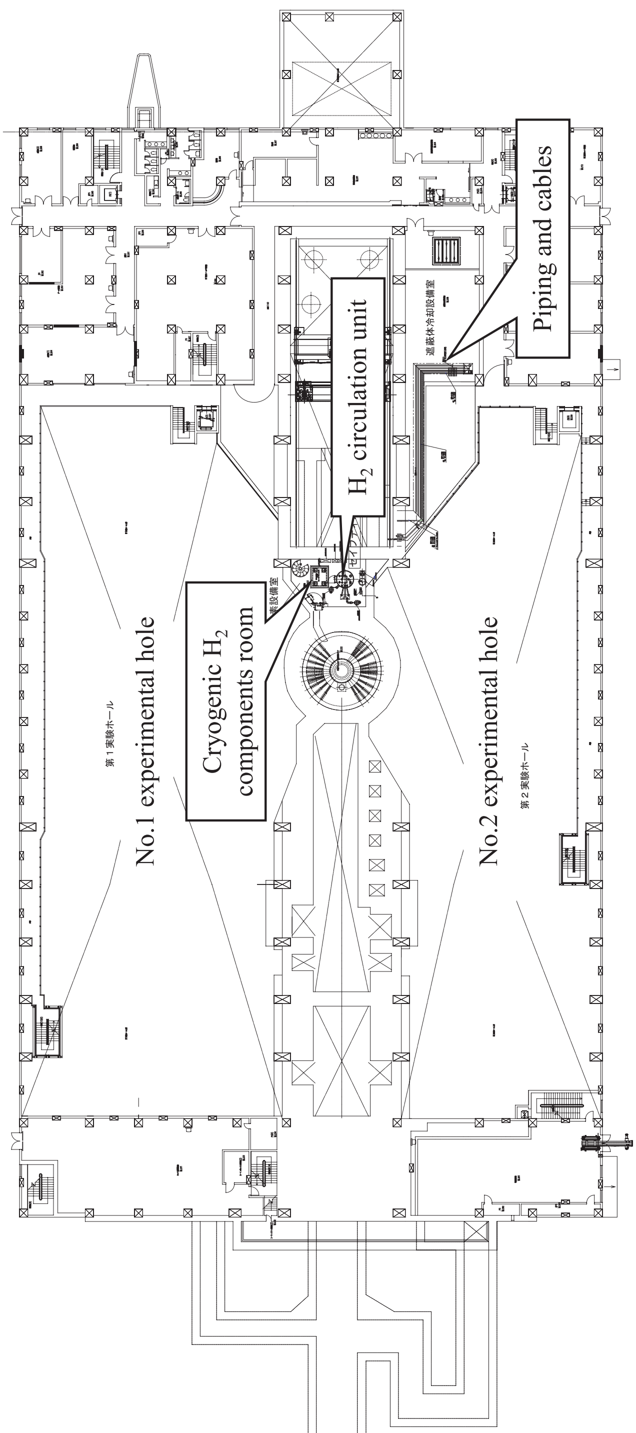

Fig. 2.4.5: Materials and Life Science Experimental Facility building (2nd floor)

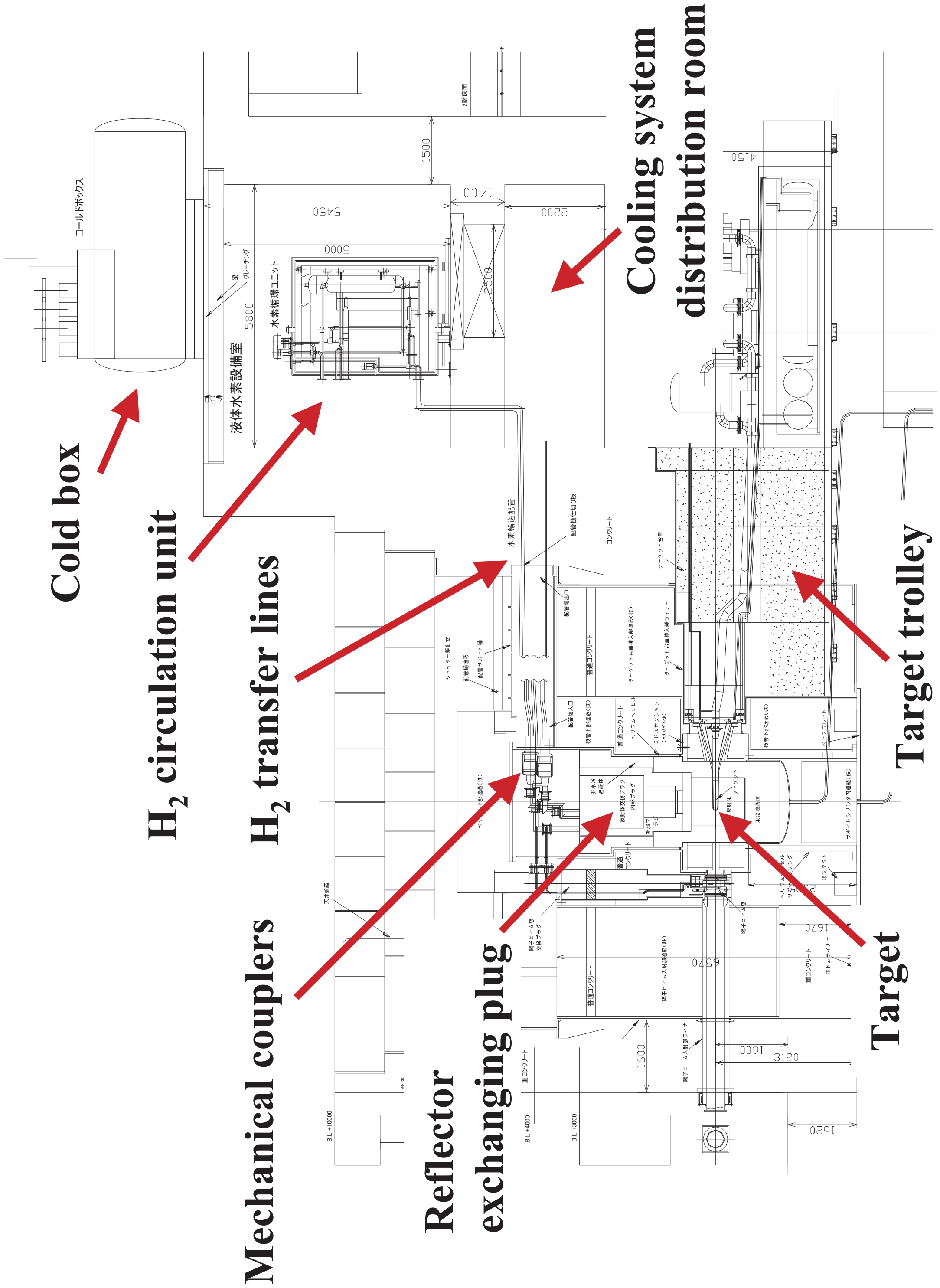

Fig. 2.4.6: Cross section around spallation neutron source

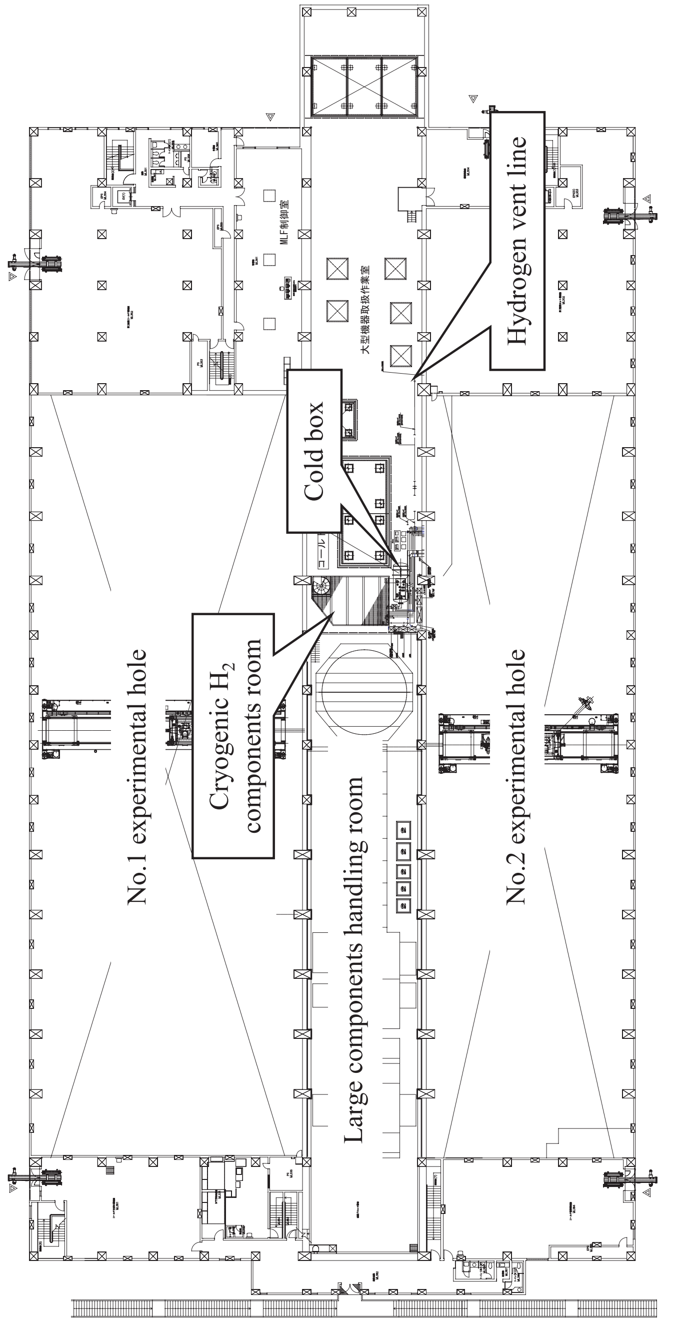

Fig. 2.4.7: Materials and Life Science Experimental Facility building (3rd floor)

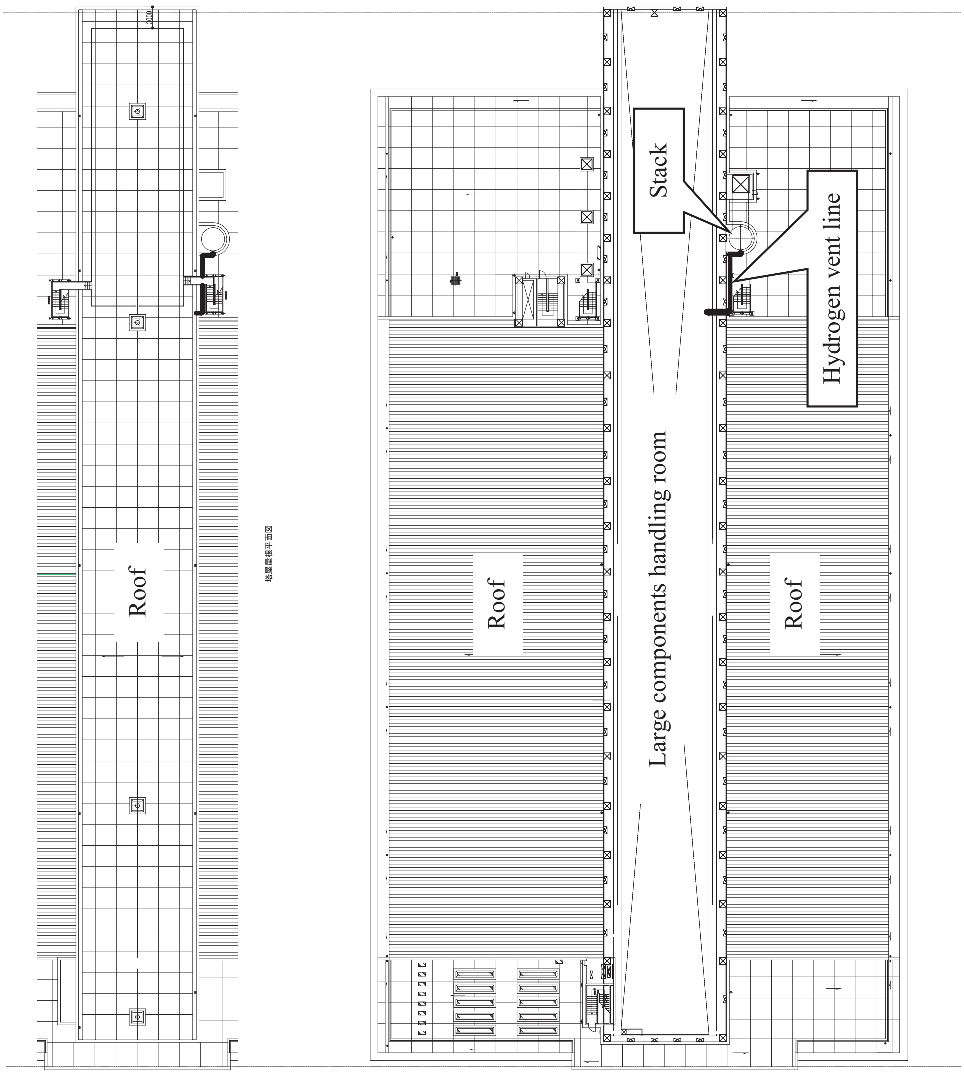

Fig. 2.4.8: Materials and Life Science Experimental Facility building (roof)

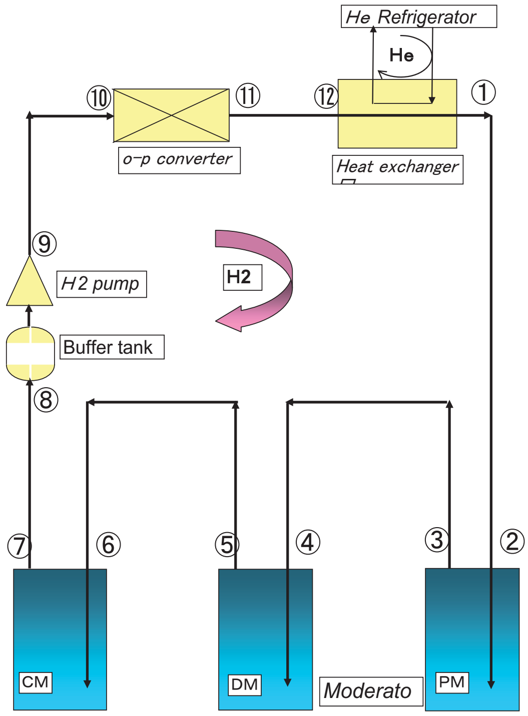

(a) Series cooling system

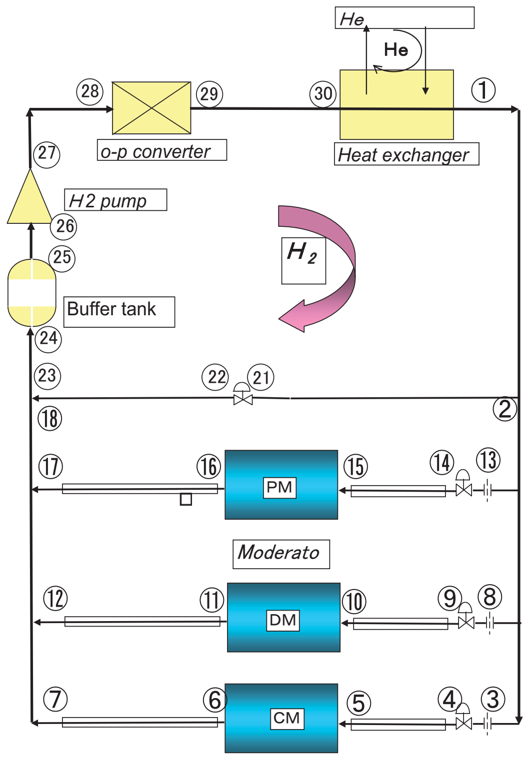

(b) Parallel cooling system

Fig.2.4.9: Analytical model

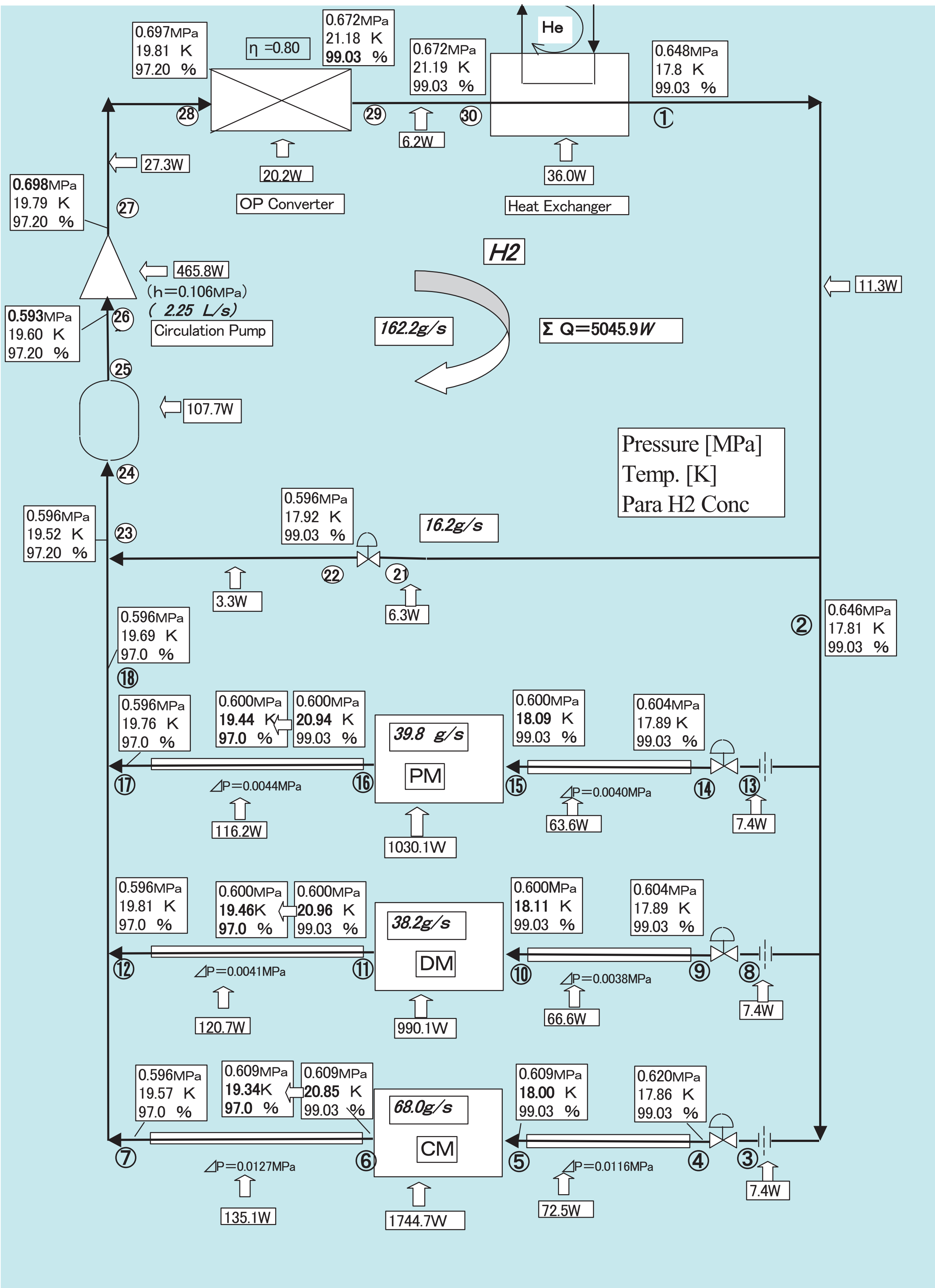

Fig.2.4.10: Process Flow Diagram in case of 0.6-MPa Operation

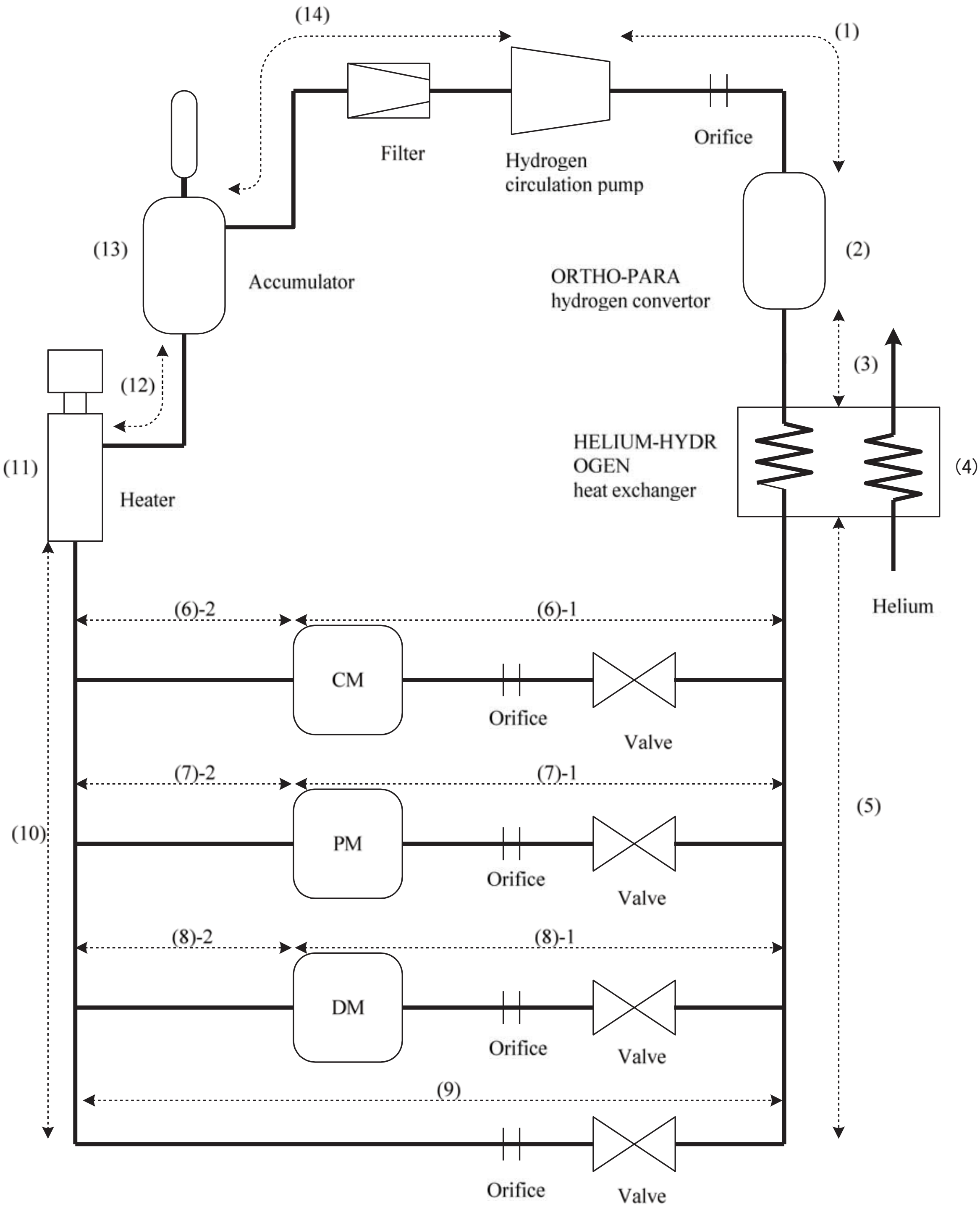

Fig. 2.4.11: Reference of the calculated pressure drops in this system

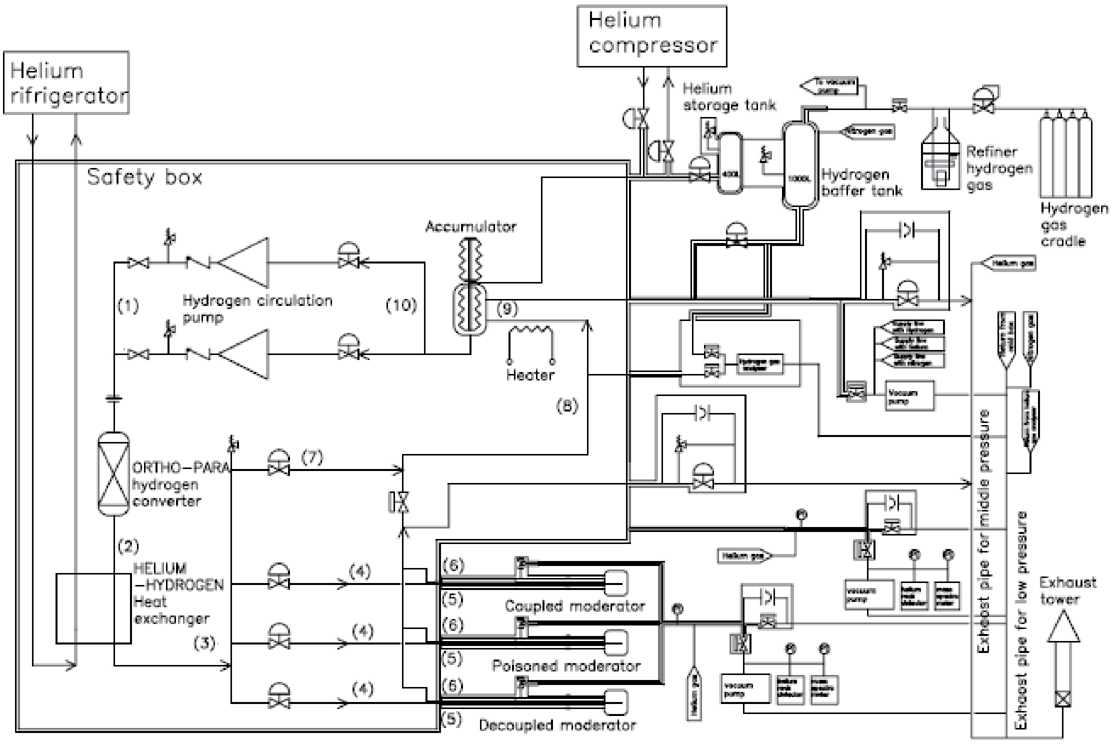

Fig. 2.4.12: Flow diagram of the hydrogen circulation system

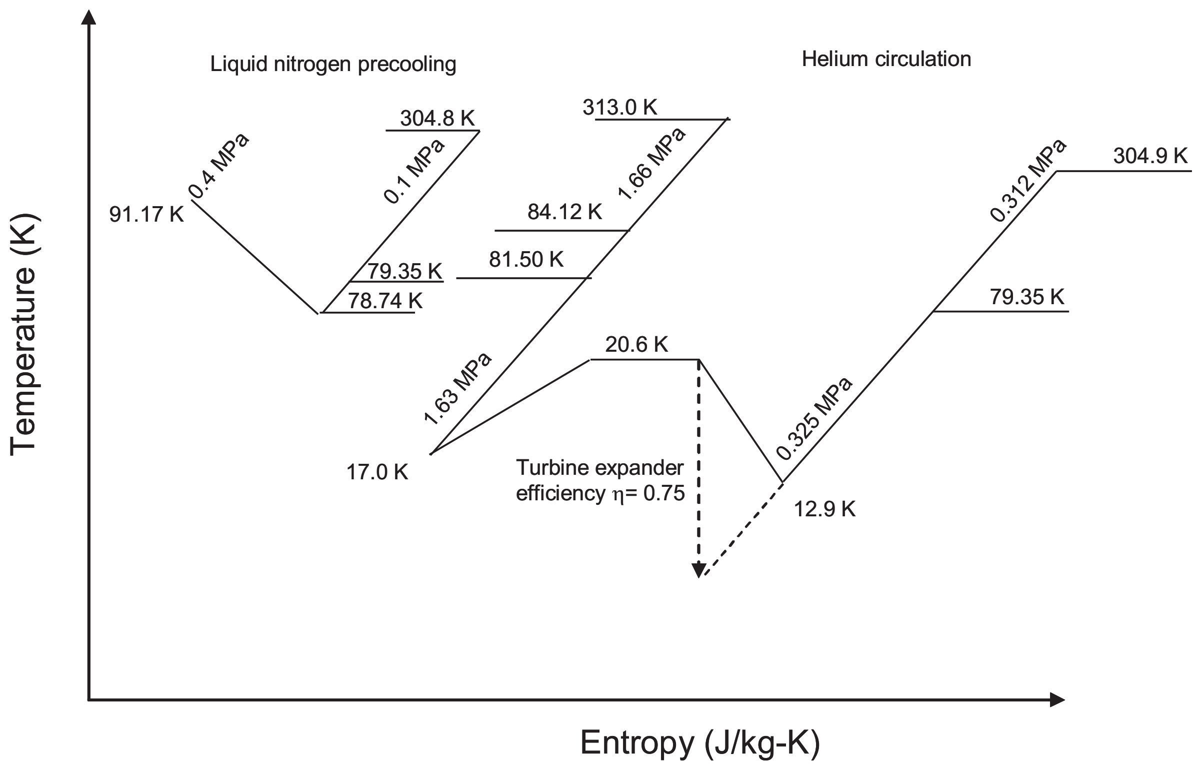

Fig. 2.4.13: T-S diagram of the helium refrigeration system

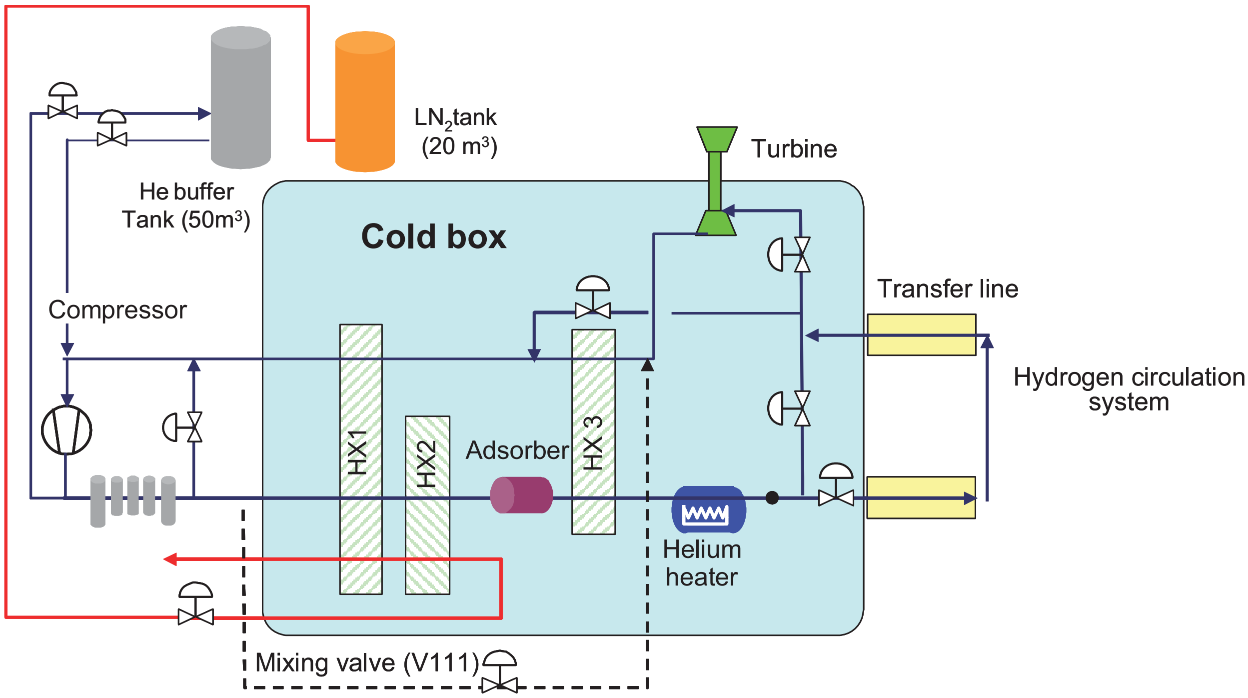

Fig. 2.4.14: Schematic of the helium refrigeration system

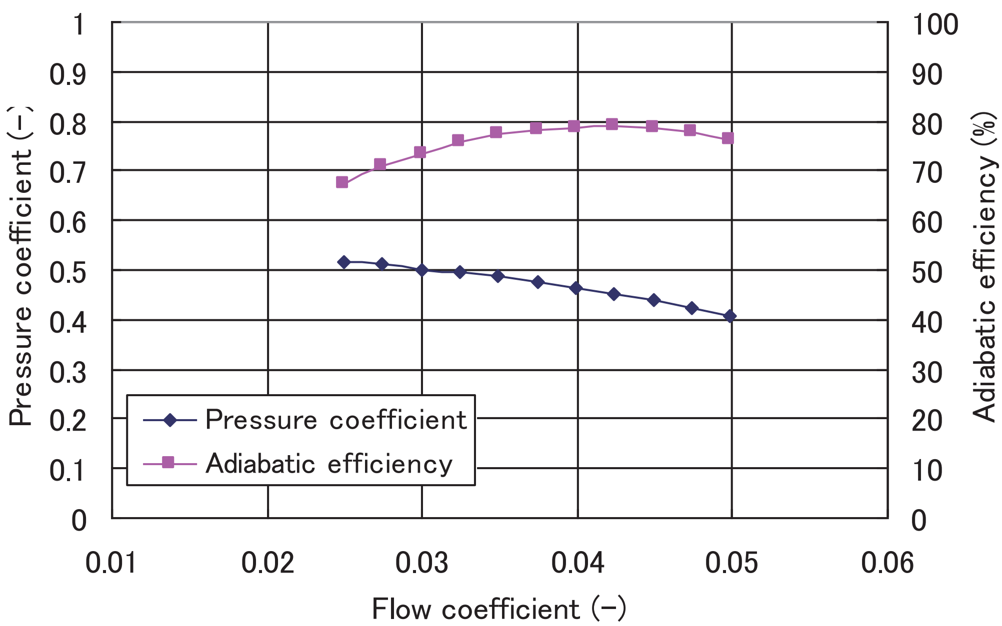

Fig. 2.4.15: Non-dimensional performance curve of the designed hydrogen pump.

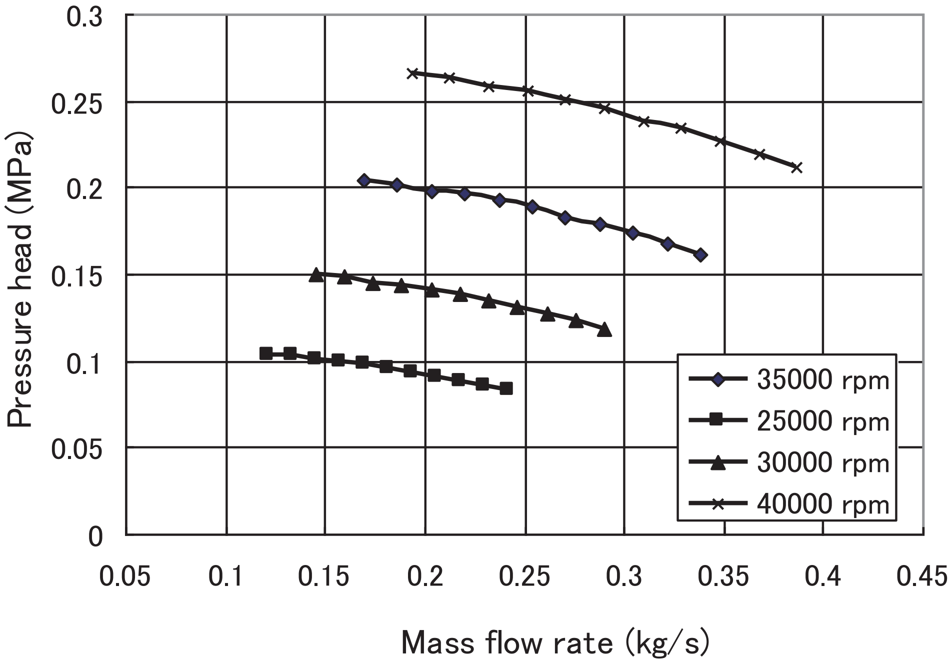

Fig. 2.4.16: Estimated pump performance with several revolutions at 1.4 MPa and 19 K.

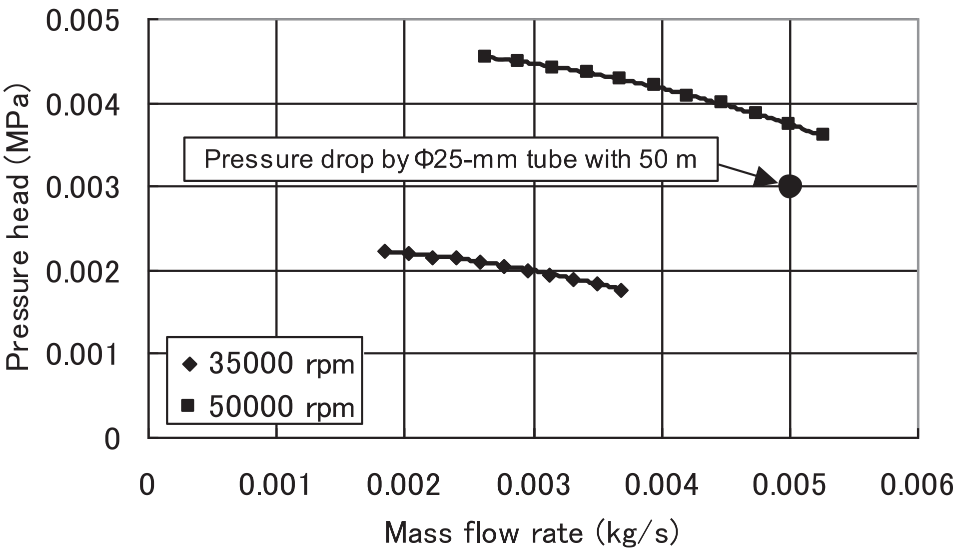

Fig. 2.4.17: Estimated pump performance at room temperature (300 K) and 1.0 MPa, the estimated pressure drop at the tube size of ϕ25-mm tube with 50 m is also over plotted.

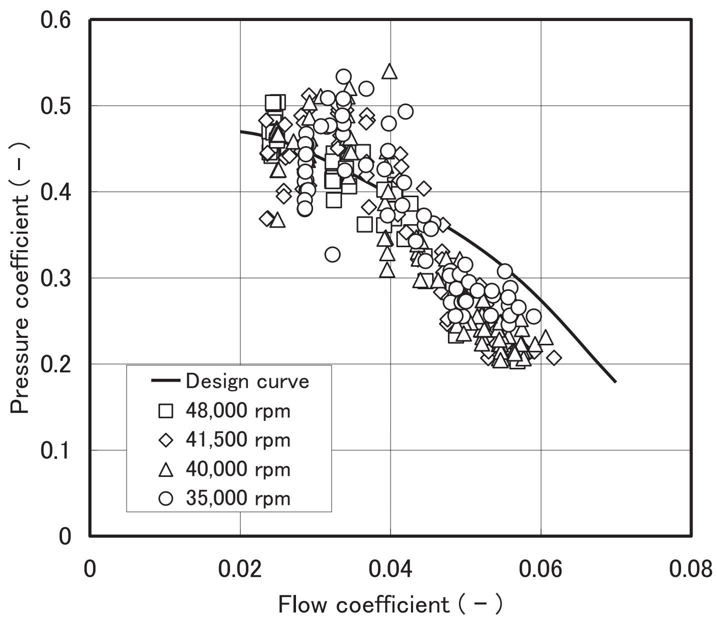

Fig. 2.4:18: Characteristics of the hydrogen circulation pump from off-beam commissioning results for helium circulation.

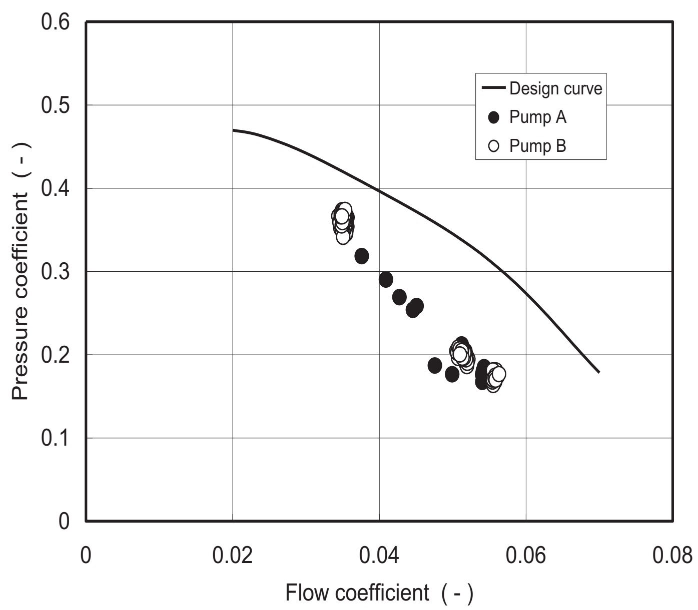

Fig. 2.4.19: Characteristics of the hydrogen circulation pump from off-beam commissioning results for hydrogen circulation after the pump improvement.

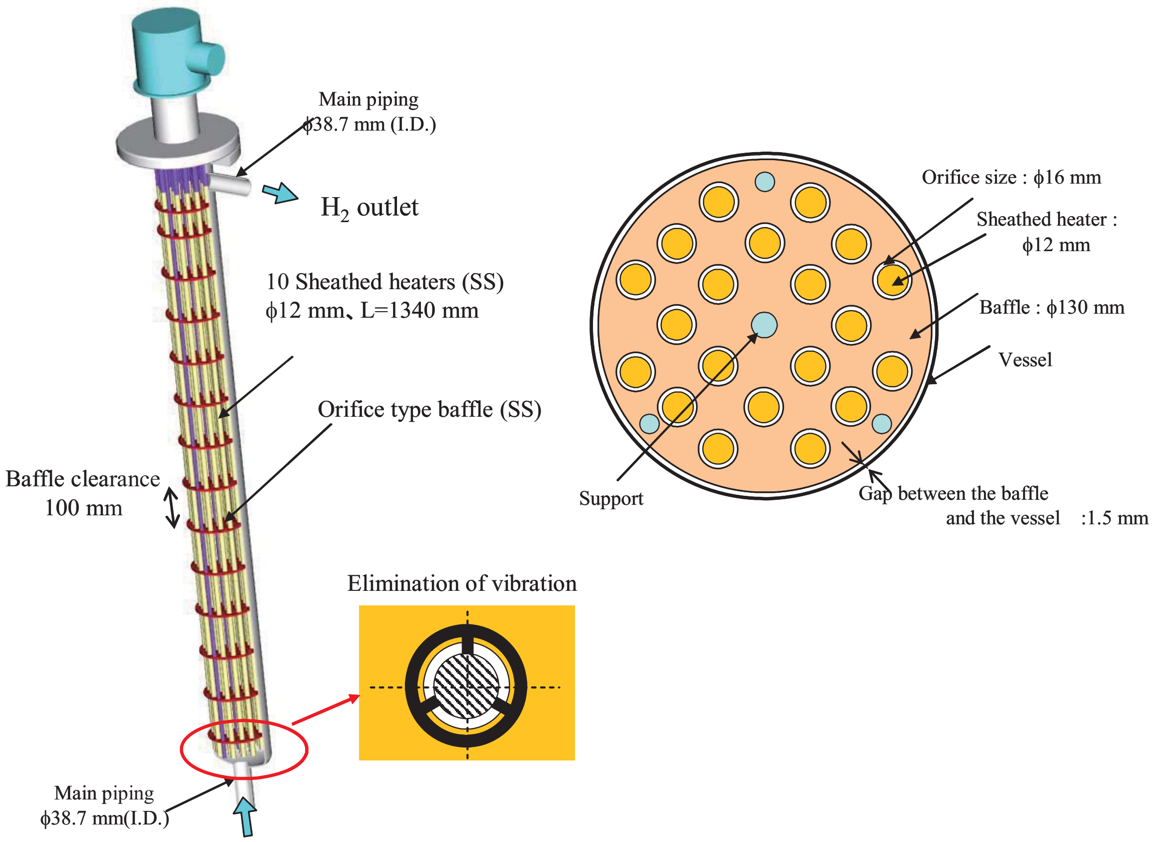

Fig. 2.4.20: Developed heater

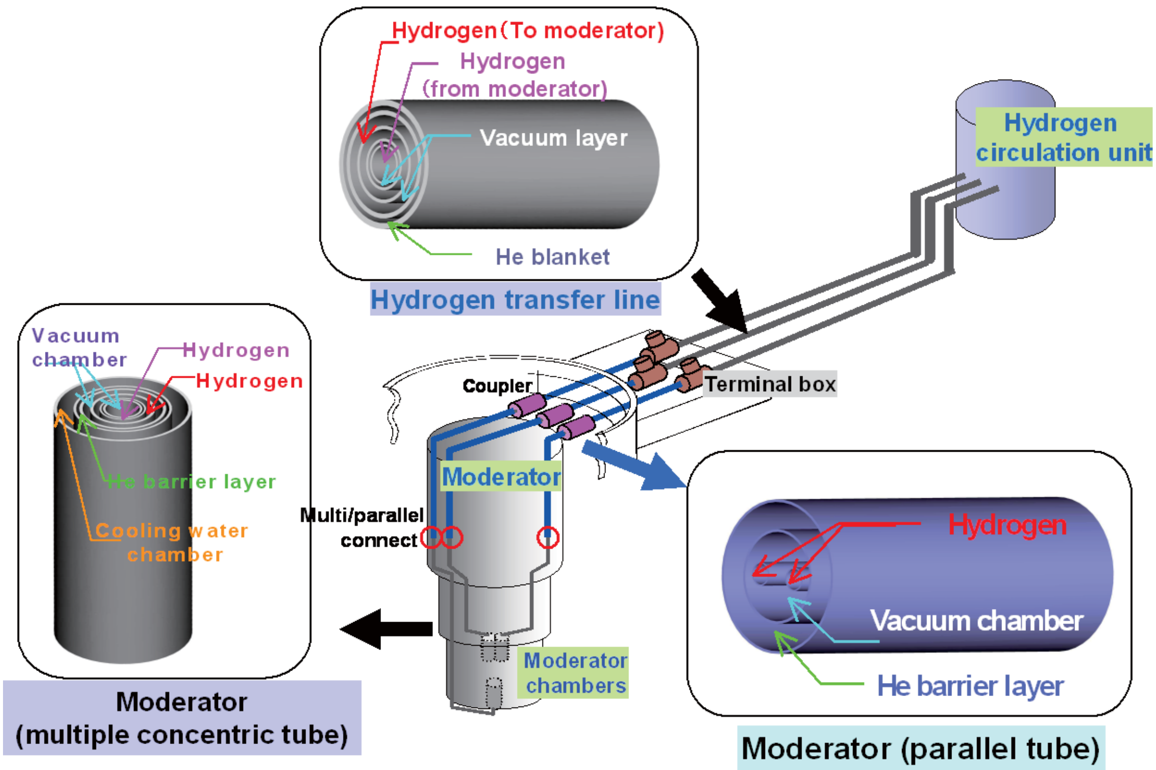

Fig. 2.4.21: Overview of the hydrogen transfer line

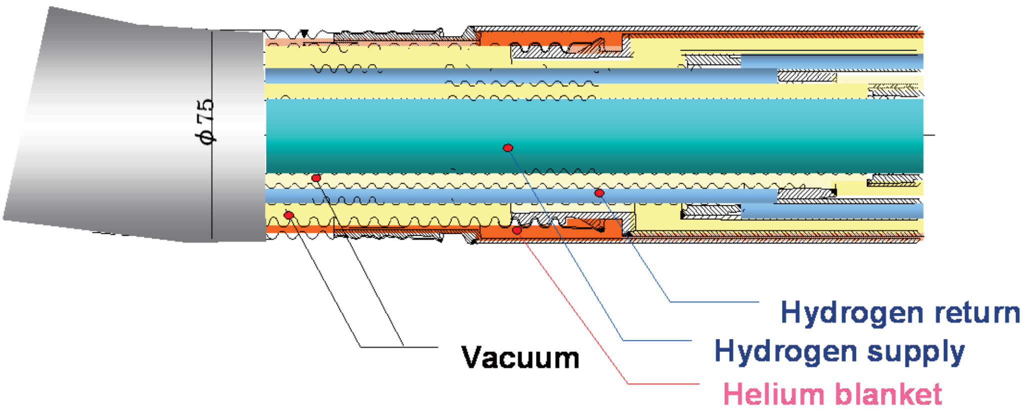

Fig. 2.4.22: Schematic drawing of the multiple layers in the line

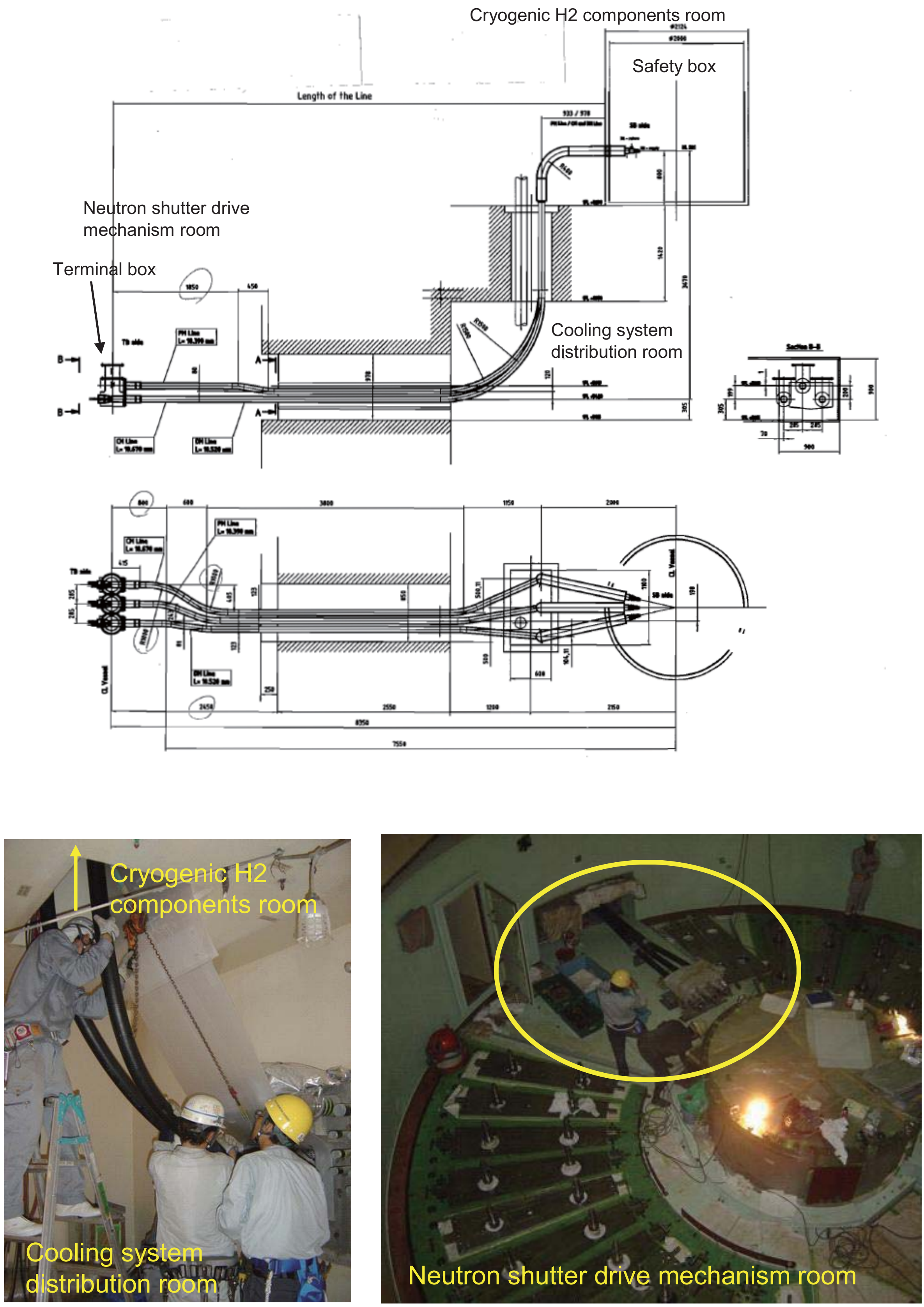

Fig. 2.4.23: Installation drawings and photographs of installation works

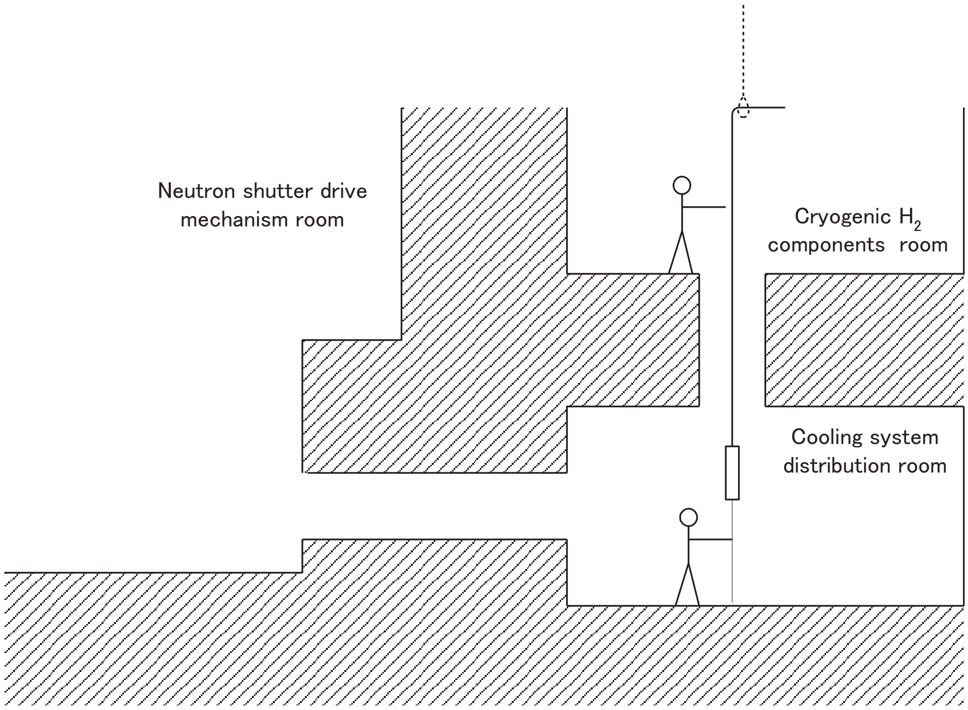

(i) Lead-in to cooling system distribution room.

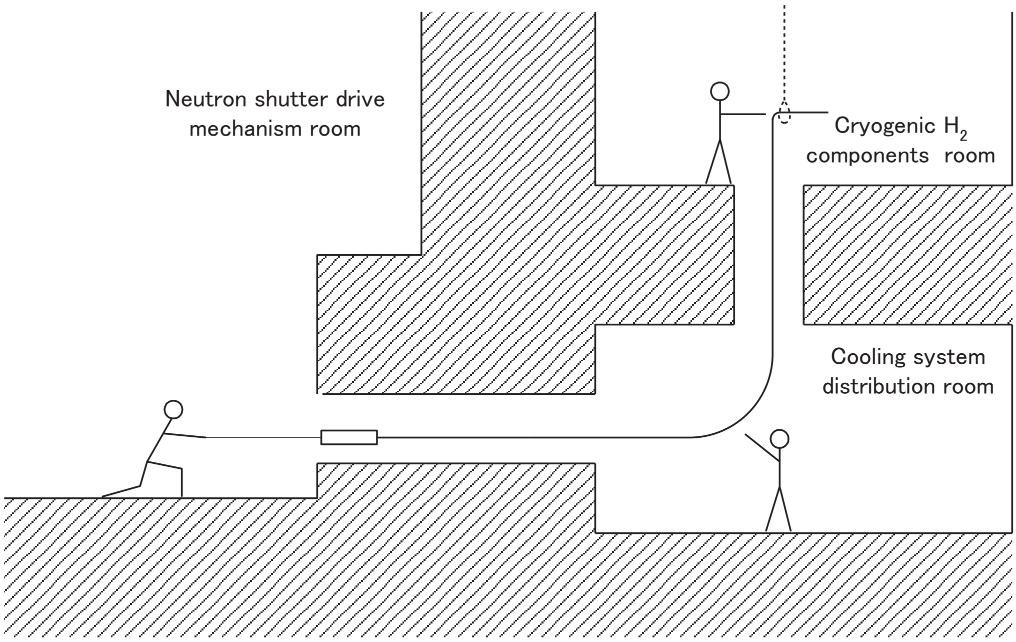

(ii) Lead-in to neutron shutter drive mechanism room.

Fig. 2.4.24: Schematic drawings of the installation process

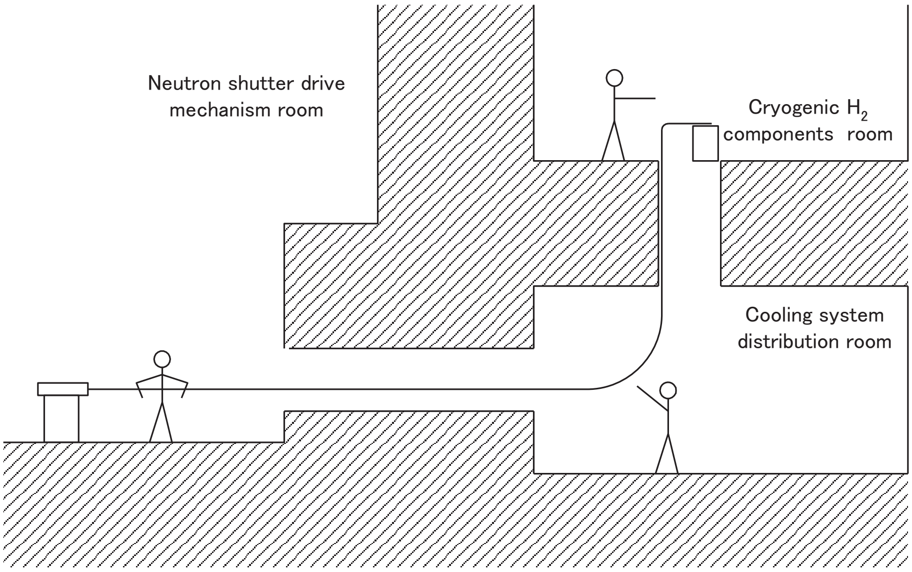

(iii) Setting supports and fix.

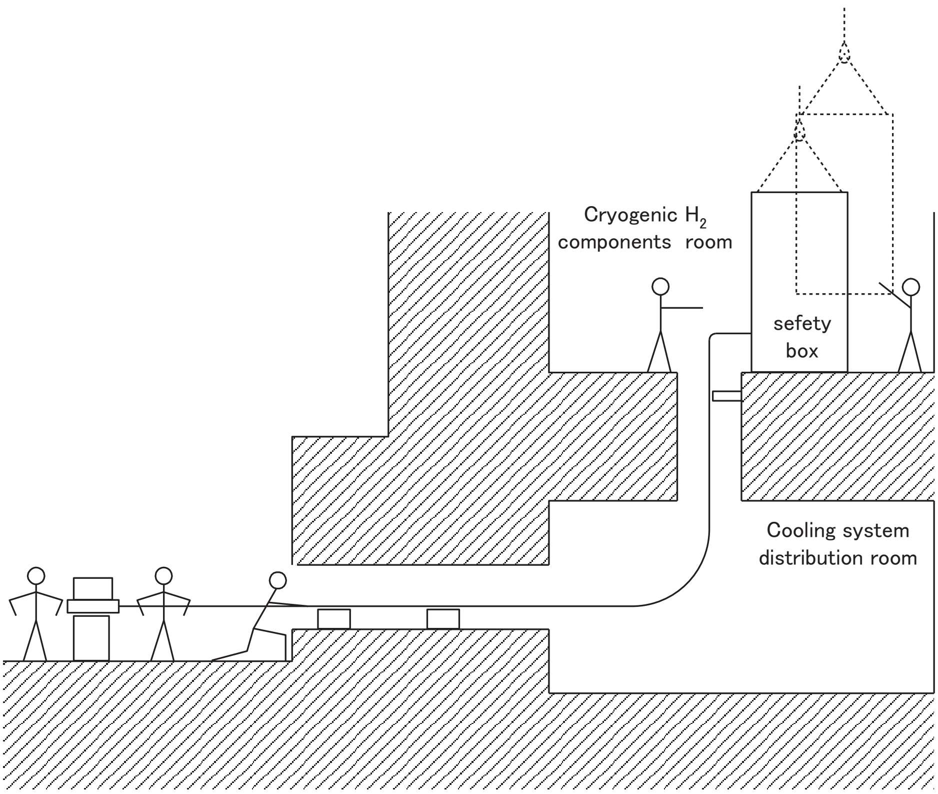

(iv) Connecting with safety box.

Fig. 2.4.24: Schematic drawings of the installation process (continued)

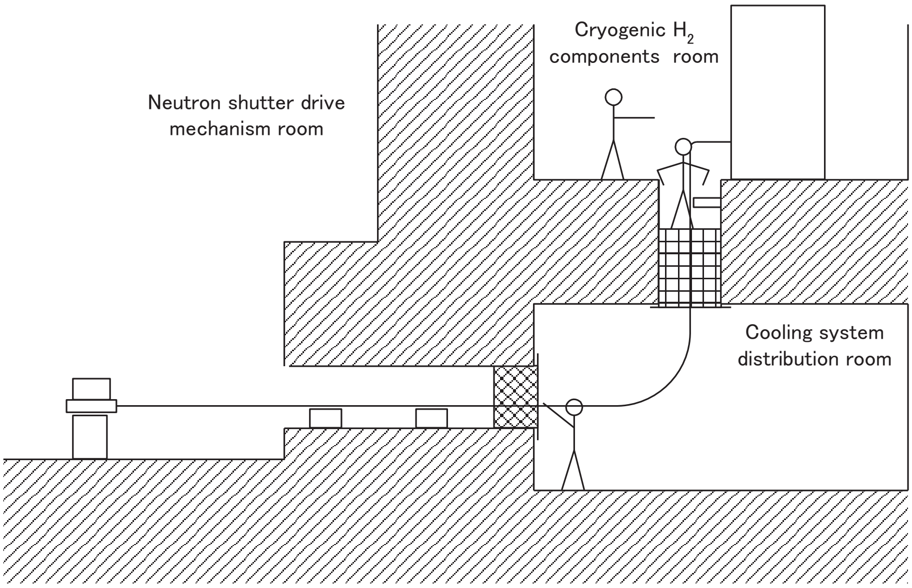

(v) Disposal of the penetration

Fig. 2.4.24: Schematic drawings of the installation process (continued)

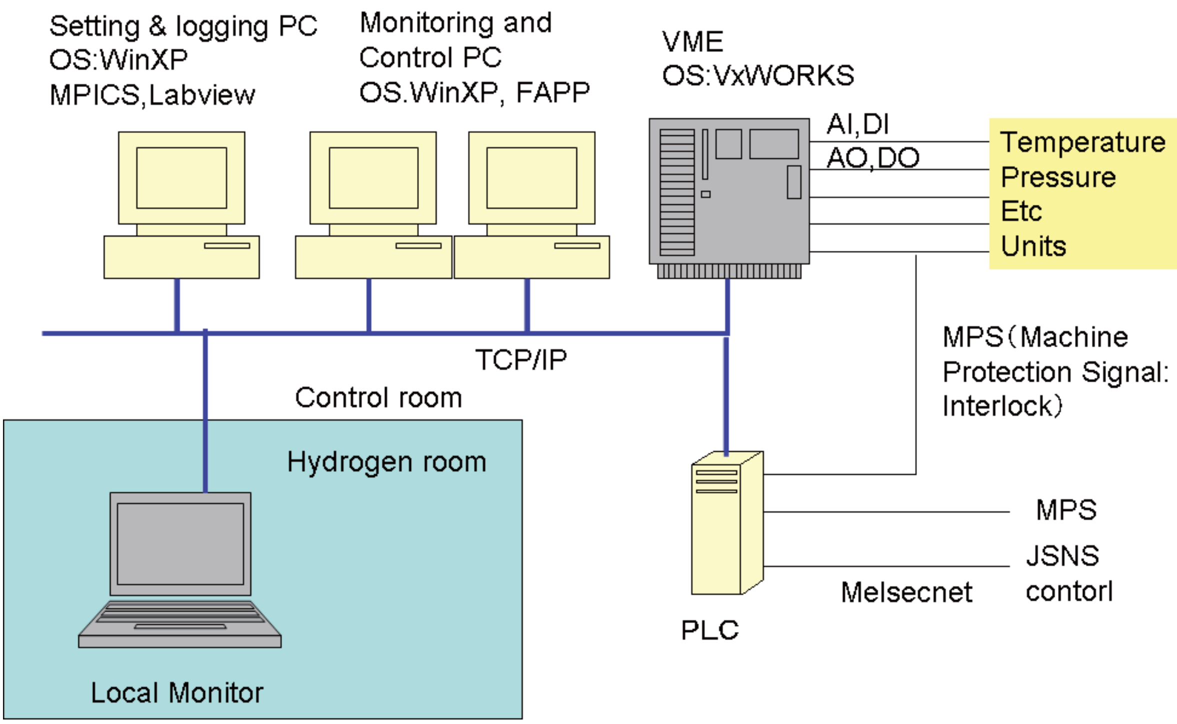

Fig. 2.4.25: Control unit of hydrogen circulation system

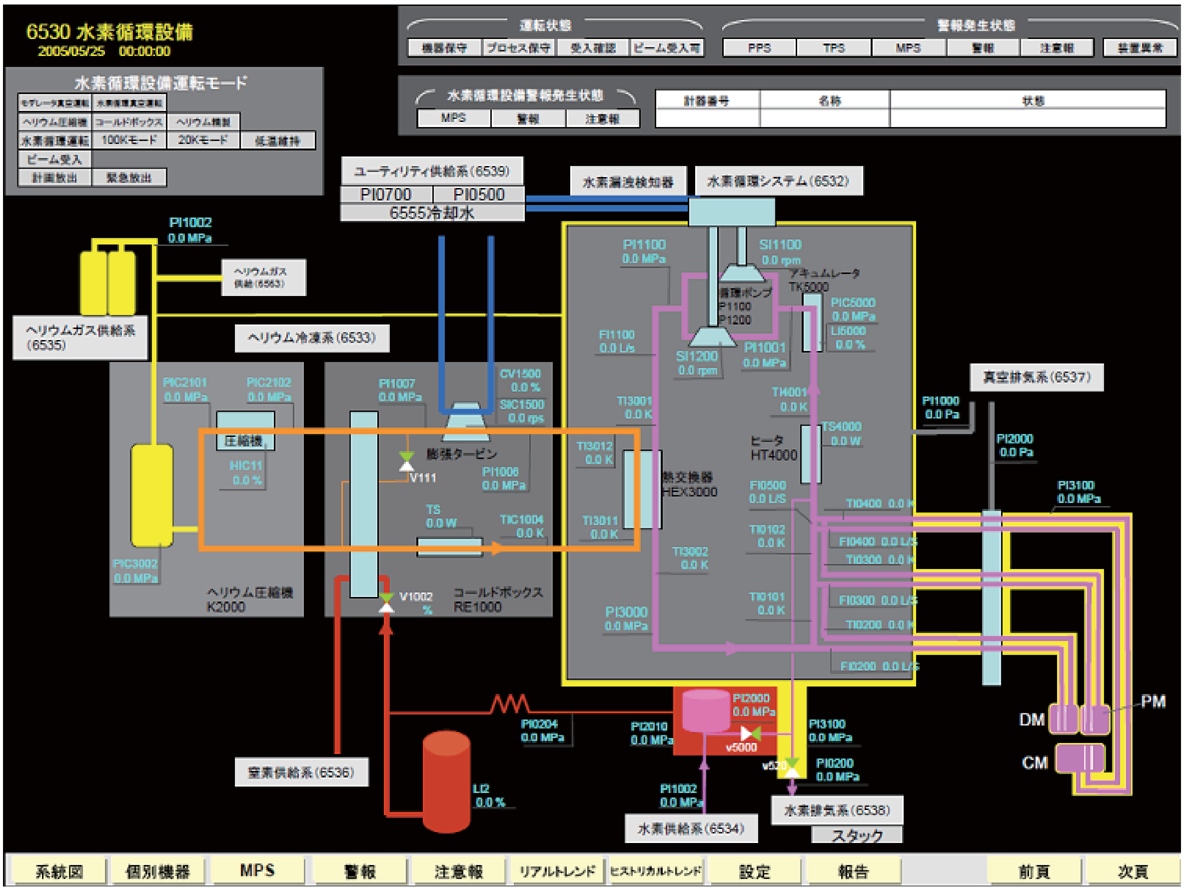

Fig. 2.4.26: Sample of FAPP control view

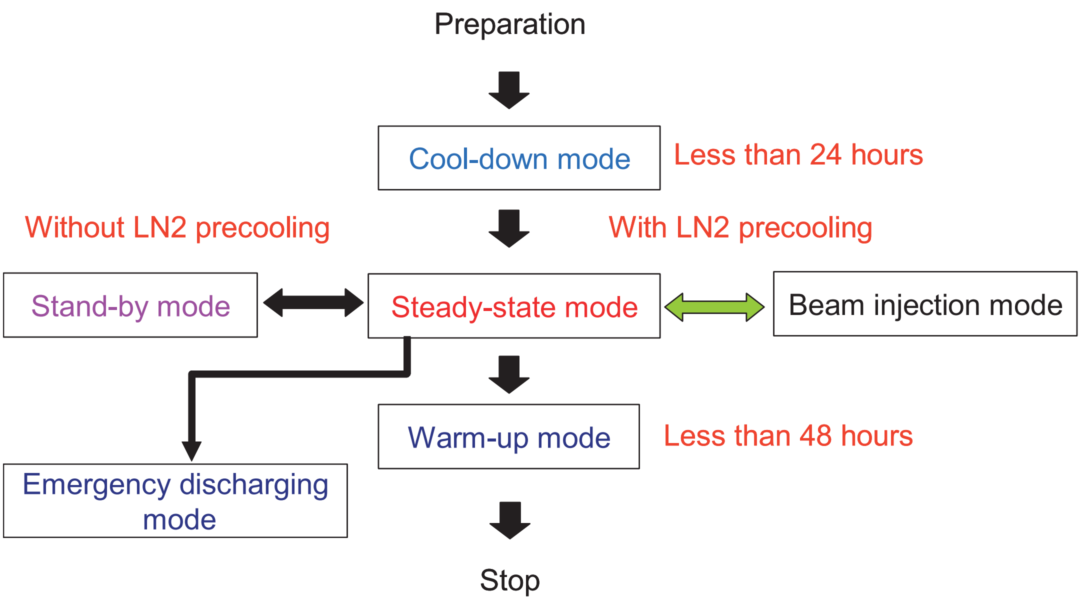

Fig.2.4.27: Schematic of an automatic operation mode

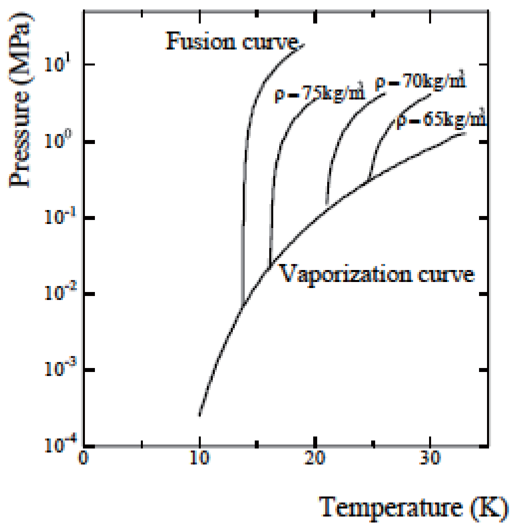

Fig. 2.4.28: Para-hydrogen phase diagram at the fluid regime

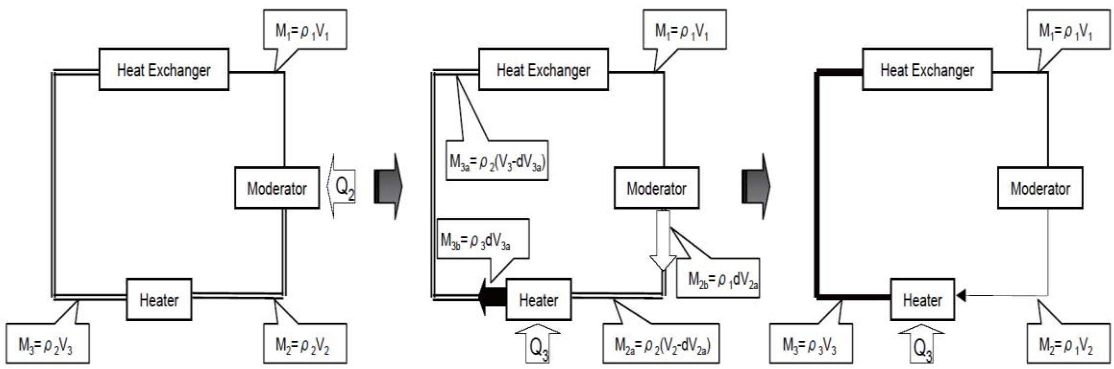

Fig. 2.4.29: Pressure calculation model for beam shutdown

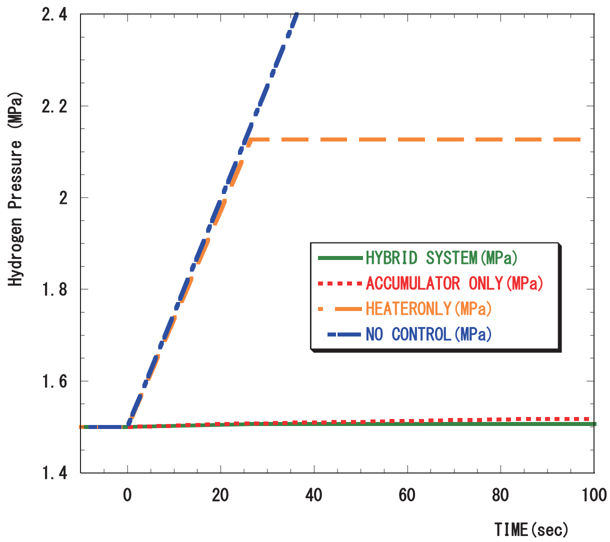

Fig. 2.4.30: Result of hybrid control system

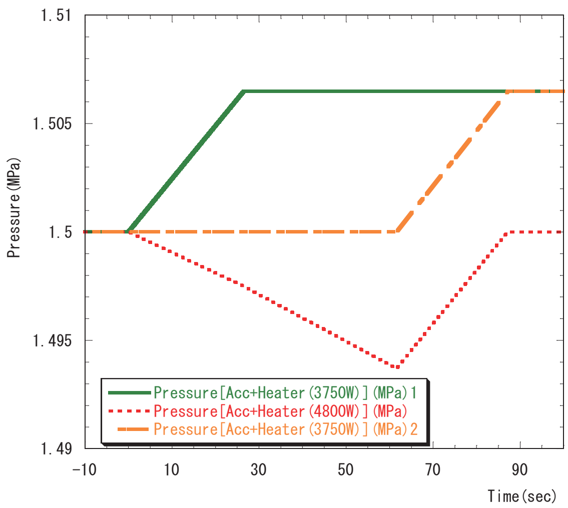

Fig. 2.4.31: Result of beam injection

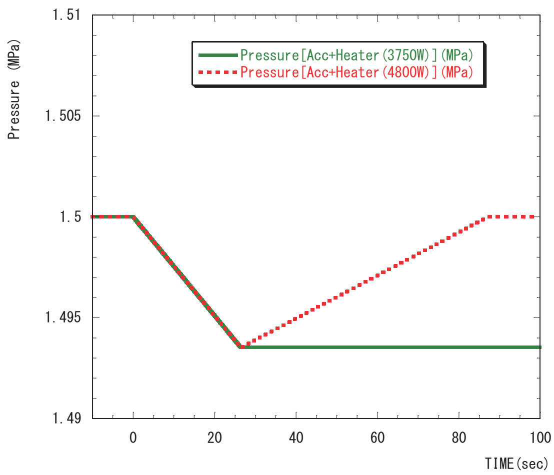

Fig. 2.4.32: Result of beam shutdown

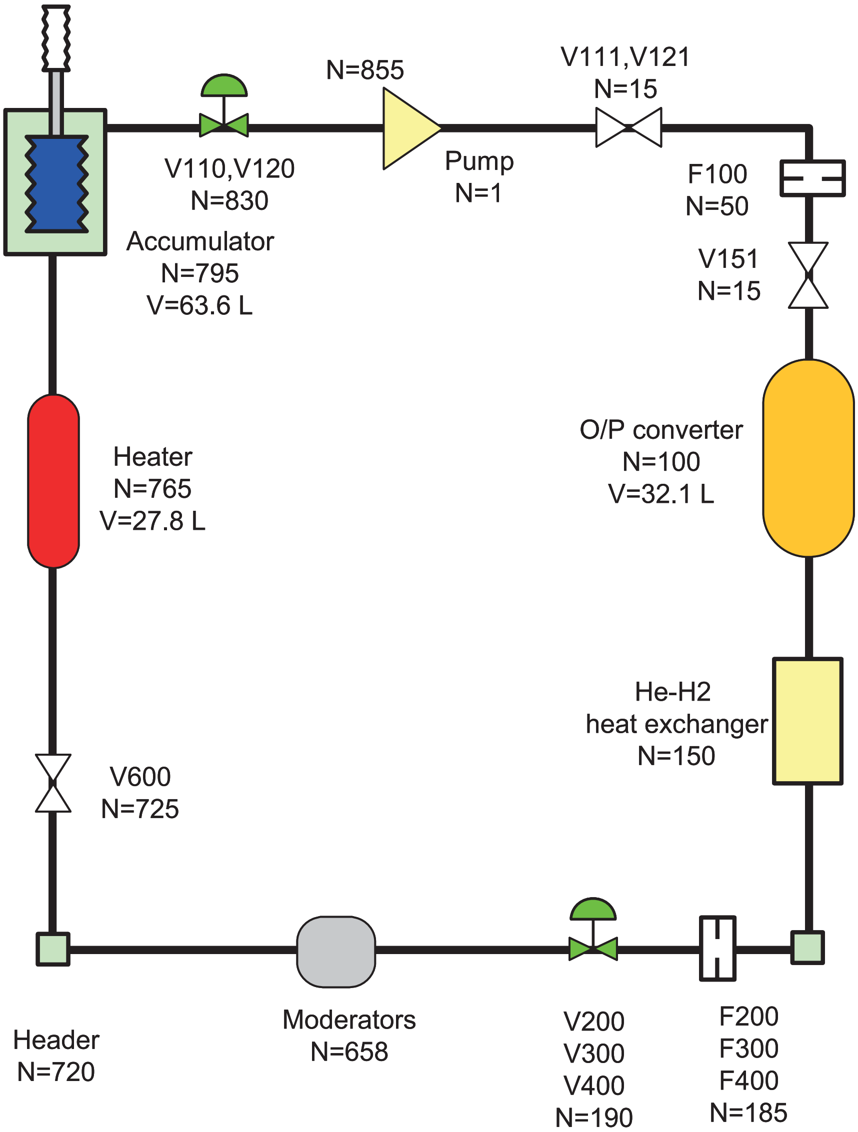

Fig.2.4.33: Simulation model

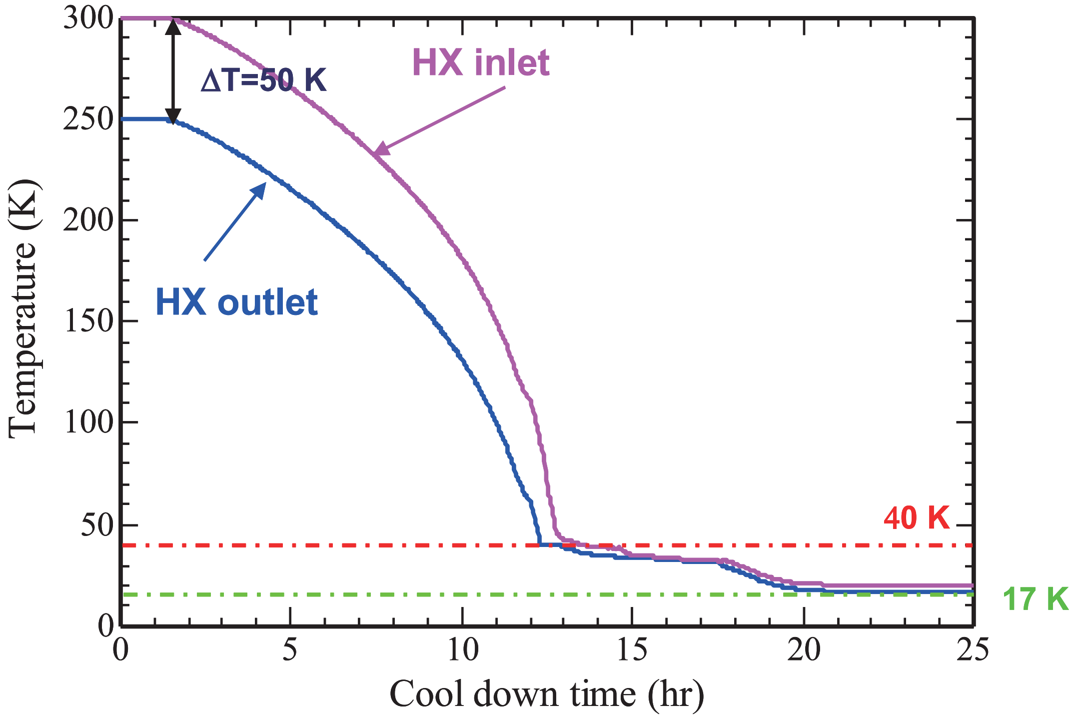

(a) Predicted cool-down curve

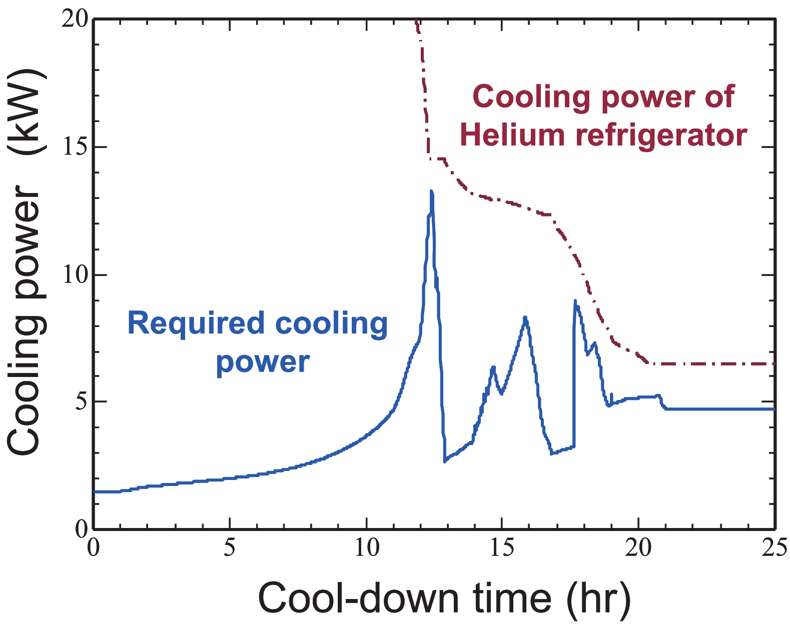

(b) Relationship between the required cooling power and the refrigeration power of the helium refrigerator

Fig. 2.4.34: Simulation results

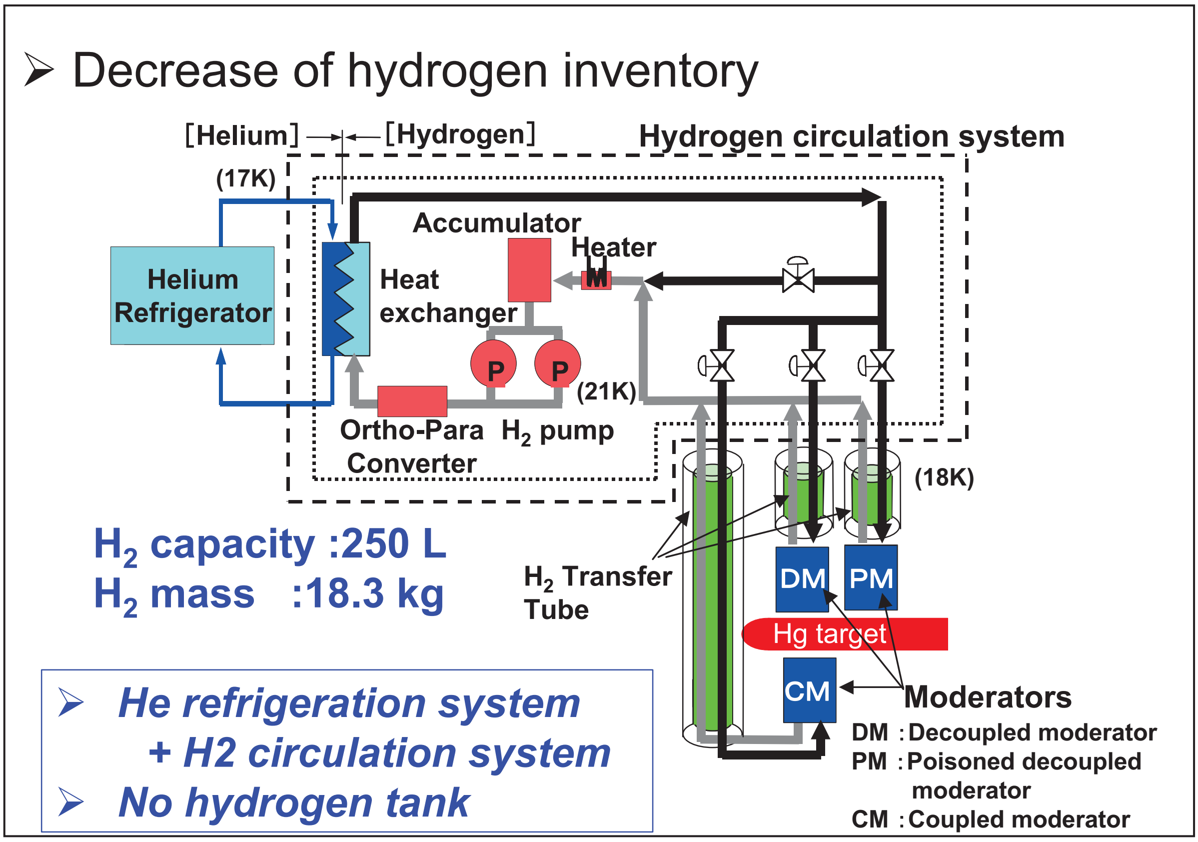

Fig.2.4.35: Flow diagram of the cryogenic hydrogen circulation system

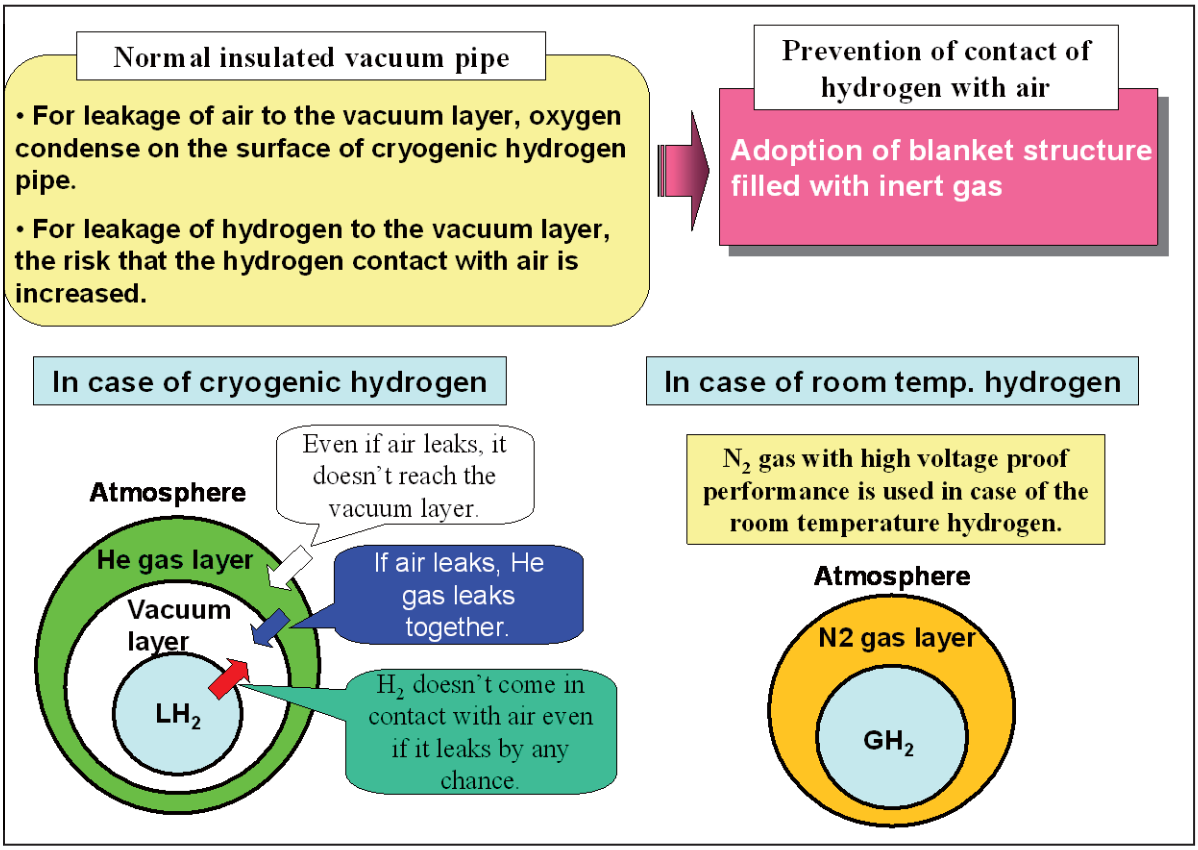

Fig.2.4.36: Concept of the blanket structure with inert gases

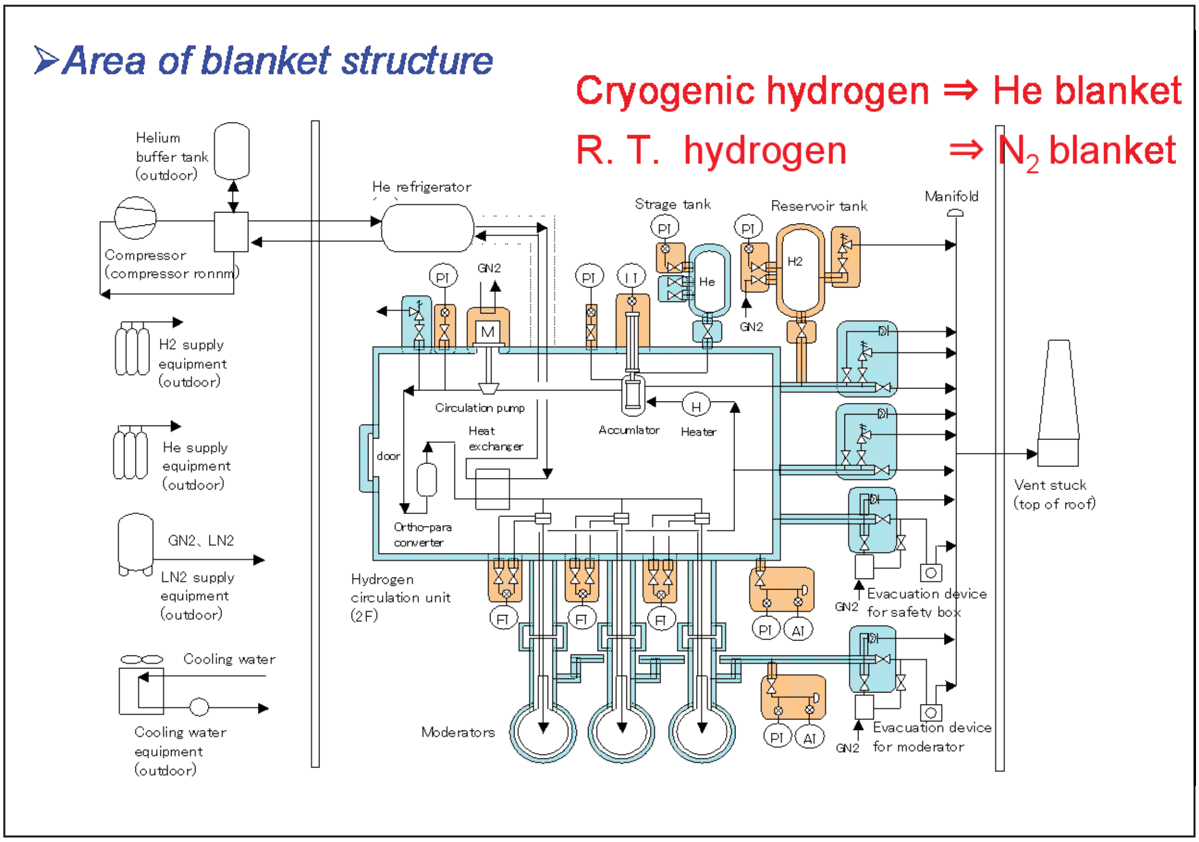

Fig.2.4.37: Area of the blanket structure

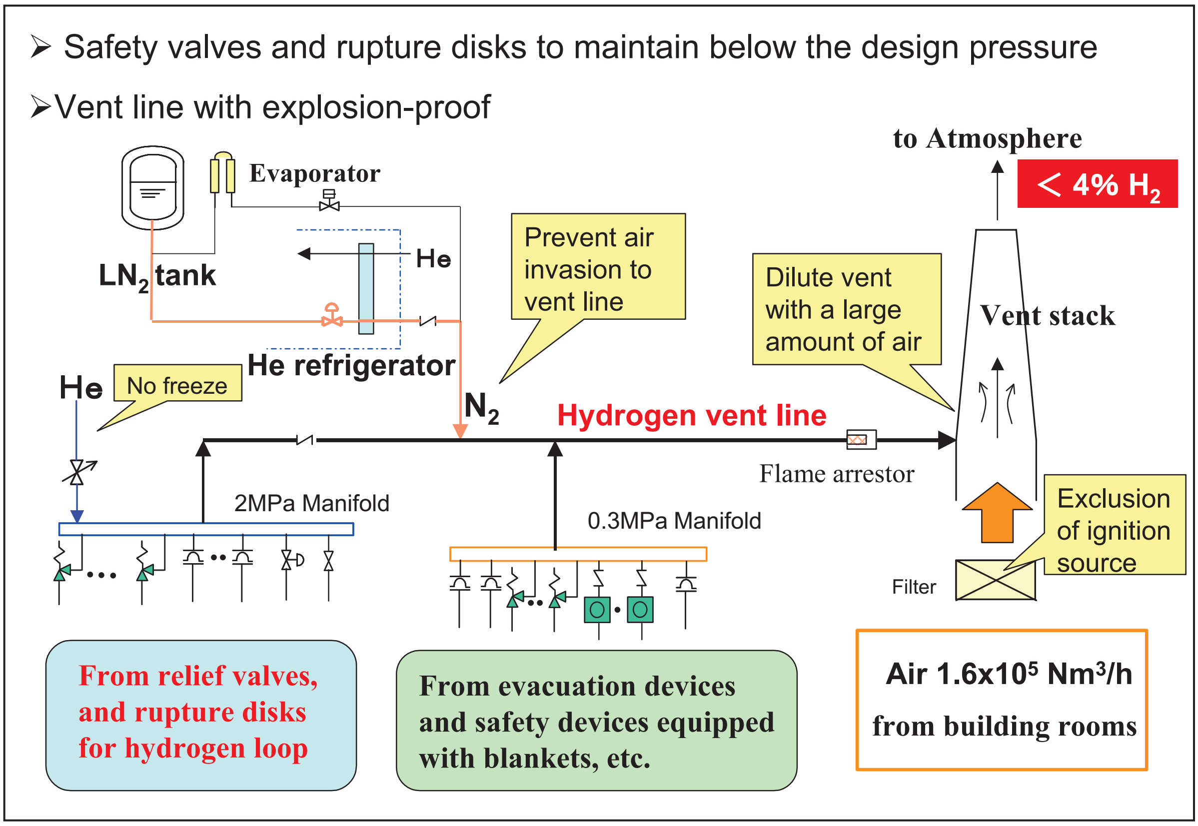

Fig.2.4.38: Overview of the hydrogen gas release system

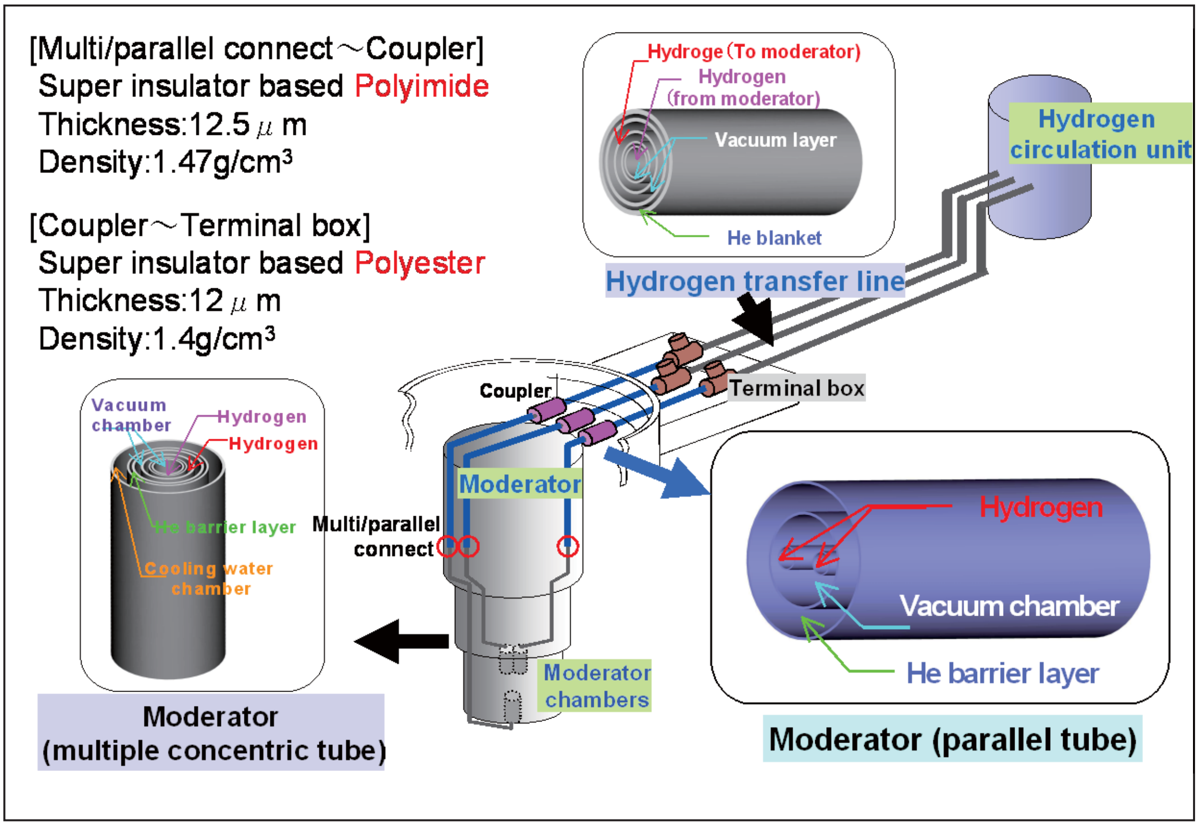

Fig.2.4.39: Specifications and installed area of Multi-Layer-Insulations (MLI)

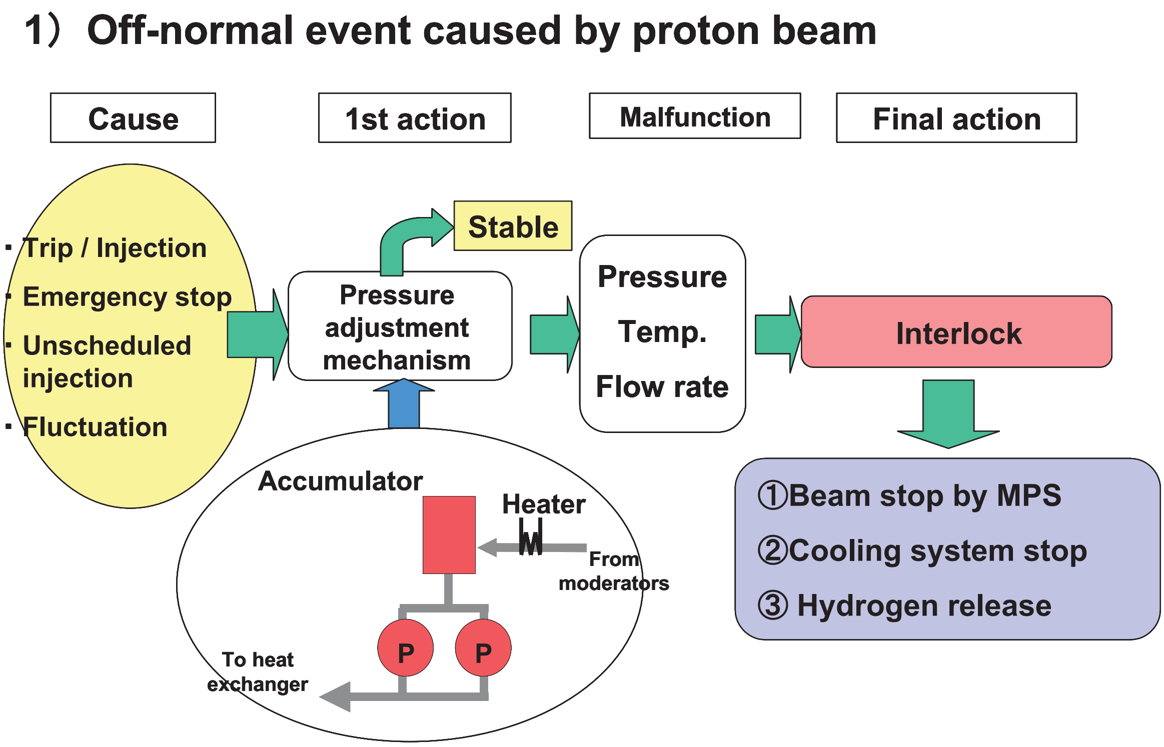

Fig.2.4.40: Basic scenario of off-normal event caused by proton beam

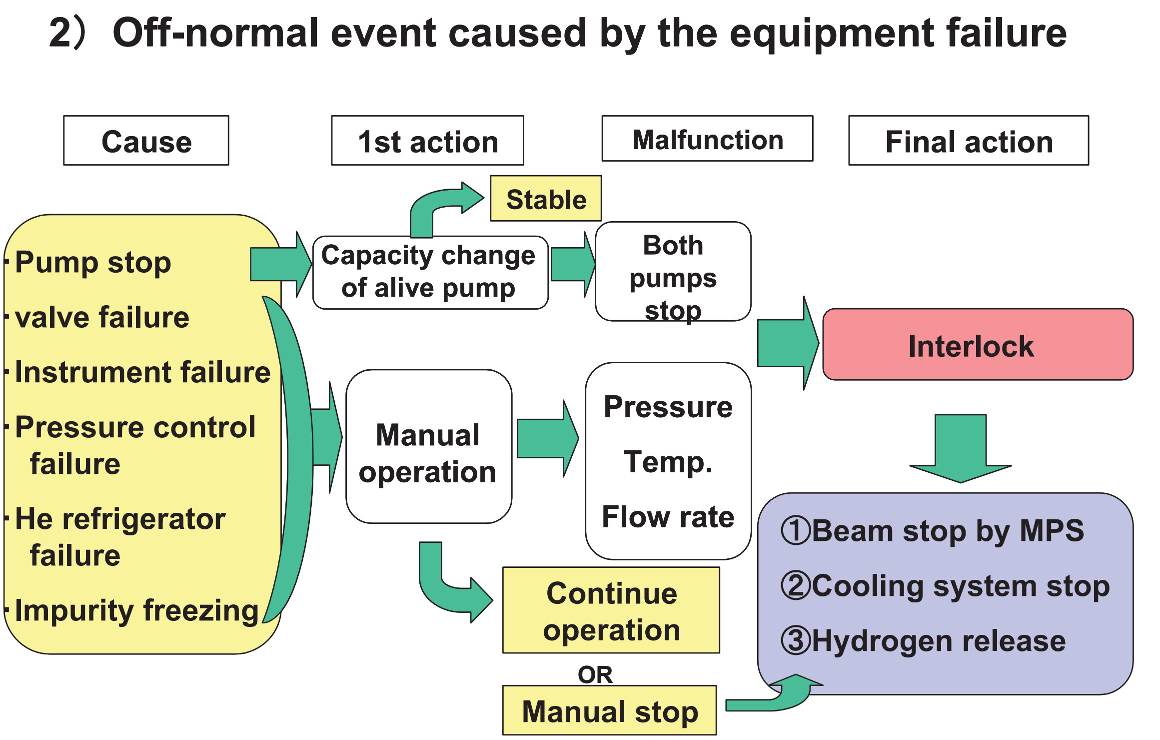

Fig.2.4.41: Basic scenario of off-normal event caused by equipment failure

3) Hydrogen leakage from piping and equipment

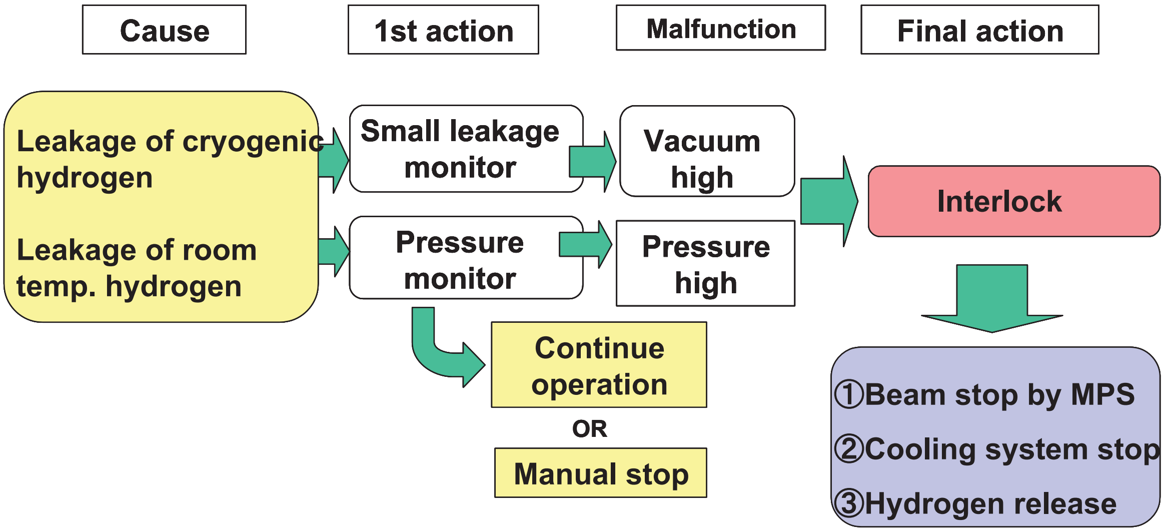

Fig.2.4.42: Basic scenario of hydrogen leakage from piping and equipment

4) Disaster

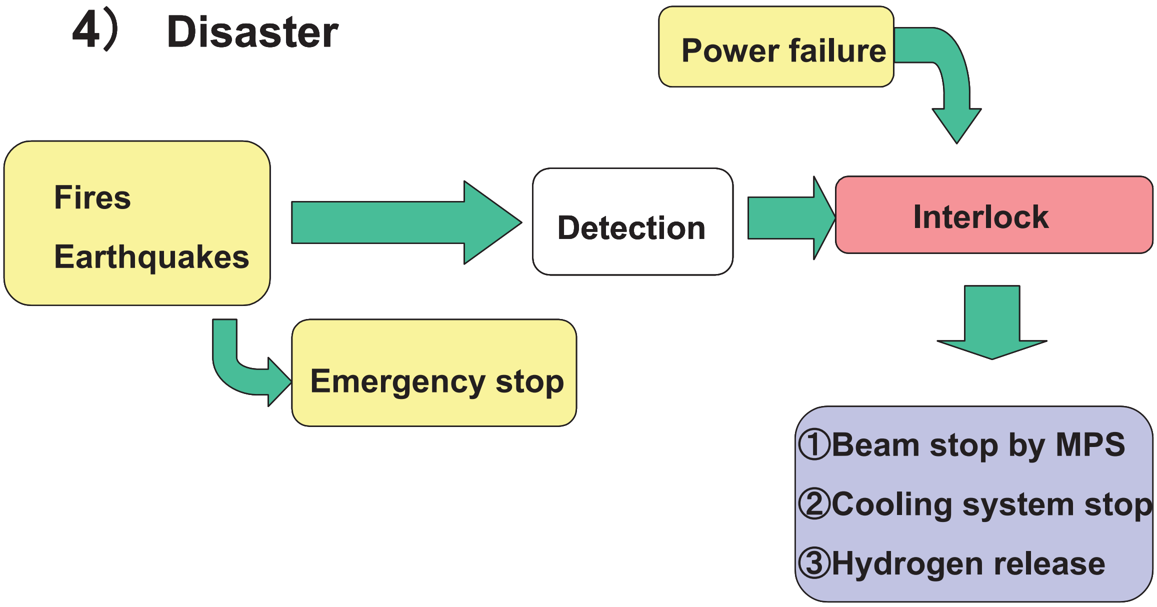

Fig.2.4.43: Basic scenario of disastert

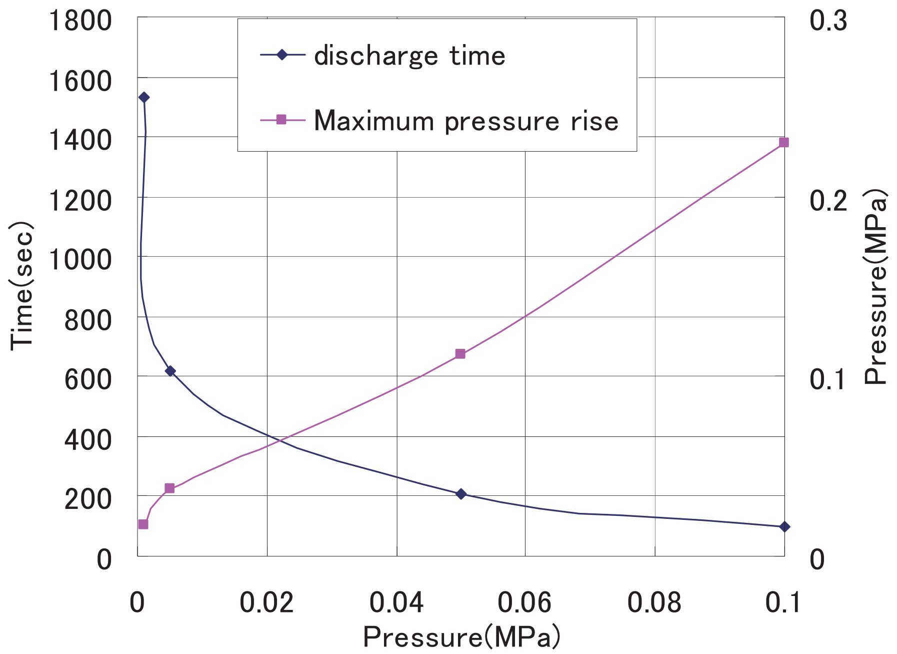

Fig.2.4.44: Hydrogen discharge time and pressure rise as a function of helium pressure injection

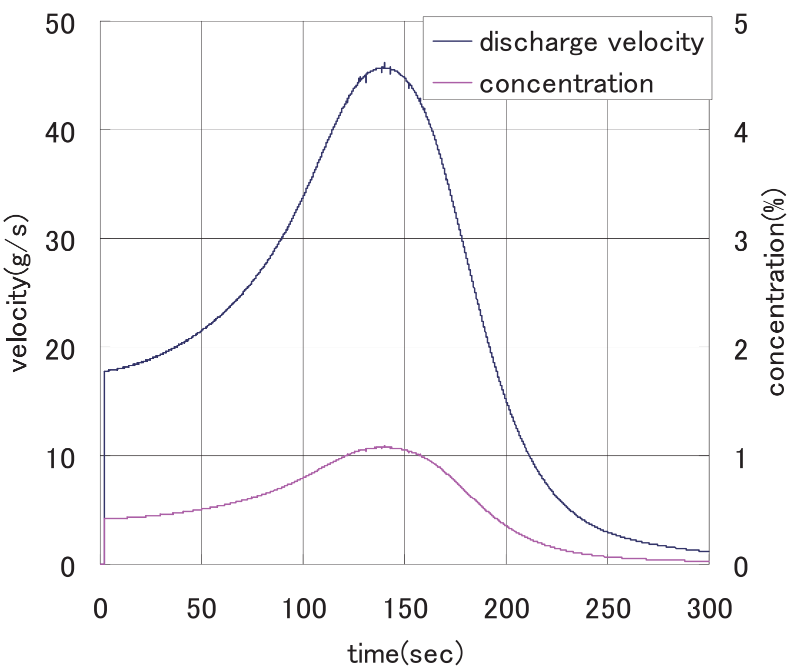

Fig.2.4.45: Mass velocity and concentration of hydrogen discharge as a function of helium pressure injection

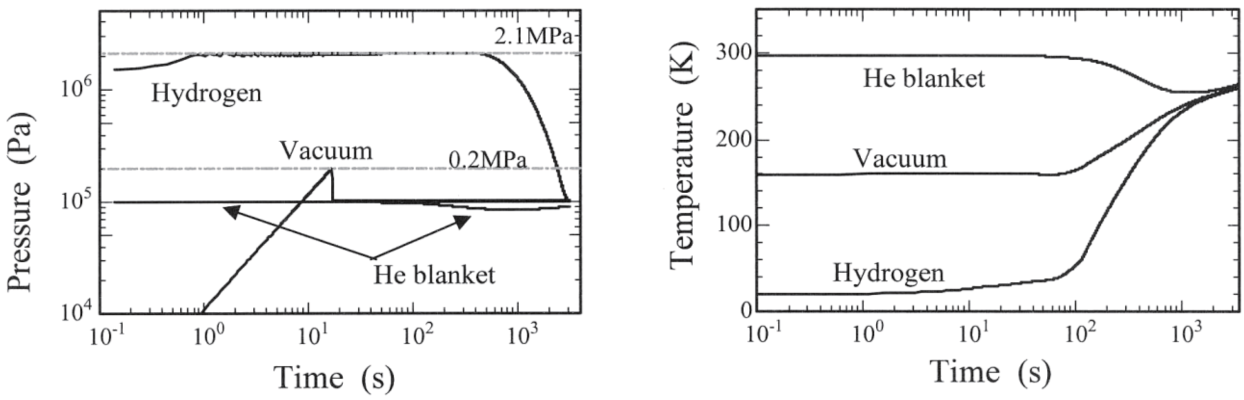

Fig.2.4.46: Pressure and temperature profiles for crack size of 0.2 mm^2

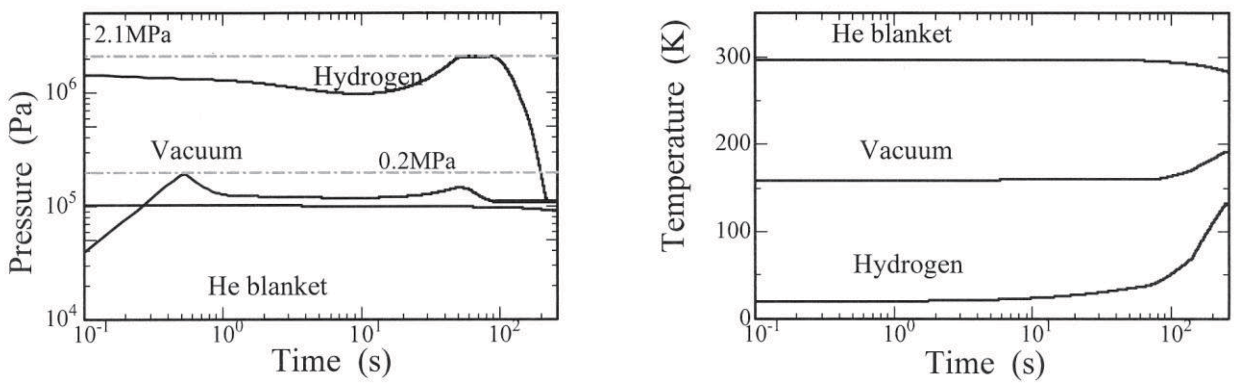

Fig.2.4.47: Pressure and temperature profiles for crack size of 10.0 mm^2

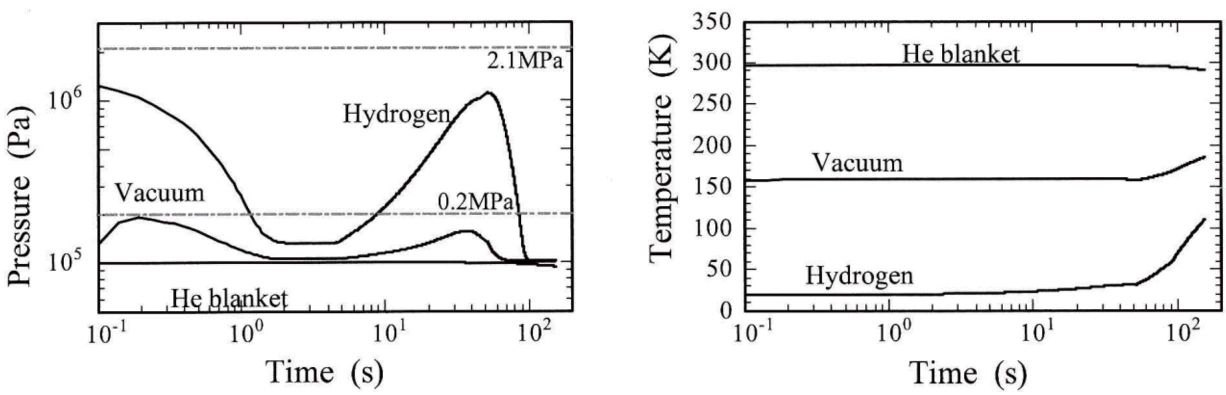

Fig.2.4.48: Pressure and temperature profiles for crack size of 27.5 mm^2 (D_t/4)

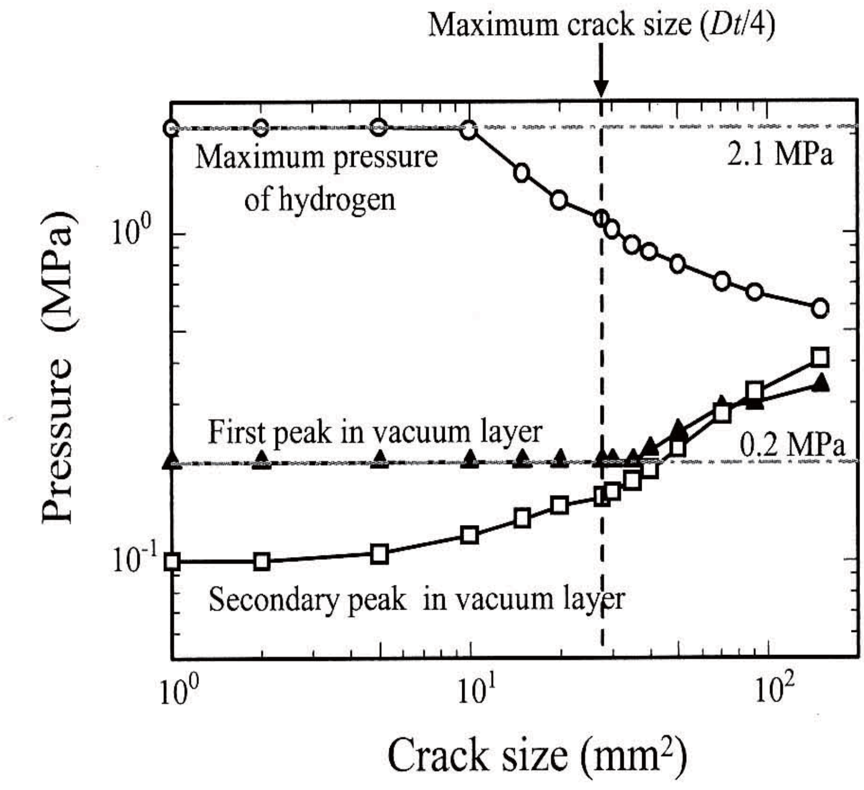

Fig.2.4.49: Maximum pressure in each layer for various crack sizes

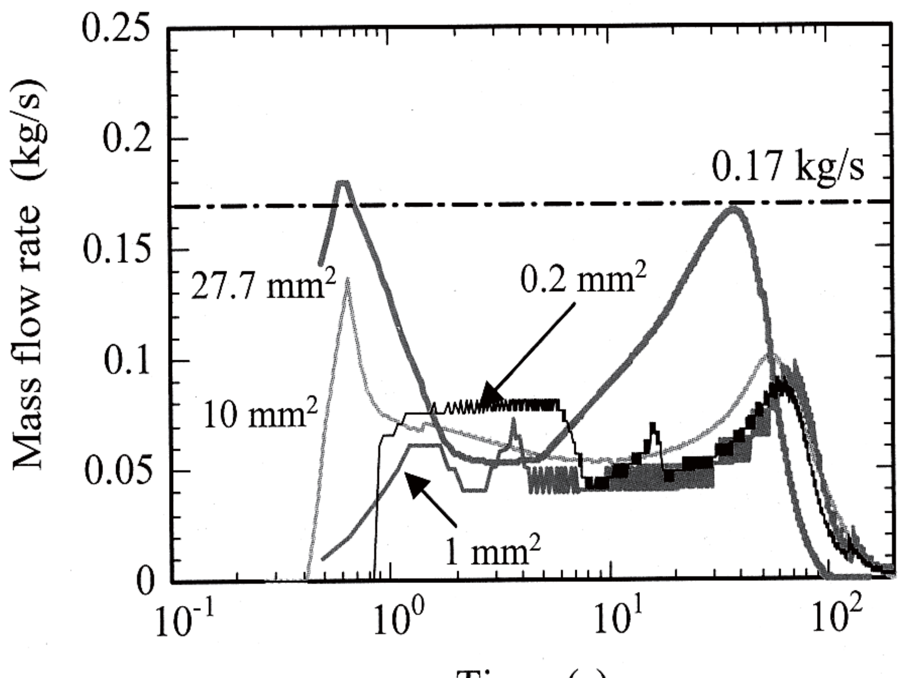

Fig.2.4.50: Mass flow rates for various crack sizes

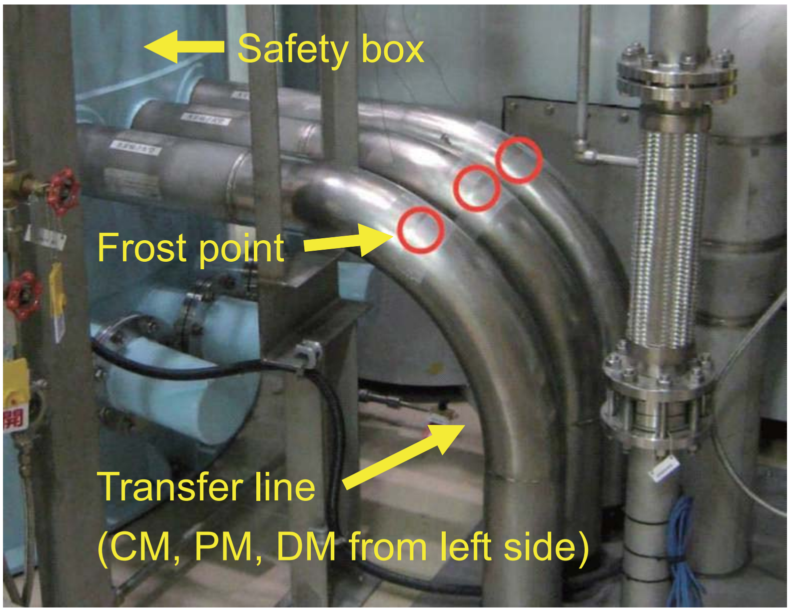

Photo. 2.4.1: Frost point of transfer line surface

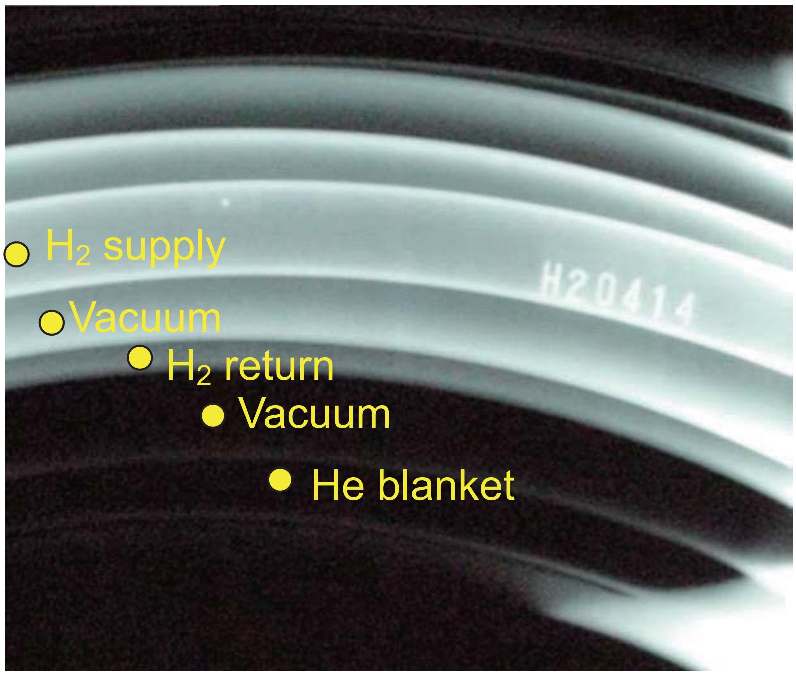

Photo. 2.4.2: X-ray radiograph of transfer line

2.5 Fundamental Components of Neutron Source Station

2.5.1 Overview

The neutron source station is an integrated system of a) bulk shield, b) neutron beam ports, c) neutron beam shutter system and d) target vessel. It plays roles of not only shielding neutron and γ-rays produced at the mercury target-moderator-reflector assembly to allowable dose rate at the boundary of the bulk shield but also furnishing neutron instruments with high quality pulsed neutron beams. Fig. 2.5.1 shows the three-dimensional (3D) layout of the neutron source station in the MLF building. The mercury target trolley in the remote handling cell, cryogenic components for providing super-critical hydrogen are also displayed for better understanding. 3D illustration of the neutron source station is shown in Fig. 2.5.2. Specifications of components were determined under design policies that

(i) made the dimension of the bulk shield as small as possible so that neutron instruments could be placed in short distance from the moderators,

(ii) made vacuum or helium filled space around the mercury target so that it could suppress the production of harmful corrosive gases such as activated gas, O_3, NO_X by means of the activation of air,

(iii) made boundaries against accidents such as leakage of hydrogen from the moderator and that of mercury from the target container in the worst case,

(iv) installed neutron beam lines as many as possible,

(v) installed only single-channel neutron beam shutter gate which enabled users to use neutron beam line independently,

(vi) the target trolley moved horizontally back to remote-handling cell at maintenance period, and

(vii) the moderator-reflector assembly was lifted up vertically to high-bay area for maintenance.

Structural highlights of major components of the neutron source station to realize those design policies are focused in this section. Details of individual components are described in the following subsections. Related components such as shields around proton beam transport line, neutron guides that are placed outside of the bulk shield and the remote handling cell at downstream of the neutron source station are reported separately from this subsection in this design report.

(1) Geometrical reference

The right-handed coordinate system was employed, in which the axis including both center lines of the proton beam and the mercury target was defined as the reference x-axis. The direction towards the upstream of the proton beam transport line is defined as 0˚. Then, the central axis of the mercury target lies on the 180˚ direction. The elevation of the center of the proton beam line is 1,615 mm from the first floor level (1FL) and it is denoted as 1FL+1,615 mm. Coordinates of origins of neutron beam lines are summarized in Table 2.5.1. The projection of those coordinates on the x-y plane is shown in Fig. 2.5.3, in which the outline of the mercury target is also illustrated for better understanding.

(2) Bulk shield

Spallation neutron sources have the neutronics characteristics that high energy neutrons with energies higher than 20 MeV are produced at the target-moderator-reflector system. The principal idea in designing the bulk shield is that high energy neutrons are shielded by iron while γ-rays and build-up low energy neutrons passed through the iron shield are shielded by materials having high number density of hydrogen such as ordinary concrete, polyethylene. We have carried out one-dimensional transport calculations to determine the shielding composition, and three-dimensional Monte Carlo calculations to determine the detailed dimension of individual components in which gaps among components were included in the geometry model to take account of the streaming effect of neutrons. In consequence, we determined to place steel components in the area with a diameter of 9.2 m and surround them with magnetite concrete.

Figs. 2.5.4 and 2.5.5 show the plane view and 3D cross sectional view of the neutron source station on the proton beam line elevation. The thickness of the magnetite concrete was optimized, so that it varied from 2.7 m at the most forward in the proton beam advancing direction to 2.2 m at the backward direction. In vertical direction, the total height of the neutron source station was designed as 11.2 m. Since there is a space for the shutter drive system on the top of the neutron beam shutter as shown in Fig. 2.5.2, the net height was about 8.6 m. The structural characteristics in vertical direction are as follows:

(i) Roof shield was installed over the concrete-based construction surrounding the target station so that their weight was unloaded upon the components inside the target station.
(ii) The roof shield was made with ordinary concrete with a height of 2 m.
(iii) 20 cm thick ordinary concrete layer was introduced in the top part of the steel components inside the target station.

The item (i) is the same structural concept as that adopted at SNS. The item (iii) is the most unique structural characteristics in the MLF neutron source station for achieving effective shielding performance and different from the design of SNS.

(3) Target vessel

In order to prevent the production of corrosive and/or harmful gases around the mercury target-moderator-reflector system, we adopted a concept that a cylindrical target vessel filled with helium was placed at the center of the station. This is the same concept as already practiced in other spallation neutron source facilities such as SNS and ISIS. Hereafter, the target vessel is denoted as helium vessel. 3D illustrations of the helium vessel and its cross sectional view are shown in Figs. 2.5.6 and 2.5.7. We have judged that the steel shield in which heat density is expected higher than 0.001 W/cc is cooled by water. Therefore, the helium vessel was designed to contain a water-cooled steel region with a diameter of 3 m and a height of 1.4 m around its center, *i.e.* the origin of the reference coordinate. This part is denoted as middle-section part. Consequently, the helium vessel plays a role of the boundary against the coolant even if it leaks at a failure accident.

It is noted that the diameter of the helium vessel becomes small as 2 m above the middle-section part. This structure bears the virtue that reduces helium gas inventory and the amount of steel shield over the moderator-reflector assembly in the helium vessel. Considering the maintenance scheme that the steel shield is lifted up by a remote handling tool for replacing the irradiated moderator-reflector assembly, the weight reduction greatly eases the design of the remote handling system and a crane equipped in the high-bay.

There are two insertion holes on the right opposite sides of the middle-section part which are set on the reference axis. One is for the mercury target which is inserted horizontally into the helium vessel at 180˚. It is sealed by a contact of a metallic O-ring with a force of 30 t. The other is for the proton beam injection at 0˚. It is sealed with a pillow seal of the proton beam window assembly placed just upstream of the helium vessel with a force of 3.5 t. 23 neutron beam ports were also mounted on the cylindrical side of the middle-section part.

(4) Liner components

The concept to suppress the production of corrosive and/or harmful gases was also applied to the atmosphere outside of the helium vessel. It is difficult and so expensive to enclose helium completely in the neutron source station because it has complicated structures such as neuron beam holes, target insertion holes, many penetration ports of coolant, cryogenic piping and cablings. Hence we chose to circulate dry air outside helium vessel. For containment of dry air, liner components were installed at the boundary from the surrounding magnetite concrete and the basement. 3D image of liner components assembled is shown in Fig. 2.5.8.

A base-plate and a bottom-liner were settled at the bottom. An outer-liner was installed upon the bottom-liner to make the boundary from surrounding magnetite concrete. Neutron beam extraction ducts are mounted on the cylindrical side of the outer-liner to assure the neutron beam lines after filling magnetite concrete. A target-trolley liner was set between the helium vessel and the outer-liner in the direction of the path of the target trolley so that it could make the boundary from the atmosphere in the remote-handling cell. For the top part of the neutron source station, some plates were arrayed on the roof shield and gaps between the plates are filled with a calking material to make a seal.

(5) Proton beam window position

The proton beam window separates the vacuum environment in the proton beam transport line from the atmosphere in the neutron source target. The layout of the proton beam window in the neutron source station is shown in Figs. 2.5.2 and 2.5.5. 3-GeV proton beams produce secondary particles at the proton beam window when passing through it. Neutronics calculations showed that the dose rate at the outer surface of the bulk shield became lower as the proton beam window position approached to the helium vessel. Moreover, additional heating by the secondary particles originated from the proton beam window is suppressed sufficiently low at the nearest position to the helium vessel because they almost injected on the water-cooled middle-section part of the helium vessel. Therefore, the proton window was designed to be right front of the helium vessel. Fig. 2.5.9 shows the overview of the proton beam window assembly.

(6) Neutron shutter system

Neutron shutter system opens and/or closes the neutron beamline at just downstream of the neutron beam ports on the middle-section of the helium vessel. The 3D view of a neutron shutter system is shown in Fig. 2.5.10. We have adopted a shutter system that drives a shutter gate vertically in a space created by a pair of interstitial blocks like a water gate. This is the same concepts as those of SNS and ISIS. However, there are some structural characteristics different from other facilities in details. For example, only shutter gate with single-channel neutron beam hole was employed so that users could utilize the corresponding neutron beam line exclusively. The shutter gate was sustained by two rods from a driving system placed above. Oilless bushes are equipped around the sustaining two rods for a kind of guide mechanism. There are no guide rails around the moving space for the shutter gate created by a pair of interstitial blocks. Adoption of the shutter gate with a width of 20 mm and its layout that the upstream edge is set at 2.32 m from the center axis of the helium vessel enabled to array 23 neutron beam lines in the neutron source station. Vertical shutter stroke and gaps around the shutter gates from interstitial blocks were determined by the three-dimensional neutron transport calculation. The resultant shutter stroke is 400 mm in the full moving space of 500 mm. The gap between the shutter gate and the interstitial block is 12.5 mm. It is also noted that the basement of the neutron beam shutter is made from magnetite concrete.

(7) Neutron beam line components

The pulsed neutron beam originating from the moderator surface passes through helium atmosphere in the helium vessel and surrounding dry air in the bulk shield. In order to achieve high neutron transmission rate in those atmosphere, vacuum region was introduced by installing the following insertion components;

(i) a rectangular-shaped vessel insert duct at the neutron beam port on the middle-section part of the helium vessel,
(ii) a rectangular-shaped shutter insert duct in the neutron beam hole in the shutter gate, and
(iii) an insert at the neutron beam duct in the magnetite concrete region.

Those ducts have thin walls (windows) at both ends and structural strength enough to contain devices such as a neutron guide (super-mirror), steel collimators. They are also designed to be exchangeable. Especially, the vessel insert duct was designed to be handled by a remote handling device from the shutter space after removing the shutter gate. The shutter insert can be replaced with a brand new one after moving the shutter gate to a maintenance area using a shutter cask. The insert in the magnetite concrete can be horizontally installed in and extracted from the neutron beam duct using equipment from outside of the bulk shield.

(8) Layout of piping and cables

The following piping and cables were laid in the target station; a) coolant pipes for the shield block installed in the helium vessel, b) those for the middle-section part of the helium vessel, c) those for the proton beam window, d) super-critical hydrogen transport tubes to three kinds of moderators, e) vacuum pipes for vessel and shutter insert ducts, and f) power cables for shutter drive motors and beam profile monitors assembled in the proton beam window, g) signal cables from shutter position detection, beam profile monitors, and thermocouples attached to the in-vessel components and helium vessel and h) utility lines for monitor cameras, lights and power supply which are equipped in the shutter drive assembly area.

Since the pipes for items a) to d) contain highly activated coolant including tritium, their route was separated from the others. Those pipes except for c) were extracted out through flanges on the upper part of the helium vessel, laid in the box-shaped piping tray towards downstream (180˚ direction) and then extracted out of the outer-liner through sleeves. In Fig. 2.5.11, the layout of pipes in the piping tray is illustrated. The sleeves were pre-assembled in a steel frame and fixed outside the outer-liner prior to pouring magnetite concrete in which the boundary at the outer-liner was sealed with a plate. The piping tray was covered with side and top plates and surrounded with steel blocks with thickness of 20 cm.

The vacuum pipes and cables, the items e) to g), were laid from their origins and to an extraction port on the way of inner surface of the outer-liner. In order to make a boundary at the extraction port, a steel panel having penetration holes for all cables and vacuum pipes was prepared to close the port. All cables and vacuum pipes were laid in a sleeve which was built from the high-bay to the extraction port.

(9) Dry air ventilation

As a result of neutronics calculations, the components in which nuclear heating is estimated less than 0.001 W/cc were excluded from water cooling. However, the estimated total heat generated in those components reaches to 8.1 kW under operation of 1-MW proton beam. Therefore, we have introduced an idea that the induced heat is removed via dry air ventilation. A 250A pipe with some openings was installed around the outer vessel shield on the base-plate. The dry air is provided with the flow rate of 2,400 m^3/h at the temperature of 35˚C. The dry air returns from upper part of the outer-liner.

(10) Component installation procedure

According to the SNS project, it was estimated to take three years to install target station components under the condition that installation works were carried out in parallel with building construction. Considering the virtue to shorten installation duration, we also adopt the installation sequence in which building construction was carried out at the same period. The installation sequence of target station components are illustrated in Appendix 2.

The installation from the base-plate to the helium vessel was carried out as field work before frames and beams of the building were constructed. They are illustrated in Figs. A.1 (2) to (9). The installation of the helium vessel was the most important milestone among them because it defines not only the center line from proton beam line to the target trolley but also the origin of neutron beam lines.

The shield blocks, neutron beam shutter system including interstitial blocks were installed after the roof of the building was completed using in-house cranes.

(11) Guidelines for materials selection

Some of fundamental components employ parts to be exchanged at a certain period due to their performance deterioration under the radiation environment. Considering the radiation distribution in the neutron source station, therefore, we made a guideline for selecting materials and estimating life time of seal material and lubricant based upon the absorption dose rate. Estimated absorption dose and selected materials are summarized in Table 2.5.2.

2.5.2 Liners

As shown in Fig. 2.5.8, the liners are composed of a base-plate, a bottom- liner, an outer-liner, a target trolley liner and proton beam duct liner. They separate the atmosphere inside the neutron source station from the outer environment together with a roof shield as shown in Fig. 2.5.1. 23 neutron beam extraction ducts which are welded on the outer-liner also act as the liner.

2.5.2.1 Base-plate and bottom-liner

The base-plate and the bottom-liner are settled upon the basement concrete so that they form the bottom of the neutron source station. The design temperature, pressure and radiation exposure are less than 60˚C, normal pressure and 1 MGy/y at maximum, respectively. Drawings of the base-plate and the bottom-liner are shown in Figs. 2.5.12 and 2.5.13. Major specifications of those components are also summarized in Table 2.5.3. The base-plate is a disk plate having a diameter of 5 m, and aligns the vessel support cylinder on which the helium vessel was settled. It also supports the shield block placed inside the vessel support cylinder and that surrounds the helium vessel with outer diameter of 2.3 m. A drain pipe of 150 A is welded at the center of the base-plate.

The base-plate is as large as 5 m in diameter and supports heavy load over 1,000 tons. Therefore, a grouting method was adopted for installation of the base-plate on the basement concrete because it is recommended for installation of a large scale apparatus. The base-plate was settled on the concrete basement with anchor bolts and filler steels. There are 12 positions to adjust elevation level of the base-plate using jack bolts. The open holes for those bolts were closed with plates by seal welding. Photos 2.5.1 to 2.5.6 show the basement, the base-plate and the bottom-liner at the MLF site.

The dimensions of the anchor bolts were determined by the following strength assessment. The conditions are as follow;

(a) Total weight of components loaded upon the base-plate: W= 1,400 t
- helium vessel including in-vessel components: 170 t
- shielding blocks: 637 t
- shutter gate and shutter top shield: 560 t
- vessel support cylinder: 19 t
- proton beam window: 10 t

(b) Horizontal load from target trolley: F =30 t

(c) Loading point of the horizontal load: h = 3.2 m

(d) Distance from the supporting point on the base-plate to center of gravity: $L = 2.5$ m

(e) Horizontal acceleration: $K_H = 0.4$

(f) Vertical acceleration: $K_V = 0.2$

The overturning moment M_F is estimated as

$$\begin{aligned} M_F &= K_H \times W \times H + F \times h - (1- K_V) \times W \times L \\ &= 0.4 \times 1400 \times 5 + 30 \times 3.2 - (1\text{-}0.2) \times 1400 \times 2.5 \\ &= 96\ (\text{t•m}) \end{aligned} \tag{2.5.1}$$

It was designed that the twelve anchor bolts were located on the base-plate as shown in Figs. 2.5.12. Suppose that the supporting point is at the edge of 0˚ direction of the base-plated. Force given to pull up the anchor bolts has a relation as

$$2R_1{\times}X_1 + 2R_2{\times}X_2 + R_3{\times}X_3 + R_4{\times}X_4 + R_5{\times}X_5 + R_6{\times}X_6 + 2R_7{\times}X_7 + 2R_8{\times}X_8 = M_F\,, \tag{2.5.2}$$

where R_i and X_I stand for the force given to the i-th anchor bolt and the distance from the supporting point to the i-th anchor bolt, respectively. From the balance of the moment,

$$R_1 : R_2 : R_3 : R_4 : R_5 : R_6 : R_7 : R_8 = 652 : 1{,}735 : 1{,}853 : 2{,}232 : 2{,}768 : 3{,}147 : 3{,}265 : 4{,}348 \tag{2.5.3}$$

From Eqs. (2.5.1) to (2.5.3), R_1 is obtained 630 kg. Then, the maximum pull-up force of the bolt is estimated as 4,201 kg. Since the cross section of the M30 bolt is 519 mm^2, the tensile stress is estimated to be 8.1 kg/mm^2. This value is allowable.

The bottom-liner was settled on the basement as its inner edge was overlapped on the outer edge of the base-plate and welded for making a seal structure. Except for the path of the target trolley, magnetite concrete with the height of 900 mm was filled upon the bottom-liner, and the neutron shutter system, the steel shield around proton beam and that on both sides of target trolley liner were installed upon the magnetite concrete. At the path of the target trolley, a pair of rails were set on a base-plate with a bolt fixed upon the bottom-liner. Then, considering the load from the target trolley carrying mercury target and a mercury circulation system, the thickness of the bottom-liner was determined.

Considering the interval of foundation bolts on the bottom-liner, it is modeled that the load is imposed on the center of the disk with a diameter of 2.5 m of which peripheral was fixed. For that model, the induced stress is given by the following expression:

$$\sigma_{\max} = \frac{P}{t^2}\{1.3(0.485\ln\frac{r}{t} + 0.52)\} \tag{2.5.4}$$

Where, P is the load, r the radius of the disk and t the thickness, respectively. According to the design of target trolley rail, the horizontal load of 40 ton is generated at the target trolley. However, it is designed that the horizontal load is absorbed by cotters which fixes the target trolley rails and is not imposed upon the bolts. Only the force of 4 ton is imposed upward upon the steel plate by a rail in case of an earthquake. Since the rail is fixed with four bolts, then the load per one bolt is 1 t. Thus, P is 1,000 kg and r= 1,250 mm, t= 20 mm. Then, the induced stress is given as;

$$\sigma_{max} = 1000/20^2\,[0.485\,ln(1250/20)+0.52]$$
$$= 8.2\ (\mathrm{kg/mm^2}) \qquad (2.5.5)$$

On the other hand, the allowable stress σ_a of type 400 steel is

$$\sigma_a = 1.5 \times F/\ 1.5 \qquad (2.5.6)$$

Where $F = min\ (\sigma_y,\ 0.7\sigma_u)$ where σ_y and σ_u represent the yield strength and the tensile strength, respectively. For type 400 steel, F=24.2 kg/mm^2. Therefore, the σ_{max} is less than the allowable stress σ_a.

Therefore, the bottom-liner has enough strength against the load induced by the target trolley at the earthquake.

2.5.2.2 Outer-liner

The outer-liner was designed to be a self supportable structure although various openings were fabricated for a target trolley entrance, twenty three neutron beam extraction ports, a proton beam transport duct, an access door, air ventilation pipes, the piping tray and so on. It was divided into lower and upper parts. The drawings of the outer-liner are shown is Figs.2.5.14 and 2.5.15. Both ends of the upper and the lower parts were designed as flange shape. The dimension of the lower part was determined on the condition that it could be transported in a completed form using a carrier on way of the bridge having a limit load of 70 t en route to the J-PARC site. The resultant dimensions of the lower and upper parts are summarized in the Table 2.5.5. The photographs of the outer-liner in installation at the MLF site are given in Photos. 2.5.7 to 2.5.10.

We have assessed the strength of the side surface against the pressure which is added at magnetite concrete pouring around. Analyses were performed using the ABAQUS code. For a wall which is higher than 3 m and a height of concrete exceeds 1.5 m but no more than 4 m, the pressure (t/m^2) given by the concrete pouring is 1.5 W_o (kN/m^3), where W_o represents the force of concrete per unit volume. In the analysis, density of the magnetite concrete is 3.5 t/m^3. Then the pressure is obtained:

$$1.5 \times 3.5 \times 9.8 = 51.5\ (\mathrm{kN/m^2}) = 0.052\ (\mathrm{MPa}) \qquad (2.5.7)$$

Figs. 2.5.16 and 2.5.17 show the displacement and von Mises stress simulated by the ABACUS code for the magnetite concrete pouring up to 1.5 m in height and that from 1.5 to 3 m. It is estimated that the induced displacement (max. 0.8 mm) and von Mises stress (max. 38 MPa) are allowable.

We describe herein the structure and the construction method of surrounding magnetite concrete region because its specification affects the dimension and the structure of the outer-liner. Steel plate reinforced concrete wall method (SC structure) was employed which had higher ductility and shorter construction period than the reinforced concrete method. Steel plates were constructed around the outer-liner. Some steel beams with thickness of 9 mm were welded on both of the outer surface of the outer-liner and inner surface of surrounding steel plates. Stud bolts with a diameter of 19 mm were welded on the outer surface of the outer-liner with a pitch of 400 mm. The magnetite concrete was poured in the space between the outer-liner and steel plates in three times.

Finally, the thermal expansion of the outer-liner is mentioned. The environmental temperature conditions are as follows:

Temperature at installation: −5 to 30°C

Temperature in operation: 40°C

The estimated thermal expansion is summarized in Table 2.5.6. Here, the thermal expansion rate for type 400 steel is 11×10^{-6} /°C

2.5.2.3 Neutron beam duct

The neutron beam duct is a part of the neutron beam line and set at the bulk shield region. 22 beam ducts were designed as annular piped configuration as shown in Fig 2.5.18. Only one beam duct for the beam line No. 16 was designed as rectangular parallel-piped as shown in Fig 2.5.19, considering that vertical separation between the center lines of upper and lower neutron beam lines are large. One end of the beam extraction duct was welded on the outer-liner and the other was set on a supporting frame. The end has a flange structure which enables us to make a seal for the inner atmosphere. All neutron beam ducts were supported by a frame which was welded on steel beams connecting between the outer-liner and the steel plates for the SC structure. (see Photo. 2.5.11)

For example, assuming that the neutron beam duct is the simple beam and a lifting power acts on it by the magnetite concrete with a density of 3.4 g/cc, the lifting power is

$$W = 3.4 \times 0.159^2 \times \pi = 0.27 \text{ (t/m)}. \quad (2.5.8)$$

The maximum deformation at the midst of the duct is estimated as

$$\begin{aligned} \delta_{max} &= 10 \times 0.27 \times 2.38^4 / 384 \times 2.1 \times 10^7 \times 5.04 \times 10^{-5} \\ &= 2.14 \times 10^{-4} \text{ (m)} \quad (2.5.9) \end{aligned}$$

This value is quite acceptable.

2.5.2.4 Target trolley liner

Figs. 2.5.20 and 2.5.21 show the assembling drawings of the target trolley liner. It has box-like configuration that fits the outline of the target trolley. It was divided into four parts. Two were installed inside and the remaining two were set outside the outer-liner. The target trolley liner creates a gap from the target trolley towards irradiated components handling room. Accordingly its horizontal and vertical dimensions change at 3,503 mm and 6,253 mm from the center, respectively, so that they could suppress neutron streaming along the gap. Inner width and height of the target trolley liner were determined under the condition that the minimum gap, in other words, battery limit between the target trolley and the target trolley liner was 10 mm and the accuracy of both components was 15 mm including installation accuracy.

Since the target trolley liner was scheduled to be installed prior to constructing magnetite concrete outside of the outer-liner, it was designed to be self-supportable structure to have enough strength against the force imposed by the concrete and assure the design gap from the target trolley. The thickness of the target trolley liner was determined 20 mm based upon the stress analyses. Fig, 2.5.22 shows the result of the stress analyses. For the part inside the outer-liner, maximum stress is induced at the forefront of the target trolley liner which contacts at the target insertion hole of the helium vessel. Since the analysis neglected neither the welding the divided two parts nor rectangular opening on both sides, the analytical results underestimated the amount of the deformation. As a matter of fact, the dimension of the shielding block of the target trolley was determined based upon the data measured after constructing magnetite concrete structure around the target trolley liner.

The bottom, the head and the tail of the target trolley liner which was installed inside the outer-liner were welded to the bottom-liner, the flange for target insertion port of the helium vessel and inside the outer-liner, respectively. Photos. 2.5.12 and 2.5.13 show the target trolley liner installed at the MLF site.

2.5.2.5 Proton beam duct liner

(1) Structure

Fig. 2.5.23 shows the assembling drawing of the proton beam duct liner. The proton beam duct liner was designed as the parallel-piped configuration with 4.73 m long to contain a proton beam pipe having a diameter of 406.4 mm. One end of the liner was set on the proton beam window support of the helium vessel (see Figs 2.5.26 and 2.5.28 of the next subsection) and the middle part of the liner was welded with a plate to the outer liner to make the boundary of the atmosphere inside the outer-liner. The proton beam pipe had flange structures on both ends and four stopper plates were mounted on the flange at downstream side at 90° interval. It was inserted into the proton beam duct liner from upstream side and rotated 45° so that the stopper plates could fit in front of the support plates mounted inside the proton beam liner. The support plate play a role of supporting a load of 3.5 t imposed on the flange of the proton beam pipe by a pillow seal of the proton beam window for making a seal.

The proton beam pipe was fixed to the proton beam duct liner at the upstream end using a bellows. The bellows also plays the role to absorb the thermal expansion of the proton beam pipe. It was designed to adjust the thermal expansion of 5 mm. Photos. 2.5.14 and 2.5.15 show the proton beam duct liner in installation at the MLF site.

(2) Structural strength assessment

Structural assessments were carried out using the ABAQUS code to determine the thickness of the proton beam duct liner. The proton beam duct was modeled with three-dimensional shell elements. As the boundary condition, the middle of the duct was rigidly fixed. The displacement and the von Mises stress predicted by the simulation are given in Fig. 2.5.24. The analytical results suggest that the thickness above 15 mm is needed for the proton beam duct.

The analytical results of the case that the horizontal load is added by the pillow seal are also shown in Fig. 2.5.24**.** Judging from those analytical results, the thickness of the liner was determined as 19 mm.

The temperature distribution, the thermal expansion and the thermal stress of the proton beam duct were also simulated under the condition that the heat generation in the duct was 159 W with environmental temperature of 40°C and the thermal transfer rate of 5 W/m^2K. Here the heat generation was factored by 1.5. The calculation model of two-dimensional axial symmetry elements was made for the most downstream 1,700 mm long part of the proton beam (*i.e.* proton beam window side). The analytical results shown in Fig. 2.5.25 suggest that the highest temperature of 83ºC appears at the end of the proton beam pipe and the largest displacement of 0.8 mm takes place at that part. The highest thermal stress of 105 MPa is induced at the portion where the proton beam duct liner is fixed to the outer-liner. Those estimated values are allowable.

2.5.3 Helium Vessel

(1) Outline of helium vessel

The helium vessel was designed to satisfy the following requirements that

(a) works as a boundary of inactive helium gas which suppresses the production of corrosive and harmful gases such as radioactive gas, ozone, NO_X *etc.*,
(b) works as an explosion-proof pressure boundary against hydrogen leakage at a failure of moderator piping,
(c) works as the third boundary for mercury although the mercury target container is designed to have a safety hull which prevents mercury from leaking to outside even though the container wall is broken,
(d) works as the second boundary for coolants provided to reflectors and steel shields where induced activities in coolants are estimated as the second highest next to mercury,
(e) has the port structure around middle-section for installing vessel insert ducts with windows from outside of the helium vessel so as to be the boundary between helium and surrounding atmosphere,
(f) has a proton beam insertion port and a supporting structure for installing proton beam window assembly just upstream of the helium vessel,
(g) has a target insertion port,
(h) has an open structure on the top for installation and extraction of a moderator-reflector assembly with shielding plug,
(i) has the reference structure to support the moderator-reflector assembly with shielding plug.

The following design guidelines were also introduced:

(a) Helium vessel is un-exchanged through the designed operational life-time of 30 years,
(b) Helium vessel contains all components which are required to be cooled, so that it could enclose activated coolants even though they were leaked,
(c) Helium vessel has neutron beam ports in which vessel insert ducts are installed,
(d) Neutron beam ports have enough cross sectional dimension to extract neutrons directly from the origin of moderator’s viewed surface with a cross section of 100×100 mm^2,

(e) Helium is enclosed in the helium vessel in slight higher pressure than outside normal atmosphere, because it is difficult to circulate helium in negative pressure.

Figs. 2.5.26 and 2.5.27 show design drawings of the helium vessel. The design conditions of the helium vessel are summarized in Table 2.5.7. It is designed that the helium vessel is exhausted to a vacuum of about 1,000 Pa to fill helium gas up to the pressure level of about 250 mmAq. It is also planned the maximum pressure in helium vessel is 0.25 MPa in a safety point of view that the pressure release mechanism by means of a rupture disk is activated to exhaust gas to a dump tank when hydrogen is leaked from moderator components.

Some of them were determined taking account of specifications of opponent compositions. Considering that the helium vessel defines the origin for installation of the proton beam line upstream, the target trolley downstream and neutron beam lines, we have designed that the bottom of the middle-section as the reference horizontal plane of the helium vessel. Major structural highlights of the helium vessel are summarized as follows.

(a) Type 316L stainless steel was chosen as material under consideration that life-time is 30 years.
(b) Resultant dimension is 6.4m in height with the maximum outer diameter of 4.4 m.
(c) The middle-section part has annular cylindrical configuration with inner and outer diameters of 1.8 m and 3.0 m respectively and height of 1.4 m, in which water-cooed steel shielding blocks are contained.
(d) The top of the inner cylindrical surface of the middle-section supports the weight of about 98 tons of in-vessel components of the moderator-reflector assembly with steel shielding plug and the surrounding water-cooled steel shielding. It also equips positioning pins of 50 mm in diameter to install the in-vessel components precisely.
(e) The inner diameter of upper part of the helium vessel enlarges from 2.0 m to 2.3 m to prevent neutron streaming along the gap between helium vessel and surrounding shielding blocks.
(f) The bottom of the helium vessel has a spatial volume of 380 litters which can afford to store the coolants and/or target fluids even if they are leaked from piping or containers. A drain pipe was welded to the bottom of the helium vessel to exhaust the ingredients to a dump tank which was set at another room downstream the target station.

Moreover, the height of vessel was determined by the concept that top of in-vessel components was located 3 m from the proton beam line height and had a certain space inside the helium vessel to access piping from in-vessel component. The piping from in-vessel components are extracted to outside through flanges on upper part of the helium vessel. The piping extracted from the in-vessel components are listed in Table 2.5.8.

(2) Neutron beam ports and insertion holes on middle-section

As shown in Fig 2.5.27, twenty-three parallel-piped neutron beam ports extend radially on the horizontal plane. The outer edge of the beam port is flange structure on which the flange of the vessel insert duct is fixed with bolts and nuts by using a remote handling device. Two positioning pins are set on the top surface of the flange to give the reference for installation of the vessel insert duct. Outer cross sectional dimension of the rectangular-shaped vessel insert duct is 112 × 112 mm^2 with thickness of 5 mm. In order to extract full cross sectional size of neutron beam from moderator's viewed surface of 100 × 100 mm^2 through the vessel insert duct, the inner dimension of the neutron beam port was designed as 124 × 124 mm^2 by taking account of its accuracies in fabrication and installation.

The required accuracy of the central axis of the vessel insert duct to the theoretical beam center line at the top surface of the flange was set within 2 mm, and the allowable deviation of the installed neutron beam line center on the viewed surface from that of the theoretical one was within 3 mm in both y and z-axis. The alignment accuracy is the sum of accuracies on manufacturing and installation. The specifications on accuracy are listed in Table 2.5.9. Table 2.5.10 shows the maximum allowable error for the positioning pin position on the top surface of the flange and allowable inclination of the flange surface with respect to both horizontal and vertical planes including the theoretical beam center line. This indicates that maximum deviation value of the positioning pin may be 4 mm that exceeds the required value of 2 mm. As a matter of fact, the flange position and the inclination of flange surface were adjusted to satisfy the required accuracy after the helium vessel was installed on the vessel support cylinder. The resultant deviation of the flange from the beam center line and inclination to the reference horizontal and vertical planes are listed in Table 2.5.11.

Fig.2.5.28 shows the drawing of the proton beam insertion part on the middle-section. A support stage for the proton beam window was mounted in front of the proton beam insertion hole. It had a rough guide and positioning holes of 29 mm in diameter for bringing down the proton beam window along vertical insertion port. The pillow seal of the proton beam window was extended by helium gas pressuring and contacted on the flange of the proton beam injection hole to make a seal. The proton beam injection hole is rectangular configuration of 250 mm in width and 120 mm in height. This size is much wider than the designed proton beam profile of 130 mm in width and 50 mm in height and accepts proton beam without causing heat deposition on the middle-section by the beam even though uncontrolled beam spill takes place .

Fig. 2.5.29 shows the drawing of the target insertion hole which is located on the opposite side from the proton beam insertion hole. The dimension of the target insertion hole gradually becomes larger along positive direction of the x-axis. It is designed to have a gap of 10 mm from the target container surface when it is inserted. There is a flange structure with outer diameter of 1,050 mm around the insertion hole at the outside. A metallic seal ring attached on the target container is pressed upon this flange so that it can make a seal between helium and the atmosphere in target handling room. The design force was set 30 kN to achieve sound seal performance. Both flange surfaces of the proton beam and the target insertion holes have precise perpendicularity within 0.5 mm to the horizontal plane.

The accuracy of the neutron beam duct on the middle-section is very important because it is the origin for alignment of the subsequent neutron beam line components arrayed on the downstream.

(3) Structural analyses of helium vessel

This horizontal load is taken into account for determining the structure of the helium vessel. The earthquake proof structural analysis was also carried out under condition that horizontal load of 0.4G was added. The analytical model is shown in Fig. 2.5.30. The following boundary condition was employed: the middle-section is completely bound to the vessel support cylinder whose base is fully fixed upon the base-plate. The total weight of the vessel support cylinder and the helium vessel is 182 t including in-vessel components.

Fig. 2.5.31 shows the displacement and von Mises stress distribution on the helium vessel caused by the dead load of the helium vessel and the external horizontal load of 30 kN at the target insertion hole for the seal. The analytical result suggests that the maximum displacement takes place at the top of the helium vessel and the maximum von Mises stress of 22 MPa arises at the target insertion port. We have selected the thickness of the helium vessel at 50 mm based on the analytical study.

As shown in Fig. 2.5.32, additional horizontal load of 0.4G, which is equal to 75 t, induces the maximum von Mises stress of 59 MPa at the upper body where the inner diameter varies from 2.0 m to 2.3 m. This value is less than the allowable stress of 100 MPa for 316L stainless steel.

The von Mises stresses induced by the internal pressure of 0.3 MPa and the cooling water pressure of 0.8 MPa were also estimated. For both cases, the maximum von Mises stress appears at the plate of the proton beam insertion hole. The resultant displacement and von Mises stress distributions are shown in Figs. 2.5.33 to 2.5.35.

(4) Detailed design of middle-section

Fig. 2.5.36 shows the cross sectional plane views of the middle-section at the upper and lower moderator elevation, respectively. Some neutron ports geometrically overlap with neighboring ones inside the middle-section. Instead of employing straight single duct, therefore, a fan-shaped block in which the rectangular holes with a dimension of 104 × 104 mm^2 was introduced on the water cooling sector and individual straight duct was welled on this block for beam lines No.1 to 6. Fan-shaped blocks without beam hole segment were also employed for beam lines No.7-11 and No.18-20.

The thickness of the beam duct and the fan-shaped block was determined based upon the structural analysis using the ABAQUS code. The analytical model is displayed in Fig. 2.5.37. The conditions used in analyses are as follows:

(a) the inner and outer cylindrical bodies, neutron beam ducts and/or the fan-shaped block are modeled by three-dimensional shell elements,

(b) the body of the middle-section is completely solidified,

(c) pressure load of coolants is 0.8 MPa,

(d) Young modulus of 316L stainless steel is 190 GPa at 100 ºC.

Figs. 2.5.38 and 2.5.39 show the analytical results of induced displacement distribution and von Mises stress for the beam duct with thickness of 25 mm. The result indicates that the maximum von Mises stress arises at the contact position of the fan-shaped block for beam lines No.7-11 with outer cylindrical body of the middle-section. Since the von Mises stress increases as the thickness of the beam duct becomes thinner, 25mm thickness was chosen.

As far as the cooling performance of the type 316L stainless steel shielding block enclosed in the middle-section part is concerned, it is necessary to suppress the temperature rise in shielding block made of SS316L as low as possible to reduce the probability of the stress corrosion cracking. The allowable maximum temperature in the steel block was set as 100°C. The pressure drop of coolant flow was selected as less than 0.2 MPa. Considering the dimensional condition that the steel block is enough thick as 900 mm, we have selected to create cooling channel by means of layer structure of plates. Fig. 2.5.40 shows the illustration of the shielding block. Fig. 2.5.41 shows a cross sectional view of the layer structure of the steel plates enclosed in the middle-section. The coolant flows into the plenum region at the bottom block and goes upward through the zigzag path formed by the steel blocks and the inner or outer cylindrical container walls. Some gaps around target insertion holes were filled with plates to make the zigzag path.

The hydraulics analysis was carried out using the STAR-CD code to determine the cooling channel structure. The middle-section was modeled by the 307 million cells of which 117 millions were for fluid region. The number of vertex was about 315 millions. The physical constants used in the analysis are listed in Table 2.5.12. Suppose that the coolant flows in the cooling channel uniformly, the Reynolds number R_e is obtained by the relation of $R_e = \rho V d_e / \eta$, where ρ stands for the coolant density, V the coolant velocity, d_e the equivalent diameter of cross section of the coolant channel and η the coolant viscosity coefficient. For the coolant velocity of 12 m^3/h, the average velocities at inner and outer channels are 0.111 m/s and 0.072 m/s, respectively. Then, the Reynolds numbers for those channels are 1,306 and 84, respectively. Since both values are less than the critical Reynolds number of 2300, the flow condition in the steel blocks is regarded as the laminar flow.

We have decided to divide the middle-section into three segments, namely the target insertion hole region, the proton beam injection hole region, and the rest of major steel layer region. This gives enough flow rate to cool the region where the maximum heat density is deposited. Therefore, three coolant inlets are made as shown in Fig. 2.5.40. The inlet flow rates are 2 m^3/h for the target insertion hole and the proton beam injection hole regions, and 8 m^3/h for the major steel layer region, respectively. The resultant temperature distribution is shown in Fig. 2.5.42. The maximum temperature was estimated as 71.2°C at the vicinity of the proton incident hole. The pressure loss between the inlet and the outlet was estimated about 3,300 Pa. These values satisfy the design criteria described above.

(5) Support components

The helium vessel is settled upon the vessel support cylinder which is installed on the base-plate. The drawing of the vessel support cylinder is shown in Fig. 2.5.43. The vessel support cylinder gives reference elevation for the helium vessel and supports its weight. Its dimension is 2,200 mm in diameter and 2,400 mm in height. Two positioning pins were fixed on the top surface of the vessel support cylinder so that the position of the helium vessel could be defined precisely. The thickness of the vessel support cylinder was determined at 150 mm based upon the structural analyses described in (3) in this subsection.

Additional strength assessment for key parts of the vessel support cylinder is reported in this part. The conditions employed for the structural strength assessment are listed in Table 2.5.13.

Moreover, four vessel support beams were installed at the elevation of 1FL+ 4,910 mm to support the load at earthquake. The layout of the vessel support beams is shown in Fig. 2.5.44. The vessel support beams were arranged asymmetrically on the horizontal plane due to the geometrical constraint and the strength assessment was conducted with the ABACUS code. In consequence, steel plate of H200 × 200 × 8 was employed as the support beam. Fig. 2.5.45 shows the analytical results considering some load conditions. The analysis predicts that the maximum von Mises stress of 94 MPa appears at the portion which the support beam is fixed on the helium vessel. This value is lower than the allowable stress for type 400 steel of 100 MPa. It is noted that one end of the support beam was fixed on the outer-liner by welding while the other end was just contacted on the helium vessel to release the excess load induced by the thermal expansion due to heat deposition in beam operation.

(a) Strength assessment for the positioning pin on the vessel support cylinder

With conditions that the helium vessel itself and the in-vessel component weigh 65 t and 94 t, respectively, the horizontal load from the target trolley is 30 t and the additional load is 0.4G at earthquake, the maximum horizontal load P (kg) is calculated as

$$\begin{aligned} P &= (65{,}000+94{,}000) \times 0.4 + 30{,}000 \\ &= 93{,}600 \end{aligned} \tag{2.5.10}$$

For the positioning pin of 40 mm diameter, the total cross section A (mm) is calculated as

$$\begin{aligned} A &= \pi 40^2/4 \times 2 \\ &= 2{,}513 \end{aligned} \tag{2.5.11}$$

Then, the shearing stress τ of the positioning pin is obtained as

$$\begin{aligned} \tau &= P/A \\ &= 37.3 \text{ (kg/mm}^2\text{)} \end{aligned} \tag{2.5.12}$$

The allowable stress is defined by $F = min(\sigma_y,\ 0.7\sigma_u)$ where σ_y and σ_u represent the yield strength and the tensile strength, respectively. According to Table 2.5.14, $0.7\sigma_u = 636$ for type 630 stainless steel, $F = 636$ (N/mm^2) = 64.8 (kg/mm^2). The allowable shearing stress is given by

$$\tau_a = 1.5 \times F/(1.5\sqrt{3}) = 37.4 \text{ (kg/mm}^2\text{)}. \tag{2.5.13}$$

From Eqs. (2.5.12) and (2.5.13), the induced shearing stress τ is less than the allowable stress τ_a. Hence, the positioning pin is enough strength against the horizontal load.

(b) Strength assessment for the welding structure

A ring-shaped plate was welded at the bottom of the vessel support cylinder so that it had a flange like structure. The butt welding method was employed in which the welding length was 30 mm.

Since the horizontal load is imposed at the elevation of 3,120 mm, the overturning moment M acting at the welding part of the bottom is obtained as

$$M = 30{,}000 \times 9.8 \times 3{,}120 = 9.18 \times 10^8 \text{ (N·mm)} \tag{2.5.14}$$

The modulus of section Z for the butt welding is obtained as follows:

$$Z = Z1 + Z2 = \frac{\pi(1960^4 - 1900^4)}{32 \times 1960} + \frac{\pi(2200^4 - 2140^4)}{32 \times 2200}$$

$$= 1.958 \times 10^8 \text{ (mm}^3\text{)} \tag{2.5.15}$$

Therefore, the bending stress σ_b is obtained as

$$\sigma_b = M/Z = 4.7 \text{ (N/mm}^2\text{)} \tag{2.5.16}$$

At design temperature of 40°C, $0.7\sigma_y = 308$, then F=225 N/mm^2. The allowable bending stress is given by

$$\sigma_a = \eta F/1.5 \tag{2.5.17}$$

where η represents the welding efficiency. Suppose that η=0.45 for the butt welding, σ_a is obtained as 67 N/mm^2. Therefore σ_b (4.7) is lower than the allowable bending stress σ_a=67 N/mm^2.

When an earthquake occurs, total horizontal load is obtained by adding the load of the vessel support cylinder itself,

$$93{,}600 + 19500 \times 0.4 = 101{,}400 \text{ kg} = 993{,}720 \text{ (N)} \tag{2.5.18}$$

Since the center of gravity of the helium vessel installed on the vessel support cylinder is 3,800 mm in elevation, the overturning moment of these components is 3.78x10^9 (N mm). Hence, the bending stress σ_b at the earthquake is obtained as

$$\sigma_b = (9.18\times10^8 + 3.78\times10^9)/\ 1.958 \times 10^8 = 24.0 \text{ (N/mm}^2\text{)} \tag{2.5.19}$$

The allowable bending stress for the earthquake is 1.5 σ_b = 100 N/mm^2. Therefore, the induced bending stress is lower than the allowable bending stress even at the earthquake.

As for the shearing stress, the cross section of the welding portion is calculated as follows:

$$A = A1 + A2 = \frac{\pi(1960^2 - 1900^2)}{4} + \frac{\pi(2200^2 - 2140^2)}{4}$$

$$= 386{,}416 \text{ (mm}^2\text{)} \tag{2.5.20}$$

Since the shearing force added by the horizontal force from the target trolley is 30,000x9.8 =294,000 (N), the shearing force is obtained as

$$\tau = F/A = 294{,}000/386{,}416 = 0.8 \text{ (N/mm}^2\text{)} \tag{2.5.21}$$

This value is lower than the allowable shearing stress of τ_a=37.4 N/mm^2. On the other hand, the shearing force F' at the earthquake is F'=294,000+993,720 = 1,287,720 (N). For this case, the shearing force is estimated as

$$\tau' = F'/A = 1{,}287{,}720/386416 = 3.4\ (\mathrm{N/mm^2}) \tag{2.5.22}$$

This value is also lower than the allowable shearing force of 1.5 τ_a = 55 N/mm^2.

2.5.4 Shield Blocks

2.5.4.1 General configuration

Figs. 2.5.46 through 2.5.48 show a general configuration of the shield blocks and related components in the target station. This section deals with shield blocks shown in thick frames in the figures and some related shield. The vessel support cylinder shield [A] is located inside the vessel support cylinder and below the He-vessel. The He-vessel is surrounded by the outer vessel shield [B, C, D]. The ring shield [E] is set on the outer vessel shield and the vessel top shield [F] is placed on the ring shield to cover the He-vessel. A space between the outer vessel shield and the outer-liner is filled by the proton beam part shield [G] for the upstream direction, and by the target trolley part shield [H] for the downstream direction. Over the proton beam window (PBW) and the PBW plug, the PBW top shield [K] is located. The piping tray is covered with the piping tray shield [J]. All the shield blocks mentioned so far are contained in the outer-liner. Whole the target station is covered by the roof shield [I], and the airtight plate above the roof shield seals atmosphere in the target station. The outer-liner is surrounded by biological shield made of heavy concrete.

Table 2.5.15 summarizes pieces, material and weight of the shield blocks. All the shield blocks except for the biological shield are made of steel and ordinary concrete. The total weight of steel exceeds 2,000 tons, and that of ordinary concrete is about 240 tons. Note that these weights do not include the He-vessel, in-vessel components, shutter system, PBW components and target system.

The maximum weight of the shield blocks is limited to 70 tons because shield blocks over 70 tons do not pass over a bridge located between the Port of Hitachinaka and the J-PARC site. If shield blocks are stored temporarily in the No.1 Experimental Hall, the maximum weight is limited to 50 tons due to the crane capacity. An earthquake acceleration of 0.25 G is adopted as a seismic design criterion. Conceptual design, configuration and installation of the shield blocks are described in references.[2.5-1, -2, -3, -4)]

2.5.4.2 Functions of each shield block

(1) Vessel support cylinder shield [A]

- Attenuate neutrons downward
- Make a space for the drain line of the He-vessel

(2) Outer vessel shield [B, C, D]

- Attenuate neutrons
- Hold the vacuum line pipes for the neutron beam extraction ports of the He-vessel
- Make a space for cooling water pipes for the He-vessel

- Make a well-shaped port for the PBW
- Make a space for the dry-air duct at the bottom
- Give a horizontal plane to install the shutter system, and bear its weight load

(3) Ring shield [E]

- Attenuate neutrons upward
- Attenuate gamma-rays mainly emitted from the ^{16}N activity in the cooling water pipes in and around the He-vessel during beam-on to protect the shutter drives from exposure dose
- Attenuate gamma-rays mainly emitted from the ^{7}Be activity in the cooling water pipes in and around the He-vessel during beam-off to protect workers from exposure dose
- Make spaces for pipes and PBW exchange work
- Give a plane to install the attachment for the floor valve, and bear weight load of the shielding cask and the in-vessel components or PBW during exchange work
- Be evacuated when pipes surrounding the He-vessel need to be maintained

(4) Vessel top shield [F]

- Attenuate neutrons upward
- Attenuate gamma-rays mainly emitted from the ^{16}N activity in the cooling water pipes in and around the He-vessel during beam-on to protect the shutter drives from exposure dose
- Attenuate gamma-rays mainly emitted from the ^{7}Be activity in the cooling water pipes in and around the He-vessel during beam-off to protect workers from exposure dose
- Be movable when the lid of the He-vessel is opened

(5) Proton beam part shield [G]

- Attenuate neutrons forward with respect to the proton beam direction
- Make a space for the proton beam line

(6) Target trolley part shield [H]

- Attenuate neutrons backward with respect to the proton beam direction
- Make a space for the target system

(7) PBW top shield [K]

- Attenuate neutrons upward
- Attenuate gamma-rays mainly emitted from the ^{16}N activity in the cooling water pipes in and around the He-vessel during beam-on to protect the shutter drives from exposure dose
- Attenuate gamma-rays mainly emitted from the ^{7}Be activity in the cooling water pipes in and around the He-vessel during beam-off to protect workers from exposure dose
- Give a plane to install the attachment for the floor valve, and bear weight load of the shielding

cask and the PBW during exchange work

- Be evacuated when the PBW is exchanged (lid of the shield)

(8) Piping tray shield [J]

- Attenuate neutrons upward
- Attenuate gamma-rays mainly emitted from the ^{16}N activity in the cooling water pipes in and around the He-vessel during beam-on to protect the shutter drives from exposure dose
- Attenuate gamma-rays mainly emitted from the ^{7}Be activity in the cooling water pipes in and around the He-vessel during beam-off to protect workers from exposure dose
- Be evacuated when pipes in the piping-tray are maintained

(9) Roof shield [I]

- Attenuate neutrons upward
- Be evacuated when components in the target station are maintained

2.5.4.3 Shielding Design

(1) Calculation method

Shielding calculation was performed with Monte Carlo particle transport codes such as MCNPX and PHITS. There are many gaps and void spaces in the target station. These shield defects can be significant streaming paths. Hence detailed 3-dimensional calculation models were employed to consider the streaming effects precisely in the calculations. Details of the shielding calculations are described elsewhere.[2.5-5, -6, -7, -8, -9, -10, -11)]

(2) Target radiation dose rate

A target radiation dose of 12.5 μSv/h, which was a value used throughout the J-PARC project, was adopted. Unlimited access is allowed for radiation workers under the target dose rate. The following correction factors and the safety margins were taken into consideration.

(a) A correction factor for underestimation of high-energy neutron fluxes in deep penetration calculation in steel with MCNPX: 3

Underestimation of 20% per shield thickness of 1 m was assumed. The correction factor to total shield thickness was $1/0.8^{4.8} \sim 3$ where 4.8 m was the radius of the outer-liner. Correction factors for concrete were not considered since high-energy neutron fluxes in concrete were overestimated, i.e., safety side, with MCNPX.

(b) A correction factor for dose by low-energy neutrons and gamma-rays : 2

In determining shield thickness, dose rates by only neutrons above 10 MeV were calculated for simplification of calculation. It was assumed that the total radiation dose including low-energy neutrons below 10 MeV and gamma-rays was lower than twice of the dose rate due to high-energy neutrons. This assumption was valid since the concrete shields surrounding the steel shields were thick enough (~2 m) to attenuate low-energy neutrons.

(c) A safety factor to the shielding evaluation with Monte Carlo codes that was commonly used in the J-PARC Project : 2

By considering the three factors, a target design dose rate of 1 μSv/h (~ 12.5/(3×2×2)) for calculated dose rate values by neutrons above 10 MeV was adopted.

(3) Source term

The mercury target that receives the 1-MW proton beam is the major source term for the shielding calculation. About 10^{17} neutrons per second are produced at the rated 1-MW operation. The PBW is another neutron source term. Although its beam power of about 3 kW is much weaker than that of the mercury target, attention should be paid for streaming effects upward along the PBW plug. The 23 neutron beam lines are also important neutron source terms because they penetrate through the bulk shield to the experimental halls.

Cooling water is highly activated by neutron irradiation. ^{16}N ($T_{1/2}$ = 7 s) in the activated water is a strong gamma-ray source along cooling water lines during beam-on. ^{7}Be ($T_{1/2}$ = 51 days) produced in water deposits inner surfaces of cooling water pipes, and is a gamma-ray source during beam-off. Although gamma-ray intensity from ^{7}Be is not as strong as that from ^{16}N, shielding against ^{7}Be has to be also considered because workers approach to the cooling water pipes for maintenance.

(4) Bulk shield

As for the horizontal direction, the target and moderators are surrounded by the reflector in which beryllium and steel blocks are contained as shown in Figs. 2.5.46 through 2.5.48. The reflector is surrounded by the water-cooled shield and the middle-section of the He-vessel both of which are made of stainless steel and cooled by water. Then the He-vessel is folded by the Outer vessel shield that fills out spaces up to R = 2.3 m from the center. Spaces outside the Outer vessel shield and inside the outer-liner (2.3 < R < 4.8 m) are filled with the Proton beam part shield, Target trolley part shield and the shutter system all of which are made of steel mostly. Accordingly, most of shielding materials in the outer-liner for the horizontal direction are steel and stainless steel that attenuate high-energy neutrons effectively due to their high density. Although small amount of water is contained in the in-vessel components and the middle-section of the He-vessel, other shield blocks do contain little hydrogenous materials, and shielding performance for low-energy neutrons below 1 MeV is not so high. The biological shield made of heavy concrete surrounding the outer-liner compensates this defect to attenuate low-energy neutrons accumulated in the steel shield blocks effectively.

As for the vertical upward direction, situation is similar to the horizontal direction. Most of shielding materials are made of steel and stainless steel in the outer-liner. A vertical distance from the proton beam height (1FL+1,600) to upper surfaces of the Proton beam part shield and the target trolley part shield (1FL+5,100) is 3.5 m. Note that the upper surfaces correspond to a floor of the neutron shutter drive mechanism room as indicated in Fig. 2.5.46. Total shield thicknesses of the roof shield are 1.00 m and 1.14

m for steel and ordinary concrete, respectively. Steel in the shield blocks inside the outer-liner and in the roof shield are effective for high-energy neutrons while the thick concrete shield in the roof shield attenuates low-energy neutrons. The steel shield in the outer-liner has an ordinary concrete layer of about 200 mm in thickness as shown in Fig. 2.5.47 with rounded squares. The concrete layer is very effective to attenuate low-energy neutrons to reduce activation level in the neutron shutter drive mechanism room. This is required because workers enter into the room for maintenance during beam-off.

(5) Measures for radiation streaming

In addition to the bulk shielding performance, suppression of the radiation streaming effects is another concern for the shielding design. Measures for radiation streaming are illustrated in Fig. 2.5.49. Bending structures are adopted at many locations in the target station as shown with rounded squares in Fig. 2.5.49. Step widths of the bending structures were determined by the 3-D Monte Carlo simulation calculations.

Three hydrogen transfer lines and many cooling water lines penetrate vertically in the reflector plug. Although these lines bend at least once in the reflector plug, bulk shielding performance to the upward direction is deteriorated due to the streaming effects through the lines as shown in Fig. 2.5.49 with the Arrow A. The vessel top shield of which thickness is 1 m suppresses the streaming effects.

Shielding structure along the arrow B is one of weak points if the ring shield [E] does not exist. This is because the path takes a route in the beryllium in the reflector, there is a shielding defect at the bending section along the path, and the vessel top shield [F] does not cover the path. The ring shield [E] compensates adequately the weak point.

Thickness of the biological shield surrounding the target station is determined by two points of view. One is for attenuation of neutrons generated in the mercury target, and the other is for that of neutrons coming from neutron beam lines as indicated as the arrow C in Fig. 2.5.49. Actually the latter condition is severer. The radius of the biological shield ranges between 7.5 m for the forward angles with respect to the proton beam direction and 7.0 m for the backward angles.

2.5.4.4 Material specifications

(1) Steel

Rolled steel for general structure (SS) of which specifications were defined in JIS (Japanese Industrial Standards) was used in many shield blocks. In addition, use of slab steel was allowed because of its low cost and availability of very thick steel plates up to 230 mm. One of demerits to use slab steel lay in warp of steel plates. When several slab steel plates were stacked to make a shield block, it was unavoidable to eliminate gaps between neighboring plates. The gaps lowered apparent density of the shield block. Accordingly, an apparent weight density of 7.6 g/cm^3 was adopted as the minimum value for every shield blocks made of steel. Note that the value is 3.3% lower than the theoretical weight density of steel, 7.86 g/cm^3.

(2) Concrete

Lower limits of weight density of 2.2 g/cm^3 and 3.4 g/cm^3 were adopted for ordinary and heavy concrete, respectively. Three cylindrical test pieces were taken at the time when concrete was poured in. Dimensions and weights of the test pieces were measured after 28 days drying period. Weight densities were deduced from the measured data and were checked whether the values exceed the lower limit value or not.

2.5.4.5 Fabrication

Steel plates were gas-cut into desired shapes. They were stacked to make a shield block. Because of the warp of the steel plate, gaps between neighboring plates were filled with steel shim plates and grout. The filling process was effective to make the neighboring plates stable, to eliminate streaming paths, and not to be compressed when many massive shield blocks were piled up. Then the neighboring plates were welded each other along their outer surface. If the shield block contained a concrete layer, concrete was poured into a vacant space prepared in advance. Finally the shield block was coated by paint.

Typical items for factory inspection were (a) quantity inspection, (b) appearance inspection, (c) dimensional inspection, (d) density inspection, (e) combinatory inspection and (f) welding inspection (PT).

References

2.5-1) H. Takada, F. Maekawa, et al.: “Target Station Design of 1 MW Spallation Neutron Source at the High Intensity Proton Accelerator Facilities J-PARC”, Proc. of the 16th Meeting of the Int. Collaboration on Advanced Neutron Sources (ICANS-XVI), May 12-15, 2003, Düsseldorf-Neuss Germany, Volume III, 2003, pp. 1115-1126.

2.5-2) H. Takada, T. Kato, M. Kaminaga, H. Natsume and Y. Hoshino: “Planning and Implementation of Large and Heavy Components of 1-MW Spallation Neutron Source for Japan Proton Accelerator Research Complex (J-PARC)”, JAEA-Technology 2006-060, 2007, in Japanese.

2.5-3) Materials and Life Science Experimental Facility Construction Team: “High Intensity Proton Accelerator Project (J-PARC) Technical Design Report, Materials and Life Science Experimental Facility”, JAERI-Tech 2004-001, 2004, in Japanese. Shield blocks are described in pp. 608-610 in Volume 1 and shielding calculation is described in pp. 1035-1088 in Volume 2.

2.5-4) K. Yoshida, F. Maekawa and H. Takada: “Basic Design of Shield Blocks for a Spallation Neutron Source under the High-intensity Proton Accelerator Project”, JAERI-Tech 2003-019, 2003, in Japanese.

2.5-5) F. Maekawa, M. Teshigawara, C. Konno, Y. Ikeda and N. Watanabe: “Shielding Design Study for the JAERI/KEK Spallation Neutron Source”, Proc. of 15th Meeting on Advanced Neutron Sources, ICANS-XV, Nov. 6-9, Tsukuba, Japan, JAERI-Conf 2001-002, 2001, pp. 907-916.

2.5-6) F. Maekawa, M. Teshigawara, H. Takada, M. Furusaka and N. Watanabe: "Study on Bulk Shielding for a Spallation Neutron Source Facility in the High-intensity Proton Accelerator Project", JAERI-Tech 2002-035, 2002, in Japanese.

2.5-7) F. Maekawa and M. Tamura: "3-D Shielding Calculation Method for 1-MW JSNS", Proc. of the 16th Meeting of the Int. Collaboration on Advanced Neutron Sources (ICANS-XVI), May 12-15, 2003, Düsseldorf-Neuss Germany, Volume III, 2003, pp. 1051-1058.

2.5-8) M. Tamura, F. Maekawa and Y. Ikeda: "3-Dimensional Shielding Design for a Spallation Neutron Source Facility in the High-Intensity Proton Accelerator Project", Proc. of the 16th Meeting of the Int. Collaboration on Advanced Neutron Sources (ICANS-XVI), May 12-15, 2003, Düsseldorf-Neuss Germany, Volume III, 2003, pp. 1077-1086.

2.5-9) F. Maekawa, M. Tamura, M. Kawai, M. Furusaka and N. Watanabe: "A New Method for Neutron-Beam-Line Shielding Calculation", Proc. of the 16th Meeting of the Int. Collaboration on Advanced Neutron Sources (ICANS-XVI), May 12-15, 2003, Düsseldorf-Neuss Germany, Volume III, 2003, pp. 1247-1255.

2.5-10) M. Tamura and F. Maekawa: "3-Dimensional Shielding Design for a Spallation Neutron Source Facility in the High-intensity Proton Accelerator Project", JAERI-Tech 2003-010, 2003, in Japanese.

2.5-11) M. Tamura, F. Maekawa, M. Harada, K. Haga and C. Konno: "Shielding Design for Target Trolley for a Spallation Neutron Source in J-PARC Project", JAERI-Tech 2005-020, 2005, in Japanese.

Table 2.5.1: Coordinates of the neutron beam-line origins and the directions with respect to the proton beam line

Beam line No.	Type of moderators*1)	Origin of beam line (x, y, z)*2) [mm]	Azimuthal angle θ*3)[deg]
1	CM	(11.5, 22.2, −163.0)	38.5
2	CM	(11.5, 22.2, −163.0)	47.5
3	CM	(11.5, 22.2, −163.0)	56.5
4	CM	(11.5, 22.2, −163.0)	65.5
5	CM	(11.5, 22.2, −163.0)	74.5
6	CM	(11.5, 22.2, −163.0)	83.5
7	PM	(−99.4, −27.5, 158.0)	90.8
8	PM	(−99.4, −27.5, 158.0)	97.5
9	PM	(−99.4, −27.5, 158.0)	104.2
10	DM	(88.3, 54.2, 158.0)	116.2
11	DM	(88.3, 54.2, 158.0)	123.7
12	DM	(88.3, 54.2, 158.0)	134.0
13	CM	(−13.4, −21.1, −163.0)	−149.0
14	CM	(−13.4, −21.1, −163.0)	−136.3
15	CM	(−13.4, −21.1, −163.0)	−123.6
16	CM	(−13.4, −21.1, −163.0)	−110.9
17	CM	(−13.4, −21.1, −163.0)	−98.2
18	PM	(−95.5, −57.2, 158.0)	−89.3
19	PM	(−95.5, −57.2, 158.0)	−82.5
20	PM	(−95.5, −57.2, 158.0)	−75.7
21	DM	(106.6, 30.4, 158.0)	−64.6
22	DM	(106.6, 30.4, 158.0)	−52.4
23	DM	(106.6, 30.4, 158.0)	−40.2

*1) PM: Poisoned decoupled moderator
DM: Decoupled moderator
CM: Coupled moderator

*2) The coordinates are based on the right-handed coordinate system in which the origin is lie on the center of the helium vessel and the advancing direction of the proton beam is defined as the positive of x-axis. Vertical upward direction is the positive of the z-axis.

*3) θ stands for the angle of a designed neutron beam line with respect to the positive direction of x-axis.

Table 2.5.2: Estimated absorption dose and materials for some parts used in components

Parts	Estimated absorption dose rate	Materials	Comment
Seal for vessel insert ducts and shutter inserts	1 MGy/y	Metal O-ring	
Lubricant for vessel insert ducts and shutter inserts	1 MGy/y	Grease Radiation resistance 100 MGy	
Polyethylene on the shutter gate	5 kGy/y		
Seal for piping on top of helium vessel	5 MGy/y	Metal seal	
Seal of lid on top of helium vessel	1.3 MGy/y	EPDM	Exchange every year

Table 2.5.3: Major specifications of the base-plate and the bottom-liner

	Base-plate	Bottom-liner
Material	Type 400 steel	Type 400 steel
diameter (mm)	5,000	9,900 (outer) 4,900 (inner)
thickness (mm)	80	20
anchor bolts, nuts and washers	M30 × 12 pairs	M24 × 24 pairs
jack bolts, nuts and washers	M36 × 12 pairs	M36 × 12 pairs

Table 2.5.4: Allowable values

Allowable stress for a bolt (σ_b)	231	154
Allowable shearing stress for a bolt (τ_b)	132	88
Allowable bond stress for concrete (M)	19.8	13.2
Allowable shearing stress for concrete	1.08	0.72
Allowable compressive stress for concrete	156.8	78.4

Table 2.5.5: Dimensional specifications of the outer-liner

Items	Upper part	Lower part
Material	Type 400 steel	Type 400 steel
Inner diameter (mm)	9,940	9,540
Thickness (mm)	30	30
Height (mm)	2,450	6,600
Openings		
for an access door	1,600 × 700 at elevation of 1,045	–
for cable ducts	750 sq. at elevation of 1,325	–
	330 sq. at elevation of 1,800	–
for piping chasing pan outlet	930 × 1,820 at elevation of 504	–
for air circulation outlet	300 diam. at elevation of 1,925	–
	167 diam. at elevation of 2,000	–
for see through		
for neuron beam ports		380 diam. at elevation of 3,258
		380 diam. at elevation of 2,937
		241 × 716 at elevation of 2,527.7
for target trolley entrance		1,820 × 3,865 at elevation of 2,062.5
for proton beam duct		685 sq. at elevation of 3,100
for air circulation inlet		300 diam. at elevation of 255
for a drain pipe from helium vessel		100 diam. at elevation of 305

Table 2.5.6: Estimated thermal expansion of base-plate, bottom-liner and outer-liner

Name of component	At installation	At operation
Base-plate	−0.8 mm (at −5°C) / 0.3 mm (at 30°C)	0.6 mm (at 40°C)
Bottom-liner	−1.4 mm (at −5°C) / 0.6 mm (at 30°C)	1.1 mm (at 40°C)
Outer-liner (radial)	−1.4 mm (at −5°C) / 2.5 mm (at 30°C)	1.2 mm (at 40°C)
(elevation)	−2.5 mm (at −5°C) / 1.0 mm (at 30°C)	2.0 mm (at 40°C)

Table 2.5.7: Design conditions of helium vessel

Items		Specification
Proton beam	Incident proton energy	3 GeV
	Injected beam power	1 MW
Design pressure	Resisting pressure of Helium atmosphere	+0.3 MPaG, −0.1 MPaG
	Resisting pressure of water-cooled shielding	+0.8 MPaG
	Horizontal load by lateral seismic factor	0.25 G
	Horizontal load by seal pressure of target trolley	300 kN
	Seal pressure by proton beam window	35 kN
Cooling of middle-section	Coolant	Light water
	Coolant pressure	0.6 MPa (max.)
	Coolant inlet temperature	35°C
	Coolant flow rate	< 15 m^3/h
	Total heat generation	30 kW
	Maximum power density	0.2 W/cc at vicinity of proton beam injection hole
Neutron beam port	No. of beam ports	23
	No. of ports for poisoned DM	6
	No. of ports for DM	6
	No. of CM	11

Table 2.5.8: List of piping and cables penetrating through the upper body of helium vessel

Origin	Name	Number	Medium	Dimension
Moderators	Liquid hydrogen transport tube for PM	1	LH_2	80A Multi-layer piping
	Liquid hydrogen transport tube for DM	1	LH_2	80A Multi-layer piping
	Liquid hydrogen transport tube for CM	1	LH_2	80A Multi-layer piping
	Coolant piping for PM	2	H_2O	25A × Sch40
	Coolant piping for DM	2	H_2O	25A × Sch40
	Coolant piping for CM	2	H_2O	25A × Sch40
Reflector	Coolant piping	2	D_2O	50A × Sch40
Reflector plug	Coolant piping for inner plug	2	H_2O	25A × Sch40
	Coolant piping for outer plug	2	H_2O	25A × Sch40
Water-cooled shielding	Coolant piping	1	H_2O	50A × Sch40
	Vacuum piping	1	Vacuum	40A × Sch40
	Hydrogen discharge piping	1	Gas	80A × Sch40
	Gas supply piping	1	Gas	10A × Sch10s
	Helium sampling piping	1	Gas	8A × Sch8s
Reflector and water-cooled shielding	Thermo-couple cables	1	Signal	feed-through (48 cores)

Table 2.5.9: Required accuracies on neutron beam ports

Items	Specifications
Required accuracy for installation of vessel insert ducts	
Center position at 2070mm from center axis of helium vessel.	< ±2 mm
Allowable shifts of center of viewed surface from that of the designed	< ±3 mm in both y and z-axis.
Required accuracy for installation of vessel insert ducts	
Accuracy of origin (center axis of vessel)	< ±1 mm
Elevation of reference plane	< ±0.5 mm
Horizontality of reference plane	< ±0.5/2070 radian
Azimuthal error	< ±0.5/2070 radian
Neutron beam ports	
Parallelization between neutron beam ports and theoretical neutron beam line	< 2 mm
Accuracy of center position of flange	< ±2 mm from center of theoretical neutron beam line
Perpendicularity of the flange surface with respect to the plane including neutron beam line and vertical to the reference plane.	< 0.2 mm

Table 2.5.10: Maximum allowable error of the positioning pin location on the flange of neutron beam ports

	Accuracy in radial direction	Accuracy on elevation
At installation	Centering error : 1 mm Azimuthal error : 1 mm	Position error : 0.5 mm Horizontality : 0.5 mm
At fabrication	Positioning pin location : 2 mm	Positioning pin location : 2 mm
Total	4 mm	3 mm

Table 2.5.11: Accuracy of each neutron beam port after installation

No. of beam line	Deviation from the center of neutron beam line in horizontal (H) and vertical (V) direction.	Perpendicularity of the flange surface to the vertical (H) and the horizontal planes (V) including neutron beam line center.
No.1	+1.8 mm (H)/ +0.6 mm (V) *1	−1.4 mm (H)/ +0.5 mm (V) *2
No.2	+1.2 mm (H)/ +0.9 mm (V)	−0.5 mm (H)/ −0.2 mm (V)
No.3	+1.5 mm (H)/ +0.7 mm (V)	−1.8 mm (H)/ +1.9 mm (V)
No. 4	+1.0 mm (H)/ +0.7 mm (V)	−0.4 mm (H)/ 0.0 mm (V)
No.5	+1.8 mm (H)/ +0.6 mm (V)	+0.7 mm (H)/ +0.2 mm (V)
No.6	+1.3 mm (H)/ +1.3 mm (H)	−0.8 mm (H)/ +0.9 mm (V)
No.7	−0.1 mm (H)/ +1.5 mm (H)	−0.4 mm (H)/ +1.8 mm (V)
No.8	−0.6 mm (H)/ −1.1 mm (V)	−0.4 mm (H)/ +0.4 mm (V)
No.9	−0.7 mm (H)/ +2.3 mm (V)	−0.2 mm (H)/ +3.8 mm (V)
No.10	−1.2 mm (H)/ +0.5 mm (V)	−1.0 mm (H)/ +0.6 mm (V)
No.11	−1.5 mm (H)/ +1.0 mm (V)	−0.3 mm (H)/ +2.5 mm (V)
No.12	−1.7 mm (H)/ −1.3 mm (V)	+0.1 mm (H)/ −4.0 mm (V)
No.13	−1.0 mm (H)/ +1.0 mm (V)	+0.1 mm (H)/ −3.5 mm (V)
No.14	−0.2 mm (H)/ +0.7 mm (V)	−0.8 mm (H)/ −3.3 mm (V)
No.15	+0.3 mm (H)/ +0.4 mm (V)	+0.1 mm (H)/ −2.3 mm (V)
No.16	/ +2.0 mm (V)	/ +1.1 mm (V)
No.17	−1.1 mm (H)/ +0.5 mm (V)	−0.1 mm (H)/ +0.1 mm (V)
No.18	+0.4 mm (H)/ −0.7 mm (V)	+0.7 mm (H)/ −1.6 mm (V)
No.19	+0.2 mm (H)/ −1.8 mm (V)	+0.9 mm (H)/ −0.8 mm (V)
No.20	−1.2 mm (H)/ −0.7 mm (V)	+0.7 mm (H)/ +0.5 mm (V)
No.21	−0.5 mm (H)/ +0.6 mm (V)	+0.9 mm (H)/ +0.4 mm (V)
No.22	+1.3 mm (H)/ −0.3 mm (V)	−1.7 mm (H)/ +1.0 mm (V)
No.23	+1.6 mm (H)/ −1.0 mm (V)	+0.2 mm (H)/ −0.3 mm (V)

Note:

*1: The "+" and the "–" marks in horizontal direction "H" indicates that the center of the neutron beam port shifts rightward and leftward from the center line of the neutron beam line viewing from inside the helium vessel, respectively. Those in vertical direction "V" mean that the center shifts upward and downward from the center line of the neutron beam line.

*2: The "+" mark on "H" means that the flange rotates clock-wise on the vertical and the "–" mark indicates the rotation counter-clock wise viewing from upper direction, respectively. The "+" mark on "V" means that the upper edge of the flange inclines towards the helium vessel and the "–" mark indicates the reverse inclination, respectively.

Table 2.5.12: Physical constants employed in the STAR-CD calculation

Items	Conditions
Coolant density	1000 kg/m^3
Coolant viscosity coefficient	854.3 μPa·s
Coolant thermal conductivity	0.6106 W/mK
Coolant specific heat	4179 J/kgK
Density of SS	7800 kg/m^3
Thermal conductivity of SS	43 W/mK
Specific heat of SS	473 J/kgK

Table 2.5.13: Materials and loading conditions for the vessel support cylinder

Items	Specification
Materials of vessel support cylinder	
-cylindrical body	Type SF440 steel
-flange at bottom	Type 400 steel
-positioning pin	Type 630 stainless steel
Diameter of the positioning pin,	40 mm
Weight of the vessel support cylinder	19.5 tons
Weight of the helium vessel	65 tons
Weight of the in-vessel component	94 tons
Horizontal load by the target trolley	30 tons
Horizontal acceleration by earthquake	0.4G

Table 2.5.14: Yield strength and tensile strength of steels employed for the vessel support cylinder

Materials	Yield strength σ_y	Tensile strength σ_u
Type SF440 steel	225 N/mm^2 at 40°C	440 N/mm^2
Type 400 steel	237 N/mm^2 at 60°C	389 N/mm^2 at 60°C
Type 630 stainless steel	793 N/mm^2 at 100°C	909 N/mm^2 at 100°C

Table 2.5.15: Materials and weights of shield blocks

Block name	ID	Piece	Weight [tons]		
			Steel	Concrete	Total
Vessel support cylinder shield	A	1	22.7	−	22.7
Outer vessel shield (lower)	B-1	2	95.3	−	95.3
	B-2	2	100.2	−	100.2
Outer vessel shield (middle)	C-1	2	39.9	−	39.9
	C-2	2	47.5	−	47.5
Outer vessel shield (upper)	D-1	2	67.9	−	67.9
	D-2	2	44.6	5.4	49.9
	D-3	2	81.2	−	81.2
Ring shield	E	1	42.7	−	42.7
Vessel top shield	F	2	89.1	−	89.1
Proton beam part shield	G-1	1	52.3	−	52.3
	G-2	1	40.1	−	40.1
	G-3	1	34.9	−	34.9
	G-4	1	55.6	−	55.6
	G-5	1	55.6	−	55.6
	G-6	1	36.2	−	36.2
	G-7	1	4.6	4.5	9.1
	G-8	1	49.3	−	49.3
Target trolley part shield	H-1	1	50.6	−	50.6
	H-2	1	42.1	−	42.1
	H-3	1	28.1	−	28.1
	H-4	1	42.5	−	42.5
	H-5	1	42.5	−	42.5
	H-6	1	4.6	4.5	9.1
	H-7	1	49.1	−	49.1
Roof shield	I-1	2	97.2	31.3	128.5
	I-2	2	95.2	30.8	126.0
	I-3	3	148.5	46.2	194.7
	I-4	2	97.8	31.3	129.1
	I-5	2	77.2	23.6	100.8
	I-6	2	97.4	30.2	127.6
	I-7	2	98.8	30.6	129.4
Piping tray shield	J	1	27.2	−	27.2
PBW top shield	K	1	21.6	−	21.6
Airtight plate	L	4	28.8	−	28.8
Total			2,008.9	238.4	2,247.3

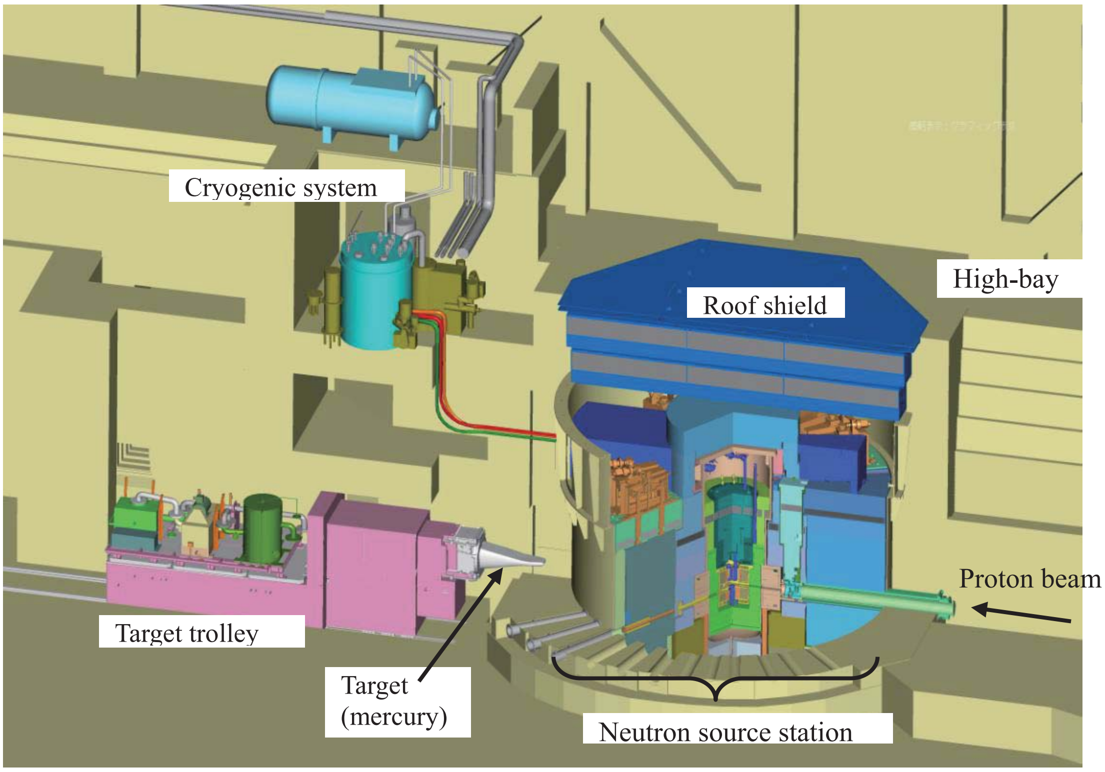

Fig.2.5.1: 3D view of neutron source station and target trolley in MLF building

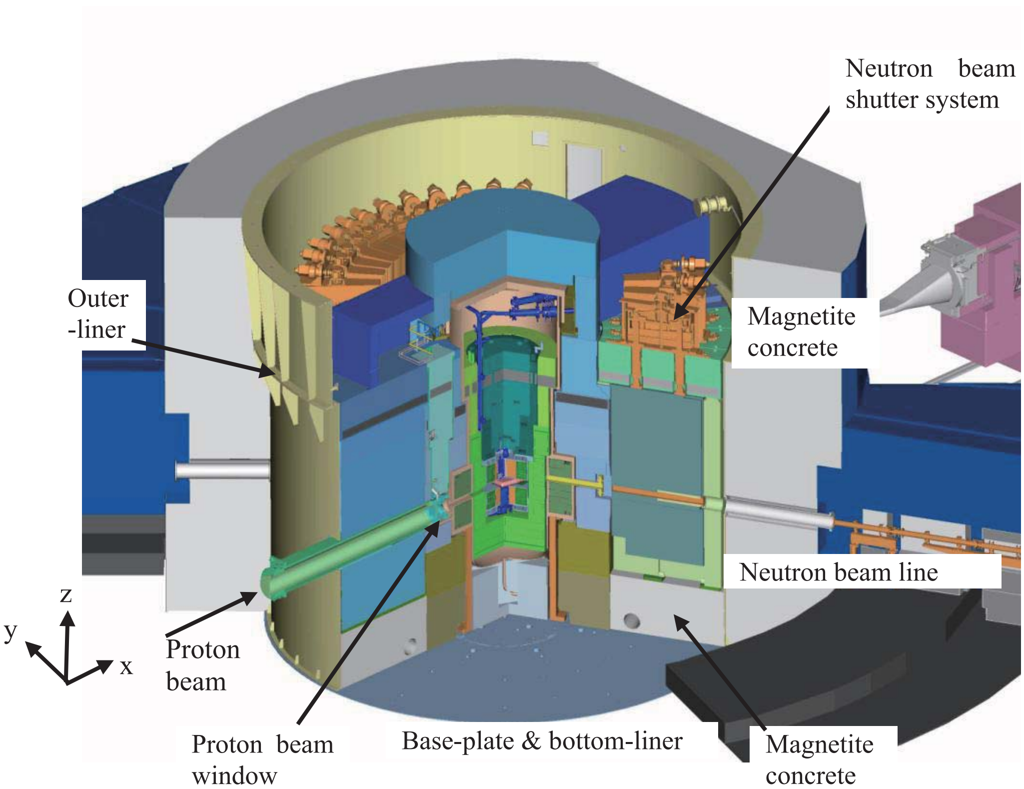

Fig.2.5.2: 3D view of neutron source station

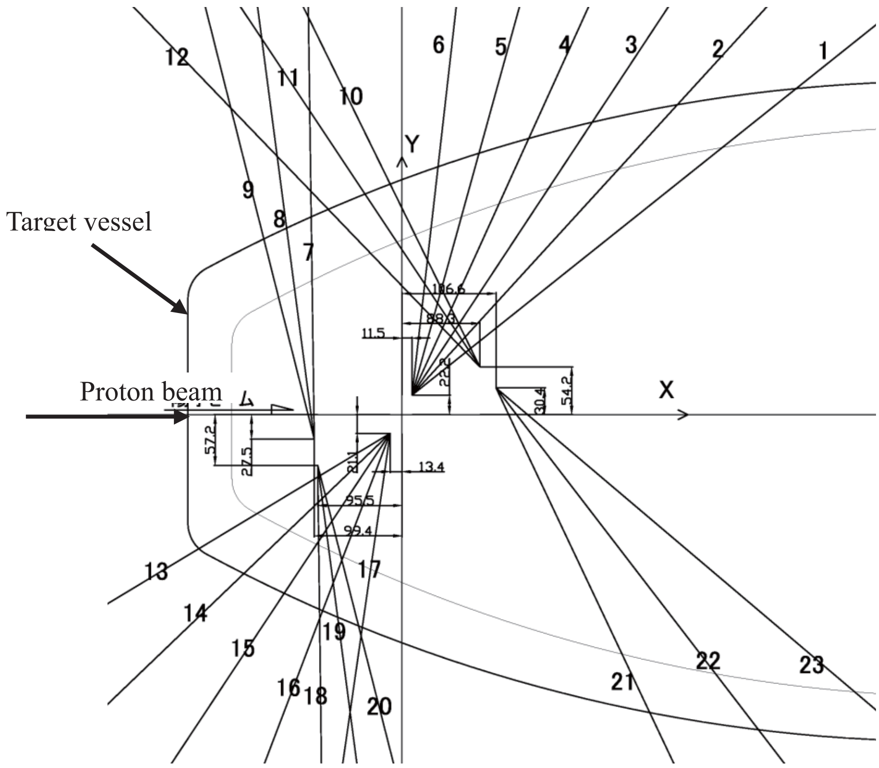

Fig.2.5.3: Projection of six origins for 23 neutron beam lines on the horizontal plane. The number from 1 to 23 indicates the neutron beam line number

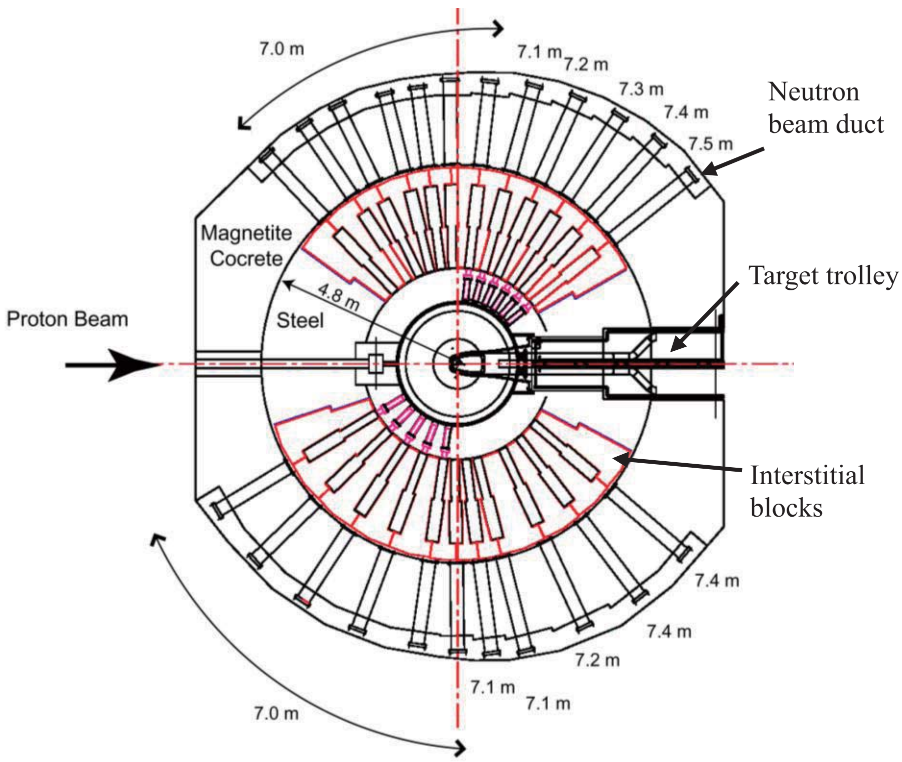

Fig.2.5.4: Plane view of neutron source station at the elevation of proton beam line

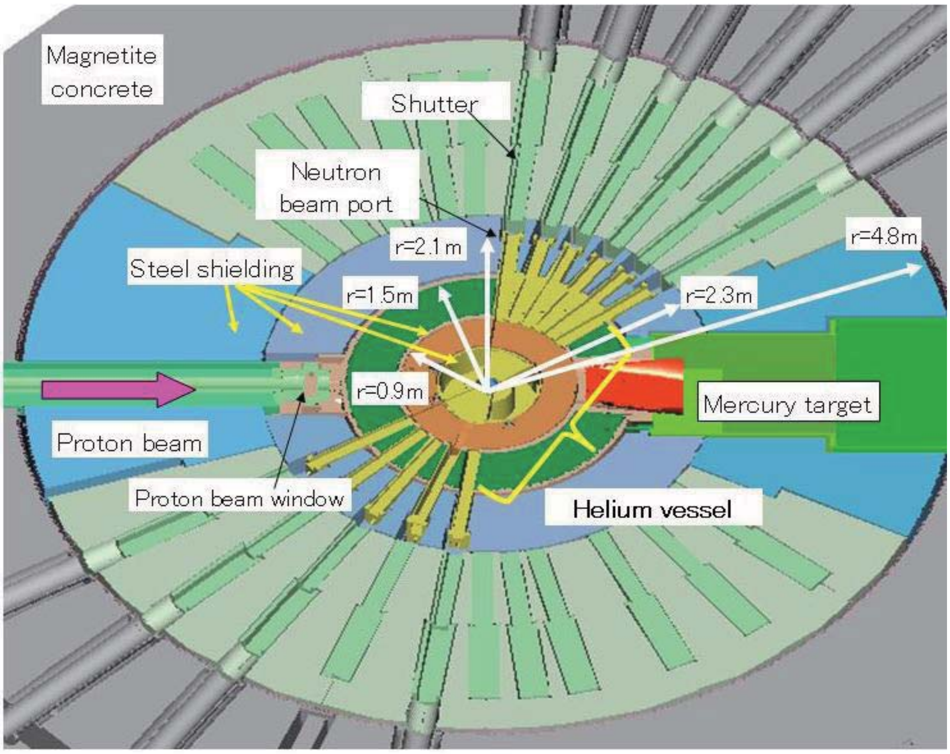

Fig.2.5.5: 3D cross sectional view of neutron source station at the elevation of proton beam line

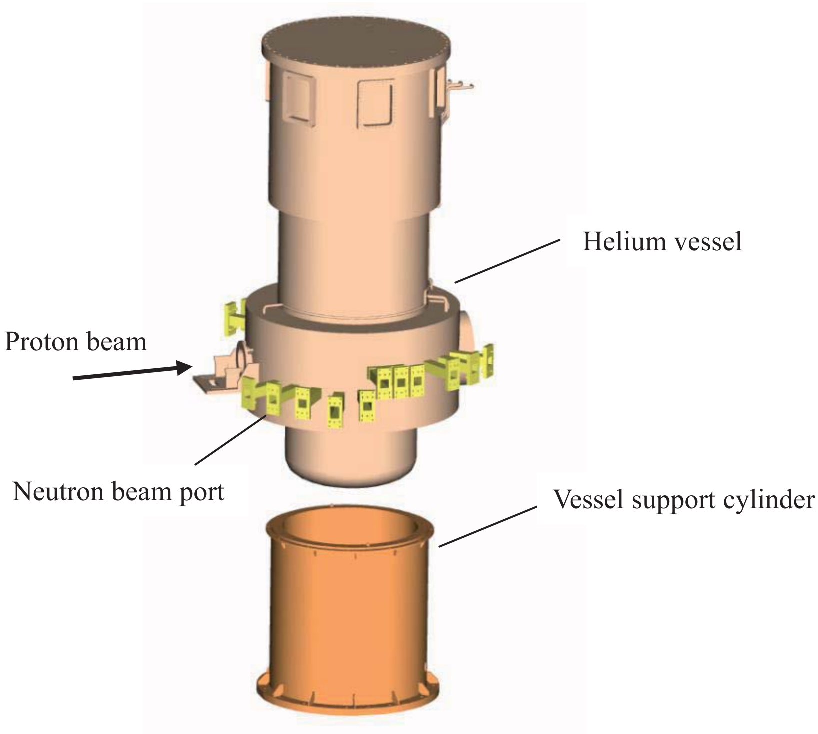

Fig.2.5.6: Overview of helium vessel and vessel support cylinder

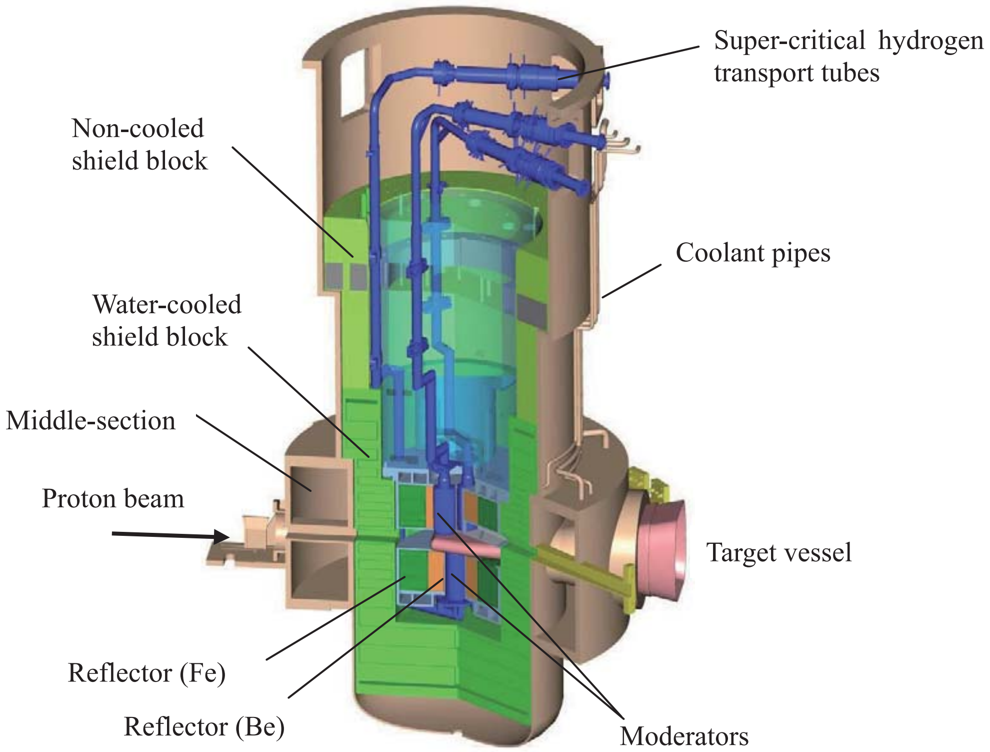

Fig.2.5.7: Cross sectional view of the helium vessel containing in-vessel components

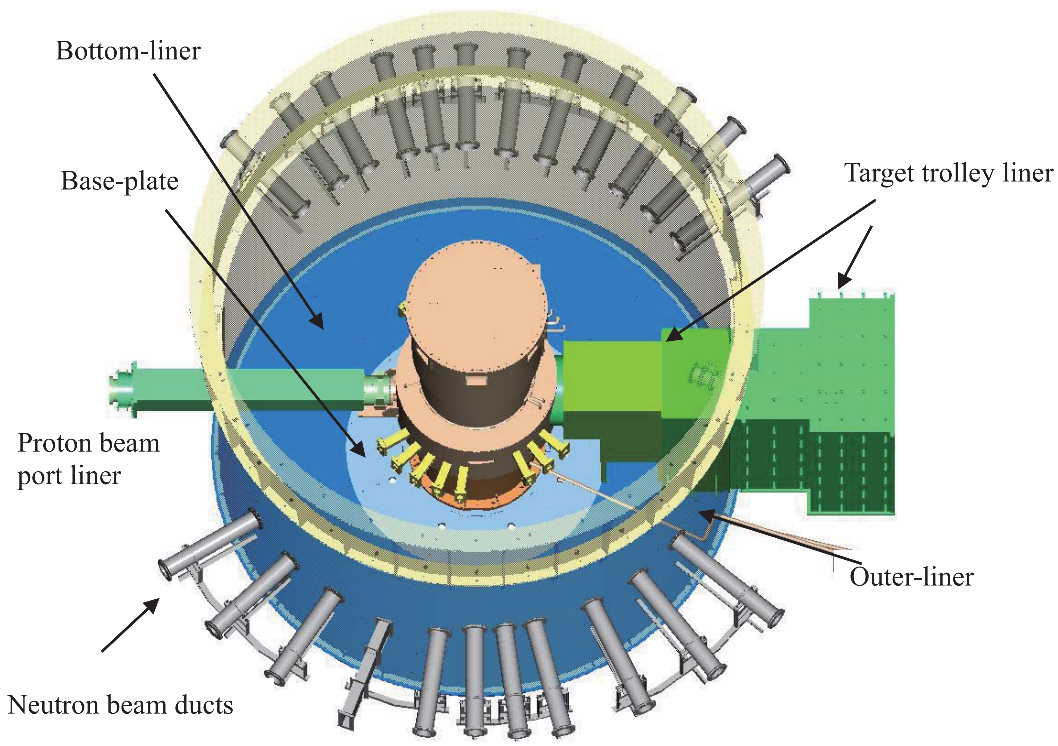

Fig.2.5.8: Overview of liner components layout in neutron source station

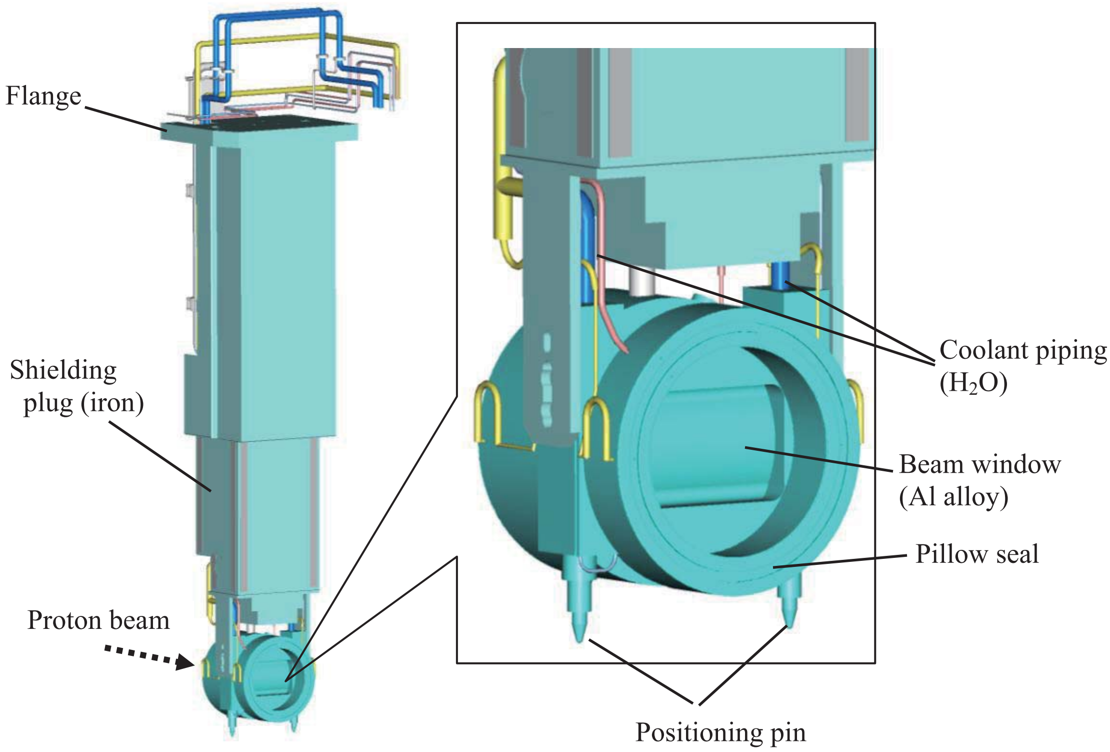

Fig.2.5.9: Overview of proton beam window assembly

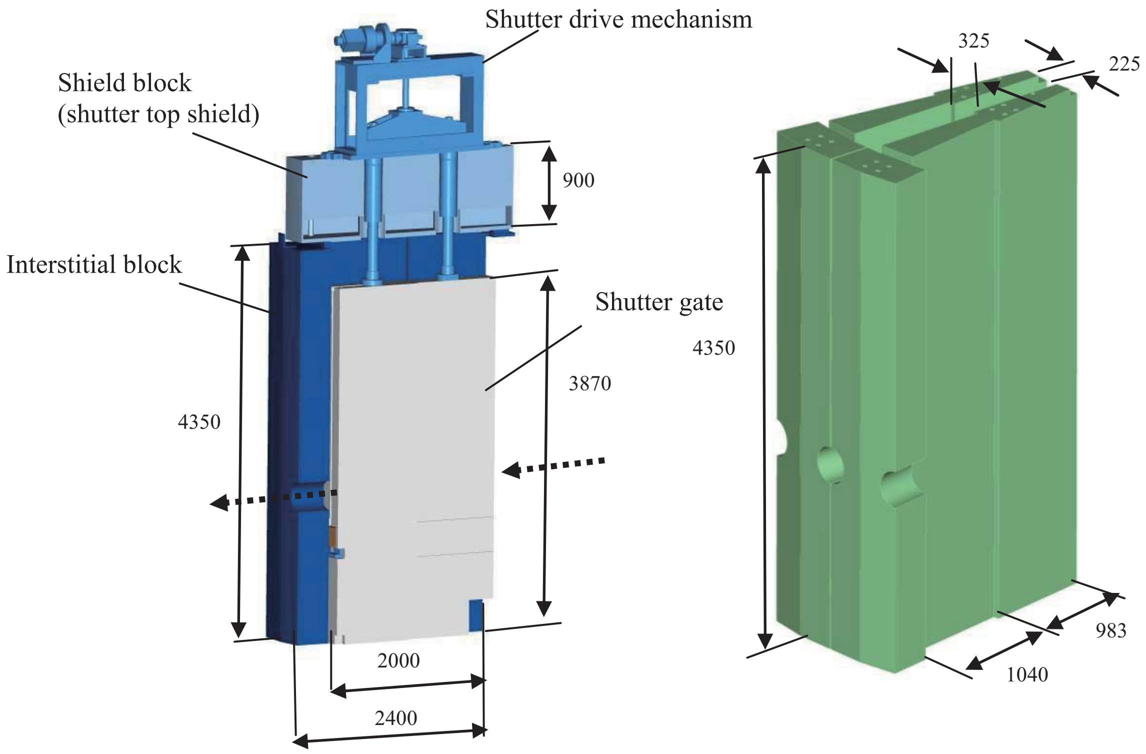

Fig.2.5.10: Overview of neutron beam shutter system. Composition of shutter system (left) and a pair of interstitial blocks creating moving space for a shutter gate (right)

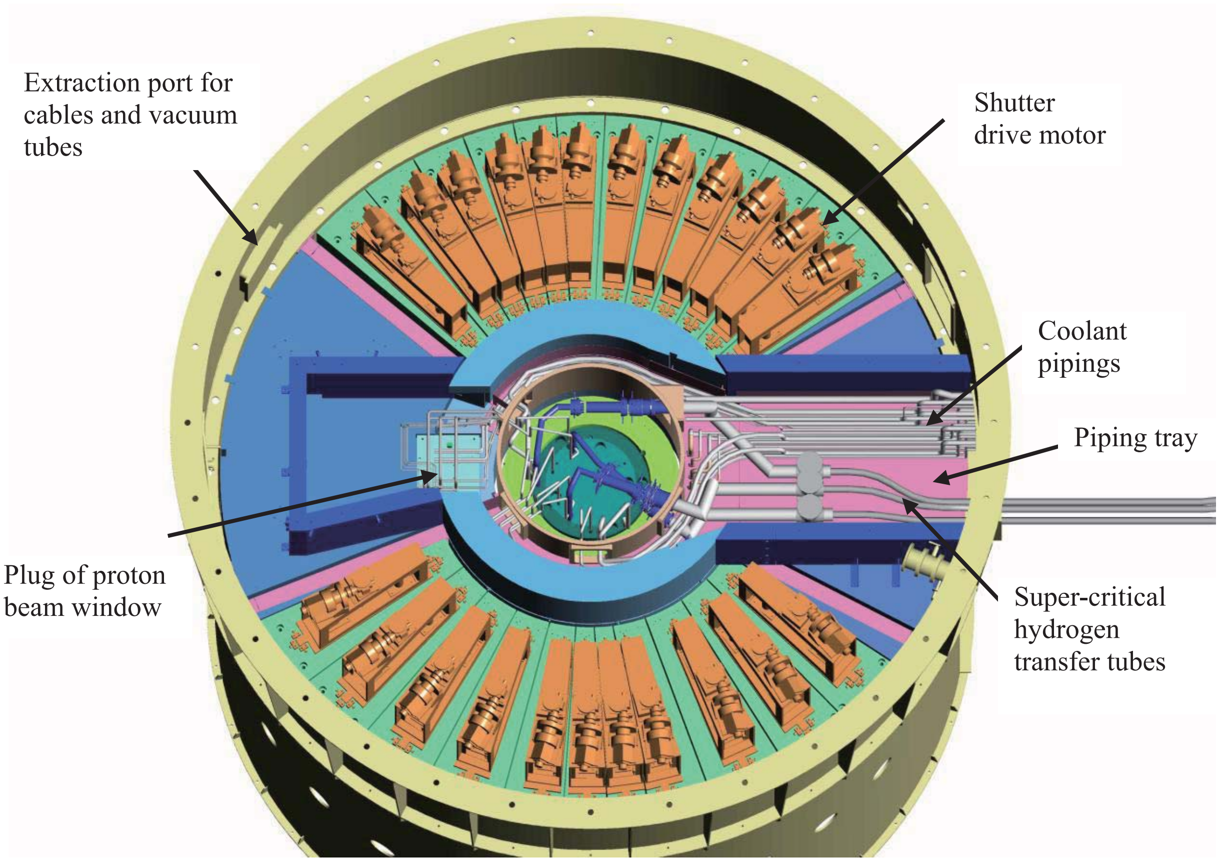

Fig.2.5.11: Overview of layout of piping in the piping tray

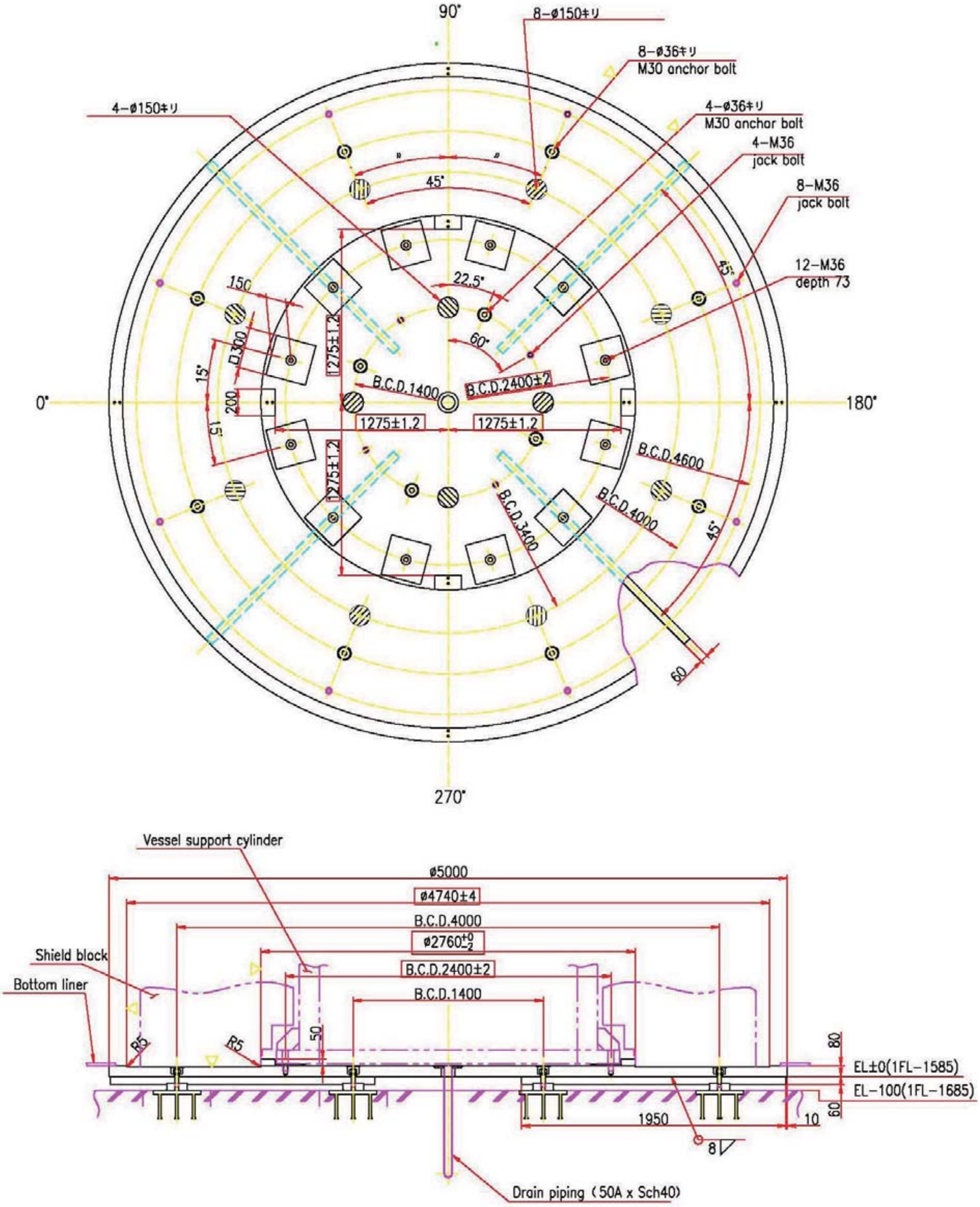

Fig. 2.5.12: Drawing of the base-plate

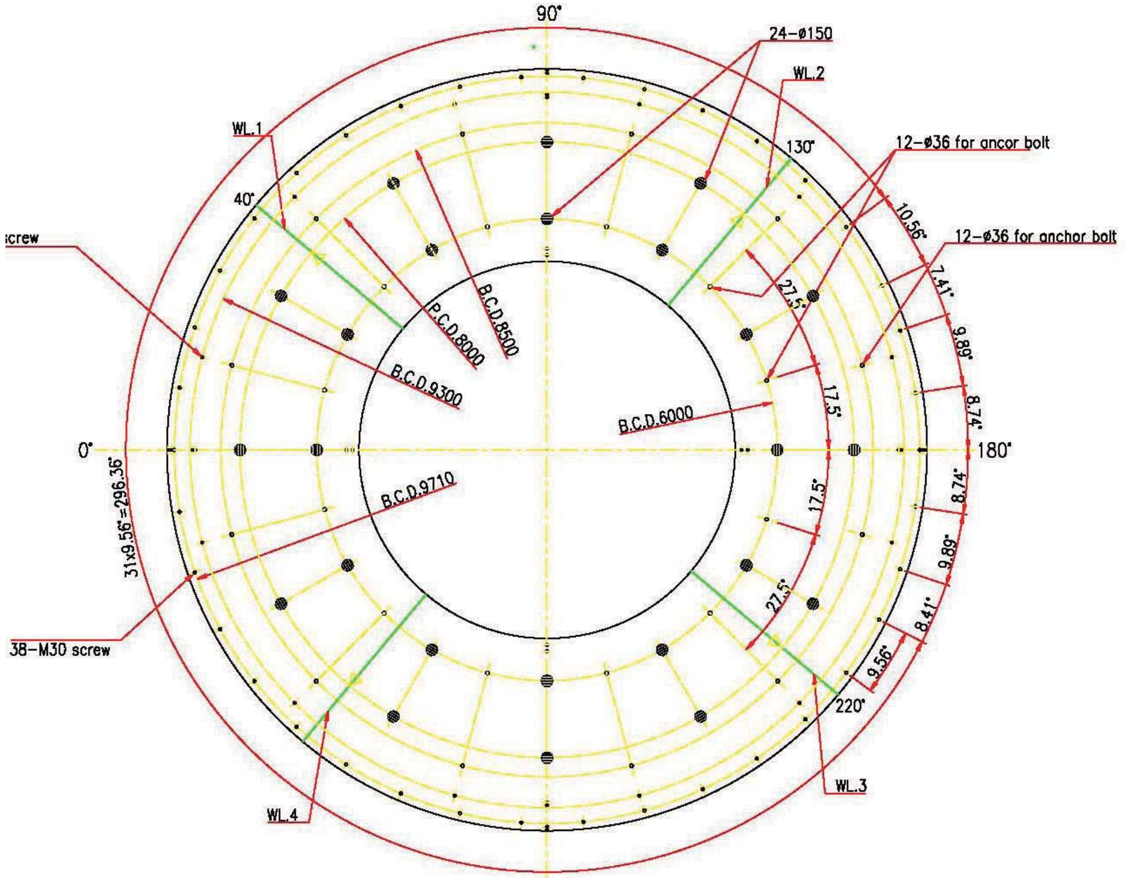

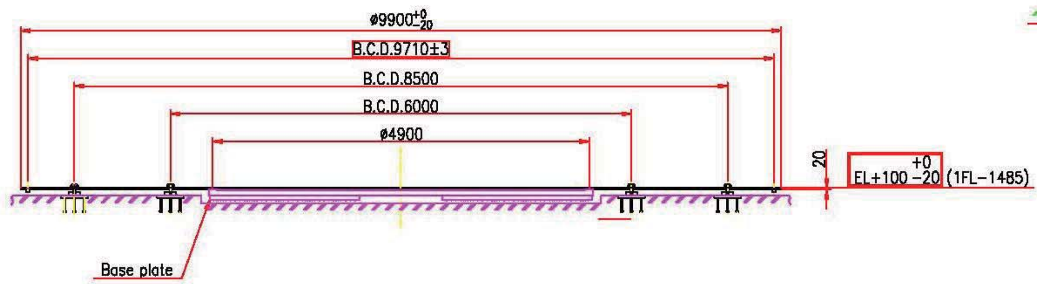

Fig. 2.5.13: Drawing of the bottom-liner

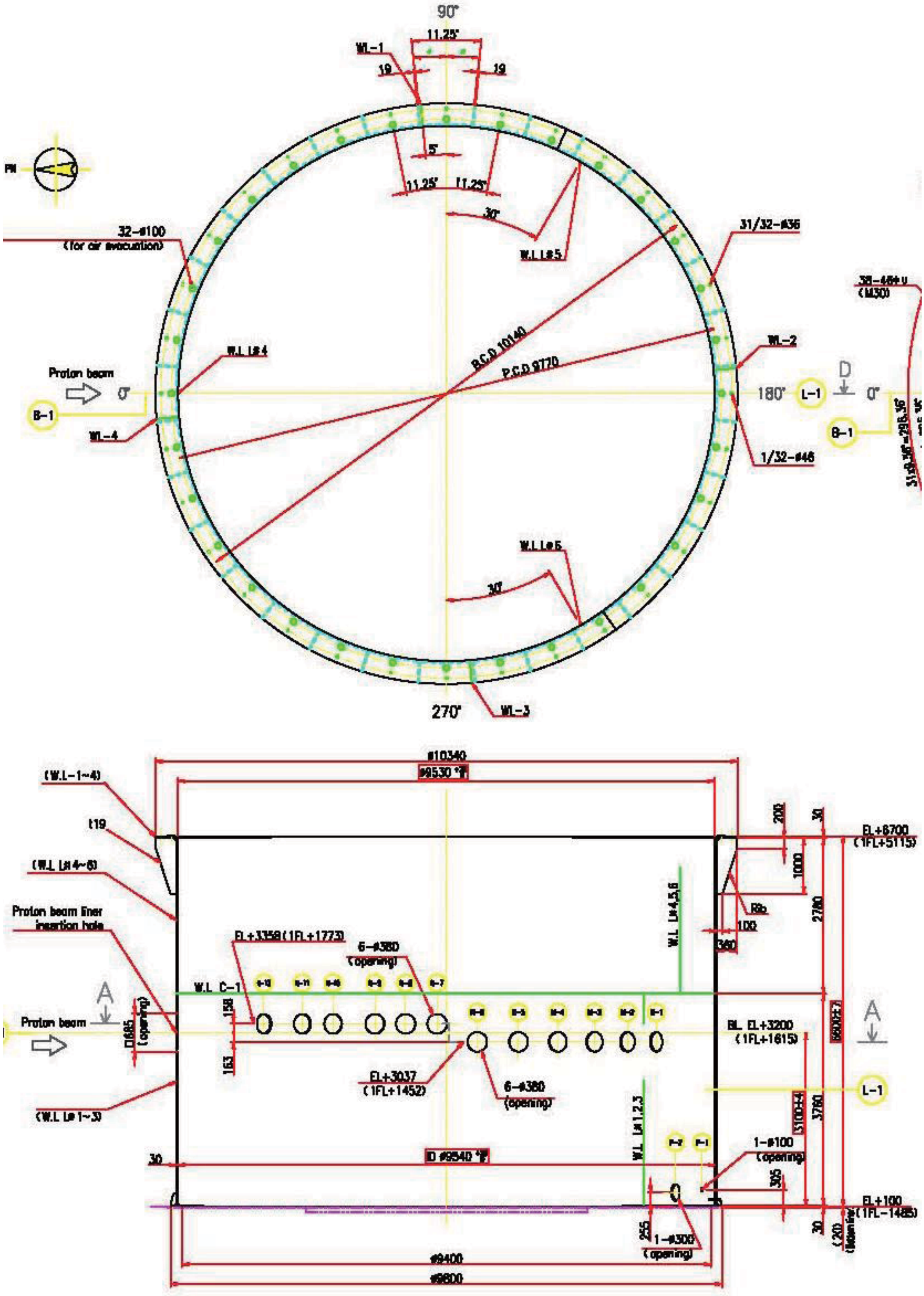

Fig. 2.5.14: Drawing of the lower part of the outer-liner

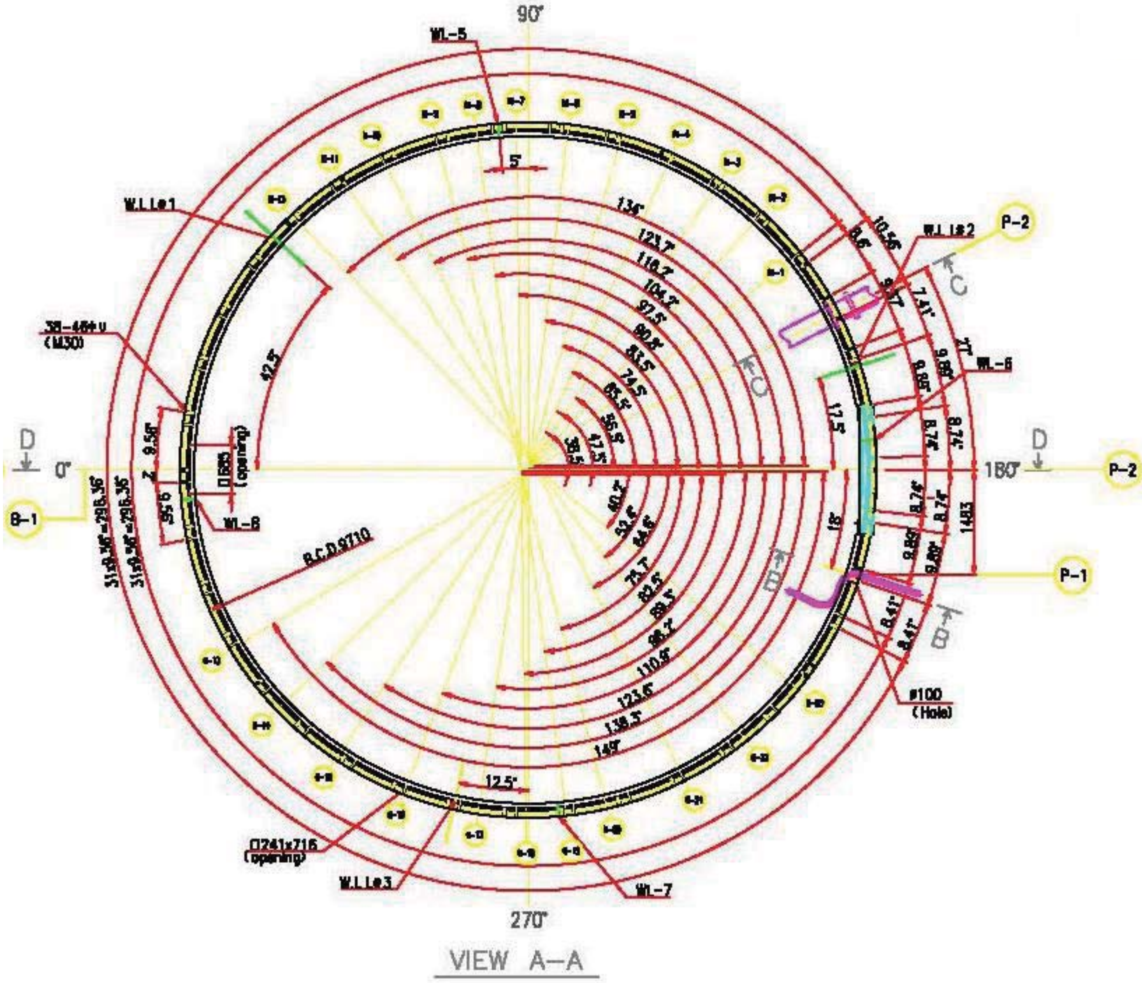

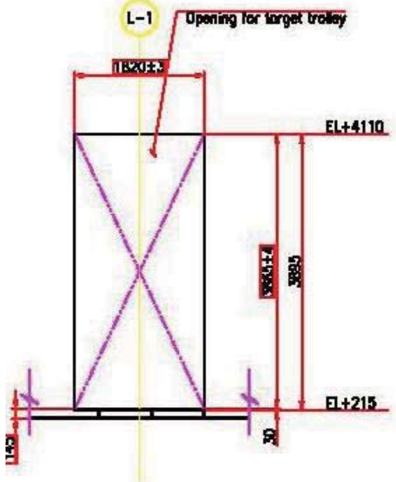

Fig. 2.5.14: Drawing of the lower part of the outer-liner (continued)

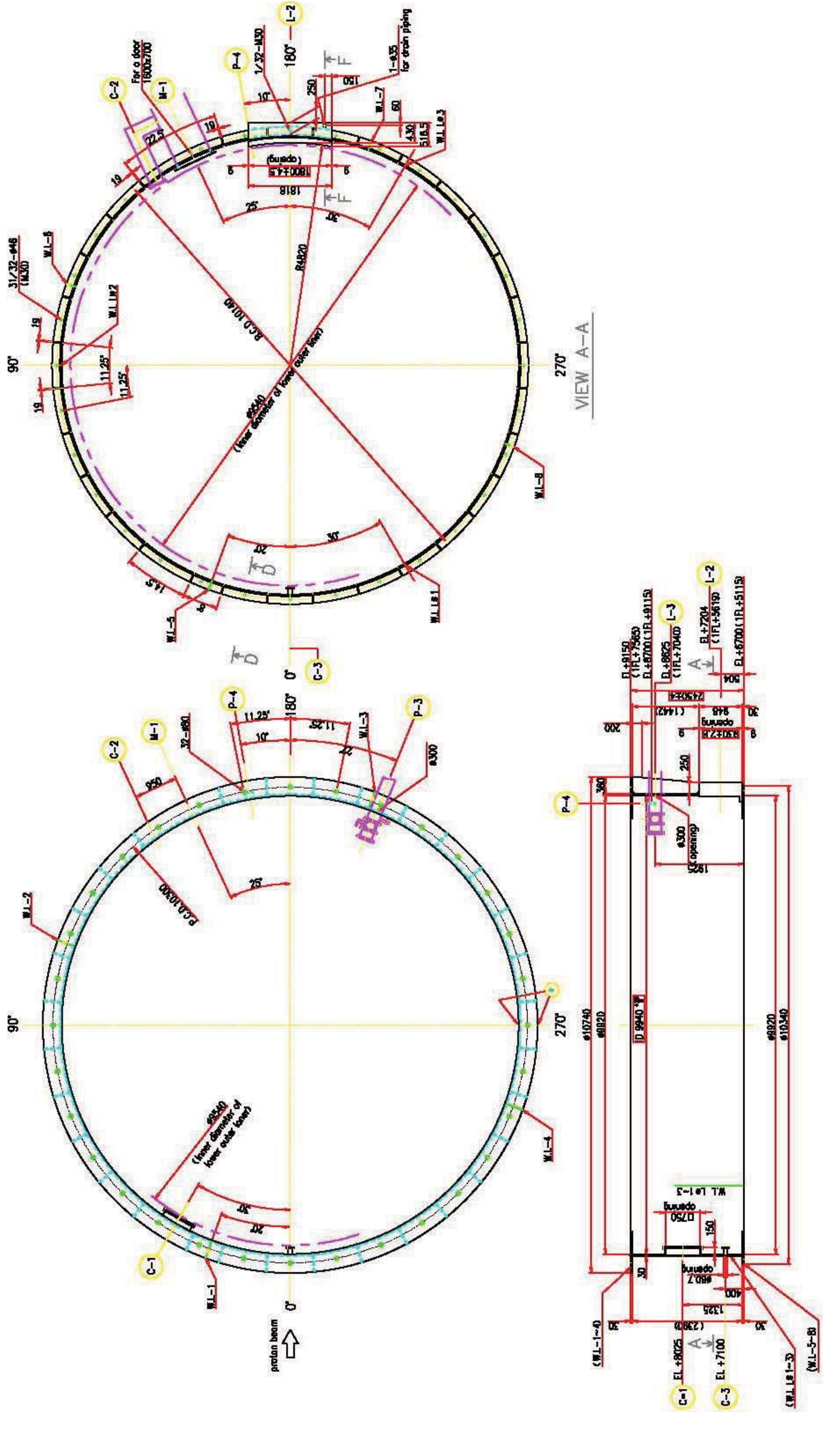

Fig. 2.5.15: Drawing of the upper part of the outer-liner

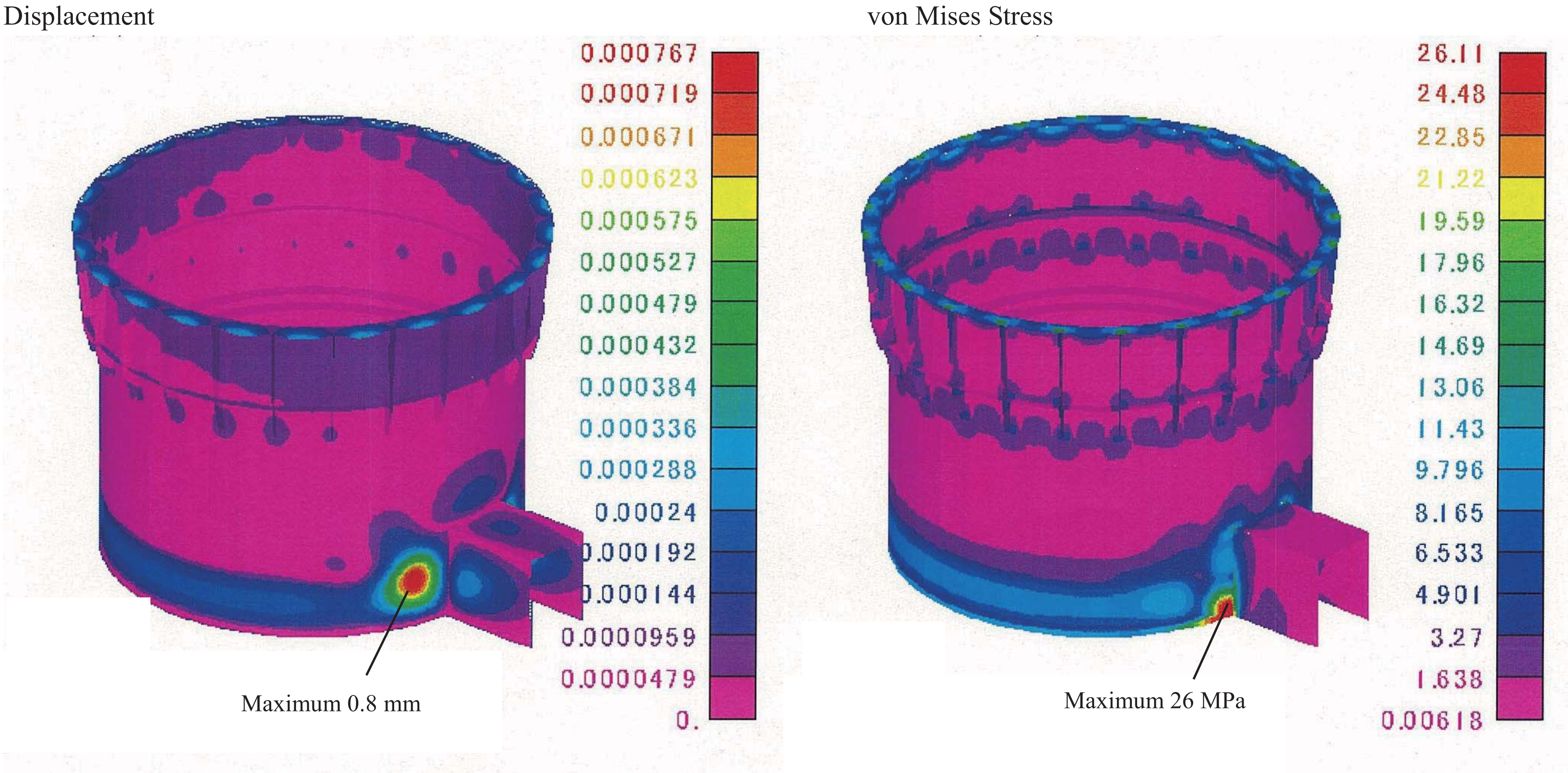

Fig. 2.5.16: Displacement and von Mises stress induced on the lower part of outer-liner calculated by the ABACUS code for magnetite concrete pouring up to 1.5 m

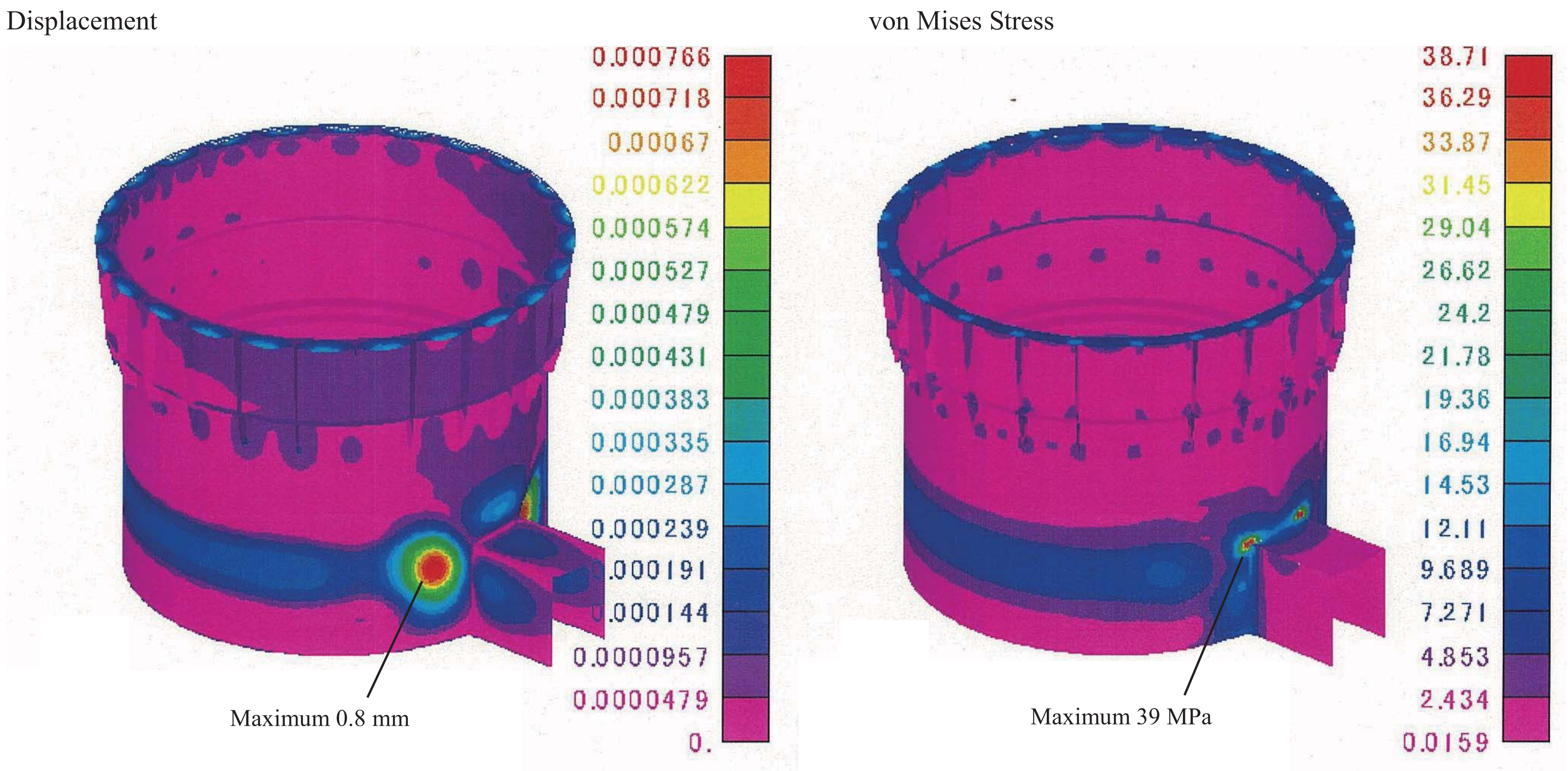

Fig. 2.5.17: Displacement and von Mises stress induced on the lower part of outer-liner calculated by the ABACUS code for magnetite concrete pouring from 1.5 to 3.0 m

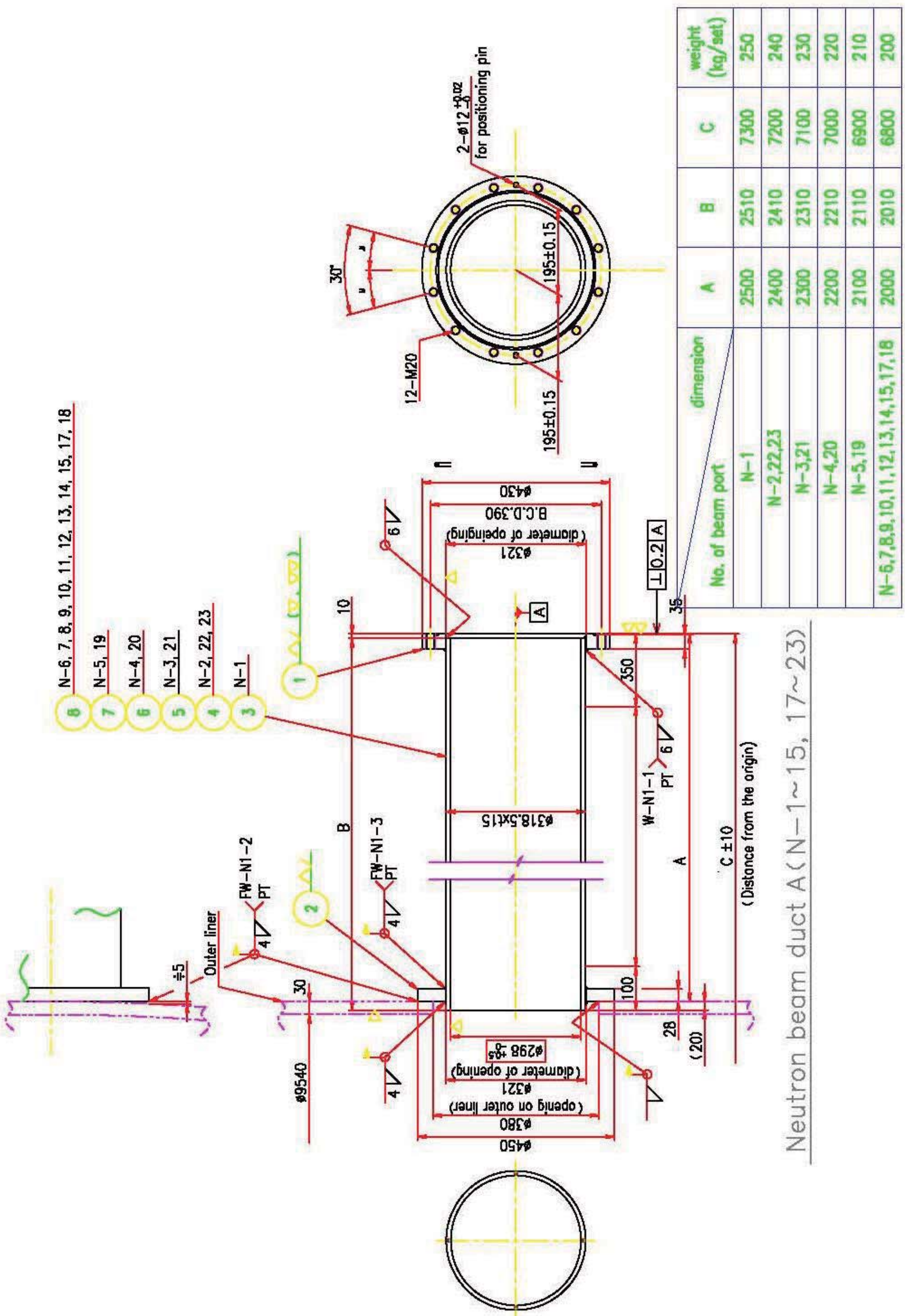

No. of beam port / dimension	A	B	C	weight (kg/set)
N−1	2500	2510	7300	250
N−2,22,23	2400	2410	7200	240
N−3,21	2300	2310	7100	230
N−4,20	2200	2210	7000	220
N−5,19	2100	2110	6900	210
N−6,7,8,9,10,11,12,13,14,15,17,18	2000	2010	6800	200

Fig. 2.5.18: Drawing of the neutron beam duct type A

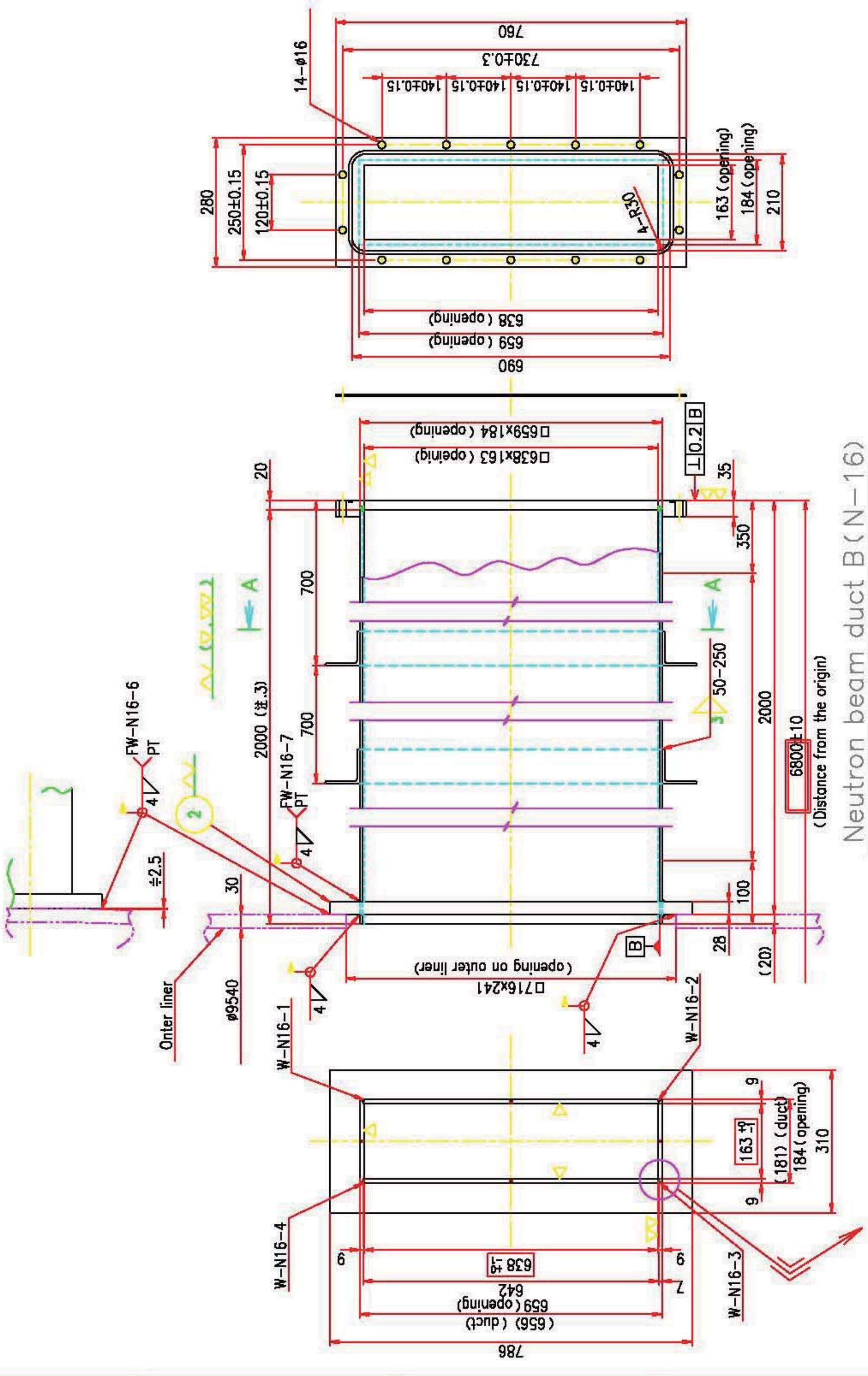

Fig. 2.5.19: Drawing of the neutron beam duct type B for BL-16

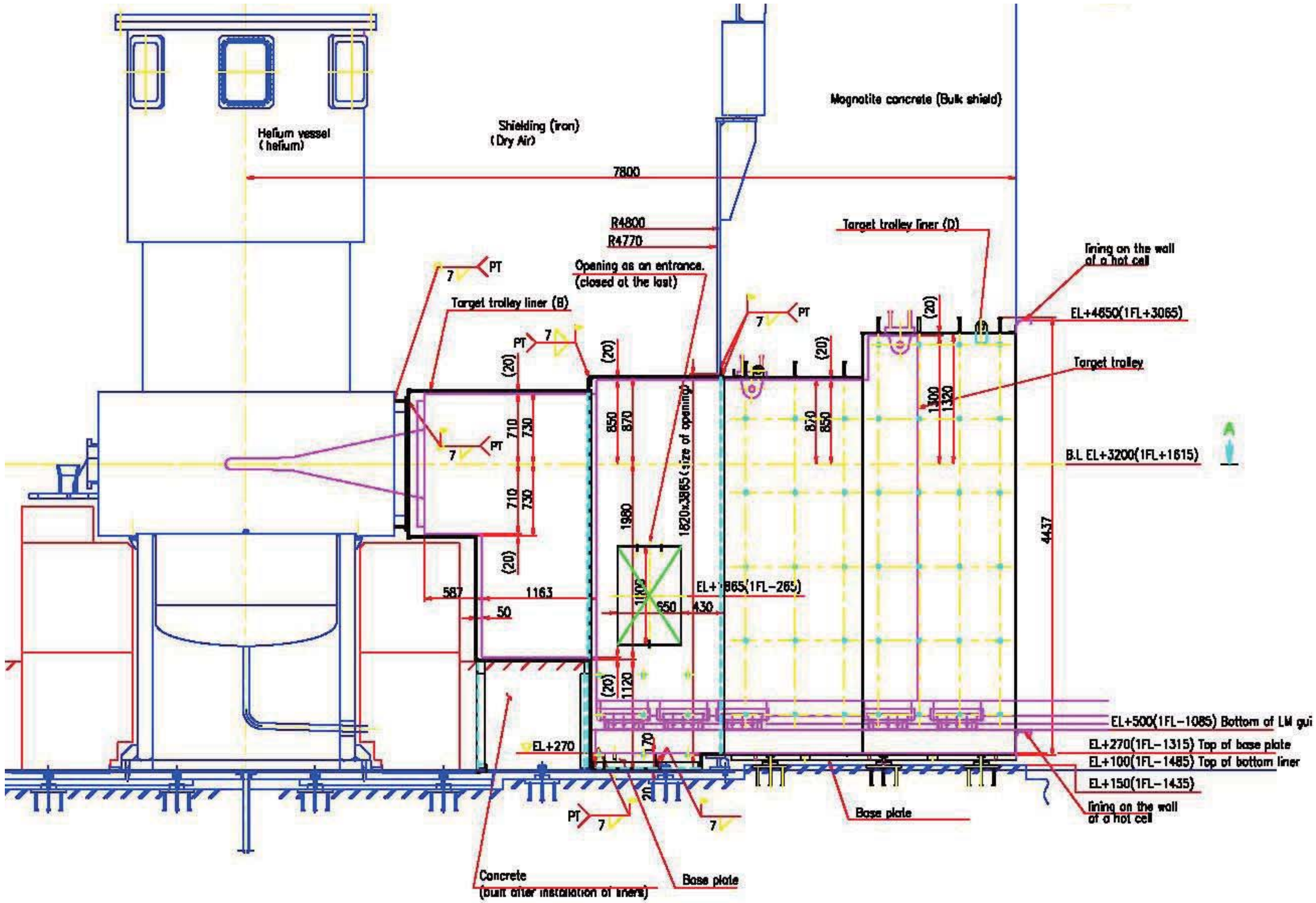

Fig. 2.5.20: Assembling drawing of the target trolley liner in vertical view

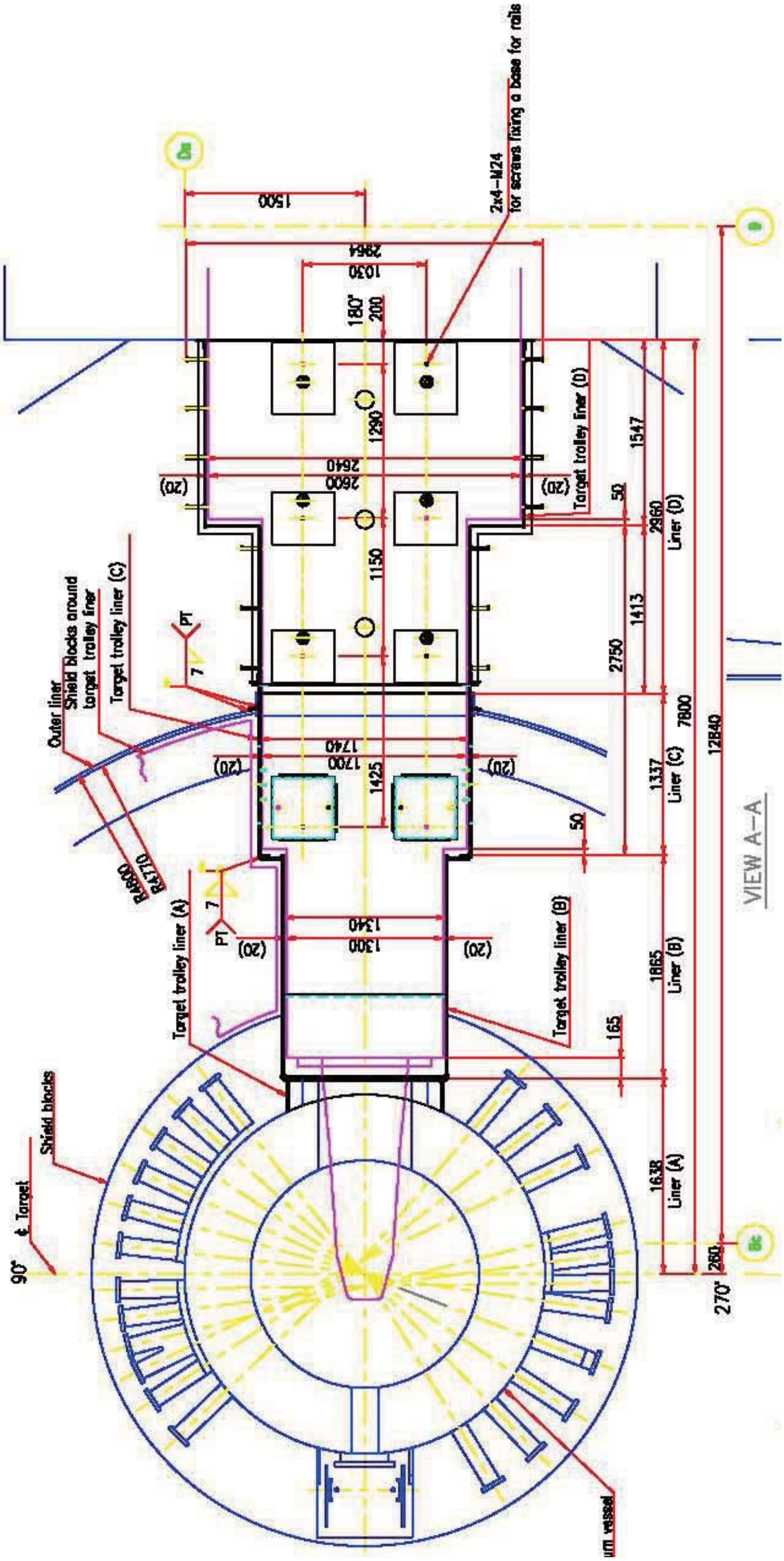

Fig. 2.5.21: Assembling drawing of the target trolley liner in plan view

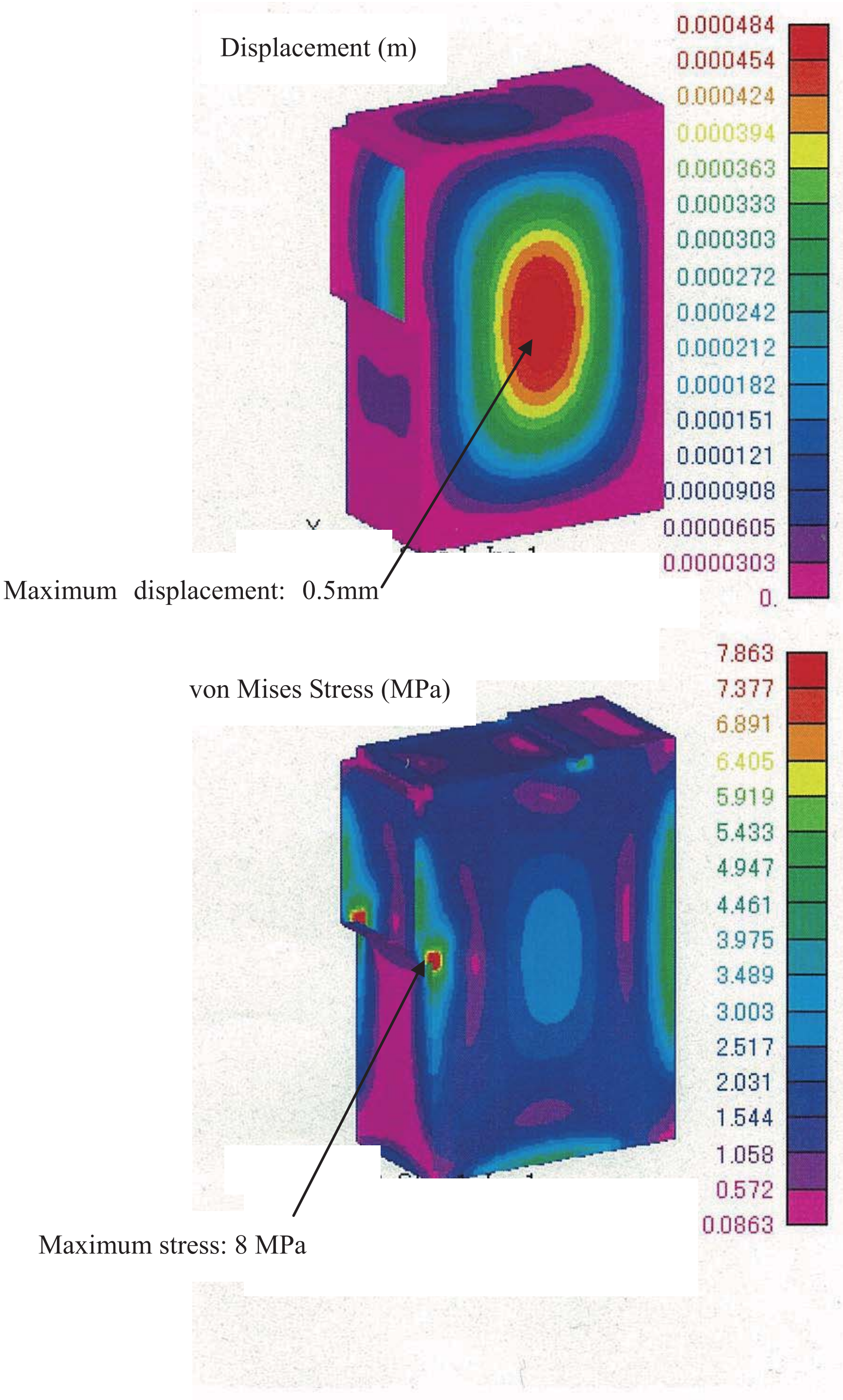

Fig. 2.5.22: Displacement and von Mises stress induced on the target trolley liner calculated by the ABACUS code for plate thickness of 20 mm

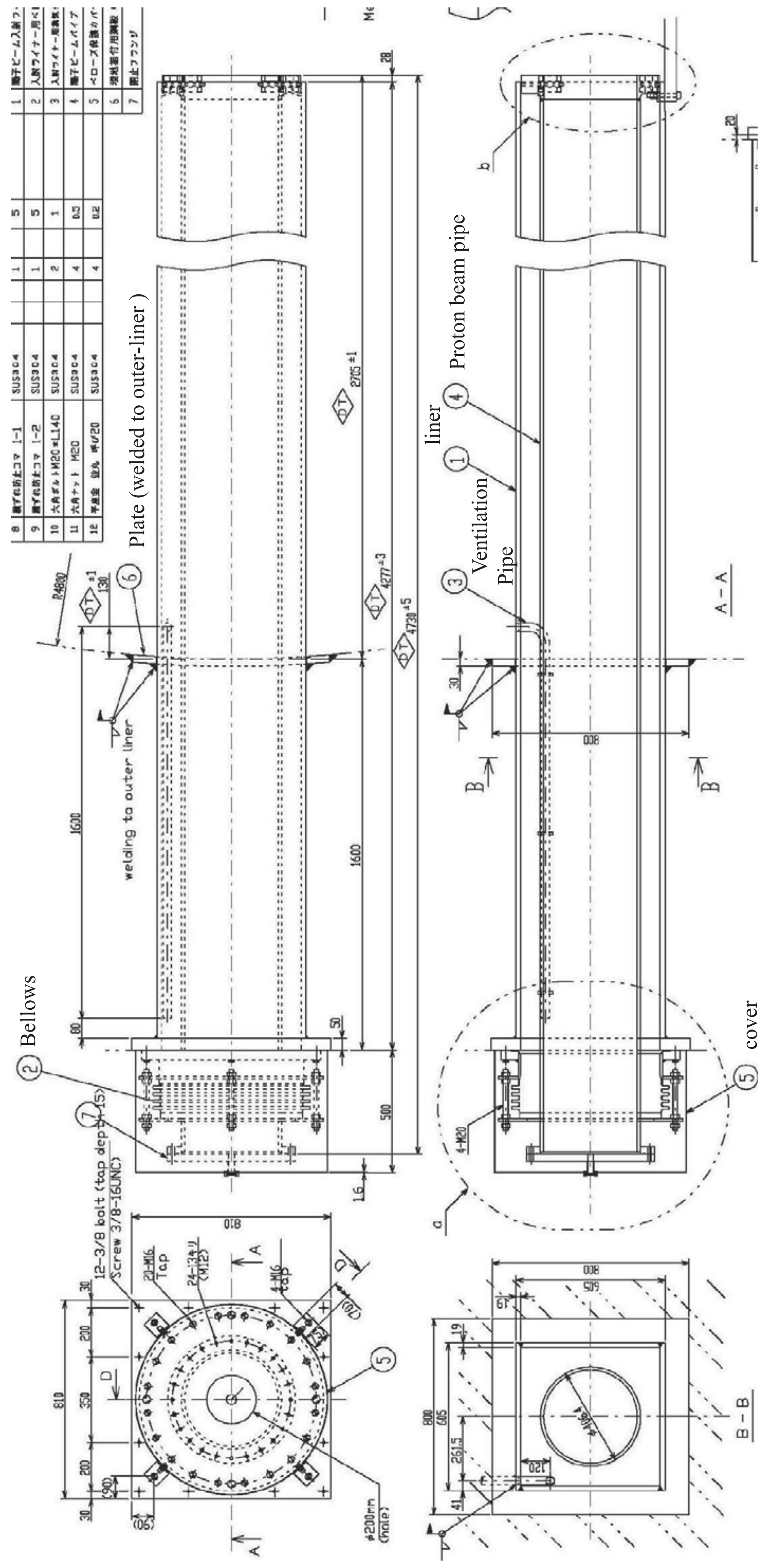

Fig. 2.5.23: Assembling drawing of proton beam duct liner

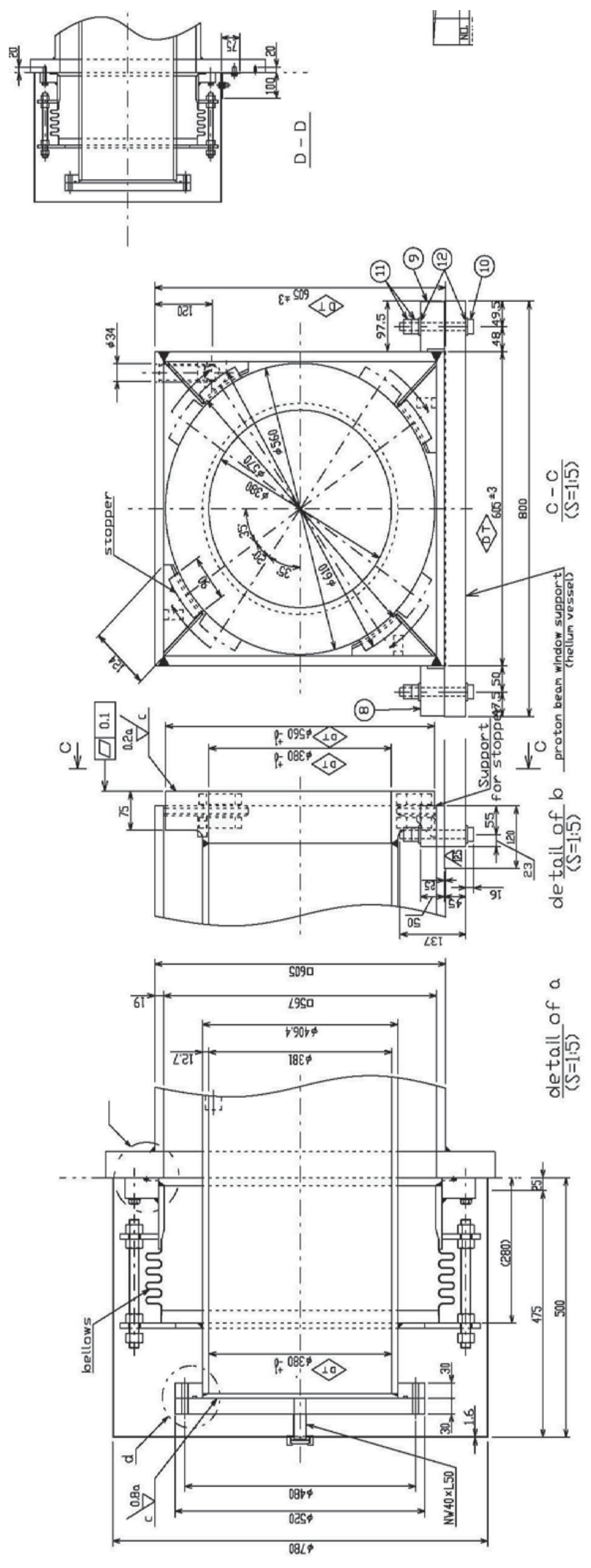

Fig. 2.5.23: Assembling drawing of proton beam duct liner (continued)

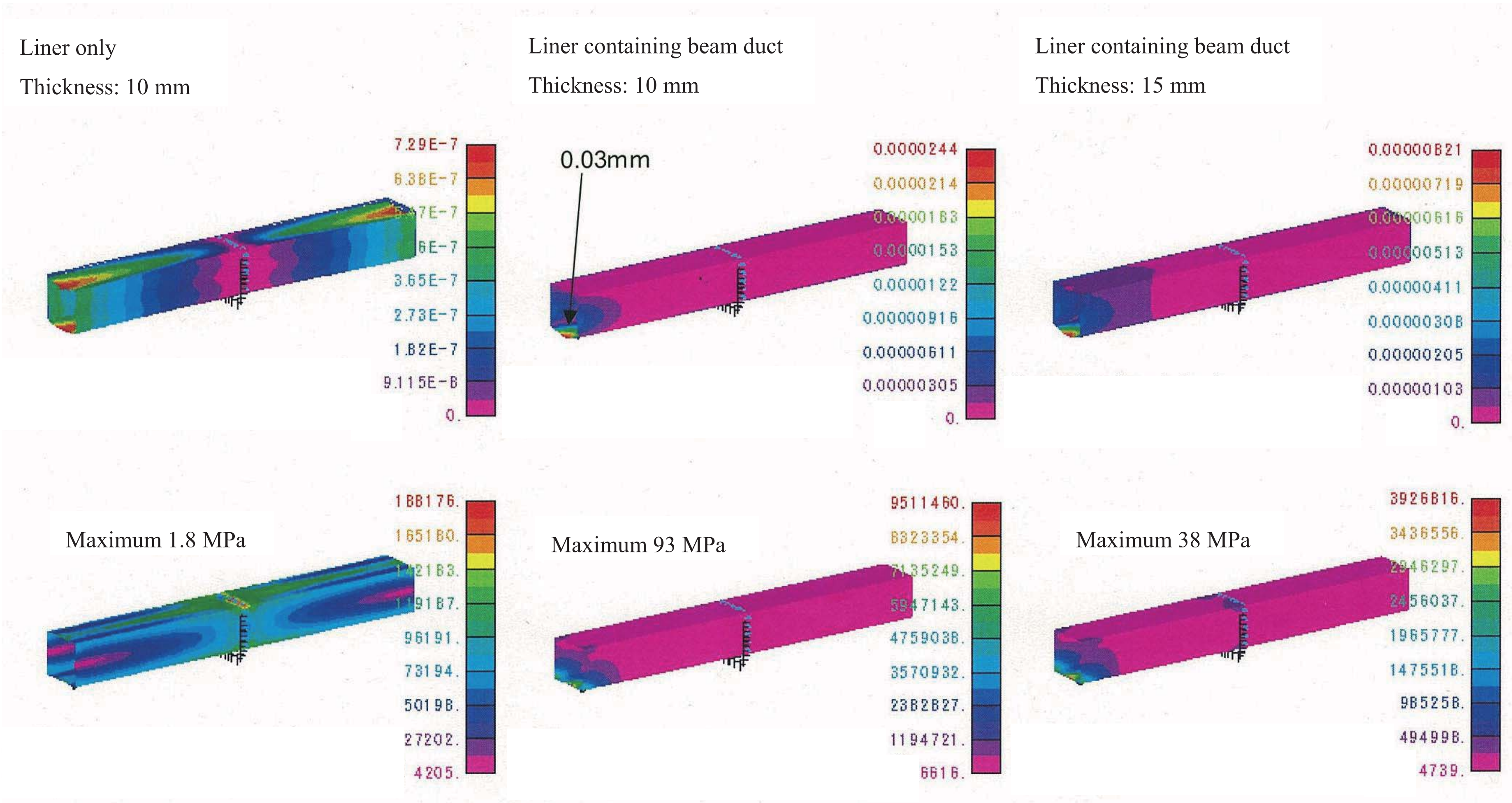

Fig. 2.5.24: Displacement and von Mises stress induced on the proton beam duct liner calculated by the ABACUS in case that only static weight is taken into consideration for liner only (left), liner with thickness 10 mm containing proton beam duct (middle) and that with 15 mm in thickness (right)

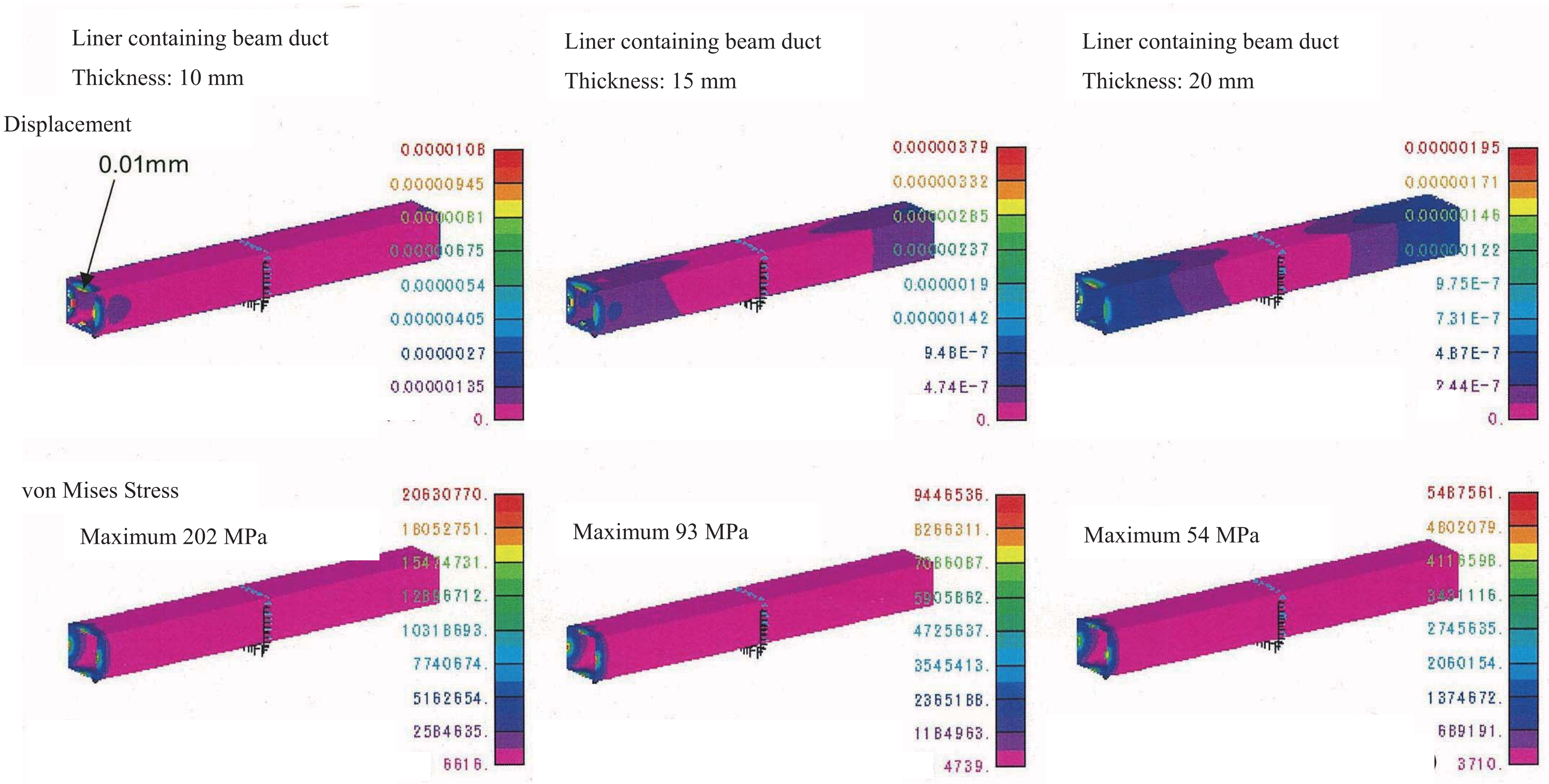

Fig. 2.5.24: Displacement and von Mises stress induced on the proton beam duct liner calculated by the ABACUS in case that static weight plus horizontal load by the pillow seal are taken into consideration for liners with thicknesses 10, 15 and 20 mm.

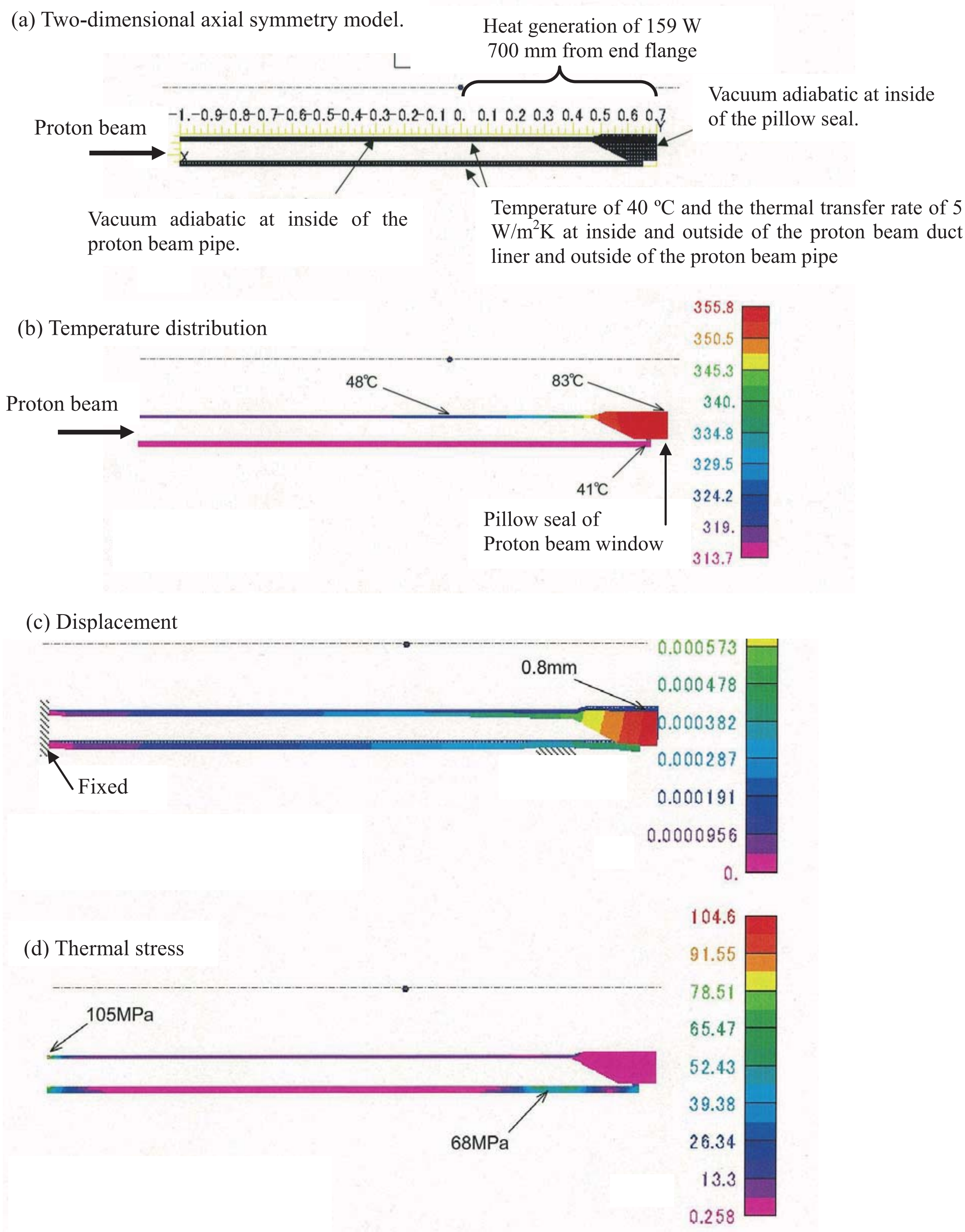

Fig. 2.5.25: Structural analyses of the proton beam duct liner containing proton beam pipe with the ABACUS code. (a) Geometry model and boundary conditions, (b) temperature distribution, (c) displacement, (d) thermal stress

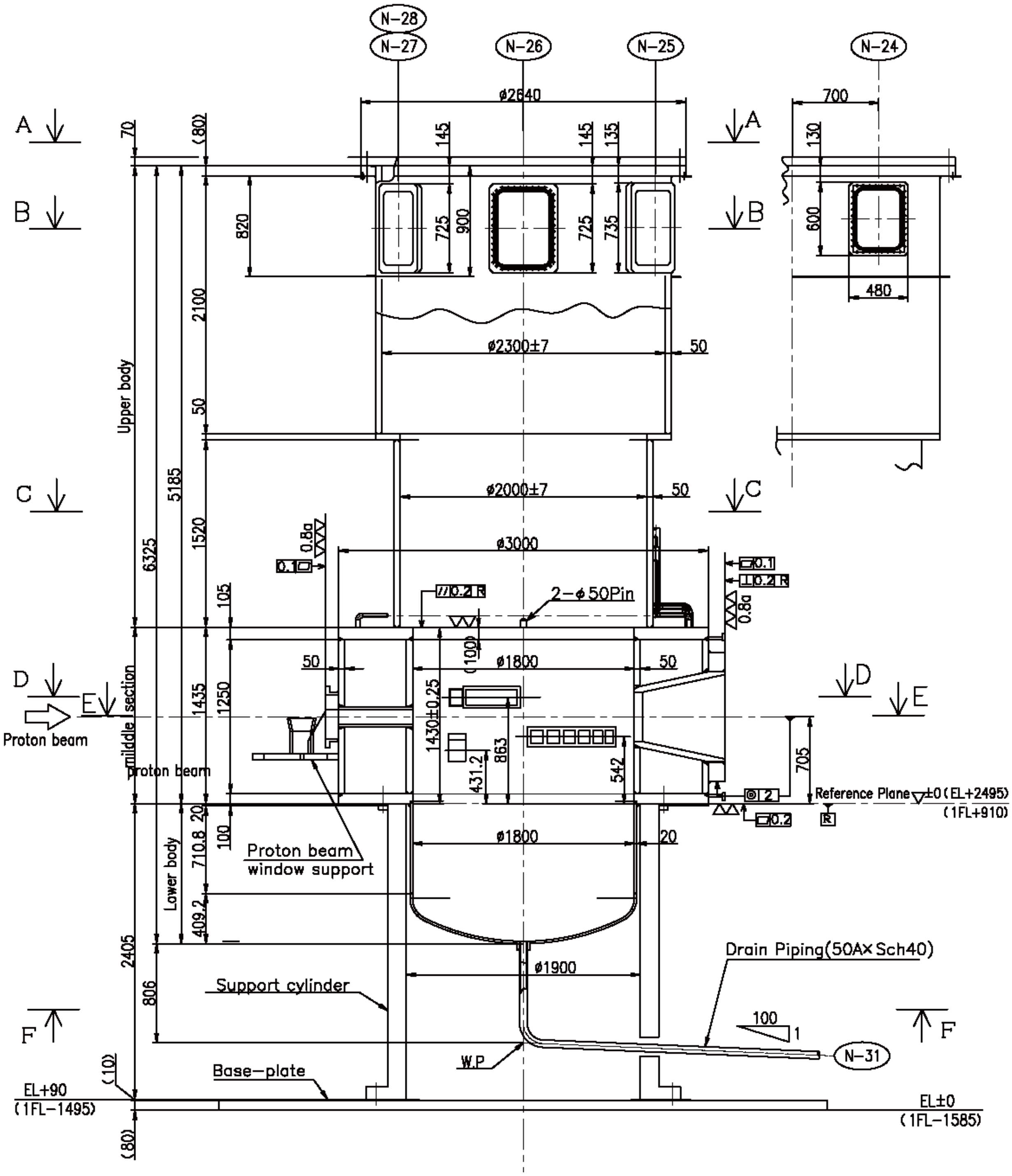

Fig.2.5.26: Front view of helium vessel

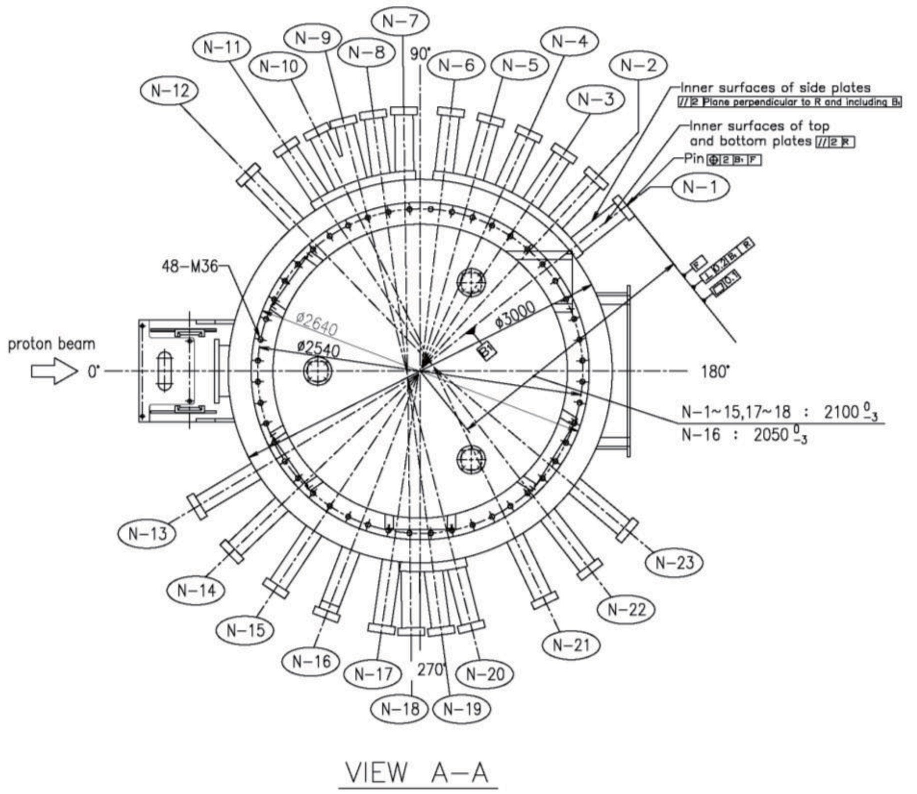

Fig.2.5.27: Horizontal cross section view of helium vessel

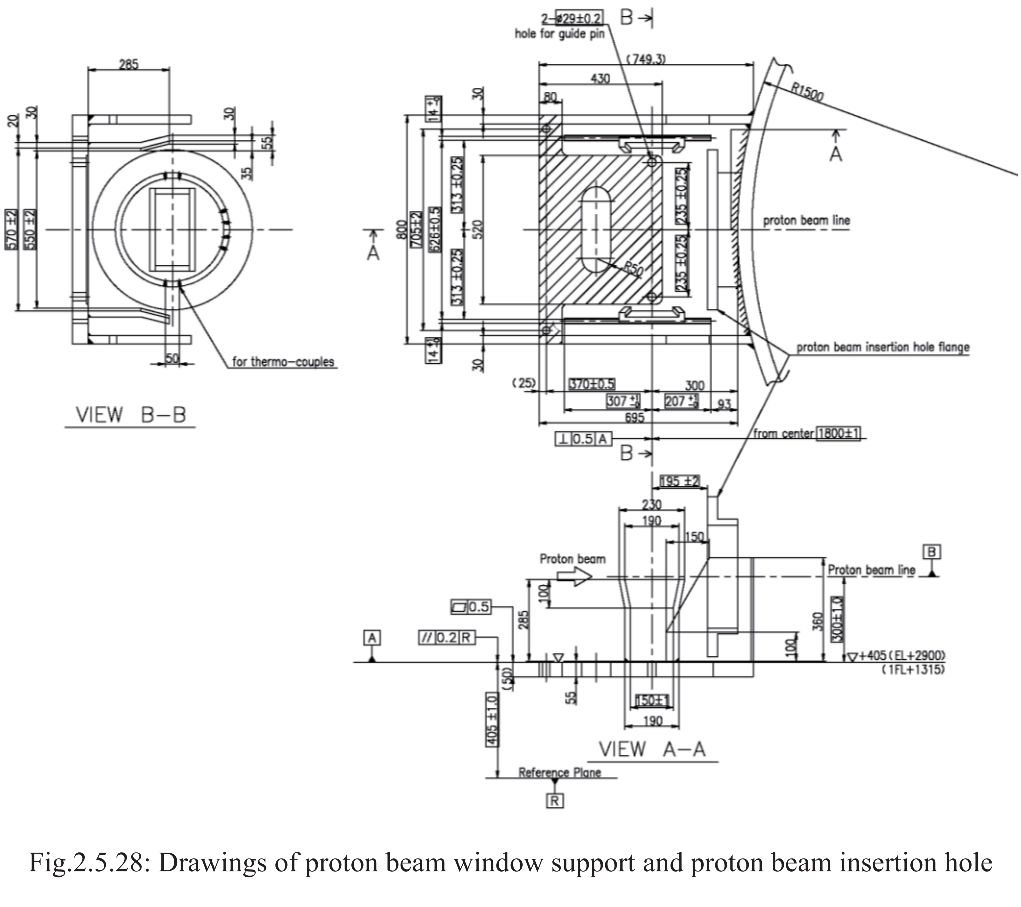

Fig.2.5.28: Drawings of proton beam window support and proton beam insertion hole

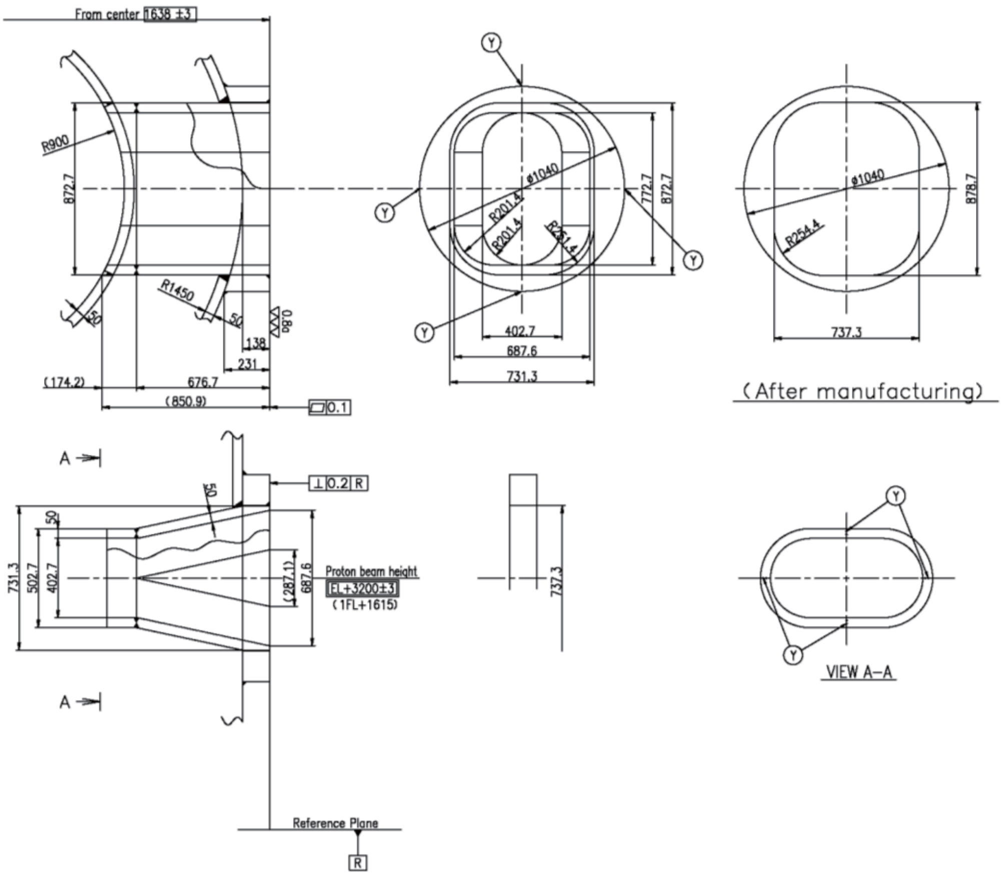

Fig.2.5.29: Drawings of target insertion hole

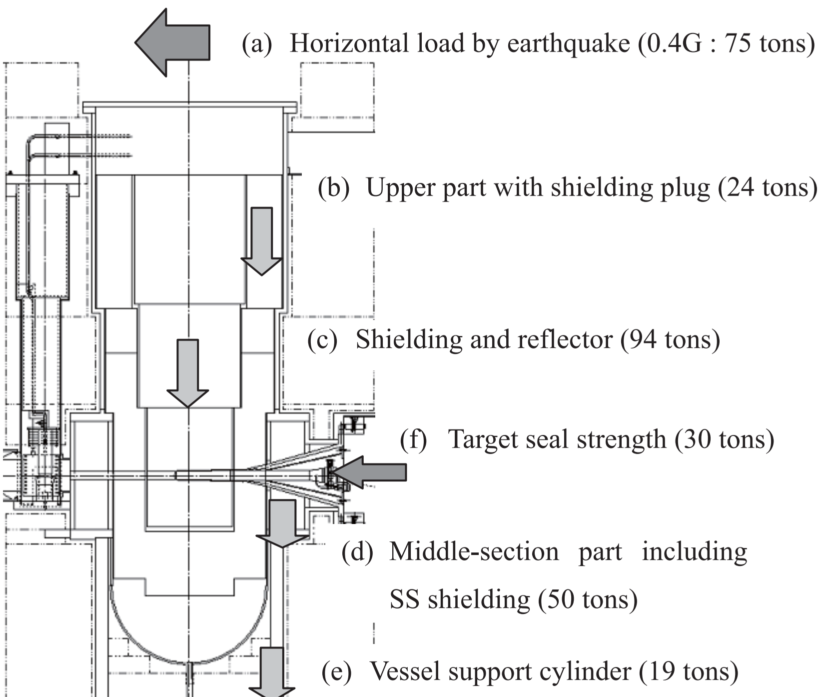

Fig.2.5.30: Analytical model of the helium vessel for earthquake-proof design

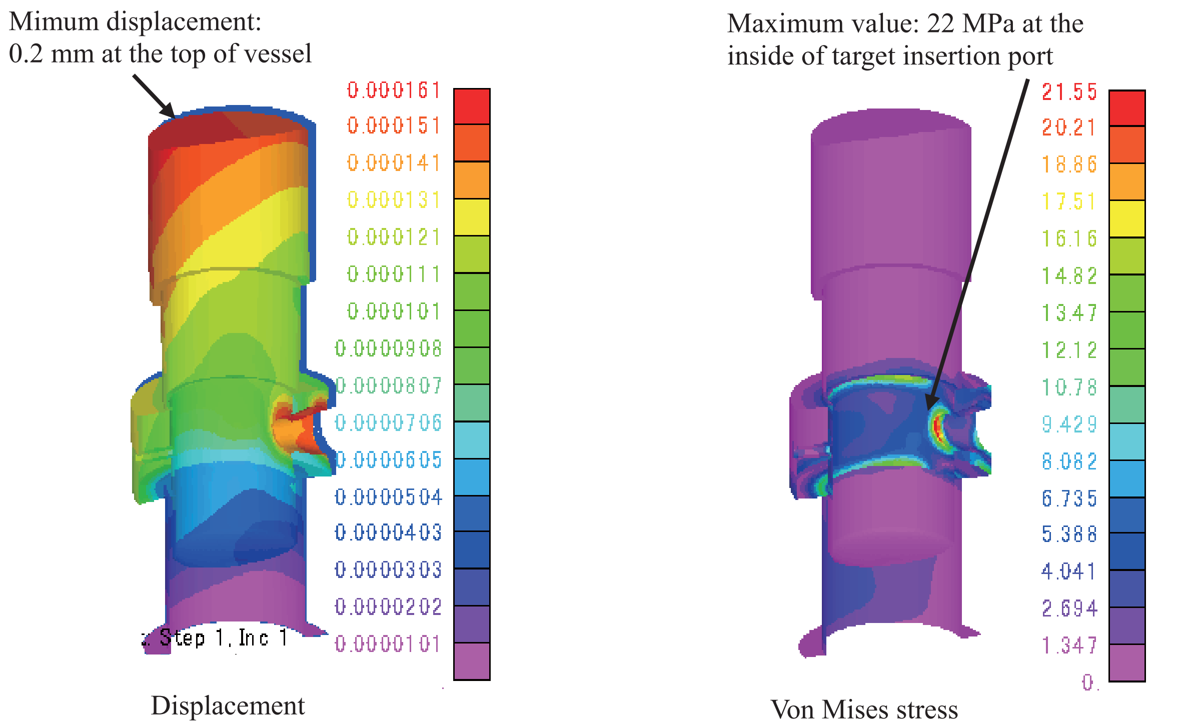

Fig. 2.5.31: Analytical results of displacement and stress distribution caused by dead load and target seal strength

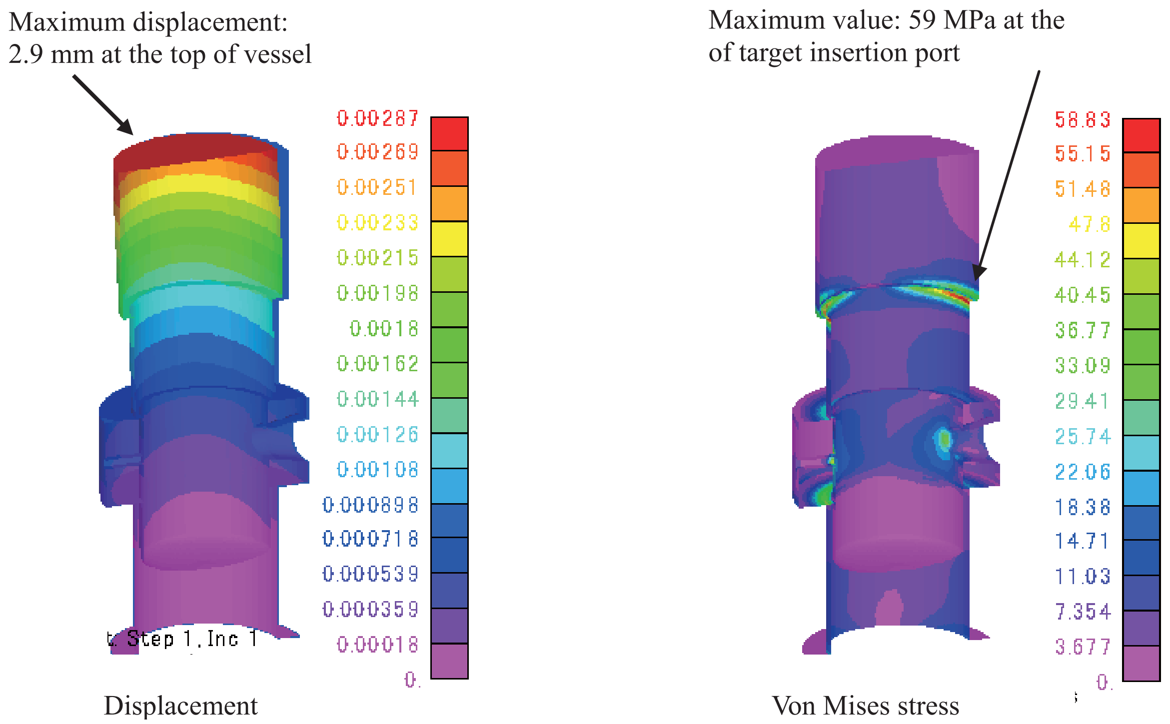

Fig. 2.5.32: Analytical results of displacement and stress distribution caused by acceleration of 0.4G in horizontal direction

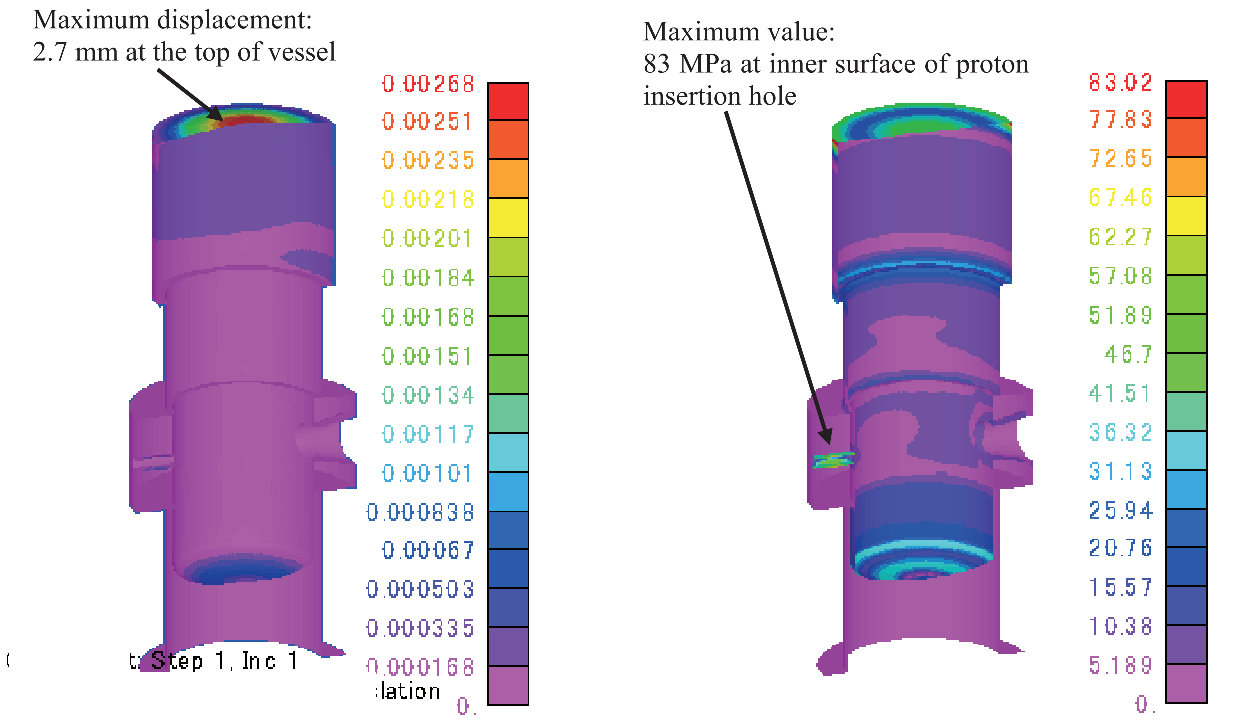

Fig. 2.5.33: Analytical results of displacement and von Mises stress distribution on helium vessel caused by inner pressure of 0.3 MPa

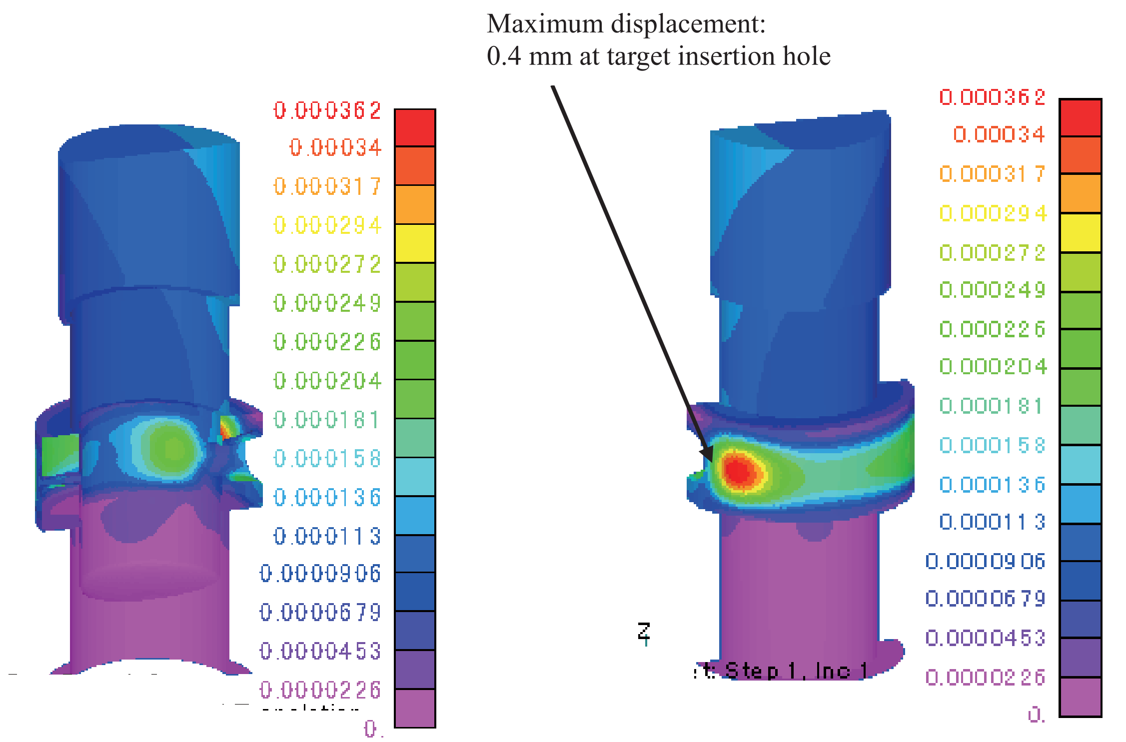

Fig. 2.5.34: Analytical results of displacement distribution on helium vessel caused by water pressure of 0.8 MPa at the middle-section part

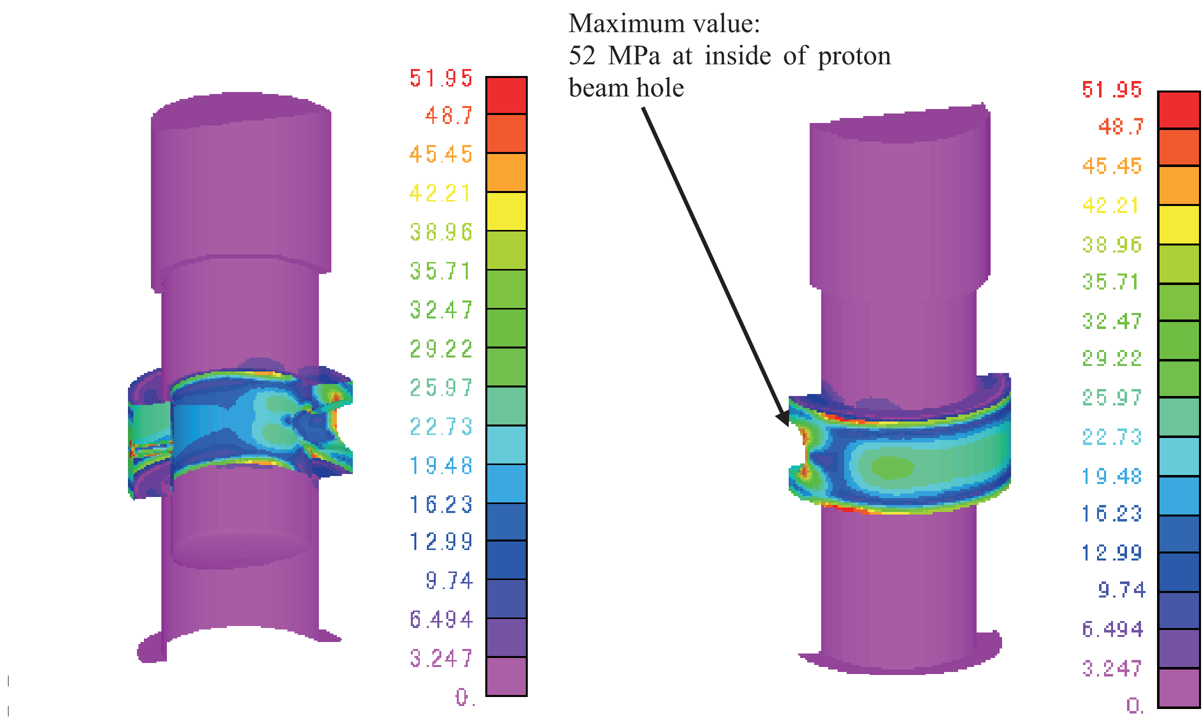

Fig. 2.5.35: Analytical results of von Mises stress distribution on helium vessel caused by water pressure of 0.8 MPa at the middle-section part

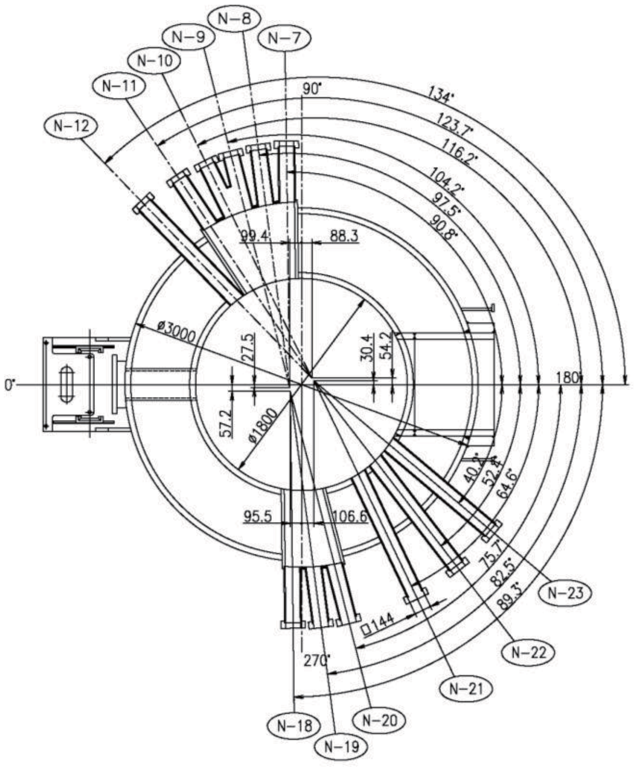

VIEW D−D

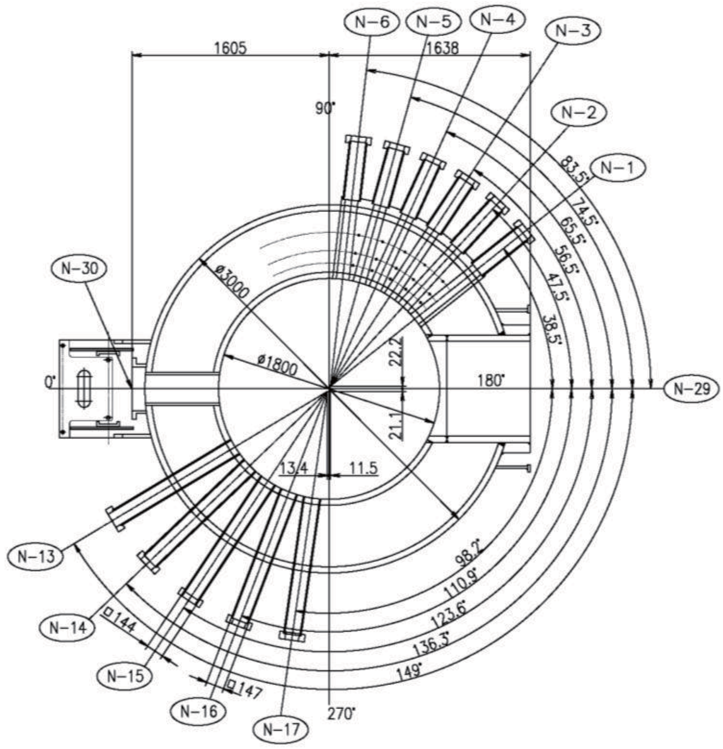

VIEW E−E

Fig. 2.5.36: Cross sectional horizontal view of middle-section part at the elevation

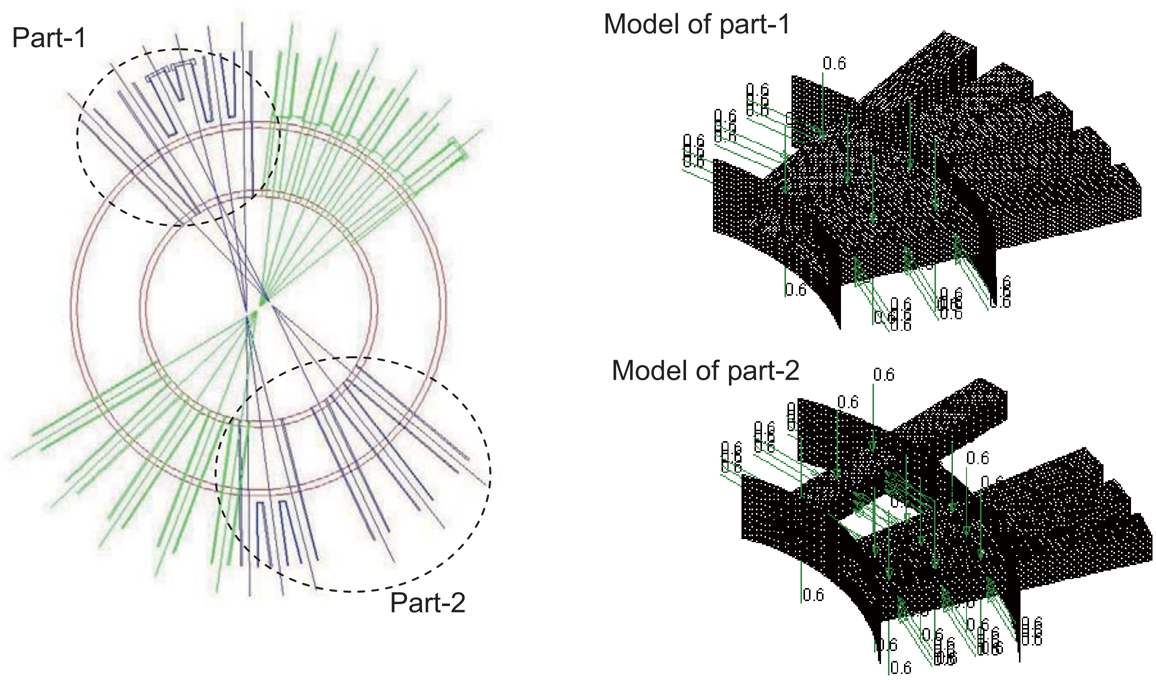

Fig. 2.5.37: Analytical models of neutron beam ports at the middle-section part of the helium vessel. Left-hand side drawing represents the cross sectional plane view of the middle-section part. The right-hand side shows the three dimensional shell models of neutron beam ports

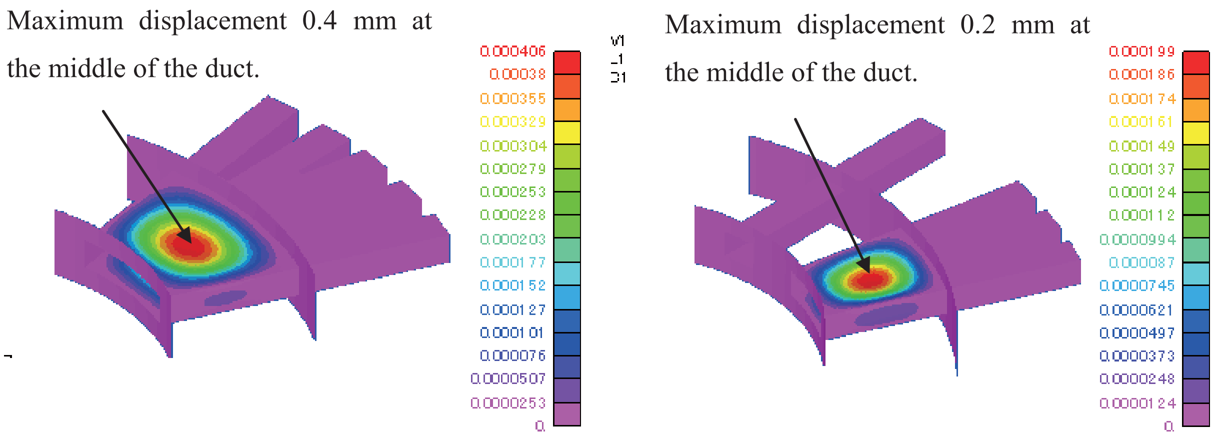

Fig. 2.5.38: Analytical results of displacement distribution on beam ducts caused by water pressure of 0.8 MPa at the middle-section part

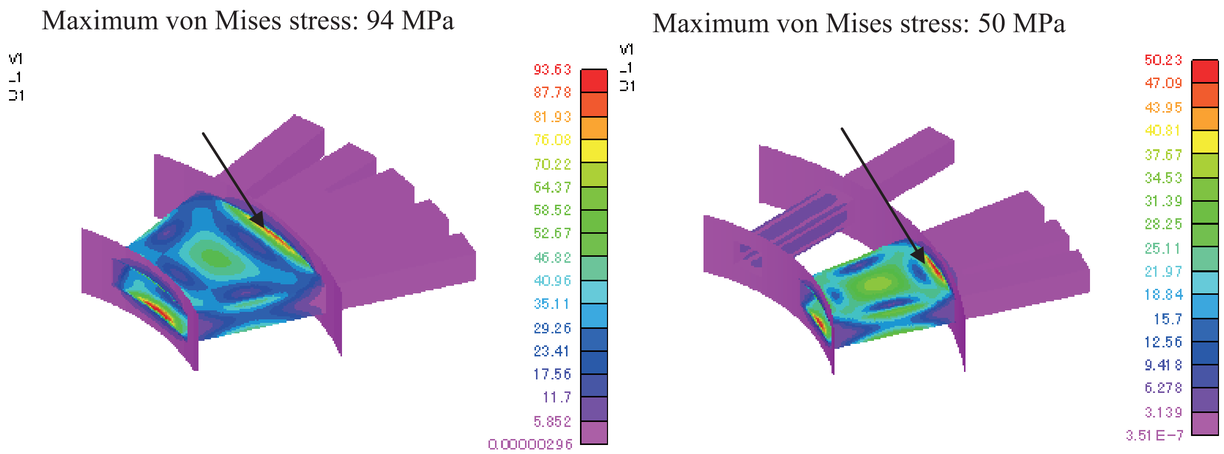

Fig. 2.5.39: Analytical results of von Mises stress distribution on beam ducts caused by water pressure of 0.8 MPa at the middle-section part

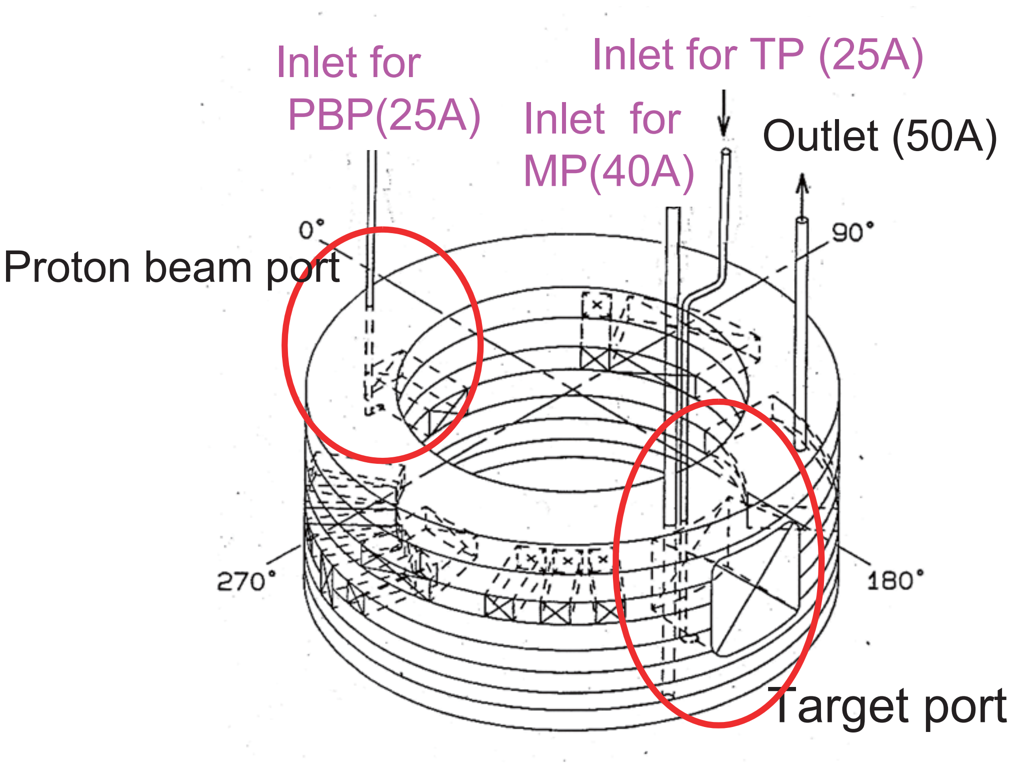

Fig. 2.5.40: Illustration of steel blocks contained in the middle-section of the helium vessel

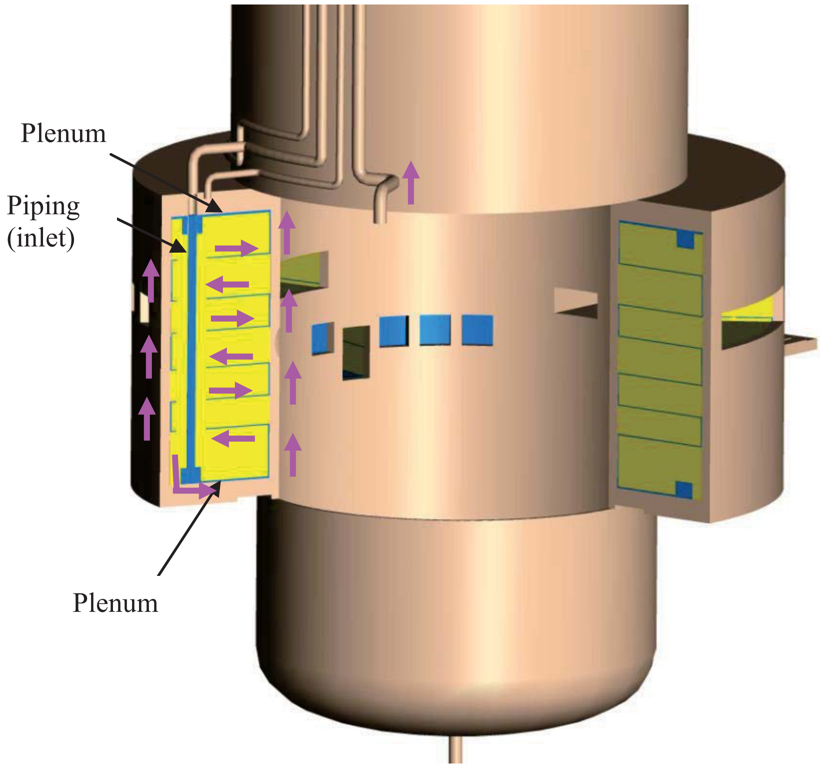

Fig. 2.5.41: 3D cut-away view of the middle-section part of helium vessel. Arrows indicate the direction of the coolant flow

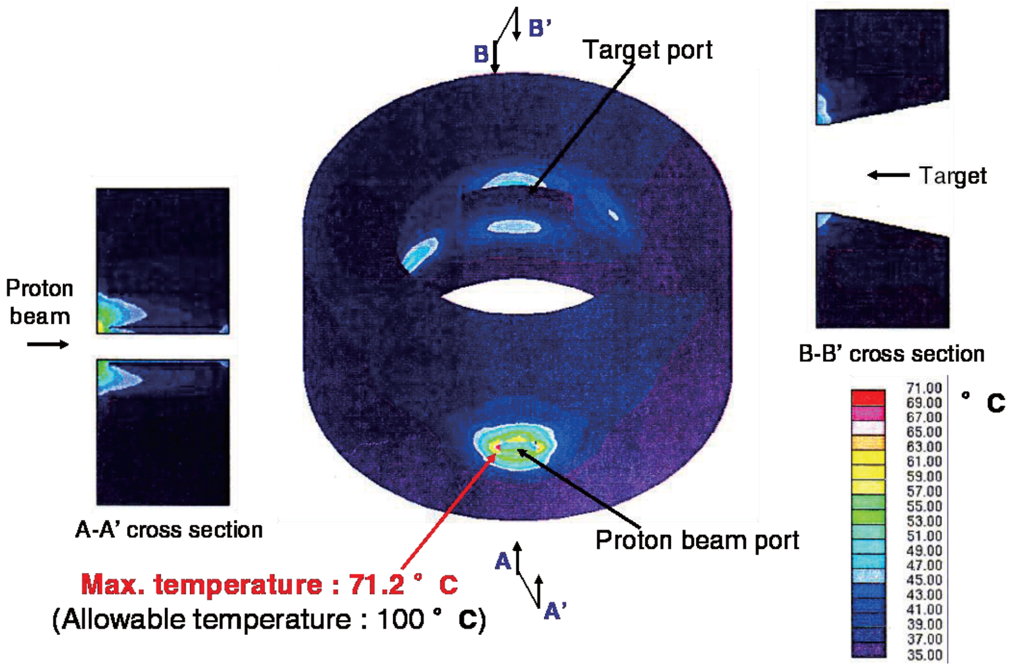

Fig. 2.5.42: 3D cut-away view of the middle-section part of helium vessel. Arrows indicates the direction of the coolant flow

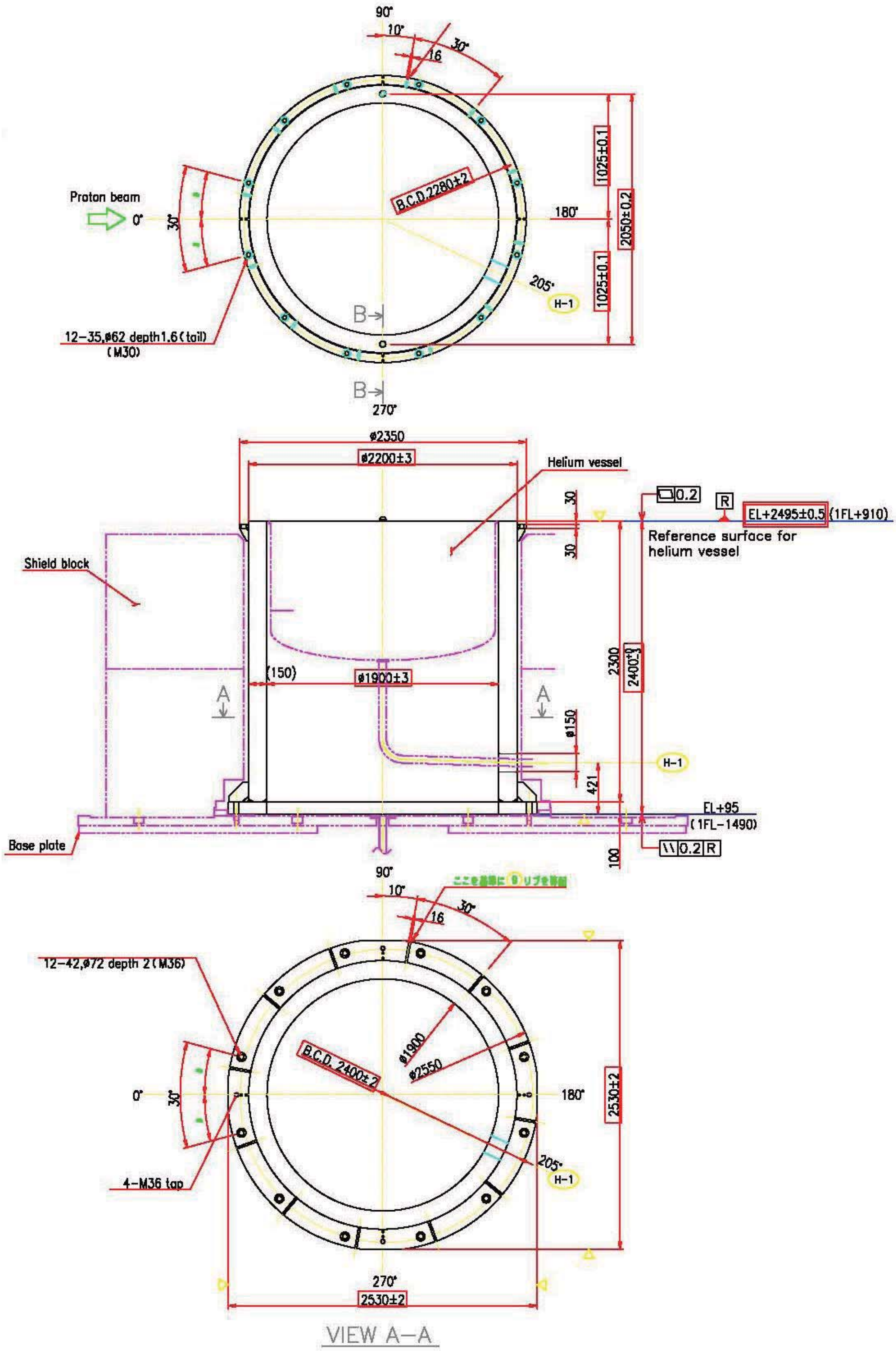

Fig. 2.5.43: Drawing of the vessel support cylinder

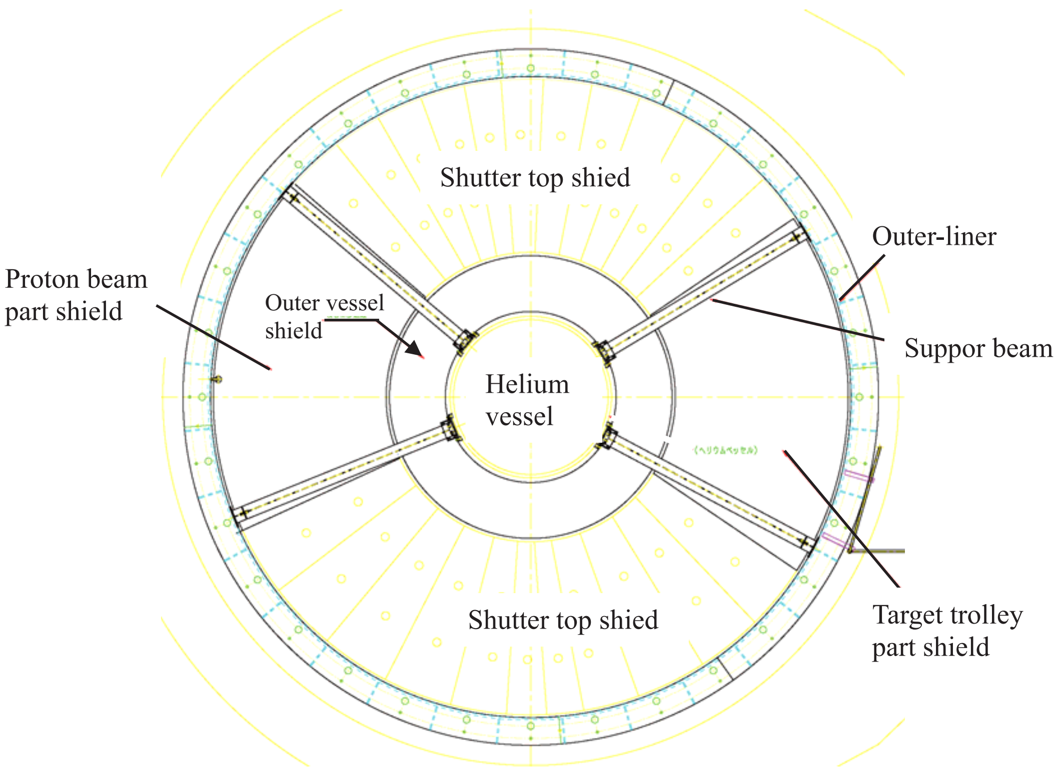

Fig. 2.5.44: Arrangement of vessel support beams viewed from elevation of 1FL+5115 mm

(1) Case 1: horizontal acceleration perpendicular to the central axis of the support beam.

(2) Case 2: horizontal acceleration along the central axis of the support beam.

(3) Case 3: case 2 plus horizontal load of 30t from target trolley.

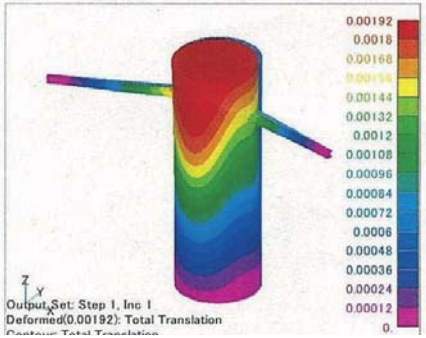

(a) displacement
maximum of 1.9 mm on top of helium vessel.

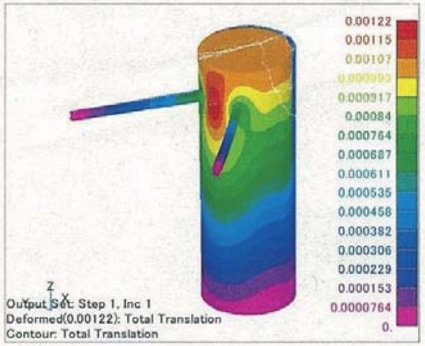

(a) displacement
maximum of 1.2 mm on side of top part of helium vessel.

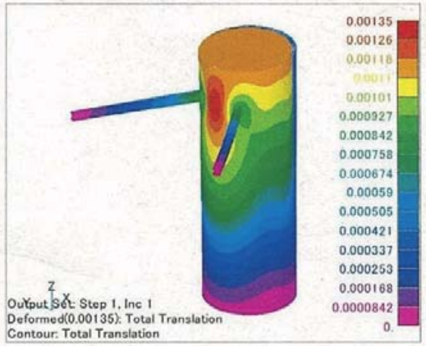

(a) displacement
maximum of 1.4 mm on side of top part of helium vessel.

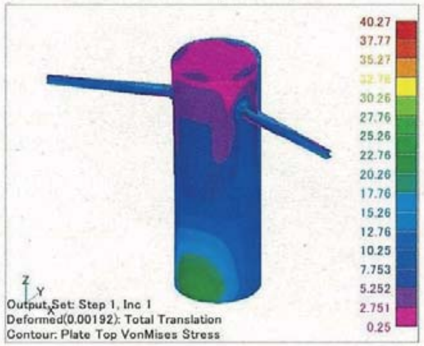

(b) von Mises stress
maximum of 40 MPa at fixed portion of support beam on helium vessel.

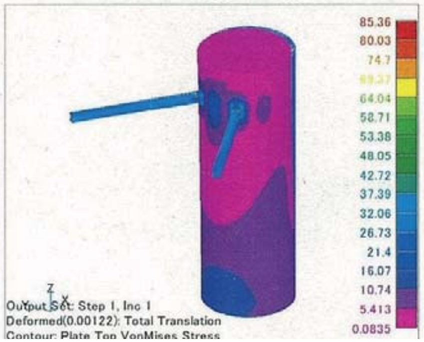

(b) von Mises stress
maximum of 85 MPa at fixed portion of support beam on helium vessel.

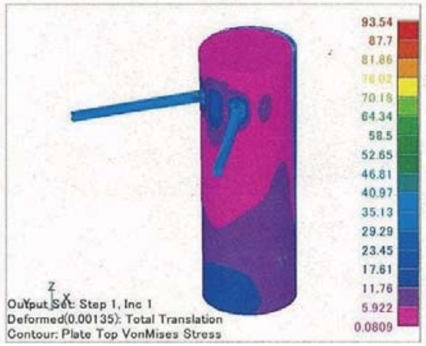

(c) von Mises stress
maximum of 94 MPa at fixed portion of support beam on helium vessel.

Fig. 2.5.45: Analytical results of displacement and von Mises stress induced on vessel support beams for horizontal acceleration of 0.4G.

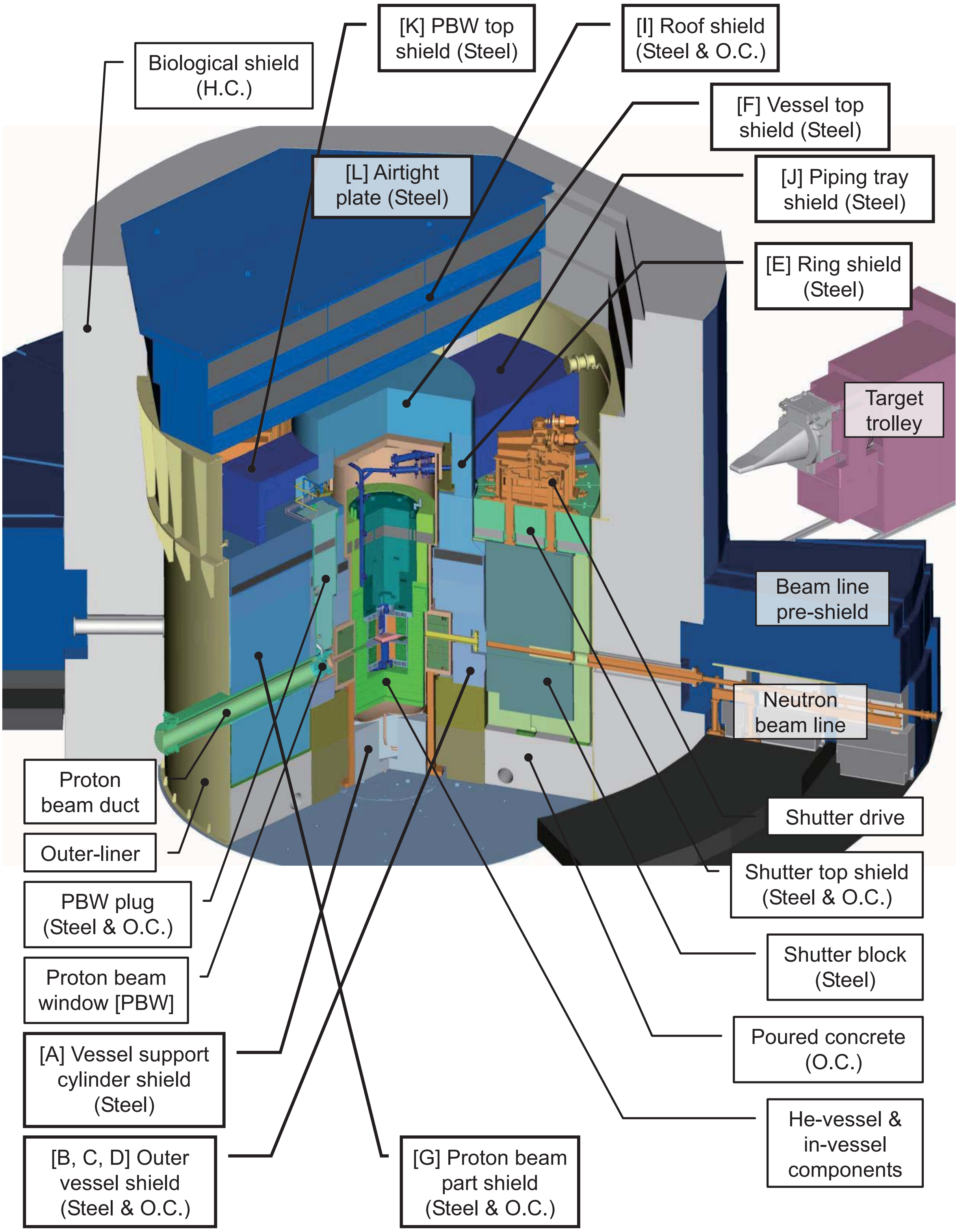

Fig. 2.5.46: General configuration of the shielding blocks and related components of the JSNS target station. Shields treated in this section are shown in thick frames. Materials are shown in parentheses where O.C. and H.C. mean ordinary concrete and heavy concrete, respectively.

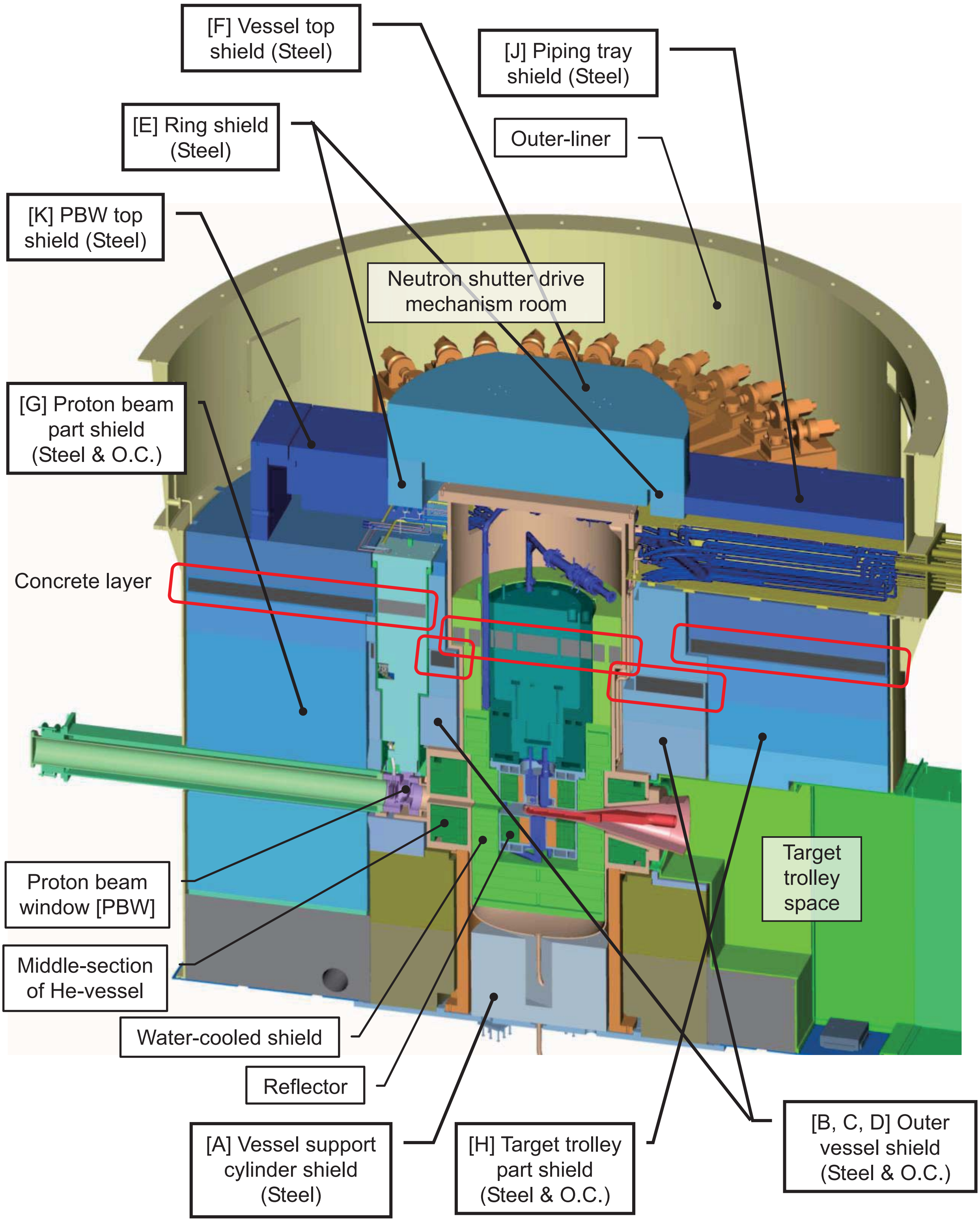

Fig. 2.5.47: Detailed general configuration of the shielding blocks and related components of the JSNS target station on a cross section of 0-180 degrees. Shields treated in this section are shown in thick frames. Materials are shown in parentheses where O.C. and H.C. mean ordinary concrete and heavy concrete, respectively.

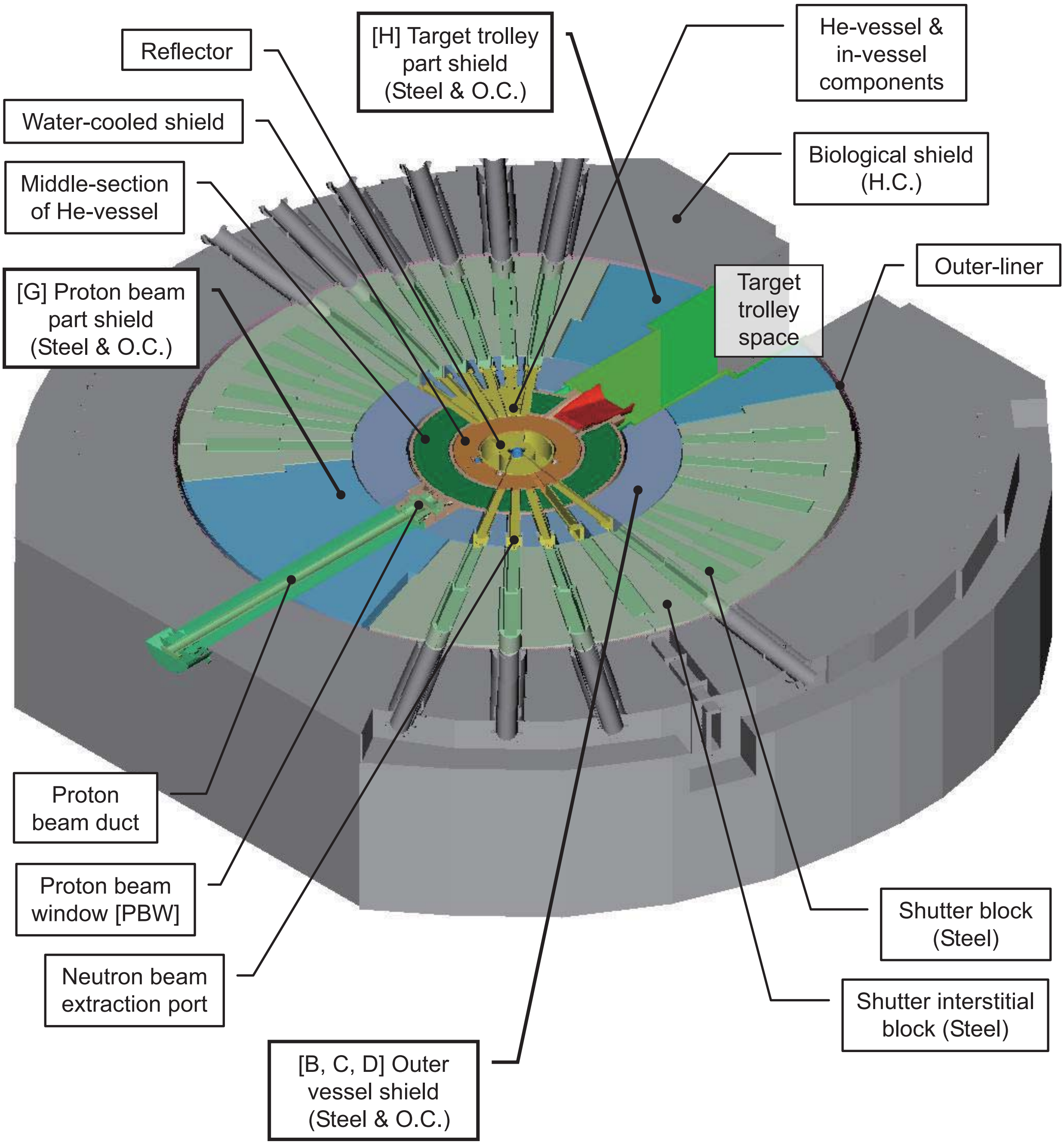

Fig. 2.5.48: Horizontal cut view of the target station at 1FL+1437 mm where neutron beam lines viewing the coupled moderator are located. Shields treated in this section are shown in thick frames. Materials are shown in parentheses where O.C. and H.C. mean ordinary concrete and heavy concrete, respectively.

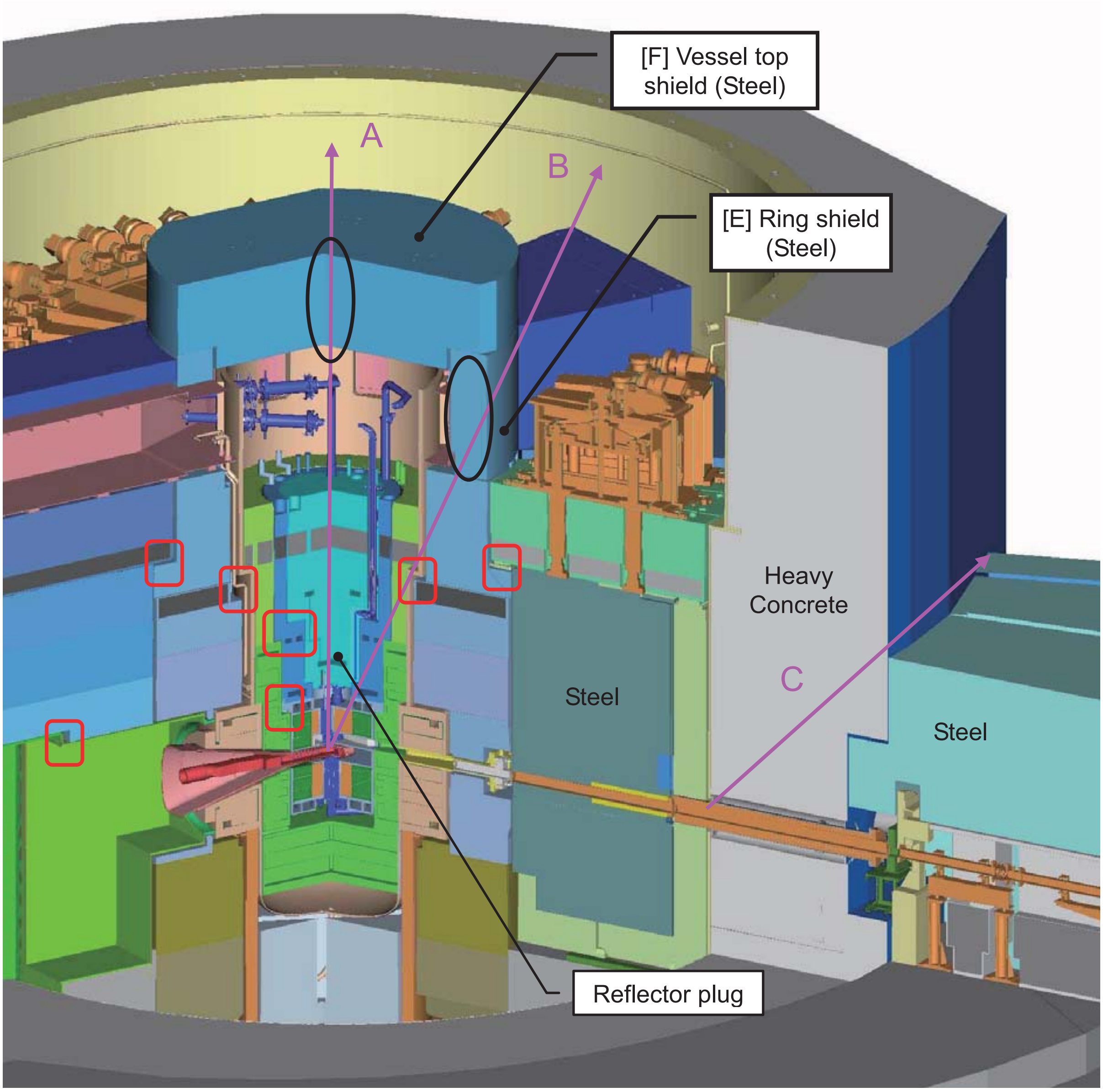

Fig. 2.5.49: Measures for radiation streaming

Photo. 2.5.1: Reference templates for the base-plate and the bottom-liner installed upon reinforcing steel bars at the basement

Photo. 2.5.2: Reference templates for the base-plate and the bottom-liner after filling concrete in the basement

Photo. 2.5.3: Steel plates welded on the template for adjusting the elevation of the base-plate with jack bolts and filler plates for anchor bolts to fixed the base-plate

Photo. 2.5.4: Base-plate installed upon the basement. Two stuffs were placed on the reference surface to measure the level of the base-plate

Photo. 2.5.5: Top surface of the base-plate installed upon the basement. Opening for anchor bolts, air evacuation at grouting and jack bolts are sealed with plates by welding.

Photo. 2.5.6: Bottom-liner installed upon the basement. Opening for anchor bolts, air evacuation at grouting and jack bolts are sealed with plates by welding.

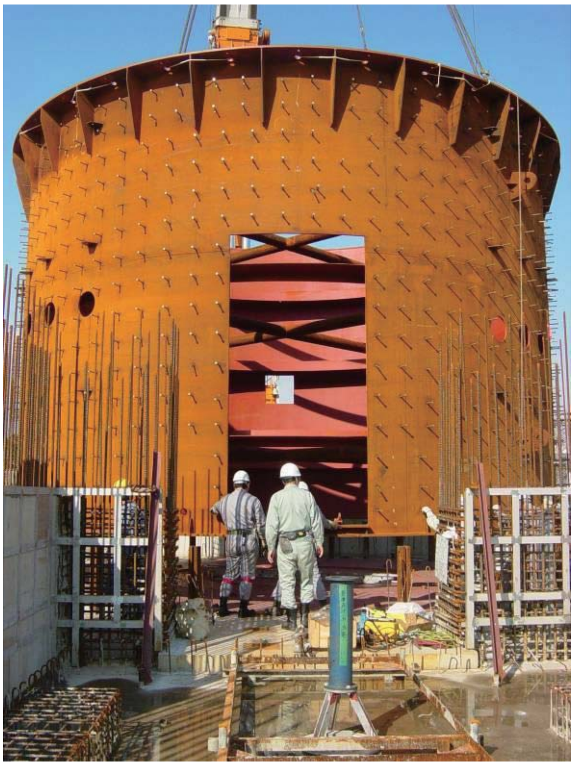

Photo. 2.5.7: Installation of the lower outer-liner on the bottom-liner

Photo. 2.5.8: Stud bolts on the outer-liner and plates welded with anchors

Photo. 2.5.9: Inspection of the seal welding on the bottom-liner and the bottom of the outer-liner

Photo. 2.5.10: Installation of upper part of the outer-liner on the lower part

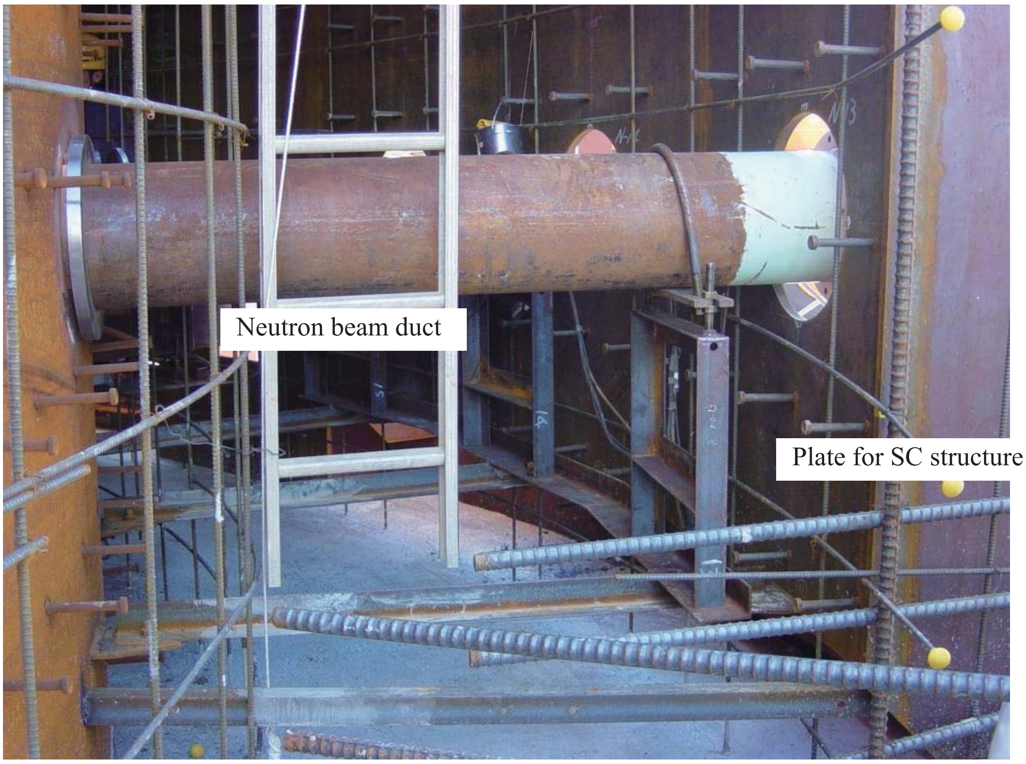

Photo. 2.5.11: Installation of neutron beam duct

Photo. 2.5.12: Target trolley liner which is installed outside of the outer-liner (view from downstream)

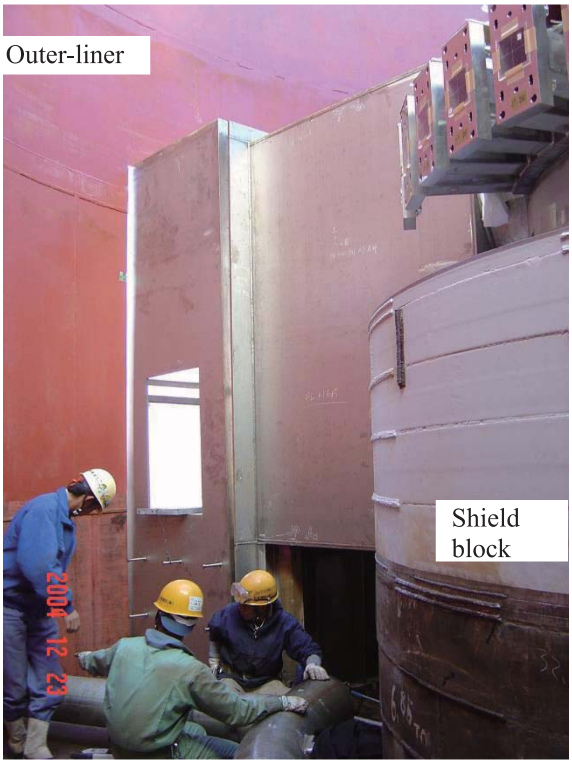

Photo. 2.5.13: Target trolley liner inside of outer-liner. The rectangular opening on side of the target trolley liner was sealed by welding a plate after completion of installation works inside the outer-liner.

Photo. 2.5.14: Upstream end of proton beam duct liner (i.e. outside of the outer-liner)

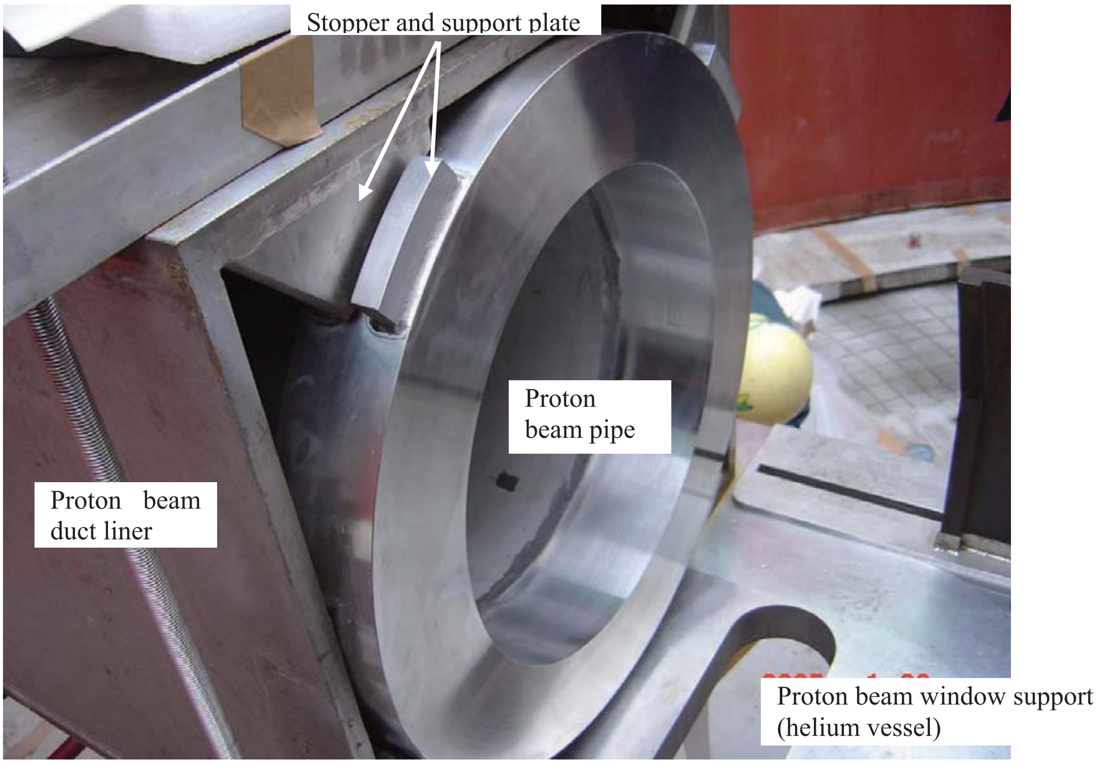

Photo. 2.5.15: End of the proton beam duct liner containing proton beam pipe at downstream side (i.e. helium vessel side)

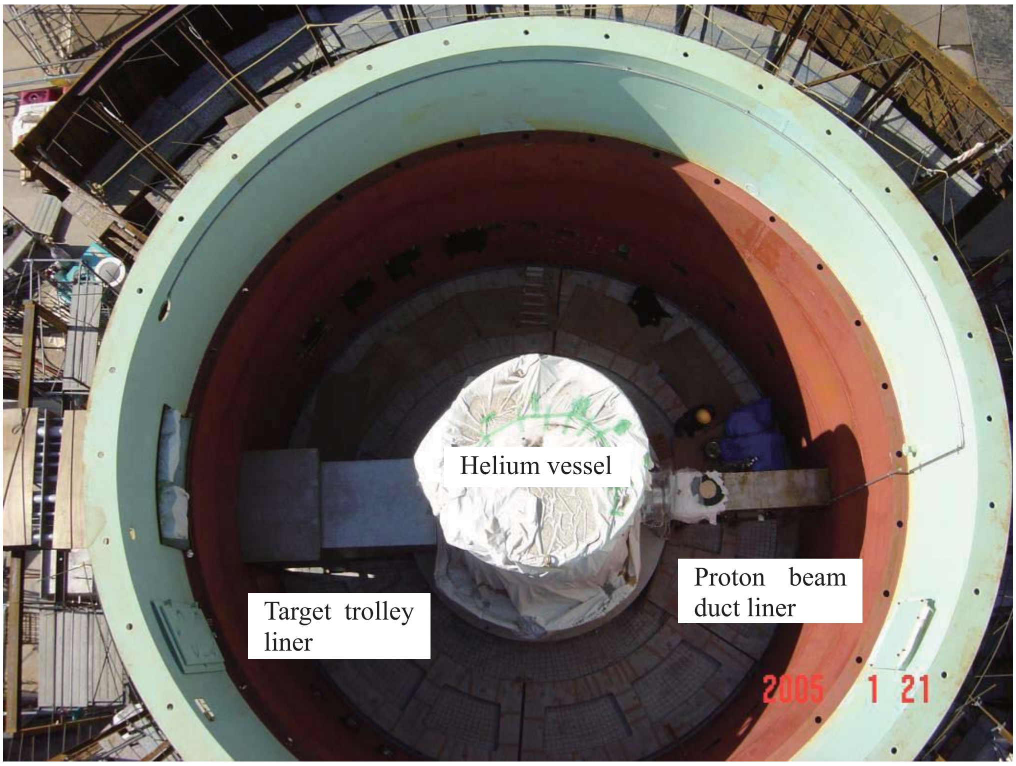

Photo. 2.5.16: View of liner components from top of the MLF building. The base-plate and the bottom-liner have been already covered with magnetite concrete

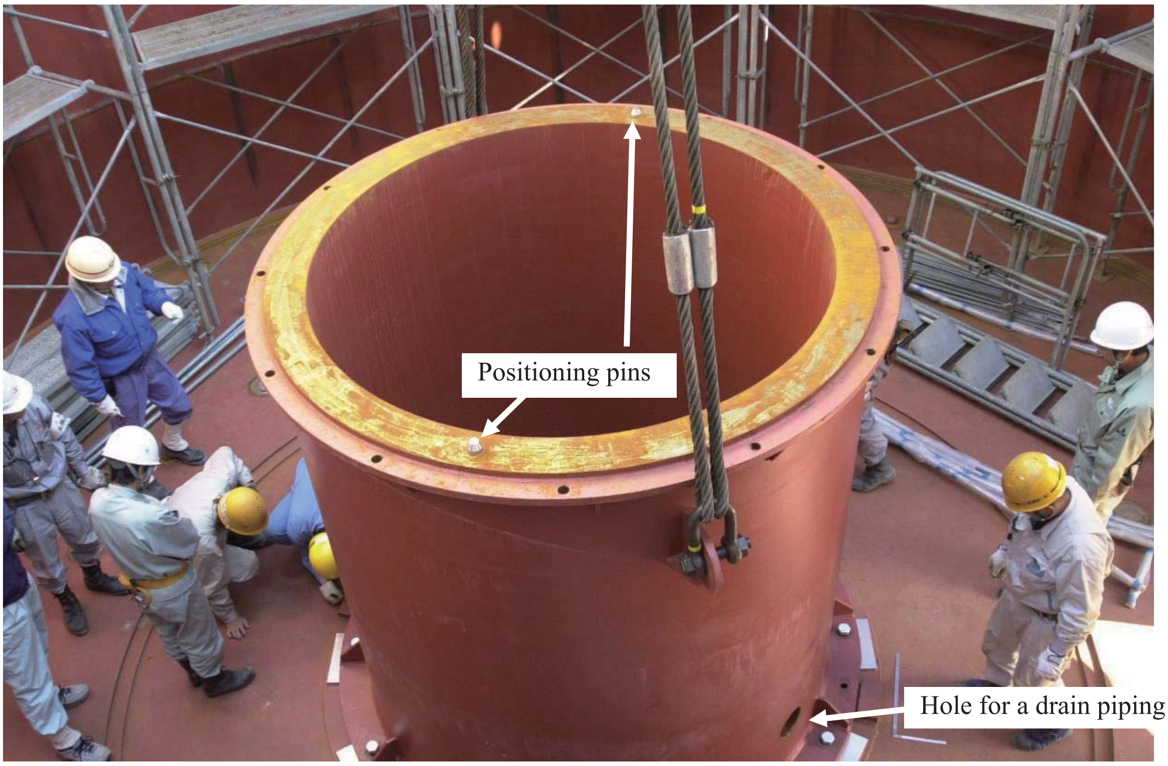

Photo. 2.5.17: Vessel support cylinder settled upon the base-plate

2.6 Neutron Beam Line Components in Neutron Source Station

Neutron beam line in neutron source station consists of "vessel insert", "shutter insert" and "bulk-shield insert". The vessel insert and the shutter insert are enclosed in each vacuum duct. Since Monte-Carlo simulations show no distinct effectiveness of neutron guide installed in the vessel insert on the neutronic performance, none of vessel insert is installed in the vacuum duct; *i.e.* the duct is empty at present except for the dual-channeled beam extraction port for the reflectometer. In contrast, a specific shutter insert is installed in the vacuum duct of each beam line, and it is followed by a respective bulk-shield insert.

Structural and functional specifications of the beam line components in the station are described in the following sections (2.6.1 ~ 2.6.3). In these sections, a right-hand coordinate system defined in Fig. 2.6.1 is applied, where z represents a neutron beam direction, x, and y the direction perpendicular to it in the horizontal and vertical planes, respectively, and θ_h and θ_v the rotation angle in horizontal and vertical planes where 0 degree corresponds to the each neutron beam direction. Dimensions are written in mm for x, y, and z, mrad for θ_h and θ_v.

2.6.1 Vessel Inserts and Window Handling Device

(1) Introduction

As described in section 2.5.1(7), neutrons cooled down in moderators pass through helium in the helium vessel and surrounding air at normal pressure in the neutron source station. Intensity of thermal and cold neutrons reduces as they pass through air region because of nuclear scattering. Let us estimate the attenuation of thermal neutron intensity in air as an example. The number density of air at normal pressure is obtained as $6.02\times10^{23}/(22.4\times10^{3}) = 2.7\times10^{19}$. The total cross sections of nitrogen and oxygen for thermal neutron with energy of 0.0254 eV are about 14 barns and 4 barns, respectively. Considering the ratio of nitrogen to oxygen composing air is 4:1, the total cross section of air is obtained as

$$0.8\times14\times2 + 4\times2\times0.2 = 24 \text{ (barns)}.$$

The relative intensity of thermal neutrons after passing through 2.2 m thick air at normal pressure is obtained as follows:

$$\begin{aligned} I/I_0 &= \exp[-24\times10^{-24}\times2.7\times10^{19}\times220] \\ &= \exp[-0.14] \\ &= 0.86 \end{aligned}$$

This means that 14% of thermal neutrons are lost on their way by the scattering in air. In order to improve the neutron transmission rate, vacuum layer was introduced at the neutron beam port on the middle section of the helium vessel and at the shutter gate. The component to make vacuum layer is defined as “duct”. Then the duct to be installed at the neutron beam port on the middle section is denoted as vessel insert duct and the one at the shutter gate is denoted as shutter insert duct.

(2) Function of vessel insert duct

The function required to the vessel insert duct is to

a) make vacuum atmosphere at the pressure of 10 torrs,
b) contain devices such as steel collimator and neutron guide (super-mirror) and
c) make the boundary from helium, inner medium of the helium vessel, at the neutron beam port flange.

In designing the vessel insert duct, the following structural conditions are taken into account:

a) The neutron beam port flange is located inside the outer surface of surrounding steel shield blocks.
b) The shutter gate moves vertically in the shutter moving space outside of the surrounding steel shield blocks.
c) Nominal gap between the steel shield blocks and the shutter gate is 20 mm..
d) The vessel insert duct has to be replaced through the shutter moving space when its window is broken to lose boundary function.
e) The design pressure of helium atmosphere is 0.2 MPa.
f) The vessel insert duct does not have cooling channel.

(3) Structural design of vessel insert duct

The vessel insert duct is designed as a rectangular-shaped duct. The conceptual illustrations of vessel insert ducts are shown with that of the neutron beam port in Figs. 2.6.2 and 2.6.3. The length of the vessel insert duct is selected as 695 mm and it is placed from 1.6 m to 2.295 m in radial distance from the center of the helium vessel. The reasons why this position is selected are as follows.

a) The cutting-edge of the ducts is placed outside of 0.9 m in radius from the center of the helium vessel to keep enough spatial distance from the neighboring duct.
b) The vessel insert duct wears no cooling system. Then the cutting-edge of the vessel insert duct is placed outside of 1.5 m in radius where nuclear heating is so small that heat removal by water cooling is unnecessary.
c) The location of the downstream cutting-edge of the vessel insert duct is the maximum to keep the gap of 20 mm towards the cutting-edge of the shutter gate. Considering that the cutting edge of the shutter gate interrupts the vessel insert duct when it comes down in the shutter space,
d) Allowable horizontal stroke of a handling devise is 800 mm to extract the vessel insert ducts to shutter space.

As shown in Fig. 2.6.3, the vessel insert duct for beam line No.16 has the configuration as a lid because the collimator is already installed in the neutron beam port to ensure the neutron beam path inclined as 2.22° and 5.17° downward with respect to the horizontal plane.

The vessel insert duct is required not only to be boundary from helium and but also to keep vacuum inside. Then, we chose double O-ring location on the vessel insert duct flange. Fig. 2.6.4 shows the cross sectional illustration of the vessel insert duct at the neutron beam port flange. A hole penetrating to the inside of the vessel insert duct was fabricated on the middle of dips for doubly allocated O-rings to evacuate inner air and also detect a leak by a failure of O-ring. To achieve helium tight seal condition under the highly radiated environment, metallic O-ring was selected.

As for the vessel insert duct material, type 5083 aluminum alloy was selected because it has better welding performance in view of manufacturing and better neutron transmission rate in view of neutronics characteristics. The neutron transmission performance for some aluminum alloys is compared in Fig. 2.6.5**.** Under the condition that the vessel insert duct is evacuated to the pressure of 10 torr and the design helium pressure is 0.2 MPa, the structural analyses were carried out by the ABAQUS code, *i.e.* finite element method. Conditions for structural analysis of the vessel insert duct are listed in Table 2.6.1. Fig.2.6.6 shows the analytical result of displacement and von Meses stress induced on 5 mm thick side plates of the vessel insert duct.

Based on the calculations, the thickness of the side plates and that of edge window were determined as 5 mm and 1.5 mm. Thinner window thickness raises neutron transmission rate. Therefore, the curve plate was selected to suppress the increase of induced stress even though the window thickness becomes thinner. The analytical results for the following three window shapes are compared in Fig. 2.6.7:

Case 1: flat plate type window,

Case 2: curve plate window with radius of curvature 100 mm,

Case 3: curve plate window with radius of curvature 200 mm.

The effect of the window thickness on the neutron transmission efficiency was also investigated by Monte-Carlo simulation using MCNP-4C and the nuclear data compiled in JENDL 3.3. For comparison, the following three cases are chosen:

Case-1 (reference): helium layer up to 210 cm from the origin and air layer from 210 to 434 cm,

Case-2: 1.5 mm thick windows are employed at vessel and shutter inserts,

Case-3: 3 mm thick plates are employed at vessel and shutter inserts.

The detailed medium compositions for case-2 and case-3 are summarized in Table 2.6.2. The calculated results of the neutron transmission rates are shown in Figs. 2.6.8 to 2.6.10 for neutron energies of 2.5 meV, 20 meV and 100 meV, respectively. The relative neutron intensities at 434 cm to the origin are summarized in Table 2.6.3. The vacuum layer with 1.5 mm thick windows reveals superior neutron transmission rate than the reference case composed of helium and air layers by 1.4%. This value becomes much larger in actual system since the neutron transmission rate for reference case would be worse because of any structural material inserted at the boundary between helium and air layers. The results with 1.5 mm thick window induces intensity gain of about 11% for 2.5 meV neutron and that of 6% even for 100 meV in comparison with the flat plate type windows, respectively.

(4) Mechanical design of bolt and nut on vessel insert duct

At the beginning of the design study, the vessel insert duct was designed to be fixed with nuts on the stud bolts on the neutron beam port flange. However, this idea does not satisfy the condition that removes bolts at a failure. Instead, alternative idea is that bolts are fixed on the vessel insert duct flange and rotate 90° to lock into cases which are mounted on the neutron beam port flange.

Fig. 2.6.11 is the drawing of bolts and nuts on the vessel insert duct. Fig. 2.6.12 shows the sequence for fastening bolts with nuts of the vessel insert duct on the neutron beam port flange. The functional points are as follows:

a) The head of the bolt has been fabricated as anchor-shaped, and the nut is attached on the tail of the bolt.
b) Adjust the vessel insert duct position so that four bolts could face to the corresponding holes on the neutron beam port flange.
c) Insert bolts in the corresponding holes on the neutron beam port flange.
d) Insert bolts till their heads are contained completely in the case mounted at the bottom of the neutron beam port flange.
e) Rotate the bolt 90˚ counter clock wise so that its head could fit a stopper fabricated on the case. This dip works as a support to fasten the nut on the tail of the bolt.
f) Fasten the nut under design torque.

Removal of the vessel insert duct from the neutron beam port is carried out in the reverse sequence from f) to b). This series of procedure is realized by the window handling device. In view of designing remote handling device, it is better to reduce the number of bolts as low as possible. However, we selected to allocate four bolts on individual corners of the rectangular-shaped flange because it is easy to take force balance in fastening them.

(5) Design of seal structure

It is noted that four bolts at corners are located at unequal intervals but in rectangular-shaped arrangement due to the geometrical constraint on account of narrow distance from neighboring neutron beam port. Therefore, it is necessary to select proper position for bolts so that metallic O-rings could be deformed enough to conduct sound seal performance when specified torque is added on bolts at fastening. We have preliminarily carried out analyses using ABAQUS code to investigate the deformation of metallic O-rings and flanges. In addition, we also carried out mock up tests to examine the seal performance of double metallic O-rings by means of four bolts. The resultant layouts of double O-rings are shown in Figs. 2.6.13 and 2.6.14. The dips for setting O-rings were fabricated on the vessel insert duct flange considering its exchangeability. The specifications of metallic O-rings and flanges are summarized in Tables 2.6.4 and 2.6.5.

2.6.2 Shutter System

Neutron beam shutter system is an integral part of the neutron source station as shown in Figs. 2.6.15 and 2.6.16. Each shutter is controlled by a remote control panel at corresponding instrument or a local integrated control panel in the station. The shutter system has been designed under a particular precondition that every shutter should be controlled and maintained independently.

The JSNS shutter system consists of the following components; i) shutter base plates, ii) 25 interstitial blocks, iii) 23 shutter gates, iv) 23 upper shielding blocks, v) 23 drive assemblies, vi) control systems, and vii) maintenance tools. A vertical view of the JSNS shutter system in the target station is shown in Fig. 2.6.16, where main components, their sizes, materials and structures, are presented.

To accomplish the feature that all the shutter gates and drive assemblies for each beam port are workable independently, a conceptual design work had been carried out at 2002. There were several methods to drive a shutter gate weighing about 15 ton. We considered not only initial installation work, but also reinstallation at maintenance phase. Table 2.6.6 summarizes comparing investigation for a conceptual design of JSNS shutter system. Finally, we selected the type of "Guided by double shafts with rigid flanges", because of "C-less" and possibility of on beam adjustment of a beam line component described in later part of this section.

2.6.2.1 Shutter base plates

(1) Specification

1) Objective

The shutter base plates define a reference level of the shutter system at 1FL−155 mm, where 1FL denotes a first floor level of the experimental hall. Flatness was required not only from plumbing of the interstitial blocks but also from self-supporting of the shutter gate on the base plate at installation. The base plates also define the position of the interstitial blocks by the positioning pins. Fig. 2.6.17 shows the layout of the shutter base plates in the outer liner. Shutter base plates were divided into five segments considering the handling in the outer liner. Supporting frames were set to mount the base plates.

2) Environmental condition

a) Temperature; less than 50°C

b) Pressure; 1 atm

c) Notes; under radiation field of 1 MGy/year

3) Loading condition

a) Load of 25 interstitial blocks, 23 shutter gates, 23 upper shielding blocks, 23 drive assemblies, and a proton beam window and its shielding

b) Seismic force at horizontal excitation; 0.25G

4) Miscellaneous

a) Number of base plates; 5 peaces

b) Densities of the materials

Apparent relative density of steel; 7.6 g/cm^3

Ordinary concrete; 2.2 g/cm^3

c) Allowable deviation from flatness; 1/1000

Allowable deviation from the reference level; 3 mm

Allowable deviation of the positioning pins from the ideal points; 1 mm

(2) Structures

The shutter base plates were mounted on frames. Magnetite concrete was poured under the base plates up to the plate surface level +0/−3 mm to support weight of the shutter system. Beam line marking was transferred from the experimental hall to the base plate and proper points inside the outer liner. These markings were transferred to higher positions in every construction step.

2.6.2.2 Interstitial blocks

(1) Specification

1) Objective

Shield in the region from 2,320 to 4,720 mm in radial direction from the center of the helium vessel and height from 1FL−155 to 1FL+4195 mm. A pair of interstitial blocks forms a space of 225/325 mm in width (see Fig. 2.6.18) and 4370 mm in depth (see Fig. 2.6.16; 4215+155 mm) where the shutter gate strokes.

2) Environmental condition

a) Temperature; less than 60°C

b) Pressure; 1 atm

c) Notes; under radiation field of 1 MGy/year

3) Loading condition

a) Dead weight (max. 50 ton) plus upper shielding block, shutter gate and drive assembly

b) Seismic force at horizontal excitation; 0.25G

4) Miscellaneous

a) Number of interstitial blocks; 25

b) Density of the material

Apparent relative density of steel; 7.6 g/cm^3

c) Supports the upper shielding block on the surface of attached plates

d) Nominal clearances; 11 mm in x and 50 mm in z

e) Allowable deviation of perpendicularity; 1/1000

Allowable deviation of the surface of the mounted plates; 4215±0.5 mm

Allowable deviation along the x-axis; ±3 mm

Allowable deviation along the y-axis; ±3 mm

Allowable deviation for each shutter gate space; ±3 mm

Allowable deviation along the z-axis; ±3 mm

(2) Structures

1) Layers

As shown in Fig. 2.6.18, each interstitial block is machined from the welded layers of steel.

2) Configuration

The angular intervals of beam lines are asymmetric, but the shutter gate structure is symmetric in each z-direction. As a result, most of the interstitial blocks are asymmetric in each z-direction (see Fig. 2.6.19).

2.6.2.3 Shutter gates and shutter insert

(1) Shutter gate

1) Specification

(a) Objective

A shutter gate shields/provides a neutron beam from a moderator to an instrument.

(b) Environmental condition

a) Temperature; less than 60°C

b) Pressure; 1 atm.

c) Notes; under radiation field of 1 MGy/year

(c) Loading condition

a) Load of a gate at normal operation; 15.5 tons

b) Seismic force at horizontal excitation; 0.25G

(d) Miscellaneous

a) Number of shutter gates; 23

b) Densities of the materials

Apparent relative density of steel; 7.6 g/cm^3

High density polyethylene; 0.95 g/cm^3

c) Nominal clearances; 20 mm in z and 12.5 mm in x

d) Difference in center of gravity; less than 1 mm (see Table 2.6.7).

e) Types;

There are two types of shutter gate; so-called type-A and -B, except one; type-C for dual-channeled beam extraction port for the reflectometer. The type-A and -B gates are used for lower and higher beam lines, respectively, as shown in left and right part of Fig. 2.6.16. The type-A extract/shield neutron beams from a coupled moderator, while the type-B extract/shield neutron beams from decoupled moderators.

2) Structures

1) Form (Figs. 2.6.20 and 2.6.21)

A stepwise width (200/300 mm) is applied in x-axis to prevent the streaming. At the close position, bulk polyethylene is attached to shield the leakage neutrons from steel; at around keV. A seesaw-like base plate for a shutter insert is mounted in the shutter gate to align the insert in a horizontal line.

2) Configuration

Each shutter gate is aligned to the beam line center, but its distance from the beam line origin is not uniform because of the six reference coordinates of JSNS beam lines.

(2) Shutter insert

1) Specification

(a) Objective

Each shutter gate includes an individual insert which provides the neutron beam of maximum size; 100 mm × 100 mm. The shutter insert is composed of insertion devices, aluminum alloy duct and supporting steel.

To prevent attenuation of neutron beam intensity, the inside of the duct is evacuated under 100 Pa.

(b) Environmental condition

a) Temperature; less than 60°C

b) Pressure; under 100 Pa (inside the duct) and 1 atm (other parts)

c) Notes; under radiation field of 10 MGy/year

(c) Loading condition

a) Load of a gate at normal operation; about 0.5 tons (weight of an insert)

b) Seismic force at horizontal excitation; 0.25G

(d) Miscellaneous

a) Densities of the materials

Supporting steel; 7.6 g/cm^3

b) Types

Type-D, E, E-2 (for BL08 only), and two special insert for shutter gate C (for reflectometer) are made.

2) Structures (Figs. 2.6.21 and 2.6.22)

Upstream beam window is welded on the square pipe, and the other side is flange structure. Because of the high radiation field, metal O-ring is used for seal.

Insertion devices, such as steel collimator or supermirror guide, were fabricated to meet the requirement of individual instrument such as beam size and divergence. Allowance of the beam line misalignment has been determined to be 1 mrad, which was estimated from the beam line simulation of some instruments using Monte Carlo simulations. In most cases, the simulation shows that slightly enlarging beam size of the insert will greatly compensate the influence of misalignment with a little sacrifice of transport performance.

2.6.2.4 Upper shielding blocks

(1) Specification

1) Objective

Shield in range of *r*; 2050 - 4720 mm from the center of the helium vessel and height; FL+4,200 −5,100 mm.

2) Environmental condition

a) Temperature; less than 60°C

b) Pressure; 1 atm.

c) Notes; under radiation field of 1 MGy/year

3) Loading condition

a) Load of a gate at normal operation; own weight (max. 10 tons) plus shutter gate and drive assembly.

b)Seismic force at horizontal excitation; 0.25G

4) Miscellaneous

a) Number of upper shielding blocks; 23

b) Densities of the materials

Apparent relative density of steel; 7.6 g/cm^3

Relative density of concrete; 2.2 g/cm^3

c) Supports the drive assembly on the surface of each block

d) Nominal clearances; 20 mm in x and 50 mm in z

(2) Structures

1) Layers

To meet the requirement for the effective shielding, a concrete layer is sandwiched at the height of 50 - 250 mm region, and the less part is composed of steel; total height is 900 mm.

2) Configuration

Because of the asymmetric angular intervals and six reference coordinates of JSNS beam lines, partitioning lines are defined as a center of the neighboring beam lines. As a result, most of the upper shielding blocks are not symmetric about each beam line center, as shown in Fig. 2.6.23.

2.6.2.5 Drive assembly

(1) Specification

1) Objective

A drive assembly moves and fixes a shutter gate to shield/provide a neutron beam from a moderator to an instrument.

2) Environmental condition

a) Temperature; less than 50°C

b) Pressure; 1 atm

c) Notes; under radiation field of 1 MGy / year

3) Loading condition

a) Load of a gate at normal operation; 15.5 tons

b) Seismic force at horizontal excitation; 0.25G

4) Miscellaneous

a) Number of drive assemblies; 23

b) Dimension of a shutter gate; 200/300 mm in x, 3,870 mm in y, and 2,000 mm in z

c) Stroke for open/close; 400 mm

d) Period of the stroke; 60 seconds

e) Reproducibility of the position; ±0.5 mm

f) Adjustment range ; ±5 mm in x, ±10 mm in y, ±5 mm in z, ±2.5 mrad in θ_h

g) Assumed frequency of usage (stroke); 2 / hour

(2) Structure and capacity

Based on the type of "Guided by double shafts with rigid flanges" in Table 2.6.6, we adopted a 5 kW AC servomotor (HC-SFS502(B)G1; Mitsubishi Electric Corporation) with a reduction gear and a 20 ton ball screw jack (JWB200DRH8U; Tsubaki Emerson Corporation) for the main component of the drive assembly, as shown in Fig. 2.6.24.

Very severe tolerances for the fabrication and assembling are applied around oilless bearings (OILES Corp.); their sizes and tolerances are shown in Fig. 2.6.25. Actually, assembling shaft(s) on each gate using flange(s) is most critical step for the installation. We carefully examined not only for the interval between two shafts, but also for the inclination of the shafts, as shown in Fig. 2.6.26.

(3) Earthquake-resistance

Earthquake-resistance strength for the components of the drive assembly, such as shaft, pedestal mounting bolt, shaft guide, shaft guide mounting bolt, shaft connecting pin, shaft-jack connecting part, pedestal, adjustment bolt, and flange bolt, is estimated under the condition of 0.25G. All the components are confirmed to be no problem, but the bending of the shaft and resultant amplitude of a gate edge swing exceed the clearance of the gate and interstitial blocks. In that case, bottom of the gate would hit the wall of interstitial blocks at around 0.1G, but the value is small enough for structural damage of the drive assembly.

2.6.2.6 Control systems

(1) Shutter local controller

Shutter control system was designed under the following basic concepts.

a) Users can operate the shutter gate individually using a shutter controller at an instrument room in the experimental hall.
b) The facility’s personnel operate shutters near the shutter drive mechanism room during the maintenance period.
c) The shutter control system is connected to the personnel protection system (PPS) to prevent the personnel from fatal radiation exposure at the instrument room.
d) The shutter status is monitored at the MLF control room on the 3rd floor.

The shutter control system is composed of shutter controllers, shutter local control boards and PPS control board. The users handle the shutter controller for open and/or close the shutter gate. It is placed near the neutron instrument room at the experimental hall. Here, the control mode for allowed users to operate the shutter controller is defined as “remote mode”.

The shutter local control board is operated by the facility’s personnel and placed near the shutter drive mechanism room in the large components handling room. The control mode for maintenance work using the shutter local control board is defined as “local mode”.

The PPS monitor is an equipment to display the shutter gates’ positions. It is set in the MLF control room.

Fig. 2.6.27 illustrates the constitution of the shutter control system. The interlock system is made on the PPS control board in the control room. The signal of the PPS is transferred by the hardwire cable in view of the reliability. The status signals such as open/close status, shutter gate position and so on are communicated by the programmable logic controller (PLC).

Table 2.6.8 summarizes the function of the switches and displays of the local control board, the remote control panel and the shutter control panels. The shutter open rejection switch on the remote control panel is employed to reject the operation of the shutter gates to protect the personnel at the shutter area from an accident during maintenance period.

Specification

(a) Objective

Drive every shutter gate independently. In normal usage, each shutter gate is controlled by the remote controller at corresponding instrument.

(b) Environmental condition

a) Temperature; less than 50°C

b) Pressure; 1 atm.

(c) Miscellaneous

a) Number of shutter local controllers; 2 (one controls No.01 − 12 shutter gates, the other controls No. 13 − 23 shutter gates)

(2) Vacuum controller

Specification

(a) Objective

Keep the vacuum level of the insert under 100 Pa.

(b) Environmental condition

a) Temperature; less than 50°C

b) Pressure; 1 atm

(c) Miscellaneous

a) Number of vacuum controllers; 4 (No. 01 − 06, 07 − 12, 13 − 18, 19 − 23)

(d) Control sequence

Each vacuum controller operates as shown in Fig. 2.6.28.

2.6.3 Neutron Beam Inserts in Biological Shield

Biological shield composed of magnetite concrete is an outer shield of the target station. Distance from the center of the target station to the wall of the biological shield is about 7 - 7.5 m in radius. The wall of the biological shield is vertically concave about 0.5 m at around the beam line height as shown in Fig. 2.6.29 to prevent the streaming. Each beam line has a beam extraction port in biological shield, where an insert can be installed from the experimental hall. Beam line center is marked on the side of the flange of the beam extraction port, and difference between the "true" beam line center and center of the each beam extraction port is less than 10 mm (most of them are <6 mm) in diameter. A function as a boundary of the air between inside target station and experimental hall is also required for the insert.

The biological shield insert starts at *ca.* 20 mm away from the end of the shutter gate (insert), and ends around 7 m, uppermost stream of the beam line in the experimental hall. The insert is composed of a housing and a beam transport device, such as collimator or neutron guide tube. The housing makes quadrate (or rectangular) aperture in the beam extraction port. Difference between the true beam line center and the center of the quadrate aperture is measured to align the beam transport device. Centering of the beam transport device is done by adjusting the spacer thickness of the roller attached on the both sides and the bottom face of it.

Specification

1) Objective

The biological shield insert is composed of a housing and a beam transport device.

To prevent attenuation of neutron beam intensity, the inside of the duct is evacuated under 100 Pa.

2) Environmental condition

- a) Temperature; less than 60°C
- b) Pressure; under 100 Pa (inside the beam transport device)
- c) Notes; under radiation field of 1 MGy / year

3) Loading condition

- a) Load of a gate at normal operation; about 1.0 tons
- b) Seismic force at horizontal excitation; 0.25G

4) Miscellaneous

- a) Beam window; Aluminum alloy (A5083)
- b) Beam transport device; SS400 or SUS
- c) Housing; SS400 or SUS

Upstream beam window is sealed by a metal O-ring, whereas the downstream one is sealed by an EPDM one considering the dose level.

Table 2.6.1: Conditions for structural analysis of vessel insert duct

Items	Conditions
Code	ABAQUS
Model	3-dimensional shell elements
Material	Aluminum Alloy (A5083)
Dimension of Duct	112 × 112 mm, 695 mm long
Young modulus of A5083	65 GPa (100°C JIS)
Load (pressure)	0.3 GPa (vacuum inside duct surrounding 0.2-MPa helium)

Table 2.6.2: Compositions of neutron beam line and their position

Position	Medium	Thin window (case-2)	Plate window (case-3)
Middle section	Helium	0 - 160 cm	0 - 160 cm
Vessel insert duct	A5083	160 - 160.15 cm	160 - 160.35 cm
	Vacuum（1 torr）	160.15 - 229.85 cm	160.35 - 229.65cm
	A5083	229.85 - 230.0 cm	229.65 - 230.0 cm
Gap	Air（normal pressure）	230.0 - 232 cm	230.0 - 232.0 cm
Shutter insert duct	A5083	232.0 - 232.15cm	232.0 - 232.25 cm
	Vacuum（1 torr）	232.15 - 431.85 cm	232.25 - 431.75 cm
	A5083	431.85 - 432.0 cm	431.75 - 432.0 cm
Gap	Air（normal pressure）	432.0 - 434.0 cm	432.0 - 434.0 cm

Table 2.6.3: Calculated relative neutron intensity at 434 cm from origin

Neutron Energy	Neutron wave length	Relative neutron intensity at 434 cm from origin		
		Case-1	Case-2	Case-3
2.5 meV	5.7 Å	0.854	0.892	0.802
20 meV	2.0 Å	0.891	0.923	0.862
100 meV	0.9 Å	0.900	0.936	0.877

Table 2.6.4: Specification of vessel insert duct flange

Items	Specifications
Material	Aluminum alloy (A5083)
Dimension	Height:450 mm, width: 208 mm, thickness:100 mm
Number of bolt holes	4
Bolts	M18, SCM435H, 4 sets
Nuts	M18, S45C H, 4 sets
Spring washer	Type 304SS, 4 sets
Dips for O-rings	Width: 3.75 mm, depth:1.25 mm (accuracy: ±0.05 mm), 2
	Surface flatness: better than 0.8S
Seal material	Type 321SS with silver coating
	Diameter: 1.57 mm, thickness: 0.25 mm,
Leak detection hole	Diameter: 3 mm

Table 2.6.5: Specification of neutron beam port flange

Items	Specifications
Material	Type 316SS
Dimension	Height:450 mm, width: 208 mm, thickness: 60 mm
Positioning pins	Type 440SS, 2 sets
Surface flatness	Better than 0.8S

Table 2.6.6: Comparison of shutter gate suspension methods (A: excellent, B: fine, C: uncertain)

Name of associated type	i) Guideless single shaft with a clevis.		ii) Guided by double shafts with rigid flanges.		iii) Guided by double shafts with clevises.	
Schematic diagram	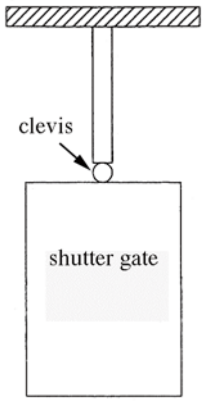		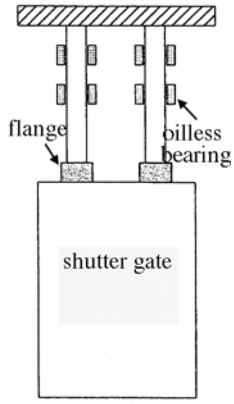		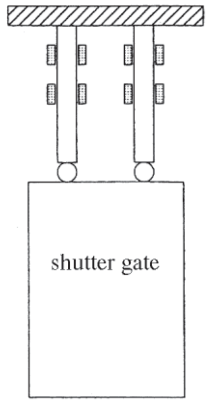	
Outline	Freely suspended by single shaft with dead weight (ISIS-type).		Suspended by double shafts. Binding with rigid flanges.		Suspended by double shafts. Binding with loose clevises.	
Type of bearing	NA		Slide bearing		Slide bearing	
Guide components	NA		Shaft and shaft guide		Shaft and shaft guide	
Posture constraint	Own weight		Shaft guide		Shaft guide and own weight	
Swing stiffness	Single shaft	C	Double shafts and rigid flanges	B	Double shafts but loose clevises	C
Impact resistance	Loose clevis	B	Stiffness optimization of shaft	B	Loose clevises	B
Accuracy and reproducibility of positioning	Low stiffness	C	Rigid flanges	B	Low stiffness	C
Alignment parts	Drive assembly	B	Drive assembly	B	Drive assembly	B
Size of drive assembly	Small	A	Medium	B	Medium	B
Cost	Low	A	Medium	B	Medium	B
Installation difficulty	Easy	A	Require centering of shafts	B	Require centering of shafts	B
Commissioning difficulty	Care for reproducibility	B	No problem	B	No problem	B
Soundness	Pay attention to sliding surfaces	B	Pay attention to sliding surfaces	B	Pay attention to sliding surfaces	B
Ease of maintenance	Simple structure	A	Drive assembly maintenance	B	Drive assembly maintenance	B
Lifetime of bearing	Contactless	A	Life of shaft guide	B	Life of shaft guide	B
Radioactivation of bearing	Low	A	Low	B	Low	B
Circumstance requirement	No problem	A	Pay attention to level of drive base	B	Pay attention to level of drive base	B

Table 2.6.6: Comparison of shutter gate suspension methods (continued)

Name of associated type	iv) Guided by support cylinders with ball casters.		v) Guided by guide rails on support cylinders with cam followers.		vi) Guided by guide rails on support cylinders with OILES bearings.	
Schematic diagram	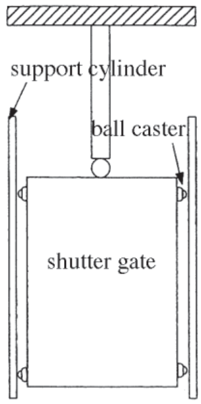		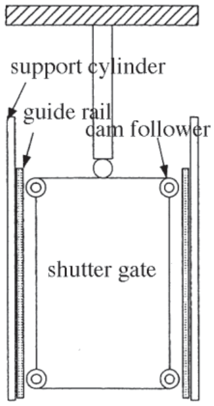		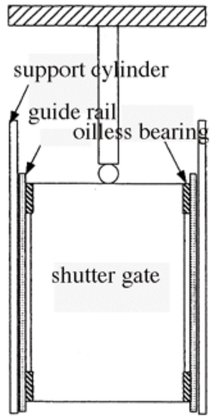	
Outline	Suspended by single shaft. Restraining with ball casters.		Suspended by single shaft. Cam followers keep in contact with guide rails		Suspended by single shaft. Oilless bearings keep in contact with guide rails.	
Type of bearing	Ball bearing		Roller bearing		Slide bearing	
Guide components	Gate (ball caster) and support cylinder		Gate (cam follower) and guide rail		Gate (oilless bearing) and guide rail	
Posture constraint	Own weight		Guide rail		Guide rail	
Swing stiffness	Require clearance between ball caster and support cylinder	C	Contiguous constraint	A	Contiguous constraint	A
Impact resistance	Limitation of ball caster	C	Contiguous constraint	A	Contiguous constraint	A
Accuracy and reproducibility of positioning	Low stiffness	C	High stiffness, depends on guide rail	A	High stiffness, depends on guide rail	A
Alignment parts	Drive assembly and ball caster	C	Cam follower	C	Oilless bearing	C
Size of drive assembly	Small	A	Small	A	Small	A
Cost	Low	A	High	C	High	C
Installation difficulty	Easy	A	Require adjustment of guide components	B	Require adjustment of guide components	B
Commissioning difficulty	Care for reproducibility	B	No problem	B	No problem	B
Soundness	Capacity of ball caster	C	Pay attention to sliding surfaces	B	Pay attention to sliding surfaces	B
Ease of maintenance	Gate (ball caster) maintenance	C	Gate (cam follower) maintenance	C	Gate (oilless bearing) maintenance	C
Lifetime of bearing	Contactless	A	Life of cam follower	B	Life of oilless bearing	B
Radioactivation of bearing	High	C	High	C	High	C
Circumstance requirement	Pay attention to level of drive base and flatness of support cylinder	C	Pay attention to level of drive base and flatness of guide rail	C	Pay attention to level of drive base and flatness of guide rail	C

Table 2.6.7: Estimation of the center of gravity of each shutter gate and insert. All the difference in center of gravity is less than 1 mm.

gate type	BL No.	duct type	insert	total weight (kg)	center of gravity from upstream edge (mm)	difference in center of gravity (mm)
A	1	D	BS-G1	14527.7	1100.3	0.3
A	3	D	BS-G03C	14575.7	1100.4	0.4
A	4	D	BS-G04C	14542.3	1100.2	0.2
B	8	E-2	BS-G08C	14582.9	1100.1	0.1
B	10	D	BS-G10C	14514.7	1100.6	0.6
B	12	D	BS-12S	14524.7	1100.5	0.5
A	14	D	BS-G14S	14597.0	1099.9	-0.1
A	15	D	BS-G15S	14563.5	1100.1	0.1
C	16 (2.22)	BS-G16SD		14707.0	1100.0	0.0
	16 (5.71)	BS-G16SF				
B	19	D	BS-G19C	14603.5	1100.3	0.3
B	20	D	BS-G20C	14620.2	1100.0	0.0
B	21	D	BS-G21C	14586.3	1100.3	0.3

Table 2.6.8: Function of local control board, shutter controller and remote control panel

Components	Function		Comment
	Operational function	Status display	
Shutter local control board	- Local/Remote selection - Move shutter gate to optional position - Position reset/ sitting position - emergency stop	- position of shutter gate - warning messages - PPS inter-lock signal	Emergency stop works all shutters. Other function works every single shutter.
Shutter controller	- On/Off of instrument safety key - Open/Close	- Open/Close status - Local/Remote mode status - warning messages	
Remote control panel	None	- Open/Close status - warning messages	

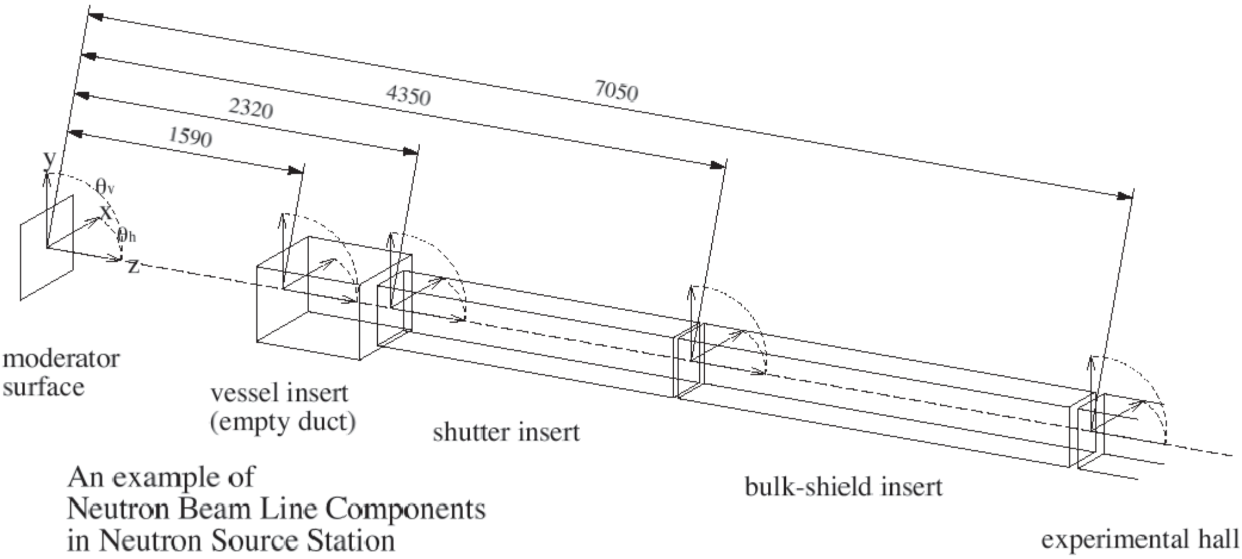

Fig. 2.6.1: Definition of a right-hand coordinate system of a neutron beam line in this section

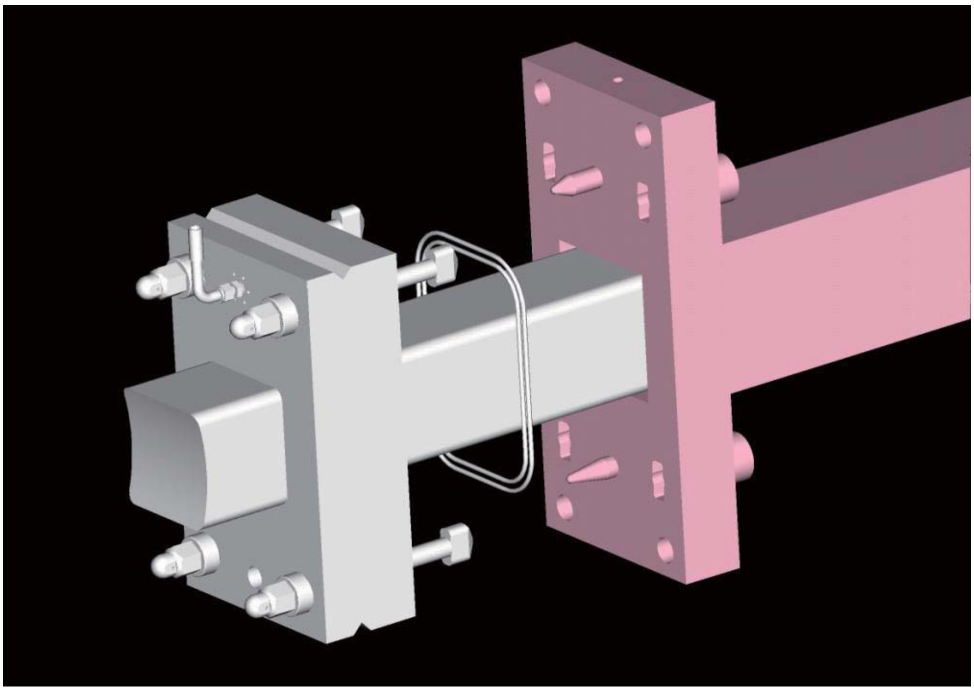

Fig.2.6.2: 3-D illustration of vessel inset and neutron beam port on the middle section except for beam line No.16

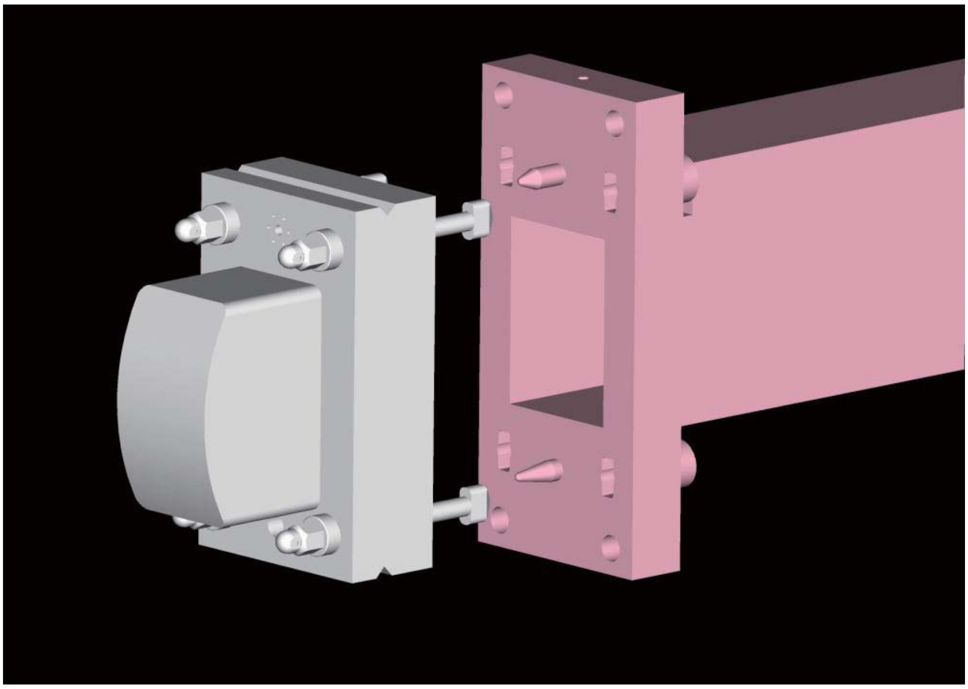

Fig.2.6.3: 3-D illustration of vessel inset and neutron beam port on the middle section for beam line No.16

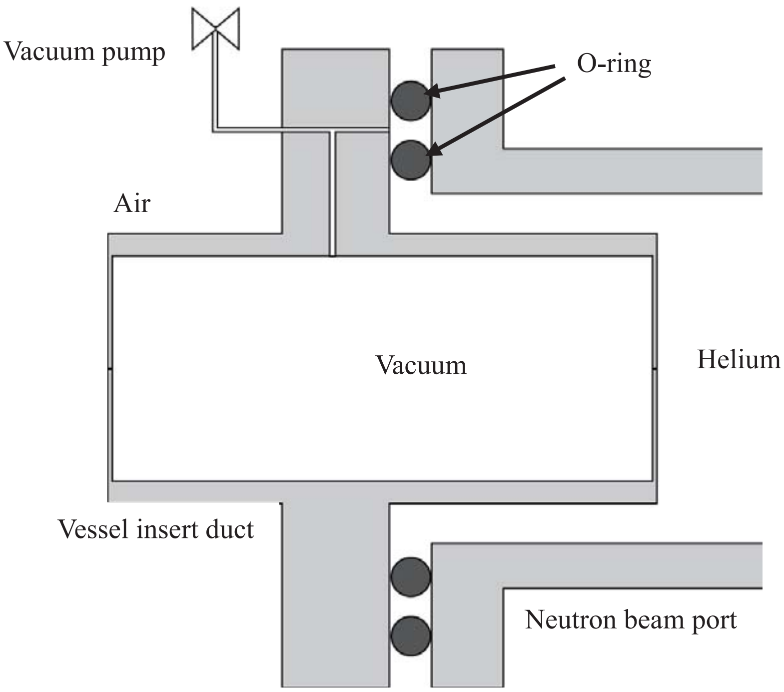

Fig.2.6.4: Cross sectional view of vessel insert duct on the neutron beam port flange

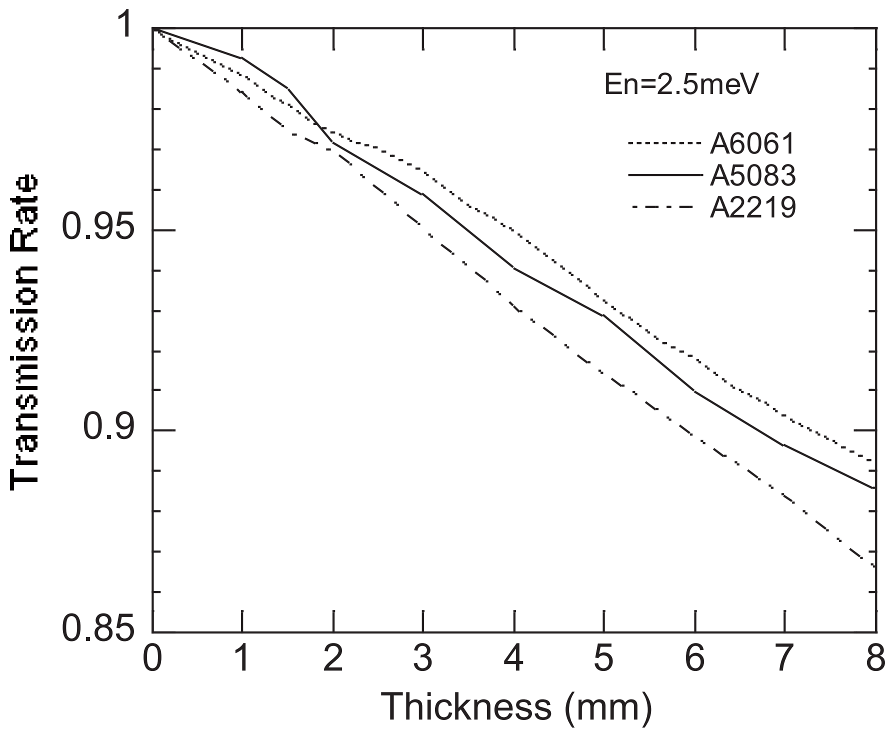

Fig.2.6.5: Transmission rate of aluminum alloys as a function of thickness for 2.5-meV neutron

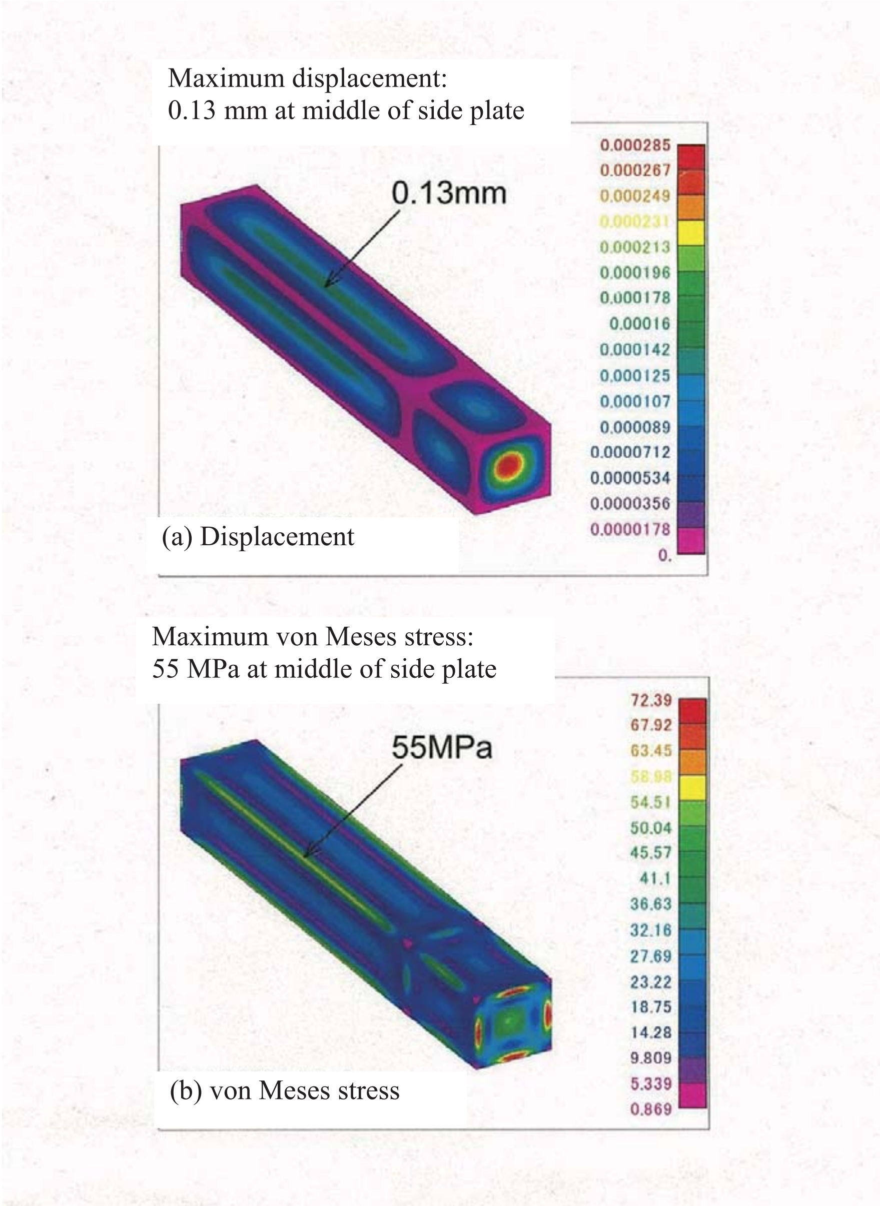

Fig.2.6.6: Analytical result of displacement and von Meses stress induced on 5 mm thick side plates of vessel insert duct for pressure difference of 0.3 MPa between inside and outside

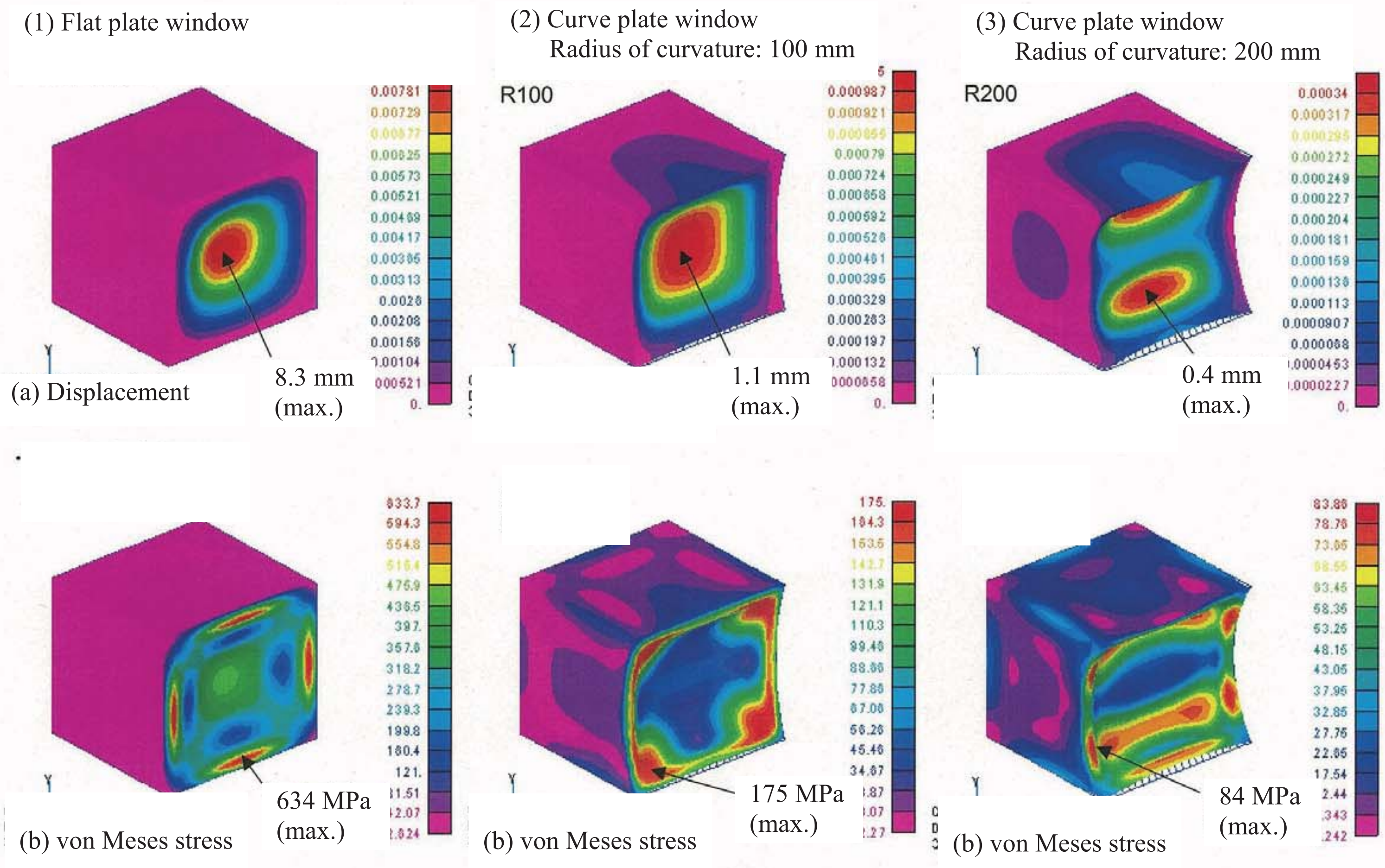

Fig.2.6.7: Analytical result of displacement and von Meses stress induced on 1 mm thick window of vessel insert duct for pressure difference of 0.3 MPa between inside and outside. Left-hand side, middle and right-hand side are for flat plate window, curve plate windows with radius of curvature 100 mm and 200 mm, respectively.

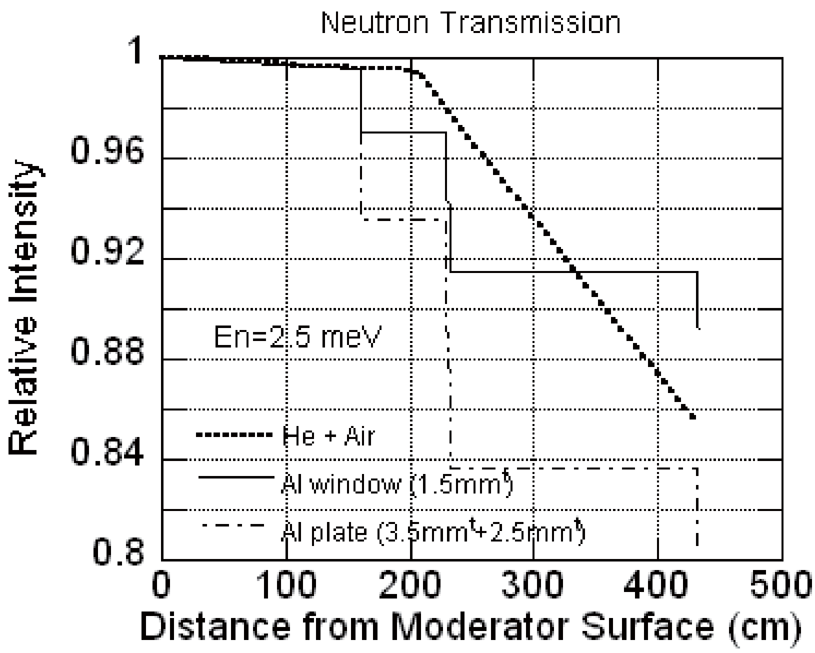

Fig.2.6.8: Attenuation of 2.5-meV neutron flying from the origin to the downstream end of shutter gate. The dotted line stands for the reference case passing through helium layer and air. The solid line represents the case that 1.5 mm thick windows are employed. The dot-dashed line is for flat plate windows.

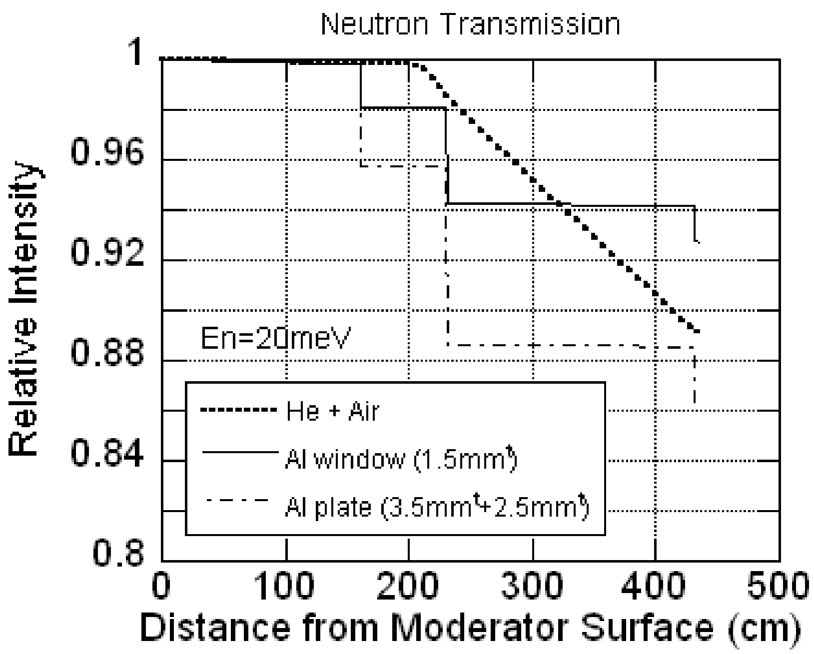

Fig.2.6.9: Attenuation of 20-meV neutron flying from the origin to the downstream end of shutter gate. The notes on the lines are the same as those in Fig. 2.6.8.

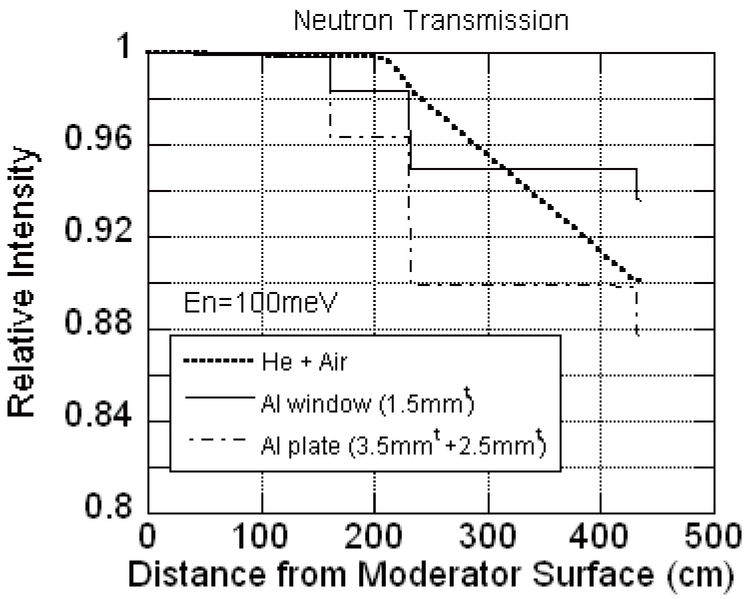

Fig.2.6.10: Attenuation of 100-meV neutron flying from the origin to the downstream end of shutter gate. The notes on the lines are the same as those in Fig. 2.6.8.

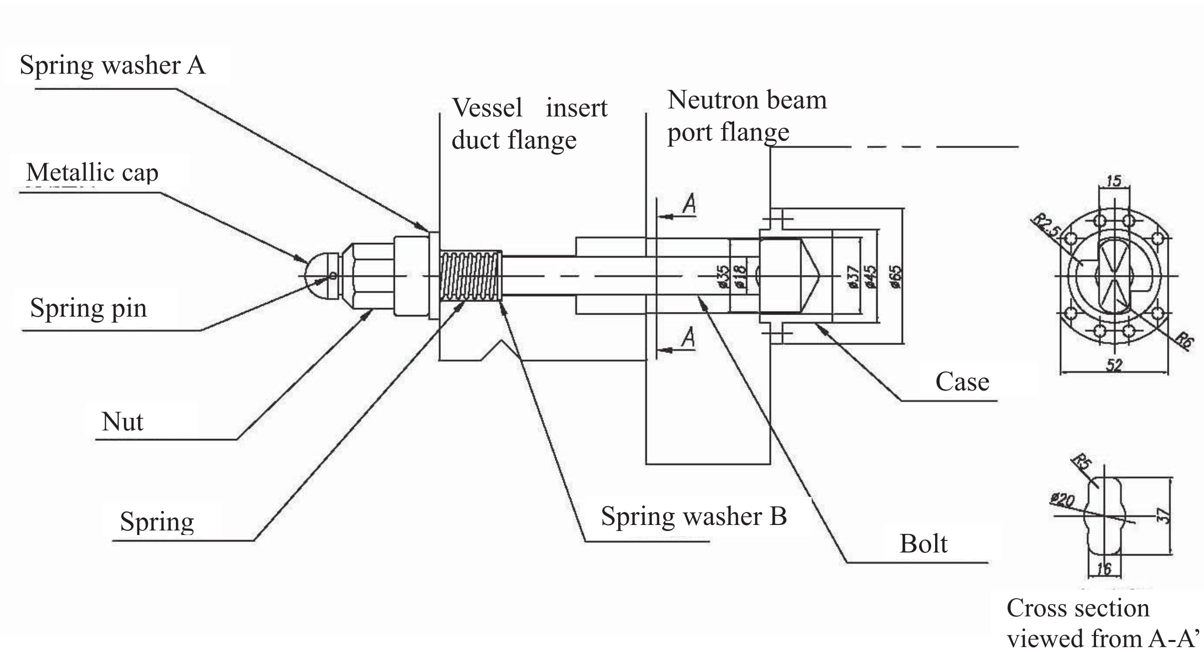

Fig.2.6.1.11: Drawing of vessel insert duct flange fixed on neutron beam port flange with bolts and nuts

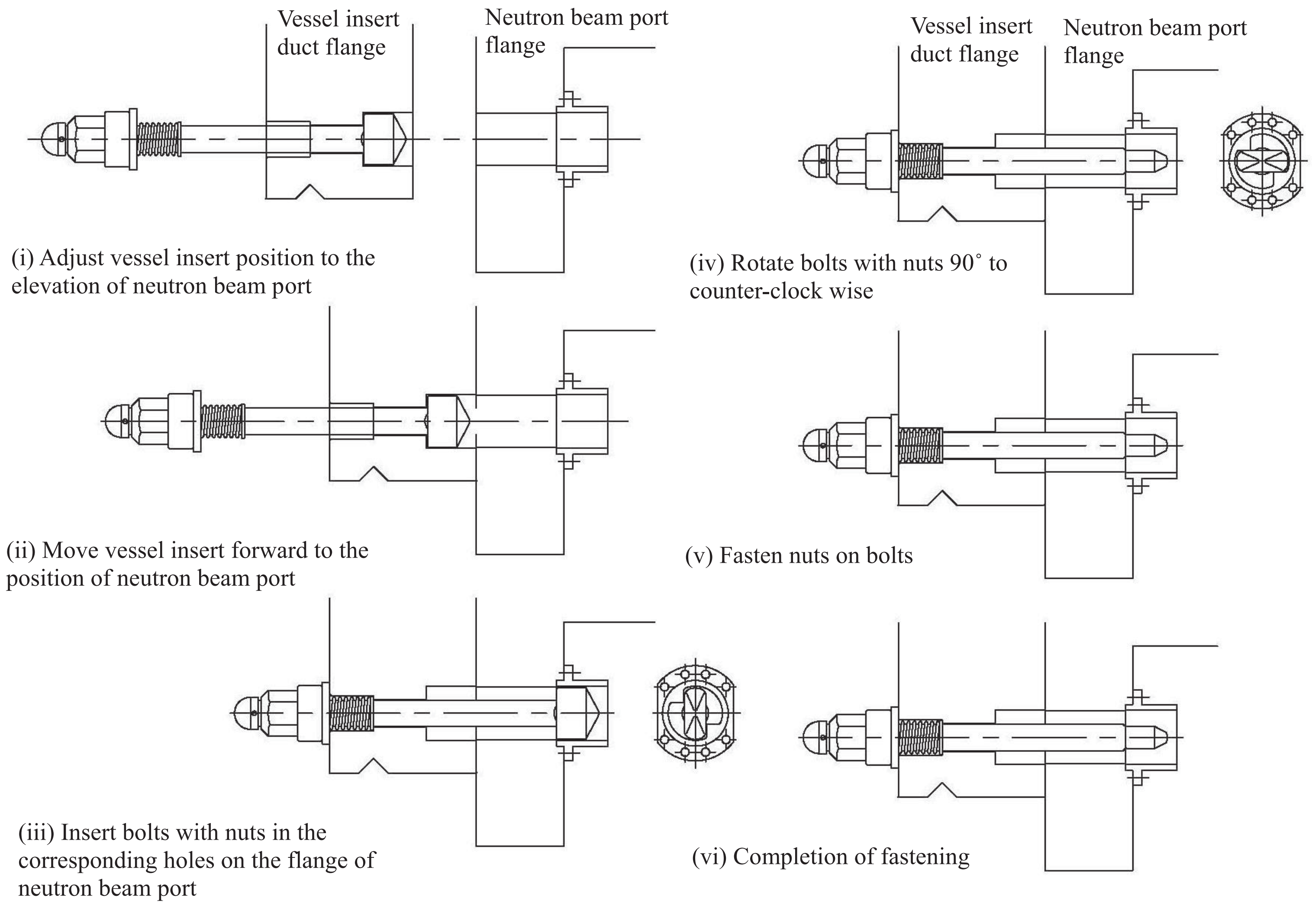

Fig.2.6.12: Attachment sequence of vessel insert duct flange on neutron beam port flange. Handling of vessel insert duct is performed with a remote handling device.

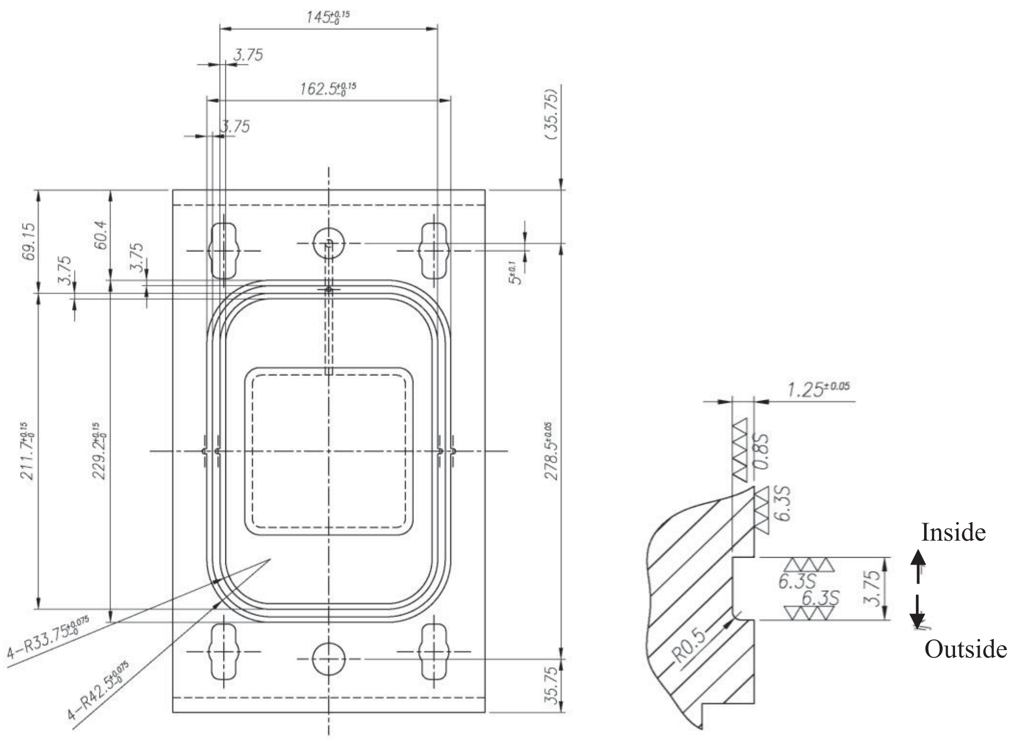

Fig.2.6.13: View of vessel insert duct flange in which dips for O-ring are fabricated. (except for beam line No.16)

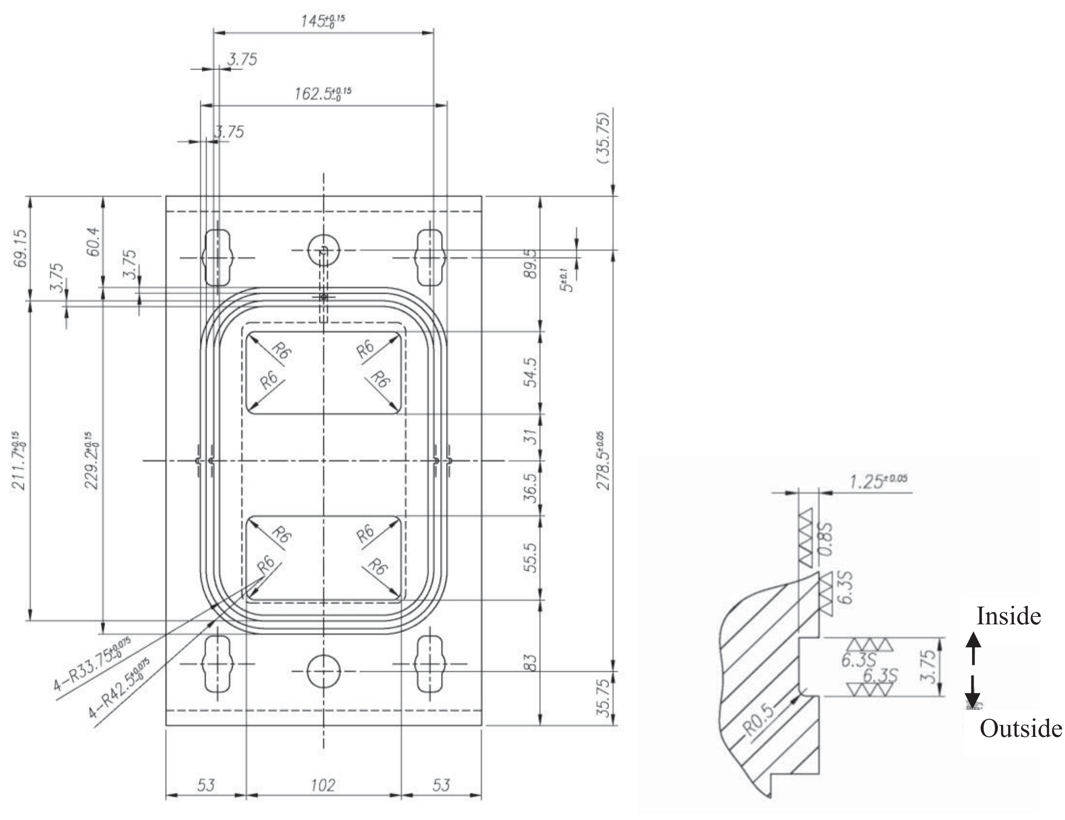

Fig.2.6.14: View of vessel insert duct flange for beam line No.16 in which dips for O-ring are fabricated.

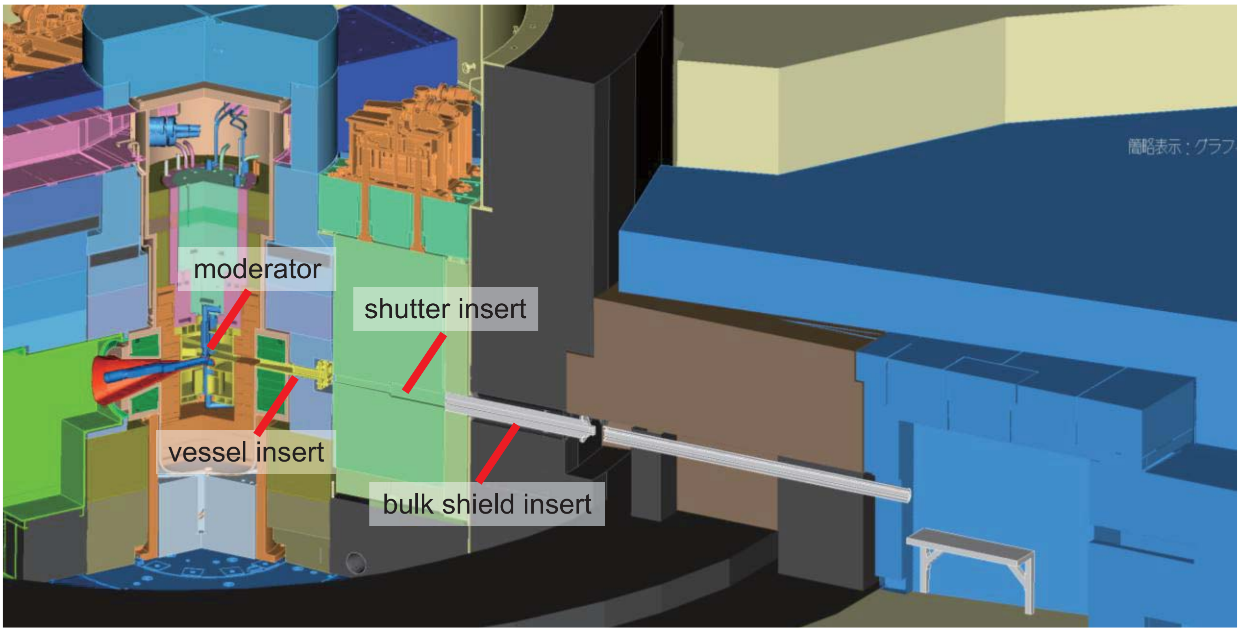

Fig. 2.6.15: 3-D image of neutron beam line components in neutron source station and an instrument in experimental hall

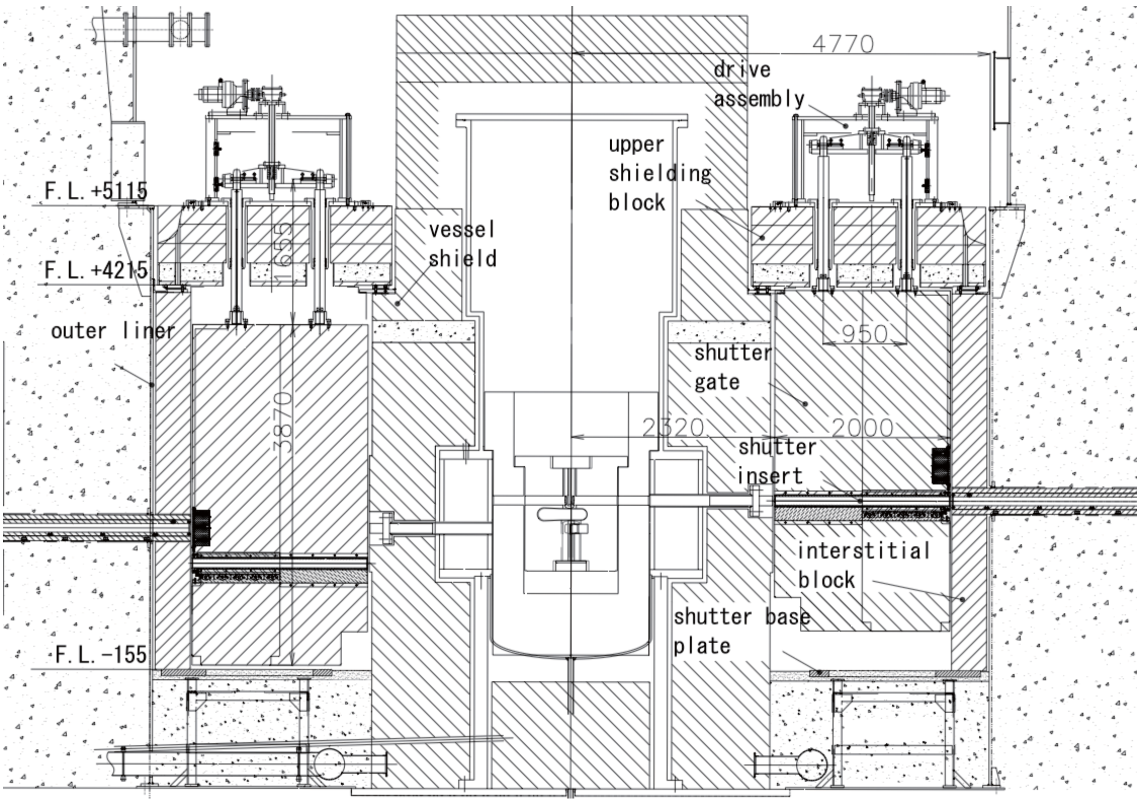

Fig. 2.6.16: Vertical view of the JSNS shutter system in the target station. Diagonal and sand-like hatch represents steel and concrete, respectively. F.L. means floor level of experimental hall of MLF.

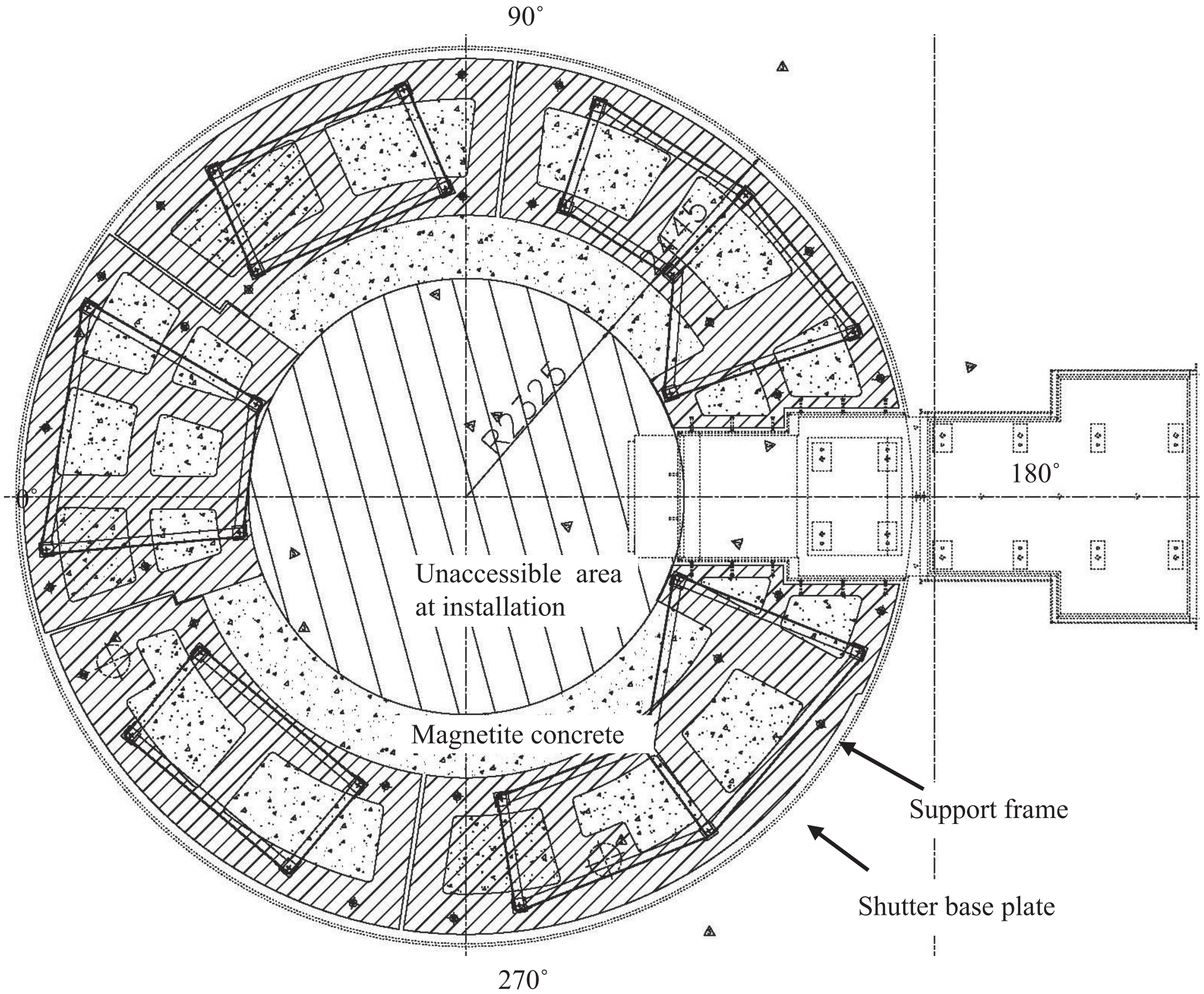

Fig. 2.6.17: Layout of the shutter base plates. The shutter base plate is shown with diagonal hatch. The sand like hatch represents magnetite concrete which is poured after setting the shutter base plate.

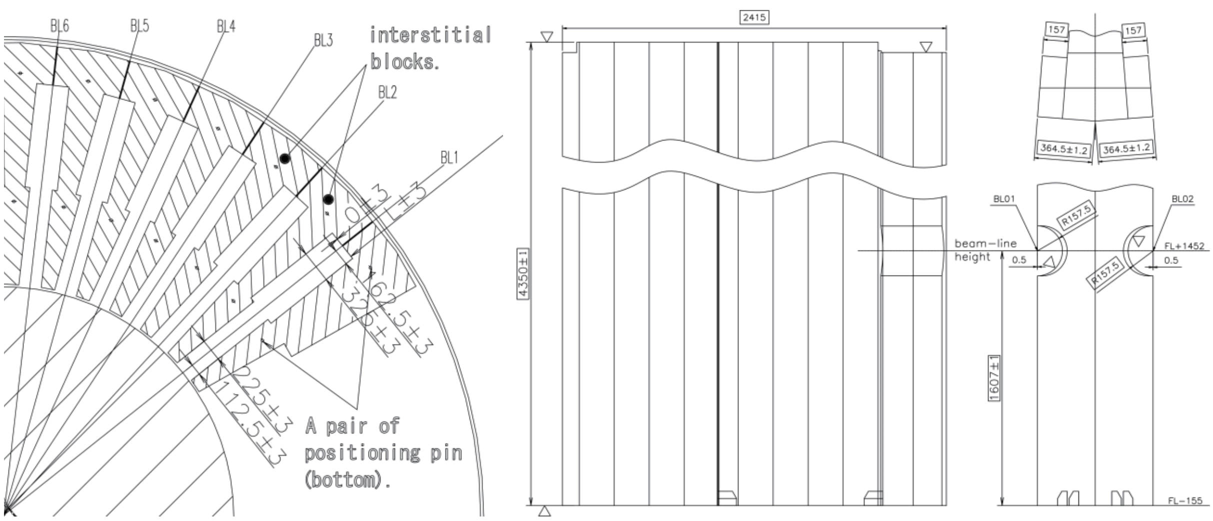

Fig. 2.6.18: A quarter-part of the layout of interstitial blocks (left) and a typical shape of an interstitial block. F. L. means floor level of experimental hall of MLF.

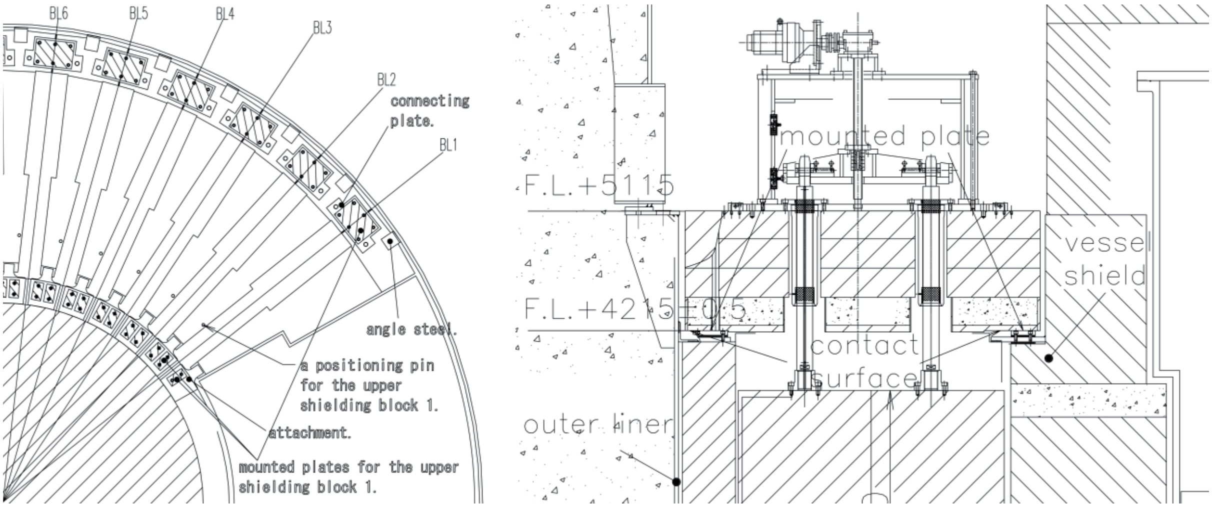

Fig. 2.6.19: A top view of the interstitial blocks (left) and a vertical cut view at around mounted plates. F.L. means floor level of experimental hall of MLF.

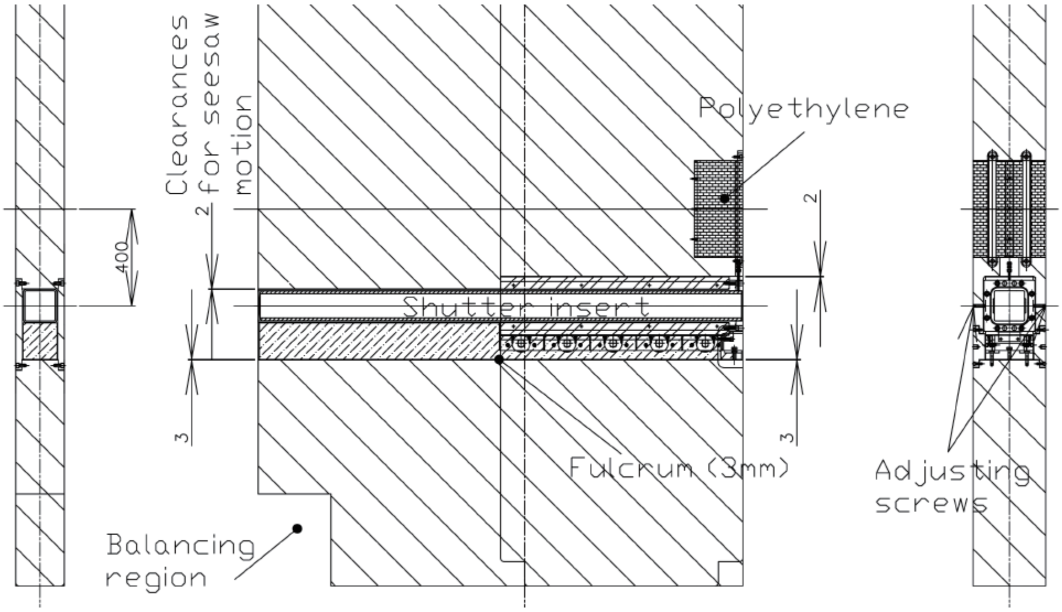

Fig. 2.6.20: An extraction view of a shutter gate and an insert; view from upstream and downstream are shown in the left and right, respectively.

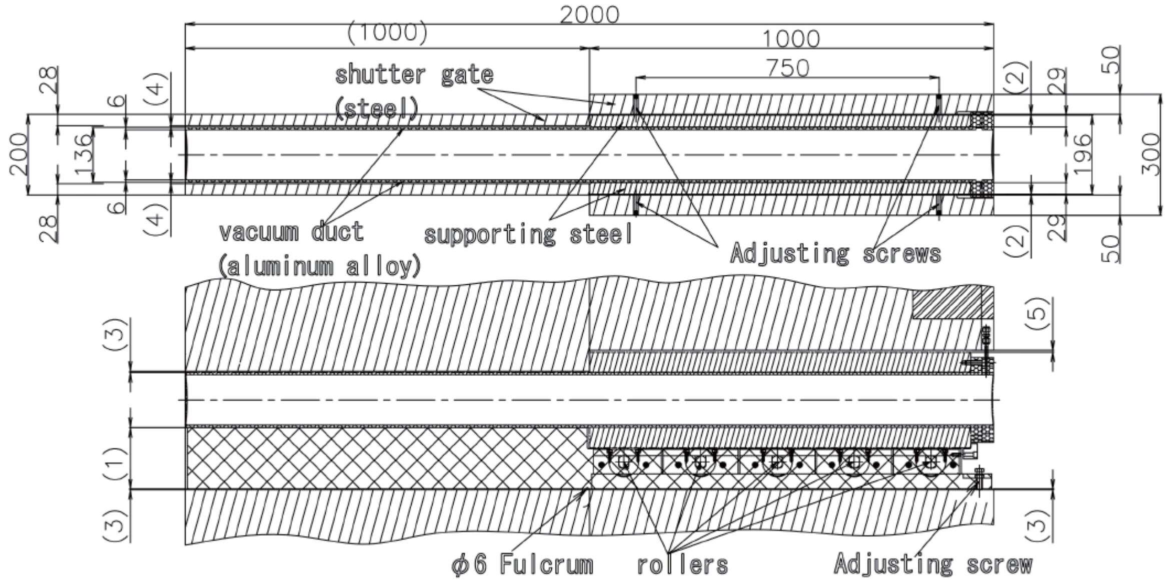

Fig. 2.6.21: An extraction view of a shutter insert and a shutter gate; view from top and side are shown. To align insert horizontally, clearances for the seesaw motion with a fulcrum are adopted. To align insert to the shutter gate, adjusting screws are applied at both sides of the gate at beam line height.

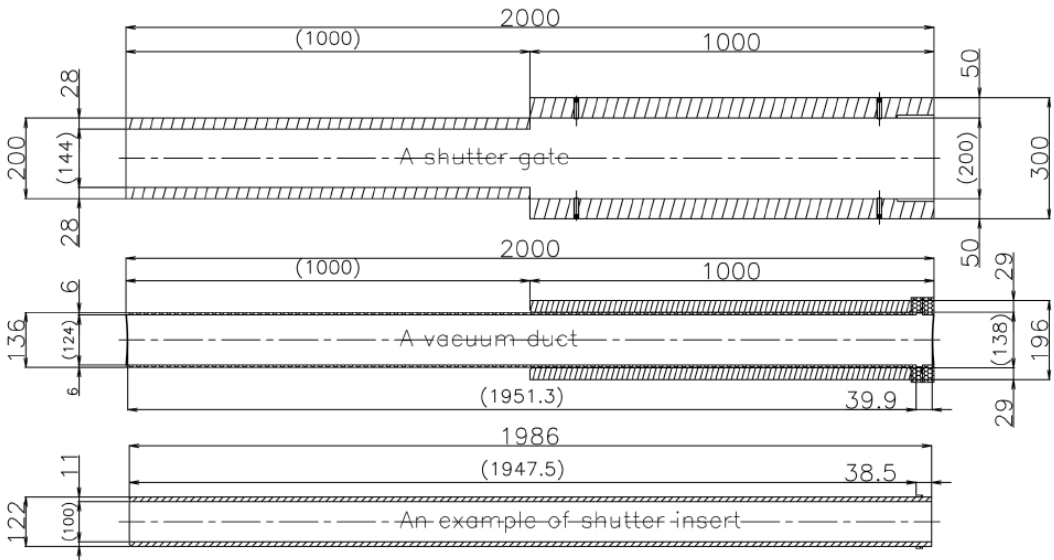

Fig. 2.6.22: Top views of a shutter gate (top), a duct with supporting steel (middle), and an insert (bottom)

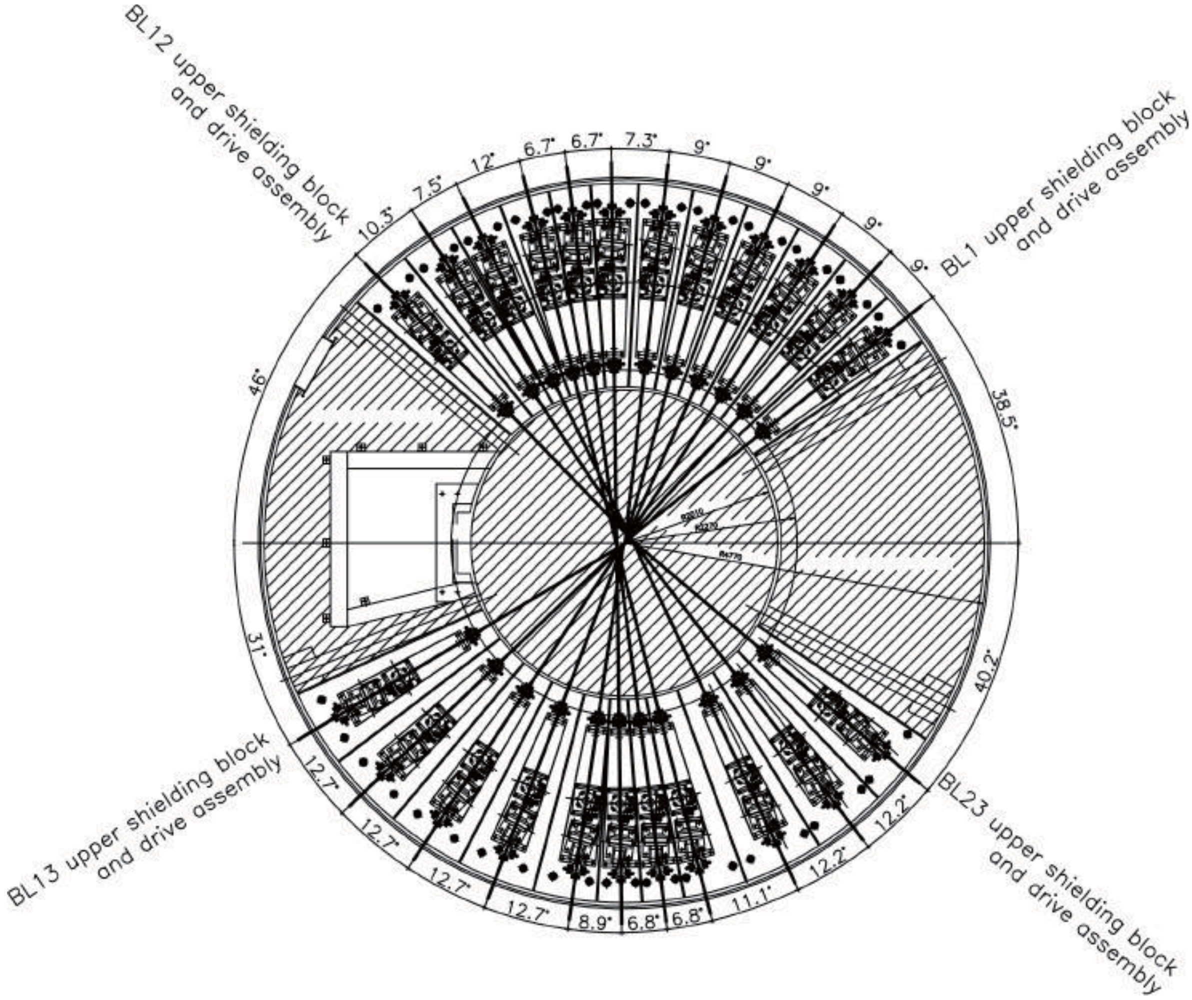

Fig. 2.6.23: Layout of upper shielding blocks with drive assemblies in the target station. Proton beam comes from left-hand side.

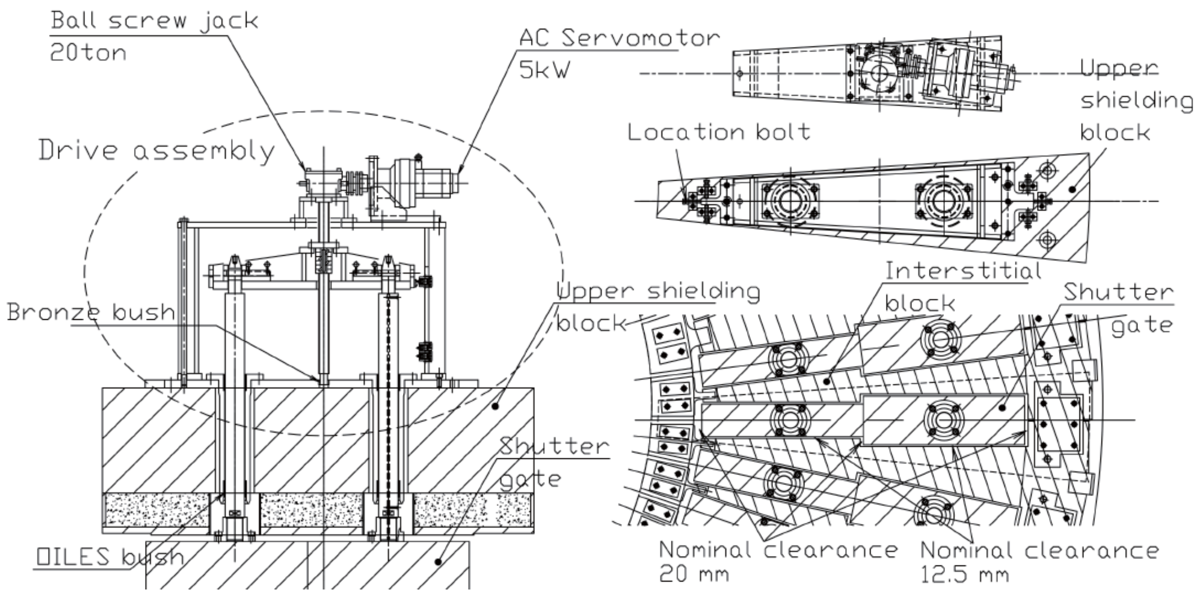

Fig. 2.6.24: Final design of a shutter drive assembly and its environment.

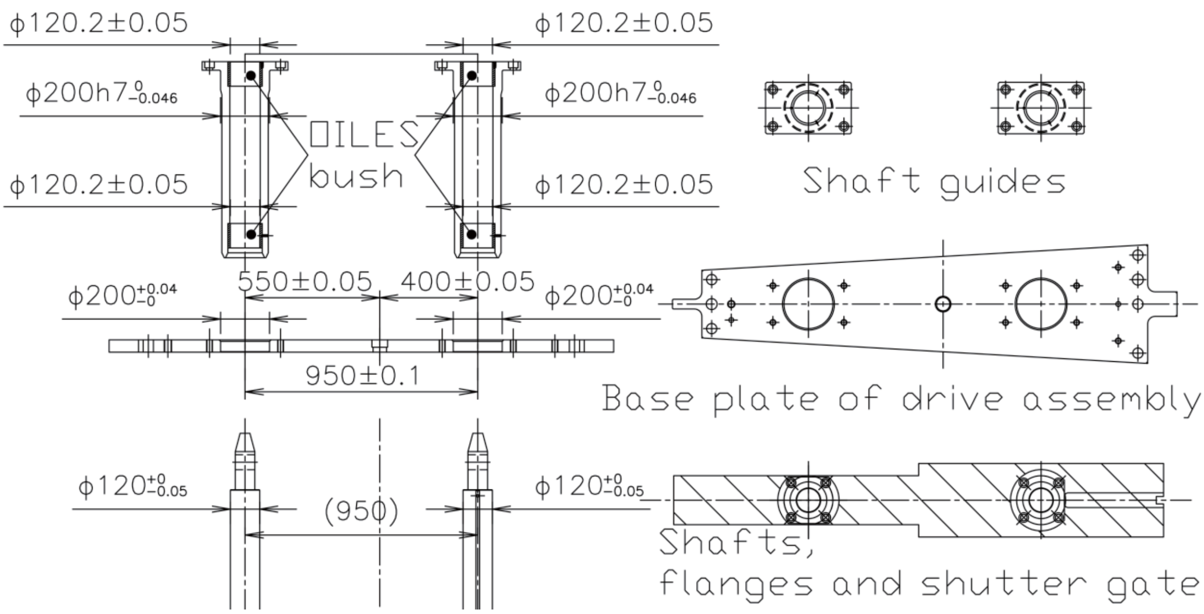

Fig. 2.6.25: Components of a shaft and shaft guide for the "Slide bearing". Their sizes and tolerances are shown in the figure.

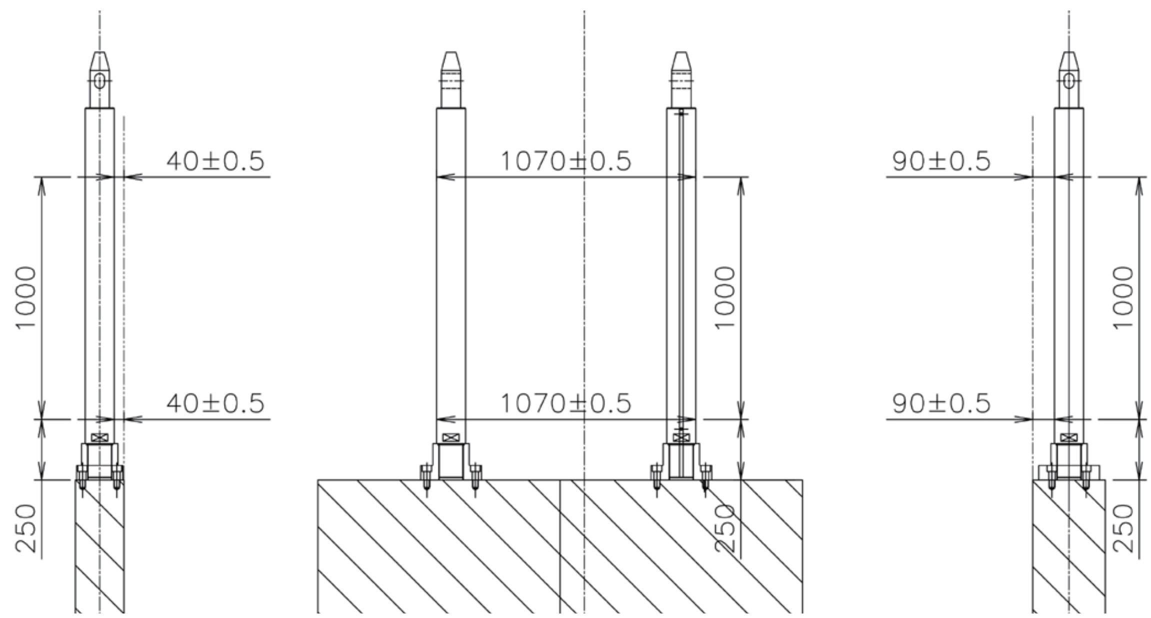

Fig. 2.6.26: Examined parts of the assembled shafts. Measured value; 1070 ± 0.5 mm corresponds to the interval of center of shaft; 950 ± 0.5 mm shown in Fig. 2.6.25 as (950).

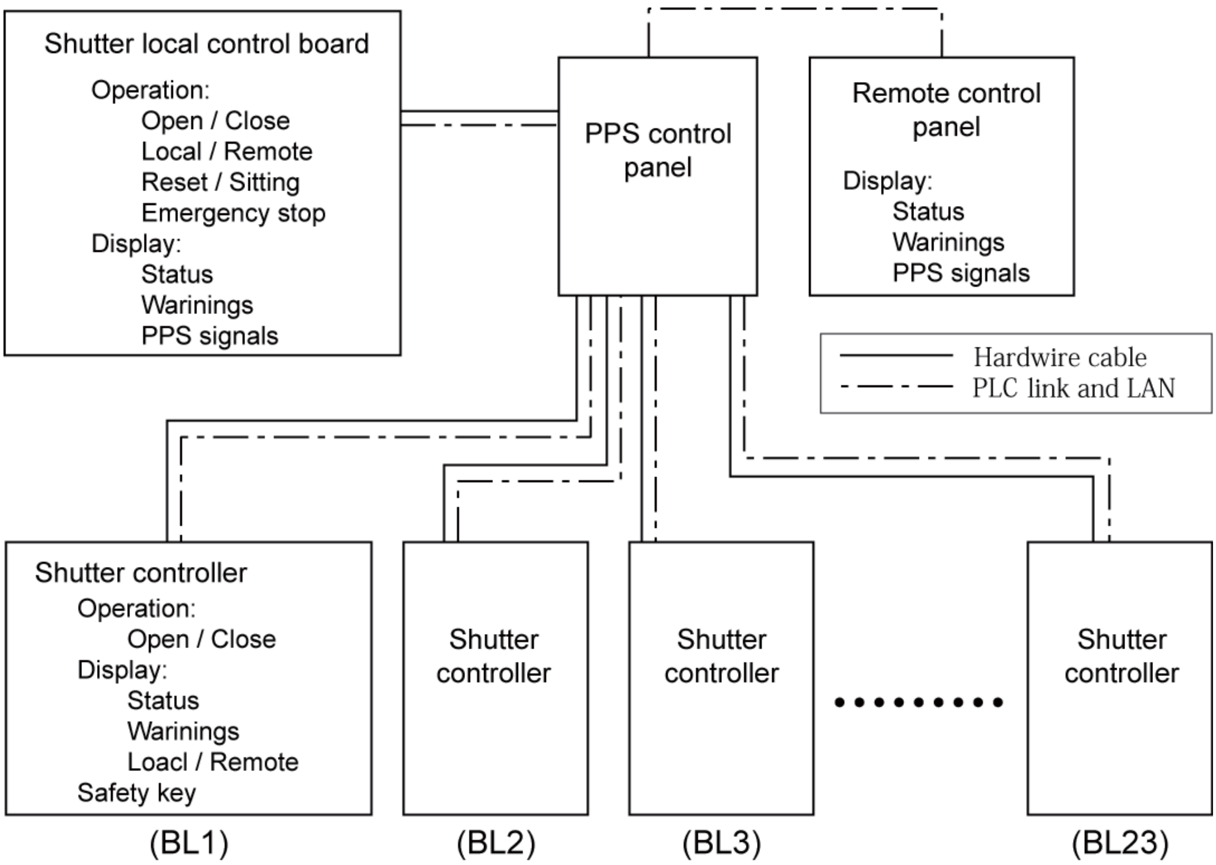

Fig. 2.6.27: Concept of shutter control system

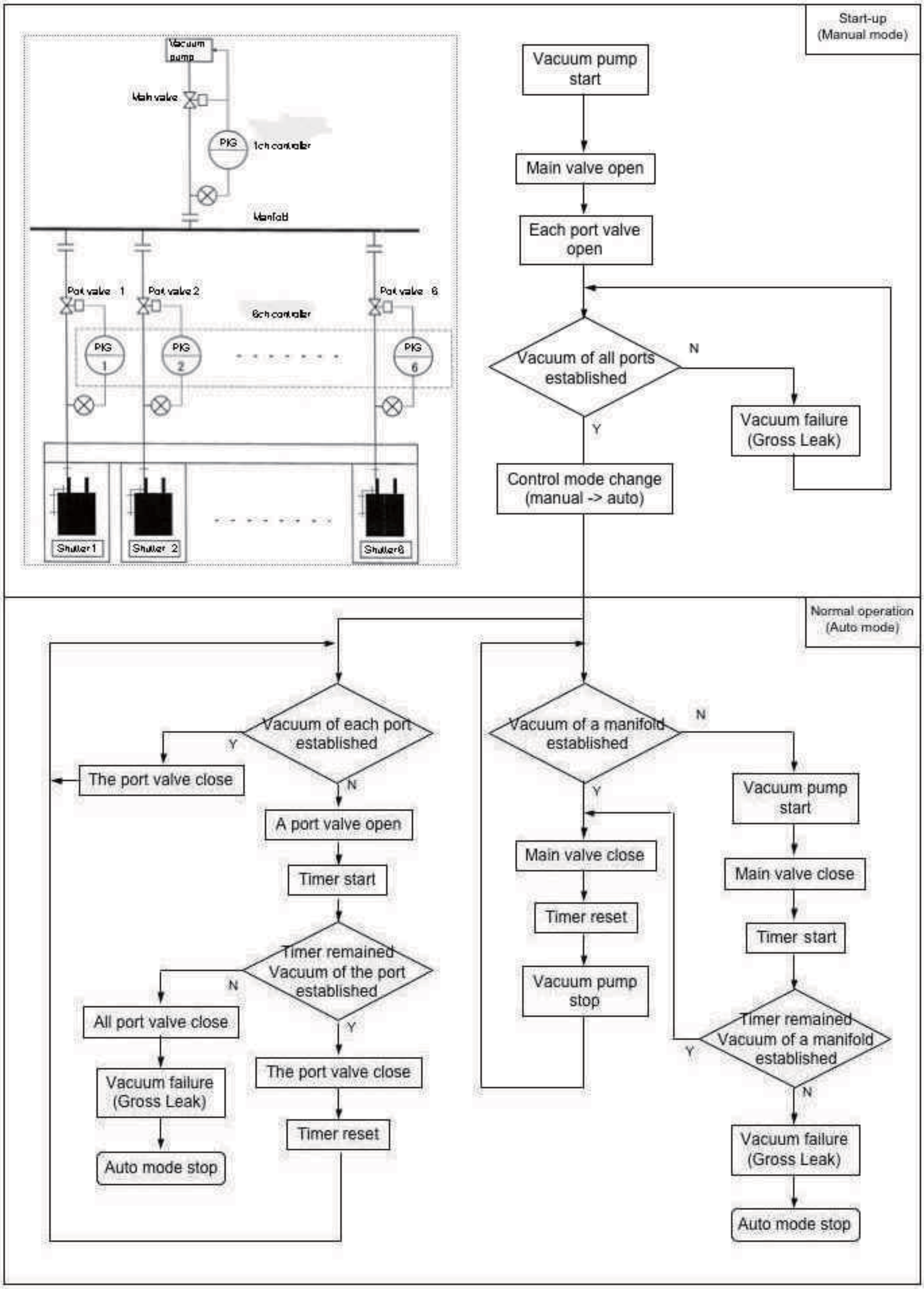

Fig. 2.6.28: Control sequence of vacuum system of the shutter system

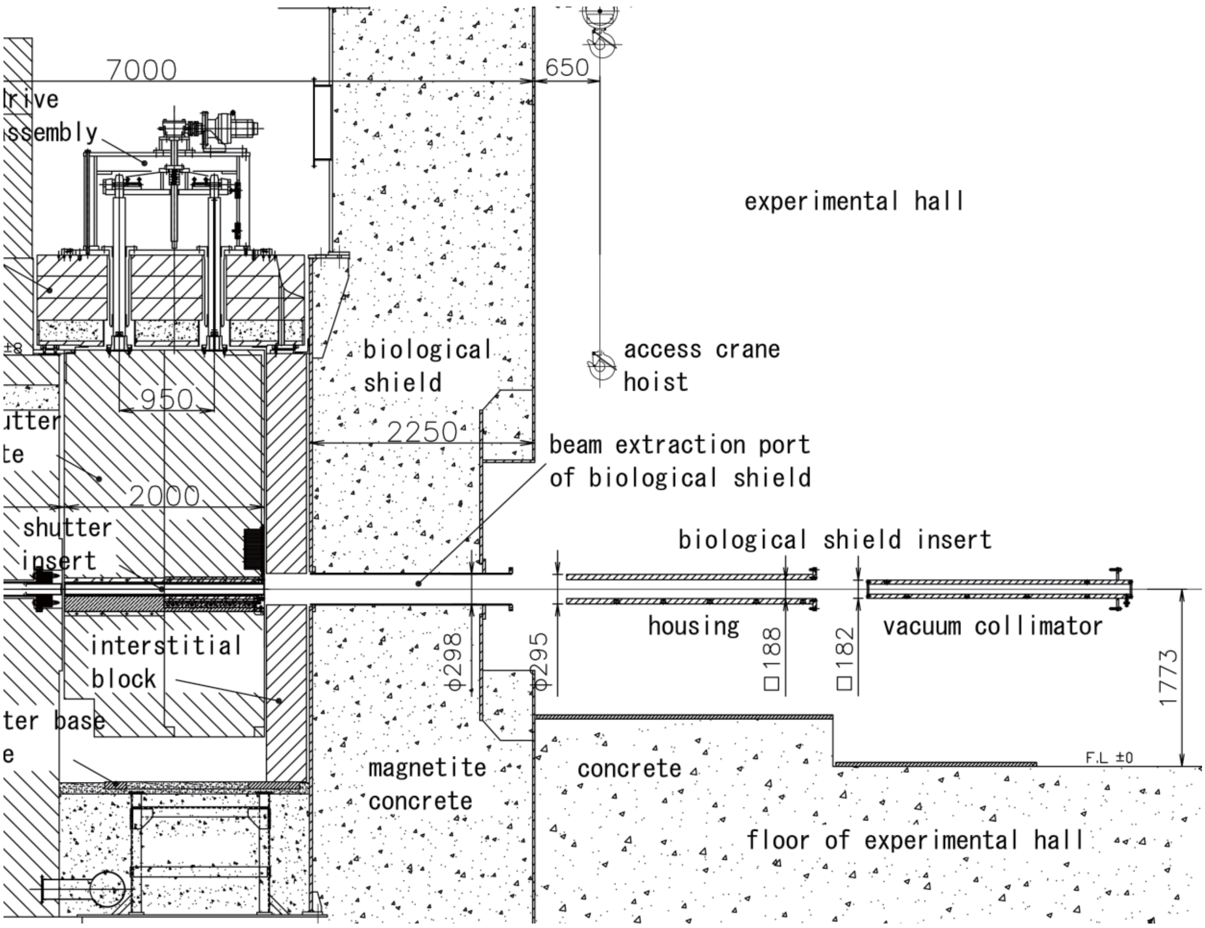

Fig. 2.6.29: Elevation view of the target station and experimental hall. Biological shield insert, composed of a housing and a vacuum collimator, is inserted from the experimental hall to beam extraction port of biological shield.

2.7 Remote Handling Facility

2.7.1 Power Manipulator

(1) Outline

Fig. 2.7.1 gives a schematic drawing of the power manipulator. The power manipulator is an overhead transport type like a ceiling crane. Fig. 2.7.2 gives a plane view of the power manipulator. The power manipulator is installed on a pair of the rails in an upper place of the irradiated components handling room, so called the hot cell. The power manipulator covers almost whole area in the hot cell as shown in Fig. 2.7.3. The overhead transported system consists of a longitude transported trolley on the railway, a traverse transported trolley on the longitude trolley and a vertical elevating device on the traverse trolley. A hand of the power manipulator is mounted under the forefront of the elevating device.

An in-cell crane is installed over the power manipulator system. Most of the components in the hot cell can be treated by the in-cell crane. The in-cell crane is places over the power manipulator system so that they can be used independently for efficient remote-handling work.

Photo. 2.7.1 is an entire view of the power manipulator. It has six-degree-of-freedom and can hold four types of tools (end-effectors) for maintenance work with the exchanging devices. A color CCD type camera and an image tube type camera are set on its wrist and shoulder, respectively.

Photo. 2.7.2 shows the four types of tools set on a tool stand; one hand and three nut runners. Two nut runners are straight for M20 and M12 bolts. The rest has a bent arm for M20 bolts. The tools can be exchanged automatically with a playback function for which motions of the exchanging have been taught to the power manipulator preliminarily.

Maintenance of the power manipulator system is designed to be conducted at the large component handling room (high bay). Accordingly, the power manipulator can be lifted up to the large components handling room (high bay) through a ceiling hatch of the hot cell. The traverse trolley can be separated into two parts, an upper part with the elevation device and a lower part with the transportation device on the longitude trolley. Cables between the upper and lower parts can be disconnected remotely with an up and down motions. Accordingly, the upper part of the traverse trolley with the elevation device and the power manipulator arm can be lifted up for maintenance full-remotely without entering into the hot cell. It is necessary to enter the hot cell to disconnect power cables, control cables, etc. between the longitude trolley with the lower part of the traverse trolley and the cableveyor for longitude transportation.

The operation of the power manipulator is controlled with an exclusive control panel as shown in Photo. 2.7.3. The power manipulator is operated manually for most of the works. But, in the case of the long transportation, operators can use a route analysis system to transport automatically to the objective point. The route analysis system analyzes the transportation route from the current point to the destination point without hitting any obstacles in the hot cell and tell the system the analyzed route. When the power manipulator is operated manually, an interference checking system in an integrated monitoring system also prevents collision with obstacles in the hot cell. The integrated monitoring system checks the motion and the position of the components in the hot cell, the large components handling room (high bay) and the irradiated components storage room. When the power manipulator is moving toward an object and might collide with it, the integrated monitoring system sends a stop signal to the power manipulator to prevent collision. As another component related with the remote handling area, the integrated monitoring system conducts the same work.

(2) General specification

1) Overhead transport system

- Type : low slung overhead type (Longitude, Traverse transport trolley)
- Operation method : manually and automatically
- Position detection : radiation resistance potentiometer (10 MGy)
  (Range : beyond each movement stroke)
- Rail span : 10.5 m
- Bridge composition : saddle and garter unit type
- Trolley composition : a manipulator elevation device and an assistant hoist loading type
- Operating range : X (longitude) ×Y (traverse) × Z (elevation)
  31.76 m × 8.1 m × 4.5 m
- Speed : Regular System X, Y, Z 4.5 m/min (manual)
  X, Y, Z 3.4 m/min (automatic with Route Analyze System)
  Rescue System X 2.6 m/min
  Y 2.2 m/min
  Z 1.3 m/min
- Positioning accuracy : X, Y and Z ±5 mm (overhead transportation part)
- Feed form : longitude and traverse cableveyor
- Main material of trolley: Carbon steel SS-400

2) Power manipulator

- Degree of freedom : 6 axes
- Drive method : Servo-motor drive
- Movement : 1st (shoulder rotation) : ± 180°
  2nd (shoulder bend) : +45° - −180°
  3rd (elbow bend) : +257° - +80°
  4th (elbow rotation) : ± 190°
  5th (wrist bend) : ± 360°
  6th (wrist rotation) : ± 190º
- Special tool : nut runner (screw machine) which has function to fasten and release bolt
- Total arm length : about 1,500 mm
- Acceptable weight : 45 kg (including weight of a tool)
- Position reproducibility : ± 0.5 mm
- Weight : about 600 kg

- Operation method : remote control with cables

3) Hoist
   - Elevation speed : Low 0.5 m/min , High 2 m/min
   - Elevation height : 20 m
   - Rated load : 480 kg

4) End-effectors
   - M12 nut runner, Straight type (Torque : Fasten 120 N・m – 60 N・m, 4steps, Loosen 150 N・m)
   - M20 nut runner, Straight type (Torque : Fasten 250 N・m – 60 N・m, 4steps, Loosen 300 N・m)
   - M20 nut runner, Angle type (Torque : Fasten 250 N・m – 60 N・m, 4steps, Loosen 300 N・m)
   - Hand (Max open width : 100 mm, Grip power : 400 N)

(3) Control interface

Control interface is consists of a control panel and a computer. A photograph of the control interface is given on Photo. 2.7.3. In addition, the route analysis system and the monitoring system are equipped in the power manipulator system.

Cameras and its controller, monitors, video recorder and switching computer are also equipped for assisting visual monitoring in the hot cell.

1) Route analysis system

The system has a 3-D map data of obstacles in the hot cell and recognizes the present position of the power manipulator. When an operator inputs an objective point, the system analyzes a route from the present position to the objective point avoiding the obstacles between them. The 3-D map can be edited to add and modify the obstacles anytime to reflect up-to-date conditions in the hot cell.

(a) Optimal route analysis software
   - Main functions : Optimal route analysis
     Map edition
     Manipulator position monitor
     Sensor monitor
     Process management
     Network communication control
     Obstacle information management
     Man-machine interface
   - Search method : Temperature distribution analogy, divergence search
   - Applicable movement area : Whole hot cell (max. coverage: 200 m×200 m)
   - Route analysis time : Less than 60 sec

(b) Computer for the route analysis system
   - Type : PC/AT interchangeable personal computer
   - OS : Windows XP
   - Communication method : Ethernet

2) Monitoring system

The monitoring system collects positions and status information of moving devices installed in the hot cell, and shows a 3-D graphic image on monitor. The system detects a collision potential between each component in the hot cell. When a component is approaching to another component too closly, the system outputs an emergency signal to stop the motion through the ethernet and sequencer link. The system has a simulation function to confirm motion of the power manipulator.

a) Monitoring system software

- Main functions : Data collection
  Collision prevention analysis
  Manipulator simulation
  Network communication control
  Man-machine interface

b) Computer for route analysis system

- Type : PC/AT compatible personal computer
- OS : Windows XP
- Communication method : Ethernet

3) ITV system

Several cameras for the ITV system are set on walls of the hot cell, on the in-cell crane garter, on the manipulator transporter, at the shoulder and wrist for monitoring the remote works in the hot cell. Views observed by the cameras can be record on a video recorder. The cameras are controlled by computer interface for on zoom, pan and tilt motions.

a) Computer for the camera, changeover vessel control

- Type : PC/AT compatible personal computer
- OS : Windows XP
- Image management board : Connection image machine NTSC form
- Interface : PCI bus or a compact PCI bus

b) Remote controlled radiation resistance cameras, a digital video recorder and monitors

- Camera type : Image tube camera
- Signal type : NTSC
- Horizontal resolution : over 470 lines
- Record form : Digital form
- Equipped functions : Pan head
  - Operation : Remote controlled
  - Tilt range : −65° - +90°
  - Pan range : 340°

  Lens function
  - Operation : Remote controlled
  - Zoom rate : 10 times
  - Focus : Manual

Iris : Auto, Manual

2.7.2 Master-Slave Manipulator

Master-Slave Manipulator (MSM) shown in Fig. 2.7.4 is used for various remote handling works in the irradiated components handling room and the irradiated components storage room. Figs. 2.7.5 and 2.7.6 shows layout of the MSM in the two rooms. The MSM is directly operated by an operator through a lead-grass window. The MSM is cooperated with the in-cell crane and the power manipulator if necessary.

Typical works of the MSM is as follows;

- Connecting/disconnecting pipings of cooling water and helium gas, and cables for sensors for the target vessel by using the exclusive tools
- Setting up hanging jigs for the in-cell crane hook
- Adjustment of rotation for components hanged by the in-cell crane

Specification of the MSM

Type :	MT 200, La Calhène, France
	Master-Slave Manipulator with electric drive system,
	Full balance, Disconnectable for 3 parts
Motion :	Handing by oeprator and electric drive
Electrically driven motion :	X, Y and Z motion
Motion lock :	X, Y and Z lock independently
	Arm turn, wrist twist and tilt, lockable hand
Material of main parts :	aluminum alloy
Capacity for handling :	about 20 kg
Master handle :	hand grip
Radiation shielding :	1,500 mm of ordinary concrete
Tong :	Remote exchange type
Max. load of the loading hook :	about 80 kg
Operational range :	see Fig. 2.7.4
Right-left motion (X) :	Manual+Electric : ± 60°
	Electric : ± 30°
Forward-backward motion (Y) :	Manual : +19°, –22°
	Electric + Manual : +90° - –22°
Up-down motion (Z) :	Master-arm length : 1,390 mm
	Slave-arm length : 1,390 mm
	Manual: 970 mm
	Electric : 910 mm
Arm turn :	±170°
Tilting of wrist :	+38° and –114°

Twist of wrist : 360°

Tong open width : max. 90 mm

Maintenance : Pulling the whole manipulator back to manipulation room or separating one to three parts

Quantity (one set with two manipulators for a schieldeng window)

Irradiated component handling room (the first floor) : 9 sets

Irradated components storage room (the basement floor) : 2 sets

2.7.3 Target Exchange Truck

(1) Outline

A target exchange truck is used to replace the mercury target vessel in the hot cell. Figs. 2.7.7 and 2.7.8 give a schematic drawing and a 3-D image view of the target exchange truck, respectively. Photos. 2.7.4 and 2.7.5 show front and side views of the target exchange truck. The target exchange truck consists of a main body with a driving system, a control box including sequencer and a LAN unit, a support rack with adjusters, a temporary rack, a battery unit and a hanger.

The target exchange truck can mount the target storage container with the target vessel on the support rack as shown in Fig. 2.7.7. A trunnion structure was adopted to the support rack to incline the storage container. The target storage container can be inclined and laid on the support rack by using the in-cell crane solely as shown in Photo. 2.7.6, which explains the handling sequence. A bottom rod of the storage container is inserted in the trunnion while the flange is mounted on the horizontal adjuster.

The target exchange truck with the storage container supports the target vessel during mounting and dismounting the target vessel to the target trolley by fastening and loosening, respectively, bolts by the power manipulator because the target vessel is fixed to the target trolley like a cantilever. Positions of the target vessel can be adjusted by the target exchange truck with respect to the target trolley. The target exchange truck moves on rails which are different from the rails for the target trolley, and all the rails are laid in parallel. The position of the support rack can be adjusted vertically and horizontally to align the position of the target vessel precisely. A temporary rack for the storage container is also furnished in the truck. The lid of the storage container in which a used target vessel is stored can be sealed with fastening bolts by the power manipulator to confine mercury vapor inside.

The target exchange truck is usually stored in a waiting area in the hot cell. When a target vessel is going to be exchanged, the target trolley is first taken back to the maintenance position. Then the target exchange truck is transported in front of the target vessel by using the in-cell crane. Photo. 2.7.7 shows the target exchange truck being hanged up by the in-cell crane.

(2) Specifications

Specifications of the target exchange truck are shown below.

・ Type : Self-driving trolley on rails

・ Material : Stainless steel, Carbon steel (with epoxy resin base paint)

- Weight : about 9.0 tons
- Driving system : Servo motor driving, radio control with wireless LAN
- Electric supply : Battery (300 Ah)
- Continuous driving time : About 80 hours
- Load weight : About 4.0 tons
- Velocity : 0.3 m/min - 0.9 m/min
- Driving reproducibility of the truck : within 2.0 mm
- Vertical stroke of support rack : 100 mm
- Horizontal stroke of support rack : 30 mm
- Support rack reproducibility : within 1.0 mm (vertical and horizontal)

(3) Control

The target exchange truck is controlled by using a touch panel and buttons on a control panel in the 1st manipulator handling room on the first floor around the hot cell. It is operated with direct watching through shielding windows and also with video monitor of the ITV cameras. A photograph of the control panel is shown in Photo. 2.7.8.

Wireless LAN is used to control the target exchange truck. A battery is equipped on the target exchange truck. Accordingly, the truck can be operated without any cabling. The battery is charged up from the control panel in the waiting area. Electrodes can be connected remotely by moving the target exchange truck on the rails.

There are three control modes for the truck; operation, battery charge and stop. The control modes can be selected by switching a mode selector by the master-slave manipulator. In the operation mode, the target exchange truck can be moved. In the battery charge mode, the battery unit is charged up from the control panel. In the stop mode, the power supply from the battery unit is inhibited.

2.7.4 Reflector-moderator Remote Handling System

2.7.4.1 Overview of moderator-reflector maintenance

The core part of the spallation neutron source consists of the target vessel, the moderators and the reflector as shown in Fig. 2.7.9. These components will be activated and damaged in the course of beam operations. Their lifetimes were estimated[2.7-1)]; 6 months for the target and 6 years for the moderators and the reflector. They are periodically replaced and finally taken out from the MLF to a storage facility. This subsection mainly focuses on the maintenance of the moderator-reflector assembly.

The moderator-reflector assembly consists of the three kinds of moderators[2.7-2)] (coupled, decoupled and poisoned moderators), the reflector, the outer plug and the inner plug as shown in Fig. 2.7.10. The moderators have a multi-layered vacuum insulated pipes of a curved shape (outer diameter of ~90 mm and length of ~4 m), made with aluminum alloy and stainless steel. The reflector consists of beryllium in the inner part and iron in the outer part, which are enclosed in an aluminum container (1 m in diameter and 1.2 m in height). The weight of the moderators and the reflector are ~ 0.3 ton and 5 ton, respectively.

The assembly is composed of two parts; the inner and the outer assemblies as shown in Fig. 2.7.10. The outer assembly consists of the coupled moderator, the reflector and the outer plug (~15 ton), which are connected with bolts and positioning pins. The inner assembly consists of the poisoned and decoupled moderators and the inner plug (~15 ton), which are connected with bolts and positioning pins. The inner assembly can be inserted into the outer assembly from the top using positioning pins as shown in Fig. 2.7.10. The total weight of these assemblies is ~36 ton.

2.7.4.2 Maintenance concept and consideration of safety handling

The concept of the maintenance is summarized in terms of the nine keywords.

(1) Confinement

Radioactive materials have to be confined and prevented from spreading out.

(2) Radiation shielding

The upper limit of the radiation dose is 12.5 μSv/h in the areas that radiation workers can access all the time. However, higher radiation dose is expected on the top of the helium vessel and the surface of a transfer cask; the radiation doses of 0.1 and 1 mSv/h are expected, respectively. The hands-on maintenance works may sometime be required in such areas. The personnel are protected by controlling the time of the radiation work so that the dose rate should not exceed the allowable limit.

(3) Vertical access to the moderator-reflector maintenance

The lifetimes of the moderators and the reflector (~6 years) are very different from that of the target vessel (~6 months). The moderators and the reflector are therefore replaced form the top of the helium vessel vertically and only the target vessel is extracted horizontally to the hot cell next to the target station.

(4) Independent replacement

The moderator-reflector assembly is separated into the inner and the outer assemblies as mentioned in the subsection 2.7.4.1. The inner assembly can be selectively pulled out, leaving the outer one and can be transferred to the hot cell by using a transfer cask. This feature leads to the reduction of unnecessary waste and the reduction of maintenance period.

(5) Full remote control maintenance

The moderators and the reflector are maintained with full remote control in the hot cell.

(6) Partial hands-on maintenance

When the cooling water pipes and the hydrogen transfer couplers are disconnected and connected again on the top of the helium vessel, those works are done by hands. On the works for the pipes, the radiation dose mainly comes from the internal exposure of tritium (^{3}H) in the cooling water, the external exposure from ^{7}Be produced by the spallation reaction of oxygen in the cooling water and the activated materials by the beam operation. The special measures for preventing the internal exposure are as follows;

a) draining the cooling water by blowing helium gas before disconnecting pipes,
b) releasing the pressure inside the cooling water pipes to prevent water splash and

c) local ventilation and using a glove bag to disconnect the cooling water pipes.

The pipes should be disconnected and connected as quickly as possible to reduce external exposure. The layout for easy access to the pipes and the simple structure of their connectors are essentially necessary. The accumulation of ^{7}Be in the beam operations of many years will make the hands-on maintenance difficult. The mechanism to do these works full-remotely will be required in due time.

(7) Transportation with transfer cask

A transfer cask is used to move the used moderator-reflector assembly and has enough radiation shield to reduce radiation dose less than 1 mSv/h on the outer surface. The used moderator-reflector assembly is pulled into the cask and transferred from the top of the helium vessel to the hot cell by using the 130-ton ceiling-traveling crane in the large components handling room (high bay). The main contribution to the radiation dose from the used moderator-reflector assembly is silver-indium-cadmium (Ag-In-Cd) alloy that is used as a thermal neutron absorber in the decupled moderator, the poisoned moderator and the reflector. At least 30 cm thick iron is required as a shield to reduce the radiation dose rate less than 1 mSv/h. The gamma rays from ^{110m}Ag mainly contributes to the dose rate, which does not diminish for 2-3 weeks because ^{110m}Ag has relatively long half-life ($T_{1/2}$ = 250 days).

(8) Replacement work in hot cell

Replacement work is performed with full remote control in the hot cell. Full-remote control devices[2.7-3, 4)] are available in the hot cell for the moderator-reflector assembly and other components, the target vessel, the proton beam window and the muon target.

(9) Cutting device

A cutting device is installed to reduce the volume of the replaced components. The cooling water pipes will be cut by using the cutting device. The drying component room is provided under the hot cell, where the water remaining inside components is dried up before cutting them. This process will prevent unnecessary contamination by tritium water.

The irradiated-components handling room (hot cell) was built next to the target station for the maintenance of highly activated components as shown in Fig. 2.7.11. The large components handling room (high bay) is located above the hot cell and the components can be sent through the hatches and the floor valves with the 65-ton ceiling-traveling crane or the 130-ton ceiling-traveling crane in the large components handling room (high bay). The used moderator-reflector assembly is transferred to the hot cell with a transfer cask. The irradiated-components storage room and the drying component room are also built below the hot cell to storage them temporarily and to dry up remaining water contaminated with tritium. These rooms are connected to the hot cell through the bottom hatches as shown in Fig. 2.7.12. The used moderator-reflector assembly is replaced in the hot cell. Four dedicated remote handling devices, namely inner and outer plug support stands, a moderator exchange device, a cutting device, are installed in the hot cell. Additional maintenance devices are prepared; a 20-ton in-cell crane, a power manipulator and 11 pairs of master-slave manipulators in the hot cell and 15-ton in-cell crane in the irradiated components storage room. The outer and inner plug support stands are installed at the corner of the hot cell near lead glass windows at different heights to improve visibility as shown in Photo. 2.7.9. The moderator exchange device is equipped between the outer and the inner plug support stands to approach them easily as shown also in Photo. 2.7.9. Five ITV remote cameras are installed in the hot cell as shown in Photo. 2.7.10. Each position was optimized for the works that will be done. Especially, two cameras are made movable with a linear motion guide to get better visibility. The design concept of the remote handling devices and their detailed maintenance scenario are described in the following subsections.

2.7.4.3 Moderator-reflector maintenance scenario

The maintenance scenario is shown in Fig. 2.7.13. It was examined and modified more efficiently to make an off-beam maintenance period as short as possible. The maintenance works are divided into two categories, replacement and disposal. In the replacement work, a new moderator-reflector assembly is prepared in advance on the outer plug support stand in the hot cell. After the pipes are removed on the top of the helium vessel, the used moderator-reflector assembly is transferred to the drying component room and the new assembly is transferred from the hot cell to the helium vessel for installation. This work is done during an off-beam period.

The disposal of the used components can be done even in an on-beam period. After the remaining cooling water inside of the used components is dried up in the drying component room, the used components are sent to the outer or the inner plug support stand. The moderators and the reflector are removed and cut into pieces with the cutting device to reduce their volumes. The cut pieces are stored in an airtight container. The container is enclosed in the cask with radiation shielding. It is stored in the irradiated components storage room and eventually transferred out of the MLF.

The remote handling devices are designed based on this maintenance scenario for the moderator-reflector assembly.

2.7.4.4 Remote handling devices for the moderator-reflector assembly

The remote handling devices were designed under the following constraints.

a) Multiple protections: double wire system for the lifting tools, manual operation for the failure of the remote handling devices and maintaining the condition at power supply loss.
b) Earthquake resistance: up to an acceleration of 0.25G
c) Radiation resistance: 1 MGy for the devices. This criterion comes from the radiation dose where no maintenance is necessary within the expected operation lifetime of the MLF. EPDM rubber is adopted for airtight seals because it has a radiation resistance of several MGy.
d) Negative pressure in hot cell: a pressure of −230 Pa to prevent the activated gases and materials such as mercury vapor and tritium water vapor from spreading out

The remote handling devices for the maintenance of activated components are described below. The transfer cask and the floor valve are provided outside the cell device and the four devices, the inner and outer plug support stands, the moderator exchange device and the cutting device in the hot cell. Used components are replaced with the full cooperation of both devices and the other remote handing devices in the hot cell, the power manipulator, the master-slave manipulators and the in-cell crane, are also made fully operational for this purpose.

(1) Transfer cask

The transfer cask has a gripper to lift an object inside and a shield door at the bottom part as shown in Photo. 2.7.11. The gripper with the rotation mechanism can lift up the inner or the outer assembly. The 130-ton ceiling-traveling crane can move the transfer cask that lifts the used moderator-reflector assembly inside. The shield of the transfer cask is designed so that surface dose rate of the transfer cask is less than 1 mSv/h when it has the used assembly inside. The thickness of the iron shielding is calculated to be about 30 cm at maximum. The total weight of the transfer cask with the used assembly inside is about 125 ton at maximum. The transfer cask is not made airtight. The transfer cask is set by hand with the 130-ton ceiling-traveling crane. Photo. 2.7.12 shows the transfer cask set on the helium vessel. The shield blocks are removed before setting the transfer cask. The transfer cask is fixed onto the floor valve with bolts and positioning pins. The dose rate on the helium vessel is expected to be ~100 μSv/h without the contribution of ^{7}Be. In order to convey the transfer cask with the 130-ton ceiling-traveling crane, the connection attachment is provided to hang the transfer cask with the crane hook as shown in Photo. 2.7.12. This connection attachment is also set by hand. The shield blocks are arranged so that the blocks of required area are to be removed for the operation. Only several shield blocks in the central region are necessary to be removed for the maintenance of the moderator-reflector assembly or the proton beam window. The maintenance period can be reduced with this wise design of the shield blocks.

(2) Floor valve

Photo. 2.7.13 shows the floor valve, which has the functions to connect transfer cask, seal the air of the room below and shield the gamma ray from there. At the maintenance, the valve is set on the helium vessel by hand before setting the transfer cask. Five floor valves are equipped on the ceiling of the hot cell as shown also in Photo. 2.7.13.

(3) Outer plug support stand

The outer plug support stand is used to replace the coupled moderator and the reflector. This device has the function to rotate and support the outer assembly. Photo. 2.7.14 shows the configuration of remote handling device for the maintenance of the moderator-reflector. The used outer assembly with the inner assembly is lifted down through the hatch on to the outer plug support stand and attached to the outer plug support stand. When the coupled moderator is replaced, the new coupled moderator with an attachment is put on the moderator exchange device with the in-cell crane as shown in Photo. 2.7.15. The moderator exchange device is moved closer to the outer plug support stand. The coupled moderator is fixed to the outer assembly with the power manipulator. In the commissioning process, all the positions of the bolts that would be accessed with the power manipulator were determined by teaching process of power manipulator as shown in Photo. 2.7.16.

(4) Inner plug support stand

The inner support stand is used to replace the decoupled moderator and the poisoned moderator, which are fixed to the inner assembly. This device can support the inner assembly with these moderators and rotate it as shown in Photo. 2.7.14. The moderator exchange device can remove either of the moderators independently from the inner assembly. The muon target assembly and the proton beam window can be also manipulated with the inner plug support by installing a dedicated attachment on the inner plug support stand as shown in Photo. 2.7.17.

(5) Moderator exchange device

This device is used to replace the moderators, the proton beam window and the muon target assembly with a dedicated attachment. This device is moved along 4 axes; travelling, traversing, lifting and rotating as shown in Photo. 2.7.14. However it does not have a fixing bolt tool such as a nut-runner. This device is moved on the linear motion (LM) guide between the inner and the outer plug support stands.

(6) Cutting device

A hydraulically-operated shear-cutting device shown in Photo. 2.7.14 is adopted as a cutting device to reduce the volume of used moderators, reflectors, proton beam windows and muon target assemblies. The main feature of this cutting method is to produce no chips, whereas other cutting methods such as a rotating saw scatter chips. Used components are cut on a storage container and their debris is dropped into the container.

2.7.4.5 Estimation of required maintenance period

It is important to estimate how long it takes to do replace the moderator-reflector assembly according to the maintenance scenario as mentioned in the previous subsections, because it is helpful to plan the replacement work. The working flow and its required time are summarized in the Table 2.7.1, where other maintenance works such as the target vessel are not taken into account. It takes 15 days in total to replace the moderator-reflector assembly, assuming 8-hour work a day. Seven days are required to transport the used moderator-reflector assembly from the helium vessel to the drying component room, and it takes 8 days to move and install a new moderator-reflector assembly to the helium vessel. In other words, beam operation should be stopped longer than 2 weeks to replace the moderator-reflector assembly, because this work cannot be done with beam on.

We already experienced the whole series of the replacement work for the moderator-reflector assembly using the real moderator-reflector assembly as shown in Photo. 2.7.18. It was planed as one of the off-beam commissioning programs to confirm the remote handling scenario. It was verified that our estimation was very reasonable. One of the lessons from this program is that experts have to be brought up for the works at hand in this replacement process, such as detaching the cooling water pipes and the hydrogen transfer couplers, to reduce internal and external exposures to radiation.

2.7.5 Cutting Device

(1) Outline

A cutting device is designed to reduce storage volume of used components such as the moderator, the reflector and the proton beam window by cutting off long pipes of the components. Fig. 2.7.14 gives a 3-D image of the cutting device consisting of upper and lower grippers, a cutter, a mast and a rack. Because the pipes of the components are complex in their shapes with several elbows, the cutting device needs to have 6 degrees of freedom; rotation and elevation of the whole body, elevation of the cutter and the lower gripper and traverse, rotation and back and forth movement of the upper gripper.

The gripper is designed not to release the component even when an accidental electric power loss. A share cutting system is selected because radioactive cutting dust can be reduced. The system is reliable due to the compact and simple design. A high pressure can be applied to the cutter with slow speed to prevent dust from scattering. The grippers and the cutter are operated by oil pressure.

The cutting device receives the used component from the moderator exchange device. Photo. 2.7.19 shows a snap that the cutting device is just receiving a dummy moderator from the moderator exchange device. Fig. 2.7.15 and Photo. 2.7.20 show the layout for the cutting device, the moderator exchange device and the inner and outer plug racks.

A typical cutting sequence is described below.

1. Positions of the grippers of the cutting device are adjusted so as to receive the individual component adequately.
2. The moderator exchange device moves toward the cutting device, and sets the component at the proper position.
3. The lower and upper grippers close their hands, and hold piping of the component.
4. The moderator exchange device moves away.
5. The cutting device rotates to the cutting position.
6. The component is cut by the cutter. Cut out component is stored into a container.
7. The cutting device changes positions for gripping, and cut off the piping into adequate lengths step by step. The cut off piping is stored into another container.

(2) Specifications

Specifications of the cutting device are shown below.

- Type : Mechanical cutting system (Shear cutter)
- Material : Carbon steel (SS400)
- Cutting method : Oil pressurized shear cutter
- Cutting objects : Moderators with multi axial piping (ϕ90 mm) made of aluminum alloy.
  Reflector with a pair of piping (50A) made of stainless steel.
  Proton beam window with several piping (40A×1, 25A×4, 10A×4) made of stainless steel.
  Muon target with several piping.

- Dimension : 2,200 mm (depth) × 2,300 mm (width)× 3,200 mm (height)
- Cutter : Blade material : Special die steel, Base: SCM440
  Open width; 150 mm
- Gripper : Material; SCM440
  Open width; 180 mm
- Movement :
  Rotation : −15° - 105°
  Elevation : 0 to 1,400 mm
  Cutter elevation : 0 to 980 mm
  Upper gripper traverse : −750 - 750 mm
  Upper gripper rotation : 0 - 180°
  Upper gripper back-and-forth : 0 - 560 mm
- Slide table : Size : 1500 × 1500 mm
  Back-and-forth moving stroke : 0 to 600 mm

If a trouble by which the operation can not be continued any more occurs during handling a radioactive component, the cutting device is rescued by the power manipulator. A rescue bolt is equipped for each movement axis, and the power manipulator rotates the rescue bolt.

(3) Control

The cutting device is controlled by using touch panel shown in Photo. 2.7.21. The touch panel can be taken off from a control panel for easy operation. The control panel is installed in the 1st manipulation room on the first floor of the MLF. An operator can take the touch panel in front of a shielding window to operate the cutting device watching its motion. A video monitor of the ITV cameras is used auxiliary to operate the cutting device.

Power and control cables are connected to the cutting device through the shielding wall. Oil pressurizer for the cutter and the grippers is located in the hot cell because an oil tube can not penetrate the shielding wall with keeping the shielding performance.

References

2.7-1) M. Harada, et al., “DPA calculation for Japanese spallation neutron source”, J. Nucl. Mat., 343, 2005, pp. 197-204.

2.7-2) M. Teshigawra, et al., “Development status of moderator-reflector system in JSNS”, Proceedings of ICANS XVI, May 12-15, 2003, Zeughaus, Germany, 2003, pp. 601-612.

2.7-3) J. Adachi, et al., “Conceptual Design of the Handling and Storage System for Spent Target Vessel, JAERI-Conf 2001-002 (KEK Proceedings 2000-22), 2001, pp. 1276-1283.

2.7-4) M. Kaminaga, et al., “Present status of MLF Building Layout and Ancillary Facilities”, Proceedings of ICANS XVI, May 12-15, 2003, Zeughaus, Germany, 2003, pp. 125-134.

Table 2.7.1: Work flow and schedule for replacing moderator-reflector assembly

			Required period (days)														
			1	2	3	4	5	6	7	8	9	10	11	12	13	14	15
		【Common tool】															
		130 ton crane															
		Transfer cask, Floor valve															
		In-cell crane (20 ton)															
		Work flow															
(1)	1	Purge in vessel															
	2	Target drain															
	3	Cooling water drain															
	4	H2 release															
	5	Move target trolley backward															
	6	Remove roof seal plate															
	7	Remove shield blocks															
	8	Remove vessel shield															
	9	Remove vessel cover															
	10	Disconnect water pipe and H2 transfer															
	11	Attach hung tool for inner plug															
	12	Attach hung tool for outer plug															
	13	Install floor valve															
	14	Tighten bolts															
	15	Connect floor valve cable															
	16	Install transfer cask															
	17	Connect transfer cask cable															
	18	Open floor shield															
	19	Open transfer cask shield															
	20	Lift down gripper															
	21	Hold outer plug hung tool															
	22	Lift up gripper into transfer cask															
	23	Close transfer cask shield															
	24	Close floor shield															
(2)	25	Remove transfer cask cable															
	26	Loosen transfer cask bolts															
	27	Transfer the cask to vessel for dry up															
	28	Install transfer cask															
	29	Connect transfer cask cable															
	30	Open hatch over dry up room															
	31	Open floor shield															
	32	Open transfer cask shield															
	33	Lift down gripper															
	34	Release inner and outer plug hung tool															
	35	Lift up gripper into transfer cask															
	36	Close hatch over dry up room															
	37	Close transfer cask shield															
	38	Close floor shield															
(3)	39	Detach transfer cask cable															
	40	Transfer to hot cell															
	41	Connect transfer cask cable															
	42	Open floor shield															
	43	Open transfer cask shield															
	44	Lift down gripper															
	45	Hold outer plug hung tool															
	46	Lift up gripper into transfer cask															
	47	Close transfer cask shield															
	48	Close floor shield															
	49	Detach transfer cask cable															
	50	Loosen transfer cask bolts															
	51	Transfer to vessel															
(4)	52	Install transfer cask															
	53	Connect transfer cask cable															
	54	Open floor shield															
	55	Open transfer cask shield															
	56	Lift down gripper															
	57	Release inner and outer prug hung tool															
	58	Lift up gripper into transfer cask															
	59	Close transfer cask shield															
	60	Close floor shield															
	61	Detach transfer cask cable															
	62	Loosen transfer cask bolts															
	63	Transfer the cask to storage position															
	64	Detach floor valve cable															
	65	Loosen floor valve bolts															
	66	Transfer floor valve to storage position															
	67	Remove floor valve attachment															
	68	Transfer floor valve to storage position															
	69	Detach hung tool of inner and outer plug															
	70	Remove inner and outer plug hung tool															
	71	Attach water pipe and H2 transfer line															
	72	Leak test of H2 transfer line															
	73	Leak test of water pipe															
	74	Circulate H2															
	75	Circulate cooling water															
	76	Install vessel cover															
	77	Move target trolley forward															
	78	Leak test of vessel															
	79	Fill He in vessel															
	80	Install vessel shield															
	81	Install shield blocks															
	82	Install roof seal plate															
	83	Leak test of outer liner															

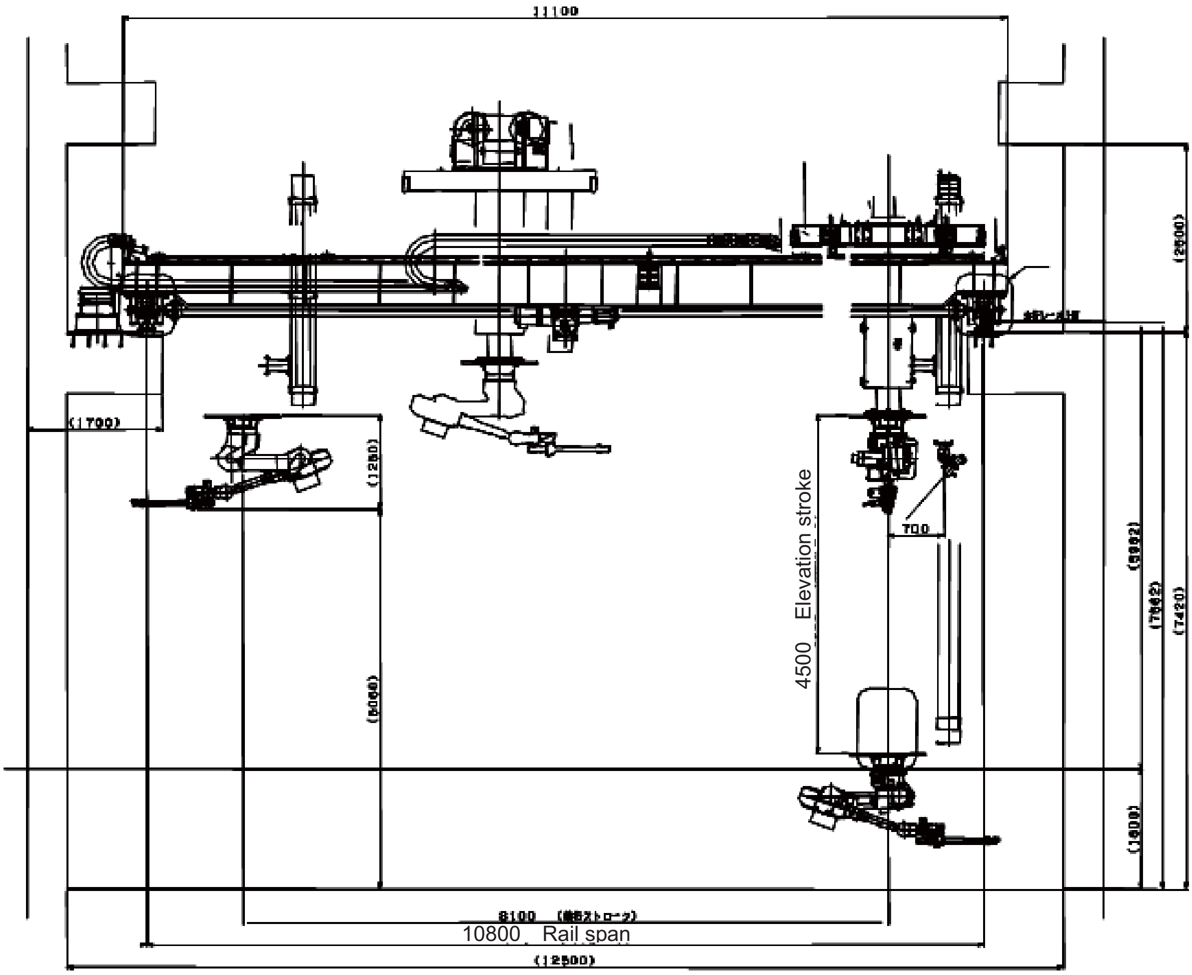

Fig. 2.7.1 Schematic drawing of the Power manipulator (PM)

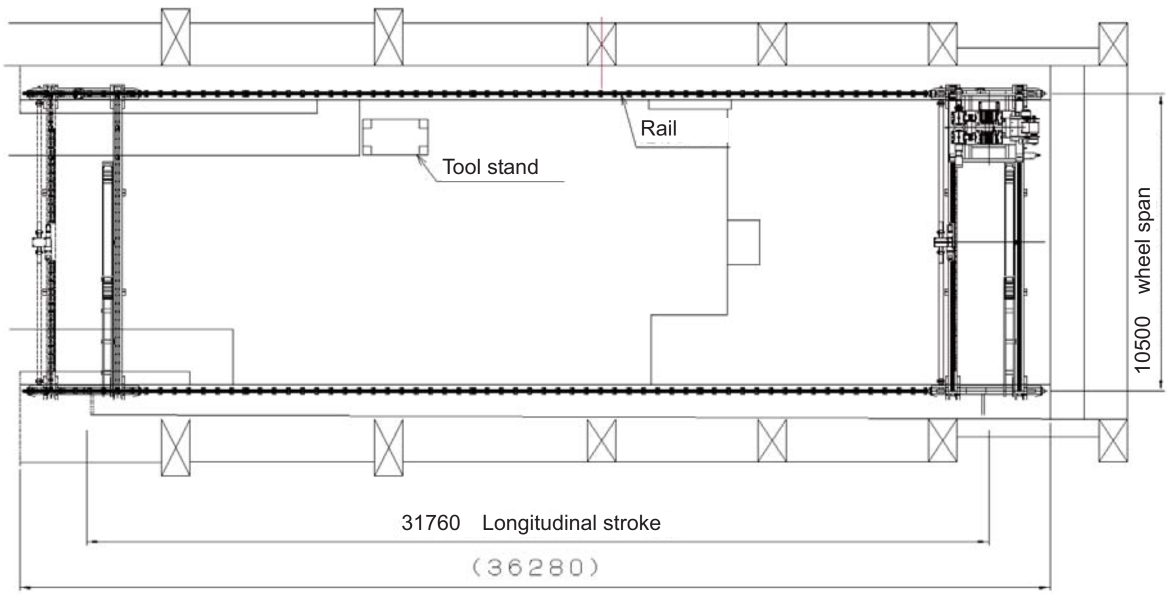

Fig. 2.7.2: Plane view of the power manipulator

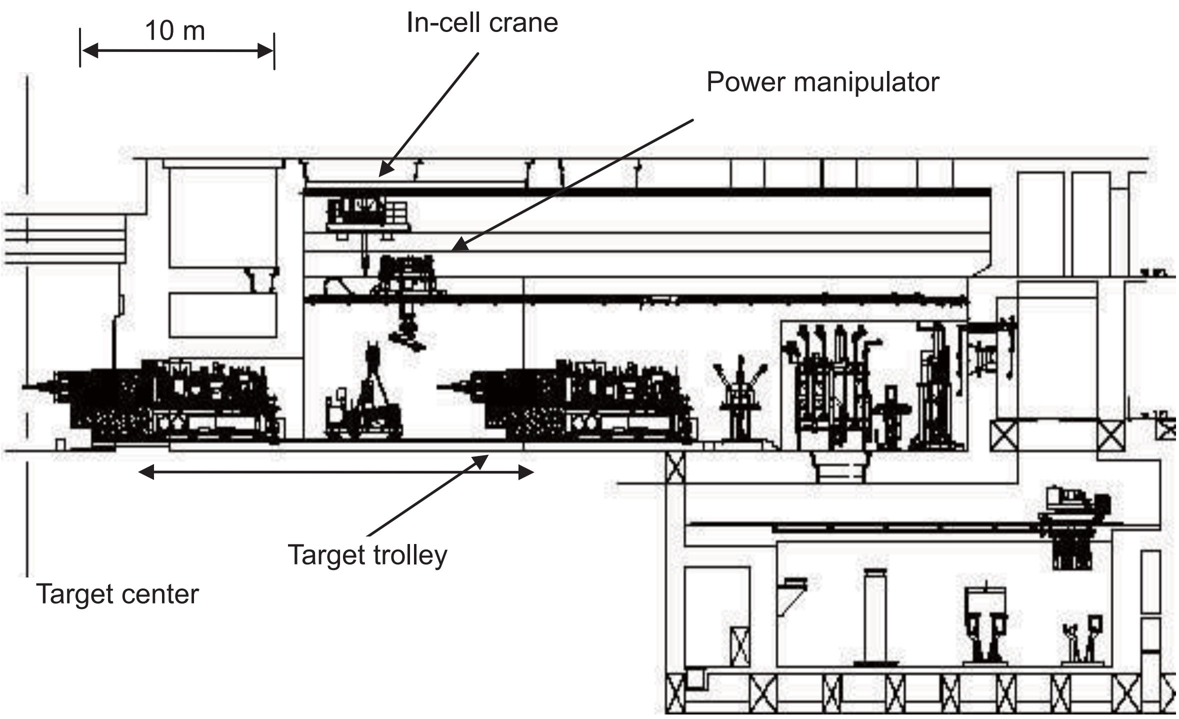

Fig. 2.7.3: Cross sectional view of the remote handling area

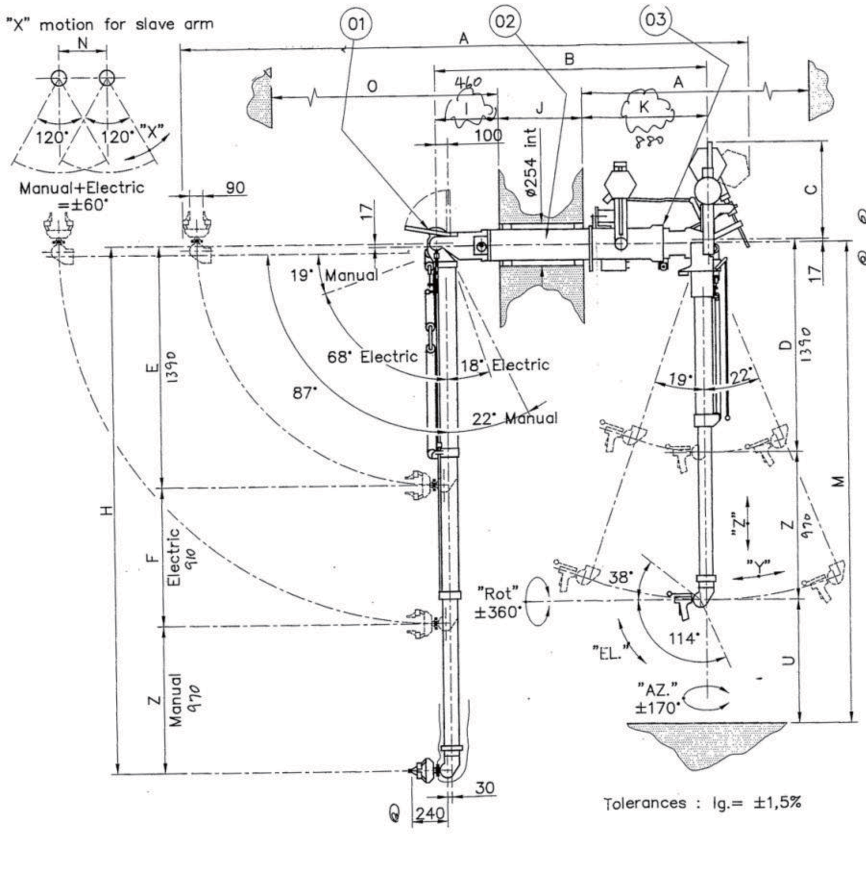

MSM		Dim. in mm
A	Withdrawal distance	4900
B	Distance between shoulder axis	2840
C	Height above shoulder pivot	616
D	Length of retracted master arm	1390
E	Length of retracted slave arm	1390
F	Z electric travel distance	910
H	Length of extended slave arm	3270
I	Slave arm overhang distance	460
J	Wall thickness	1500
K	Master arm overhang distance	880
M	Height of axis above floor	3050
N	Distance between two machines	800
O	Minimum depth of cell	1950
U	Pistol-grip guard to floor with master arm extended	707
Z	Z manual travel distance	970

Fig. 2.7.4: Schematic drawing of the MSM (MT200)

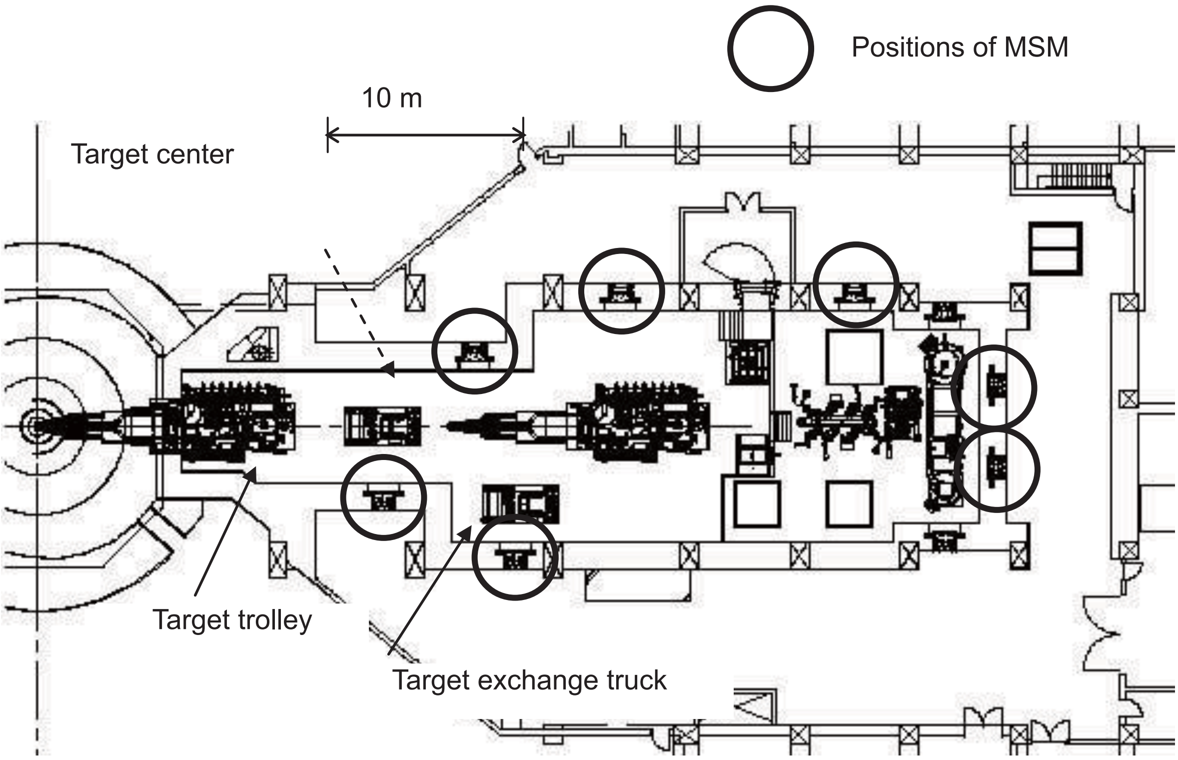

Fig. 2.7.5: MSM layout in the irradiated components handling room (1F)

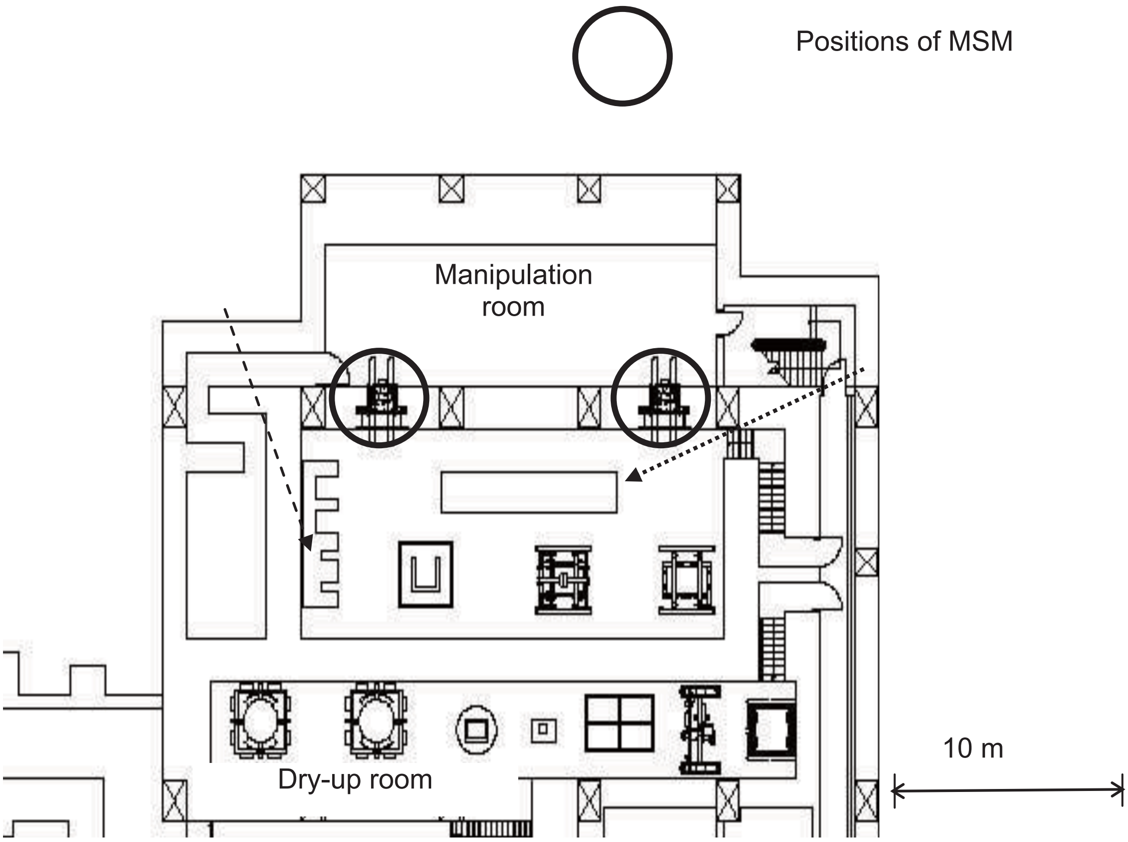

Fig. 2.7.6: MSM layout in the irradiated components storage room (B1F)

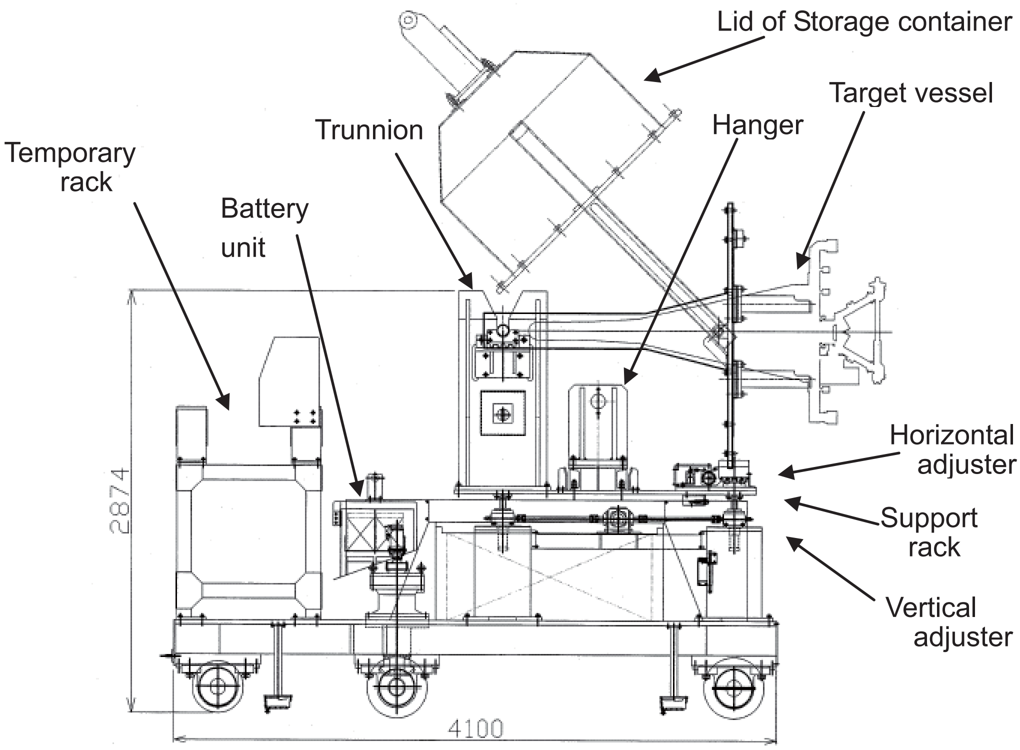

Fig. 2.7.7: Schematic drawing of the target exchange truck

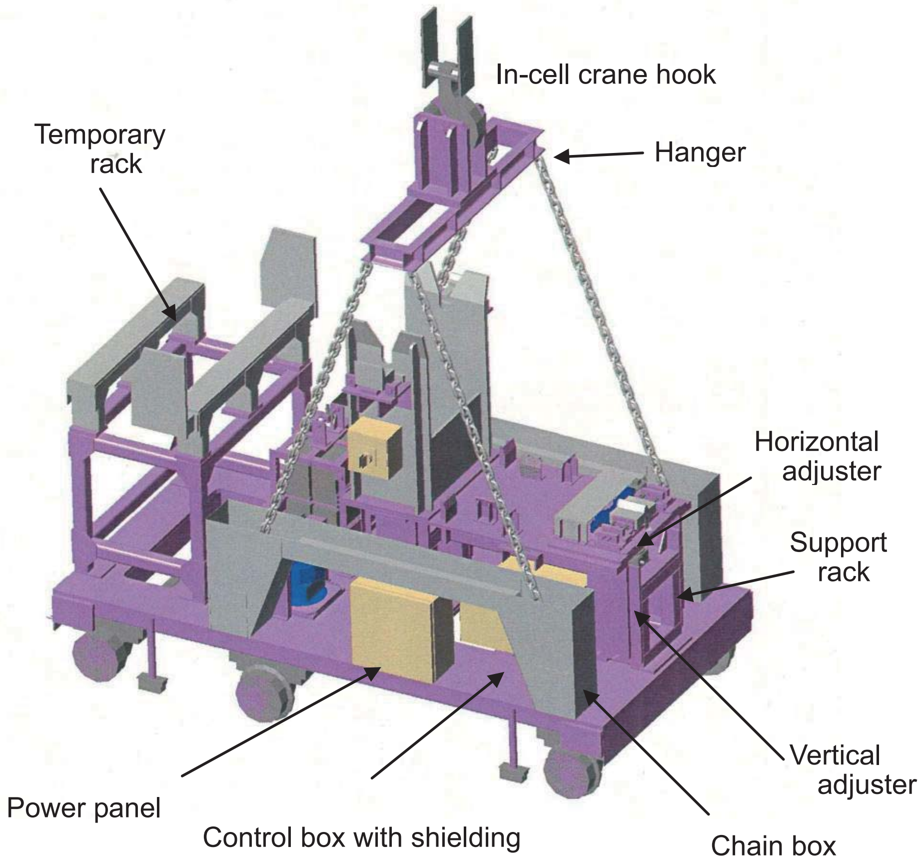

Fig. 2.7.8: 3-D image view of the target exchange truck

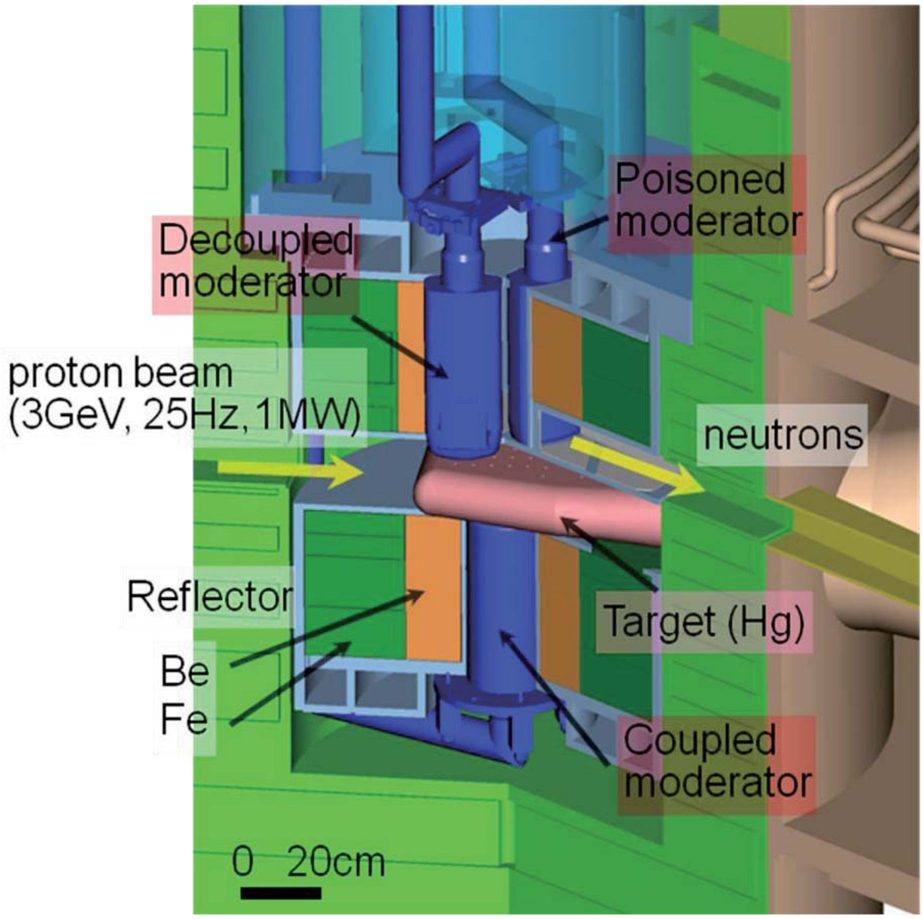

Fig. 2.7.9: Cross sectional view of target-moderator-reflector system

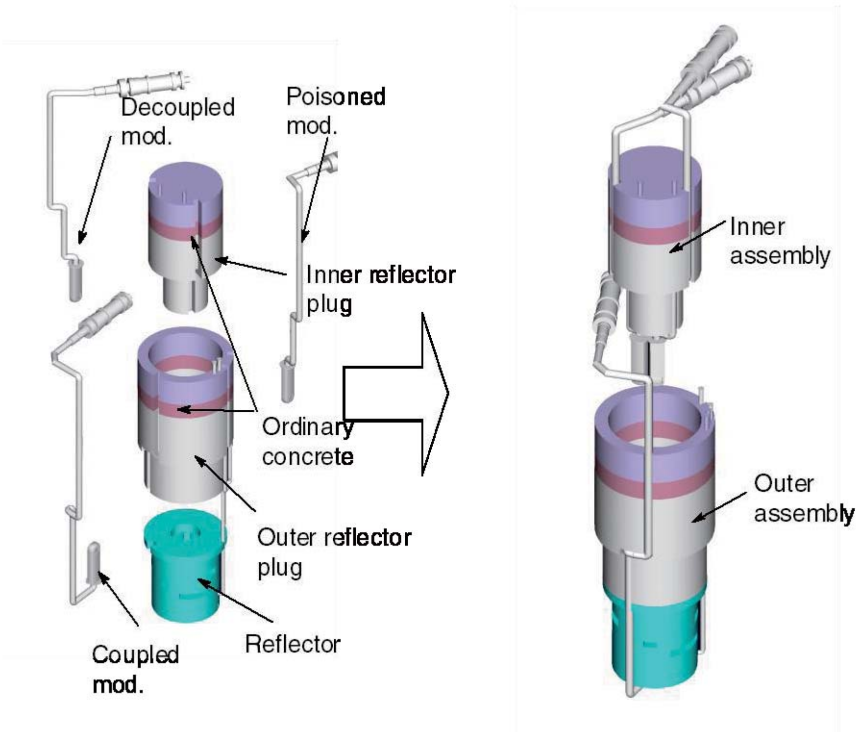

Fig. 2.7.10: Structure of moderator-reflector plug.

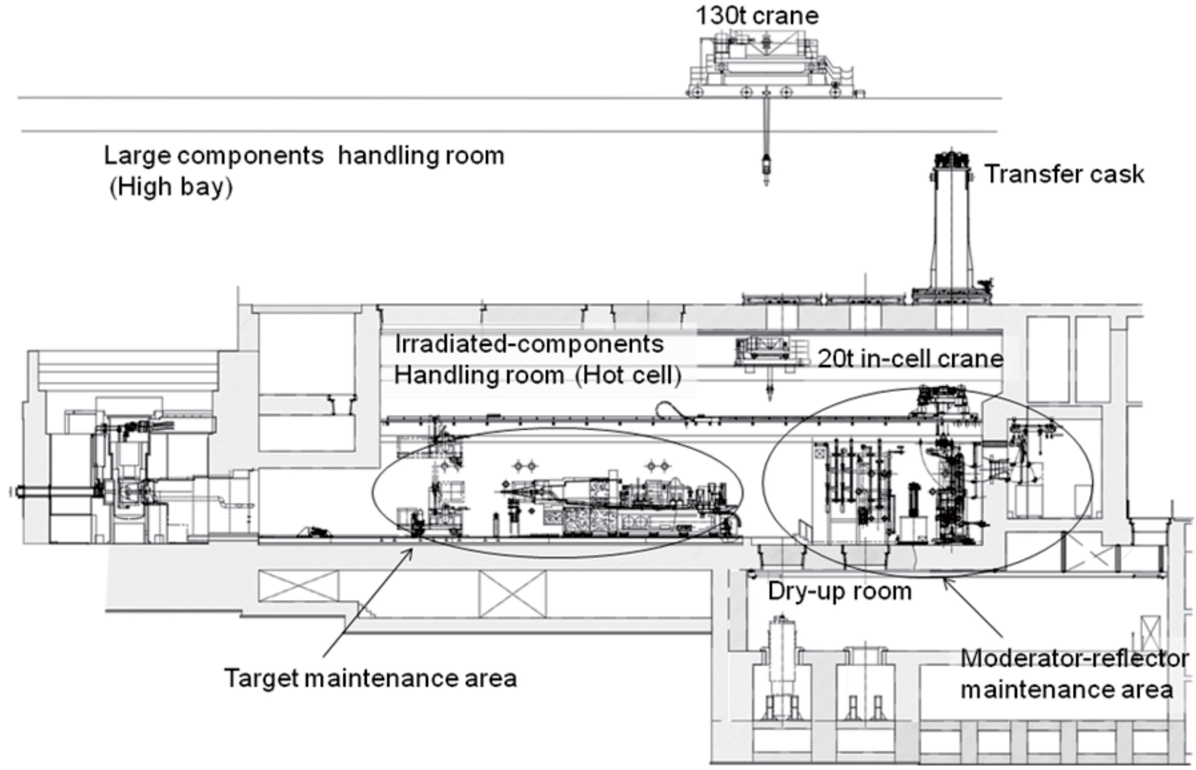

Fig. 2.7.11: Vertical cross section of target station and its related rooms

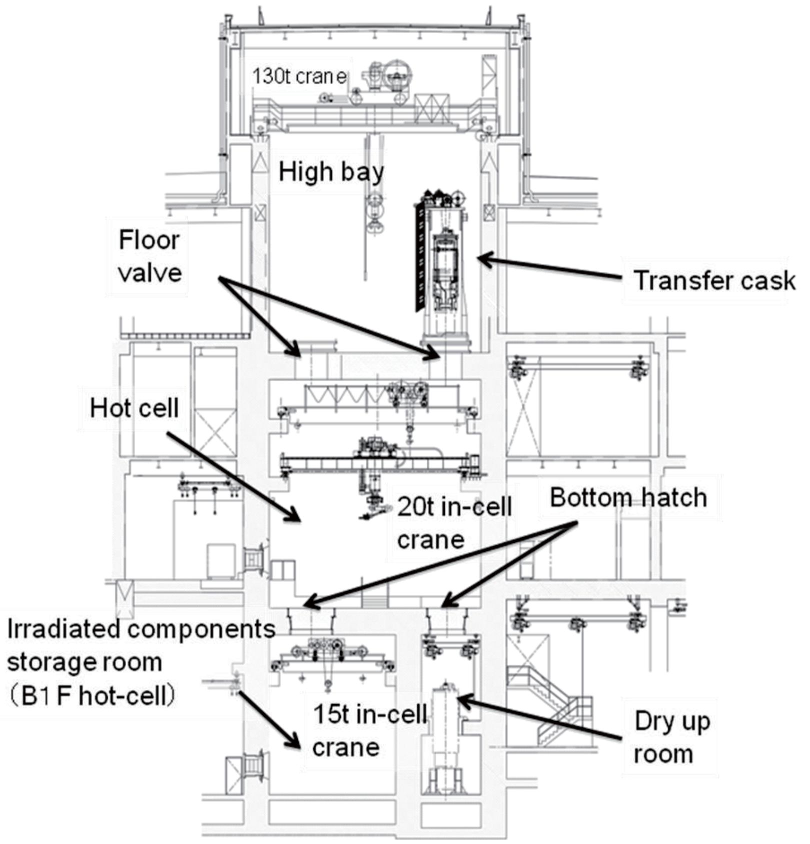

Fig. 2.7.12: Another vertical cross section of target station and its related rooms

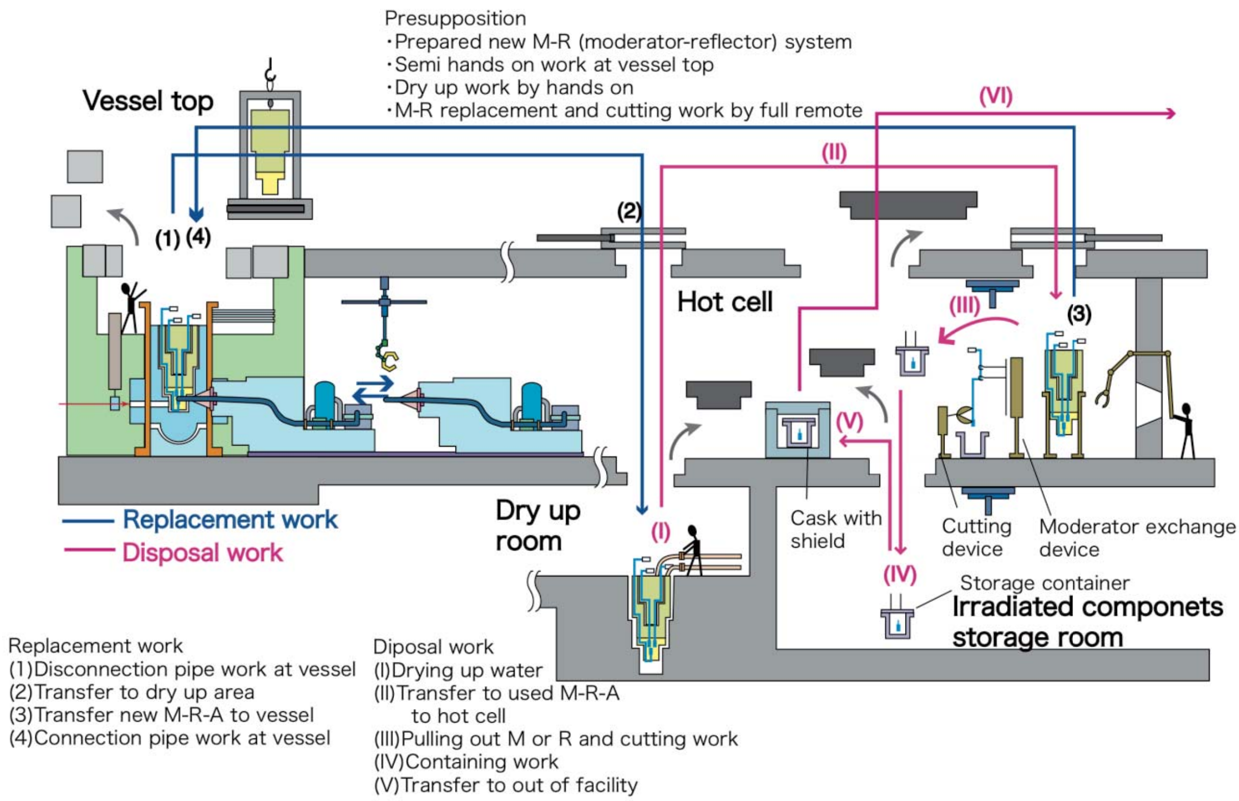

Fig. 2.7.13: Replacement scenario of moderator-reflector assembly

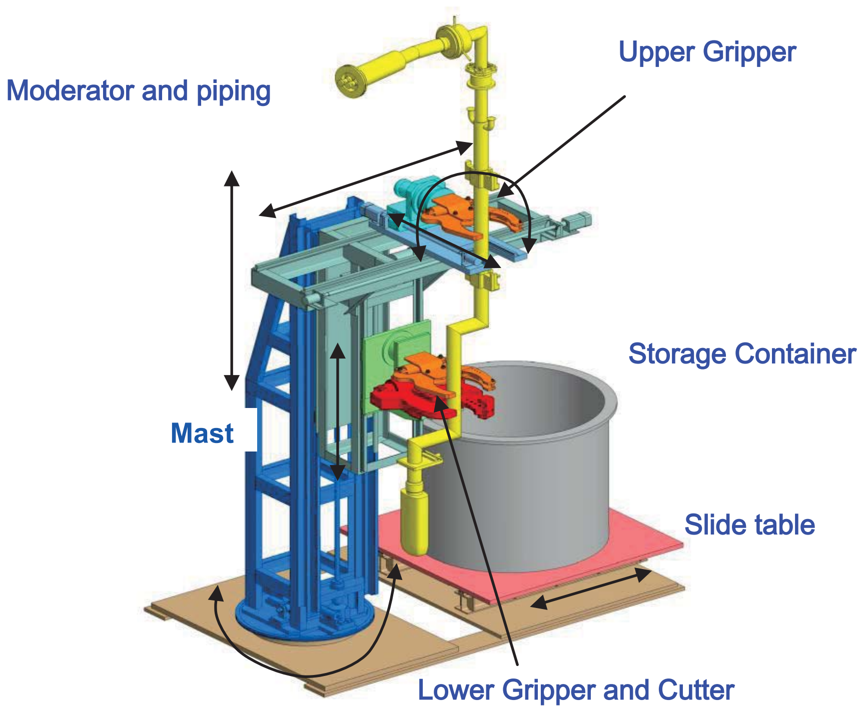

Fig. 2.7.14: Image of the cutting device

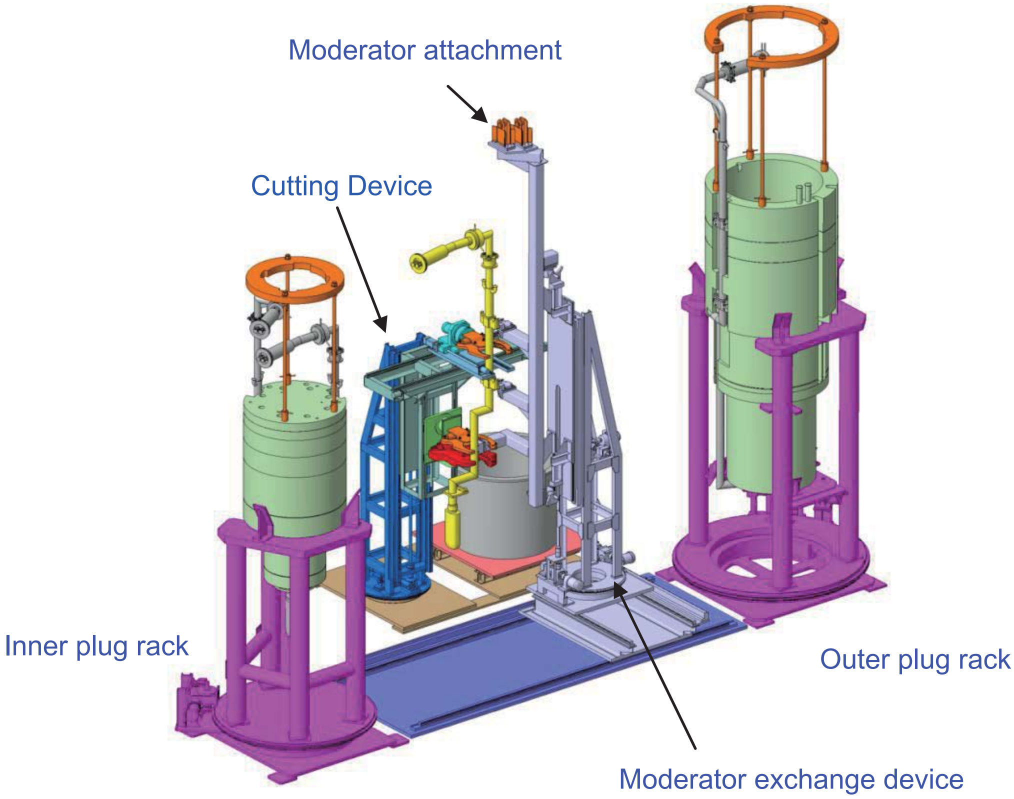

Fig. 2.7.15: Image of the cutting device and related devices layout

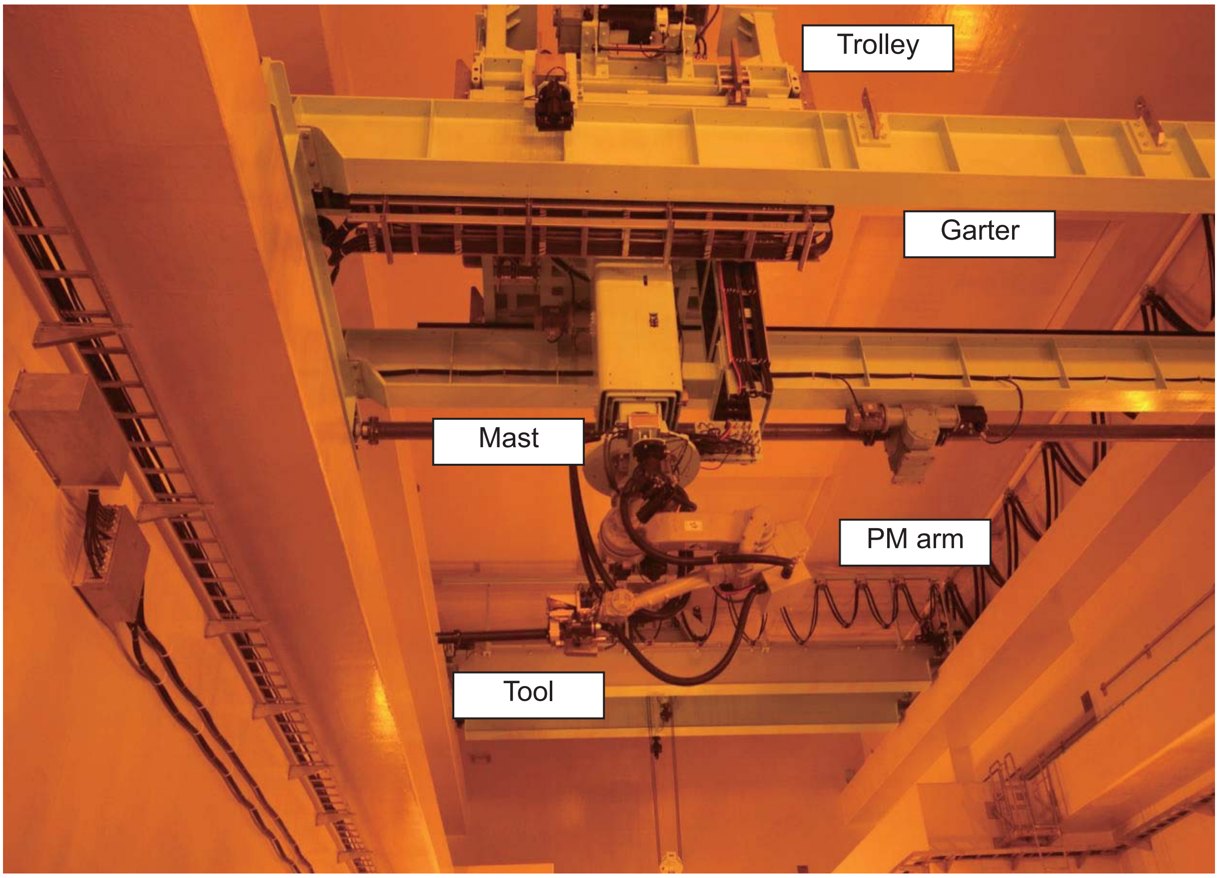

Photo. 2.7.1: Power manipulator

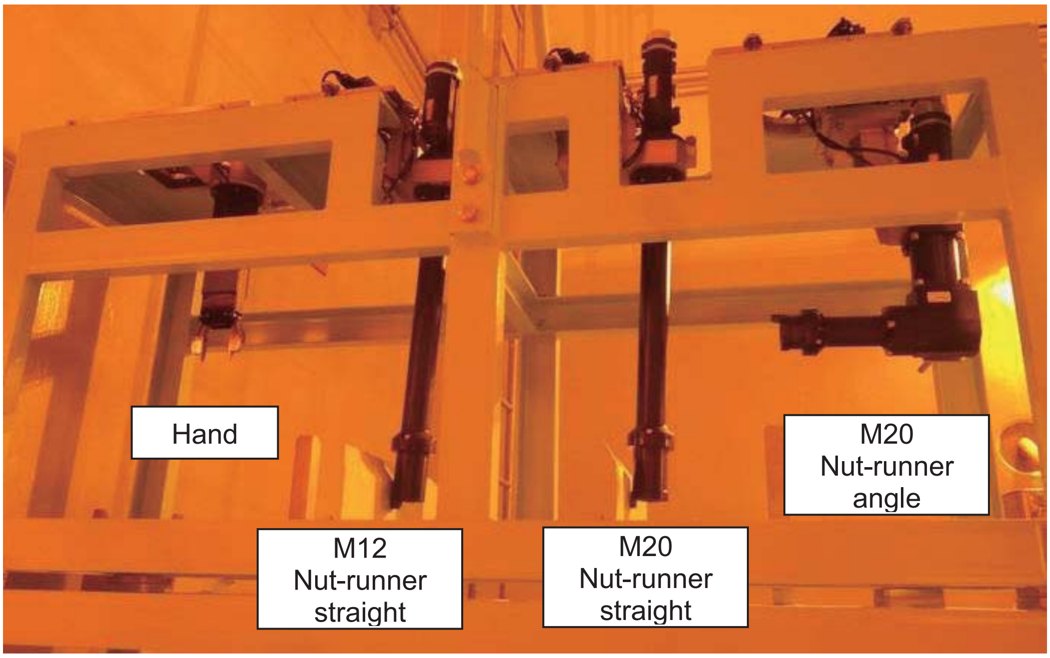

Photo. 2.7.2: Tools (end-effectors) for the power manipulator

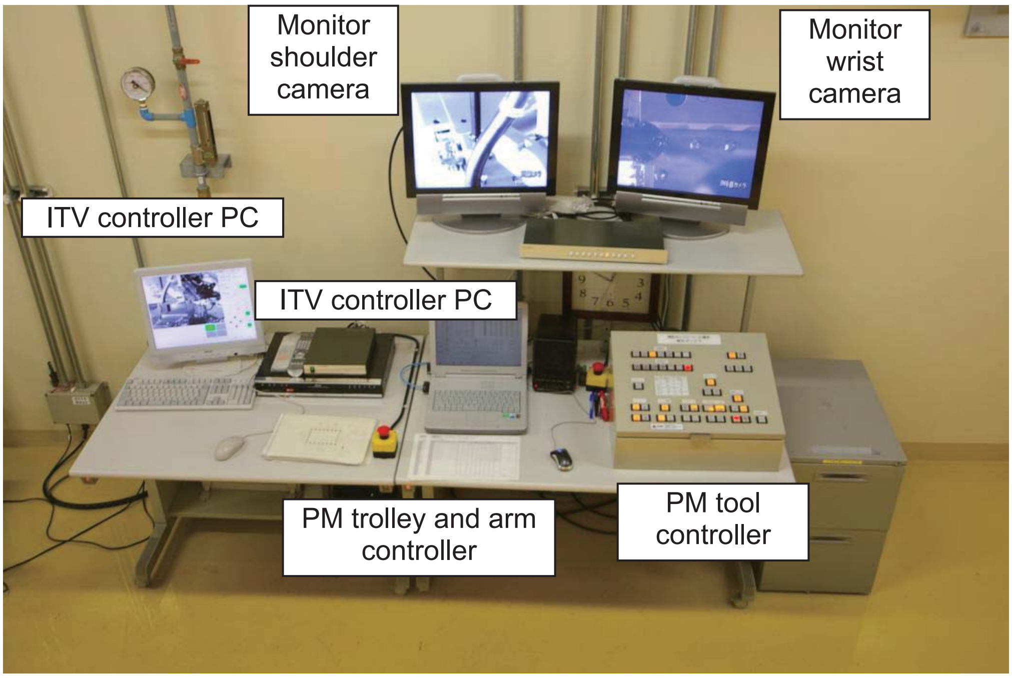

Photo. 2.7.3: Control panel for the power manipulator

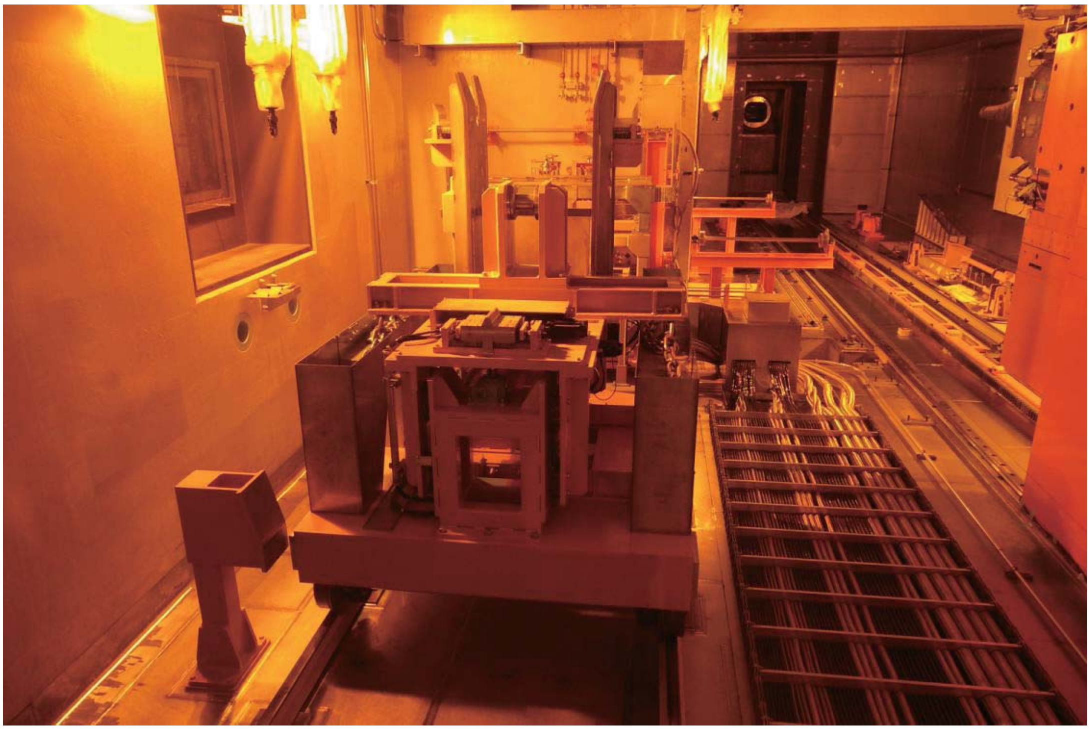

Photo. 2.7.4: Front view of the target exchange truck

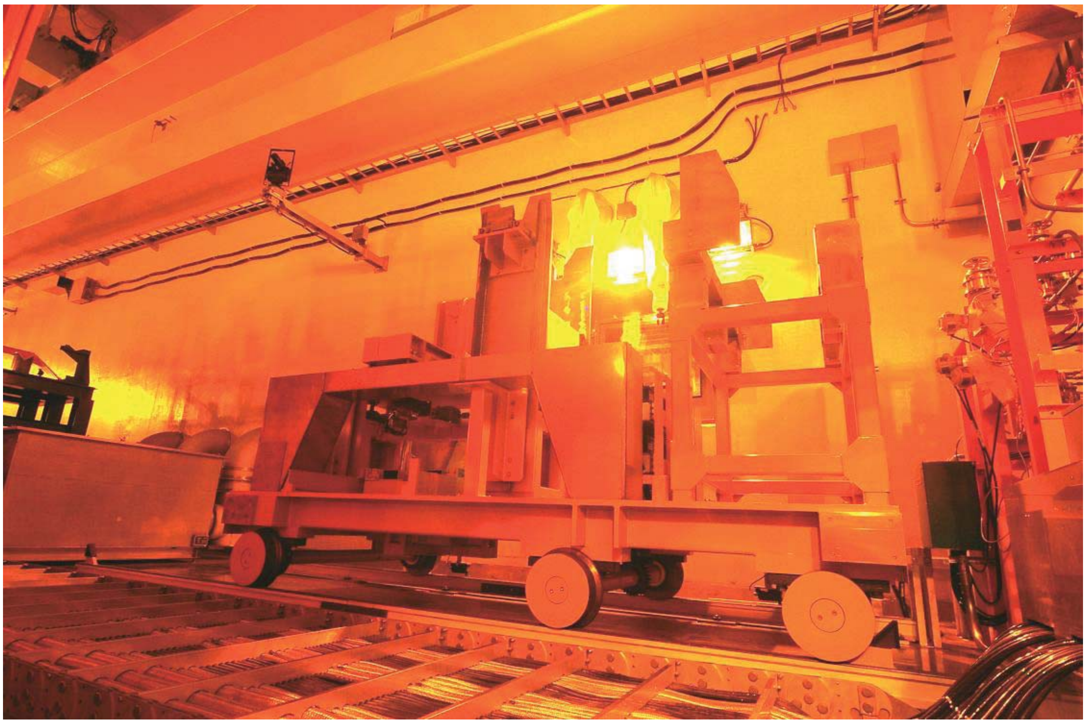

Photo. 2.7.5: Side view of the target exchange truck

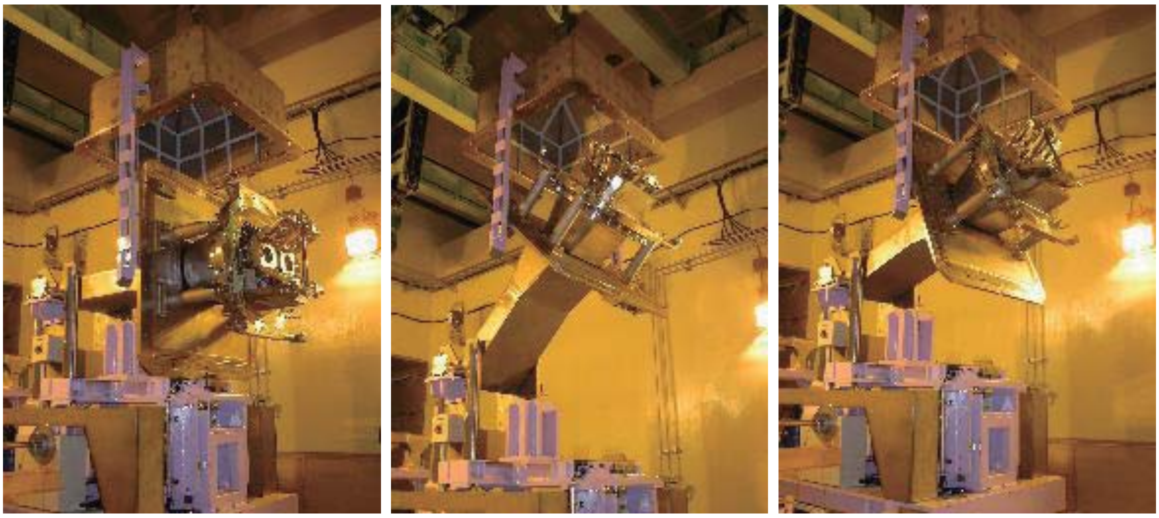

Photo. 2.7.6: Setting sequence of the target storage container on the target exchange truck

Photo. 2.7.7: Target exchange truck being hanged up by the in-cell crane

Touch Panel

Operation button

Photo. 2.7.8: Control panel for the target exchange truck

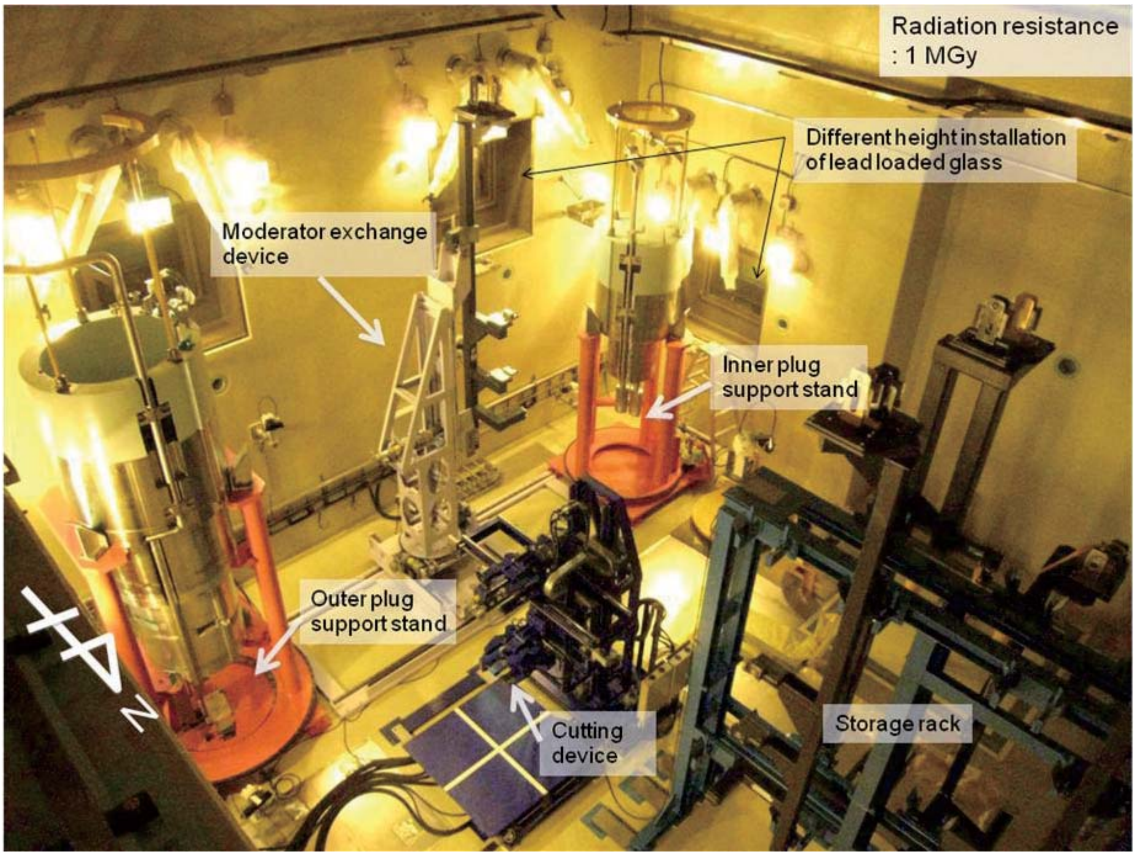

Photo. 2.7.9: Remote handling devices for moderator-reflector maintenance

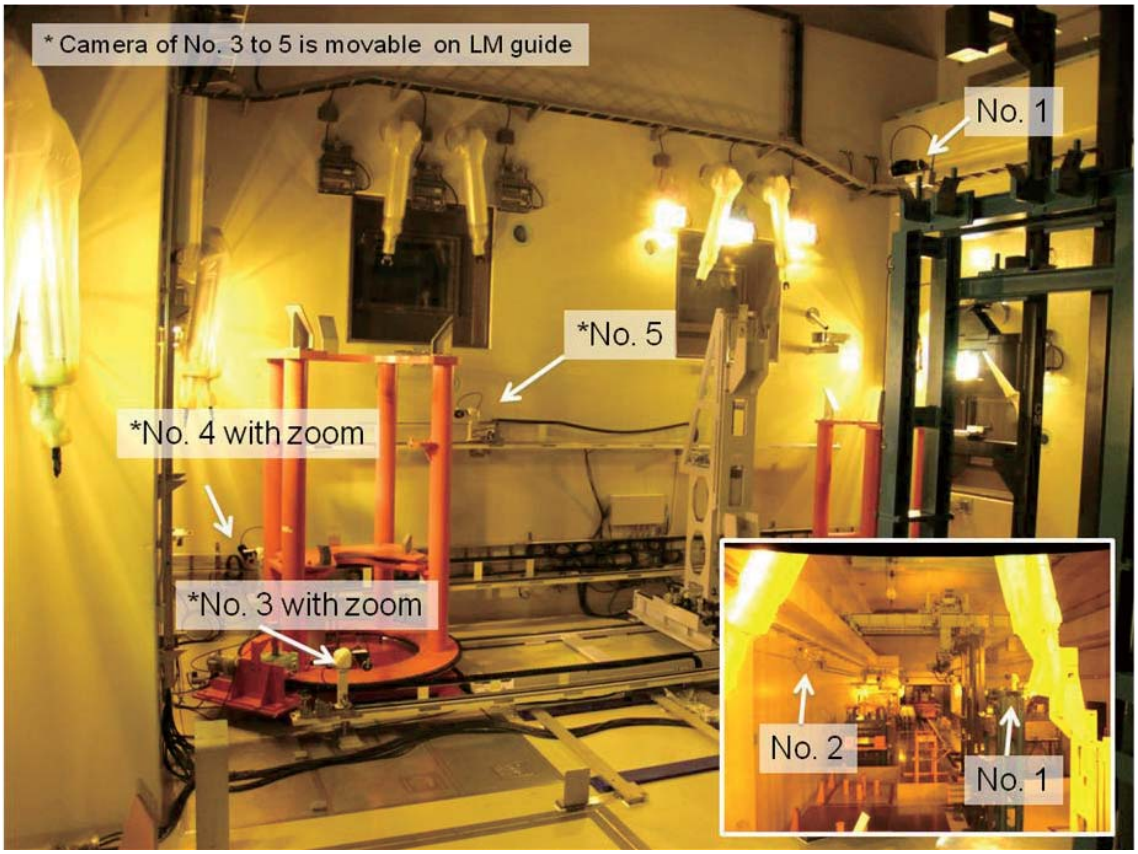

Photo. 2.7.10: Arrangement of ITV remote cameras

Photo. 2.7.11: Sepcification of transfer cask

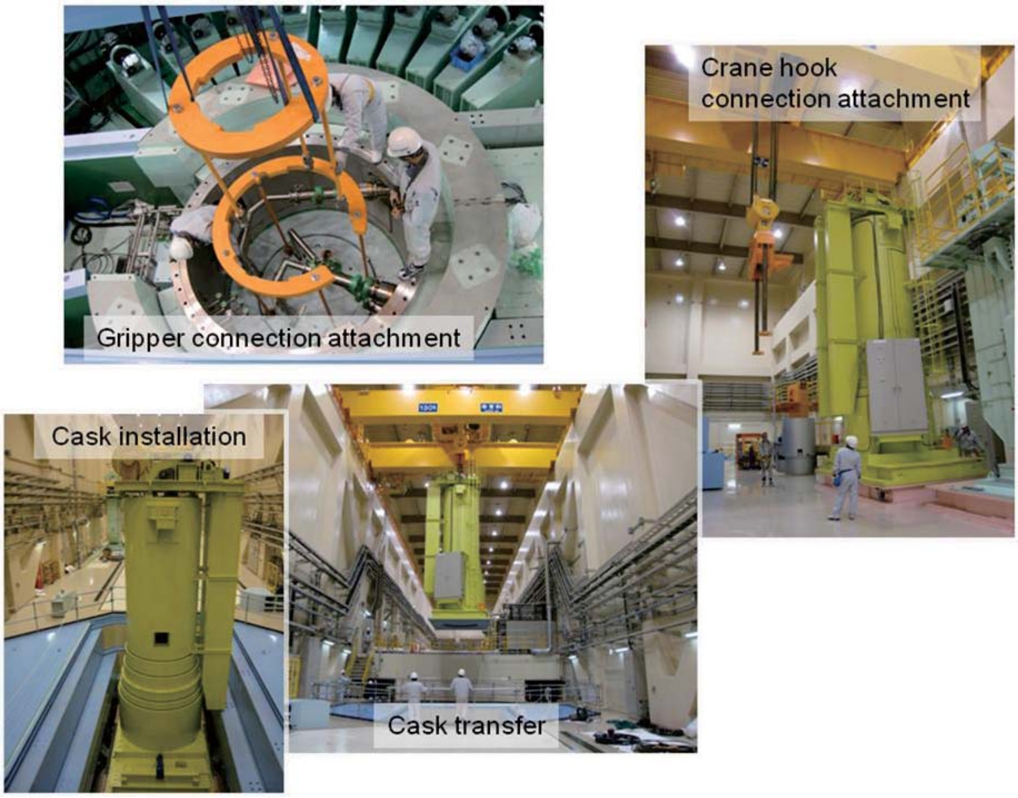

Photo. 2.7.12: Installation flow of transfer cask onto helium vessel

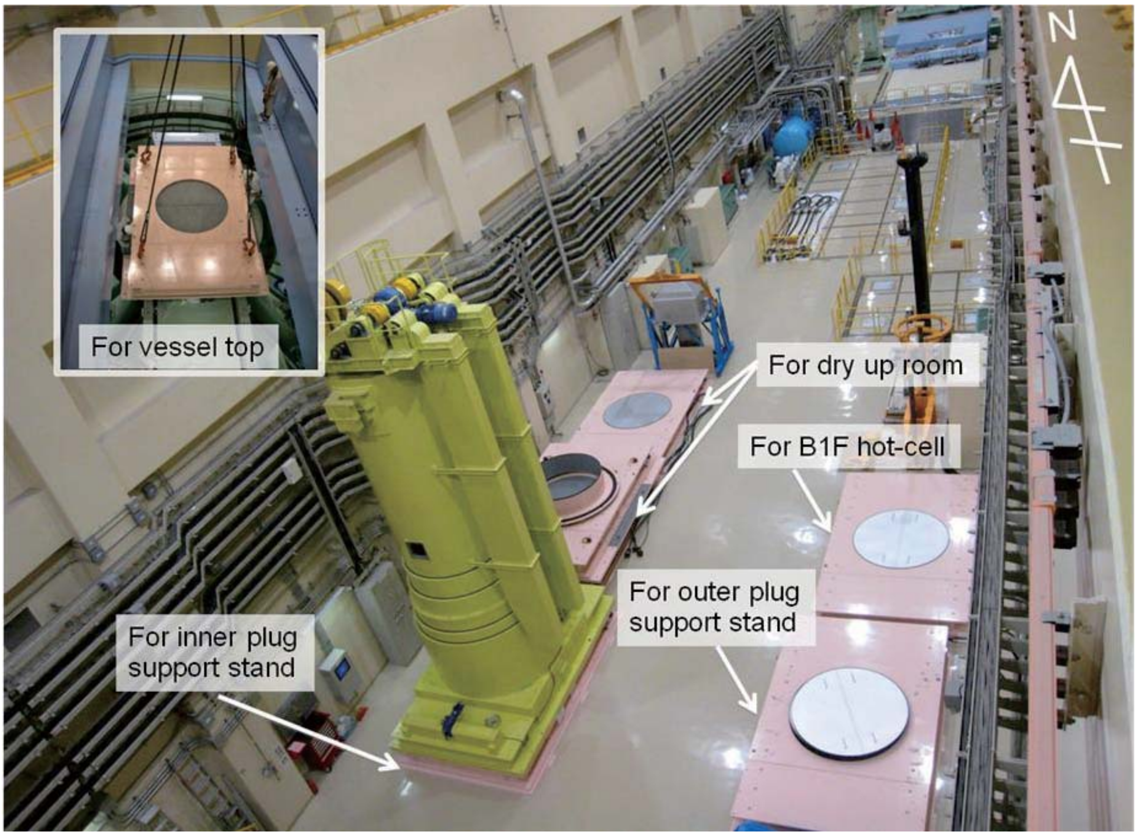

Photo. 2.7.13: Six floor valves were installed in large component handling room (high bay)

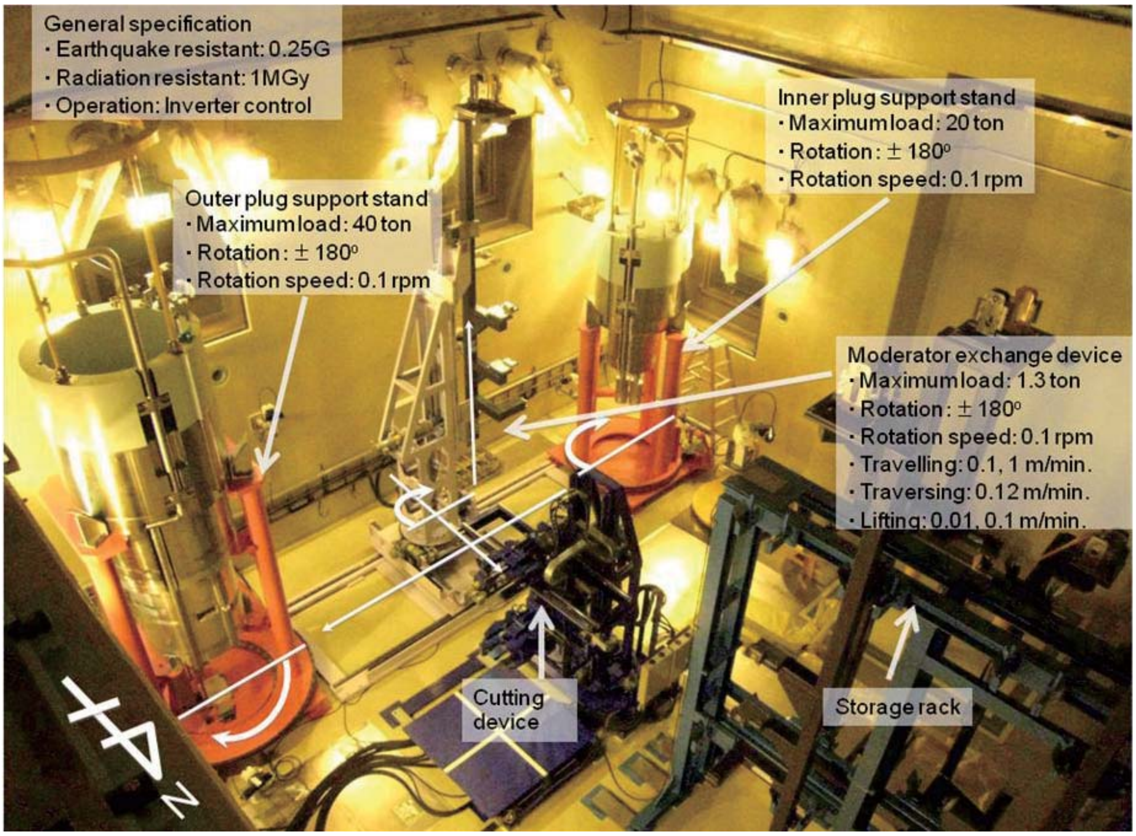

Photo. 2.7.14: Configuration of remote control devices in hot cell

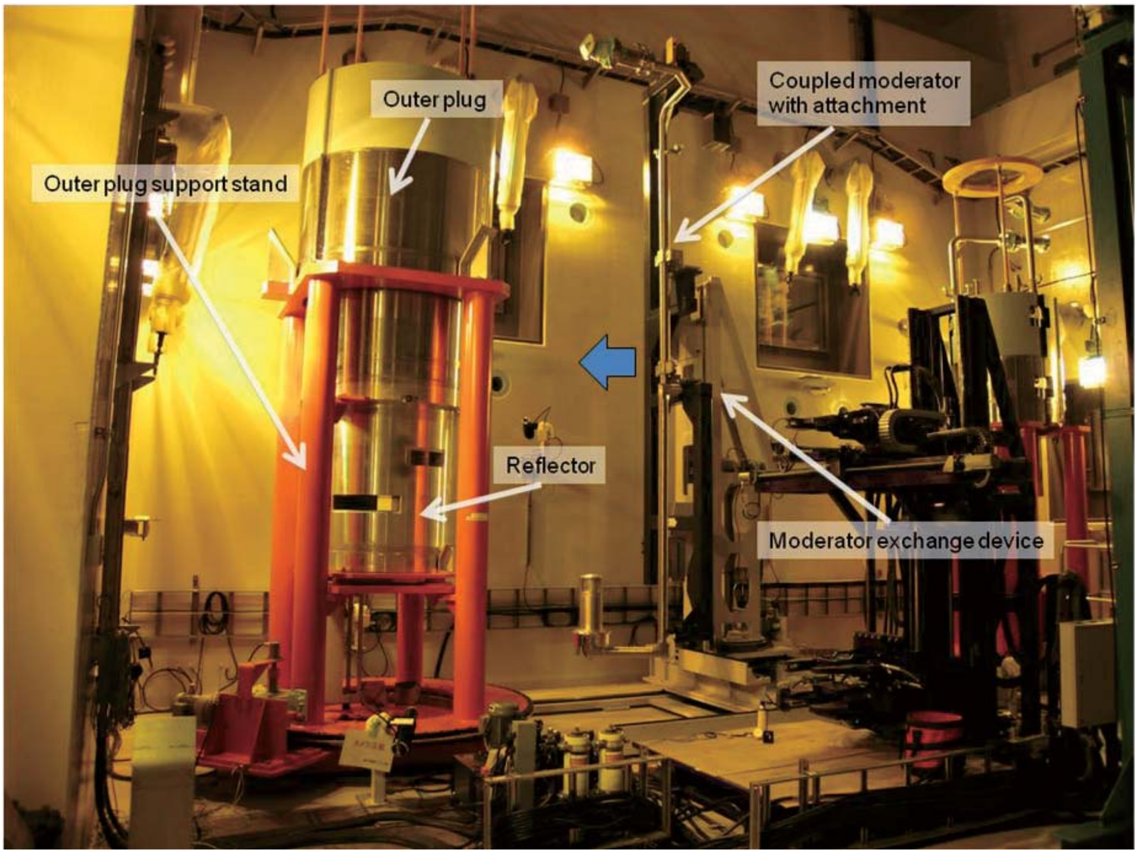

Photo. 2.7.15: Replacement of coupled moderator with moderator exchange device

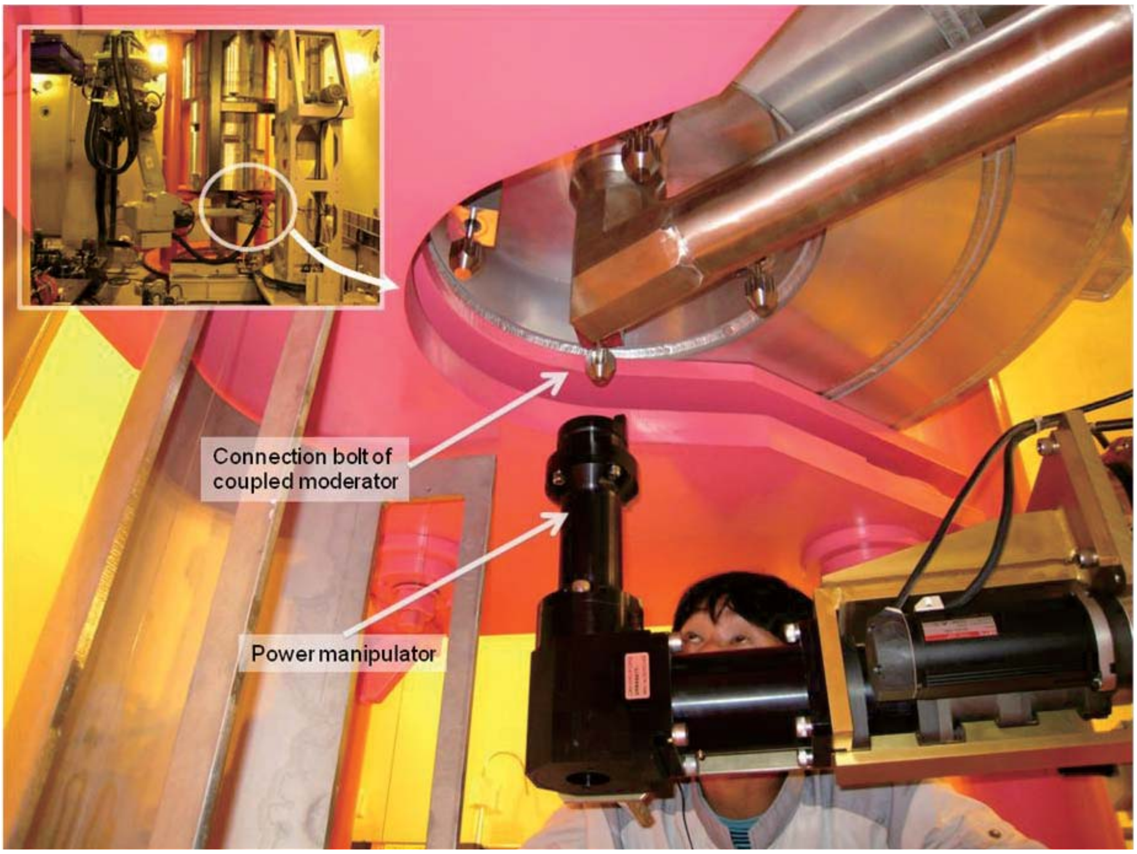

Photo. 2.7.16: Access of power manipulator to connection part of coupled moderator

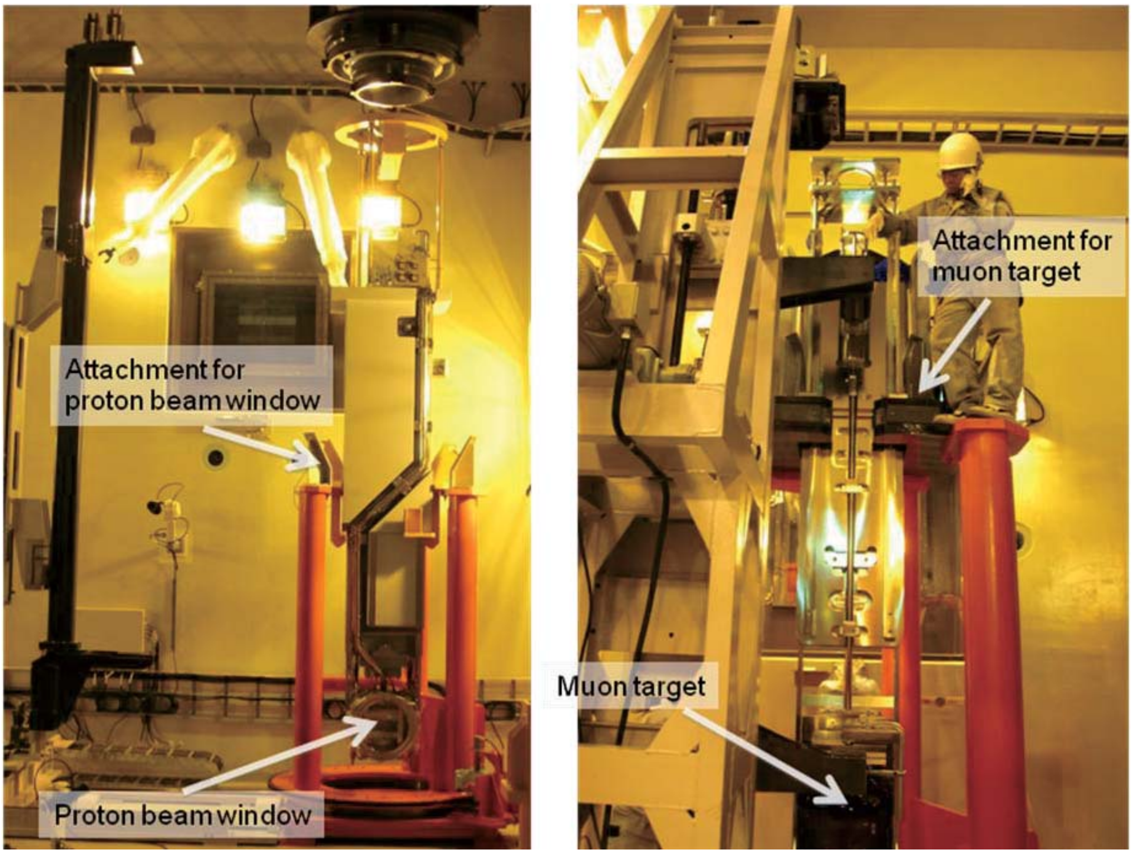

Photo. 2.7.17: Dedicated attachments for proton beam window and muon target assembly

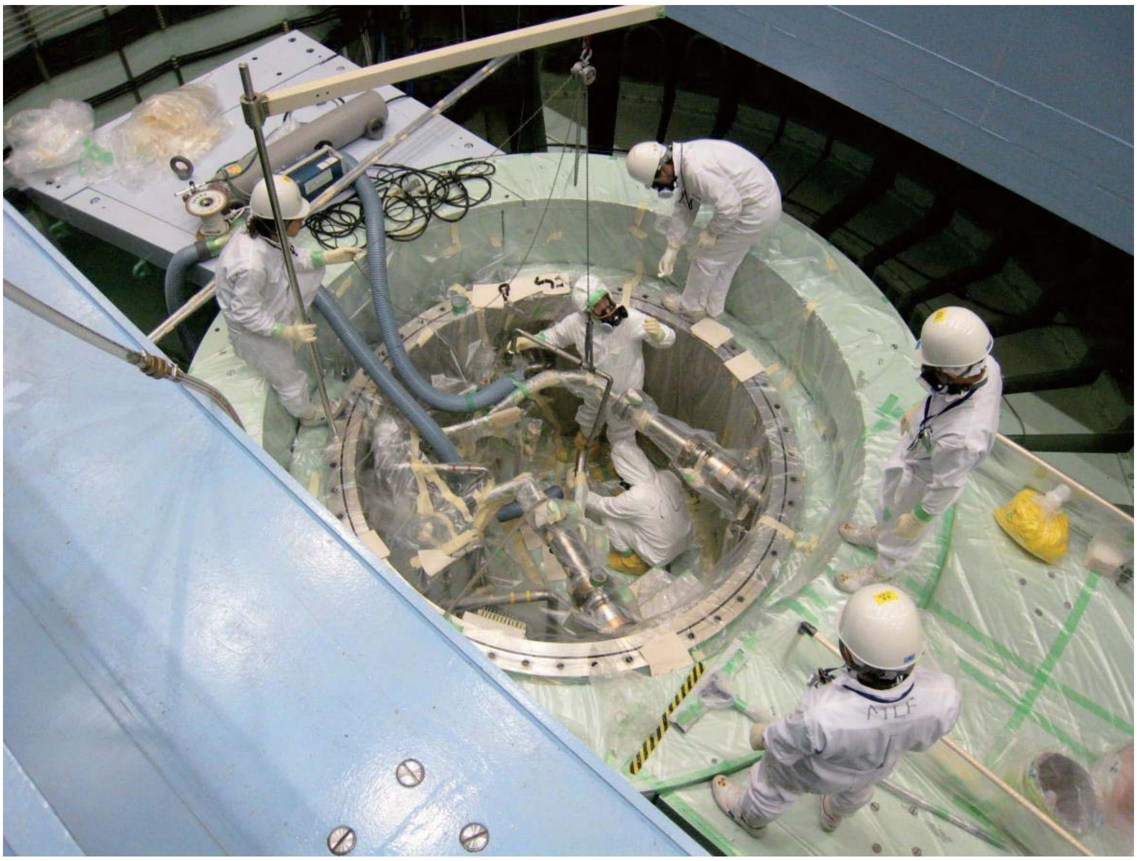

Photo. 2.7.18: Off-beam commissioning to detach cooling water pipes

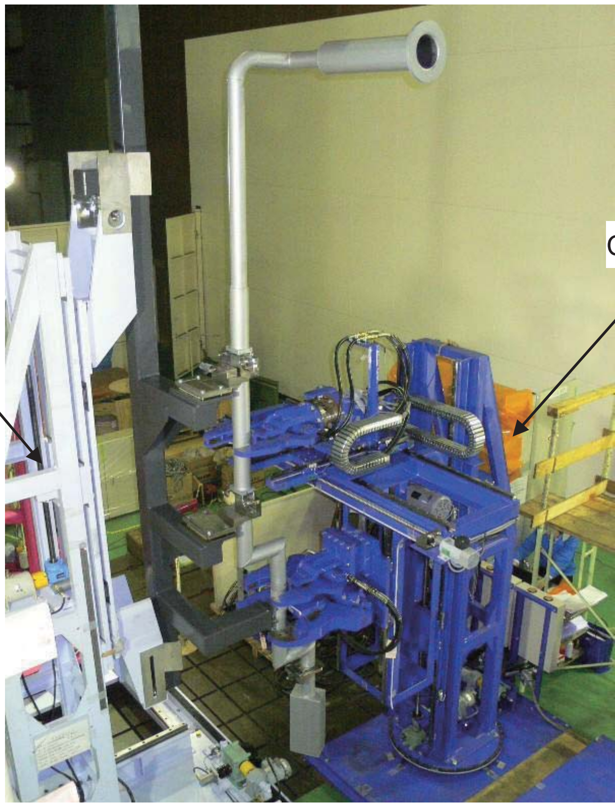

Photo. 2.7.19: The cutting just receiving a dummy moderator by the moderator exchange device

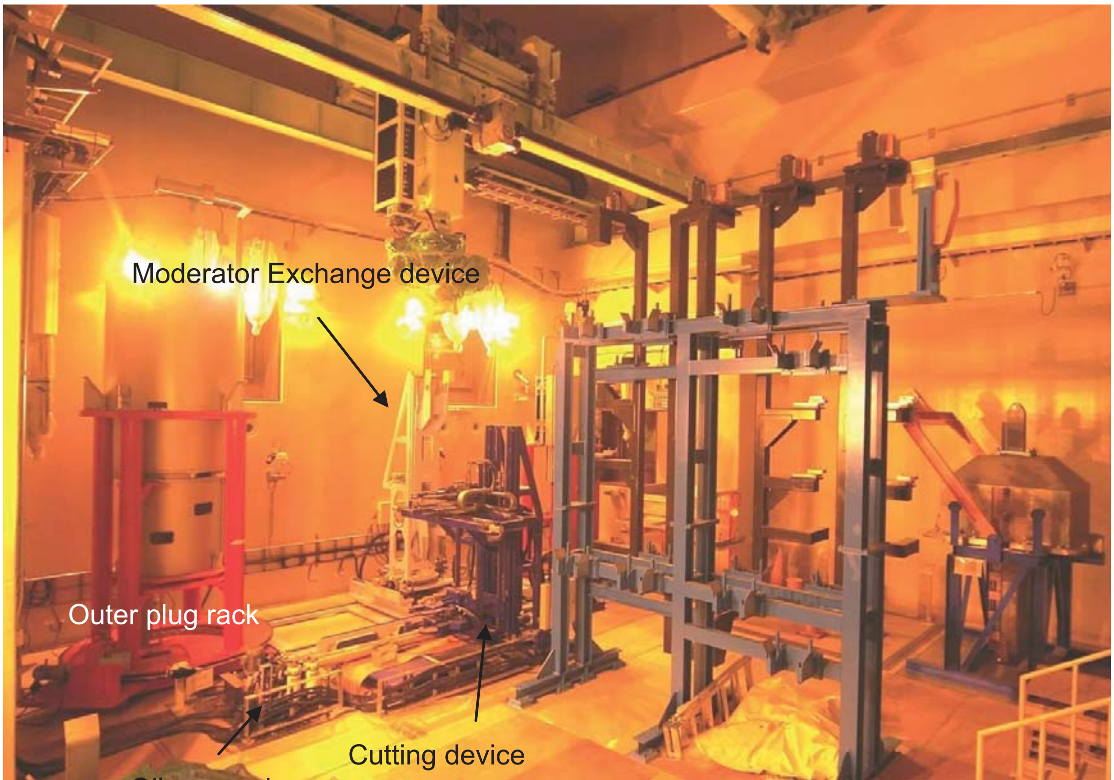

Photo. 2.7.20: Cutting device and related devices in the hot cell

Photo. 2.7.21: Control panel for the cutting device

2.8 Proton Beam Transport Line

2.8.1 Layout and Structure

High-intensity proton beams that generate neutrons in the mercury target is produced at the 3-GeV rapid-cycling synchrotron (RCS). Its characteristics are summarized in Table 2.8.1. The proton beam is transported through a beam line that connects the accelerator and the MLF building. The 3-GeV proton beam transport (3NBT) line[2.8-1, 2, 3] plays an indispensable role to accept the high-intensity proton beam from RCS synchrotron, transport it with extremely low beam loss rate (< 1 W/m) and finally tailor it in the optimal condition for secondary beam production targets in MLF. The layout of the 3NBT line (Figs. 2.8.1 and 2.8.2) is not necessarily ideal, since J-PARC is a multi-purpose research facility with accelerator complex and was built in the open site close to existing buildings and the site boundary with several geometrical constraints. The MLF building is located inside the 50-GeV synchrotron (MR) tunnel rather than close to the RCS. As a result, the 3NBT line extends 258 m long from the RCS synchrotron tunnel till the MLF building. The beam transport line in the most upstream section is branched to the beam injection line to the 50-GeV synchrotron (MR).

The 3NBT tunnel is thin and long and both ends connected to massive structures, RCS tunnel and MLF building. The 3NBT tunnel is rather fragile from the viewpoint of civil engineering. Therefore, both ends of the tunnel were joined "softly" with elastomer materials as an expansion joint. These isolate the tunnel from the movements of the adjacent structures and keep its structure in good shape. The beam line magnets, on the contrary, may go out of alignment because of uneven settlement among the tunnels and the building, even though they were built on many strong piles. The MR tunnel and the neutrino decay volume are crossed beneath the middle of the 3NBT tunnel. The 3NBT tunnel is disconnected completely and its weight is supported with its own piles. The floor of the 3NBT tunnel and the ceiling of the MR tunnel have enough thickness in terms of radiation shield and the personnel access to a tunnel is not restricted with the beam operation in the other tunnel.

The beam dump is placed in the upstream of the 3NBT tunnel and is used for beam study and beam tuning of RCS. The beam dump was buried under the floor of the tunnel and the proton beam was bent vertically to the beam dump. The pathway in the 3NBT tunnel is not interrupted with the beam duct to the beam dump, which increases the maintainability of the beam line components. The amount of the shielding for the beam dump decreased as compared with other configurations and the sky shine was decreased substantially.

The beam line inside the MLF building is further 57 m long to a neutron production target. A muon production target lies in cascade[2.8-1, 3, 4, 5, 6] along the proton beam line just before a neutron production target (M2 tunnel) in the MLF building shown in Fig. 2.8.3. The proton beam has interaction with the muon production target and primary protons are scattered or secondary particles are generated. Large beam loss is, hereby, expected and poses serious measures to high-radiation environment for beam line components and facilities.[2.8-5, 6] It is necessary to localize the beam loss rather than scatter it all along the M2 tunnel. The beam line components have to be designed to stand for high radiation circumstance and to be maintained semi-remotely without getting close to high dose points. The air in high-radiation tunnel, furthermore, imposes intricately intertwined problems, such as activation and corrosive gas formation. The realization of the cascade target system largely depends on the realistic solution to this issue.

The M1 tunnel between the 3NBT tunnel and the M2 tunnel has been reserved for the second muon production target in future. For the time being the M1 tunnel is treated in the same manner as the 3NBT tunnel in terms of the beam transportation.

The major parameters of the proton beam line are summarized in Table 2.8.2 and the layout of the beam line components are depicted in Fig. 2.8.2. The beam line tunnel around straight section B and vertical bend section is shown in Photo. 2.8.1. In this section the 3NBT facility is described mainly in terms of the following components.

a) proton beam optics
b) beam line magnets and their DC power supplies
c) proton beam monitors and data acquisition system
d) vacuum beam duct and vacuum components
e) proton beam window
f) beam dump
g) coolant system
h) control and interlock system

2.8.2 Proton Beam Optics

The beam optics[2.8-3, 4, 5] is the very basis for designing the beam transport facility. The beam transport line consists of two parts of very different characteristics, quite low beam loss rate in the 3NBT tunnel and high radiation environment in the M2 tunnel. The design policies of the beam optics are optimized for respective requirements.

The beam optics was studied with calculation codes of TRANSPORT[2.8-7] and MAD.[2.8-8] We developed a calculation code that gives us the data file of the coordinates of beam line magnets from the results of TRANSPORT and MAD. The data file can be read with CAD software VECTORWORKS and shows the drawing of the optics calculation instantly. This method was extended to the 3-50 BT lines and the beam optics and the layout of the magnet were efficiently determined for both 3NBT and 3-50 BT lines.

(1) Beam optics in 3NBT line

The layout of the beam transport line was determined so that it had been arranged with dipole magnets of the same bending angle. This was expected to reduce design cost, manufacturing cost and maintenance cost of the bending magnets. As a result a bending angle of 7.5° was adopted. The beam is elevated with a dipole magnet of 7.5° vertical bending angle and the 30° horizontal bend section consists of 4 dipole magnets of 7.5° vertical bending angle. The exceptions are the most upstream bending magnet, which has the bending angle of 10.3°, and the vertical bending magnet to the beam dump, that has the bending angle of 11.8°

The pulse bending magnet is installed just the most upstream bending magnet, which switches the proton beam to the injection beam transport line (3-50BT line) into 50-GeV synchrotron (MR).

The beam line components in the 3NBT tunnel, such as magnets and beam monitors, have to be maintained in hands-on manner. The beam loss rate should be smaller than 1 W/m to keep residual radiation activity in the components below certain level. This upper limit is extremely low enough, compared with the beam of 1 MW that is to be transported though this line. Therefore the beam optics has to be designed to show no beam loss in any possible situations.

The emittance of the beam extracted from the RCS, which is 324π mm·mrad, is determined by the aperture of the collimator located at the RCS. The beam orbit may be disordered with several factors; the instability of the kicker magnets at the extraction section of the RCS, the non-uniform magnetic field of the bending magnets and the quadrupole magnets and the misalignment of the magnets. The beam radius will be also expanded with these factors. If the beam radius is smaller than the aperture of the beam duct all the way along the beam line, no beam will be lost in theory. The beam optics was designed with the possible distortion factors taken into account.

At the extraction section of RCS, the beam is extracted by using the eight kicker magnets. When the power supplies are turned on, the output currents oscillate for a while. This causes 1% instability[2.8-9] in each kicker magnets. In the worst case, the angle and the position of the beam may be distorted by 0.33 mrad and 1.6 mm, respectively, at the exit of the extraction septum magnet of the RCS. These instabilities are intrinsic value and impossible to be reduced substantially. The allowable uniformities of the beam transport magnets were, therefore, determined so the effect on the distortion of the beam orbit would been comparable to that of the kicker magnets. The non-uniformity in $B{\cdot}L$ product (the integration of the magnetic flux density B along the beam path) of the bending magnets was required to be smaller than 5×10^{-4} and the non-uniformity in G·L product (the integration of the magnetic field gradient G along the beam path) of the quadrupole magnets was required to be smaller than 2×10^{-3}. The effects of these non-uniformities are verified with some simple 3-D tracking calculations.

The allowable misalignments of the beam line magnets were also investigated in similar manner. In the analysis, the center orbit of the beam was assumed to be able to be corrected by exciting steering magnets properly with the information from beam monitors. It was found that the alignments of the beam line magnets should have been better than the accuracy of 0.5 mm in position and 0.5 mrad in direction.

It is known that the momentum bite of the beam will be about 1%. The dispersion functions D were made zero for both horizontal and vertical directions[2.8-3, 8] with double-bend-achromatic (DBA) method to minimize the momentum spread effect on the beam radius.

In Fig. 2.8.4, beam optics parameter along beam line shows that the dispersion becomes to zero at all the place except bending area. By this design, we aimed to avoid cost up due to large enhancement on beam radius by the momentum spread.

(2) Beam optics in M2 tunnel

The muon production target is inserted in the proton beam line of the M2 tunnel. The protons have interaction with a 20 mm thick graphite disc and muons and pions are generated. Several percents of the proton beam is dissipated in the target[2.8-10)], which causes enormous radiation. Reduction of the effect of the beam scattering was very important issue in early stage of the beam optics design. When the proton beam is focused on the muon target, the beam diverges after passing through the target even though the beam does not interact with the target material. The growth of divergence due to the scattering is, therefore, kept relatively smaller. The small spot of the proton beam is also good for making muon beam of small beam emittance. The maximum field gradient of the quadrupole magnets was turned out to be 8 T/m with this optics design.

In the downstream of the muon production target, collimators are located to localize the beam loss. The acceptances of the collimators were made larger than the emmitance of the maximal beam halo (324π mm·mrad), taking into account the distortion of the beam central orbit and the growth of the beam emittance, as mentioned in previous part (Beam optics in 3NBT line). Two 700 mm long collimators were employed, which were made of oxygen-free copper and cooled with pure water. The hole of the collimator has conical shape, whose inner diameter ranges from 74.2 mm to 81.6 mm in the first collimator and from 85.2 mm to 92.6 mm in the second collimator. They are placed at 395 mm and 1,222 mm from the muon production target along with the beam direction, respectively.

2.8.3 Electromagnets

The electromagnet system of the beam transport line consists of bending magnets, quadrupole magnets and steering magnets. All the magnets are operated with DC current. The magnets have been designed[2.8-2)] to satisfy the requirements from the beam optics as described in section 2.8.2.

The beam loss was designed to be smaller than 1W/m. The cumulative dose for 30 years operation was found to be approximately 1 MGy with the calculation of radiation. Radiation-resistant components were adopted as much as possible for all the electromagnets and other devices placed in the beam tunnel as well.

(1) Bending magnets

Six horizontal bending magnets are installed in the beam line. Their bending angles are 7.5° except the most upstream one, which has bending angle of 10.3°. Vertical bending magnets are placed at both ends of the slope section. Their coils and yoke have the same design parameters as the horizontal bending magnets. The magnetic field of the bending magnets requires high uniformity, that is $\Delta B{\cdot}L/B{\cdot}L < 5{\times}10^{-4}$ ($B{\cdot}L$ is the integral of magnetic field along beam path) within 100 mm of both sides of the central beam orbit. Several design schemes are adopted to obtain utterly high field uniformity for limited magnet size as follows; window frame type of yoke, magnetic poles of sector type, shims at both edges of the poles along the beam axis and end plates at the beam entrance and exit sides. Their sizes and parameters were carefully optimized with three-dimensional field calculations using OPERA code. The faithful computation models had to be extended well outside of the magnet because the leakage of the magnetic field is not negligible to aim at the uniformity of 10^{-5} level. The magnetic properties of the yoke iron offered by a steel manufacturer were used to increase reliability of the computation. The parameters of the bending magnets are summarized in Table 2.8.3.

The bending magnets were manufactured and installed (Photo. 2.8.2) by NEC TOKIN Corporation (Sendai, Japan). Their magnetic field was measured at the nominal operation point and its $\Delta B{\cdot}L/B{\cdot}L$ is plotted as a function of the distance from the beam axis in the horizontal plane with the result of the calculation (Fig. 2.8.5). The measurements show good agreement with the design calculation and also satisfy the design criterion well.

In order to perform cross check of the magnetic field distribution, we also carried out field measurements by ourselves (Photo. 2.8.3). A simple 3-D stage has been developed, which is controlled by GPIB. As for the magnetic field measurement, 3-D hall probe was utilized. In order to compensate temperature property, a small thermocouple is attached on the hall probe and the result is corrected for the temperature behavior in off-line analysis. It is found that the measurements by us agree very well with the result by the magnet maker. In early stage, for the quadrupole magnet, the number of mapping points by the magnet vendor is not enough so that the wrong shape of end shim plate attached magnet was missed. By the cross check measurement, such miss design can be easily found and revised by attaching appropriate end shims.

(2) Quadrupole magnets

The beam optics design requires wide range of magnetic field gradient and bore diameter for quadrupole magnets. Those parameters are classified into three groups in terms of bore diameter and pole length. Quadrupole magnets in the 3NBT tunnel have either 220 mm or 300 mm of bore diameter. Quadrupole magnets in the M2 tunnel have 260 mm of bore diameter with mineral insulation cable (MIC) for coils. They have a radiation shield plug on their yoke. Quadrupole magnets require the uniformity of $\Delta G{\cdot}L/G{\cdot}L < 3\times10^{-3}$ ($G{\cdot}L$ is the integral of magnetic field gradient along beam path) inside their bore. The poles of the quadrupole magnets are of hyperbolic shape. They also have shims at their both edges along the beam axis and 45° cut at the edges of the beam entrance and exit sides to achieve very high uniformity of field gradient. Their sizes and parameters were carefully optimized with three-dimensional field calculations using OPERA code. The faithful computation models had to be extended well outside of the magnet because the leakage of the magnetic field is not negligible to aim at the uniformity of 10^{-4} level. The magnetic properties of the yoke iron offered by a steel manufacturer were used to increase reliability of the computation. The parameters of the quadrupole magnets are summarized in Table 2.8.4.

The quadrupole magnets were manufactured and installed (Photo. 2.8.4) by Tokin Machinery Corporation (Sendai, Japan). Their magnetic fields were measured at a few typical operation points and their $\Delta G{\cdot}L/G{\cdot}L$ is plotted as a function of the distance from the beam axis in the horizontal and vertical planes with the results of the calculations (Fig. 2.8.6). The measurements show good agreement with the design calculation and also satisfy the design criterion well.

(3) Steering magnets

Steering magnets, which correct the proton beam orbit, have two types, horizontal bending and vertical bending dipole magnets. They are of wind-frame type and their pole gaps are either 220 mm or 300 mm in the 3NBT tunnel. The steering magnets in the M2 line have 260 mm of pole gap with MIC coils and a radiation shield plug on their yoke. The parameters of the steering magnets are summarized in Table 2.8.5.

(4) DC power supplies

High stability and low ripple current are required for the DC power supplies. High reliability is also a key to performance of high-quality beam transportation. The drift of output current and the ripple current of power supplies for bending magnets were designed to be smaller than 1×10^{-5}, which is better than the uniformity in $B{\cdot}L$ of the bending magnets. The stabilities for power supplies to quadrupole magnets and steering magnets were 10^{-4}.

The power supplies over 100 kW of output power for bending magnets have adopted a 12-phases psyristor and a transistor dropper for rectifier. Those below 100 kW of output power have an insulated gate bipolar transistor (IGBT). The power supplies for steering magnets have bipolar output and their rectifier is either an IGBT or a transistor dropper, depending on their output power. Output current is read with a DCCT (DC current transformer). The power supplies for bending magnets have two DCCT's to control output current to achive higher stability.

The power supplies have simple self-diagnostics system to increase reliability. It monitors output current in terms of setting value and actual readout and gives alarm if they show discrepancy larger than threshold. It also monitors the temperatures and performance of indispensable parts. This enables us to replace parts before breakdown or find out trouble point easily.

Each beam line magnet is connected to an individual DC power supply, whose output current can be set independently. Two adjacent quadrupole magnets and their power supplies are connected with three cables rather than four cables as shown in Fig. 2.8.7. The currents to two magnets in the common cable will cancel to some extent, which reduces the amount of the heat generation in the cables as well as the quantity of cables. It was confirmed that those two power supplies could be operated without any interference even though one of them had tripped.

All the power supplies can be monitored and controlled remotely. The operating data inside power supplies, ADC readout of output current and setting data of output current are communicated in parallel with programmable logic controllers (PLC), which are connected to the main control system in J-PARC accelerator, EPICS (Experimental Physics and Industrial Control System) [2.8-11)] via network.. The exceptions are an interlock signal for Personnel Protection System (PPS), an interlock signal for Machine Protection System (MPS) and a signal on beam operation mode, which are connected directly with hard wires.

2.8.4 Proton Beam Monitors

Proton beam monitors plays a very important role for the beam diagnostics on the beam transport line[2.8-12]. The condition of beam loss has to be watched all along the beam line to clear the important criterion for hands-on maintenance. The beam orbit is adjusted by looking at beam positions and beam halo. It is important to monitor beam profile in the high-intensity accelerator facility since excessive beam current density might cause serious damages in beam line components. The monitor system developed 3-GeV beam transport line (3NBT) summarized in Table 2.8.6.

.

(1) Beam intensity monitor (CT)

Integration current transformer (CT) was developed with a commercially available beam charge monitor (BERGOZ Instrumentation). The CT is decoupled from titanium chambers with ceramic insulator along beam direction to avoid the effect of wall current in the monitor. Nine CT's are installed in the main beam line and one CT is in the branch line to the beam dump. The signal from CT is fed to local control room (LCR) with a SUCOFEED corrugated coaxial cupper cable of flame-resistant type to diminish noises. The signal is attenuated and read with a charge integrated ADC developed by Technoland Co. Ltd. The characteristics including the cable and the readout system were measured with one turn coil in the center of the CT and a high voltage switch in advance of installation. It was found that the present system had good linearity in the dynamic range corresponding to the intensity of the proton beam. The beam current is calculated with this coefficient. The measurement of the CT characteristics is shown in Photo. 2.8.5.

(2) Beam profile monitor (PM) and halo monitor

The proton beam profile can be obtained by measuring the secondary electrons emission from wires placed in proton beam.[2.8-13] Eleven monitors are installed in the 3NBT tunnel and the M1 tunnel. These monitors have 32 wires tensed on a ceramic frame at intervals of 6 mm both in horizontal and vertical directions. Silicon carbide (SiC) wires have been adopted because of longer lifetime than tungsten wires that had been normally used for profile monitors. The aperture of the ceramic frame is 220 mm × 220 mm, which is determined to avoid hit of the beam peripheral. The ceramic frame has 0.2 mm thick aluminum electrodes on its four sides to observe the secondary electrons if the beam halo hits an electrode. The proton beam profile monitor is shown in Photo. 2.8.6. The monitor head was designed to be retracted to prevent unnecessary irradiation. In normal beam operation, the monitor head is swung off the beam orbit position. Signals of multi-wire profile monitor and halo monitor are fed to the LCR with a flameproof twisted pair cable and a coaxial cable, respectively. These cables are typically ~300 m long.

Three profile monitors were placed in the M2 tunnel. One of them was integrated into the muon production target assembly. Twenty-three SiC wires are tensed with the pitch of 3 mm on the frame, which has the aperture of 80 mm × 80 mm. The target assembly can be moved vertically and either the muon target or the profile monitor is selected at the beam position. The other two monitors are installed solely at the monitor position. They have the frame aperture of 220 mm × 220 mm and 23 SiC wires with the pitch of 6mm. Mineral Insulation (MI) cables were adopted for signal cables in the M2 tunnel because of high radiation environment.

A prototype of the profile monitor was manufactured and tested with 500-MeV proton beam at KEK to obtain the characteristics of signals from SiC wires and design electronics for data acquisition system. It is found that the signal termination with high impedance gives good S/N. Widely available ADC modules of CAMAC (Computer Automated Measurement and Control) standard [2.8-14] have negative signal input. The multi-wire profile monitor provides positive signals and inverter amplifiers are necessary before putting the signals to an ADC module. Noise reduction function was incorporated into the inverter amplifier module, which can diminish a common mode noise by subtracting the signal from the cable without connection of a sensor wire.

(3) Beam loss monitor (LM)

The beam losses in the 3NBT line are monitored all the time during beam operation. If one of the amounts of the beam losses exceeds a threshold, the proton beam has to be stopped immediately. Quick response and high reliability are required for the protection system.

The beam loss monitors in the 3NBT tunnel and the M1 tunnel are proportional gas counters of 30 cm long cylindrical shape, which is filled with PR10 gas of 0.11 MPa. Photo. 2.8.7 shows a loss monitor when gas is being filled. The beam loss monitors were placed at every quadrupole magnet since the beam size gets larger there. A set of four monitors are placed on top, bottom, right and left of the beam duct at upstream side of the magnet, as shown in Photo. 2.8.7. When PR10 gas in loss monitors is degraded by radiation, it can be easily refilled. An air-ionization chamber is adopted for loss monitors in the M2 tunnel, since the maintenance work is quite difficult. There are 54 quadrupole magnets in total and 54 sets of loss monitors were installed.

The response to radiation was checked with gamma-rays from ^{241}Am before actual operation. It was found that the low energy gamma-rays at a level of several keVs produce a photo peak in the output signal.

The signal from the loss monitor is directly transmitted to a local control room via a high-voltage cable without a preamplifier to minimize the number of cables and to prevent the cables from breaking down due to radiation. The signals are amplified and divided with an amp-divider module and then fed into a charge sensitive type of ADC's and a comparator module in Machine Protection System MPS (see Section 2.8.10). If the signal from loss monitor gets higher than a threshold level of the comparator, MPS interlock signal is generated and the proton beam will be stopped within 40 ms.

(4) Beam position monitor (BPM)

The principle of beam position monitor is that an electrode generates induction current when beam passes through nearby. The amplitude of the current is proportional to the distance between the electrode and the beam. In a beam position monitor four electrodes are placed the inner surface of a beam duct surrounding the beam (Phot. 2.8.8). The centroid of the beam can be estimated by comparing the amplitudes of the induction current from the electrodes facing each other. When the amplitudes differ by 1% the beam lies 0.2-0.3 mm off the center of the beam duct. The signals from the beam position monitors are transmitted with thick coaxial cables of 8D type (impedance of 50 Ω) to diminish any distortion in the signal. Those cables were carefully arranged to be of exactly equal length. The signals are fed into a digital storage oscilloscope (DSO6014L of Agilent Technologies, Inc.), which can be connected to network and operated in EPICS. The peak to peak amplitudes of the signal voltages are compared and the beam position is deduced.

Two beam position monitors were inserted in the quadrupole magnets QX1 and QX3 in the most upstream area and they are mainly used to adjust the extraction beam from the RCS. Two monitors BPM1 and BPM2 were placed both sides of the pulse bending magnet (PB), which switches the beam to the MR. These monitors watch the effect of residual magnetic field of the PB.

The proton beam pulse from the RCS has normally two bunches separated by ~600 ns. The beam positions of the bunches might be different because the magnetic field of the RCS extraction kicker magnet has ringing in the early stage of the flat top time region. It is necessary to know the difference for better beam operation. Two time frames were, therefore, set in DSO and each of them was adjusted to synchronize one of the bunches. The beam position of each bunch was successfully obtained by switching the time frame alternatively.

(5) Beam monitor system at the proton beam window

The most downstream beam monitors were integrated into the proton beam window that divides the vacuum of the beam transport line and the helium vessel of the neutron station, rather than installed solely. This decision helps us to improve maintenability and reduce the cost of radiation shielding. Two profile monitors and two halo monitors are introduced as shown in Photo. 2.8.9. The profile monitors cannot be extracted from the beam line because of no space for this motion and quite high radiation. As a result, the proton beam hits wires all the time and radiation damage is inevitable. In the point view of the reliability, two profile monitors were decided to be inserted, one with SiC wires and the other with tungsten wires. These will provide useful information on the lifetime of profile monitor for higher intensity beam operation in future.

The proton beam profile is oblong at the proton beam window and the aperture of the profile monitors is 234 mm wide and 100 mm high accordingly. The numbers of the sense wires are 32 and 14 wires in horizontal and vertical directions, respectively and the wire pitch is 7 mm in both directions. The signal cables are selected in terms of radiation-resistivity, namely mineral insulation (MI) cable outside of the vacuum region and polyimide cables covered with small ceramic sheathes inside the vacuum region. The latter has the merit of low gas emission rate in vacuum.

Two kinds of beam halo monitors were also integrated into the proton beam window. The one detects secondary electrons and the other is a set of thermocouples that measures temperature rise. The apertures of both beam halo monitors is 190 mm wide and 75 mm high, which are slightly smaller than those of the beam profile monitors and the beam entrance hole of the reflector in the neutron target station

(200 mm × 90 mm).

(6) Beam monitor at 3NBT dump

A fixed type of beam profile monitor and a beam halo monitor are located at the entrance of the 3NBT beam dump. The maximal beam power allowable for the beam dump is limited by the temperature. Thermocouples were placed around the beam dump and their signals were monitored all the time during the beam operation. If the temperature exceeds a certain level, the proton beam is immediately stopped with the MPS.

(7) Electronics and data acquisition system

The signals from the beam monitors are processed mainly with NIM (Nuclear Instrumentation Module) standard modules and then measured and/or controlled with modules having CAMAC (Computer Automated Measurement And Control) bus. Their design was based on the well-established system in the proton beam transport facility of KENS, KEK. Some modules were too old to reproduce and their substitute were newly designed and manufactured for J-PARC. They were verified and tuned with proton beam in KEK and the gains and the termination impedances of the modules for beam profile monitor and beam loss monitors were obtained.

The design criteria for the DAQ system were the capacity to acquire the data from all the beam monitors for every beam pulse of 25-Hz repetition. This would be very useful to analyze the data off line and to study any causes for possible failure events. The ADC modules and signal comparators are CAMAC bus modules and amplifier modules and signal divider modules are NIM standard modules. Several CAMAC crate controllers CC/NET (TOYO Corporation, Tokyo, Japan) are incorporated in the system. They have an onboard personal computer and work as EPICS field I/O modules (see subection 2.8.10).

The ADC CAMAC modules have 16 inputs and of single width. A crate controller CC/NET can handle 23 modules in a crate at maximum. One has to read 352 data at 25 Hz when a crate is filled with the ADC modules. Considering the CAMAC bus speed and CAMAC command operation speed; it takes longer than 40 ms for a crate controller to read all the data individually. A programmed I/O (PIO) technique is used to read ADC data effectively. The whole data are treated as single waveform data and read with one command session. This method can reduce the read time and the CPU load of the crate controller by one third. It can also lighten the network load among EPICS IOC's.

A CC/NET crate controller also controls loss monitor comparators, loss monitor high voltage supplies, output registers and attenuators for CT. The temperature of 3NBT beam dump is monitored directly with EPICS. If the temperature of the beam dump gets higher than a threshold, an MPS signal is generated with an output register. Expanded EPICS waveform records are written for these modules.

The high voltage power supplies to the loss monitors are controlled with an exclusive CAMAC interface module. Their voltages can be set at the front panel of the module. Switching them on and off and monitoring the voltages can be done with a CAMAC crated controller.

A digital oscilloscope module DSO6014L does not have a control panel or a display on its own body. One is controlled and monitored with EPICS.

Fig. 2.8.9 shows the PC components of the 3NBT monitor system. The 3NBT facility has two control rooms, one in the 3NBT building and the other is in the 3NBT downstream part of the MLF building. In the control room of the 3NBT building, there are three CC/NET crate controllers, an EPICS IOC server and several DSO6014L digital oscilloscope modules. In the control room of the 3NBT downstream part, there are four CC/NET crate controllers, an EPICS IOC server and several DSO6014L digital oscilloscope modules. All these modules are connected to a private Ethernet LAN.

The DAQ system for beam monitors is synchronized with the timing signal of proton beam pulse from the central control room (CCR). This timing signal is divided, delayed and sent to the ADC modules as a signal gate and to the CC/NET crate controllers as an operation trigger.

The EPICS IOC servers are used as OPI and data server as well. They receive monitor data from CC/NET crate controllers and process them for OPI and data archive. PostgreSQL is used as database software. Monitor data records are archived with the data of year, date, time and tag number. The tag number is allocated to every proton beam for identification.

JAVA program and EDM, which is EPICS extension program, are used as an operator interface. These OPI programs enable us not only to watch real time data but also to display snapshot data and archived data. The archive data are read from the data server by selecting date/time or a tag number. The EPICS IOC servers are also used as an NFS server for CC/NET crate controllers.

In some accelerator studies 181-MeV proton beam is transported directly from the Linac to the 3NBT beam dump without acceleration in RCS. The timing and its structure are totally different from those in the normal operation. The timing system has two timing mode, which can be selected remotely.

2.8.5 Vacuum System

The proton beam pulses turns tens of thousand times in the ring of the RCS. Ultra high vacuum, such as 1×10^{-6} Pa, is required for the vacuum system in RCS to reduce the amount of scattering with the residual gas in the beam duct. The vacuum pumping system for the beam ducts is designed to get the vacuum better than 1×10^{-6} Pa.

Achievable gas pressure was estimated in the following way. The outgassing rate Q is expressed with the following equation,

$$Q = A\cdot L\cdot R$$

where A is the surface area of a beam duct per unit length, L the length of a beam duct and R an outgassing rate per unit surface area. The outgassing rate (R) depends largely on surface finishing of a beam duct and is reasonably assumed 1×10^{-8} Pa·m^3/s/m^2 with proper surface treatment and removing grease. When the diameter of a duct is approximately 0.3 m and the L is 320 m, the outgassing rate Q is 3×10^{-6} Pa·m^3/s. In the case of the system with 7 pump units distributed along the beam duct in equal spacing, Q is 4.3×10^{-7} Pa·m^3/s for each pump unit.

The achievable pressure P is estimated with the following equation,

$$P = Q/\nu_e$$

where ν_e is an effective pumping speed. It is expressed as

$$1/\nu_e = 1/\nu + 1/C$$

where ν is a pumping speed and C is a conductance of the pump. The conductance is shown as

$$C = 121 \times D_p^3/L_p$$

where D_p is the diameter of a pump entrance and L_p is the length between the duct and the pump. In the case of the 3NBT vacuum system, D_p is 0.3 m and L_p is 0.5 m. The effective pumping speed ν_e is, therefore, 0.5 m^3/s and the achievable pressure turns out to be 8.7×10^{-7} Pa. The outgassing rate can be reduced by pumping the duct for many hours. The vacuum in the upstream section of the 3NBT line is improved furthermore by getting the distance between the pump units shorter.

The criterion of outgassing rate is set better than 1×10^{-8} Pa $m^3/s/m^2$ after 50-hours pumping. This is applied not only for the beam duct but also all other vacuum components such as the proton beam profile monitor and the beam stopper. Two candidates were compared, stainless steel (SS 316L) with electrochemical buffing (ECB) and pure titanium (JIS type-2) without special surface treatment, as material of vacuum beam ducts. Although the outgassing rate and the cost are comparable, pure titanium is superior to stainless steel in terms of maintenance and magnetic properties. Titanium is lighter and more elastic, and residual radiation dose is expected much lower, which surely reduces the burden of the maintenance work. The conclusive factor was that the magnetic susceptibility (χ) of pure titanium is very small (3.19×10^{-6} cm^3/g) even at welding parts and does not distort magnetic distribution at all. All the beam ducts are made of pure titanium. They were baked at 150 °C for 24 hours after fabrication and typical outguessing rate turned out to be ~8×10^{-9} Pa $m^3/s/m^2$. Pure titanium was adopted as the material of other vacuum components such as beam profile monitors as much as possible.

Based on the calculation above, seven pump units were installed in the 3NBT vacuum system (Fig. 2.8.10), which were distributed at narrower intervals in the upstream region to get better vacuum. Each pump unit consists of a sorption ionization pump (SIP), a turbo molecular pump (TMP) and a roots pump. SIP is preferable in radiation circumstance because it does not have any dynamical mechanism. A sorption ionization pump of Low Profile 800LX manufactured by Gamma Vacuum has been adopted. A turbo molecular pump of TG900MRKAB of Osaka Vacuum is employed, which has the exhaust velocity of 1000 ℓ/s and a multi stage roots pump ACP28S manufactured by Alcatel Vacuum Technology is attached as backing pump of the TMP. In the M1 tunnel, the TMP has to run all the time because of the large leak rate in the M2 line.

All metallic gate valves made by VAT, which are resistant for absorbed dose of 10^8 Gy, are used in the beam line. Fast closing valves are also required for emergency. One of possible failures is that the water-cooled proton beam window of the neutron target or the muon production target is broken and the cooling water rushes into the beam duct. It takes 27 ms to close a fast closing valve of flap type. Since water molecules fly for ~15 m before the valve is closed, the fast closing valve is located at least 20 m upstream of the proton beam window. A fast closing valve (FCV) from VAT is installed in the downstream part of the 3NBT tunnel and additional fast closing valve (FCV) is placed in the upstream part near the 3-GeV RCS to minimize possible damage to the accelerator. Two HV sensors that activate FCV's are located on the top of proton beam window assembly and in the M1 tunnel for redundancy.

Metal seals are used in the beam line and delta type of HELICOFLEX seals are used to connect vacuum ducts and other vacuum components. The standard of the vacuum flanges are made common in J-PARC accelerators and beam transport lines to use aluminum chain clamps from CEFILAC.

In the M2 tunnel a new seal technique, a pillow seal, was adopted since the vacuum components have to be connected and disconnected remotely in the high radiation environment. The principle of seal mechanism is that a diaphragm of a pillow seal is inflated with compressed gas and pressed onto a counter flange. In our case a pillow seal has two diaphragms and the gap between the inner and outer diaphragms is evacuated with differential pumping to obtain better seal performance. This type of pillow seal was found to provide leak rate better than 1×10^{-6} Pa·m^3/s. The pillow seal with double diaphragms are adopted for the proton beam window as well.

The control system of vacuum is also incorporated into the system run by EPICS.[2.8-11)] All the signals from the vacuum pump controllers, the vacuum valves and the vacuum gages are fed into PLC and all the devices can be operated remotely via network. The trends of these signals can be easily read from the database and plotted on a screen, which would be of great help for the diagnostics of the system. If the vacuum gets worse than 1×10^{-4} Pa, the MPS interlock signal is generated and the proton beam stops immediately.

2.8.6 Proton Beam Window

A proton beam window (PBW) is one of the very important components in the spallation source, which separates the accelerator region of ultra-high vacuum and the target region filled with helium gas of 0.1 MPa. The whole assembly of the proton beam window (PBW) is shown in shown in Photo. 2.8.10. Since the PBW is continuously irradiated with high intensity proton beams, extreme high radiation resistance is required for its material. The seal performance is also important for the selection of the material. The PBW is expected to be highly activated. It has to be handled with remote handling manipulators for exchange with new one.

A schematic view of the whole assembly of the proton beam window is shown in Fig. 2.8.11. Since the shielding plug is attached on the top of the window, the PBW assembly is as heavy as 10 t. A cross sectional view of the PBW is shown in Fig. 2.8.12. The window consists of 2.5 mm thick aluminum alloy plates with 3-mm gap between, where cooling water flows in horizontal direction. The cooling water is supplied with the coolant system for the reflector and the moderators.

(1) Window material

The selection of the window material is very important. The first candidate was INCONEL alloy, which has been used in LANSCE. 1.5 mm thick plates were required for the 3NBT line from the viewpoint of structural strength. The optics calculation indicated that the beam scattering in the INCONEL plates was not small enough. Aluminum alloy ($AlMg_3$) was then studied for window material, which has been used in PSI. Its experience showed the high endurance of radiation up to 7 dpa. Although thicker plates are required for the window, not only the beam scattering but also the heat deposition is expected to be reduced. The heat deposition in two 2.5 mm thick $AlMg_3$ plates decreases from 1.7% to 1.2% and the beam loss gets smaller from 1.7 % to 1.2% accordingly.

The result of the heat analysis is shown in Fig. 2.8.13. In this analysis, the flow speed of the cooling water was 1.6 m/s and the heat transfer coefficient was 9,000 W/m^2K. The beam profile was assumed to have a uniform distribution in phase space. The maximum temperature was 60°C, which is lower than the allowable temperature of 100°C. The maximum stress in the window is 23 MPa, which is much smaller than the allowable stress of 90 MPa. Considering the results mentioned above, aluminum alloy ($AlMg_3$) has been selected as the window material and the alloy A5083 specified by JIS (Japanese Industrial Standards) was used for its manufacturing.

(2) Pillow seal

A new type of pillow seal was developed to connect and disconnect the vacuum remotely. The detail of pillow seal is described in section 2.8.5. The beam radius is expanded at the neutron target to decrease the peak beam current density. A pillow seal of 0.6 m in diameter was required, which was much larger than conventional products. The seal performance was tested by the manufacturer, as shown in Photo. 2.8.11. It showed that the flatness of diaphragm was important to get good seal performance. After the PBW was installed in its housing of the neutron target station, the seal performance was tested again. Helium gas was fed from the top of the shield plug to the outside of the pillow seal and the leak rate was measured through the multi-purpose hole, which was connected to the vacuum side of the PBW. It was found that the leak rate was 7×10^{-7} Pa m^3/s, which satisfied the criterion of the vacuum system.

(3) Beam monitors

The beam monitors in the PBW are described in section 2.8.4. All the monitors are assembled in the vacuum region of the PBW. The signals from the beam monitors are extracted from the top of the shielding plug with mineral insulation (MI) cables. The calculation suggested that the radiation dose around at the signal cables was extremely high and standard insulator cannot stand for it. The radiation dose on the top of the shielding plug is expected less than 1 mSv/h after irradiation, which allows hands-on maintenance. The signal cables can be connected and disconnected there with hands.

(4) Installation of the PBW

If the pillow seal and/or the counter flange are scratched during the installation, it may spoil the seal performance. Guide rails are put on the housing of the PBW and guide pins on the shielding plug to avoid such serious scratches. Furthermore, a counter weight is placed on the shielding plug to keep the PBW assembly exactly upright, Fig. 2.8.14 shows the clearance between the pillow seal and the counter flange during the installation, which is estimated at least 3 mm.

(5) Remote handling system for maintenance

Avoiding excessive radiation exposure to personnel is one of the quite important issues to design components that may get highly activated. A special cask dedicated for the maintenance of the PBW assembly has been developed and manufactured. The PBW assembly can be lifted up into the cask remotely with the combination of the special gripper of the cask and the attachment on the top of the shielding plug. The gripper and the attachment can be connected and disconnected safely with a key and a keyway. The cask has massive radiation shielding around its body.

The sequential work for replacing the PBW assembly was demonstrated before beam operation. The PBW assembly is pulled into the cask and transported into the drying room, where the residual cooling water in the PBW is purged completely. The PBW is hoisted again into the cask and moved to the hot cell. The bolts that fix the PBW to the shielding plug are unscrewed with a power manipulator. The PBW is then replaced with a new one by using the remote exchanging system, which is commonly used for the reflector and the moderators of the target station. The pipes of the used PBW can be cut into small pieces with the specially developed cutting device to reduce the volume of radiation waste. The assembly with the new PBW is installed into the housing with the cask as shown in Fig. 2.8.14. The whole sequence was successfully demonstrated except for cutting pipes.

2.8.7 Beam Dump

(1) Outline

The beam dump[2.8-16)] used for the beam commissioning and the beam study of RCS was located in the most upstream section of the 3NBT lines. The conceptual drawing is shown in Fig. 2.8.15. The proton beam is bent downward with a vertical bending magnet and injected into the beam dump. The major roles of the beam dump are to stop the proton beam, to shield the secondary particles such as neutrons and to minimize the activation of the soil and the groundwater around the beam dump. The beam dump is made of iron slabs covered with concrete walls. An active cooling system was not adopted because the maximal injection beam intensity was limited to 4 kW. The beam duct of the main beam line branches at the vertical bending magnet and the beam duct is embedded in the center of the assembly of iron slabs. The vacuum of the beam duct is separated from that of the main beam duct with a thin window because the vacuum in the main line is much better than that of the dump duct. A pumping port is placed in the upper part of the beam duct above the tunnel floor. The beam duct is evacuated down to less than 10 Pa with the roots pump before a beam operation period starts. The beam duct is then shut off with the gate valve and the roots pump is left turned off during the beam operation period.

(2) Design condition

Design conditions of the beam dump are summarized.

1) Beam operation

The proton beam energy injected to the beam dump is 3 GeV[1]. The maximal beam intensity is 4 kW. The continuous beam operation for the beam dump is less than 48 hours.

2) Shielding during the operation

J-PARC project set the design limit of dose in soil area to be less than 11 mSv/h and the safety factor of 2 for detailed calculation code such as MCNPX.[2.8-17)] This means that the target dose outside the concrete area is less than 5.5 mSv/h.

3) Temperature and heat expansion

The iron slabs are heated with the proton beam injection. The heat transfers from the iron slabs to the concrete walls and finally diffuses to the air in the beam line tunnel and the soil around the beam dump. The strictest limitation comes from the structural strength of concrete, which gets weaker by continuous heating higher than 60°C. The structure of the beam dump was designed so that the temperatures of the concrete parts would not exceed 60°C. The concrete walls were set to have just enough spaces to the assembly of iron slabs not to be pressed destructively when the iron slabs expanded at maximum.

(3) Analysis

1) Shielding

The calculation model is shown in Fig. 2.8.16. The neutron doses[2] were averaged over the soil regions with 1 m thickness at the backward (region I in Fig, 2.8.16), the bottom (region II), and the sides (region III), respectively. In this calculation, the density of iron was assumed to be 7.2 g/cm^3, which was an effective value taking account of gaps among iron slabs. The densities of concrete and soil used for the calculation were 2.2 g/cm^3 and 1.5 g/cm^3, respectively.

The doses were calculated mainly with MCMPX code,[2.8-17)] and the nuclear data file of LA-150 was used for simulating the nuclear interactions less than 150 MeV.

Table 2.8.7 shows the calculated neutron dose rate in each region.[3] The result shows that the calculated values are lower than the design target.

2) Heat and Stress

The calculation model is shown in Fig. 2.8.17 and the physical constants of the construction materials are shown in Table 2.8.8. The calculation model contains 3 m thick soil region around the concrete walls. The temperature on the outer boundary of the soil region was set to be 16°C as the boundary condition. An adiabatic boundary was set between the concrete wall and the space of the service tunnel because the air temperature in the tunnel is relatively high due to the low ventilation rate. The heat

---

[1] Injection beam energy is 400 MeV when the non-acceleration mode is operated on RCS.

[2] Gamma-ray dose was not added because gamma-ray does not contribute to the activation of soil.

[3] The injection point of the proton beam was moved upstream from the original design just before the fabrication to have room for the increase of the injection beam intensity in future. As a result, the forward shielding got thicker by 250 mm and the evaluated doses were decreased to 1.4, 0.35 and 0.38 mSv/h in the region I, II and III, respectively.

transfer from the concrete surface into the main tunnel, where the air temperature was fixed to be 30°C all the time, was considered. The heat transfer coefficient to the air in the main tunnel was evaluated to be 1.14 W/m^2K from the cross section of the tunnel and the averaged wind speed in the tunnel, which was estimated to be 0.38 m/s from the ventilation rate. The effective heat conductivity of iron was evaluated by considering the contact resistance between the slabs and supposed to be 200 W/m^2K for each contact. The air gaps between the iron slabs and the concrete walls are set to be 3 mm. As the initial condition of the calculation, we put the temperatures distributed linearly so that the boundary conditions would be satisfied, namely, 30°C on the surface of the main tunnel floor and 16°C on the outer boundary of the soil region.

The proton beam profile in the beam dump was calculated with DECAY-TURTLE code.[2.8-10)] The heat distribution in the dump was evaluated with NMTC/JAM code,[2.8-18)] using the calculated beam profile as input. The heat conduction on non-stationary condition was calculated with ABAQUS code[2.8-19)] using the calculated heat distribution as an input. The temperature distribution was evaluated on the condition of continuous beam operation for 48 hours with 4-kW beam power.

In Fig. 2.8.18, the trends of the temperatures at the hottest points of the iron slabs and the concrete region are shown respectively. The highest temperature in the iron region was found at the proton injection point and estimated to be 220°C at the end of the beam operation. The temperature then rapidly decreases just after the termination of beam operation. In the concrete region, the highest temperature was found on the surface of the iron region just above the beam injection point, shown in Fig. 2.8.17. The temperature increases even after the termination of the beam operation and gets to the maximum about 1 day later. During the beam operation and the cooling interval, the concrete temperature has to be kept lower than the maximum allowable temperature of 60°C.

The heat expansion of the iron region was estimated to be 3 mm at most from the calculated temperature distribution. It is expected that the heat expansion does not give destructive stress to the concrete walls because the heat expansion of the iron slabs will be absorbed with the gaps among the iron slabs.

The specification determined by these analyses is shown in Table 2.8.9.

(4) Construction

The fabrication of the beam dump was started in September 2003 at the factory in Oita city.[4] The iron slabs were assembled at the factory in advance to make the beam dump on trial. After disassembling them, those were transported to J-PARC site by ship in November. The installation of the beam dump and the beam duct was finished at the beginning of December (Photo. 2.8.12). Those were covered with concrete and buried under the floor of the main tunnel in February 2004.

2.8.8 Coolant Facility

The 3NBT coolant facility provides cooling water for the beam line magnets and their DC power

[4] The vendor of the beam dump was Mitsui Engineering & Shipbuilding Co., Ltd.

supplies, as well as the muon production target system and the magnets in muon beam lines. The circulation water has to be pure in terms of the electrical resistivity and the concentration of oxygen.

(1) System Organization

The facility consists of the primary coolant system that cools down loads directly (e.g. magnets and power supplies) and the secondary coolant system that releases the heat conducted from the primary coolant systems. The coolant facility was built both in the 3NBT building and in the 3NBT section of the MLF building, according to the location of heat loads. The system organization is depicted in Fig. 2.8.19.

1) Primary Coolant Systems

The cooling water passes through hollow conductors of magnets where 1,000 A of electrical current is posed. The circulation water has to be of very low electrical conductivity, i.e. less than 0.1 μS/cm. This purity is good for low residual activity. Five percent of the circulation water is bypassed to a water purifier. The system is provided pure water of very low dissolved oxygen to prevent corrosion. The water pass was carefully designed for circulation water not to be exposed to air.

The primary coolant systems are composed of a circulation pump that circulates pure water and supplies one to heat loads, a heat exchanger that transfers the heat to a secondary coolant system, a surge tank that absorbs pressure change in a system and a water purifier that keeps the purity of water. They also have a drain line and a drain pump to discharge water.

The primary coolant system I is placed in the 3NBT building and circulates pure water to the magnets in the 3NBT lines and the M1 lines. The primary coolant system II is located in the MLF building (Photo. 2.8.13) and circulates pure water to the magnets of the proton beam line and muon beam lines in the M2 tunnel and the muon production target chamber. The primary coolant system III is also located in the MLF building (Photo. 2.8.13) and circulates pure water to the magnet and their power supplies of muon beam lines in the experimental halls of the MLF building.

2) Power Supply Coolant Systems

They are essentially primary coolant system and have the same components as the primary coolant systems. The requirement for electrical conductivity is not so sever as primary coolant system. The heat loads are magnet power supplies that are placed in a non-radiation-controlled area.

The power supply coolant system I is placed in the 3NBT building and circulates pure water to the power supplies for magnets in the magnet power supply room of the 3NBT building. The power supply coolant system II is located in the MLF building and circulates pure water to the power supplies for magnets in the magnet power supply room of the MLF building

3) Secondary Coolant Systems

The secondary coolant systems are composed of a circulation pump that circulates water and supplies one to a heat exchanger, cooling towers that release the heat transferred from the primary coolant system and a surge tank that absorbs pressure change in a system.

The secondary coolant system I is located in the 3NBT building and plays a role as cooling source for the primary coolant system I and the power supply coolant system I. The secondary coolant system II is placed in the MLF building and plays a role as cooling source for the primary coolant system II, the primary coolant system III and the power supply coolant system II.

4) Water Purifier Systems

The water purifier systems are composed of a water purifier and an oxygen removal device. The water purifier system I is located in the 3NBT building (Photo. 2.8.13) and supplies pure water to the primary coolant system I and the power supply coolant system I. The water purifier system II is placed in the MLF building and supplies pure water to the primary coolant system II, the primary coolant system III and the power supply coolant system II.

5) Nitrogen Gas Supply Systems

The surge tanks are supplied with nitrogen gas that is used as cover gas. The nitrogen supply systems have nitrogen gas cylinders and a pressure regulator. The nitrogen gas supply system I is located in the 3NBT building and supplies nitrogen gas to the surge tanks of the systems. The nitrogen gas supply system II is located in the MLF building and supplies nitrogen gas to the surge tanks of the systems.

(2) Specifications

The loads estimated for designing the coolant facility are summarized in Table 2.8.10. The main parameters of the constituent systems are determined with minimal margin.

1) Primary Coolant Systems

fluid :	pure water
electrical conductivity :	<0.1 μS/cm
fluid path :	confined circulation
discharge pressure of circulation pump :	0.7 MPa
outlet temperature of heat exchanger :	35 ± 1°C
rated flow rate of main path :	168 m^3/h (I), 107 m^3/h (II), 130 m^3/h (III)
rated flow rate of water-purifying bypath :	8.0 m^3/h (I), 5.1 m^3/h (II), 6.2 m^3/h (III)
expected heat load :	4,035 kW (I), 1458 kW (II), 1429 kW (III)
expected temperature rise of main path :	21°C (I), 12°C (II), 10°C (III)
capacity of surge tank :	1.0 m^3
capacity of drain tank :	2.0 m^3
main materials :	stainless steel (SUS304)

2) Power Supply Coolant Systems

fluid :	pure water
electrical conductivity :	<1.0 μS/cm
fluid path :	confined circulation
discharge pressure of circulation pump :	0.7 MPa
outlet temperature of heat exchanger :	35 ± 1°C

rated flow rate of main path :	41 m^3/h (I), 44 m^3/h (II)
rated flow rate of purifying bypath :	1.9 m^3/h (I), 2.1 m^3/h (II)
expected heat load :	374 kW (I), 391 kW (II)
expected temperature rise of main path :	8°C (I), 8°C (II)
capacity of surge tank :	0.5 m^3
main materials :	stainless steel (SUS304)

3) Secondary Coolant Systems

fluid :	water for industrial use
fluid path :	confined circulation
discharge pressure of circulation pump :	0.4 MPa
rated flow rate of main path :	758 m^3/h (I), 564 m^3/h (II)
cooling capacity of cooling towers :	500 RT × 2 (I), 400 RT × 2 (II)
outlet temperature of cooling towers :	32°C
rated flow rate of cooling towers :	379 m^3/h (I), 282 m^3/h (II)
expected temperature rise of main path :	5°C (I), 5°C (II),
capacity of expansion tank :	0.85 m^3
main materials :	carbon steel

4) Pure Water Supply Systems

purifier :	ion exchange resin (cartridge type)
electrical conductivity :	<1.0 μS/cm
degasser module :	hollow fiber membrane
dissolved oxygen :	~10 ppb
fluid path :	one pass
process capacity :	3 m^3/h
water temperature :	30°C
main materials :	stainless steel (SUS304)

5) Requirements for supply water

neutrality :	pH 5.8 - 8.7
muddiness :	<15
temperature :	<30°C
pressure :	0.2 - 0.3 MPa

6) Electric power

pumps and cooling towers :	AC 420V, three-phase, 50 Hz, 440 kVA (3NBT building), 460 kVA (MLF building)
degassers and others :	AC 210V, three-phase, 50 Hz, 10 kVA (3NBT building), 10 kVA (MLF building)

7) Compressed air supply

pressure :	0.60 ± 0.05 MPa

dew point of air :	<12°C
filter mesh size :	0.01 μm

(3) Operation

The coolant facility was designed to be operated continuously without major maintenance work. It may be halted only in the long machine down period for maintenance and overhaul. The facility is envisaged to be operated soundly at least for 30 years.

The facility can be operated either with the touch panel of a control rack or a PC connected to a network. The latter displays the status of the facility graphically, stores the values from all the meters and gauges in the facility and displays their trend.

The circulation water in the primary coolant systems may contain radioactive nuclei during operations. The amounts of activity are estimated with realistic model, assuming 3-weeks beam cycles and 5,000-hours beam operation a year. The result is summarized in Table 2.8.11. The circulation water is planned to be replaced in the following manners

1) Primary coolant system I

The concentrations of radioactive nuclei after 5000-hours beam operation are below the legal limit for discharge. The circulation water is therefore used for a year and replaced in the long machine down period. The circulation water is discharged to the drain tank and new pure water is supplied from the pure water supply system. The amount of discharged water is estimated ~10 m^3.

2) Primary coolant system II

The concentrations of radioactive nuclei are relatively high and the circulation water is replaced after 3-weeks beam operation. The circulation water is discharged to the drain tank and new pure water is supplied from the pure water supply system. The amount of discharged water is estimated ~7 m^3.

3) Primary coolant system III

Radioactive nuclei are not expected to be produced in the circulation water. The system has a function to replace the circulation water nevertheless.

2.8.9 Air Conditioning Facility for M1 and M2 Tunnels

The proton beam line in the M2 tunnel is buried completely with radiation shield because large beam loss is expected at an intermediate target. Even the beam line magnets themselves have shield plug on their yokes. Air circulation around the beam line magnets is, on the other hand, essential[2.8-1, 6)] to cool down their coils and prevent the magnets from the damage due to the corrosive gases such as NOx, which are formed with radiation. The dedicated facility of air cooling and circulation was designed[2.8-2)] for the M1 and M2 tunnels.

2.8.9.1 Basic Design Principles

(1) Design temperature and humidity

The design temperature and relative humidity in the M1 tunnel are set at the same condition as the accelerator tunnels and the beam transport tunnels of J-PARC, as shown in Table 2.8.12. The design temperature in the M2 tunnel is determined by the highest temperature tolerable for concrete (60ºC), since mineral insulation cables that are used for the coils are highly temperature-resistant. The preferable temperature in the service space, the upper part of the M2 tunnel, is below 30ºC because of a lot of power cables are laid on cable trays.

(2) Cooling method

The cooling method for the M1 and M2 tunnels is as follows,

1) Individual air cooling apparatuses are dedicated for the M1 tunnel and the M2 tunnel respectively. The heat sources (coolant) are supplied from a common apparatus.
2) The M1 tunnel is cooled down with air circulation method.
3) In the M2 tunnel sufficient cooling air is supplied once into the service space above the beam line and transferred down through the narrow gaps between the magnets and the shield bricks. It is then circulated back along the channels (concrete ducts) at the bottom of the M1 tunnel.

(3) Setup and layout of facility

The air circulation facility is composed and arranged as follows,

a) Dynamic components such as circulation fans have their spares and can be switched to their spare anytime.
b) Circulation filters (pre-filters and HEPA filters) are set in the path of air out of the M1 and M2 tunnels to reduce contamination as much as possible on the surfaces of the apparatus and the ducts during beam operation period. This would lower personnel exposure dose substantially.
c) All the apparatuses are installed in the M1 tunnel, except the coolant apparatus.

(4) Operation method during beam operation period

The air in the M1 and M2 tunnels is confined and is circulated inside. The option for additional continuous air discharge apparatus is reserved. The air leak rates from the tunnels will be measured and air-tightness will be improved while the beam intensity is low. The air leak could be eliminated by keeping the tunnels at negative pressure with the continuous air discharge apparatus if the amount of radioactivity in the air leaked from the tunnels cannot be neglected.

(5) Operation method during personnel access period

When personnel enter the M1 and M2 tunnel without removing shield bricks above the tunnels, the tunnels are ventilated so that the whole volume of the air in the tunnels are replaced less than an hour.

2.8.9.2 Structure of facility

(1) System composition

The facility consists of an air circulation system of the M1 tunnel, an air circulation system of the M2 tunnel, ventilation systems, an air discharge system and a coolant system, as shown in Fig. 2.8.20.

1) Air circulation system of M1 tunnel

The system is composed of a circulation fan, a cooling coil unit and a circulation filter unit. The apparatuses are installed in the M1 tunnel (Fig. 2.8.21). Air is cooled down with the cooling coil unit and supplied into the M1 tunnel uniformly with the circulation fan and an air supply duct. The air returns directly to the circulation filter unit. The flow rate is controlled with a flow rate sensor in the air supply duct and a volume damper in a return air duct so that the flow rate could be kept constant even though the filters are clogged. The thermometer in the return air duct monitors the return air and controls the flow rate of coolant to the cooling coil unit to keep the temperature in the M1 tunnel at the design temperature. The condensed water in the cooling coil unit is drained into the sump pit of the M1 tunnel and pumped up to disposal tanks.

2) Air circulation system of M2 tunnel

The system is composed of a circulation fan, a cooling coil unit and a circulation filter unit. The apparatuses are also installed in the M1 tunnel (Fig. 2.8.21). Air is cooled down with the cooling coil unit and supplied into the service space. It is circulated through the narrow gaps between magnets and shield bricks to the concrete duct on the floor. The air flow rates and their distribution at air outlets and inlets are determined according to the amount of heat generation from the magnets and their power cables. The air flow rate is controlled with a flow rate sensor in the supply air duct and a volume damper in a return air duct so that the flow rate should be kept constant even though the filters are clogged. The thermometer in the return air duct monitors the return air and controls the flow rate of coolant to the cooling coil unit to keep the temperature in the M2 tunnel at the design temperature. The apparatuses and the ducts are made highly air-tight to prevent the air circulating in the M2 tunnel from leaking into the M1 tunnel. The condensed water in the cooling coil unit is drained in the sump pit of the M1 tunnel and pumped up to the disposal tanks.

The air duct in the M1 tunnel has an outlet and a volume damper for the continuous air discharge system.

3) Ventilation systems of M1 and M2 tunnels

The ventilation systems are installed in the M1 and M2 tunnels for personnel access into the tunnels. The supply of fresh air and the treatment of discharged air rely on the air conditioning system for the high bay above the M1 and M2 tunnels and those ventilation systems don’t have any ventilation fans or filter units. An inlet and an outlet are placed in the M1 tunnel and the service space of the M2 tunnel and the ventilation operation can be started just by opening dampers. The ventilation rates are set so that the whole volumes of air in the tunnels are ventilated once an hour. The ducts of the ventilation systems are made highly air-tight to prevent the air from leaking out of the tunnels.

4) Continuous air discharge system of M1 and M2 tunnels

The amount of radioactivity in the air that leaks from the M1 and M2 tunnels might have the possibility to exceed the limit as the proton beam power increases. Continuous air discharge system keeps the tunnels at negative pressure to prevent the air firmly from leaking to the high bay or the experimental halls. This system extracts the part of the circulating air in the M2 tunnel to the M1 tunnel and keeps it there diluting the radioactivity and waiting for decay of shot-lived radioactivity as well. The air in the M1 tunnel is then discharged outside of the building through a stack after proper treatment. The path and the inner diameter of the air discharge duct are selected so that it would take about 30 seconds for the air to transfer from the M1 tunnel to the stack. The ducts and the fans are made highly air-tight. The maximal air discharge rates from the M1 tunnel and from the M2 tunnel are 40 m^3/h and 20 m^3/h, respectively, which are determined to keep the density of radioactivity in the air released from the stack below the legal limit. The negative pressures of the M1 and M2 tunnels are controlled with those flow rates by looking at their pressure differences between the inside and outside of the M1 and M2 tunnels.

5) Coolant system

This facility does not have own heat source. Coolant is generated with a heat exchanger using the heat source of the air conditioning facility of the MLF building and supplied to the cooling coil units of the air conditioning systems of the M1 and M2 tunnels. This system is composed of a heat exchanger, a water pump and an expansion tank and installed in the 3NBT hot-area cooling water facility room near the M1 tunnel. The valves are attached onto the cooling coil units, which control the coolant flow rates as the heat load may be changed.

(2) Operation mode of facility

The operation mode of the facility is shown in Table 2.8.13.

a) beam operation period

The air is confined and circulated in the M1 and M2 tunnels. The continuous air discharge system will be operated only when the tunnels are necessary to be kept at negative pressure.

b) personnel access period

The circulation systems and the ventilation systems are operated in parallel to provide sufficient cooling power for the heat load in the tunnels.

(3) Capacity of facility

The capacities of the systems are summarized in Table 2.8.14. The heat loads of the M1 and M2 circulation systems show those in beam operation period. The flow rates of the ventilation system are those supplied from the air conditioning system of the building.

The cooling power of the coolant system is shown in Table 2.8.15. It was given small margin since extra power may be required for humidity escaping from the concrete wall of the building for the first year or so after the completion.

2.8.10 Control and Interlock System

(1) General control system

A general control system of the proton beam transport line had been developed aiming at operating the magnet power supplies, the vacuum system, the movement system for the heads of the beam profile monitors. The control system has included the functions of monitoring the status of the cooling water system, the water leakage detectors and the ground-fault circuit interrupter as well. The control system was developed using Experimental Physics and Industrial Control System[2.8-11)] (EPICS). Programmable Logic Controllers (PLC) are additionally introduced to communicate with the magnet power supplies, the vacuum system, the water leakage detectors and the ground-fault circuit interrupter using hard wire connections. For the movement system for the heads of the beam profile monitors and the cooling water system, PLC's are used both for local control and the communication with the general control system. The PLC's are connected to a control network and are remotely controlled through four Input/Output Controllers (IOC) running on Linux. The IOC's have a silicon disk rather than a hard disk to reduce failure rate. The silicon disk is configured to be read-only to allow power-off without shutdown. Two IOC's are used for the magnet power supplies and the other two for other systems.

The software for operators (named OVAMA: Operating software for 3NBT VAcuum, MAgnet and other systems) in an operator interface (OPI) was developed with JAVA on Scientific Linux[2.8-20)]. The initial window of OVAMA shows simplified status of each system and provides buttons to open a detailed window for each system. Standard Linux boxes are used for OPI. All the analog data and the events of status transition are recorded by a database server developed with PostgreSQL. OVAMA directly sends IOC commands, but reads data from the database server to refer not only current data but also past ones. The flow of data is shown in Fig. 2.8.22.

(2) Machine protection system (MPS)

The Machine Protection System (MPS) was introduced in the 3NBT facility. Ready signals were connected to MPS modules,[2.8-21,22)] which had been originally developed for the Linac of J-PARC. Two blocks of MPS modules were prepared for the operations to two different proton beam destinations: the 3NBT dump and the mercury target of the Material and Life Science Experimental Facility (MLF). All the relevant signals have to be ready before accepting the proton beam to the 3NBT facility and the proton beam will be stopped immediately if any of MPS signals fail. The following ready signals are monitored: the magnet power supplies, the ordinary and fast-closing valves and the degrees of vacuum in the vacuum beam ducts, the beam loss monitors and the beam plug position. The statuses of all the signals are monitored as EPICS records through IOC working in VME modules.

(3) Personnel protection system (PPS)

The personnel protection system (PPS) had been developed in J-PARC to protect personnel from excessive doses of radiation using Programmable Logic Controllers (PLC). For this purpose, PPS prohibits personnel from entering interlock areas during beam operation and do not allow beam operation if personnel remains in the interlock areas. The PPS of the 3NBT facility is a part of the entire PPS of J-PARC and is controlled only by the operators in the Central Control Room (CCR). RCS and 3NBT are defined as the same interlock area in PPS since there is no boundary for personnel between tunnels of RCS and 3NBT.

A beam stopper (Photo. 2.8.14) was installed downstream of the vertical bending magnet to the 3NBT dump not to allow the proton beam for being transported to MLF. The beam plug in the beam stopper (Photo. 2.8.14) is made of a block of stainless steel that is 0.5 m long along the beam direction. It takes about 30 seconds to insert or extract the beam plug. Two bending magnets downstream of the beam plug are defined as safety magnets to be included in PPS.

References

2.8-1) S. Sakamoto et al.: “Advanced design of high-intensity beam transport line in J-PARC”, Nucl Instr. and Meth Phys Res. A 562, 2006, pp. 638-641.

2.8-2) S. Sakamoto et al.: “Design Report on the 3-GeV Proton Beam Transport Facility (3NBT) of High Intensity Proton Accelerator Facility Project (J-PARC),” JAERI-Tech 2004-020, 2004, in Japanese.

2.8-3) S. Meigo et al.: “Evaluation of the 3-GeV proton beam profile at the spallation target of the JSNS,” Nucl Instr. and Meth. Phys. Res., A 562, 2006, pp. 569-572.

2.8-4) S. Meigo: “A Study on a 3-GeV Proton Beam Transport Line at the NME Facility in the Joint Project for High-Intensity Proton Accelerator,” JAERI-Tech 2000-088, 2001, in Japanese.

2.8-5) S. Meigo et al.: “Study on 3 GeV Proton Beam Transport Line for JSNS,” Proc. Int. Collaboration on Advanced Neutron CANS-XV, Tsukuba, Japan, 6-9 Nov. 2000, JAERI-Conf 2001-002 & KEK Proc. 2000-22, 2001, pp. 314-324.

2.8-6) S. Sakamoto et al.: “Study of Technical Issues on Proton Beam Line Tunnel in Material/Life Science Experimental Facility of High Intensity Proton Accelerator Project,” JAERI-Tech 2001-075, 2001, in Japanese.

2.8-7) K.L. Brown et al.: “TRANSPORT, a computer program for designing charged particle beam transport systems,” CERN 80-04, 1980.

2.8-8) H. Grote and F.C. Iselin: "The MAD Program Version 8.16 User's Reference Manual," CERN/SL/90-13.

2.8-9) S. Meigo et al.: “Design of Beam Optics in the Proton Beam Transport Line from Synchrotron to Spallation Neutron Target,” Proc. Int. Collaboration on Advanced Neutron Sources ICANS-XVI, Dusseldorf-Neuss, Germany, 12-15 May 2003, 2003, pp. 967-976.

2.8-10) K.L. Broun and Ch. Iselin : “DECAY TURTLE, a computer program for simulating charged particle beam transport systems, including decay calculations,” CERN 74-2, 1974.

2.8-11) http://www.aps.anl.gov/epics/

2.8-12) S. Meigo et al.: “Design of Beam Incident Monitor for Spallation Neutron Target of JSNS,” Proc. Int. Collaboration on Advanced Neutron Sources ICANS-XVI, Dusseldorf-Neuss, Germany, 12-15 May 2003, 2003, pp.1175-1180.

2.8-13) S. Meigo et al.: “JSNS Proton Beam Profile Monitor Using Silicon Carbide Wire,” Proc Int. Collaboration on Advanced Neutron Source ICANS-XVII, 24-29 Apr., 2005, LA-UR-06-3904, 2006, pp. 455-462.

2.8-14) IEEE (1976) CAMAC Instrumentation and Interface Standards, IEEE Document No. SH06437. Wiley-Interscience (New York).

2.8-15) M. Ooi et al.: “Development of Beam Monitor DAQ system for 3NBT at J-PARC,” 10th ICALEPCS Int. Conf. on Accelerator & Large Exp. Physics Control Systems, 10-14 Oct, 2005 PO1.024, 2005.

2.8-16) Y. Kasugai and H. Kogawa : "Study on 3-GeV beam dump - Analysis of its temperature and stress," 3NBT Internal Report 3NBT 2001-10, Nov. 2001, in Japanese.

2.8-17) L.S. Waters (Ed.) : “MCNPX User's Manual,” TPO-E83-G-UG-X-00001, Los Alamos National Laboratory, 1999.

2.8-18) K. Niita et al. : "High Energy Particle Transport Code NMTC/JAM," JAERI-Data/Code 2001-007, 2001.

2.8-19) "ABAQUS/Standard ver.5.8," Hibbit, Karlsson & Sorenson, Inc.

2.8-20) https://www.scientificlinux.org/

2.8-21) H. Sakaki, N. Nakamura, H. Takahashi, H. Yoshikawa: “Performance test of the prototype-unit for J-PARC Machine Protection System,” JAERI-Tech 2004-021, 2004, in Japanese.

2.8-22) H. Sakaki, N. Nakamura, H. Takahashi, H. Yoshikawa: “Design of prototype unit for J-PARC Machine Protection System,” JAERI-Tech 2004-022, 2004, in Japanese.

Table 2.8.1: Main parameters of proton beam. The numbers in parenthesis show the values when the injection energy from the LINAC to the RCS is 181 MeV.

proton beam energy (E)	3 GeV
proton beam momentum (p)	3.8249 GeV/c
proton beam velocity (β)	0.97121
magnetic rigidity ($B\cdot\rho$)	12.758 T·m
beam current (I)	333 (200) μA
beam power	1.0 (0.6) MW
number of protons per pulse	8.33×10^{13} (5.03×10^{13}) ppp
beam emittance (ε)	81π (54) mm·mrad (beam core) 324π mm·mrad (max. beam halo)
longitudinal beam emittance	3.5 (2.7) eV·s
momentum bite ($\Delta p/p$)	<±1%
repetition	25 Hz
number of bunches	2 /pulse
bunch width	~140 ns
bunch separation	~600 ns

Table 2.8.2: Main parameters of 3NBT line

total length of beam line in 3NBT tunnel	258 m
typical internal dimension of 3NBT tunnel	5.0 m (W) × 4.5 m(H)
total length of beam line in MLF Building	57 m
bend angle of 3NBT tunnel	30°
elevation of 3NBT tunnel	4.8 m with gradient of 7.5°
number of horizontal bending magnets	6
number of vertical bending magnets	3
number of quadrupole magnets	54
number of steering magnets	45
inner diameters of beam ducts	204, 242, 282 mm
number of vacuum pump units	7

Table 2.8.3: Main parameters of bending magnets

	unit	D16150H/V	D16150H_10	D16180C
bending angle	deg	7.5	10.3	11.8
magnetic field	T	1.11	1.53	1.46
pole gap	mm	160	160	160
pole length	mm	1,500	1,500	1,800
pole width	mm	580	580	360
number of turns in coil	/coil	120	126	100
current	A	591	900	1,110
voltage	V	162	180	125
conductor		hollow conductor of oxygen-free copper	hollow conductor of oxygen-free copper	hollow conductor of oxygen-free copper
conductor size	mm	□13-Φ9	□16-Φ10	□17-Φ11
insulator		polyimide	polyimide	polyimide
cooling		direct water cooling	direct water cooling	direct water cooling
total weight	ton	14.0(H) / 15.7(V)	18.0	22.2
quantity		5(H) / 2(V)	1	1

Table 2.8.4: Main parameters of quadrupole magnets

	unit	Q2260	Q3060_G6	Q3060_G8	Q2690	Q2690MIC
bore diameter	mm	220	300	300	260	260
maximal magnetic field gradient	T/m	8.0	6.0	8.0	8.0	8.0
pole length	mm	600	600	600	900	900
pole width	mm	239	297	297	262	262
number of turns in coil	/coil	84	129	129	95	49
current	A	458	416	605	630	1,200
voltage	V	81	111	127	138	126
conductor		hollow conductor of oxygen-free copper	hollow conductor of oxygen-free copper	hollow conductor of oxygen-free copper	hollow conductor of oxygen-free copper	hollow conductor of oxygen-free copper
conductor size	mm	□12−ϕ8	□12−ϕ8	□12−ϕ8	□13−ϕ7	□19.8−□7.3
insulator		polyimide	polyimide	polyimide	polyimide	MgO
cooling		direct water cooling	direct water cooling	direct water cooling	direct water cooling	direct water cooling
total weight	ton	5.1	7.7-7.8	10.4	14.2	13.8
quantity		30	14	4	3	3

Table 2.8.5: Main parameters of steering magnets

	unit	S2240AC	S2260AC	S3060	S2630	S2640MIC
bending angle	deg	0.172	0.172	0.172	0.172	0.172
magnetic field	T	0.0638	0.0638	0.0638	0.1276	0.0957
pole gap	mm	220	220	300	260	260
pole length	mm	400	600	600	300	400
pole width	mm	230	229	340	270	270
number of turns in coil	/coil	176	168	60	36	12
current	A	31.7	33.0	127	220	520
voltage	V	14.3	17.1	18	7.74	5.33
conductor		rectangular copper wire	rectangular copper wire	hollow conductor of oxygen-free copper	hollow conductor of oxygen-free copper	hollow conductor of oxygen-free copper
conductor size	mm	4.5×8	3.5×10	□9− ϕ 6	□12− ϕ 8	□19.8−□7.3
insulator		polyimide	polyimide	polyimide	polyimide	MgO
cooling		natural convection air cooling	natural convection air cooling	direct water cooling	direct water cooling	direct water cooling
total weight	ton	0.76-0.81	0.81	0.98	0.40	0.52
quantity		24	6	11	2	2

Table 2.8.6: Specifications of proton beam monitors

Types	Spec	Material	quantity
Intensity monitor (CT)	Primary line	Ti	9
	Dump line	Ti	1
Profile monitor(PM)	Retractable frame type:		
	Upstream of M2 (wire pitch 6mm)	Ti	12
	Muon target (wire pitch 3mm)	SS	1
	M2 line (wire pitch 6mm)	SS	2
	Fixed frame type:		
	Beam dump (wire pitch 6mm)	Ti	1
	Proton beam window	SS/$AlMg_3$	2
Beam loss monitor(LM)	Beam line to M1	SS	192
	M2 tunnel	SS	24
Beam halo monitor(HM)	Primary line	Al	14
	Dump line	Al	1
Beam position monitor (BPM)	Upstream of the beam dump	SS	4
	Downstream of the beam dump	SS	10

Table 2.8.7: Evaluated Neutron dose in each region

Region	I (Backward)	II (Bottom)	III (Side)
Neutron Dose (mSv/h)	4.1	0.69	0.36

Table 2.8.8: Physical constants used for the heat analysis

Material	Density [g/cm^3]	Heat transfer coefficient [$W\ m^{-1}K^{-1}$]	Specific heat [$kJ\ kg^{-1}\ K^{-1}$]	Physical condition
Iron[1)]	7.8	47.8	0.529	500K
Concrete	2.2	1.6	0.9	
Soil	1.6	1.3	0.5	Dry density: 1.5 g/cm^3 Water content: 10%
Air	0.0011763	0.02614	1.007	300K, 0.1MPa

Table 2.8.9: Specification of beam dump and beam duct

Beam dump	
General Feature	Assembly of iron slabs sealed by stainless steel[1)]
Dimension	Whole length, width and height: 3.5 mm × 3 m × 3 m Beam-duct hole: 72 cm on each side
Iron density	7.83 g/cm^3 [2)]
Total weight	255 ton [3)]

Beam duct	
Feature	Stainless steel duct
Dimension	15 m long and 60 cm in diameter
Material	SS304 with 5 mm in thickness
Accessory	Flange, Welded stainless cover, Vacuum port Temporary duct supporters

1) For preventing groundwater contamination of radioactivity because installation position of the beam duct is lower than the groundwater level. Iron sand was used for filling gasp between iron slabs for preventing neutron duct streaming and improving the heat transfer

2) By sampling measurement.

3) Estimation from the actual dimensions of each slabs and the measured density of 7.83 g/cm^3.

Table 2.8.10: Loads for coolant facility

system	flow rate (ℓ/min)	temperature rise (°C)	heat load (kW)	pressure drop (MPa)	tolerant pressure (MPa)
primary coolant system I	2607.7	21.7	4035.3	0.5	1.0
primary coolant system II	1705.7	12.2	1457.7	0.5	1.0
primary coolant system III	2066.9	9.9	1428.9	0.5	1.0
power supply coolant systems I	643.5	8.3	374.1	0.5	1.0
power supply coolant systems II	701.8	8.0	391.3	0.5	1.0

Table 2.8.11: Concentrations of radioactive nuclei in coolant

1) Major radioactive nuclei immediately after 3-weeks beam operation

	Primary coolant system I	Primary coolant system II
^{15}O	270 Bq/cc	7700 Bq/cc
^{16}N	150 Bq/cc	3800 Bq/cc
^{11}C	90 Bq/cc	2700 Bq/cc
^{14}O	44 Bq/cc	2200 Bq/cc
^{13}N	41 Bq/cc	1300 Bq/cc

2) Major radioactive nuclei after 15 hours since 3-weeks beam operation

	Primary coolant system I	Primary coolant system II
^{7}Be ¶	0.084 Bq/cc	2.5 Bq/cc
^{3}H	0.9 Bq/cc	23 Bq/cc
^{14}C	0.0005 Bq/cc	0.01 Bq/cc

3) Major radioactive nuclei after 15 hours since 1-year (5,000-hours) beam operation

	Primary coolant system I
^{7}Be §	1.0 Bq/cc
^{3}H	11.0 Bq/cc
^{14}C	0.006 Bq/cc

Inventories of coolant in primary coolant system I and II are assumed 20.2 m^3 and 6.4 m^3, respectively.

¶ 1% of generated nuclei is assumed to be remained in coolant and other 99% are captured in filters and ion exchange resin.

§ Decay of nuclei during 1-year operation is ignored.

Table 2.8.12: Design temperature and humidity in M1 and M2 tunnels. The numbers in the parentheses indicate preferable values.

area	design temperature (ºC)		design humidity (%RH)	
	beam operation period	personnel access period	beam operation period	personnel access period
M1 tunnel	≤30	≤28	≤60	≤60
M2 tunnel (service space)	≤55 (≤30)	≤28 (≤28)	no control	no control

Table 2.8.13: Operation modes of the systems

system \ mode	beam operation period	personnel access period
air circulation systems of M1 and M2 tunnels	operation	operation
ventilation systems of M1 and M2 tunnels	stop	operation
continuous air discharge system of M1 and M2 tunnels	operation	stop

Table 2.8.14: Capacities of systems

system		design temp. (ºC)	supply temp. (ºC)¶	ΔT (ºC)	heat load (kW)	flow rate (m^3/h)	duct size (mm)	pressure drop (mmAq)
circulation system	M1 tunnel	30	13	17	16.5	3,000	400×400	150
	M2 tunnel	55	13	42	68.5	5,000	450×450	200
ventilation system	M1 tunnel	—	(25)	—	—	700	250A	20
	M2 tunnel	—	(25)	—	—	400	200A	20
continuous discharge system	M1 tunnel	—	—	—	—	40	65A	100
	M2 tunnel	—	—	—	—	20	—	—

¶ : outlet temperature of cooling coil unit

Table 2.8.15: Capacity of coolant system

coolant supply		coolant system				
inlet and outlet temp. (ºC)	flow rate (ℓ/min)	inlet and outlet temp. (ºC)	flow rate (ℓ/min)	cooling power (kW)	main pipe size (mm)	pressure drop (mAq)
7/12	300	8/13	300 M1 : 60 M2 : 240	102	65A	40

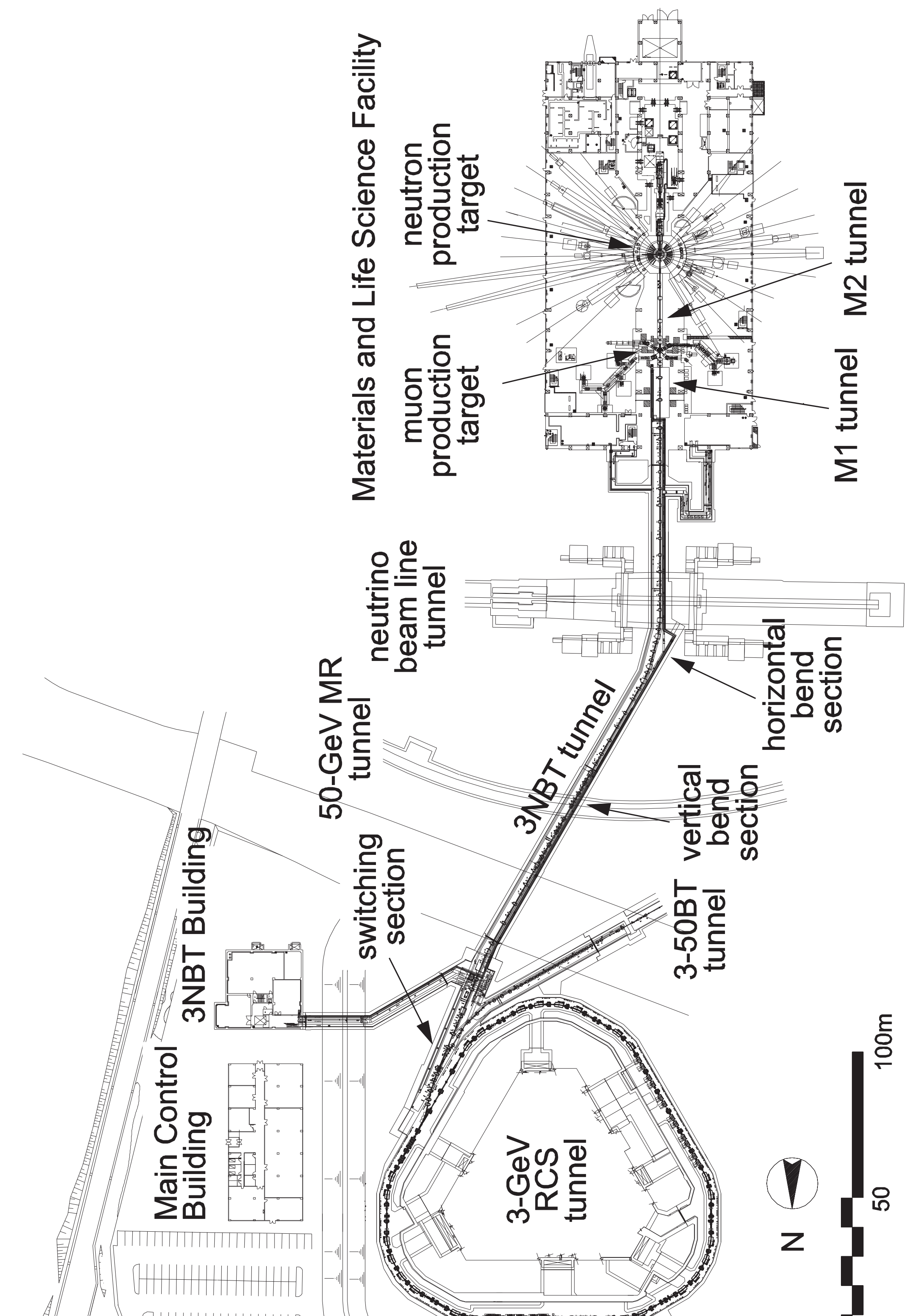

Fig. 2.8.1: Layout of beam transport to neutron and muon production targets (3NBT)

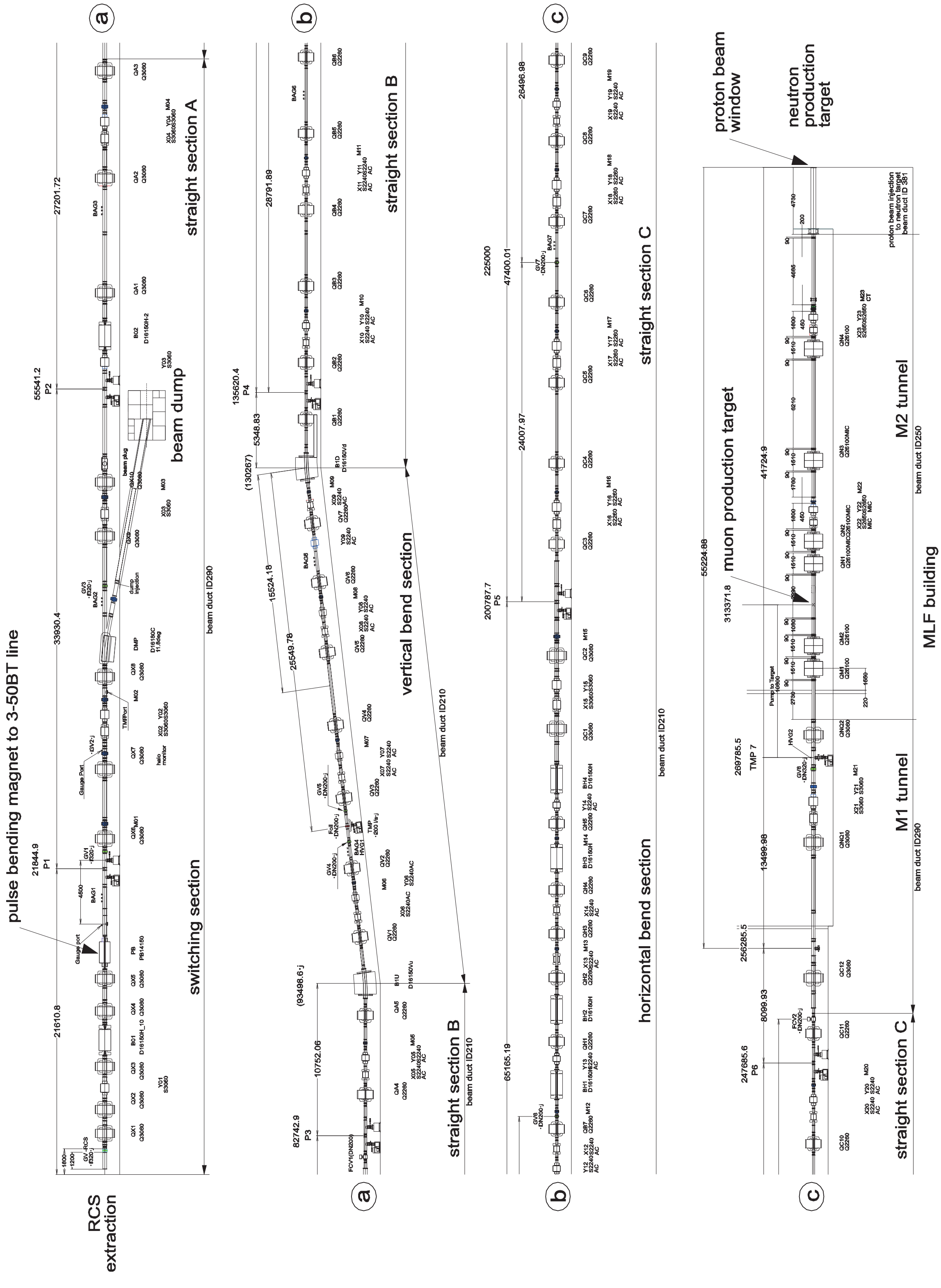

Fig. 2.8.2 : Layout of beam line components (vertical cross section)

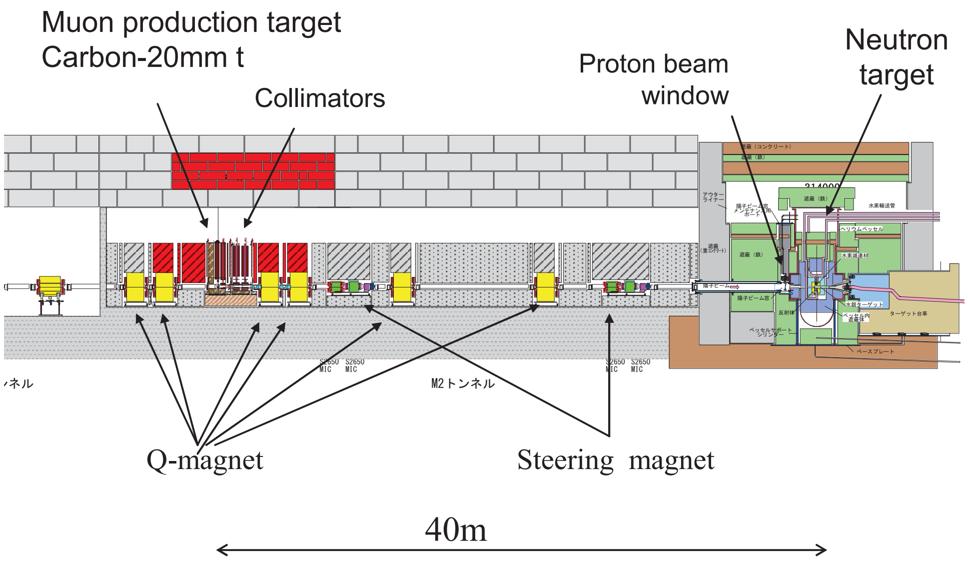

Fig 2.8.3: Vertical cross sectional view of beam transport line around muon and neutron production targets

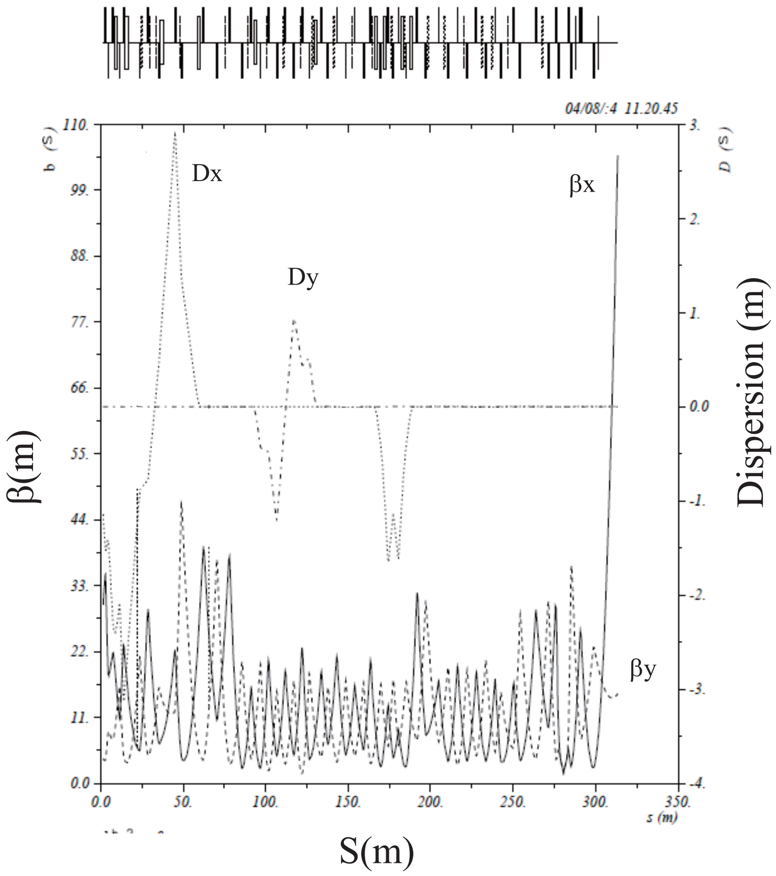

Fig 2.8.4: Beam optics parameter of beta(β) and dispersion function (D) at 3NBT. The symbol of x and y stands for horizontal and vertical, respectively.

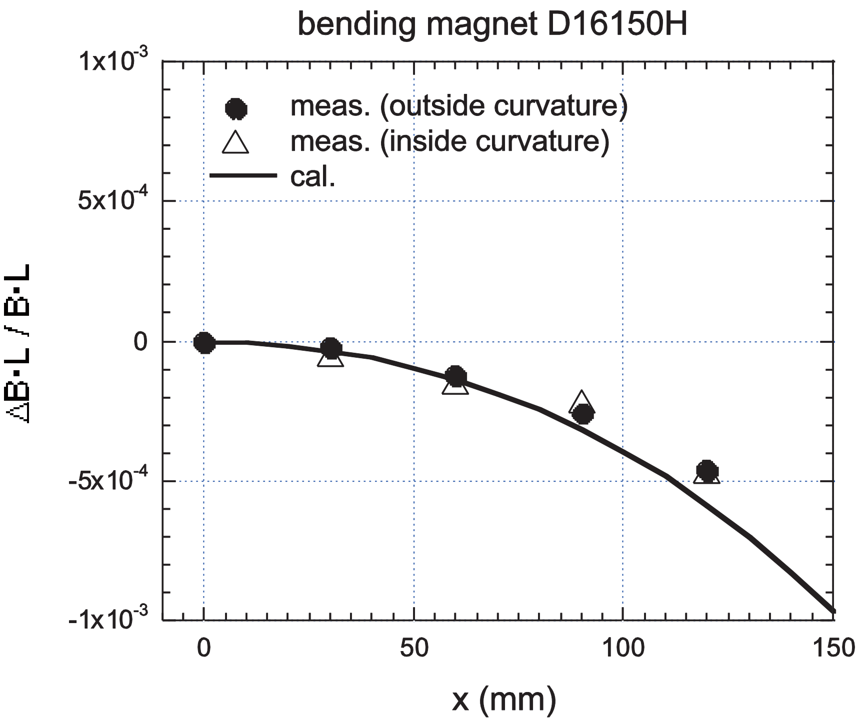

Fig. 2.8.5: Relative deviation of B·L product along the horizontal axis perpendicular to the beam direction (D16150H)

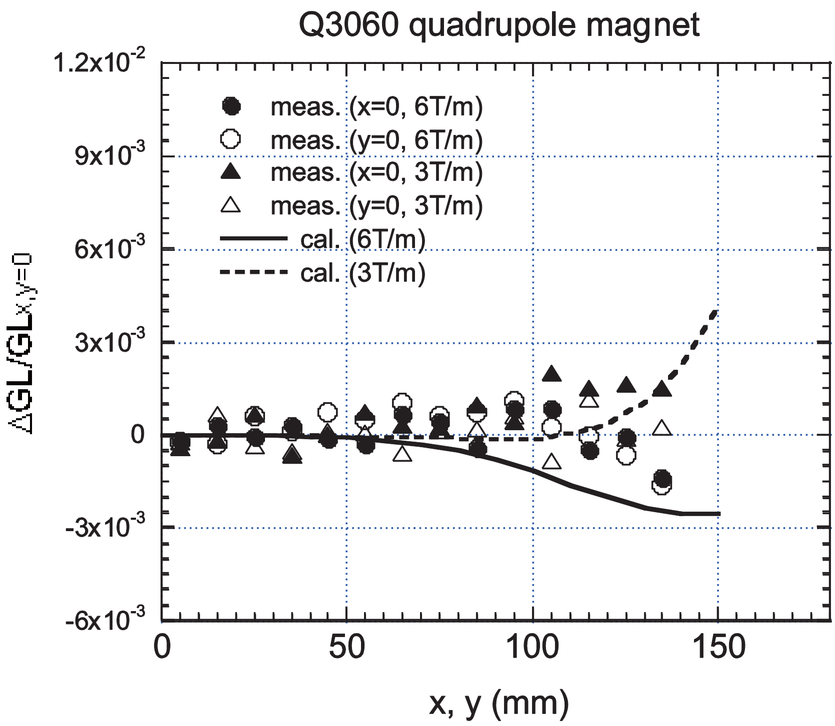

Fig. 2.8.6: Relative deviations of field gradient along the horizontal axis and the vertical axis perpendicular to the beam direction (Q3060)

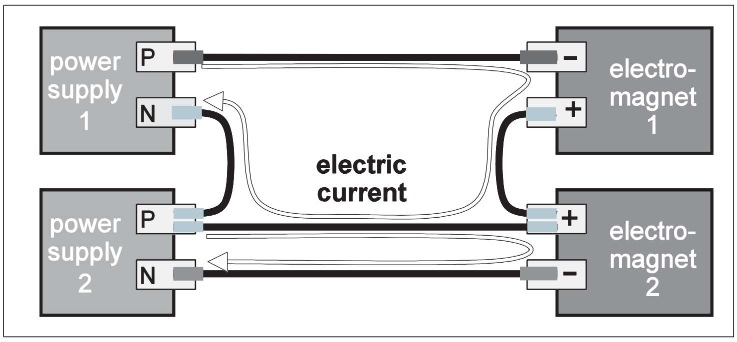

Fig. 2.8.7: Three-cable connection

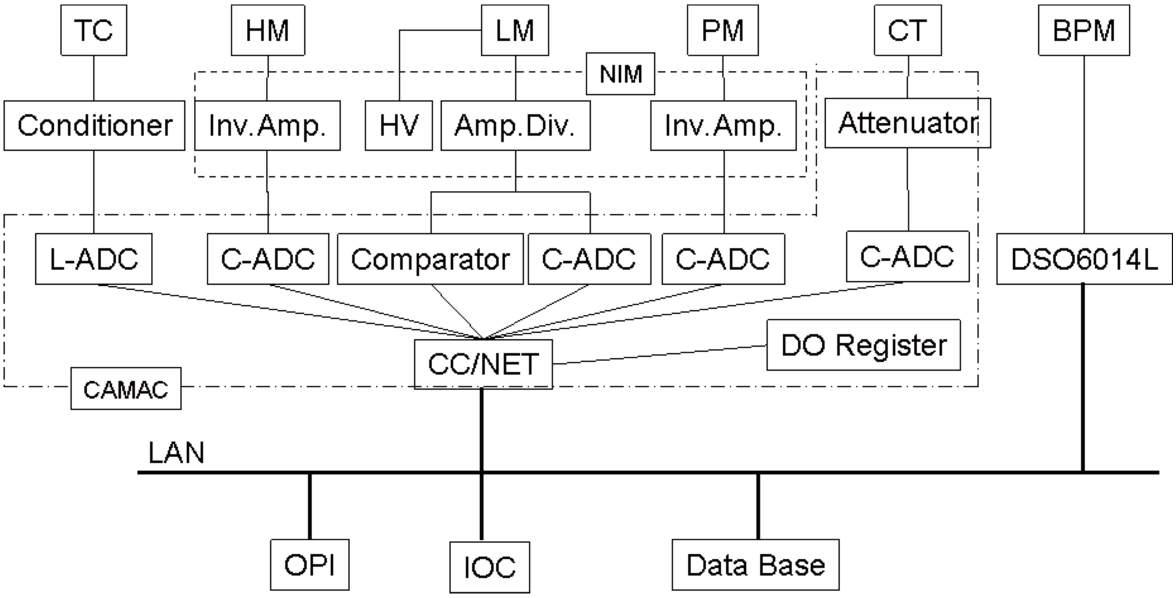

Fig. 2.8.8: Outline of 3NBT beam monitor data acquisitions system

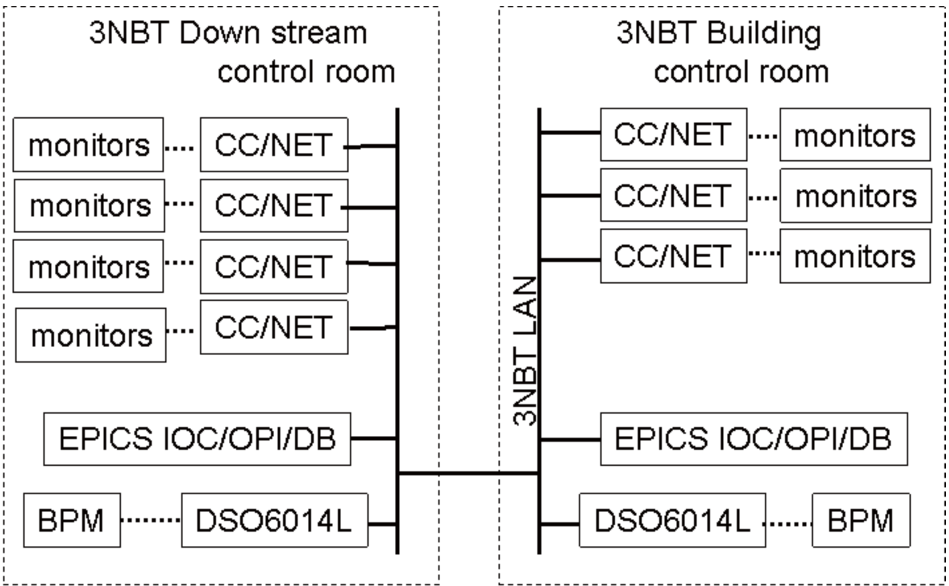

Fig. 2.8.9: PC components of 3NBT monitor system

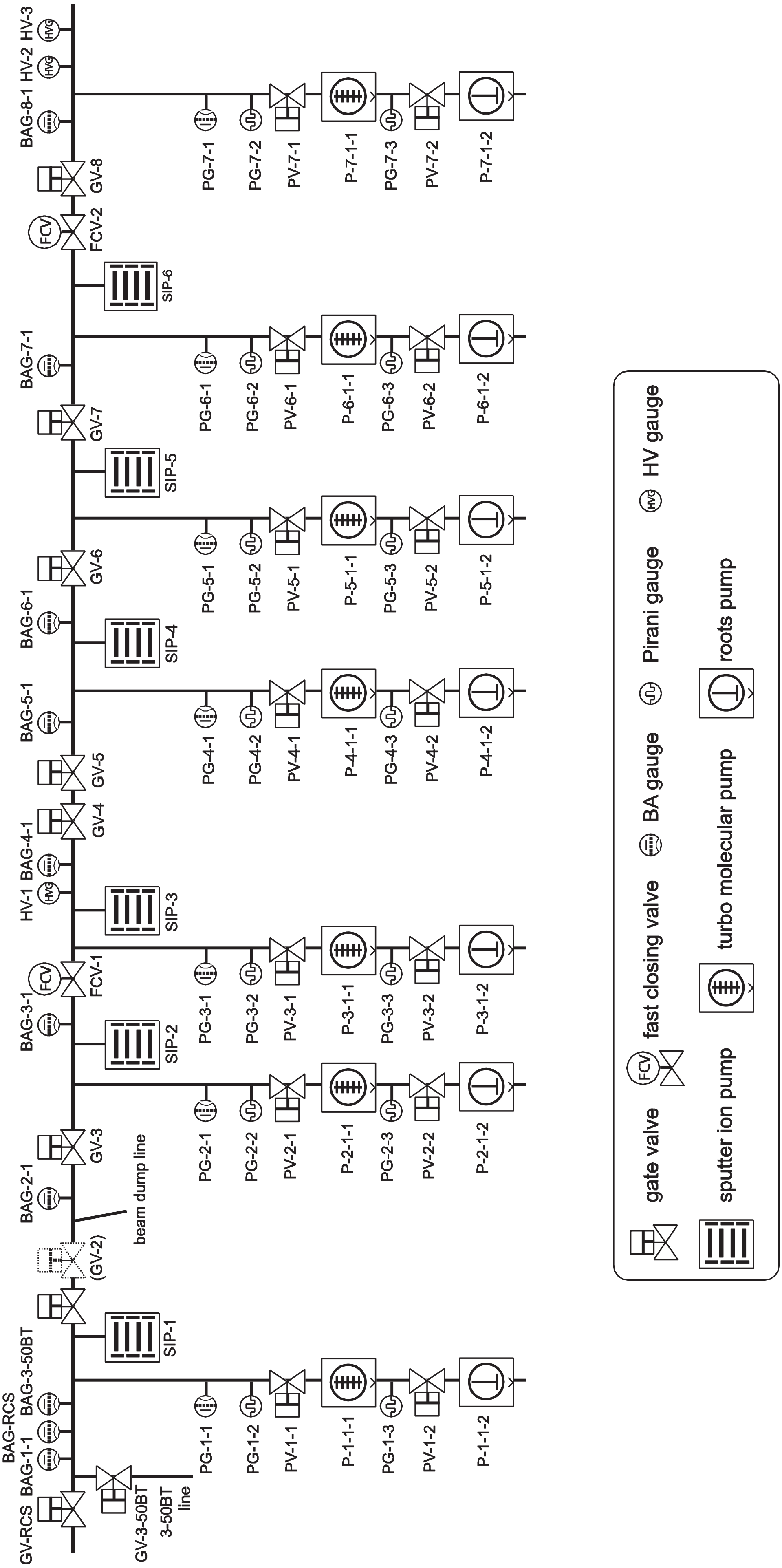

Fig. 2.8.10: Block diagram of 3NBT vacuum system

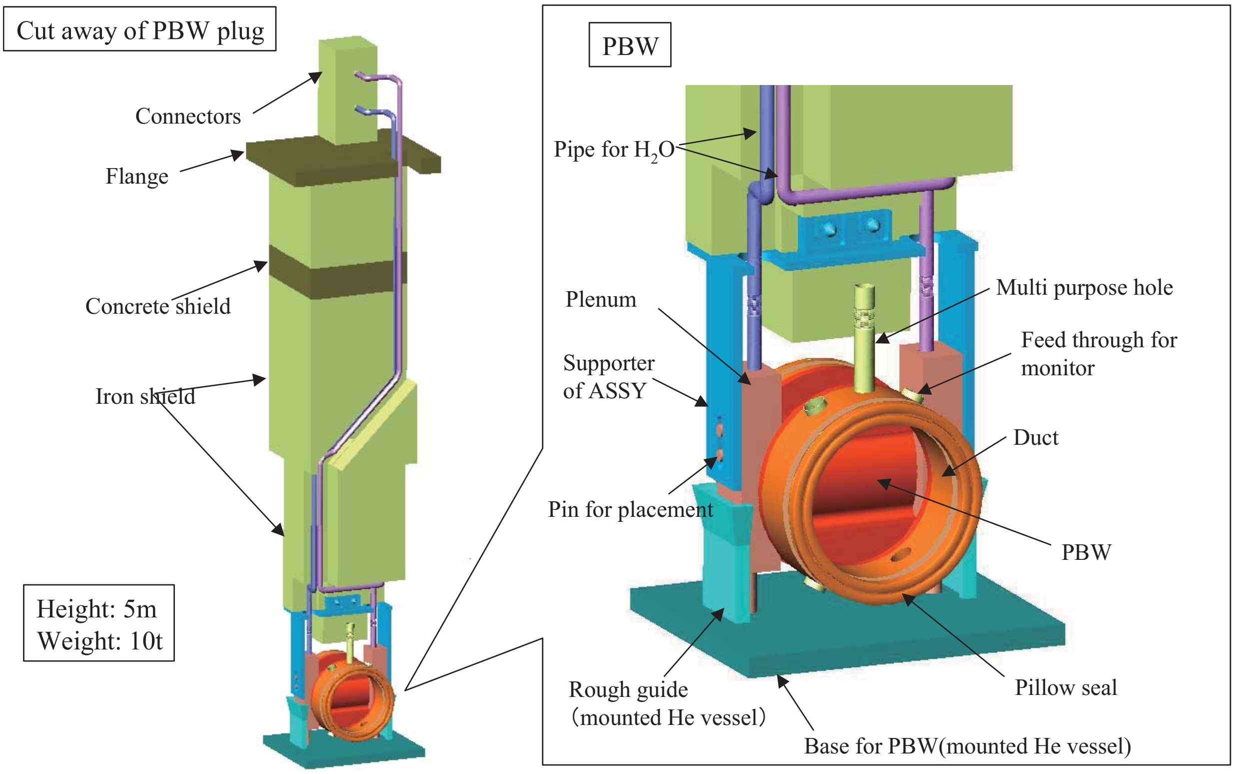

Fig. 2.8.11: Schematic view of the proton beam window assembly

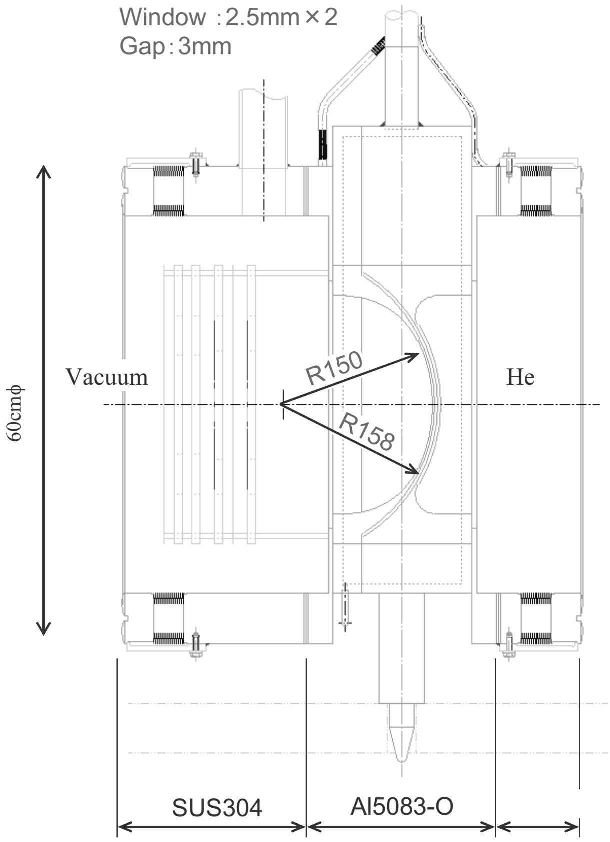

Fig. 2.8.12: Vertical cross sectional view of the PBW

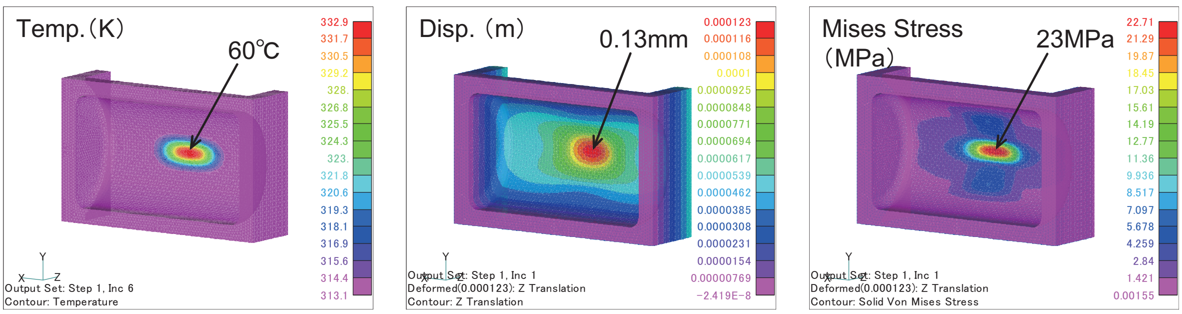

Fig. 2.8.13: Result of temperature and stress analysis on the PBW introduced by proton beam of 1MW. Beam profile is approximated to have uniform in phase space which has peak intensity of 8.3 $\mu A/cm^2$.

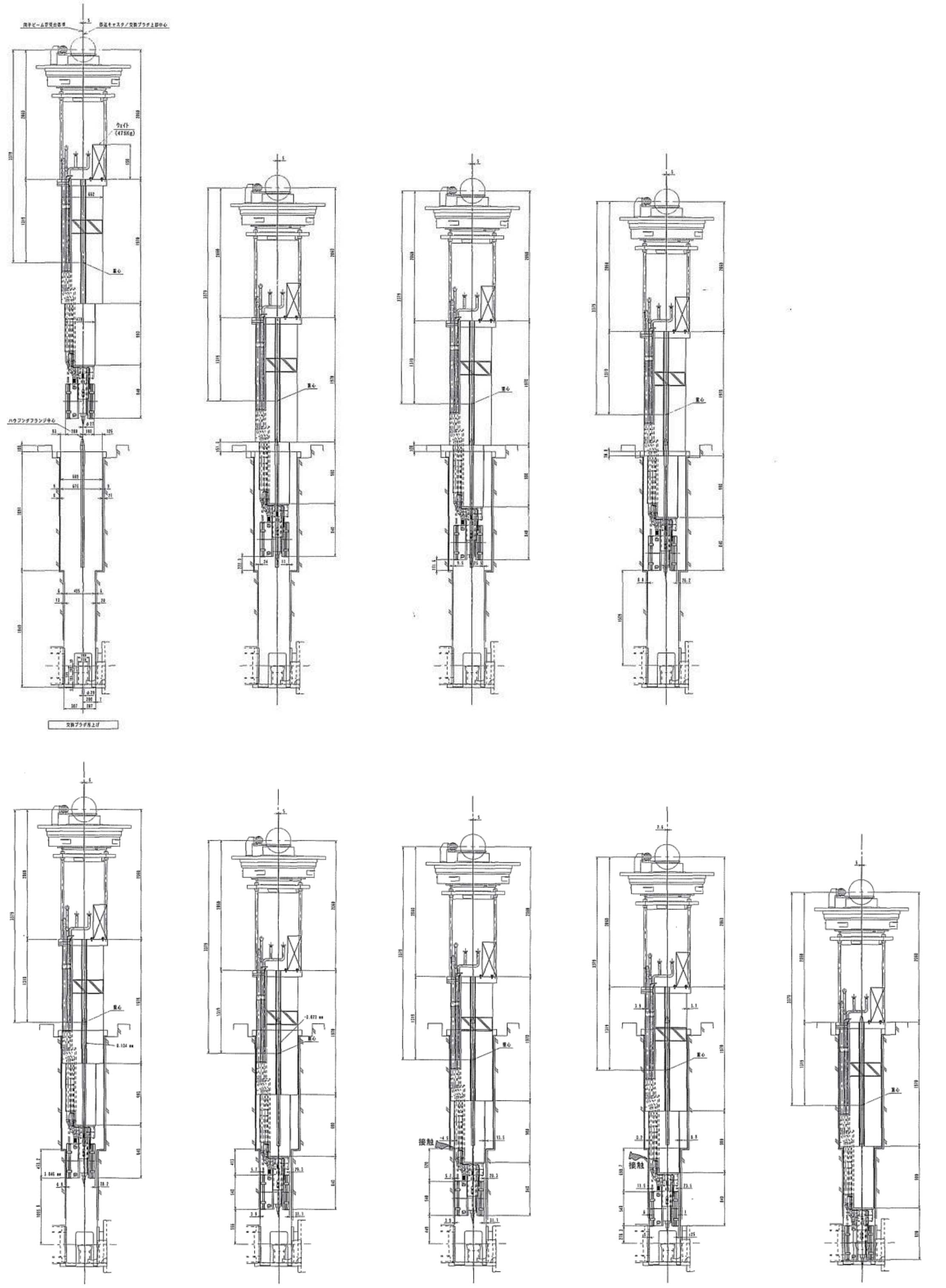

Fig. 2.8.14: Relationship of clearance between the PBW pillow seal and the counter flange during installation. Motion of the PBW follows from left to right and top to bottom.

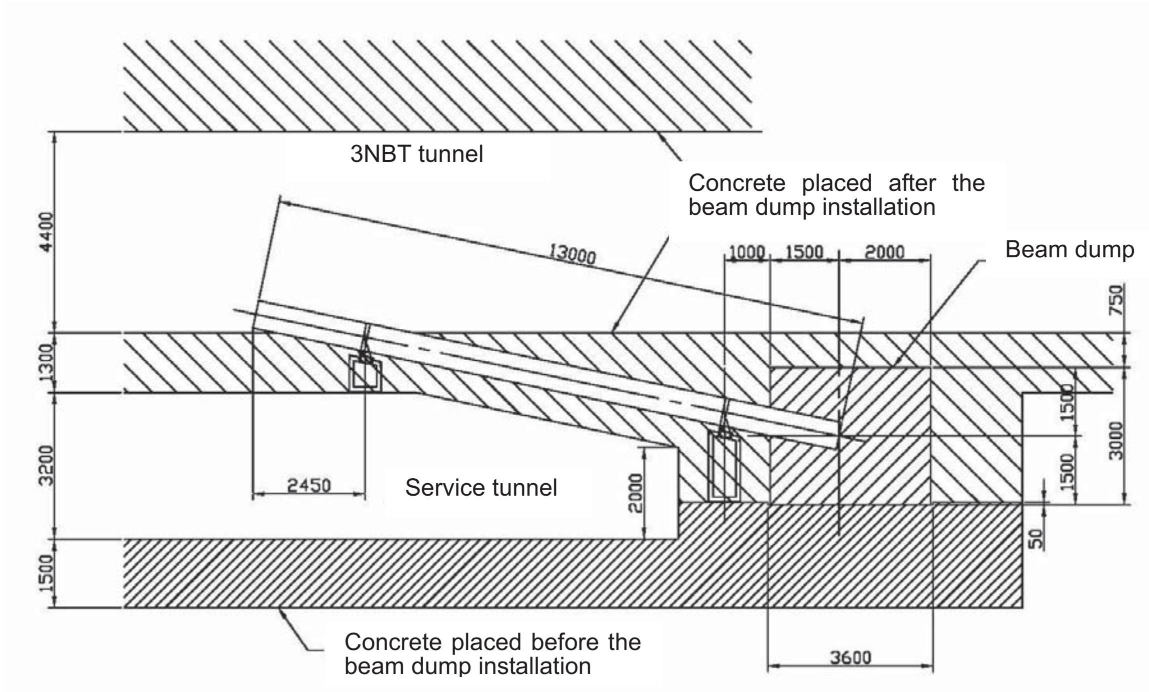

Fig. 2.8.15: Conceptual drawing of 3-GeV RCS extraction beam dump. Unit of the dimensions is in mm.

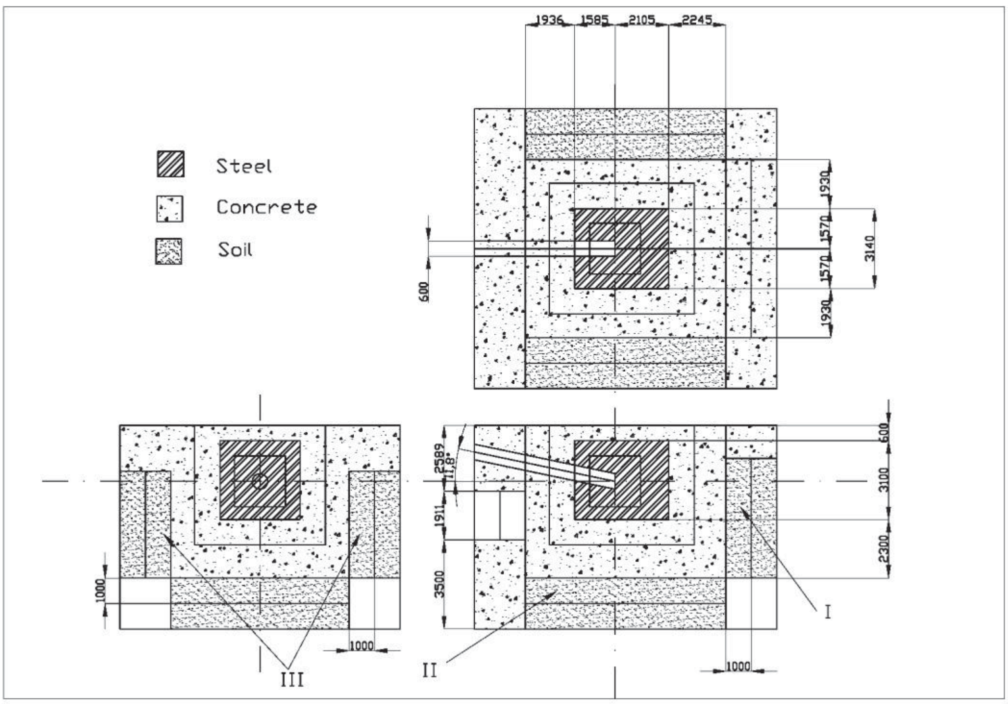

Fig. 2.8.16: Calculation model for shielding. Unit of the dimensions is in mm.

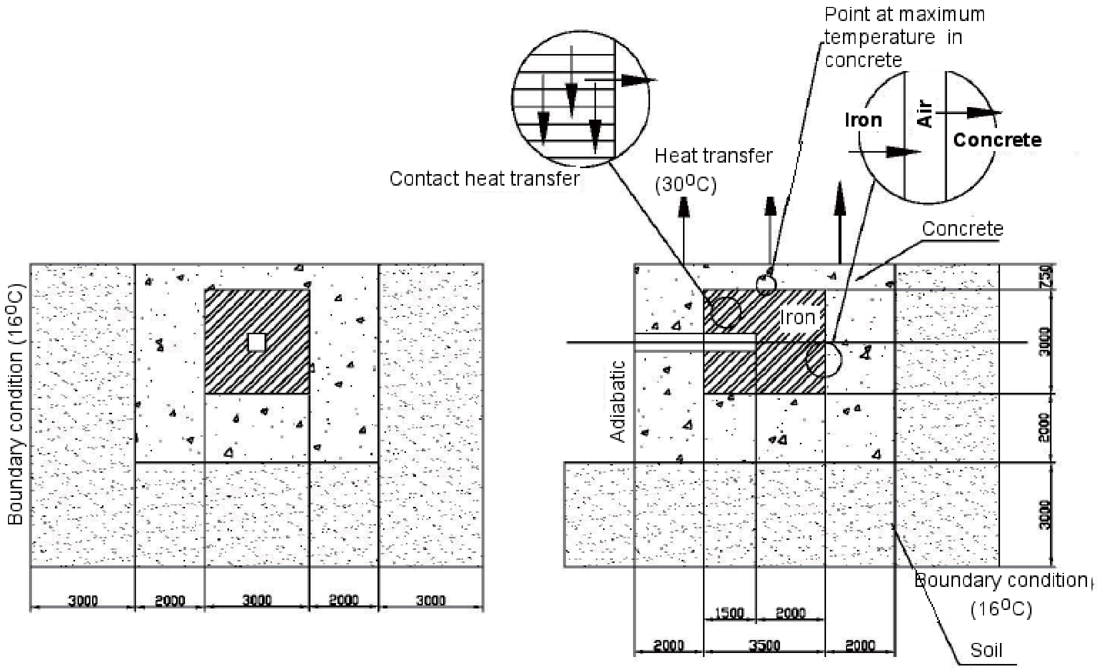

Fig. 2.8.17: Calculation model for heating analysis. Unit of the dimensions is in mm.

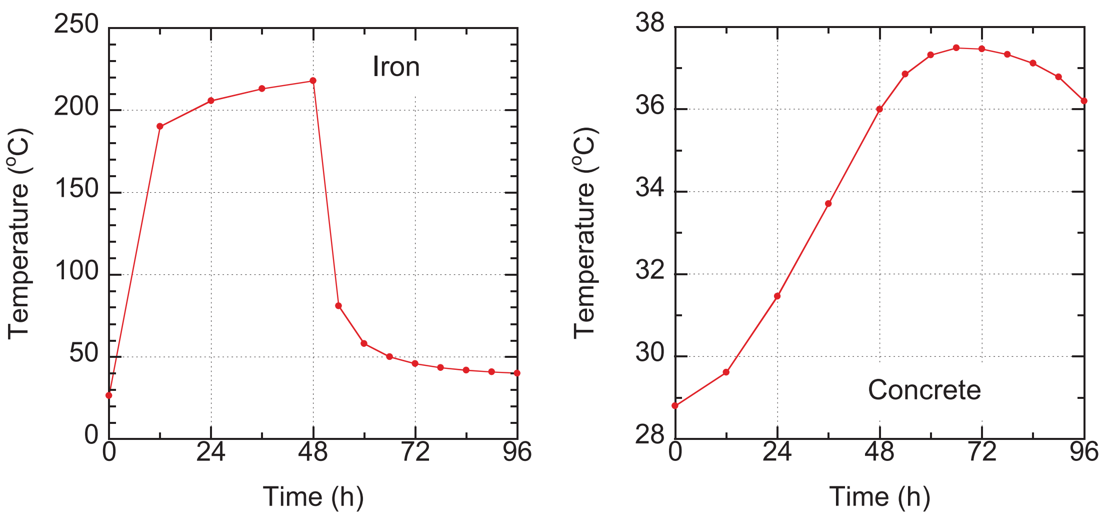

Fig. 2.8.18: Calculated temperature history at the points showing maximum temperature in iron and concrete region, respectively

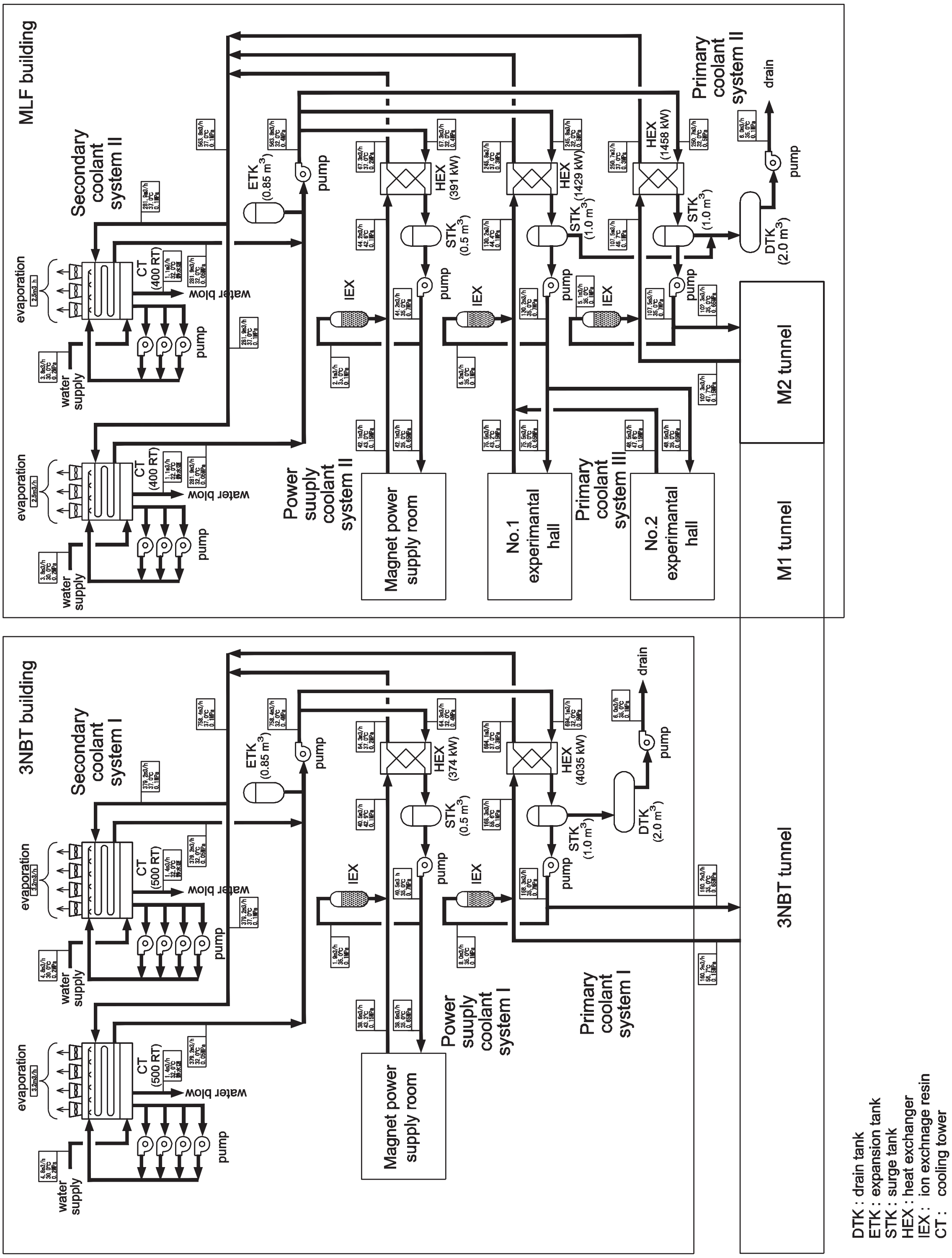

Fig. 2.8.19: Block diagram of 3NBT coolant facility

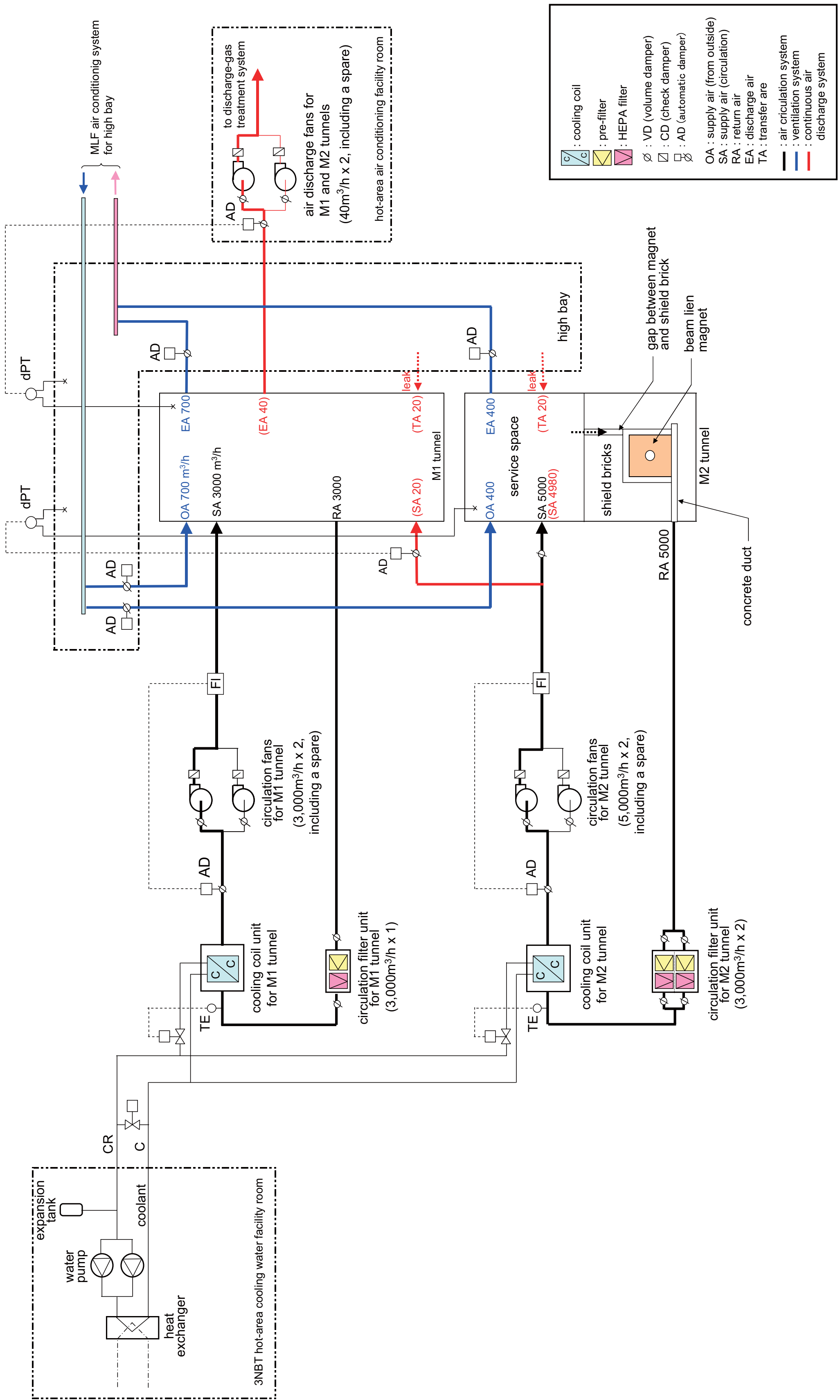

Fig. 2.8.20: Systematic diagram of air conditioning facility for M1 and M2 tunnels

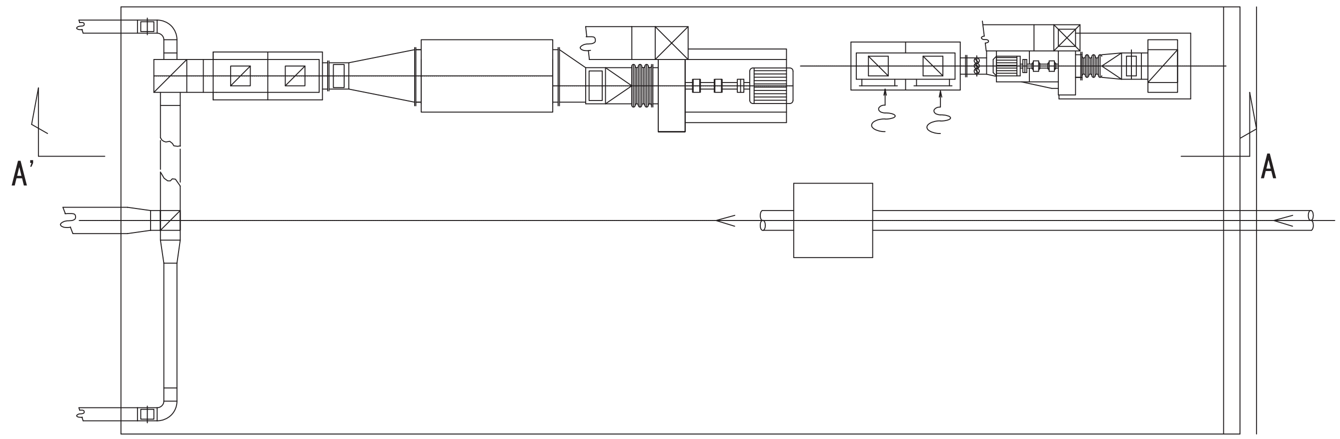

air conditioning apparatus for M1 and M2 tunnels (plan view)

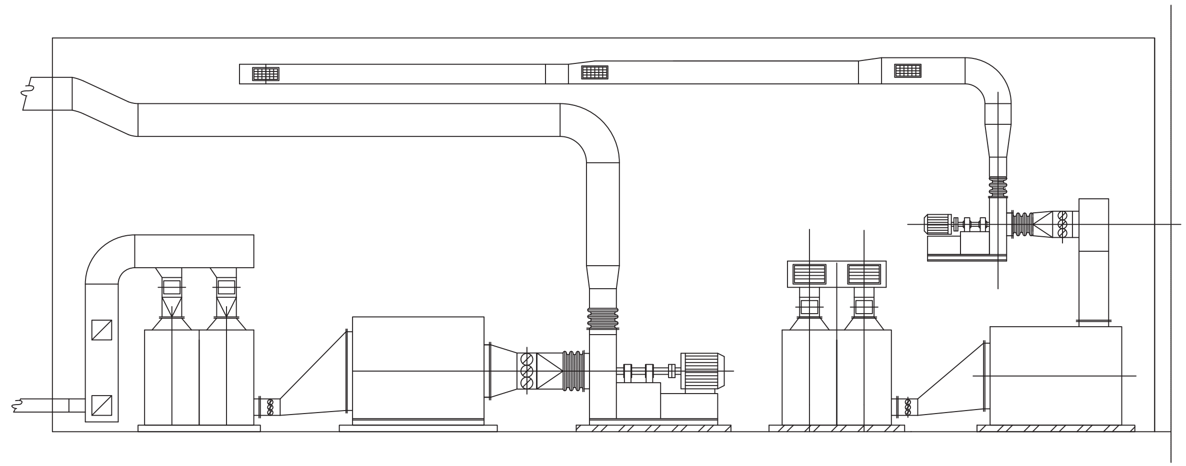

air conditioning apparatus for M1 and M2 tunnels (A-A' cross section)

Fig. 2.8.21: Air conditioning apparatus installed in M1 tunnel (top: plan view, bottom: cross section)

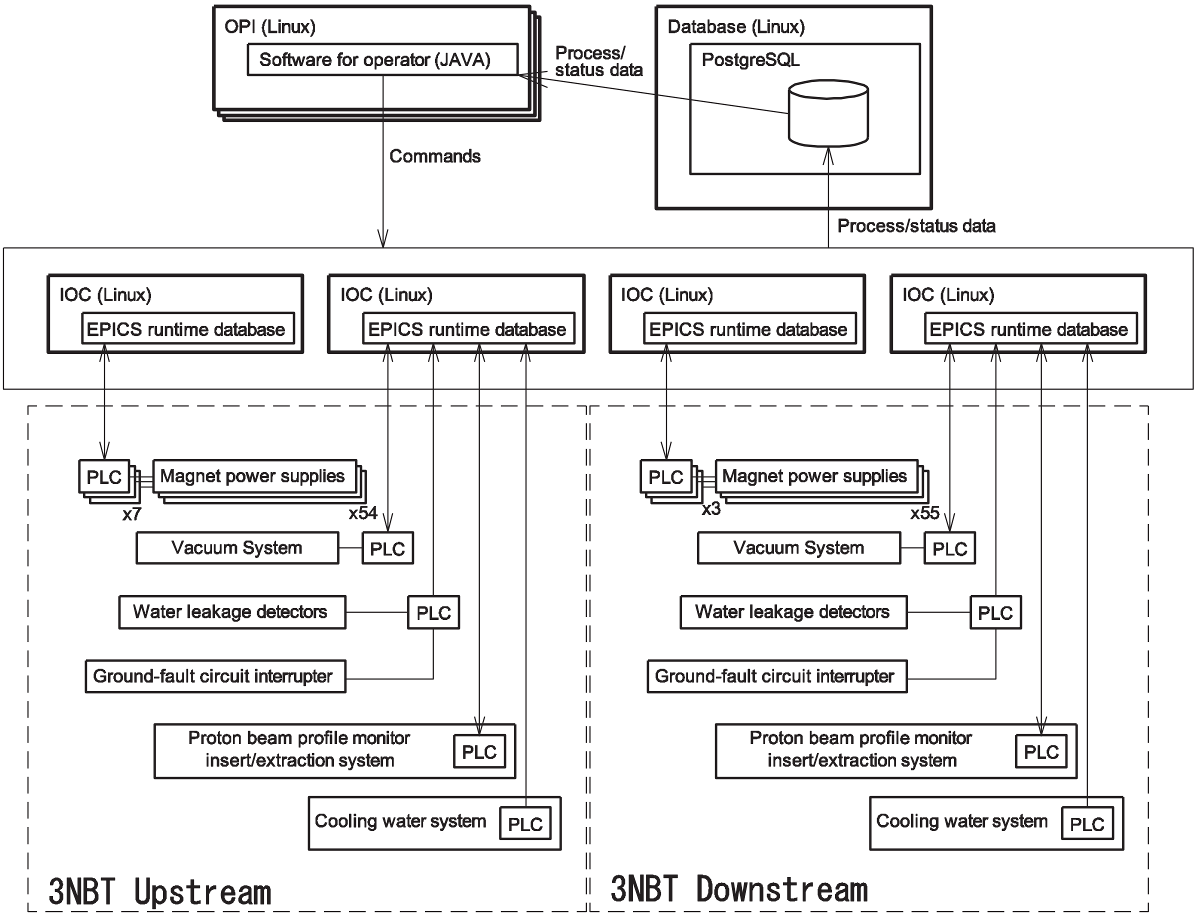

Fig. 2.8.22: Data flow of 3NBT control system

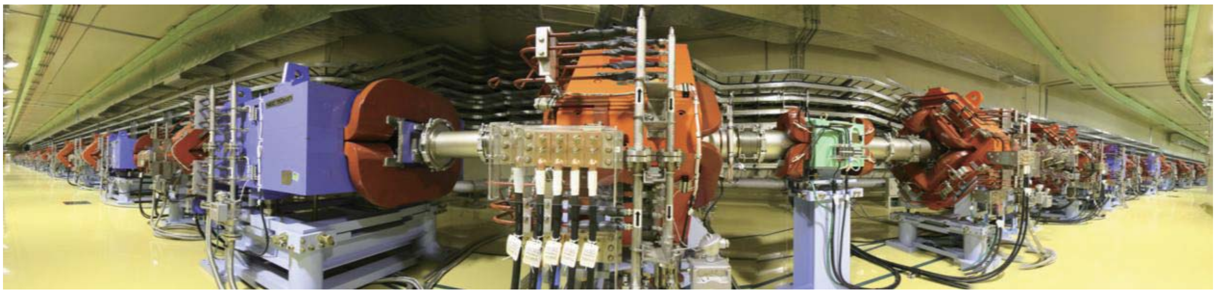

Photo. 2.8.1: 3NBT line around straight section B and horizontal bend section. The proton beam is transported from right to left.

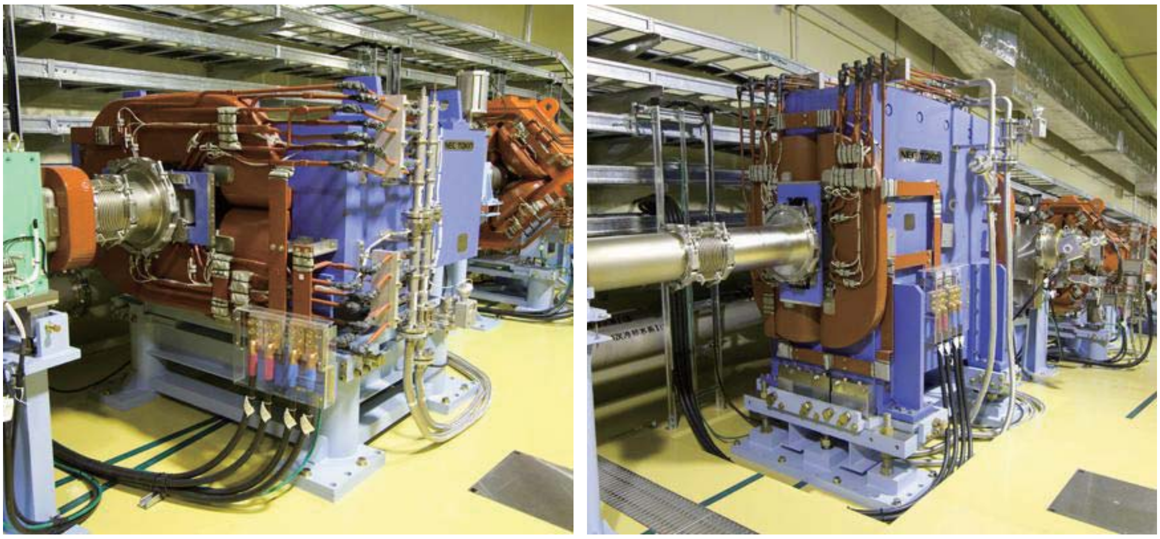

Photo. 2.8.2: Bending magnets D16150H (left) and D16150Vd (right)

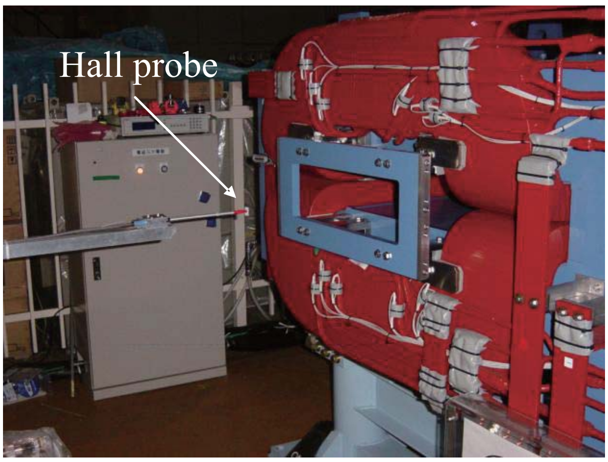

Photo. 2.8.3: Typical viewing of magnetic field measurement for the bending magnet by hall probe at JAEA

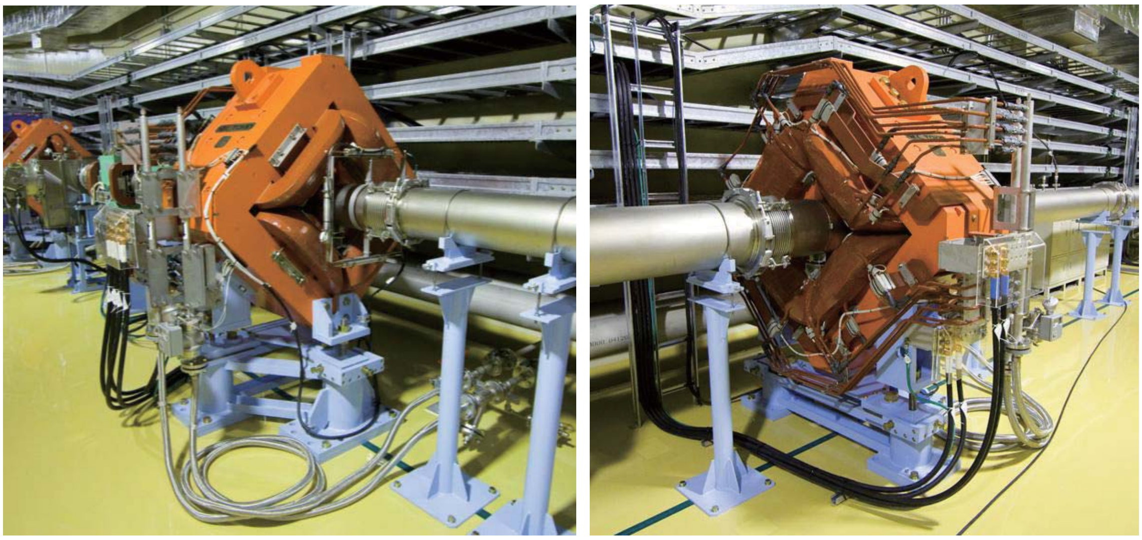

Photo. 2.8.4: Quadrupole magnets Q2260 (left) and Q3060_G6 (right)

Photo. 2.8.5: Vendor’s test of integration current monitor (CT)

Photo. 2.8.6: View of profile monitor (PM) at the 3NBT tunnel. (Top: sensor wire frame, Bottom: whole image of the profile monitor). Ellipse shown in above stands for the sensor wire frame.

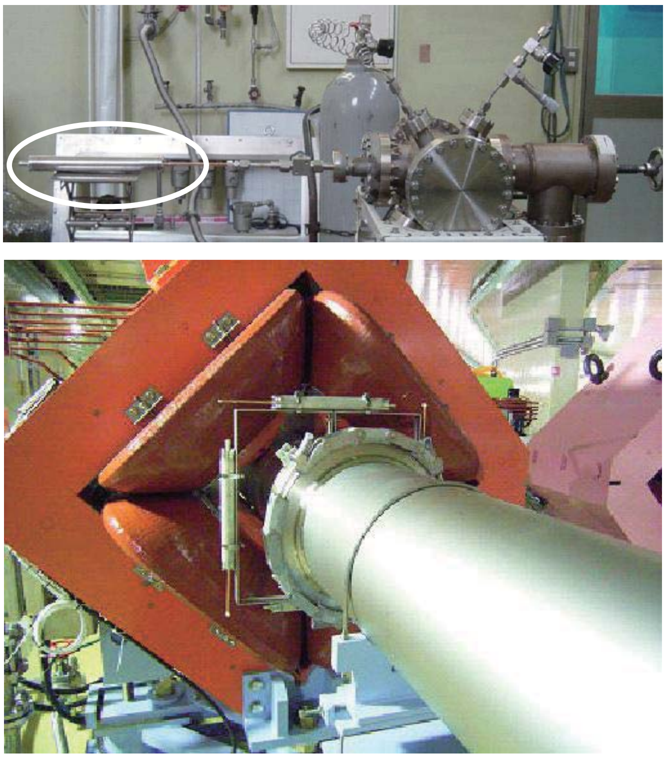

Photo. 2.8.7: View of beam loss monitor (LM). (Top: monitor coupling with gas filler, Bottom: whole image of the beam loss monitor) Ellipse shown in above stands for the monitor head.

Photo. 2.8.8: View of beam position monitor (BPM) (Top: whole image of the beam position monitor, Bottom: electrode in the BPM)

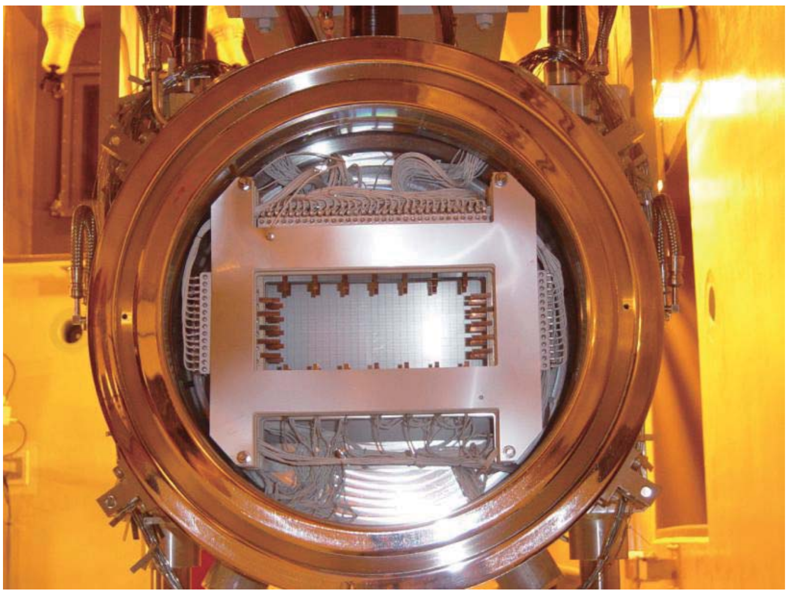

Photo. 2.8.9: View of the proton beam monitors located on the proton beam window

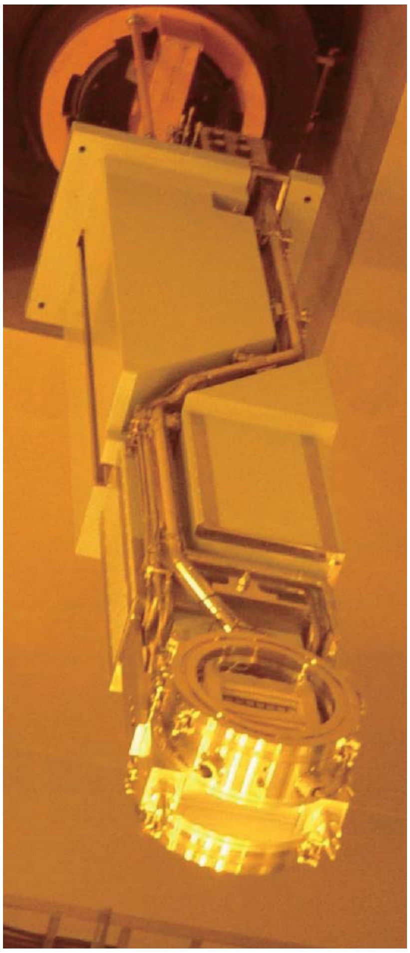

Photo. 2.8.10: View of the total assembly of the PBW at the hot cell. The assembly is hoisted by the cask.

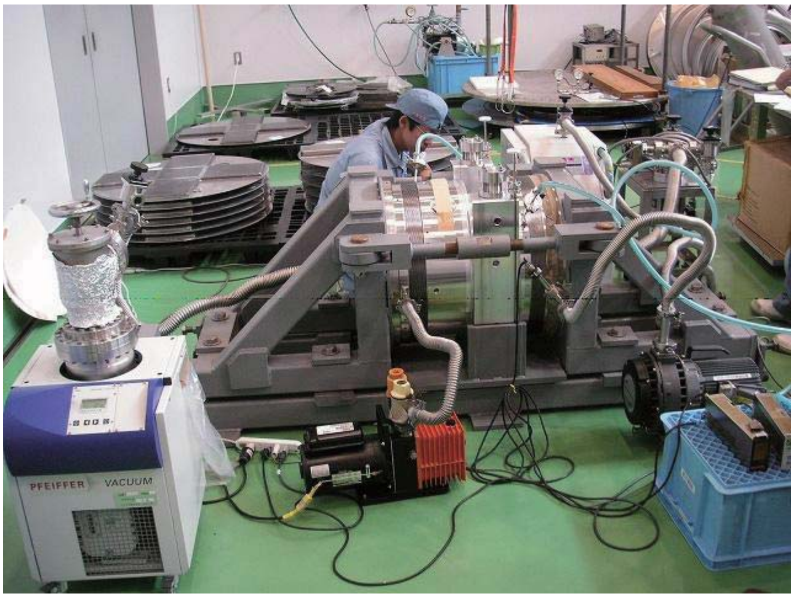

Photo. 2.8.11: Pillow seal performance test at vendor factory

Photo. 2.8.12: Iron slabs were assembled to a beam dump (left). The beam dump was completely covered with a stainless container and a long beam duct was connected (right).

Photo. 2.8.13: Primary coolant system II and III (left) and pure water supply system I (right)

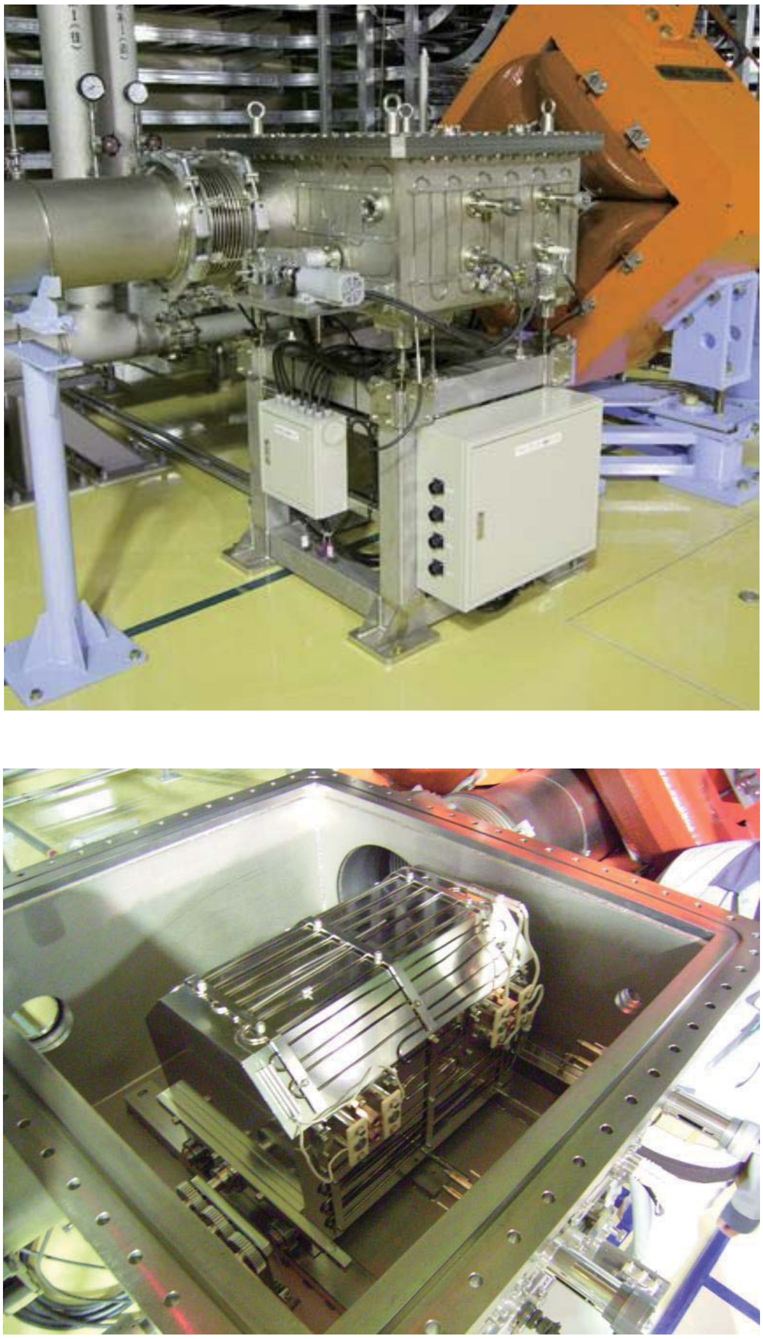

Photo. 2.8.14: The beam stopper (top) and the beam plug in the beam stopper (bottom)

2.9 Storage Facility for Activated Components

2.9.1 Basic Concept

The main components of the spallation neutron source, as a mercury target vessel, moderator vessels, a reflector, a proton beam window, have to be exchanged in certain periods on account of the material damage of proton and neutron injection. But the components cannot be exported from the MLF building immediately, because the radiation level is very high. Then the activated components must be stored temporarily in the MLF building for cooling down. The storage facility is planed to keep the activated components temporarily in safety by remote handling devices. Fig. 2.9.1 gives the flat plan of the irradiated components storage room. Fig. 2.9.2 gives the image of storage components in the irradiated components storage room. The concepts of the storage facility are shown as follows.

(1) Components to be stored

The components for storage in the MLF are highly activated and contaminated by the activated mercury, which cannot be exported from the MLF immediately after the replacement. These components have to be periodically replaced because of damage by irradiation.

The storage components in the MLF are shown below; (replacement period)

a. Mercury target vessel (0.5 years)
b. 3 type moderators (6 years)
c. Proton beam window (2 years)
d. Reflector (6 years)
e. Muon target (0.5 years)
f. Pump, Heat exchanger and other components of the mercury circulation system contaminated by irradiated mercury.

(2) Components not to be stored

The components showed below will not be stored in the MLF. However, in the case of accident, the storage facility should store these components for a short period.

a. Shielding plug (reflector and moderators plug, proton beam window plug, muon plug, etc.)
b. Electrical magnet (Exclusive storage pits are set near muon line.)
c. Neutron shutter

(3) Capacity of storage facility

The storage periods for each component are decided by the radiation level after cooling down. Capacity of the storage facility for each component is as the following.

a. Mercury target vessel :	2 (Max.3)
b. Moderators :	3 (1 set)
c. Proton beam window :	1
d. Reflector :	1

e. Muon target : 2 (in the storage facility)

Other exclusive pits are built in the M2 tunnel.

f. Pump, heat exchanger, and other components of the mercury circulation system : 1 set

(4) Storage configuration

Storage configuration of the each component is as the following.

a. Mercury target vessel

The vessel is inserted in the storage vessel without shielding and sealed to prevent the mercury vapor leakage, set on the storage rack at the irradiated components storage room.

b. Moderators

The piping is cut into 3 or 4 parts to reduce the storage space and stored in a container, set on the floor of the storage room.

c. Proton beam window

The piping and cables are cut into 3 or 4 parts to reduce the storage space and stored in a container, set on the floor of the storage room.

d. Reflector

The piping of the reflector is cut away and the reflector itself is stored in a container, which is placed on the floor of the storage room.

e. Muon target

The piping, cables and rod are cut into 3 or 4 parts to reduce the storage space and stored in a container, set on the floor of the storage room.

f. Components of the mercury circulation system

They are stored in the container with seal, set on the floor of the storage room.

Table 2.9.1 shows objective components, replacement period, capacities of storage, sizes and weights.

2.9.2 Handling of Activated Components

Outline of replacement and storage scenario for each activated component is as follows.

(1) Mercury target vessel

A new mercury target vessel, which is stored in the storage container, is transported by the ceiling crane (130 t) in the large components handling room and is put down through a ceiling hatch of the irradiated components handling room (hot-cell) and replaced for the used one by using the power manipulator and the target exchange truck. The storage container with the used target vessel is transported by the in-cell crane (20 t) to the irradiated components storage room and set on the temporary rack. The storage container is transported to a mercury target vessel storage rack by the ceiling crane (12 t) in the storage room.

(2) Moderators

New moderators are set on the attachment in the large components handling room and transported and put down by the ceiling crane (130 t) through a ceiling hatch of the hot-cell. The new moderators with attachment are transported by the in-cell crane to set the temporary rack in the hot-cell. Used moderators and reflector are transported from the target station, stored in the shielding cask by the 130t crane, and set on the floor hatch connecting the dry-up room. The used moderators and reflector with shielding plug are put down to the dry-up room. The cooling water remained in the moderators and reflector is removed by a dry-up system. The dry-up system is a compressed air circulation system with heater and dryer (chiller). After dry-up, the moderators and reflector are pulled up to the large component handling room by the shielding cask. The moderators and reflector are put down on the rack in the hot-cell. The new moderators and reflector are replaced for the used ones by using the power manipulator and the moderator exchange device. The used moderators and reflector are cut by using cutting device in the hot-cell and the used components and piping are separated and stored in the storage containers. The storage containers are put down to the irradiated component storage room by the in-cell crane (20 t). The storage containers are transferred to the common area by the in-cell crane (12 t) and stored. The shielding plug can be stored in the dry-up room.

(3) Proton beam window

Storage sequence for the proton beam window is almost the same as the moderator. But the attachment and the storage container are exclusive for the proton beam window. The Shielding plug can be stored in the irradiated component storage room.

(4) Reflector

Storage sequence for the reflector is almost same as the moderator. But the attachment and the storage container are exclusive for the reflector.

(5) Muon target, etc.

Storage sequence for the muon target is almost same as the moderator. But the attachment and the storage container are exclusive for the muon target. The Shielding plug can be stored in the irradiated component storage room.

Table 2.9.1: Main components stored in a storage facility of the MLF

Irradiated component considered to be stored	Storage capacity	Frequency	Dimension (mm), Weight (ton) (Storage container dimension, weight)
a. Mercury target vessel	2 (Max. 3)	2 / year	1150 × 1300 × H2200, 0.7 t (2100 × 1820 × H3200, 0.5 t)
b. Moderator	3 (1 set)	1 / 6 year	1400 × 850 × H4400, 0.25 t
c. Proton beam window	1	1 / 2 year	860 × 980 × H4510, 10 t (including beam plug)
d. Reflector	1	1 / 6 year	ϕ1900 × H4785, 20 t
e. Muon production target	2	2 / year	1020 × 1120 × H3200, 10t (including beam plug)
f. Mercury cooling system components, sensors	1 set	–	

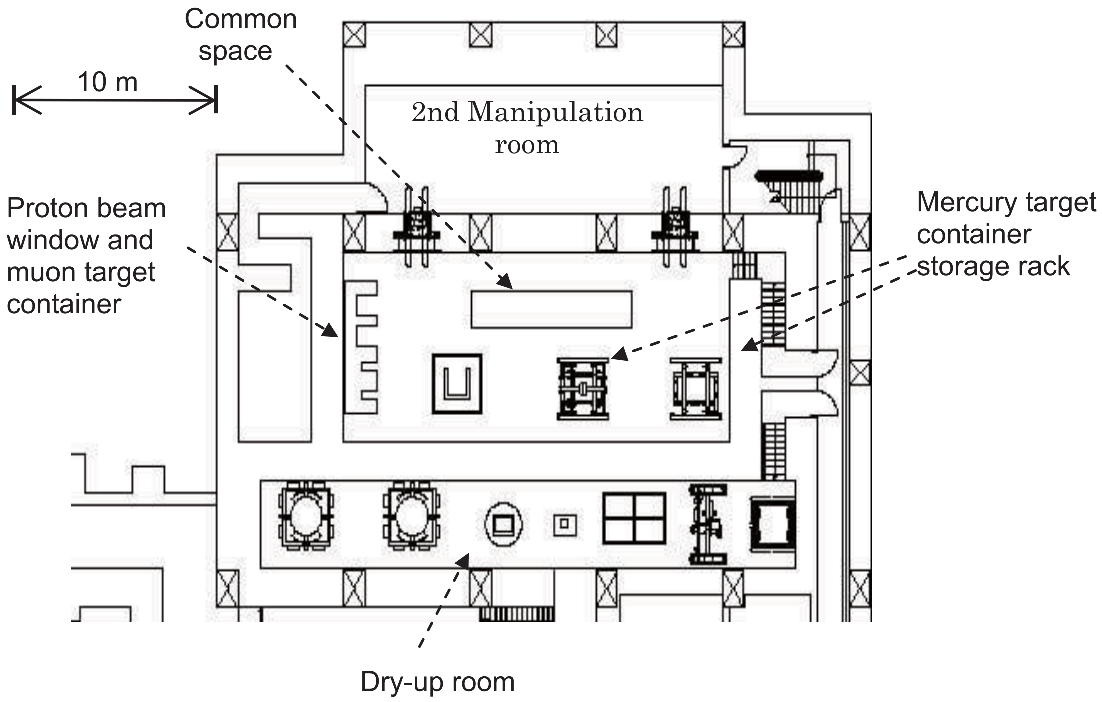

Fig. 2.9.1: Layout of the irradiated components storage room

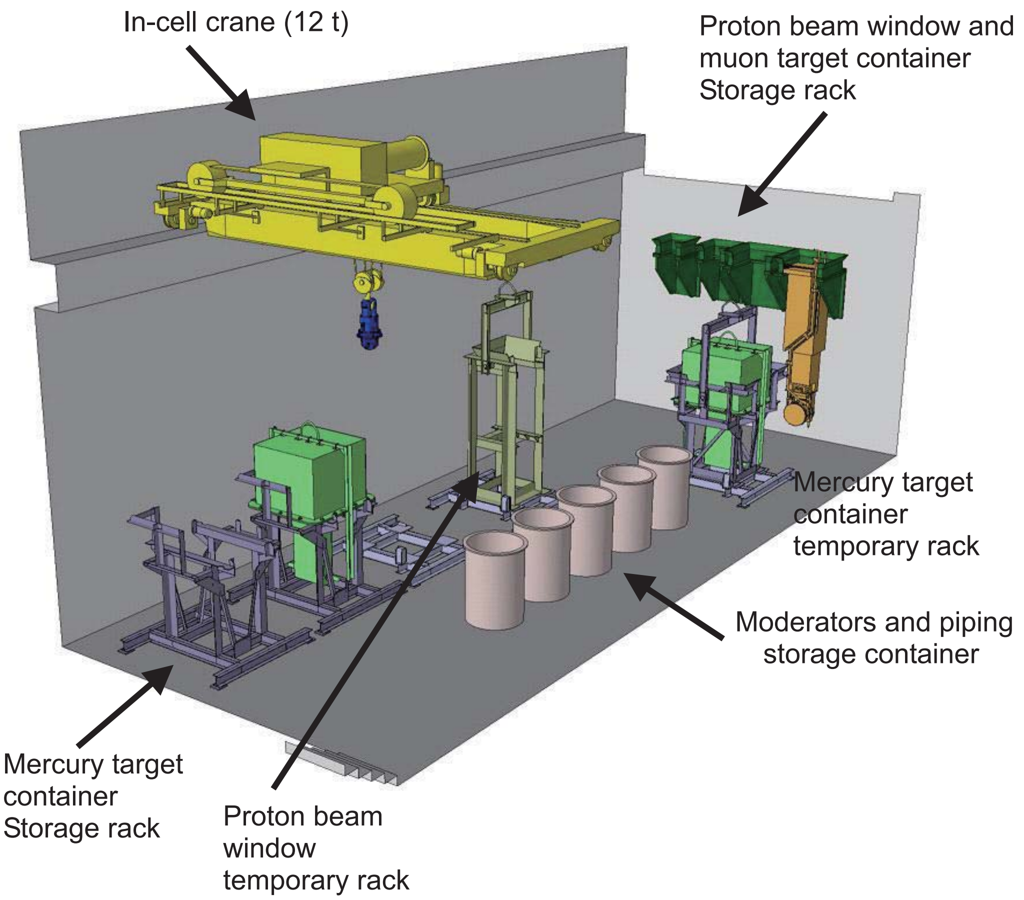

Fig. 2.9.2: Image of the storage components in the irradiated components storage room

2.10 Utility

2.10.1 Outline of Utility

The utility system in MLF is roughly composed of three systems, the cooling system for the neutron source, the electric power supply system and the building equipment including a ventilation and air conditioning system, a pressurized air supply system, a water supply and drainage system.

The cooling system is aimed to realize suitable removal of the heat generated by the primary proton beam and the secondary particles, such as neutron and gamma-ray. It also refrigerates main components of the neutron target system and the experimental apparatus in the experimental halls, by means of the light water cooling system, the heavy water cooling system, the air cooling system, the secondary cooling system, the unit to accept heavy water, the helium gas supply and exhaust equipment, the cooling water and cover gas analysis equipment, and so on.

The electric system receives high voltage (6,600 V) power from the electric power substation in Tokai Establishment and supplies adequate electricity to several systems in MLF. It consists of the transformation devices, such as the transformer and the breaker, etc., the distribution boards, the back-up generator for the emergency, the uninterruptible power source (UPS) and so on, to transform and supply electricity for each system.

The building equipment supplies air and water for the facility operation and experimental activities. The ventilation and air conditioning system keeps negative pressure of the radiation controlled area to prevent outflow of radioactive materials in the leakage accident. It will keep temperature in facility to remove heat of devices, which is not corresponded by cooling system. To reduce the volume of the exhaust from the radiation controlled area, the ventilation and air conditioning system equips blowers and filters for intake and exhaust, respectively, and the damper to control negative pressure and so on. It also includes the pressure air supply system to control valves or dumpers in MLF.

The components of the utility system are shown as follows;

1) Cooling system – Items in parenthesis are coolant fluid and radiation category*.

- Safety hull cooling unit (heavy water, high radiation)
- Reflector cooling unit (heavy water, high radiation)
- Target trolley cooling unit (light water, high radiation)
- Helium vessel cooling unit (light water, high radiation)
- Proton beam window cooling unit (light water, high radiation)
- Light water pre-moderator cooling unit (light water, high radiation)
- T0 chopper cooling unit (light water, low radiation)
- Neutron instruments cooling water supply unit (light water, no radiation)
- Air circulation for biological shielding cooling unit (dry air, low radiation)
- Secondary cooling unit (light water, no radiation)
- Heavy water acceptance unit
- Dump tank unit

- Pure water supply unit
- Helium gas supply and exhaust unit
- Water and gas analysis equipment

*Radiation category

High: Coolant will not be discharged and will be stored in the MLF during its facility lifetime.

Low: Coolant can be discharged outside the MLF.

2) Electric power supply system

- Transformation device
- Distribution board
- Generator for the emergency
- Uninterruptible power supply (UPS)

3) Building equipment

- Ventilation and air conditioning system
- Pressurized air supply system (intake, exhaust)
- Water supply and drainage system
- Control panel

2.10.2 Cooling System

(1) System composition

The constitution of the cooling system is shown in Fig. 2.10.1. The specification of each system is shown in Table 2.10.1.

The composition of the cooling system is as follows:

1) The primary cooling system

- Safety hull / Reflector cooling system
- Target trolley / Helium vessel cooling system
- Proton beam window / Light water pre-moderator cooling system
- T0 chopper cooling system
- Neutron experimental device cooling water supply system
- Biological shield cooling air circulation system

2) The secondary cooling system

3) Heavy water acceptance system

4) Helium gas supply and exhaust system

5) Water and gas analysis system

6) Purify water supply system

This system is composed of the primary cooling system to remove the heat directly from the target station components, the secondary cooling system to transfer the heat from the primary cooling system and diffuse to atmosphere, the heavy water accept system, the helium gas supply and exhaust system, the water and gas analysis system and the purify water supply system and so on.

The safety hull / reflector cooling system, the target trolley / helium vessel cooling system and the proton beam window / light water pre-moderator cooling system are set in the primary cooling system room at basement. The T0 chopper cooling system and the neutron experimental device cooling water supply system are set in T0 chopper cooling system room at 1st floor. The biological shield cooling air circulation system is set in shield cooling system room at 2nd floor. The heavy water acceptance system is set in high level irradiated water waste system room at basement, the purify water supply system and secondary cooling system are set in secondary cooling system building at the south-east outside of MLF, and the helium gas supply and exhaust system is set with the each system. The floor layouts of the MLF building and the piping route of the water cooling system are described in the section 3.5.

Some cooling systems supply coolant to two different components. The coolant is divided with the header component to assure adequate flow rate to each component, since the pump, the heat exchanger and the surge tank are common. The safety hull and the reflector are provided with the same cooling system. The target trolley and the helium vessel share the cooling system and the proton beam window and the light water pre-moderator also get coolant supply from the same system. The specifications of the cooling systems are summarized in Fig. 2.10.1.

(2) System composition and expected radiation level

1) Primary cooling system

a) Safety hull / Reflector cooling system

This system removes the heat generated in the safety hull and the reflector. Heavy water is employed as a coolant from the viewpoint of maximizing the neutron performance at the target-moderator-reflector system. Cooling water is highly irradiated. Tritium will be 10^{12} – 10^{13} Bq/cm^3 after 30 years operation (5,000 h/year).

b) Target trolley / Helium vessel cooling system

This system removes the heat generated in the front side of the target trolley shield and the shield in the helium vessel, the middle section shield, and the inner- and outer- reflector plugs for the reflector and the pre-moderators handling. This system circulates light water. Cooling water is highly irradiated. Tritium will be 10^{12} – 10^{13} Bq/cm^3 after 30 years operation (5,000 h/year).

c) Proton beam window / light water pre-moderator cooling system

This system removes the heat generated in the proton beam window and the pre-moderators for three kinds of moderators. This system circulates light water. Cooling water is highly irradiated. Tritium will be 10^{12} – 10^{13} Bq/cm^3 after 30 years operation (5,000 h/year).

d) T0 chopper cooling system

This system is set for the T0 choppers installed outside the biological shield in the neutron beam lines at the experiment halls. This system circulates light water. Since the T0 choppers are placed 8 – 10 m away from the origin of the neutron beam line. The irradiation level of the cooling water is comparatively low. It will be lower than the upper limit of the regulation.

e) Neutron experimental device cooling water supply system

Main cooling water is supplied for the neutron experimental device in the first experiment hall and the second experiment hall, but a small part of cooling water is supplied to the cryogenic hydrogen circulation system. This system circulates light water. The cooling water is not irradiated.

f) Biological shield cooling air circulation system

This system circulates dry air to remove the heat generated in the shield blocks surrounding the helium vessel. It is composed of the blower, the heat exchanger, the filter unit and so on. It also have the supply line and the ventilation line that can be used to ventilation the top of the helium vessel for maintenance works on and be connected to a local ventilation system.

2) The secondary cooling system

This system circulates light water to the heat exchangers of the primary cooling system and the mercury circulation system. It is composed of the circulation pump, the cooling tower, the cooling water purifier, the expansion tank, and so on.

3) Heavy water acceptance system

We have the precondition that heavy water is transported from the other facility. Therefore, this system accepts heavy water from drums and transfers them to the heavy water acceptance tank. And then, this system transfers it from the acceptance tank to the drain tank of the safety hull / reflector cooling system.

Heavy water is transferred to the acceptance tank in the highly irradiated waste water room by pressurizing the heavy water drum (transportation container) in the T0 chopper cooling system room on the first floor. The heavy water is transferred from the acceptance tank to the safety hull / reflector cooling system by pressurizing the acceptance tank with helium gas as well. To measure and record the inventory of heavy water, a level meter is installed in the acceptance tank.

4) Pure water supply system

Pure water supply equipment is composed of the ion-exchange resin unit, filters, and the pipes for the supply to each system. It is installed in the secondary cooling system pump building outside MLF. Purified water is supplied to the safety hull / reflector cooling system, the target trolley / helium vessel cooling system, the proton beam window / light water pre-moderator cooling system, T0 chopper cooling system, neutron experimental device cooling water supply system, the secondary cooling system and a gas waste processing system. Electrical conductivity of supplied water from the purifying system is less than 1.0 μS/cm.

This system is composed of the ion exchange resin cartridge and the filter to keep the water quality, the flow separation header, the flow meter, the degas device, and so on. The water quality meter is set at an exit to measure the water quality of pure water.

5) Helium gas supply and exhaust system

The helium gas supply system supplies helium gas for the target station devices and the cooling systems in the facility. Helium gas is supplied to the systems to keep the pressure constant to match the system specifications. This system is composed of the pressure control valve, the remote control breather valve, the flow meter, etc. Helium gas is also used for the pressurized test of the tanks or the leakage test of the pillow seal system. Therefore, this system is designed to correspond to the several pressure conditions. The pressure of helium gas is 0.15 MPa (for surge tank of water cooling system) to 0.98 MPa (for the target pillow seal).

The helium gas exhaust system manages the cover gas and the purge gas used in the cooling systems and target station devices. This system is composed of 3 systems, the heavy water system (cover gas of safety hull / reflector cooling system, etc.), the light water system (cover gas of target trolley / helium vessel cooling system, cover gas of proton beam window / pre-moderator cooling system, cover gas of T0 chopper cooling system, cover gas of neutron experimental device cooling water supply system, etc.) and the mercury system (cover gas of mercury circulation system, gas filled in safety hull, gas filled in helium vessel, etc.). Each water system has the condensation vessel cooled by chilled water. Then, the exhaust gas is dried so that almost of the tritium water would be collected. The collected water returns to the cooling system by the gravity effect. The mercury system is connected to the waste gas processing system at the waste gas processing room at first floor. The exhaust gas including mercury and rare gas is processed to remove radioactive elements. Exhaust gas is blown down to the facility ventilation system and discharged through the stack with the filter unit of the ventilation system. Moreover, this system has vacuum pump to conduct vacuum purge for the connected components.

6) Water and gas analysis system

The cooling fluids (circulated water and cover gas) are irradiated during operation. Especially, the three systems in the primary cooling system room at the basement (safety hull / reflector cooling system, target trolley / helium vessel cooling system, proton beam window / pre-moderator cooling system) are relatively highly irradiated. Therefore, the water and gas analyses are necessary to measure their radioactivity levels and the amount of impurities before exhausting the cover gas. For this purpose, the analysis system is installed in the water and gas analysis system room at the basement. Cover gas and cooling water are pulled in the hood and the device by the sampling line, and analyzed. Gas chromatography analysis system is set at the water and gas analysis system room.

The cover gas in the mercury circulation system, the helium gas filled in the helium vessel and the helium gas filled in the safety hull have to be analyzed before discharge.

A liquid waste transportation vessel is installed in the bottom part of the hood to transfer the liquid waste, which is produced in the analysis equipment. Gas is sent to the facility ventilation sysytem through the exhaust blower of the sampling food.

(3) Common specification

The specification of the cooling system is shown in the following. Especially, the system is designed to reduce the outside leakage of the radioactive substance as low as possible.

1) Vessels and tanks
   a) The material used for the vessel should have better corrosion resistance than type 304 stainless steel since it contacts to the liquid.
   b) The vessel or tank, in which the radioactive substance is involved, is fabricated in cylindrical shape with welding. The soundness of the welded sections can be confirmed by the visual observation or by the other leakage tets.
   c) In consideration of the long-term use (more than thirty years), more than 1.5-mm wall thickness is sellected.
   d) The fixation part of the container is designed under the condition that the earthquake-proof is 0.25G.
   e) The tanks are designed to drain almost inside water.
   f) As for the decay tank, the internal structure (baffle board and so on) is devised to get rid of the stagnant region or recirculation, and then the necessary time (2 minutes) to decay the short-lived radioactive nuclide must be secured.
2) Pumps and blowers
   a) In principle, a self-water-inject type canned pump is employed for the transportation and circulation of the primary coolant.
   b) The pump of the primary cooling system is installed on a catch pan for leakage liquid to prevent the expansion of the leakage. Therefore it can detect leakage with a resistance line and so on.
   c) A remote shaft abrasion detector is put on the pump so that it can remotely watch the conditions of the shaft.
3) Heat exchangers
   a) The heat exchanger used for the primary water cooling system is the all welded-plate type heat exchanger. The multiple piped heat exchanger is used for the air cooling system.
   b) The catch pan for leakage liquid is installed under the heat exchanger, which is used for the primary water cooling system circulating the high radioactive coolant, and it can detect leakage.

(4) Refrigerators
   a) Refrigerator is constructed so that it would not require "the freezing preservation of order and public safety personnel” who is prescribed by “the high pressure gas preservation of order and public safety law".
   b) CFCs or HCFCs aren't used for refrigerant.

(5) Cooling tower
   a) The cooling tower is an enclosed type to decrease effluent capacity of the radioactive to atmosphere.

(6) Piping and valves

a) All the pipes that include highly activated substances are the seamless ones.

b All the remote valves that attach highly activated substances are air-operating type and the valves installed in the main piping of the primary water cooling system are metal bellow seal type ones.

c) The connection of the piping must be welded in principle. But, the flanges are used for the piping connection with the machine.

d) The velocity of the liquid in the piping should be less than 2.5 m/s from the viewpoint of preventing the fluid inductive vibration and the cavitation. The velocity of gas should be less than 10m/s.

e) In all systems, the part exposed to liquid or gas is made of type 304 stainless steel or equivalent material.

f) All the air operation valves should close normally, and operating pressure is less than 0.5 MPa・G.

g) The open rate of the air-operating valve, which needs to control the open rate, is adjusted remotely by watching the indicator on the control panel.

(7) Instrumentations

a) Thermometer should be K-type sheathed thermocouple. Precision is JIS class-1 equivalent (JIS-0.4 degree). The sheath material is NCF600 or type 316 stainless steel equivalent. The compensating lead wire should be of precise class with the electromagnetic shield. Double element type should be used. And it can be switched to another one, when the one being used is failed.

b) An orifice-type or other pressure difference sensing type is adopted for the flow meter of liquid .

c) When the supply of electricity or pressurized air is lost, the sensors detect it and the system would be shut down to the safety side.

d) A leakage detection is the resistance detection type.

(8) Common equipment

Industrial water, compressed air and so on are supplied in the facility as common equipment. The specifications are shown as follows.

a) Industrial water

P.H. :	5. 8 - 8. 7
Turbidity :	less than 15
Temperature :	less than 30°C
Pressure :	About 0. 3 MPa (0. 2 - 0. 4 MPa)

These qualities are based on Ibaraki Prefecture industrial water service regulations.

b) Compressed air

Supply pressure :	0. 6 ±0. 1 MPa
Dew point :	less than 10°C (under pressurized condition)
Filter :	less than 0.01 mm

(9) Operation control equipment

a) We can watch and operate the whole system in the neutron source target station using the general operator console installed in the MLF control room on the third floor. If necessary, when the operation mode is changed to local mode, the independent equipment operation can be conducted by using the local control panel of each system.

b) When the operation mode is changed to the other mode, the operator can confirm the operation status step-by-step interactively through the man-machine interface.

c) The fundamental monitoring items of each cooling water system are flow rate, pressure, temperature, etc.

d) The alarm signals concerned to the low flow rate of cooling water, low pressure, pump stop and leakage detection are duplicated. One of each is transmitted by using the PLC network and the other is sent to a PLC module with metal wires independently. Those signals are transmitted to the MLF control room and connected to the indication panel and the interlock system.

e) If the power supply is lost, this system has the UPS, then the system can stop safely.

2.10.3 Electric Power Supply System

(1) Composition outline

The electric room of the MLF is located on the southeastern side of the 1st floor, and the electric power supply system accepts 6,600-V electric power in 3 lines from the 50-GeV special high voltage substation. This system transforms the voltage down to the loads of the facilities in the MLF and distributes the electricity with cables to them. An emergency power generator is connected to the 6,600-V feeder line for the dedicated facilities. The common UPS (Uninterrupted Power Supply) is connected to important systems that need continuous power supply anytime even when power outage takes place. The PPS is equipped with its own UPS, because the PPS is essential to radiation safety and is necessary to be maintained independently from the other systems. As for the muon and the neutron experimental instruments, the dedicated power supply circuits are installed to suppress high harmonic distortion and noise for precise experimental measurements. The composition of the electric supply power system is shown in Fig. 2.10.2.

(2) General properties

1) Earthquake-proof design

Design horizontal seismic intensity (K_H) is 0.4.

2) Cable specifications

Cables have to pass the test of “JIS C 3005 4.26 − 60° inclination test” and they do not generate Dioxin gas or Halogen gas at the event of the combustion. Furthermore, the cables are designed with careful consideration for the fireproof countermeasure.

3) Earth system circuit

This system is classified into the general (commercial) purpose circuit and the dedicated experimental instrument circuit for the purpose of avoiding high frequency noise. The general purpose circuit is isolated from the experimental instrument circuit. Therefore, these two circuits have each independent earth electrode and bus line.

4) Penetration management of the area boundary

The cable penetration parts of the wall or the floor are sealed according to the legal fire protection division. As for the part where airtight is required, airtight treatment is done additionally. Moreover, the parts where shielding is needed are penetrated by using concealed pipes with curve form.

(3) Detail of the power supply system

1) General (commercial) circuit

The system doesn’t have any backups of spare power supply for blackout event. The systems that are not connected to the emergency generator, such as the common UPS, experimental devices, PPS circuit, are connected tothis circuit. The power supply to the primary coolant circulation pumps is not connected to the emergency generator, because it is assecced that the heat from nuclear reactions is not neccesary to be removed once the proton beams stop.

2) Emergency power generator circuit

The emergency power genetrator system is installed in the generator room on the southeastern side of the 1st floor. When the general circuit system detects power outage, the emergency power genetrator is started automatically and some lines are switched to emergency power genetrator. It takes about 40 seconds for the lines to be fed with electricity again. The main specifications of the emergency power generator are as follows;

- Type : gas turbine generator
- Rated spec : 500 kVA, 6,600 V and 50 Hz
- Fuel : Heavy oil
- Volume of the tank : 1,950 ℓ (7.5 hours rated operation, equivalent)

The main machines connected to the generator are

- The sensors and the CCD camera system of the reflector remote control system
- The exhaust blower and control machine of the ventilation system for the basement floor radiation component storage room, 1st floor radiation component handling room (hot cell).
- The monitors of the facilities radiation safety system
- The safety light.

3) UPS circuit

The UPS circuit system is installed in the electric room. It.has batteries and is to supply electricitly without any momental stop even if general circuit has outage. The emergency power generator takes over when it is started and the electricity is fed from the emergency power generator. The electricity won't be interruped even for very short momonet. The main specifications of the UPS are as follows;

- A rated input : 3 phases 200 V, 50 Hz
- A rated output : 3 phases 200 V, 100 kVA
- Storage battery type : Sealed lead battery (MSE)
- Blackout compensation time : 10 minutes

The main machines connected to UPS are

- The control systems of the primary and the secondary cooling systems and the air circulation system for Biological-shield cooling
- The control system of the mercury circulation system
- The circulating pumps and control system of the cryogenic hydrogen circulation system
- The control system of the helium refrigerator
- The control panels and operation indication panels of the MLF control system

4) Experimental device circuit

It has the system to avoid the inflow of the high harmonic distortion and noise from the power supply system to the experimental device. To reduce the noise flowing into the experimental device, the transformer bank is independent from that of the systems since it can become a source of the noise by itself.

The main machines connected to this circuit are

- The experimental devices
- The measuring machine of the in-cell monitors

5) PPS circuit (independent UPS circuit)

Because high reliability is demanded, exclusive UPS is installed in the power supply system of the PPS in the control room at 3rd floor. The input of the UPS is supported with a generator. The main specifications of the UPS are as follows;

- Rated input : single phase 200 V, 50 Hz
- Rated output : single phase 200/100 V, 15 kVA
- Storage battery form : Sealed lead battery (MSE)
- Blackout compensation time : 10 minutes

The machines connected to the PPS circuit are mainly related to the radiation safety.

- Entrance control system of the PPS areas
- The PPS control panels
- The control system of the neutron shutters and the muon blocker

2.10.4 Building Equipment

(1) Composition outline

Building equipment consists of the ventilation and air condition system, pressurized air supply system and water supply and drainage system and so on. The ventilation and air condition system adjusts the pressure of the radiation controlled area. It also controls temperature and humidity in the building. The pressurized air supply system is set in the air compressor room at the first floor. The pressurized air is used to operate the valves and dumpers in the MLF. The water supply and drainage system supplies water to anywhere in the MLF and drains water to the storage tank (water from the radiation controlled area) and outside of the building (water from non-controlled area).

(2) Ventilation and air condition system

The ventilation and air condition system consists of the air supply system and the exhaust system. The air supply system includes the blower filter chiller and heater. The supply system removes dusts from the intake air and adjusts temperature and humidity in the building. The exhaust system includes the blower and filter. The exhaust system reduces dusts in the exhaust air from the radiation controlled area. Those systems adjust the balance of the supply and the exhaust by controlling the dumper to keep the pressure of the radiation controlled area in negative. Figs. 2.10.3 - 2.10.10 show diagrams of duct flow in the MLF. The system is separated into eight lines, in which, 6 lines are connected to the radiation controlled area and 2 lines are connected to the non-controlled area. Lines of the radiation control area are east No. 1, east No. 2, west No. 1, west No. 2, experimental hall No. 1 and experimental hall No. 2. The capacities of these lines is as follows;

- East No. 1 : 11,030 m^3/h
- East No. 2 : 20,800 m^3/h
- West No. 1 : 47,890 m^3/h
- West No. 2 : 15,230 m^3/h
- Experimental hall No. 1 : 32,000 m^3/h
- Experimental hall No. 2 : 25,000 m^3/h

Total amount of exhaust air is over 160,000 m^3/h.

The negative pressure level in the MLF is categorized in 4 levels;

Level I : −280 mmAq (Irradiated components handling room (Hot-cell), Irradiated components storage room)

Level II : −60 mmAq (Primary cooling system room, Dry up system room, Gas processing system room, etc.)

Level III : −30 mmAq (Manipulation room, Primary cooling system power supply room, etc.)

Level IV: −10 mmAq (Experimental hall)

(3) Pressurized air supply system

The pressurized air supply system consists of compressors、pressure control valves, accumulation tanks and so on. The pressurized air is supplied to operate the air operation valves of the neutron source related systems and ventilation system in the MLF building. The pressurized air is also supplied to the experimental halls for the experimental use.

Specification of the pressurized air supply system is as follows;

- Pressure : 0.6 MPa for neutron source and experimental hall
  0.39 MPa for ventilation system
- Volume of the accumulate tank : 3.25 m^3/h for neutron source and experimental hall
  190 m3/h
- Compressor : 2.9 m^3/min
  0.65 m^3/min

(4) Water supply and drainage system

The water supply and drainage system consists of the piping, taps and sinks, catch basin, pumps and tanks. Water from the filtration plant is introduced to the taps and sinks in the MLF. The used water from sinks in the radiation controlled area flows down to the catch basin or the drain tanks, if necessary, the water in the catch basin is pumped up to the drain tanks. Drain tanks also accept the drainage water from the cooling system in the MLF.

Table 2.10.1: Specification of cooling systems

<table>
<tr><th>component</th><th>type</th><th>volume [m^3]</th><th colspan="2">1st flow rate [m^3/h]</th><th>2nd flow rate [m^3/h]</th><th colspan="2">heat exchange* [kW]</th><th>1st piping</th><th>2nd piping</th><th>main piping velocity [m/s]</th><th>temp. (in/out) [°C]</th></tr>
<tr><td>safety hull (D_2O)</td><td rowspan="2">combined</td><td rowspan="2">5</td><td>12</td><td rowspan="2">32</td><td rowspan="2">47</td><td>36</td><td rowspan="2">266</td><td>50A</td><td rowspan="2">125A</td><td>1.53</td><td>35/37.3</td></tr>
<tr><td>reflector (D_2O)</td><td>20</td><td>230</td><td>80A</td><td>1.16</td><td>35/43.9</td></tr>
<tr><td>target trolley (H_2O)</td><td rowspan="2">combined</td><td rowspan="2">5</td><td>6</td><td rowspan="2">32</td><td rowspan="2">31</td><td>6</td><td rowspan="2">171</td><td>40A</td><td rowspan="2">100A</td><td>1.25</td><td>35/36.0</td></tr>
<tr><td>helium vessel (H_2O)</td><td>26</td><td>165</td><td>80A</td><td>1.51</td><td>35/42.2</td></tr>
<tr><td>proton beam window (H_2O)</td><td rowspan="2">combined</td><td rowspan="2">5</td><td>5.4</td><td rowspan="2">23.4</td><td rowspan="2">5</td><td>5</td><td rowspan="2">27</td><td>40A</td><td rowspan="2">40A</td><td>1.13</td><td>35/35.8</td></tr>
<tr><td>pre-moderator (H_2O)</td><td>18</td><td>22</td><td>80A</td><td>1.04</td><td>35/36.1</td></tr>
<tr><td>T0 chopper (H_2O)</td><td>single</td><td>5</td><td colspan="2">18</td><td>38</td><td colspan="2">220</td><td>50A</td><td>65A</td><td>1.27</td><td>35/45.6</td></tr>
<tr><td>neutron station (H_2O)</td><td>single</td><td>10</td><td colspan="2">125</td><td>180</td><td colspan="2">1,130</td><td>125A</td><td>150A</td><td>1.38</td><td>35/42.8</td></tr>
<tr><td>bio-shielding (air)</td><td>single</td><td>10</td><td colspan="2">2400</td><td>15</td><td colspan="2">12</td><td>300A Sch20</td><td>25A</td><td>9.09</td><td>35/51.4</td></tr>
<tr><td>secondary cooling system (H_2O)</td><td>single</td><td>12</td><td colspan="2">500</td><td></td><td colspan="2">3000</td><td></td><td>300A</td><td>1.99</td><td>30/35.2</td></tr>
</table>

*: Proton beam power is 1 MW.

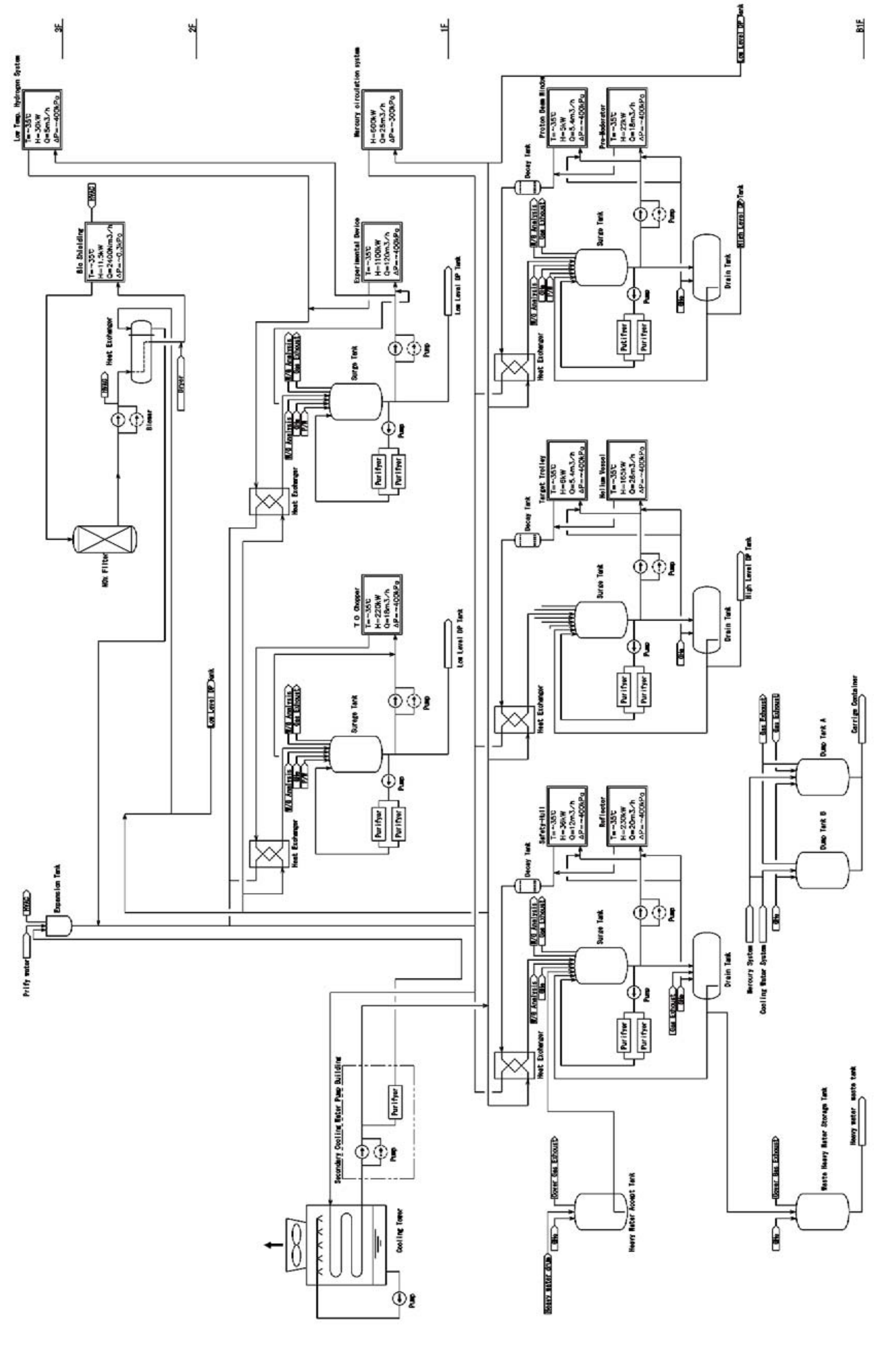

Fig. 2.10.1: Constitution of the cooling system for the neutron source

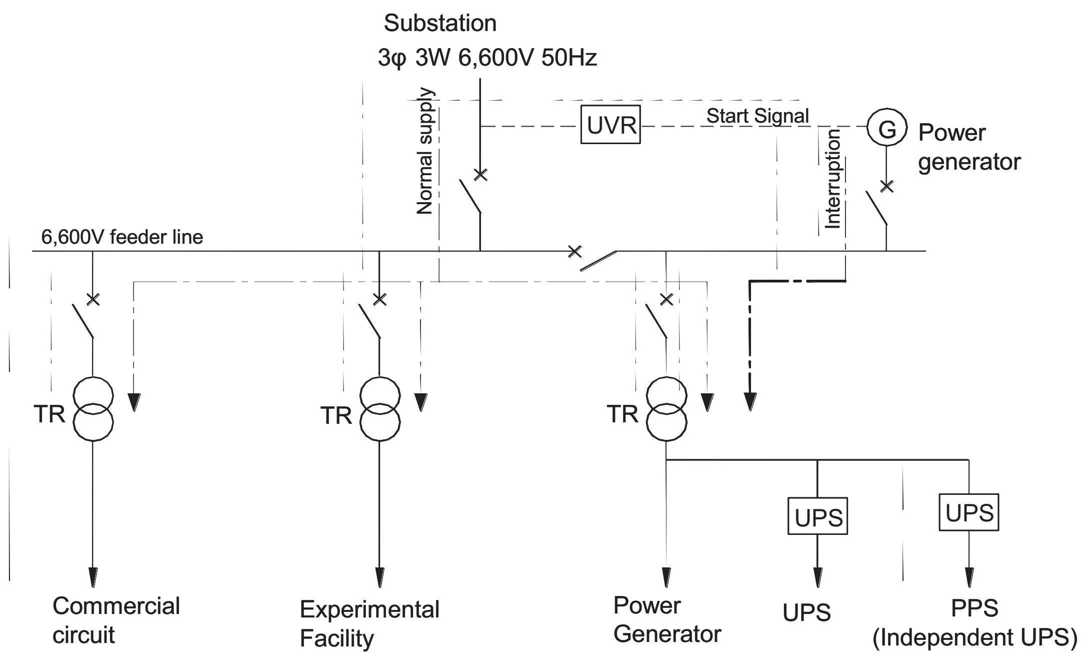

Fig. 2.10.2: Outline of power supply system

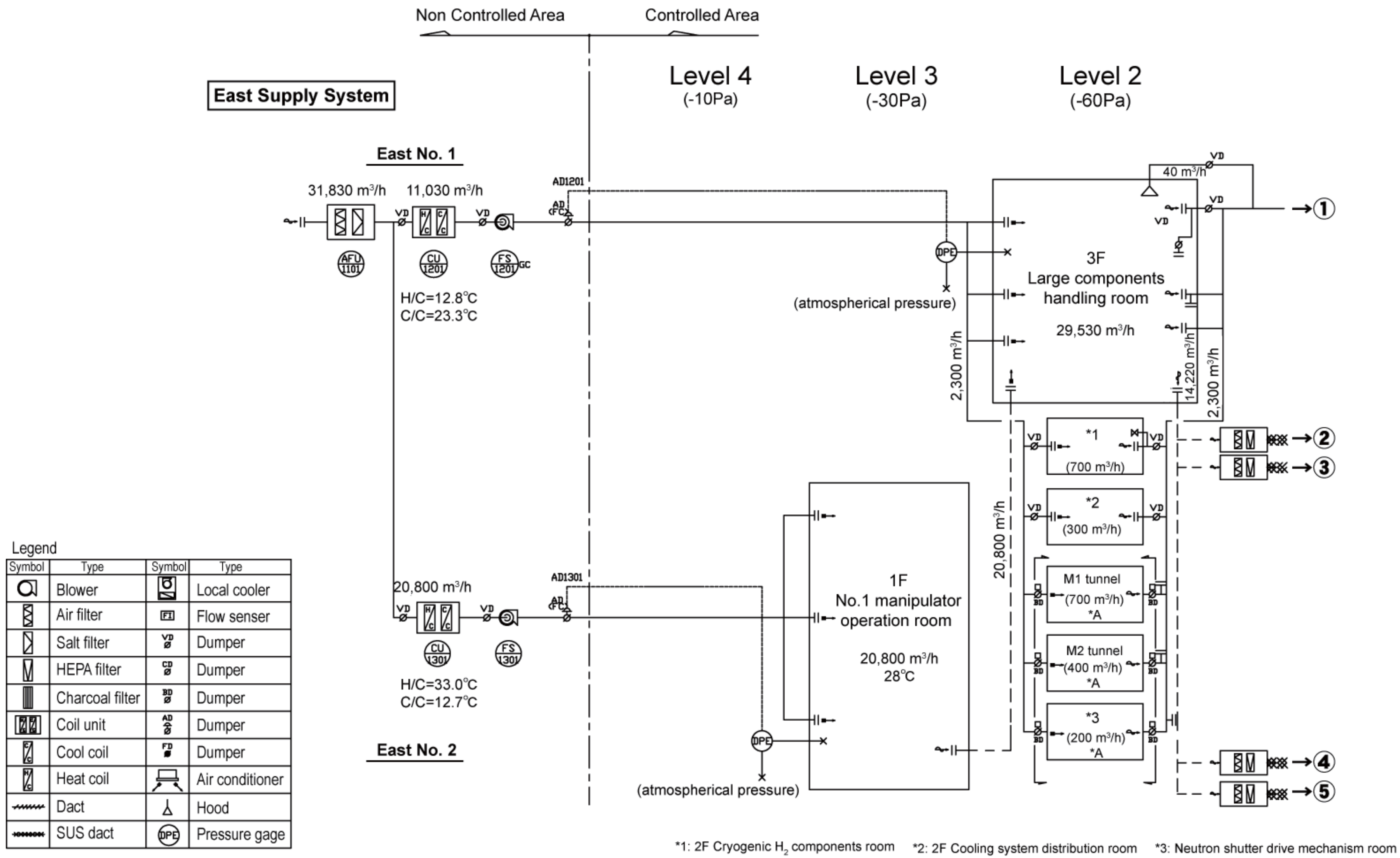

*1: 2F Cryogenic H_2 components room *2: 2F Cooling system distribution room *3: Neutron shutter drive mechanism room

Fig. 2.10.3: Duct flow of east controlled area (1)

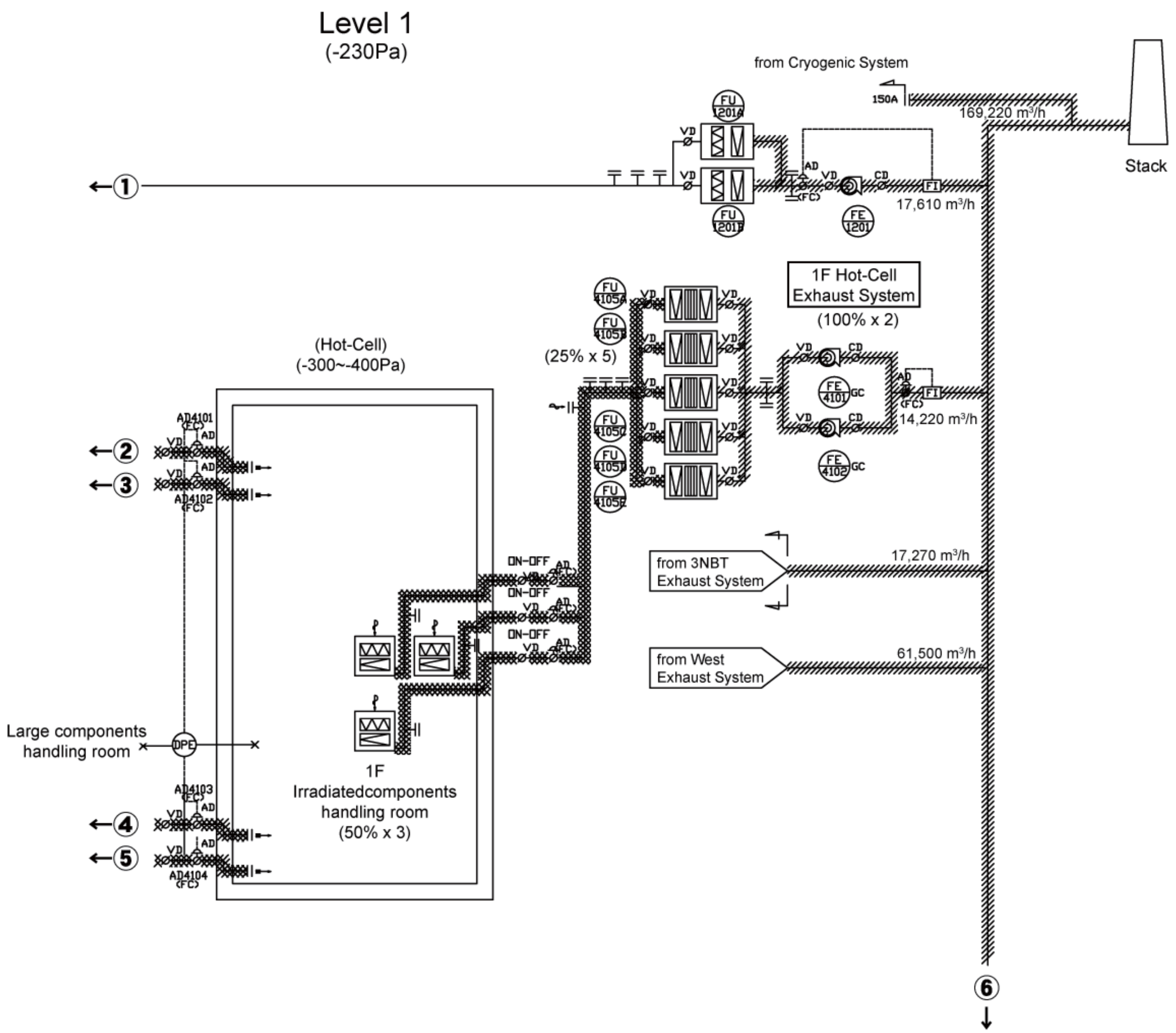

Fig. 2.10.4: Duct flow of east controlled area (2)

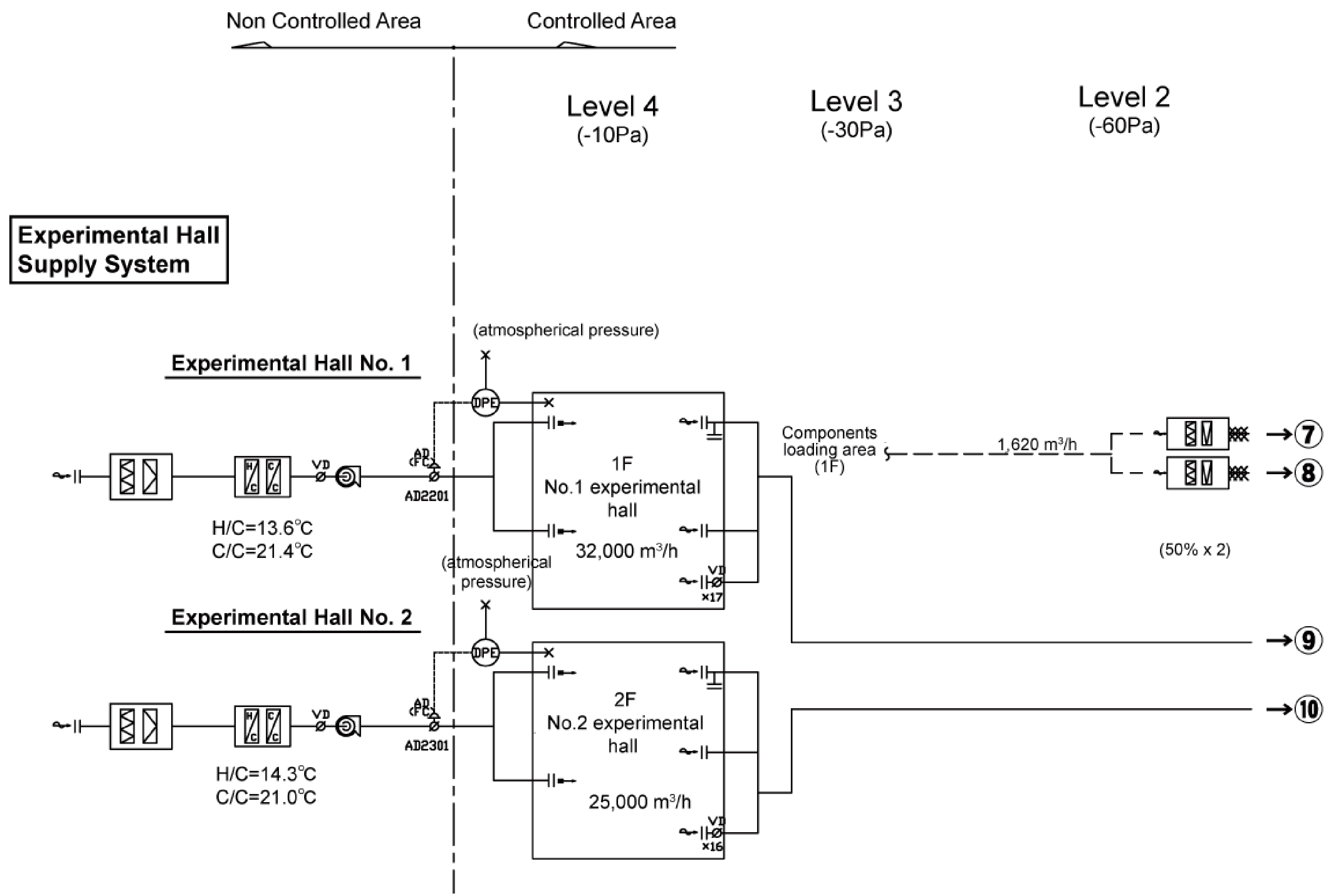

Fig. 2.10.5: Duct flow of east controlled area (3)

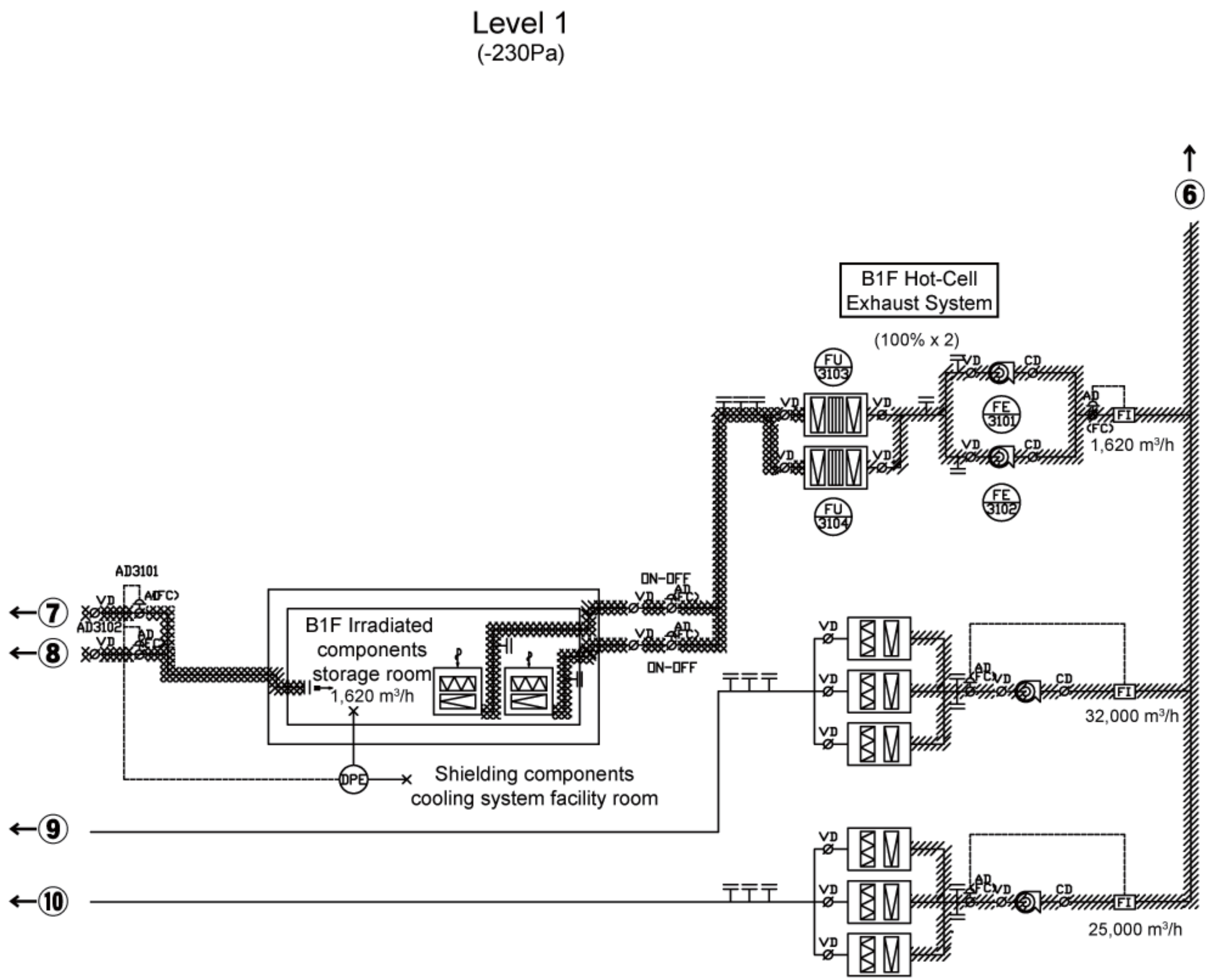

Fig. 2.10.6: Duct flow of east controlled area (4)

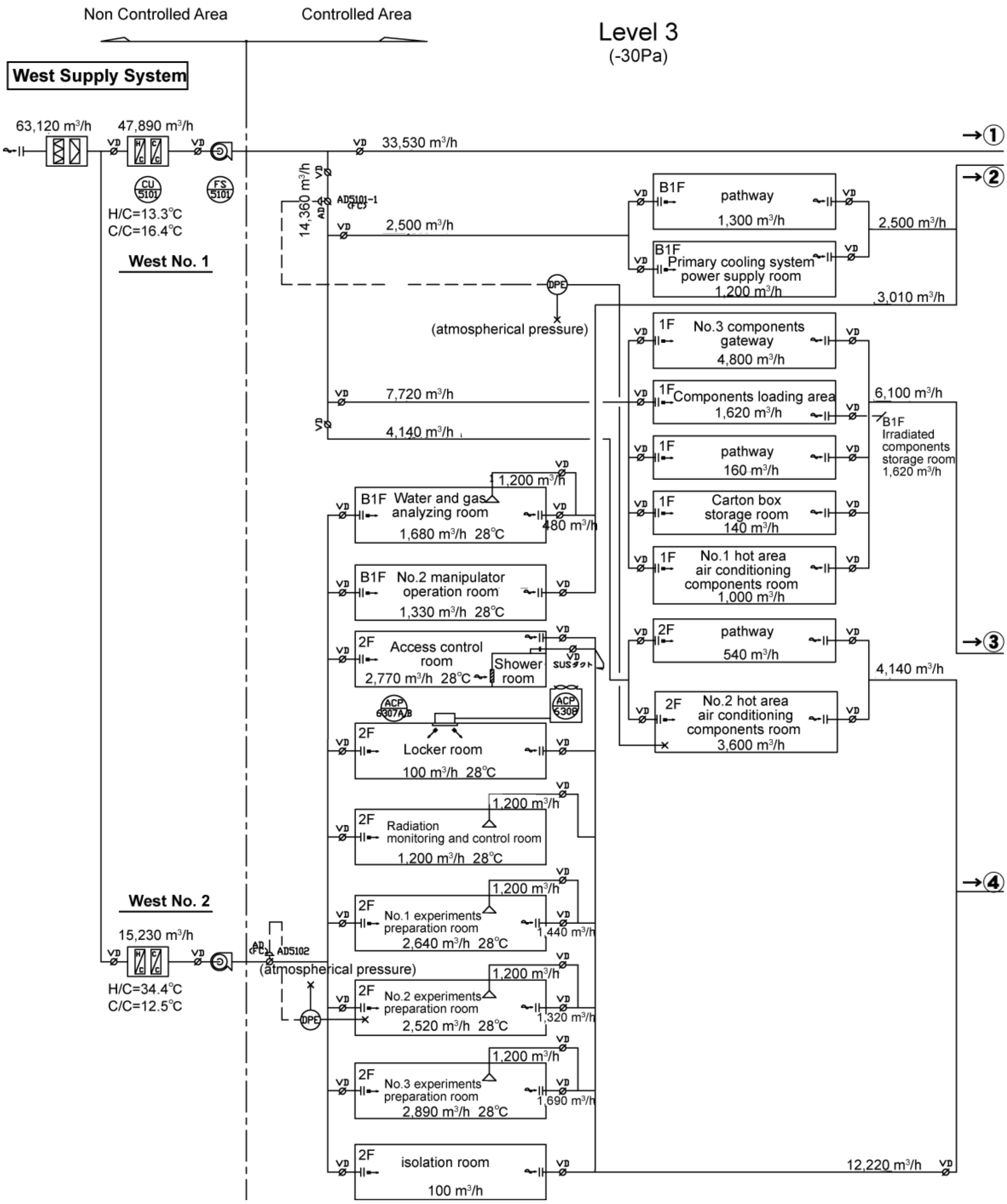

2.10.7: Duct flow of west controlled area (1)

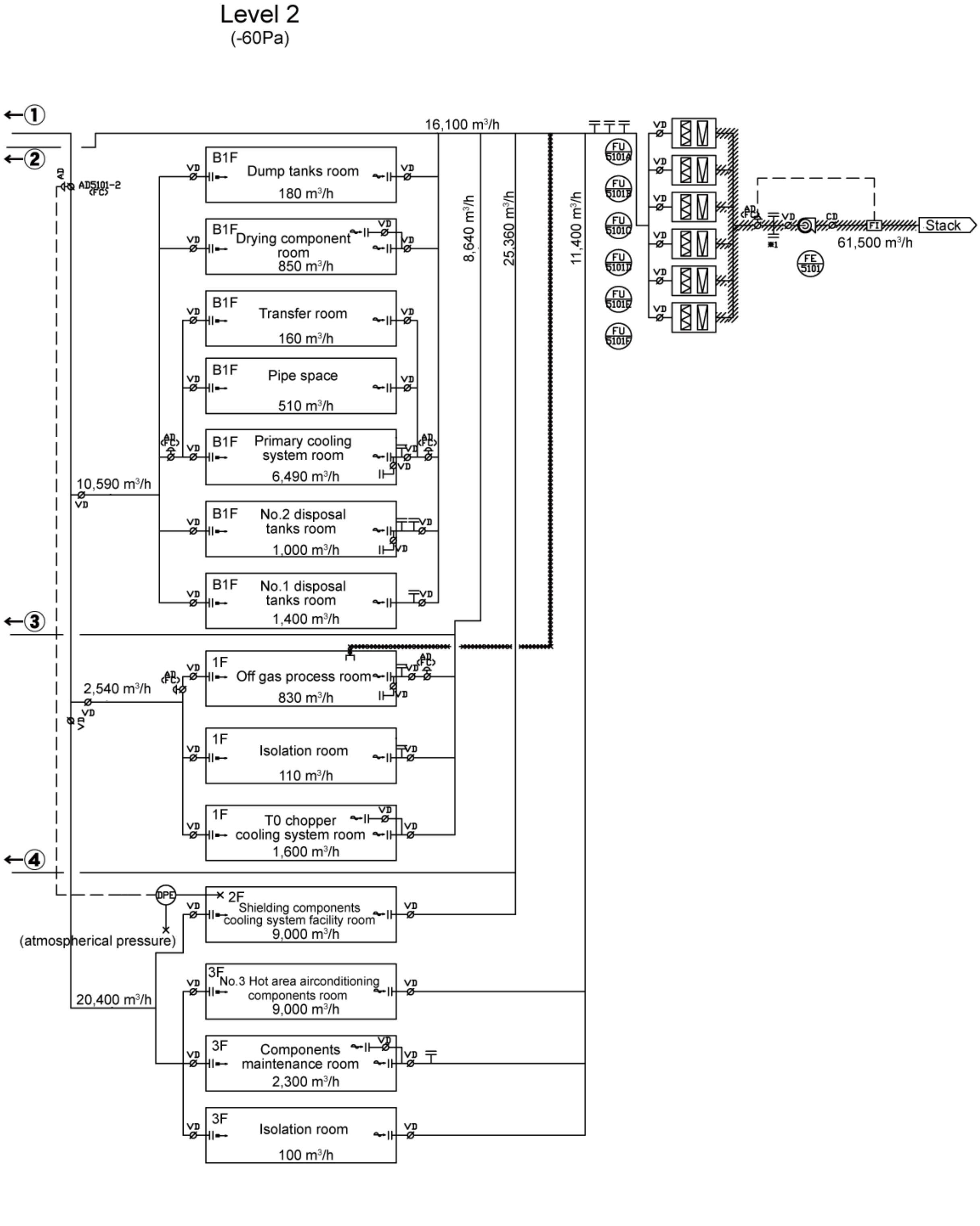

2.10.8: Duct flow of west controlled area (2)

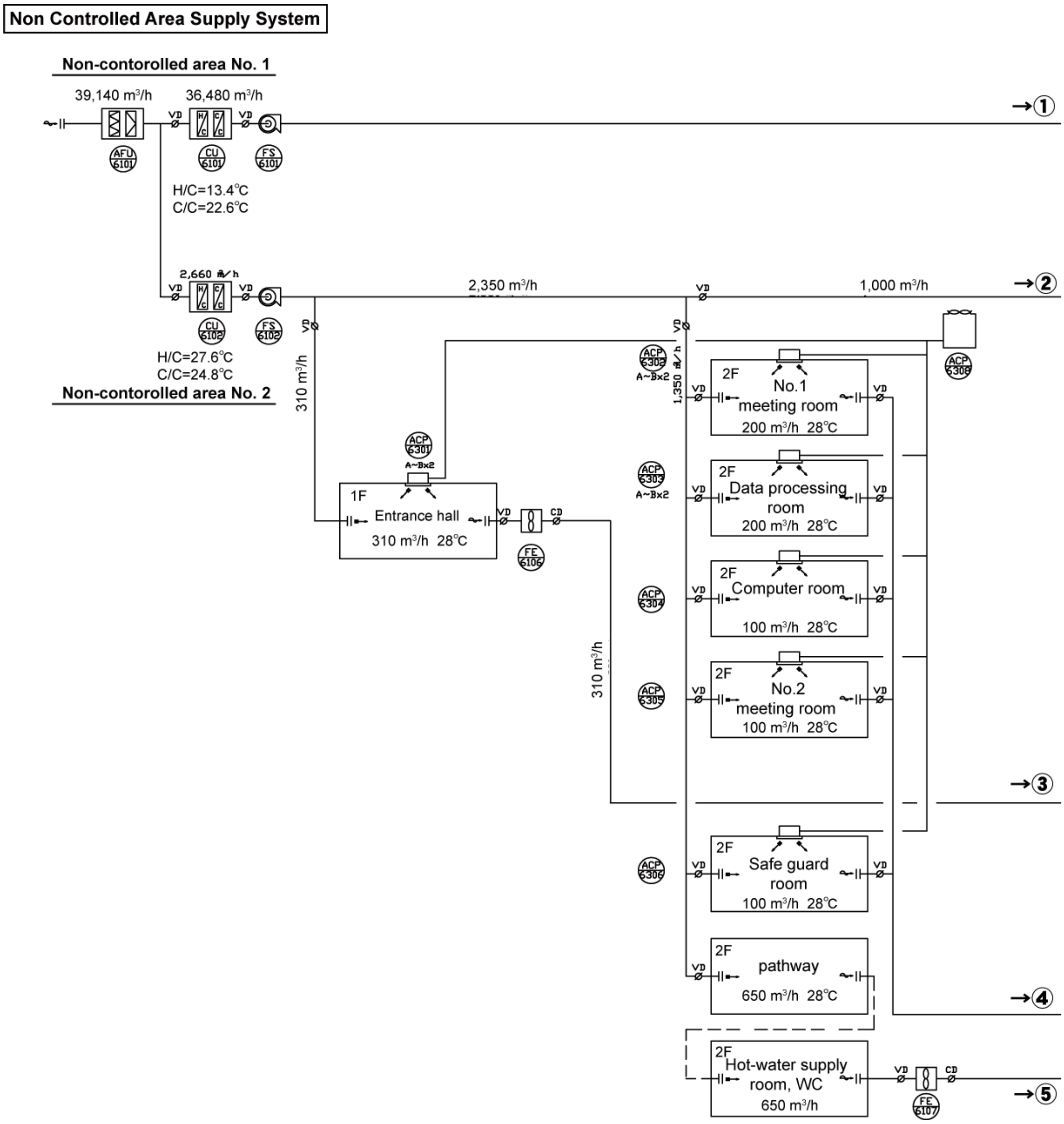

2.10.9: Duct flow of non-controlled area (1)

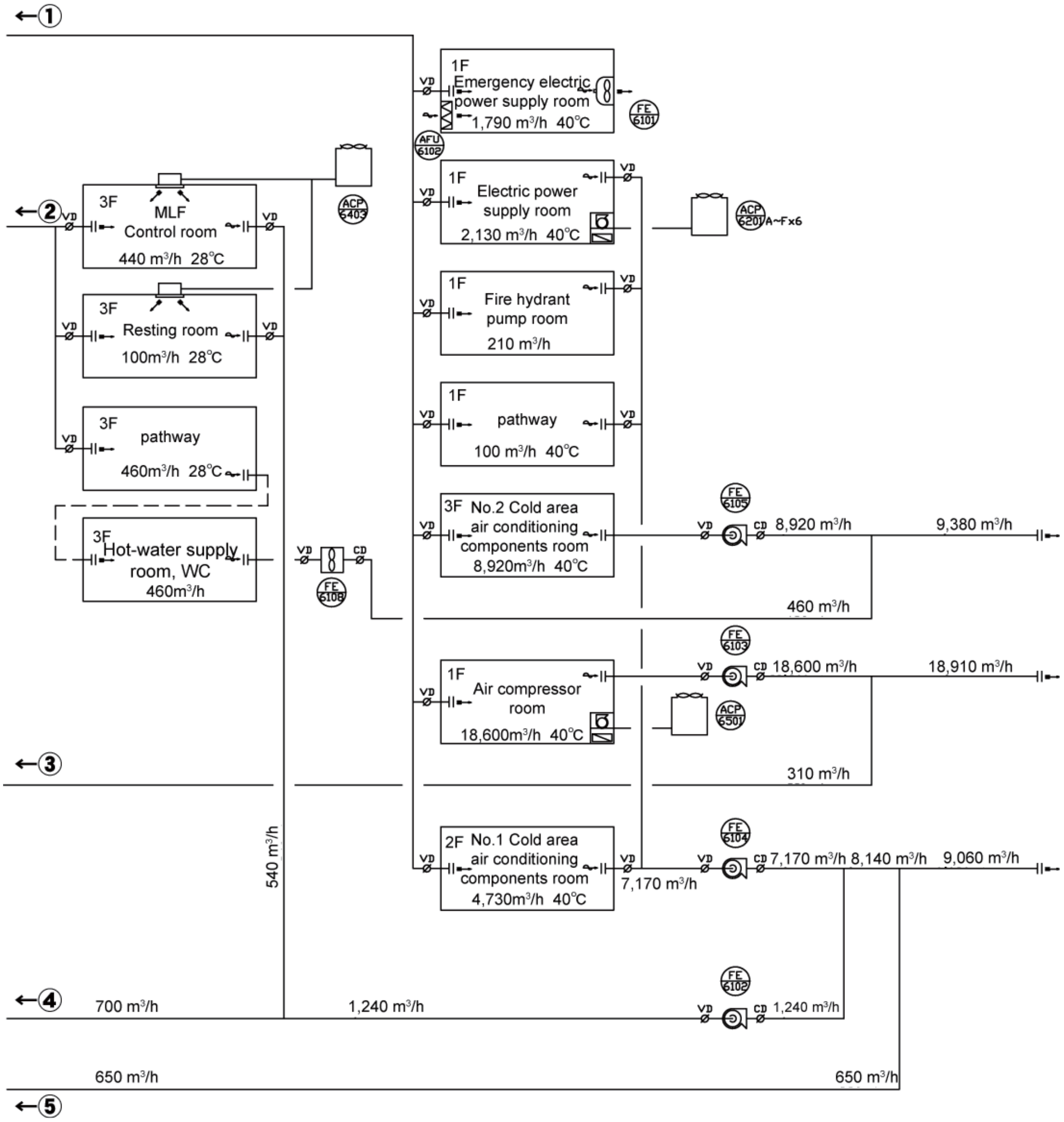

2.10.10: Duct flow of non-controlled area (2)

2.11 Control and Interlock System

In order to operate all the equipment of the MLF safely and efficiently, the MLF general control system (MLF-GCS) is designed to have several subsystems such as the facility control system centering on the control of the targets, interlock systems for protecting personnel, machine and the neutron target, and so on. The MLF-GCS has an advanced and independent system for control of the neutron target, including a large amount of mercury, three moderators with supercritical hydrogen and cooling systems with radioactive light and heavy water. It administers the instruments and operating processes according to the various MLF operating states such as the beam irradiation, adjustment of the source, and target exchange. Although the MLF-GCS is an independent system, it has to work closely with the control systems of accelerator and other facilities in J-PARC.

The construction of MLF-GCS and its performance test to check and adjust remote operations and integral interlocks from the control room of MLF have been completed. This chapter explains an outline of the MLF-GCS including interlock systems.

2.11.1 Structure of MLF-GCS

The structure of the MLF-GCS is shown in Fig. 2.11.1. The rectangle of broken lines in Fig. 2.11.1 shows the control room of MLF (MLF-CR), located on the 3rd floor of the facility. This structure, based on the concept of a distributed digital control system (DCS), has the advantage of allowing modification and addition of instruments flexibly in the future. In Fig. 2.11.1, personal computers (PC) and programmable logic controllers (PLC) such as an administrative control panel (ACP), general control panel (GCP) and local control panels (LCP) are connected through a looped and duplicate optical network system for PLC links named MELSECNET-H (NET-H). The ACP and GCP are also connected to Information View PCs (IV-PC) and Web, Data Base (DB) and EPICS servers through a duplicate Ethernet system of the MLF-GCS. These servers are also connected to a control network system (C-LAN) in J-PARC, which is administered by the central control room (CCR) to control the accelerators and facilities. The C-LAN is a duplicate Ethernet system of star topology and its core switch in the CCR is directly connected to a 1st edge switch in each facility. The C-LAN of the MLF consists of edge switches, the 1st edge switch connected to the CCR, network hubs and devices. A monitoring network system (M-LAN) of the MLF is included in the C-LAN and is connected to the 1st edge switch of the C-LAN. In addition, J-PARC has also a network system for general users (J-LAN). The C-LAN is connected to the J-LAN extending from the CCR through a firewall.

2.11.2 Functions of MLF-GCS

The ACP consists of four PCs installed with the SCADA (Supervisory Control and Data Acquisition) system, and the GCP consists of PLCs, I/O devices and touch panels. In MLF-CR, the ACP and GCP administer the entire MLF by monitoring status, executing processes, warnings and interlocks of systems, displaying trend information and acquiring data through MELSECNET-H. They also control local instruments indirectly through LCPs or directly through remote I/O panels. To enable many operating processes using the equipment in the MLF, the ACP and GCP are designed as parts of a centralized control system, and coordinate controls executed by the LCPs.

The operating data from the ACP are shown on two large plasma displays (PDP) in the MLF-CR, managed by IV-PCs. The DB server stores operating data and the Web server distributes several kinds of operating information through the C-LAN. For general users of the MLF, the information such as status, schedule and beam on/off areas is shown on exclusive terminals mounted at several places in the MLF as information displays. More detailed information is distributed to authorized PCs in the format of a Web browser or database on demand. Contents of this detailed information are determined depending on the aim of utilization such as experiment or facility maintenance. Here, the information for experimental users is distributed through the CCR and the J-LAN because their PCs are connected to the J-LAN.

Comprehensive control of J-PARC is carried out with the EPICS (Experimental Physics and Industrial Control System) protocol through the C-LAN. The EPICS server of the MLF consists of PCs for the Input/Output Controller (IOC) and Operating Interface (OPI). It is connected as one of the EPICS terminals of J-PARC, and mediates between the MLF and CCR as an EPICS interface. For monitoring the entire MLF, about eighty cameras are placed in normal and high-radiation areas. Their images are digitalized by IP cameras and IP encoders, transmitted to the MLF-CR through the M-LAN, and shown on three large plasma displays managed by the ITV control PCs.

2.11.3 Timing System

Independently of the structure shown in Fig. 2.11.1, the MLF-GCS distributes some kinds of signals for synchronizing with the incident period of proton beam in order that users in the MLF could operate and adjust their experimental instrument, and acquire and analyze experimental data. The structure of MLF timing systems is shown in Fig. 2.11.2. In J-PARC, a scheduled timing system based on high-precision 12 MHz Master Clock (MLCK) signal generated in the CCR is adopted as a standard timing system. According to the scheduled timing system, the Master Clock and 25-Hz trigger pulse (MLF Reference; MLFREF) produced by this scheduled timing system are distributed to users in the MLF.

In addition, the MLF-GCS also distributes the timing signals named as “RCS Trigger Tag (RCSTG)”, “3NBT –CT Trigger (3NCT)“ and “RCS Extraction Kicker Trigger (RCSXT)”, where “3NBT” and “RCS” represent the 3GeV proton beam transportation tunnel and 3GeV rapid cycling synchrotron, respectively. The RCSTG represents the common number of a primary proton beam tagged by the CCR. The 3NCT represents the proton beam signal which is detected by the current transformer mounted upstream of the target. The RCSXT is the signal for starting up the power of kicker magnet in order to eject proton beam from the RCS to the facilities. The RCSXT will be important for the experimental apparatus that requires the timing signal for synchronizing with the proton beam ejection high-precisely. Users can utilize these timing signals according to their request.

2.11.4 Interlock System

Interlocking systems, each of which has a veto to stop the proton beam supply, play an important role for ensuring the safety of persons and machines in the MLF. The MLF-GCS has three kinds of interlock systems named MPS, TPS and PPS. The instruments of each interlock system are connected with duplicate metal cables. Fig. 2.11.3 represents the structure of interlock systems within the MLF-GCS more concretely rather than Fig. 2.11.1.

MPS (Machine Protection System) is a system for preventing trouble in important machines due to unusual irradiation by a proton beam. After the sensors detect interlock signals, the signals are collected in each LCP and are transmitted to an exclusive MPS controller in the MLF-CR. After receiving the signals, the controller sends a request for proton beam stop to the CCR through an exclusive route. In J-PARC, the devices of the MPS were originally developed for protecting accelerators from thermal shock caused by the proton beam, and the MLF also utilizes these devices. After transmitting the MPS signal to the CCR, the radio frequency (RF) power to a linear accelerator (LINAC) is terminated and beam-shutters between the ion-source and RFQ (a type of LINAC) are closed.

PPS (Personnel Protection System) is a system for preventing exposure of personnel to high-radiation. In the maintenance of the MLF, there are two kinds of areas requiring PPS. One is the area of high-radiation generated directly by the primary proton beam and the other is the area of high-radiation generated by radioactive components such as the target vessels. Entrance into these PPS areas is controlled with keys and an interlock system operating in response to radiation levels. In addition, entering into the PPS area related to the proton beam is also restricted according to the beam operation mode as defined by the accelerator state. In Fig. 2.11.1 and Fig. 2.11.3, the PPS in the MLF consists of a PPS monitoring PCs, a PPS management device, a user PPS management device, PPS local instruments and so on. Entering into the PPS areas for the facility maintenance is administered by the PPS management device. On the other hand, entering into experimental rooms of secondary beam lines is administered by the user PPS management device. The PPS of the MLF also terminates the proton beam, if necessary, to protect personnel from high-radiation during proton beam irradiation. The PPS interlock signals collected in the PPS management device are transmitted to the CCR through an exclusive route. Since the beam stop function of the PPS requires higher reliability than the MPS, not only the beam shutter close function but also the ion-source termination, are included in this procedure.

TPS (Target Protection System) is an interlock system for preventing troubles related to the mercury target from expanding to become serious if the beam stop operation executed by the MPS ends in failure. Since the beam stop by the TPS is required to have the same reliability as the PPS, the TPS interlock signals are collected in the PPS management device, and the beam is terminated by utilizing the beam stop procedure of the PPS. In Fig. 2.11.3, 5 LCPs emit MPS interlock signals, with 3 of those LCPs of also emitting TPS signals. In addition, information on the 97 MPS and 11 TPS interlocks is displayed on the ACP through NET-H.

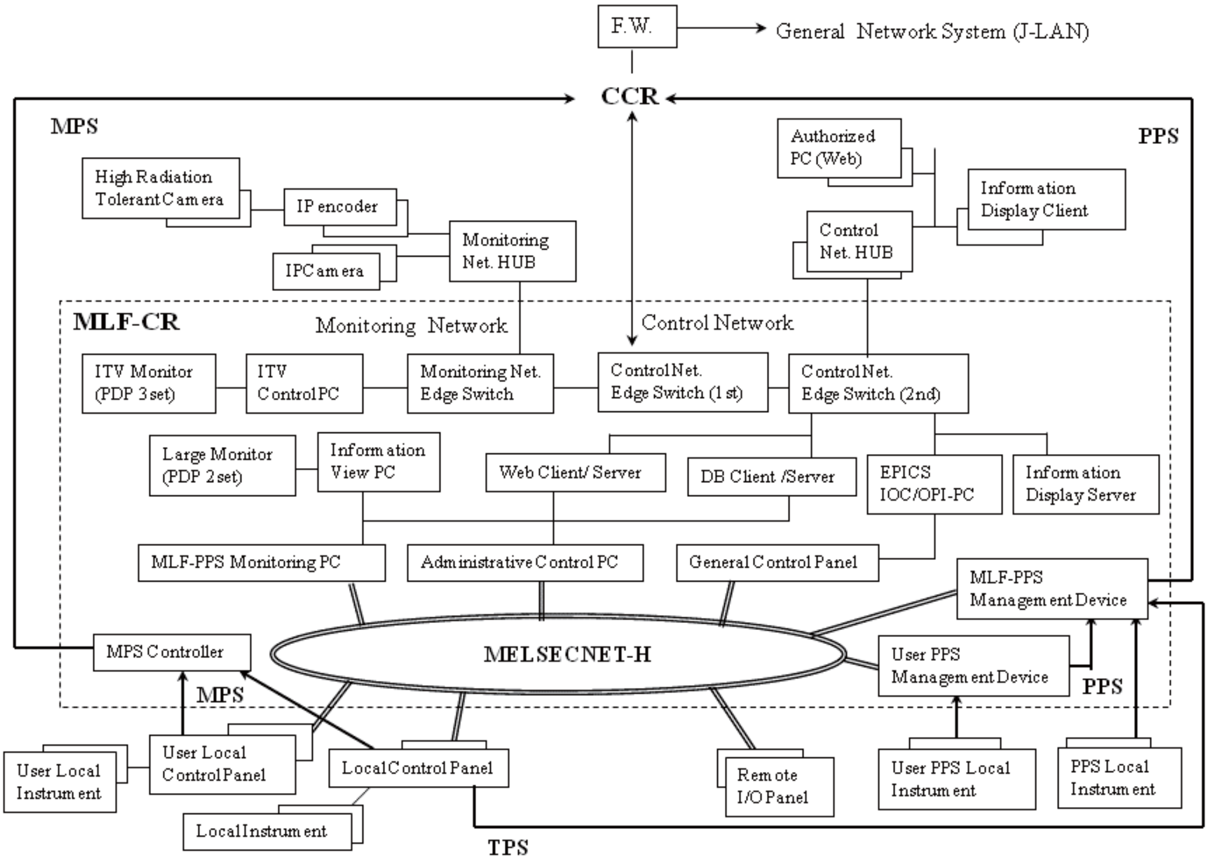

Fig. 2.11.1: Structure of MLF general control system

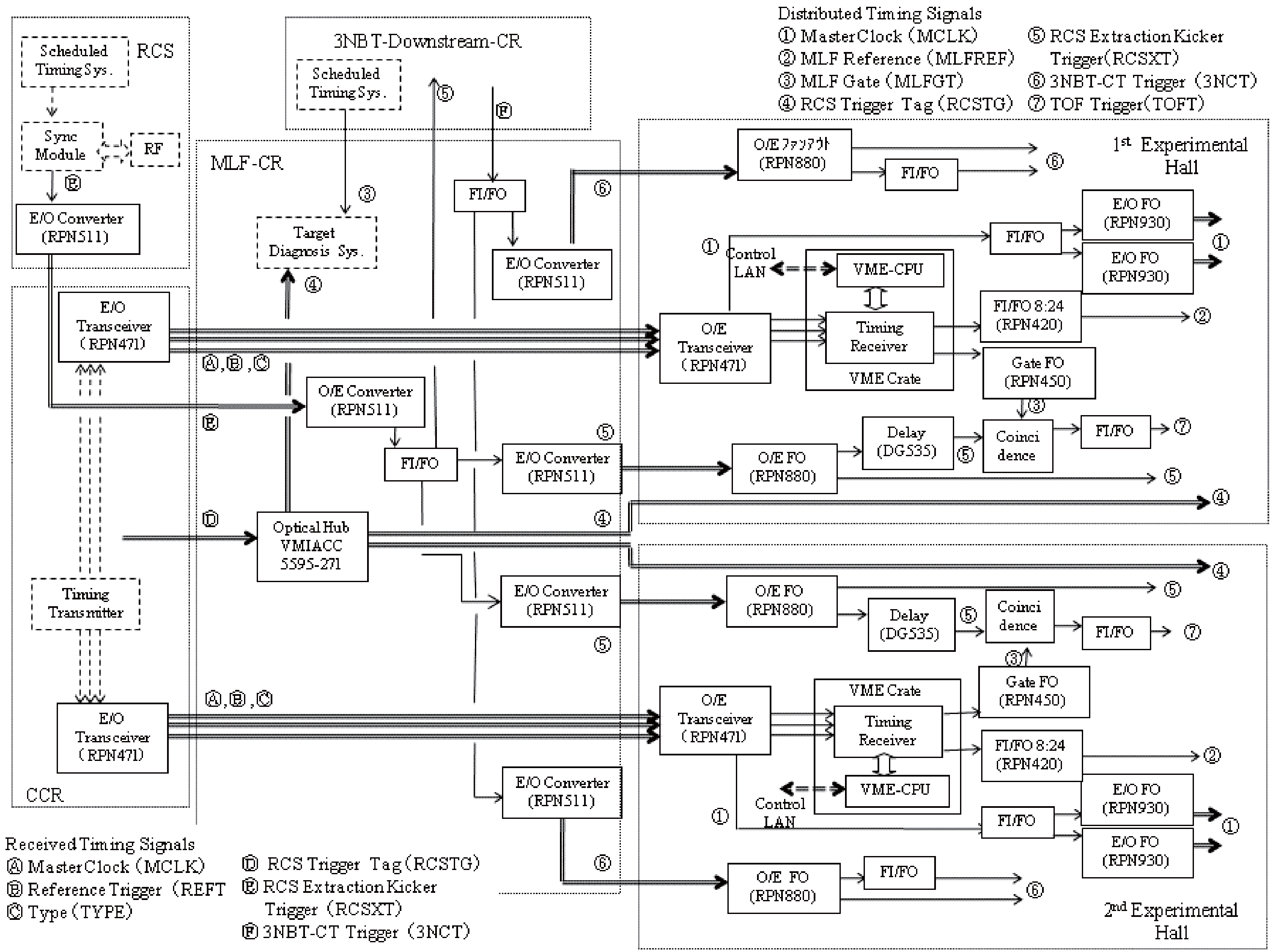

Fig. 2.11.2: Structure of MLF timing system

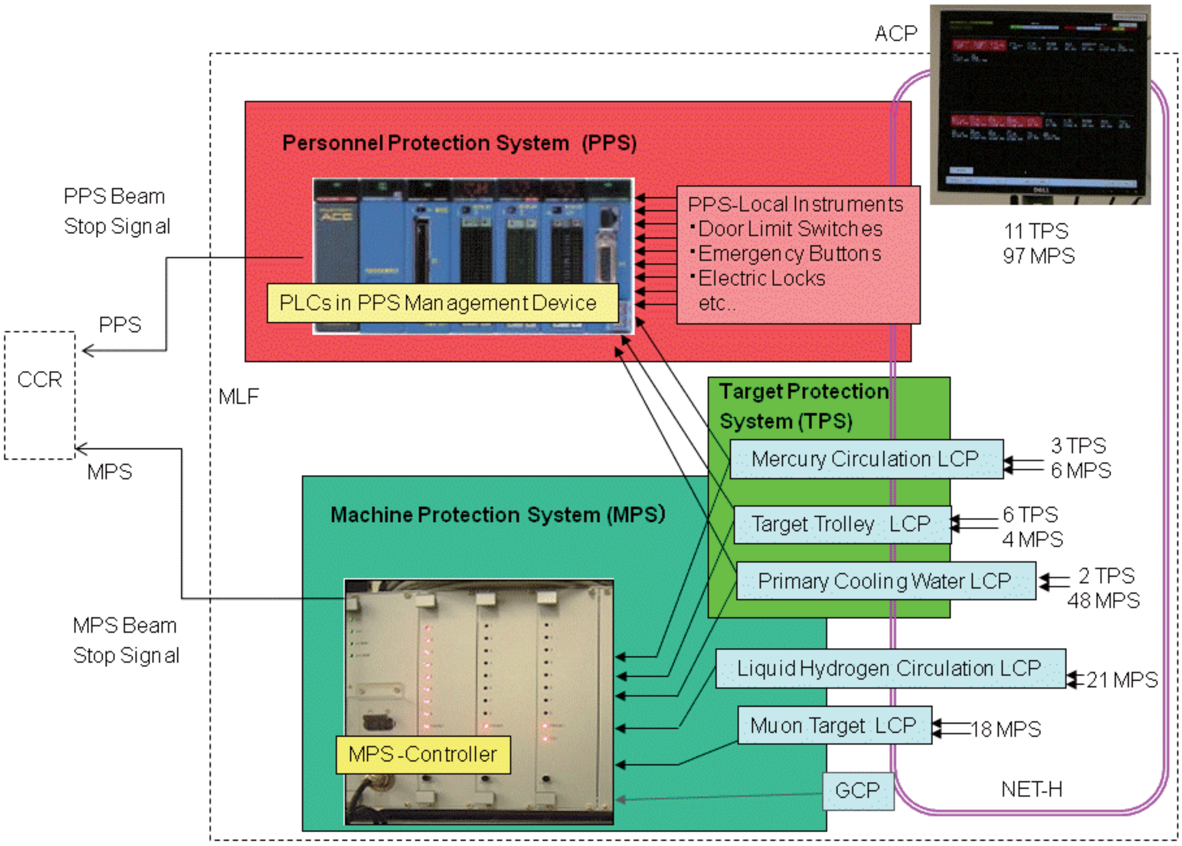

Fig. 2.11.3: Structure of ML F interlock system

2.12 Neutron Beam Evaluation Instrument

2.12.1 Outline

NOBORU, NeutrOn Beam-line for Observation and Research Use, has been constructed at the beam line number 10 (BL10) in the Materials and Life Science Experimental Facility. NOBORU was designed to "observe" a 1MW Japan Spallation Neutron Source, i.e. to study neutronic performance of JSNS. The characteristics of the neutron source will be measured to provide high-quality and high-intensity neutron beams to the JSNS users. The mission is classified into the following five;

a) comprehends the correlations between various control parameters and the properties of neutron beams,

b) delivers the information of neutron beams to users,

c) diagnoses the neutron source equipment,

d) confirms the validity of neutron source design, and

e) develops the techniques for neutron measurement.

NOBORU is also used for "research" activities, i.e. a test port for R&D activities and trial users who have new ideas. The optical devices, detectors, data acquisition system, etc, will be tested using a real neutron beam. These devices will make ambitious experiments feasible in the next decade.

2.12.2 Design of Instrument

The distance between a moderator and a sample (L1) and the size of a experiment cave, which was related to the distance from the sample to a detector (L2), were first considered to accomplish the mission of NOBORU. NOBORU should not have any neutron guide system in its beam-line to observe the moderator directly. On the other hand, a high-intensity beam with large cross-section was required to expand the versatility of experiments. Then beam-line number 10 (BL10) with L1 = 14.0 m was selected taking account of its own workspace and the spatial relation to other instruments.

One of the important features of NOBORU is that experimenters can enter the experiment cave from an entrance through a 600 mm wide corridor as shown in Figs. 2.12.1 and 2.12.2. To accept various experiments, NOBORU does not have a specific sample chamber, a stationary goniometer, a detector array, or any other equipment. A 30 mm thick experimental table (load capacity of 1 ton) and a compact 5-axis goniometer (load capacity of 20 kg) are equipped instead. The goniometer, and even the experimental table can be removed when they are not used.

The experiment cave of NOBORU is shielded by layers of hydrogenous absorber and steel. The hydrogenous absorber is a resin (10 wt%) bonded mixture of borax (45 wt%) and rice-grain sized polyethylene (45 wt%). The concrete floor of the experiment cave is covered with a 50 mm thick steel plate to reduce a considerable number of thermalized neutrons produced in the concrete. In contrast, the beam stop of NOBORU is composed of B_4C, lead, polyethylene, steel and concrete. Detailed shielding was analyzed using MCNPX and PHITS code as shown in Figs. 2.12.3 and 2.12.4.

NOBORU was the first beam line in MLF whose detailed shielding was designed. Since the target dose rates of shielding calculations had not been defined, temporal target dose rates were assumed. There are three general criteria for the target dose: a dose rate at site boundaries, a dose rate at boundaries of radiation-controlled areas and a dose rate for non-limited access to radiation-controlled areas. These general criteria were converted to the target dose rates for NOBORU, which can be compared directly with calculated results as follows.

Source: NOBORU itself (when the NOBORU shutter is opened)

a) maximum dose rate on outer surfaces of NOBORU: 2.5 μSv/h

b) averaged dose rate on outer surfaces of NOBORU: 0.5 μSv/h

c) maximum dose rate on the exterior wall of MLF: 0.025 μSv/h

Source: adjacent beam line (when the NOBORU shutter is closed, but the shutter of the adjacent beam line is opened)

d) maximum dose rate in the sample room of NOBORU when a T0-chopper for the adjacent beam line is in normal operation: 6.25 μSv/h

e) maximum dose rate in the sample room of NOBORU when a T0-chopper for the adjacent beam line is out of phase (experimenters should evacuate immediately from the sample room in this case): 500 μSv/h

These target dose rates ware reconsidered from the viewpoint of ALARA and the new target doses are now applicable to other instruments as follows.

Source: NOBORU itself (when the NOBORU shutter is opened)

a') maximum dose rate on outer surfaces of NOBORU: 12.5 μSv/h

c') maximum dose rate on the exterior wall of MLF: 0.25 μSv/h

Source: neighboring beam lines (when the NOBORU shutter is closed, but both shutters of the neighboring beam lines are opened)

d') maximum dose rate in the sample room of NOBORU: 12.5 μSv/h

To assure the radiation safety of experimenter in NOBORU, the personal protection system (PPS) is introduced. Fig. 2.12.5 shows the conceptual drawing of the interlock system of NOBORU. Photo 2.12.1 shows the components of the interlock system of NOBORU. The doses of neutron and γ-ray are measured with the area monitor installed in the cave and the measured values are displayed near the entrance.

2.12.3 Specification

Main specification of NOBORU is summarized in Table 2.12.1.

Table 2.12.1: Specification of NOBORU

Beam Line Number	BL10 (decoupled moderator)
Viewed Surface of the Moderator	100 mm × 100 mm
Maximum Beam Size at Sample Position	100 mm × 100 mm
L1 (moderator-sample distance)	14.0 m
L2 (sample-detector distance)	1- 2 m
Experimental Cave	2.5 m (W) × 3.5 m (L) × 3.0 m (H)
Cold Neutron Flux at Sample Position	4.8×10^7 neutrons/s·cm^2
Neutron Peak Intensity at 10 meV	1.5×10^{12} neutrons/eV·s·cm^2
Neutron Pulse Width at 10 meV	33 μs
Available Bandwidth	9 Å (possible to shift using BWC)

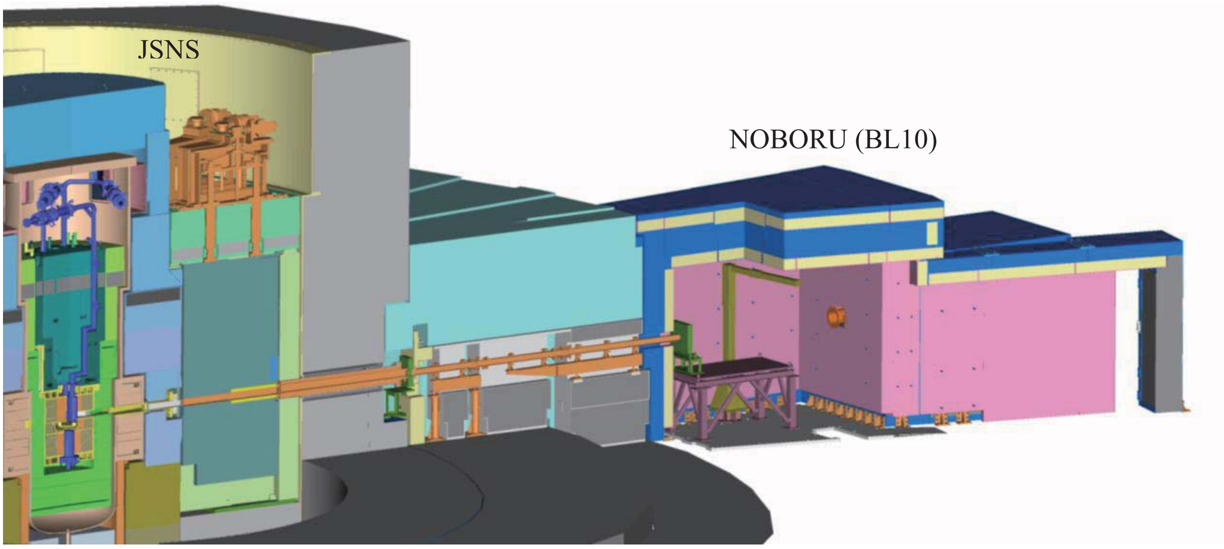

Fig. 2.12.1: A 3-D image of NOBORU and the spallation neutron source

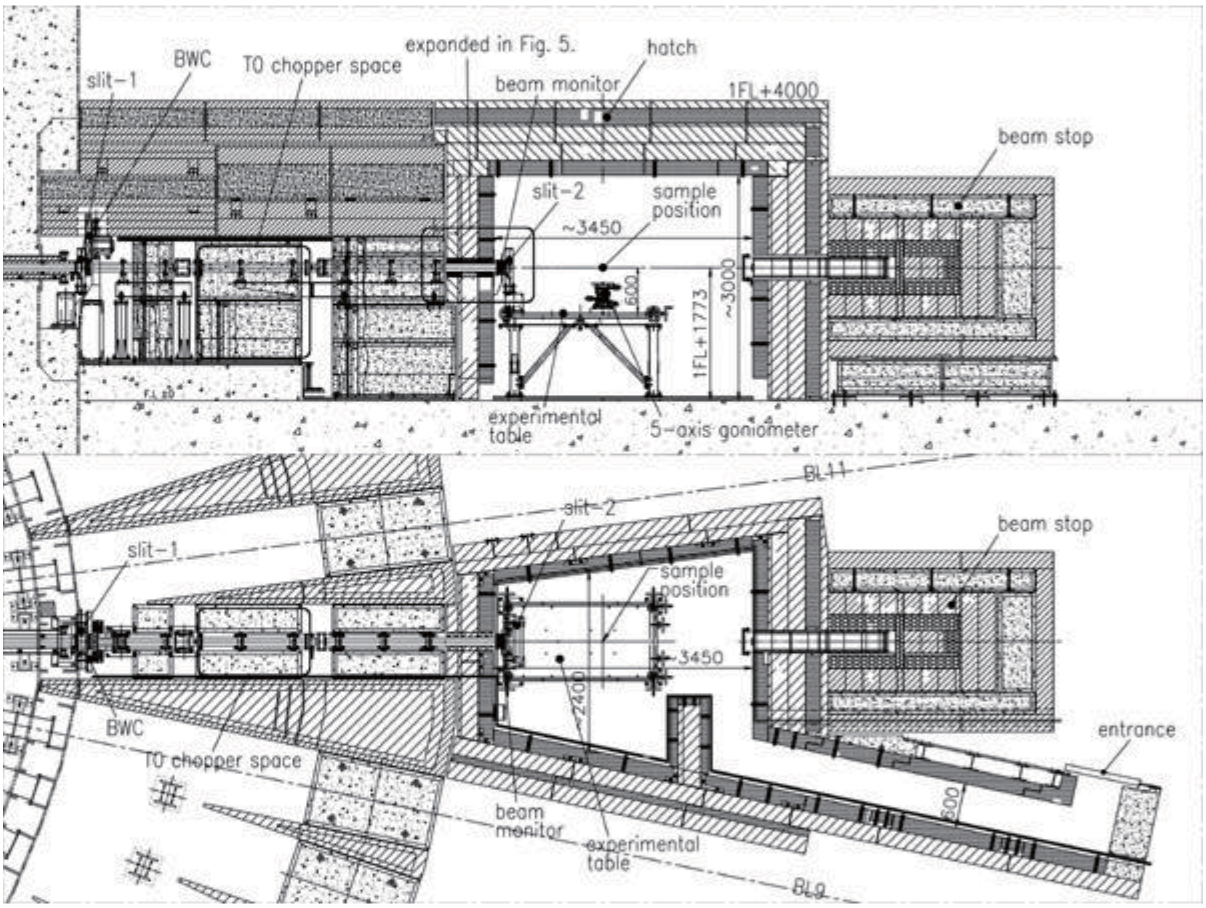

Fig. 2.12.2: Vertical and horizontal views of NOBORU

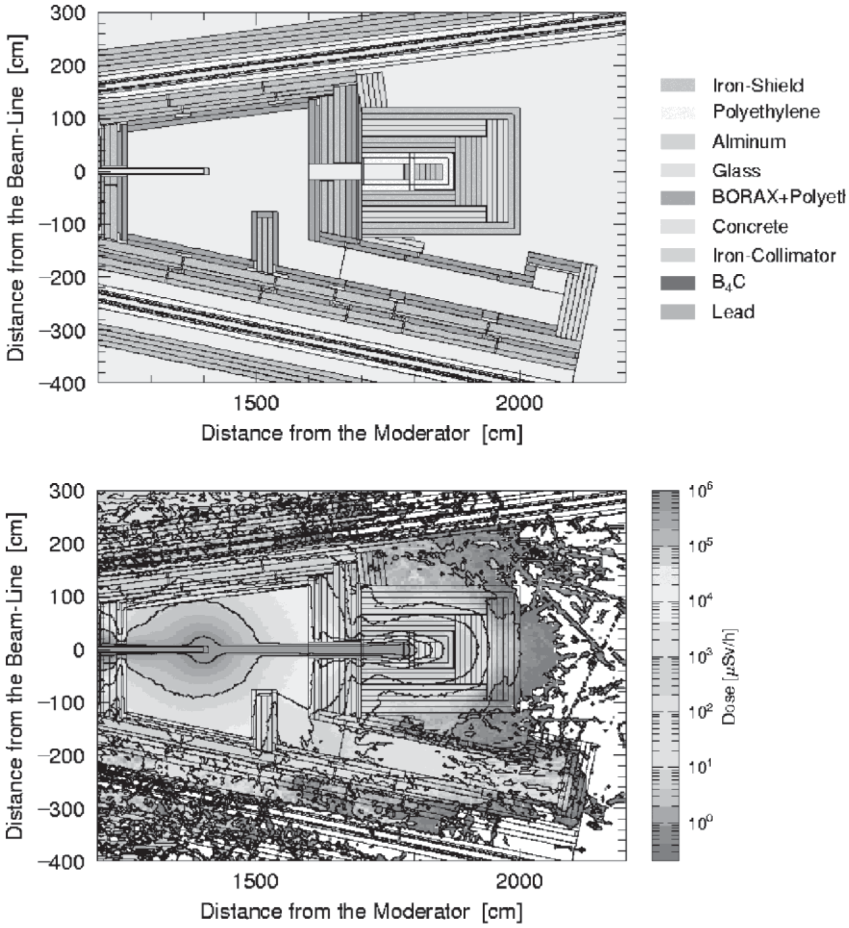

Fig. 2.12.3: Calculation model (upper) and an example of dose map (lower) in the case with a 100-mm cube of steel sample

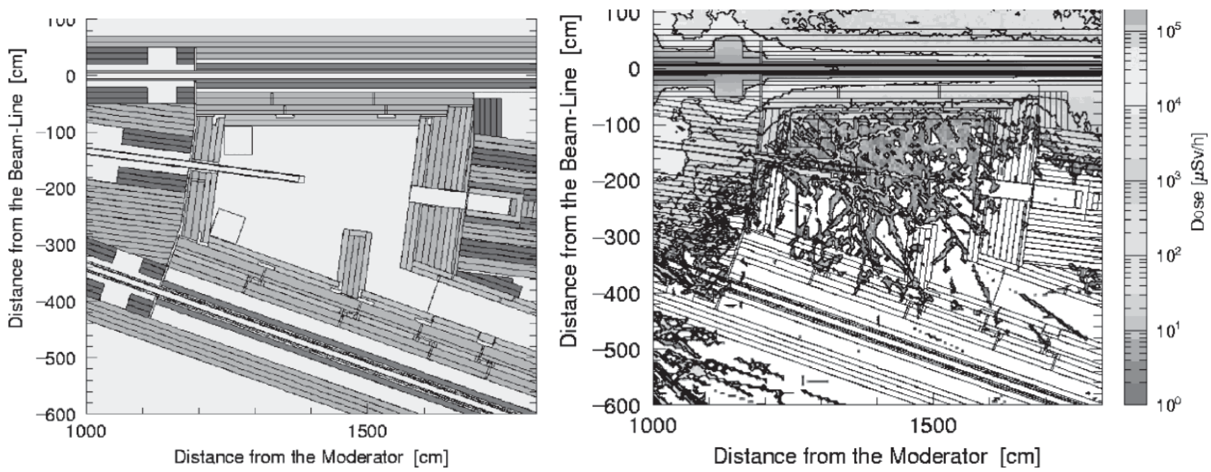

Fig. 2.12.4: Calculation model (left) and an example of dose map (right) without a T0 chopper in BL11

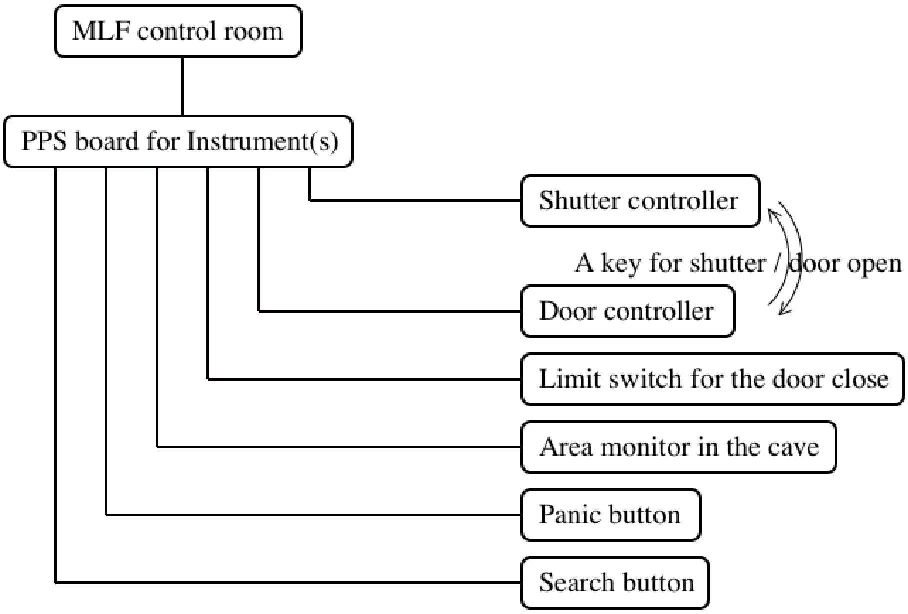

Fig. 2.12.5: Interlock system of NOBORU

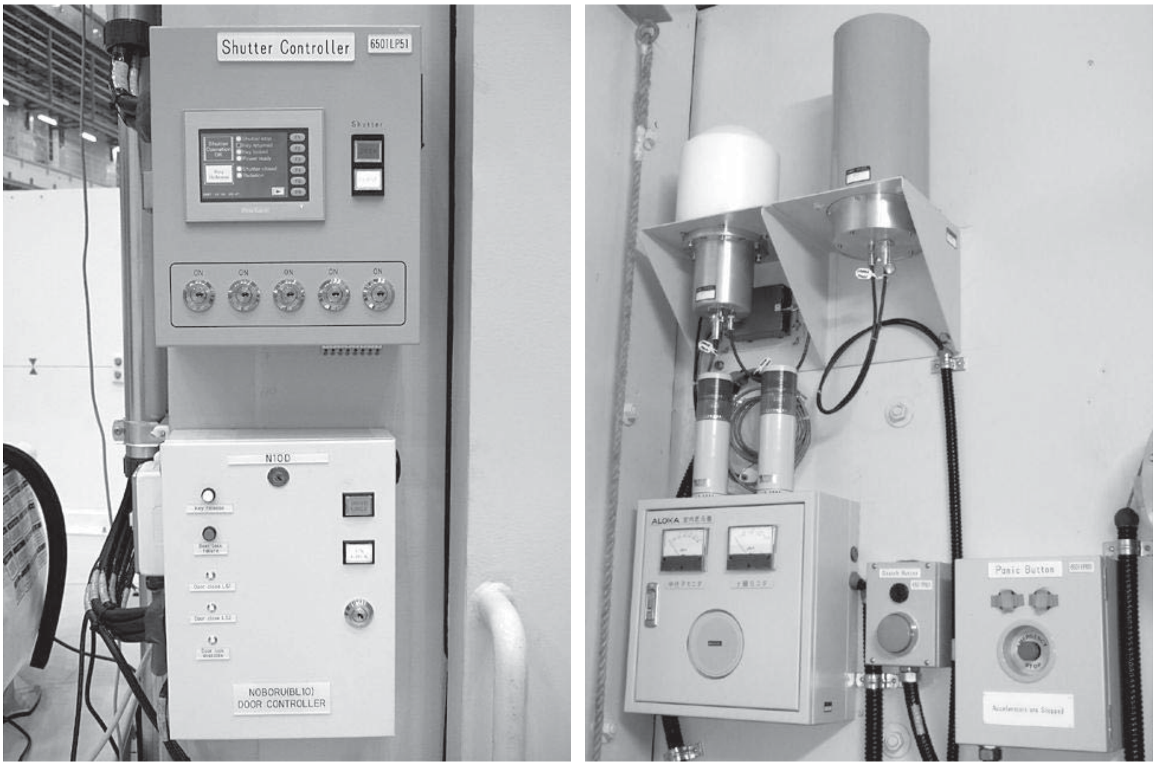

Photo. 3.12.1: The shutter controller and the door controller at the entrance of NOBORU (left). The area monitor, the search button and the panic button in the cave of NOBORU (right).

3 Safety and Building

3.1 Dose Estimation on Beam Operation

The shielding design of MLF building and the identification of the radiation generators were carried out on the basis of the design target in Table 3.1.1. In this section, we will describe the estimation of the dose rate we have done for the applications of beam operation with intensity of 250 kW.

In order to estimate the dose rates during the beam operation, the beam losses, which generates radiation field, were considered. The loss points and their amounts of the beam losses are tabulated in Table 3.1.2.

We assumed three kinds of beam losses: (1) Full beam loss, (2) Point loss and (3) Line loss. "Full beam loss" means that whole beam is lost in one point, which corresponds to the beam loss at neutron source. "Point loss" means that a small part of the proton beam is lost for generating secondary particles or beam loss happened locally due to unintended spread of proton beam profile, which corresponds to the beam losses at M2 line including the muon target. The amount of point losses was estimated by the beam optics where beam losses were taken into account. "Line loss" means the beam loss at the beam transport lines. The amount of line loss should be kept lower than 1 W/m for hands-on maintenances of beam line devices, which is determined on the basis of experience of maintenance of existing similar facilities such as 12-GeV synchrotrons at KEK. The line loss corresponds to the beam loss of M1 line. For the estimation on safe side, we supposed that the beam losses are focused on quadruple magnets where the beam profile tends to spread wider than other places.

The dose rate estimation for the neutron beam lines was carried out as an origin of the neutron generation from the moderators. The devices in the neutron beam lines such as collimators, T_0 choppers, experimental samples and beam stops were considered for the calculation. If some devices are removable from the neutron beam lines, the case with the highest dose rate was adopted for each estimation point. So far, twelve neutron beam lines have been installed in MLF and the licensing for the neutron beam lines and the beam operation of 250-kW power has been obtained. The neutron beam lines with licensing are tabulated in Table 3.1.3.

In the dose calculation in MLF, the Monte Carlo codes of PHITS[3.1-1)] and MCNPX[3.1-2)] were mainly used since the structure of radiation source and shielding are too complicated to apply the simplified calculation method; the simplified method with Moyer formula is applied only for M1 line. Since the shielding structure around the neutron source is so complicated, it is time-consuming, and not reasonable and impossible, that the real shielding structure is simulated in the Monte Carlo calculation. For example, the shielding blocks around the neutron source were constructed with stacks of steel and concrete layers. The complicated structures were simplified by using average densities mixed with different materials. In addition, gaps between shielding blocks were not considered in the simulation model because the gap structures were designed to prevent streaming effect. The estimation results of the dose rates are shown in Fig. 3.1.1.

References

3.1-1) H. Iwase et al.: "Development of General-Purpose Particle and Heavy Ion Transport Monte Carlo Code", J. Nucl. Sci. Technol., 39, 2002, pp. 1142-1151.

3.1-2) MCNPX version 2.1.5, CCC-705, RSICC Computer Code Collection, Oak Ridge National Laboratory, 1999.

Table 3.1.1: Design target for radiation shielding

Area classification	Dose rate of design target	Allowable limit defined by law
Site boundary	< 50 μSv/year	< 250 μSv/3 months [a]
Boundary of controlled area	< 0.25 μSv/hour	< 1.3 mSv/3 months [b]
General access area	< 12.5 μSv/hour	< 1 mSv/week [c]

a) "3 month" is defined as 2184 hours by law.
b) In this case, "3 months" is defined as 500 hours, considering the average annual working time of 2,000 hours.
c) "1 week" is 40 hours, which means weekly working time deduced as "daily working time" (= 8 hours) times "weekly working days" (= 5 days).

Table 3.1.2: Points and amount of beam losses

Position	Amount of beam losses	Length of loss region
M1 line	1 W/m	17 m
M2 line [a]	15.63 kW	33 m
Neutron Source	250 kW	

a) Including the beam loss of the muon target

Table 3.1.3: Licensed neutron beam lines on April 2009

No.1 Experimental hall		No.2 Experimental hall	
No.	Name	No.	Name
1	4D space access neutron spectrometer	14	Cold neutron disk chopper spectrometer
3	IBARAKI biological crystal diffractometer	16	High performance neutron reflectometer with a horizontal sample geometry
4	Neutron-nucleus reaction instrument	19	Engineering material diffractometer
5	Neutron optics and fundamental physics	20	IBARAKI materials design reflectometer
8	Super high resolution powder diffractometer	21	High intensity total diffractometer
10	Neutron beam line for observation and research use		
12	High resolution chopper spectrometer		

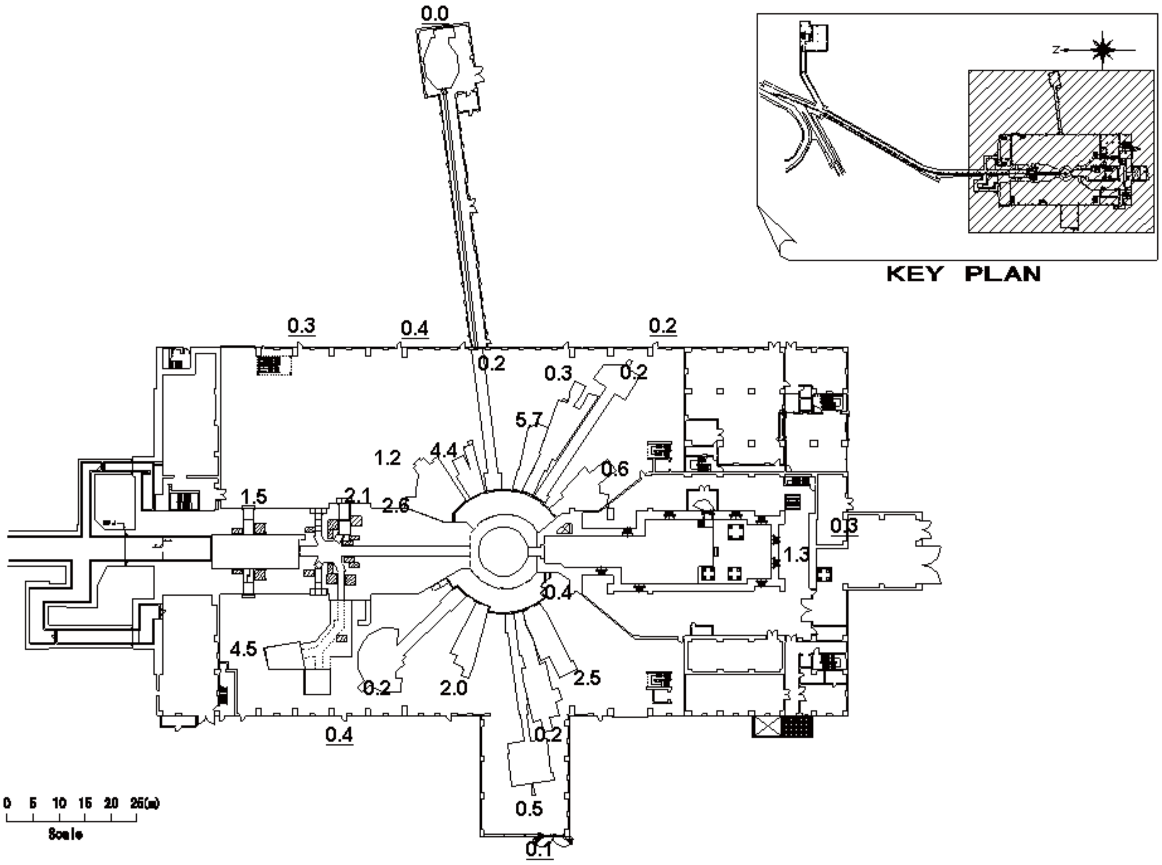

Fig.3.1.1 Calculation results of the dose rates on the beam operation with 250 kW. The calculated dose rates are shown in the unit of μSv/h on the map of the MLF first floor. The numbers with underbars show the dose rates at the boundary of controlled area, and others show those in accessible controlled areas.

3.2 Handling of Activated Air and Water

Various kinds of radioactive products are induced by bombarding incident protons with devices, such as the neutron target, the muon target, the magnets in the proton beam line. Gas products and activated cooling water are periodically exhausted as waste from the building. The concentration of radioactive isotopes in the gas and water wastes need to be lower than the allowable limits specified in the laws concerning the prevention from radiation hazards due to radioisotopes. In order to keep the concentrations lower, the disposal scenarios should be made on the basis of radioactivity evaluations. In this section, the evaluations of radioactivity and the disposal scenarios of activated gas and water in MLF are indicated.

The evaluation of radioactivity is carried out by setting various assumptions in some steps. Consequently, the calculation includes large margin due to ambiguities of the assumptions. Therefore, the evaluations are carried out mainly by using scaling method on the basis of measurement data in other facilities, such as 12-GeV proton synchrotron at KEK, if such data are available. If there is no measurement data available, the code calculation is utilized.

In our facility, we have three kinds of evaluations which are categorized by the origins: Air, Cooling water and Mercury. Each evaluation and handling scenario will be described below.

3.2.1 Air

The amount of radioactive products in air in the neutron source room and the beam tunnels, which include the downstream region of the 3NBT tunnel, M1 and M2 tunnel, were evaluated using primary and secondary flux in air and activation cross sections. The amounts of radioactive products for 13 isotopes, which are expected to be produced in the air, were evaluated. The major short-lived products are ^{13}N with a half-life $T_{1/2}$ of 9.97 minutes, ^{11}C (20.4 minutes), ^{15}O (2.03 minutes) and ^{41}Ar (1.83 hours), and the long-lived products are ^{3}H (12.3 years) and ^{7}Be (53.3 days). The fluxes of protons and neutrons were evaluated using PHITS or MCNPX code. As for the activation cross sections, the experimental data of INC/GEM[3.2-1)] or the calculated values with LAHET[3.2-2)] codes were used. The amounts of the products were deduced by multiplying between the flux of particles and the cross sections.

The concentrations of the radioactive products in the air of rooms and those in the exhaust air were evaluated along with the operation and exhaust scenario. In our exhaust scenario, the air in the rooms and the tunnels are exhausted after cooling the short-lived products. The concentration of products D in the air can be deuced using the following expression:

$$D = N\sigma\phi\left(1 - e^{-\lambda t_1}\right)e^{-\lambda t_2},$$

where N is the atomic concentration of air, σ is the activation cross section, ϕ is the mean value of the flux in the room or tunnels, λ is the decay constant of the product, and t_1 and t_2 are the operation and cooling times. The evaluation results for 20-days operation and no cooling and 12-hours cooling are shown in Table 3.2.1.

For the evaluation in 3NBT and M1 tunnels, the beam loss by 1 W/m was assumed. For M2 tunnels, the beam loss at the muon target and the M2 tunnels were evaluated using PHITS code and for the neutron source room, full beam stop, which means 250-kW beam loss, was assumed.

Since we can expect that significant radioactivity will be produced in the gas, the air circulation system for M1 and M2 tunnels, neutron source room was installed in radiological control areas, and the radioactive gases are controlled with the same level as unsealed radioactive materials.

The circulation systems of air in M1 and M2 tunnels and the neutron source room are operated in the circulation mode, not releasing the gas to public during the operation. Having enough cooling time to decrease short-lived activities after the operation, the circulation system is operated with gas-release mode.

3.2.2 Cooling Water

The major products in the primary water are short-lived products such as ^{13}N ($T_{1/2}$=9.97 minutes), ^{11}C (20.4 minutes) and ^{15}O (2.03 minutes) and long-lived products such as ^{3}H (12.3 years) and ^{7}Be (52.3 days). In addition, the radioactive products induced from Fe, Mn and Ni, which are dissolved from the piping wall by erosion, exist in the cooling water. The estimation of the radioactivity concentration in the cooling water was carried out by multiplying the production cross sections for the radioactive products, σ, and the proton and neutron fluxes at the region where the cooling water flows, ϕ, which were calculated using the Monte Carlo codes of PHITS, MCNPX, etc. The radioactivity for the erosion products was estimated by scaling the measurement data of 12-GeV synchrotrons at KEK and LAMPF at LANL in US.

The long-lived radioactivity for annual operation is deduced by the formula as

$$A = N_0 \sigma \phi \left(1 - e^{-\lambda t_{op}}\right),$$

where N_0 is a number of water molecules in the radiation filed at flux ϕ, t_{op} is the annual operation time. Since the short-lived radioactivity in the cooling water depends on the parameters of the water circulation, such as residence time in the radiation field and the transfer time from the radiation filed to the estimation point, the equilibrium radioactivity can be deduced as

$$A_{\infty} = n_0 N_0 \sigma \phi e^{-\lambda t_{cool}} \left(1 - e^{-\lambda t_{op}}\right) \Big/ \left(1 - e^{-\lambda T}\right),$$

where n_{o} is a number density of water molecules which flows in the radiation field per unit time, t_{cool} is the transfer time of the cooling water from the radiation field to the estimation points, t_{op} is the residence time in the radiation field, which also means the irradiation time, and T is the periodic time for circulating the cooling water. The concentration of radioactivity in a tank of cooling water can be estimated by integrating the above formulae for t_{cool}.

The calculation results in the cooling water are shown for the long- and short-lived products in Tables 3.2.2 and 3.2.3 respectively.[1], and the equilibrium concentrations for short-lived products are shown

[1] The tables do not include the estimation at the downstream region of 3NBT and M1 tunnel since those are included in 3GeV RCS.

in Table 3.2.4.

For the short-lived products, the equilibrium activities at water tanks and return pipes from radiation areas were separately estimated. The estimation was carried out under 250-kW operation. Though we did not care about removal effect of products of ^{7}Be, Co, Ni and Fe by ion-exchange resin and piping wall in the estimation, we can assume that those products will be removed from the cooling water by considering the experiences in other facilities. Consequently, the concentration of ^{3}H is the most important issue.

Measurement of radioactivity concentration in the cooling water will be carried out with adequate frequency. Used cooling water is exchanged to virgin water before the concentration of radioactivity becomes higher than the allowable disposal limit defined by law. The used water for disposal is transferred to the temporal storage tanks in MLF. The used water in the storage tanks is discharged to the outlet. In 1-MW operation, the cooling water for the neutron source devices, such as the proton beam window, moderator, helium vessel etc., are expected to be highly activated and the concentration of radioactivity becomes higher than the allowable limits for disposal in the regulation in Nuclear Science Laboratory of JAEA. Therefore the cooling water of the neutron source region needs to be used semi-permanently.

3.2.3 Mercury

The radioactivity of gas products in the mercury was estimated[3.2-3)] using PHITS and DCHAIN-SP codes. The calculation was carried out for the case when the mercury was stationary in the target vessel. We also assumed that all gas products were transferred to the cover gas in the surge tank and the concentration of the mercury vapor was saturated in the cover gas. The beam power in the calculation was 250 kW. The operation time and the cooling time were 5,000 hours and 48 hours, respectively.

We made a scenario that the off gas from the mercury was going to be processed by the off gas process system, whose functions will be described in Section 3.3. Radioactivity concentration of the released gas was estimated under the assumptions as follows:

- Cover gas will be kept in the gasholders in the offgas process system for about one year in order to decrease the radioactivity of ^{127}Xe with a half-life of 36.4 days.
- Radioactivity of tritium will be decreased to 1/1,000 by using the tritium removal process in the offgas process system.
- 99% of mercury vapor are removed at the mercury absorption column in the offgas process system.
- The processed gas will be released slowly for 3 months.
- The total exhaust rate from the MLF stack is 160,000 m^3/h.

In order to reduce the concentration of T and ^{127}Xe in the released gas, the offgas is required to be processed with the offgas process system. The estimation results for the radioactivity for the offgas exhaust are shown in Table 3.2.5.

References

3.2-1) S. Furihata, "Statistical Analysis of Light Fragment Production from Medium Energy Proton Induced Reactions", Nucl. Instr.. Meth., B171, 2000, pp. 251-258.

3.2-2) R.E. Prael and H. Lichtenstein, "User Guide to LCS: the LAHET Code Systems", LA-UR-89-3014, Los Alamos National Laboratory, 1989.

3.2-3) T. Kai et al.: "Induced-radioactivity in J-PARC Spallation Neutron Source", Proceedings of the 2nd iTRS International Symposium on Radiation Safety and Detection Technology, J. Nucl. Sci. Technol., Supplement 4, 2004, pp. 172-175.

Table 3.2.1: Calculation results of the concentration of radioactivity

Nuclide	$T_{1/2}$	Radioactive concentration [Bq/cm^3]					
		M1 tunnel		M2 tunnel		Neutron source room	
		No cooing	12-h cooling	No cooing	12-h cooling	No cooing	12-h cooling
^{14}C	5730 y	7.2×10^{-4}	7.2×10^{-4}	8.2×10^{-4}	8.2×10^{-4}	1.5×10^{-6}	1.5×10^{-6}
^{3}H	12.3 y	2.1×10^{-3}	2.1×10^{-3}	1.1×10^{-2}	1.1×10^{-2}	1.5×10^{-6}	1.5×10^{-6}
^{7}Be	53.3 d	1.6×10^{-2}	1.6×10^{-2}	1.1×10^{-1}	1.1×10^{-1}	8.8×10^{-7}	8.8×10^{-7}
^{37}Ar	35.0 d	1.2×10^{-3}	1.2×10^{-3}	5.9×10^{-3}	5.9×10^{-3}	9.3×10^{-4}	9.2×10^{-4}
^{41}Ar	1.83 h	1.1×10^{-1}	1.1×10^{-3}	4.4×10^{-1}	4.7×10^{-3}	9.3×10^{-2}	9.8×10^{-4}
^{11}C	20.4 m	1.2×10^{-1}	2.8×10^{-12}	8.4×10^{-1}	2.0×10^{-11}	5.3×10^{-2}	1.2×10^{-12}
^{13}N	9.97 m	2.1×10^{-1}	-	1.9×10^{-0}	-	3.8×10^{-1}	-
^{15}O	2.04 m	7.2×10^{-2}	-	6.7×10^{-1}	-	4.3×10^{-1}	-
^{14}O	1.18 m	1.4×10^{-2}	-	2.6×10^{-1}	-	1.1×10^{-2}	-
^{10}C	19.3 m	1.2×10^{-2}	-	-	-	1.8×10^{-2}	-
^{11}Be	13.8 m	1.8×10^{-3}	-	2.2×10^{-5}	-	1.7×10^{-2}	-
^{16}N	7.13 s	6.8×10^{-2}	-	2.4×10^{-1}	-	1.7×10^{-2}	-
^{15}C	2.45 s	9.3×10^{-4}	-	1.7×10^{-6}	-	1.3×10^{-2}	-
Ratio[a)]		5.9	0.047	36.02	0.29	7.22	0.0098

a) Sum of the ratios of radioactive concentrations for allowable limits determined for each isotope by law

Table 3.2.2: Long-lived radioactivity in the cooling water of MLF

Nuclide	$T_{1/2}$	Radioactivity for each cooling system [Bq/cm^3]				Total
		M2 line [a]	6551 system [b]	6552 system [c]	6553 system [d]	[Bq]
T	12.3 y	1.3×10^{1}	4.1×10^{4}	2.5×10^{4}	1.3×10^{4}	3.0×10^{11}
^{7}Be	53.3 d	1.4×10^{2}	1.6×10^{5}	1.0×10^{5}	4.5×10^{4}	1.1×10^{12}
^{14}C	5730 y	6.9×10^{-3}	2.8×10^{1}	1.8×10^{0}	8.8×10^{0}	2.0×10^{8}
^{22}Na	2.602 y	1.4×10^{-3}	2.6×10^{1}	1.7×10^{1}	7.5×10^{0}	1.9×10^{8}
^{46}Sc [e]	83.8 d	9.3×10^{-1}	5.8×10^{1}	3.6×10^{1}	1.9×10^{1}	4.3×10^{8}
^{54}Mn	312.21 d	4.0×10^{-2}	2.4×10^{2}	1.6×10^{2}	7.0×10^{1}	1.8×10^{9}
^{59}Fe	44.6 d	2.9×10^{-3}	2.6×10^{0}	1.8×10^{0}	7.7×10^{-1}	1.9×10^{7}
^{56}Co	77.1 d	4.9×10^{-2}	7.6×10^{1}	5.1×10^{1}	2.2×10^{1}	5.6×10^{8}
^{57}Co	271.77 d	4.0×10^{-2}	2.1×10^{2}	1.4×10^{2}	6.0×10^{1}	1.5×10^{9}
^{58}Co	70.8 d	2.5×10^{-1}	3.5×10^{2}	2.4×10^{2}	1.0×10^{2}	2.6×10^{9}
^{60}Co	5.271 y	9.9×10^{-3}	3.6×10^{2}	2.4×10^{2}	1.0×10^{2}	2.6×10^{9}
^{65}Zn	244.1 d	1.1×10^{-3}	5.2×10^{0}	3.5×10^{0}	1.5×10^{0}	3.8×10^{7}

a) The cooling system of M2 line has 6.8-m^3 water.
b) 6551 system has 4.1-m^3 water for cooling the target vessel and the reflectors.
c) 6552 system has 2.6-m^3 water for cooling the proton beam window and the moderators.
d) 6553 system has 5.1-m^3 water for cooling the helium vessel and the target trolley.
e) The estimation for the origins of erosion material shown below ^{22}Na in the table was carried out by scaling the measurement data of KEK except ^{46}Sc, whose radioactive concentration was estimated using LAMP data.

Table 3.2.3: Short-lived radioactivity in the cooling water of MLF

Nuclide	$T_{1/2}$	Radioactivity for each cooling system [Bq/cm^3]				Total
		M2 line [a)]	6551 system [b)]	6552 system [c)]	6553 system [d)]	[Bq]
^{10}C	19.3 s	4.6×10^{2}	8.9×10^{3}	5.9×10^{3}	4.3×10^{2}	6.0×10^{9}
^{11}Be	13.8 s	6.5×10^{1}	5.8×10^{2}	3.3×10^{2}	4.2×10^{1}	4.0×10^{8}
^{11}C	20.4 m	3.0×10^{3}	3.0×10^{5}	1.4×10^{5}	1.2×10^{5}	2.3×10^{11}
^{13}N	9.97 m	2.2×10^{3}	2.1×10^{5}	1.1×10^{5}	7.8×10^{4}	1.6×10^{11}
^{14}O	1.18 m	2.9×10^{3}	3.2×10^{5}	2.4×10^{5}	3.9×10^{4}	2.3×10^{11}
^{15}C	2.45 s	1.6×10^{-1}	3.6×10^{-9}	3.2×10^{-9}	7.7×10^{-11}	1.1×10^{-5}
^{15}O	2.04 m	1.1×10^{4}	1.7×10^{6}	9.3×10^{5}	5.1×10^{5}	1.3×10^{12}
^{16}N	7.13 s	7.8×10^{2}	2.9×10^{2}	2.0×10^{2}	8.2×10^{0}	7.0×10^{8}
^{24}Na	15.0 h	3.0×10^{1}	3.5×10^{-1}	1.6×10^{-1}	1.4×10^{-1}	2.0×10^{7}
^{52}Mn	5.59 d	3.0×10^{1}	3.2×10^{0}	1.4×10^{0}	1.2×10^{0}	2.2×10^{7}

a) The cooling system of M2 line has 6.8-m^3 water.
b) 6551 system has 4.1-m^3 water for cooling the target vessel and the reflectors.
c) 6552 system has 2.6-m^3 water for cooling the proton beam window and the moderators.
d) 6553 system has 5.1-m^3 water for cooling the helium vessel and the target trolley.

Table 3.2.4: Equilibrium concentration of short-lived radioactivity in the cooling water of MLF

Nuclide	$T_{1/2}$	Radioactivity for each cooling system [Bq/cm^3]			
		M2 line [a)]	6551 system [b)]	6552 system [c)]	6553 system [d)]
^{10}C	19.3 s	1.9×10^{3}	6.7×10^{5}	4.4×10^{5}	3.2×10^{4}
^{11}Be	13.8 s	4.5×10^{2}	2.4×10^{5}	1.4×10^{5}	1.7×10^{4}
^{11}C	20.4 m	3.1×10^{3}	3.2×10^{5}	1.5×10^{5}	1.3×10^{5}
^{13}N	9.97 m	2.3×10^{3}	2.4×10^{5}	1.2×10^{5}	9.0×10^{4}
^{14}O	1.18 m	4.3×10^{3}	1.0×10^{6}	7.7×10^{5}	1.3×10^{5}
^{15}C	2.45 s	8.8×10^{3}	2.0×10^{6}	1.8×10^{6}	4.4×10^{4}
^{15}O	2.04 m	1.4×10^{4}	3.3×10^{6}	1.8×10^{5}	1.0×10^{6}
^{16}N	7.13 s	3.3×10^{4}	3.4×10^{7}	2.3×10^{7}	9.7×10^{5}

a) The cooling system of M2 line has 6.8-m^3 water. The flow rate is 2.1×10^{4} cm^3/s.
b) 6551 system has 4.1-m^3 water for cooling the target vessel and the reflectors. The flow rate is 8.9×10^{3} cm^3/s.
c) 6552 system has 2.6-m^3 water for cooling the proton beam window and the moderators. The flow rate is 8.9×10^{3} cm^3/s.
d) 6553 system has 5.1-m^3 water for cooling the helium vessel and the target trolley. The flow rate is 6.5×10^{3} cm^3/s.

Table 3.2.5: Estimation of radioactivity for the offgas exhaust

Nuclide	$T_{1/2}$	Radioactivity transferred to the gas phase [Bq]	Reduction rate by the offgas system	Radioactivity concentration of exhaust gas (averaged for 3 months) [Bq/cm^3]	Ratio of the concentration to the allowable limit
^{3}H(HTO)	12.3 y	1.9×10^{13}	1/1000	5×10^{-5}	1×10^{-2}
^{37}Ar	35 d	3×10^{10}	1/500	2×10^{-7}	3×10^{-10}
^{39}Ar	269 y	1×10^{8}	1	3×10^{-7}	1×10^{-6}
^{42}Ar	32.9 y	3×10^{8}	1	1×10^{-6}	5×10^{-6}
^{81}Kr	2×10^{5} y	2×10^{6}	1	5×10^{-9}	5×10^{-8}
^{85}Kr	10.8 y	3×10^{9}	1	1×10^{-5}	1×10^{-4}
^{127}Xe	36.4 d	3×10^{12}	1/500	2×10^{-5}	6×10^{-3}
^{194}Hg	520 y	2×10^{3}	1/100	8×10^{-14}	3×10^{-8}
^{203}Hg	46.6 d	3×10^{-7}	1/100 × 1/135	8×10^{-12}	3×10^{-7}
Total					2×10^{-2}

3.3 Offgas Process System

3.3.1 Outline

Many kinds of spallation products will be produced in the mercury as a target material. The whole of mercury is going to be used without the renewal until the termination of the MLF facility. Most of the spallation products will be accumulated in the mercury. The spallation products contain volatile elements, such as tritium, rare gas, etc. The mercury circulation system has a surge tank with the volume of ~0.7 m^3. Helium gas will be used as cover gas in the tank. Most of the volatile gases are expected to pass into the helium gas from the mercury surface in the surge tank. The mercury circulation system will be open periodically due to exchange of the mercury target vessel. Before doing so, the cover gas must be properly processed because it is expected that, if the radioactive gas is directly released from the exhaust stack without any process, radioactivity concentration of the exhaust gas will exceed the regulation values in law. In order to reduce the exhaust radioactivity, the offgas process system was installed in the MLF facility.

Major radioactive sources needed to be processed with the offgas process system are tritium, noble gas and mercury vapor. In the noble gas, which contains argon, krypton and xeon, the most important source is ^{127}Xe from the viewpoint of radiation safety. The offgas process system was designed to reduce tritium, ^{127}Xe and Hg vapor with certain reduction rates. The target reduction-rate values for tritium, ^{127}Xe and Hg vapor are 1/1000, 1/500 and 1/100, respectively.

Schematic drawing of the offgas process system is shown in Fig. 3.3.1. The whole system consists of the following four subsystems:

- Cover gas transfer system,
- Gasholder
- Tritium removal system,
- Exhaust system.

Each system has the following function, respectively:

- Transform of the cover gas from the surge tank to a gasholder and reduction of mercury vapor,
- Keeping the gas for spontaneous disintegration of xenon activity
- Reduction of tritium,
- Slow exhaust of the processed gas.

The detailed designs of the individual subsystems are shown in the next subsection.

3.3.2 Subsystem

(1) Cover-gas transfer system

Cover-gas transfer system has two pumps and a mercury adsorption column. One pump of two will be used for the backup. During cover-gas transfer process, mercury vapor is removed by the adsorption column in which charcoal filter processed especially for mercury absorption[2] is bedded. In order to assure the reduction rate of mercury vapor at 1/100 or less, it is required that the cover gas stays for more than 10 seconds in the column. Therefore, the gas flow rate is controlled at 30 ℓ/min or less with a flow controller[3] installed just after the absorption column.

The operation of cover-gas transfer is conducted in two steps; the first step is pressure equalization and second is vacuuming. Since the gasholder is normally depressurized to less than 100 Pa before operating the transfer process, the operation begins with pressure equalization between the surge tank and the gasholder using a bypass line. After that, the surge tank is depressurized to ~100 Pa using the vacuum pump. The flow rate is limited to 30 ℓ/min in both steps. It can be estimated that it takes about one hour to depressurize the cover gas in the surge tank from 0.1 MPa to 100 Pa by the both steps.[4]

(2) Gasholder[5]

Cover gas received from the surge tank via gas transfer system will be kept in the gasholder about a year mainly for reduction of ^{137}Xe. Four stainless-steel tanks, which were named TK3100~3400, were used as the gasholders. The volume of each tank is 2.4 m^3. Since gamma-ray dose from the cover-gas is quite high, these tanks are shielded with iron slabs with 20 cm thickness so that workers can get into the offgas process system room. In the normal operation, TK3100 and 3200 are mainly used for keeping the cover gas. TK3300 is a spare in the normal operation. After the cover-gas transfer operation, radioactive gas remains in the pipes between the pumps and the inlet valve of the gasholder tank. The residual gas is transferred to TK3300 in order to reduce the gamma-dose in the offgas process room. TK3400 is used in emergency such as leakage from the mercury circulation system, failure of a gasholder, etc. In the case of such kinds of emergency, the cover gas in the surge tank or the stored gas in the failed tank is urgently evacuated to TK3400. (When the leakage from the mercury circulation system happens, the cover gas is urgently transferred to TK3400 without the limitation of the flow rate. It takes half an hour to depress the surge tank to 100 Pa in case of no flow limitation.)

In the system operation, holders are controlled by giving a status name of "Waiting", "Transferring", "Not processed" and "Processed" in order to prevent operators from releasing unprocessed high-radioactive gas carelessly.

The tanks are always used with negative pressure at less than 80 kPa to prevent radioactive-gas leak even in unexpected failure. If the pressure exceeds 80 kPa, which means that outer gas breaks into the

2 The charcoal was impregnated with sulfur so that mercury vapor is strongly absorbed by chemical reaction of $Hg + S \rightarrow HgS$.

3 The controller is a device for keeping a mass flow constant. In order to keep the volume flow constant at 30 ℓ/min, the setting value of the mass flow rate is changed depending on the fluid pressure from the system controller.

4 The required time to complete the cover-gas transfer process is determined by the limited flow rate of 30 ℓ/min since the conductance between the surge tank and the gasholder is enough low and the exhaust velocity of the pumps is much higher than the limited flow rate. In the estimation, the volume of the cover gas in the surge tank is supposed to be 0.2 m^3.

5 Though, in the early design, the noble gases would be collected by hollow-fiber membrane method and cold condensation, we finally adopted the gasholder method from the viewpoint of technological issue.

tank, the gas in the failed tank is evacuated to a spare by using a vacuum pump in the gas transfer system.

(3) Tritium removal system

The gases stored in the gasholders are processed with the tritium removal system. The tritium removal system has a circulation pump, oxidation catalyst column, gas cooler and molecular sieve column. It is expected that tritium exists in chemical forms of HT and HTO in the off gas. In the tritium removal process, the HT component is oxidized to HTO by the oxidation catalyst at first, cooled by the gas cooler and absorbed by molecular sieve in the molecular sieve column. The component that exists in HTO originally is also absorbed by molecular sieve after passing through the oxidation column and gas cooler.[6]

The oxidation catalyst column is normally operated at 300°C to accelerate the reaction.[7] The gas warned at the column is cooled at the gas cooler to 30°C.

In order to assure the reduction rate of water at 1/1,000 or less in the molecular sieve column, it is required that the gas stays for more than 20 seconds in the column. Therefore, the gas flow rate is controlled at 30 ℓ/min or less with a flow controller installed just after the circulation pump.

Humidity in the system needs to be kept more than10% in order to keep the absorption capacity of the molecular sieve. Therefore, H_2 and O_2 gases are injected into the system from the injection ports at the constant flow rate.

(4) Exhaust System

The gas exhaust system has an exhaust pump and a mass-flow regulator. In order to decrease the exhaust radioactivity concentration below the regulation in law, the processed gas in the tank needs to be slowly exhausted for about 3 months. This system is also used to exhaust low-activated gas directly from the mercury circulation system without holding it in the tank.

3.3.3 Commissioning

The standard work sequence of cover-gas processing using this system is carried out in three steps: cover gas transfer process, gas holding and tritium removal process and gas exhaust process. In the commissioning period, we need to check the sequence. In addition, in order to validate our system design we will obtain the data as follows on the commissioning period.

- Efficiency of the mercury filter
- Efficiency of the tritium removal process
- Radioactivity measurement for the irradiated mercury

[6] The regulation for HT concentration in the exhaust gas is much higher than that for HTO. We estimated that, even if we suppose that whole amount of tritium exists in HT, whole of HT gas can be exhausted under the regulation in law. This means that HT component does not need to be oxidized to HTO by operating the oxidation catalyst column.

[7] It was pointed out, at the special committee on neutron source in J-PARC, that existence of tritium methane should be considered. Tritium methane can be changed to water by operating the oxidation column at 500°C while the normal operation is carried out at 300°C.

- Radioactivity measurement for offgas
- Performance of exhaust of the vacuum pumps

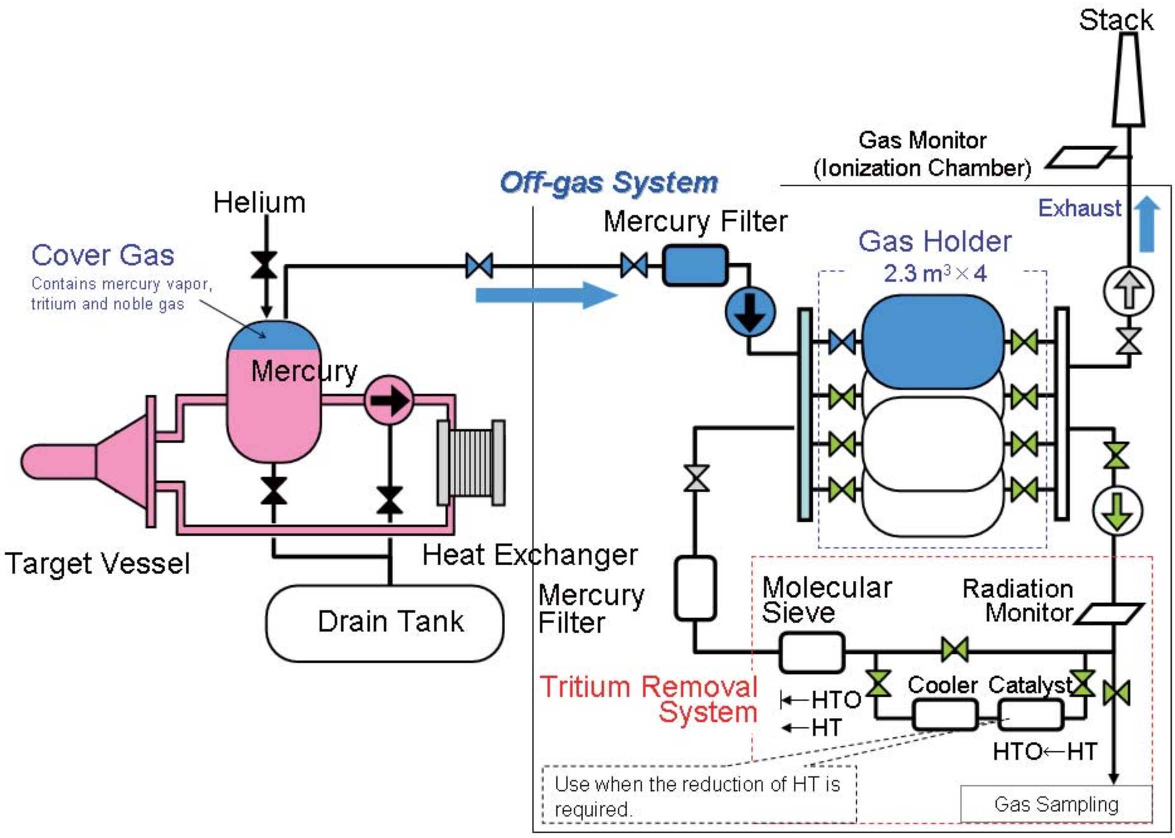

Fig. 3.3.1: Schematic drawing of the offgas process

3.4 Analysis of Off-normal Events

The mercury used as neutron target is highly activated by beam operation. If the mercury leaks from the circulation system, it is possible that the activated products are released to public via the air exhaust system from the stack. Radioactive gas products, which include tritium, noble gas and mercury vapor, are most releasable. The worst scenario is that the whole of the activated gas produced in mercury is released to public. In this section, making assumption that the whole of the gas products is released to public due to the mercury leak during 1-MW operation, radiation dose at the site boundary will be evaluated for risk assessment.

3.4.1 Event Scenario

The scenario we assumed is the following:

- Piping wall of the mercury circulation system fractured.
- All the amount of mercury leaked to the catch pan on the target trolley, and the whole amount of gas including tritium and noble gas in the surge tank is released in the hot cell.
- The gas is released to public via the ventilation system of MLF.

3.4.2 Radioactivity Evaluation in Mercury

Radioactivity in mercury was evaluated using PHITS and DCAHIN-SP codes [3.4-1]. The evaluation conditions are as follows:

- Proton beam energy: 3 GeV
- Beam intensity: 1 MW
- Irradiation time: 5000 h
- Cooling time: 0 h

3.4.3 Evaluation of the Amount of Released Gas

We assumed that mercury vapor, tritium and noble gases including argon, krypton and xenon, are released to public. Evaluations of the total amount of production and release for each material were carried out as follows.

(1) Mercury

The following assumptions were made to evaluate the amount of mercury vapor released from the stack.

- The whole amount (1.4 m^3) of mercury in the circulation system leaks and is kept on the catch pan.

- Mercury vapor from the catch pan is released from the stack of the MLF building via the ventilation system.
- The dumper of the ventilation system is closed one hour later and the gas release stops.

The evaporation rate of mercury on the catch pan was estimated to be 0.3 g/min by considering diffusion of mercury gas due to boundary layer of the gas concentration gradient made by wind on the surface of leaked mercury. The parameters used in the estimation were set as follows:

- Mercury temperature: 80°C
- Temperature in the hot cell: 40°C
- Wind speed: 0.1 m/s
- Stability of atmosphere: F (the most stable state)

The wind speed was roughly evaluated by taking the ventilation speed and the cross section of the hot cell into account. The area of the catch pan is 16 m^2. It can be estimated that the total amount of the released mercury vapor within the interval between the mercury leak and dumper close for one hour is 18 g. [3.4-2)]

(2) Nobel gas and Tritium

We assumed that the whole amount of noble gas and tritium is released to public.

3.4.4 Dose Evaluation at the Site Boundary

The outer dose D_γ of gamma-ray by isotopes of noble gas and mercury is deduced as

$$D_\gamma = (D_\gamma / Q_\gamma) Q_\gamma$$

where D_γ/Q_γ is a relative dose for atmospheric diffusion, and Q_γ [Bq·MeV] is a product of an activity of a released isotope in Bq and the effective gamma-ray energy for the isotope. The inner dose D_I by inherent of mercury and tritium (HT) is evaluated as

$$D_I = KMQ(\chi / Q)$$

where K is an effective dose coefficient [mSv/Bq], M is a breathing rate as 1.2 m^3/h, and Q is an activity of a released isotope, and χ/Q is a relative concentration for atmospheric diffusion.

The coefficients for atmospheric diffusion were deduced under the conditions as follows:

- Distance between the stack and the site boundary: 310 m
- Height of the stack from the ground: 0 m (released from the ground)
- Projected area of the building wall from the evaluation point: 1640 m^2
- Wind speed: 1.0 m/s

- Stability of atmosphere: F (the most stable state)

It was estimated that the relative dose and the relative concentration was 7.2×10^{-12} $\mu Sv\cdot Bq^{-1}\cdot MeV^{-1}$ and 2.5×10^{-7} h/m^3, respectively.

3.4.5 Results of the Evaluation

The results of the dose evaluation are shown below:

Outer dose

Noble gas:	100 μSv
Mercury:	1×10^{-2} μSv

Inner dose

Tritium:	5×10^{-2} μSv
Mercury:	10 μSv

The maximum dose for a person in public is about 100 μSv and the annual dose limit defined by law for general public is strictly observed.

References

3.4-1) T. Kai et al.: "Induced-radioactivity in J-PARC Spallation Neutron Source", Proceedings of the 2nd iTRS International Symposium on Radiation Safety and Detection Technology, J. Nucl. Sci. Technol., Supplement 4, 2004, pp. 172-175.

3.4-2) Y. Kasugai and T. Kai: "Risk Assessment of the Mercury Leak at Materials & Life Science Experimental Facility of J-PARC", JAEA-Technology 2009-010, 2009, in Japanese.

3.5 Building

3.5.1 Overview

The Materials and Life Science Experimental Facility (MLF) consists of a 1-MW pulsed spallation neutron source and a muon source for various experiments in materials and life sciences. Fig. 3.5.1 shows final construction image of the MLF. The dimensions of the facility building are 150 m in length, 70 m in width and 30 m in height as shown in Fig. 3.5.1. MLF receives 3-GeV, 333-μA, 25-Hz pulsed proton beam through a proton beam line as shown in Fig. 3.5.2. About 6% of the proton beam is dissipated at a muon production target and collimators, which are located just after the muon production target. The rest of the beam is injected into a mercury target. The construction of the MLF building was started January 2004 and was finished April 2007.

Fig. 3.5.3 shows a cutaway view of the target station, the part of irradiation components handling room and the large components handling room. The mercury target and a mercury circulation loop are installed on a target trolley. The mercury circulation loop supplies mercury to the target vessel at the maximum flow rate of 60 m^3/h. The reflector-moderator assembly is fixed on the bottom of an exchanging plug and set in a helium vessel. Neutrons generated in the target are slowed down to appropriate energy with moderators and the neutron beams are supplied to the users' apparatuses through neutron beam lines. Twenty-three neutron beam lines will be eventually installed in the experimental halls. The cryogenic H_2 circulation system is located just down stream of the target station in the large components room. The moderator vessels and the reflectors can be removed vertically from the target station with a reflector plug. A transfer cask with 130 ton crane is used to pull up the moderator vessels and the reflectors and transfer them into the irradiated components handling room for maneuvers with their remote handling. Spent components such as the mercury target vessel, the moderator vessels and the mercury circulation components will be stored temporally in the irradiated components storage room on the basement.

3.5.2 Building Layout

Fig. 3.5.4 shows the layout of the 1st floor of the building. The 3-GeV proton beam transportation line is located in the center of the building. Two huge experimental halls were designed to be located on both sides of the proton beam line. Each experimental hall is divided into two areas of "Muon science" and "Neutron scattering". The first priority of the facility design is to accommodate sufficient experimental instruments for their best performance. The outside space of the MLF building is reserved for future extension of the building and neutron beam lines. In this facility, most radioactive products stay in the hot cell located just down stream of the target station. Therefore, the air conditioning system to keep the air in the hot cell at negative pressure is connected to the emergency electric power supply. In Fig. 3.5.4, the whole area other than the rooms in gray is radiation-controlled.

Fig. 3.5.5 shows the 2nd floor level of the MLF building. The radiation controlled area is further divided into the area that general user can enter and the area that only the facility staff can access for operation and maintenance. On the 2nd floor, an access control room is located. All the personnel have to pass through the access control room to enter the radiation-controlled area.

Fig. 3.5.6 shows the 3rd floor level of the facility building. The control room of the facility is located on this floor level. When we need to access the target station and the proton beam transportation line, we will access from the large components handling room which is located in the center of the MLF building.

Fig. 3.5.7 shows the basement floor level of the facility building. Utility rooms, such as an irradiated components storage room and a primary cooling system components room, are located on the basement.

3.5.3 Design Policy

The basic design policies on the facility arrangement of MLF were established based on the characteristics of the facility as the experimental user facilities as well as the 1-MW spallation neutron source.

As user facilities for neutron and muon experiments;

- experimental use → provide the experimental area
- prevention of radiation exposure to experimental users due to spallation neutron source operation → separation of experimental area and operation & maintenance area, neutron source shielding and access control

As 1-MW spallation neutron source;

- neutron source operation → provide the operation & maintenance area
- production of highly irradiated components → handling and storage facilities
- heat generation → cooling system
- radiation generation, prevention of radiation exposure → shielding, access control
- control release of radioactive materials → collect radioactive materials, maintain negative pressure in radiation-controlled rooms
- use of mercury (harm material) and hydrogen (combustible gas) → decrease total amount of mercury and hydrogen

Based on the above characteristics of MLF, the following nine policies on facility arrangement design were set up.

(1) Policy 1: Provide user areas necessary for experiments as the experimental user facility

Experimental user areas should be decided based on user's request. The design results are shown in Fig. 3.5.8 and summarized as follows.

a) Twnty-three independent neutron beam lines are accommodated in the No.1 experimental hall (32 m in width and 61.6 m in length) and the No.2 experimental hall (24.5 m in width and 61.6 m in length) of the facility building based on the instruments arrangement plan proposed from the neutron users.

b) The muon experimental areas are also arranged in the No.1 experimental hall (32.0 m in width and 29.0 m in length) and the No.2 experimental hall (24.5 m in width and 29.0 m in length) of the facility building based on the experimental apparatuses arrangement plan proposed from muon users. Those areas include the spaces for the apparatuses of the second muon target.

c) A neutron experimental area and a muon experimental area are arranged in the same experimental hall to share cranes and gateways.

(2) Policy 2: Provide the operation and maintenance area necessary for 1-MW spallation neutron source

The areas for the variety of cooling equipments and the exchange area of the irradiated components have to be provided sufficiently and properly. The design results based on the policy 2 are shown in Fig. 3.5.9 and summarized as follows.

a) The target station, which consisted of 1-MW spallation neutron source and biological shielding and so on, is arranged in the center of the MLF building. The irradiated components handling room (a hot cell) for maintenance and exchange of components such as a target vessel, a moderator vessel and so on, is arranged downstream of the target station and the large components handling room is arranged on the top of the hot cell by considering the best layout for the maintenance.

b) A maintenance and exchange space for a muon target, beam line electromagnets and so on is provided upstream of the target station coupled with the large components handling room.

c) The minimum spaces necessary for a cooling components room, an irradiated components storage room and radioactive liquid waste tanks rooms are arranged on the basement.

d) Air conditioning components rooms necessary for air exhaust, air ventilation and maintenance of negative pressures are arranged in the radiation-controlled area. Air conditioning components rooms for non-radiation-controlled areas are also arranged.

e) Goods gates are prepared and carefully arranged for handling large components.

(3) Policy 3: Clear separation and classification of the experimental user area and the operation and maintenance area

The experimental user area and the operation and maintenance area have to be classified and separated to prevent unnecessary radiation exposure to experimental users by entering the operation and maintenance area and enable experimental users and facility operators to work individually. The design results based on the policy 3 are shown in Fig. 3.5.10 and summarized as follows.

a) The experimental halls are arranged on both sides of the proton beam line running through the center of the building from the north to the south, which is connected to the target station. The space over the proton beam line and the target station is clearly separated from the experimental user areas with the biological shielding walls of the maintenance and exchange working area of the irradiated components.

b) All the experimental user areas are located in the radiation-controlled area except for the user's waiting room and the computer room. The cooling system components rooms for the spallation neutron source and the maintenance and exchange areas of the irradiation components are also located in the radiation-controlled area. Therefore, only one access control room to these radiation-controlled areas is set up in the building to inspect contamination and do intensive radiation control. The entrances to the radiation-controlled areas for experimental users and those for operators are provided individually. The authentication process with a card key and an APD (alarmed pocket dosimeter) is required to enter the operation and maintenance area.

(4) Policy 4: The efficient arrangements of the radiation-controlled and non-radiation-controlled areas

The access control to the radiation-controlled area has to be managed individually for the experimental users and the operators. The hot area air conditioning components rooms and the cold area air conditioning components rooms have to be arranged efficiently. The design results based on the policy 4 are shown in Fig. 3.5.10 and summarized as follows.

a) The arrangements of rooms for users and operators, machine rooms and storage rooms are concentrated in the downstream of the MLF building. The non-radiation-controlled areas are arranged in the east part of the building and the radiation-controlled areas are arranged in the west part of the building.
b) The access control room (contamination inspection room) is set up in the center between the east and west of the second floor. Users and operators enter the radiation-controlled areas and leave them after contamination inspection.

(5) Policy 5: Appropriate and effective facility layout for any exchange works of major components during maintenance period

The exchange work of the target vessel, which is scheduled most frequently, has to be done independently from works of other major components such as the reflector, the moderator vessel and the proton beam window for efficient maintenance or exchange works. The design results based on the policy 5 are shown in Fig. 3.5.11 and summarized as follows.

a) The mercury target vessel is expected to be exchanged most frequently. It is fixed in the front of the target trolley and drawn out from the beam operation position into the hot cell horizontally for maintenance and exchange works. Accordingly, the hot cell was located just downstream of the target station.
b) The reflector and moderator vessels are mounted on the bottom end of the reflector plug. The reflector plug is moved vertically into a reflector plug cask by using the crane inside the cask when the reflector and/or the moderator vessels are exchanged. The reflector plug cask is transferred to the top of the hot cell by the 130-ton overhead crane in the large component handling room. They are moved down from the reflector plug cask to the reflector stand mounted on the hot cell floor for exchange work.
c) A proton beam window is mounted at the bottom of a proton beam window plug. The proton beam

window plug is moved vertically into the reflector plug cask by using the crane inside the cask when the proton beam window is exchanged. The reflector plug cask is transferred to the top of the hot cell by the 130-ton overhead crane in the large component handling room in the same way as the exchange work for the reflector. The proton beam window is exchanged in the hot cell after moving down to the reflector stand with the proton beam window supporting tool.

(6) Policy 6: Providing the hot cells for handling highly irradiated components

In order to prevent radiation exposure of operation and/or maintenance personnel, the hot cell has an independent exhaust system that can keep the air at negative pressure, since one of the main uses is the exchange works of highly irradiated components such as the mercury target vessel, reflector, moderator vessels, proton beam window, muon target, etc. Remote handling devices are installed in the hot cell for these exchange works. The design results based on the policy 6 are shown in Fig. 3.5.11 and summarized as follows.

a) The irradiated components handling room was designed as a hot cell and set up to exchange the mercury target vessel, the reflector, the moderator vessels, the proton beam window and so on. The hot cell was located just downstream of the target station to minimize the movement distance of irradiated components inside the facility. The components of the mercury circulation system are also handled inside the hot cell because the mercury circulation system is installed inside of the irradiated components handling room. The negative pressure of the air in the irradiated components handling room was set to −230 Pa, referring to the negative pressure design value of existing hot cells. Furthermore, charcoal filters were decided to be installed to remove mercury vapor from hot cell exhaust air.
b) Highly irradiated components are stored in the irradiated components storage room for several years to lower the radiation level. The irradiated components storage room is also designed as the hot cell and located just under the irradiated components handling room. The irradiated component storage room is designed in the same way as the irradiated components handling room and components are handled by remote handling devices there.

(7) Policy 7: Careful arrangement of components which contain radioactive materials

Components that contain radioactive materials should be arranged carefully to limit or prevent spreading contamination by radioactive materials. The design results based on the policy 7 are shown in Fig. 3.5.12 and summarized as follows.

a) The mercury circulation system components including the mercury target vessel are decided to be handled inside of the irradiated components handling room (hot cell).
b) The 3 primary cooling systems (heavy water and light water cooling system) whose radiation levels of water are expected to increase are arranged in the primary cooling system components room located on the basement of the building. All the radioactive liquid waste tanks (high level liquid waste tanks, low level liquid waste tanks, a heavy water storage tank and a spent heavy water

disposal tank) are also arranged on the basement. The design value for the negative pressure in the rooms which contain radioactive materials is set to be lower than other rooms and areas to limit or prevent the diffusion of the contaminations.

(8) Policy 8: Appropriate layout of systems or components to reduce inventory of mercury, heavy water, light water and hydrogen

Components should be arranged properly and efficiently to reduce the inventory of mercury, heavy water and light water that contain radioactive materials. Components should be also arranged properly and efficiently to reduce inventory of hydrogen, combustible gas. The design results based on the policy 8 are shown in Fig. 3.5.12 and summarized as follows.

a) Mercury circulation system components are designed to be arranged on the mercury target trolley to reduce the total length of mercury piping and the mercury inventory is eventually reduced down to 1400 ℓ.
b) Based on the tritium concentration of light water or heavy water, six primary cooling systems are sorted out and integrated into three systems and the total inventory of water is reduced down to about 5000 ℓ.
c) Cryogenic hydrogen circulation system for cold moderator vessels is designed to be located near the target station to reduce the total piping length and the liquid hydrogen inventory is reduced down to about 260 ℓ.

(9) Policy 9: Providing exclusive piping route for primary cooling system

Exclusive piping routes surrounded by shielding walls should be provided for primary cooling system piping where radioactive materials are contained and their levels get high during beam operation. The design results based on the policy 9 are shown in Fig. 3.5.13 and summarized as follows.

a) Exclusive piping route for primary cooling system from the primary cooling system components room on the basement to the primary coolant distribution room on the second floor is specially designed. The piping rote is designed so that the piping of the primary cooling system has to avoid passing through other components rooms or passages.
b) The piping route was surrounded by shielding walls to reduce radiation level and meet the shielding design criteria.

3.5.4 Negative Pressure Ventilation

Negative pressure classification is established so that it can control release of the radioactive materials during normal operation and prevent contamination to circumference when contamination occurs. An air conditioning and ventilation system was designed based on the following negative pressure classification of the radiation controlled area.

1) Negative pressure zone 1: −20 Pa

Negative pressure zone 1 is applied to the experiment halls which are used as experimental user areas. Negative pressure of −20 Pa is determined so that the air should always flow toward inside a radiation controlled area when the gateway between a radiation controlled area and a non-radiation controlled area in the experimental hall is opened.

2) Negative pressure zone 2 : −30 Pa

Negative pressure zone 2 is applied to the passage and working spaces where no contamination source exists in the room, such as a power supply room, a manipulator operation room. Workers and operators were assumed to enter this zone for usual maintenance work or operation. Negative pressure of −30 Pa is determined by referring to the precedents on the negative pressure values in the manipulator operation rooms of the existing hot cells.

3) Negative pressure zone 3 : −60 Pa

Negative pressure zone 3 is applied to machine rooms such as the primary cooling system components room where there is some possibility of contamination (contamination source : tritium, radioactive air). Negative pressure of −60 Pa was determined by taking the value between Zone 2 and Zone 4 to make clear differences of negative pressure to Zones 2 and 4.

4) Negative pressure zone 4 : −400 Pa

Negative pressure zone 4 is applied to the hot cell where there is high possibility of contamination during maintenance or exchange works (Contamination sources: radioactive mercury, tritium). Negative pressure of −400 Pa is decided by referring to the precedents on the negative pressure values in the existing hot cells and the air ventilation system design of MLF.

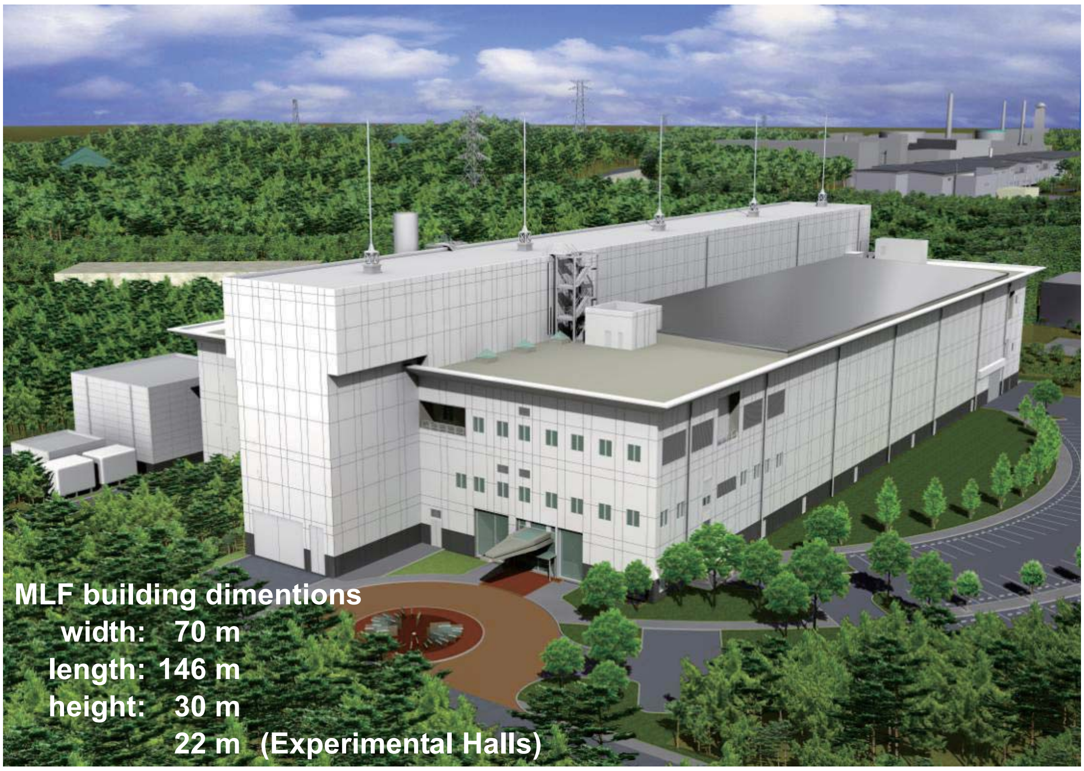

Fig. 3.5.1: Construction image of the Materials and Life Science Experimental Facility building

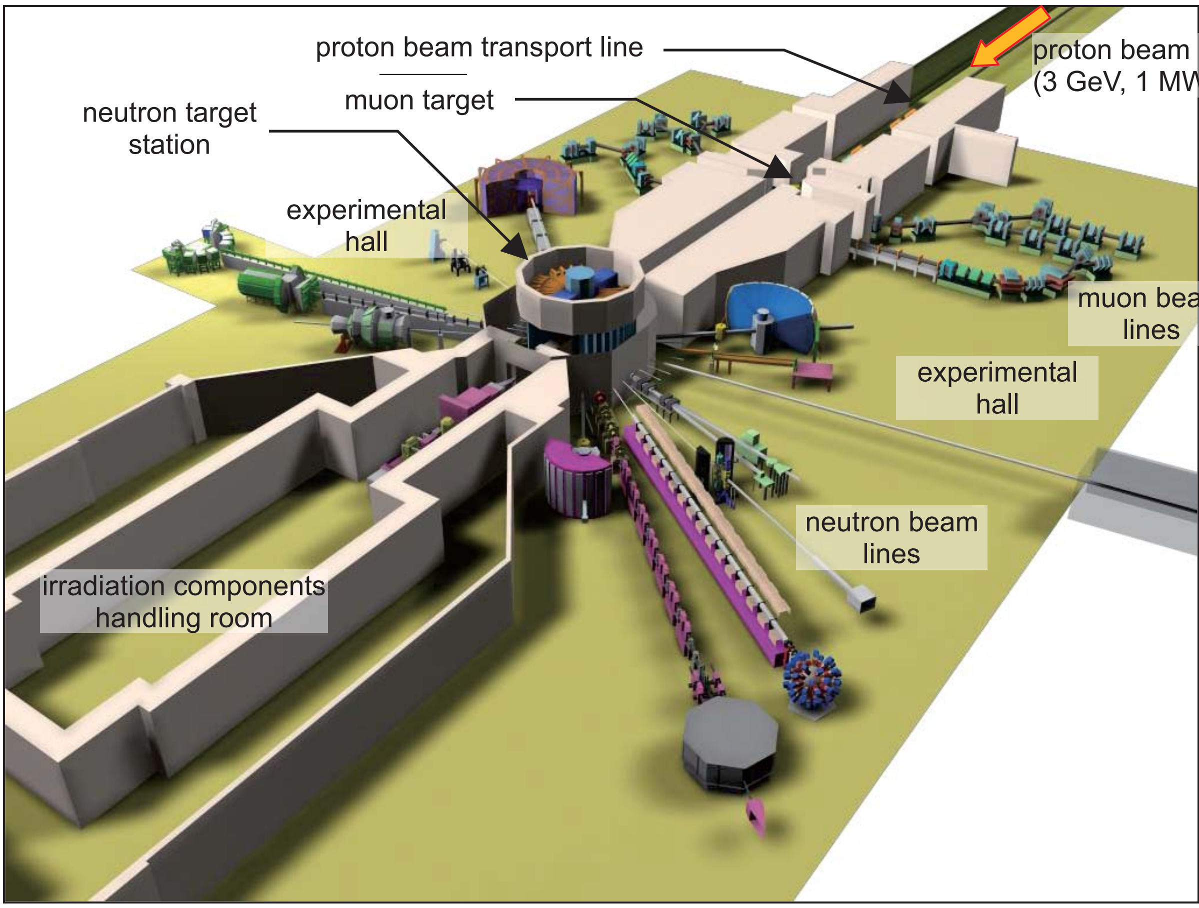

Fig. 3.5.2: Cutaway view of the Materials and Life Science Experimental Facility building

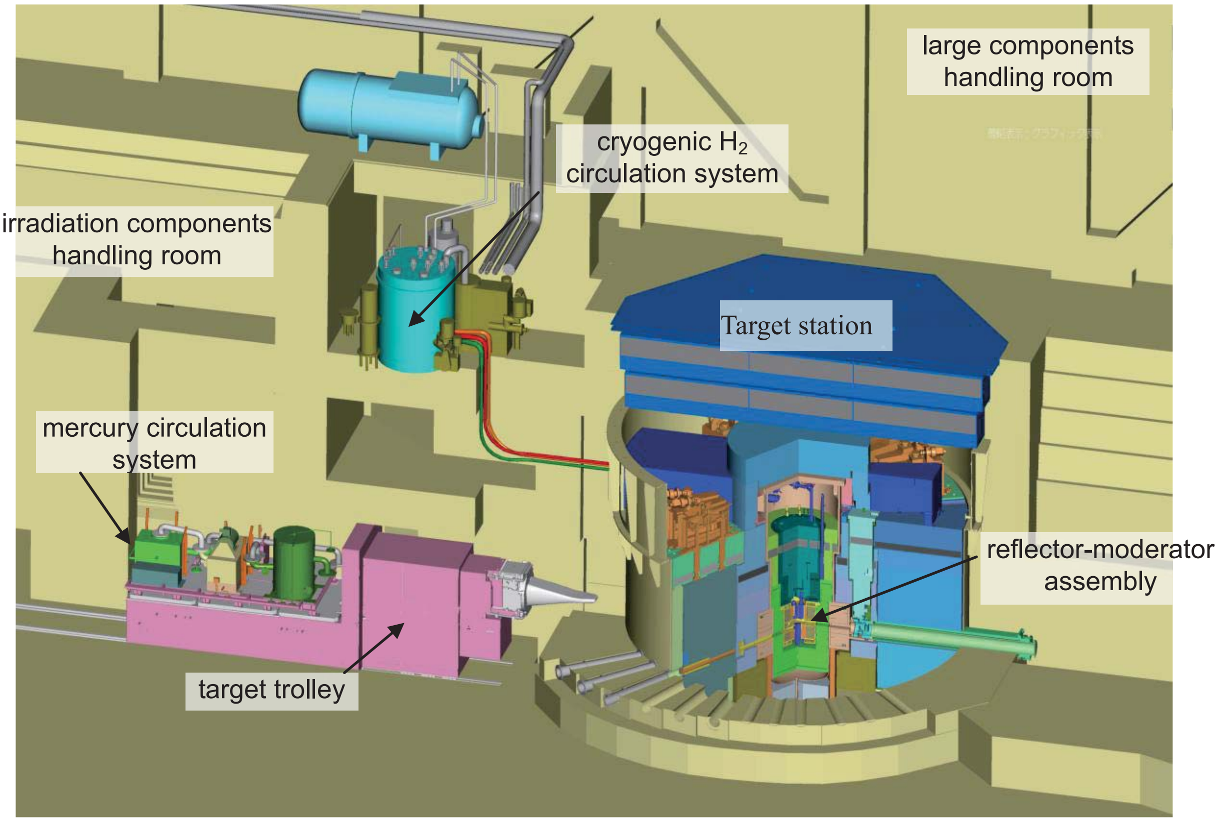

Fig. 3.5.3: Cutaway view of neutron target station and irradiation components handling room

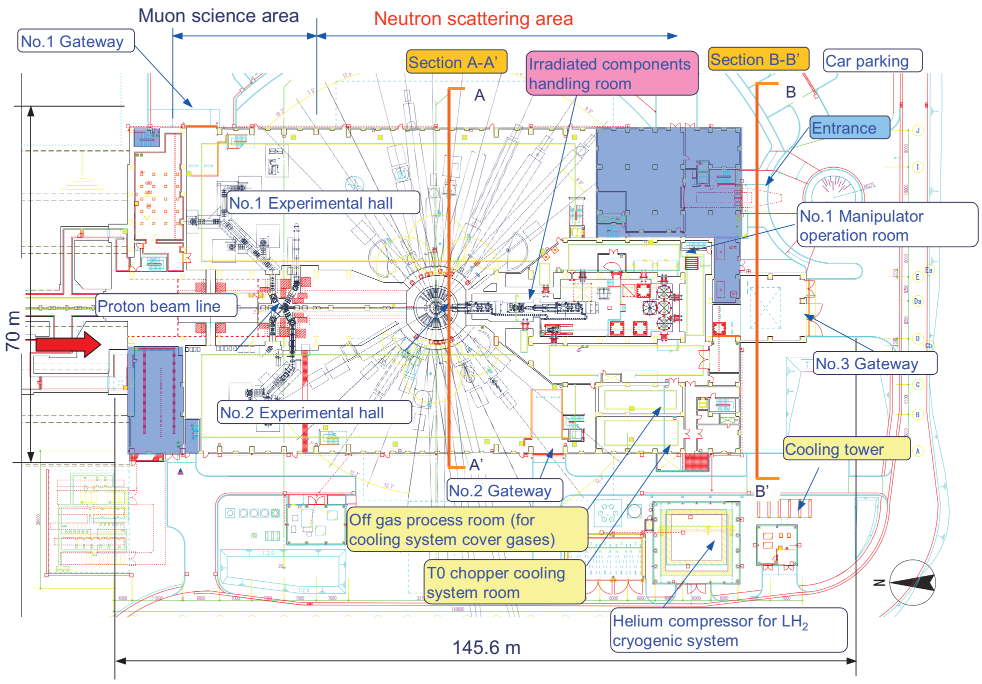

Fig. 3.5.4: First floor layout of the Materials and Life Science Experimental Facility building

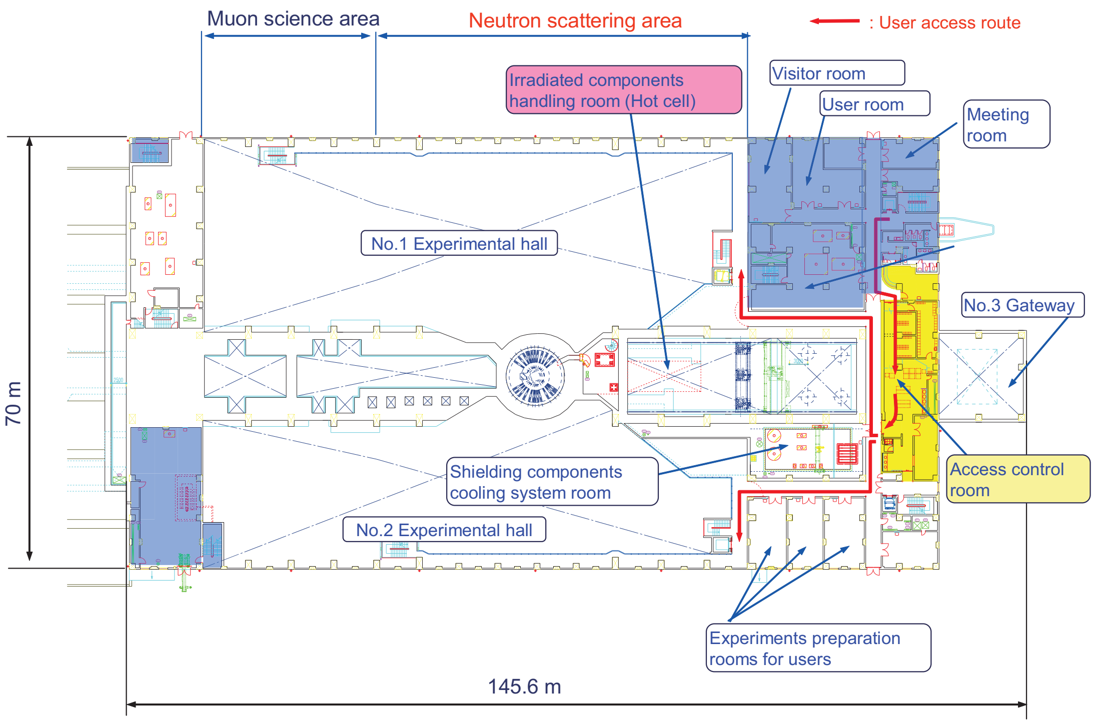

Fig. 3.5.5: Second floor layout of the Materials and Life Science Facility Experimental building

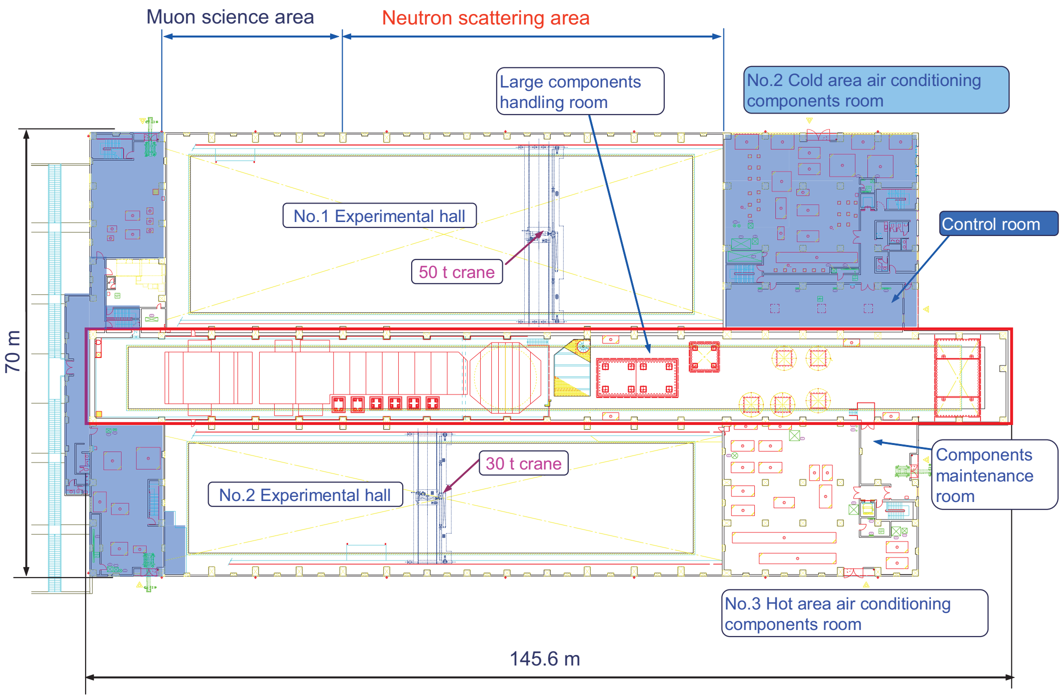

Fig. 3.5.6: Third floor layout of the Materials and Life Science Facility Experimental building

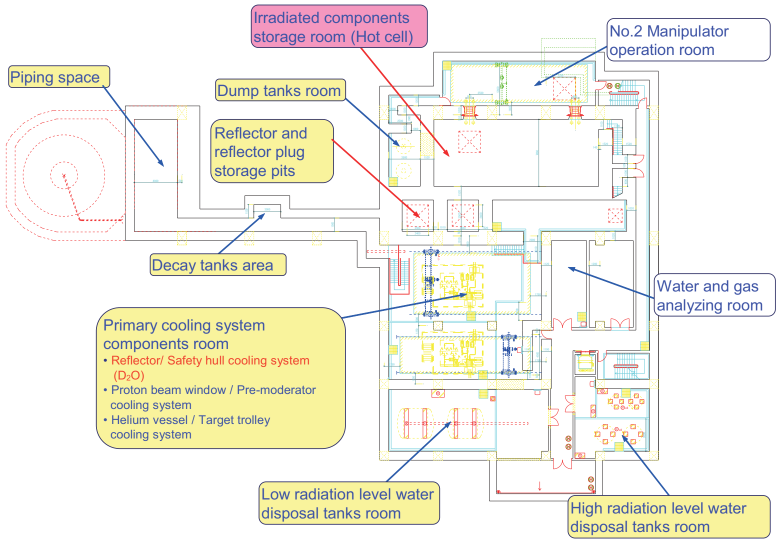

Fig. 3.5.7: Basement floor layout of the Materials and Life Science Facility Experimental building

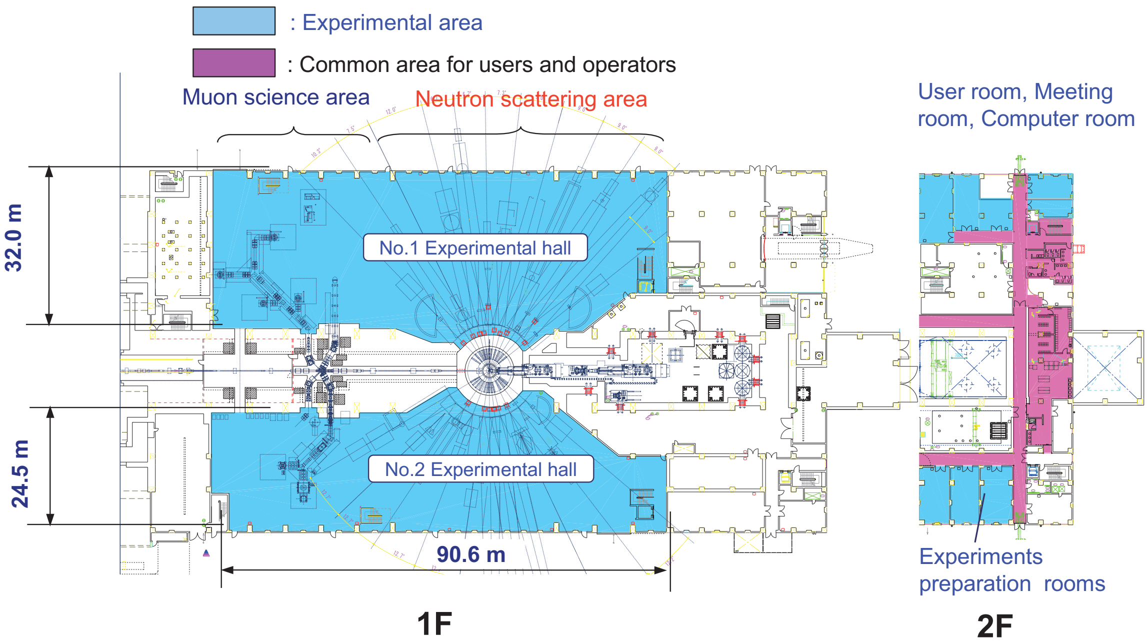

Fig. 3.5.8: MLF experimental user area and common area for both users and operators

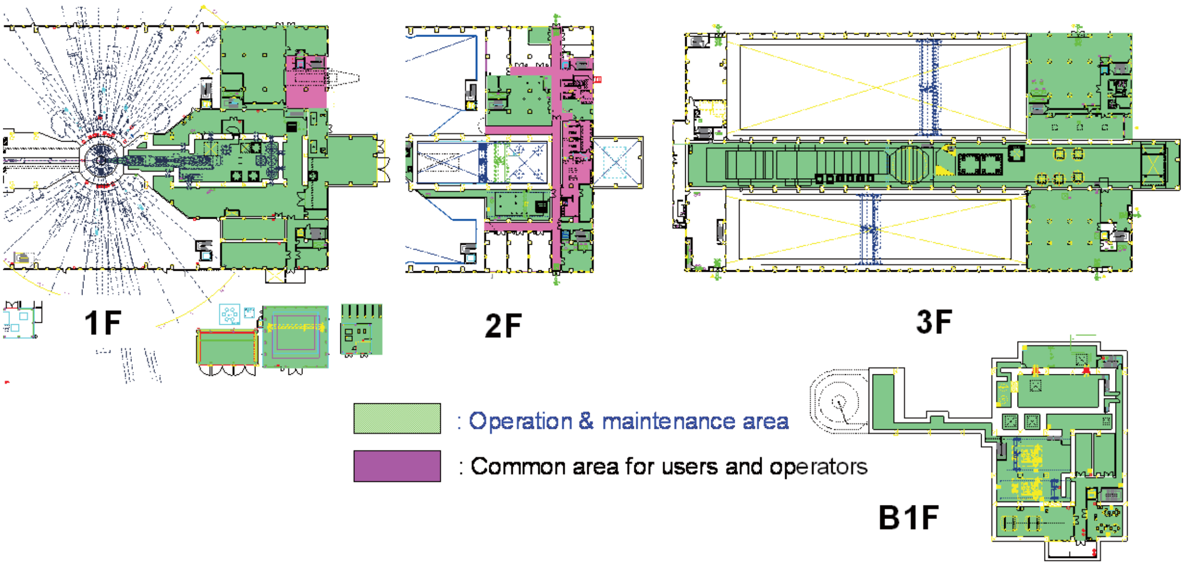

Fig. 3.5.9: MLF operation & maintenance area and common area for both users and operators

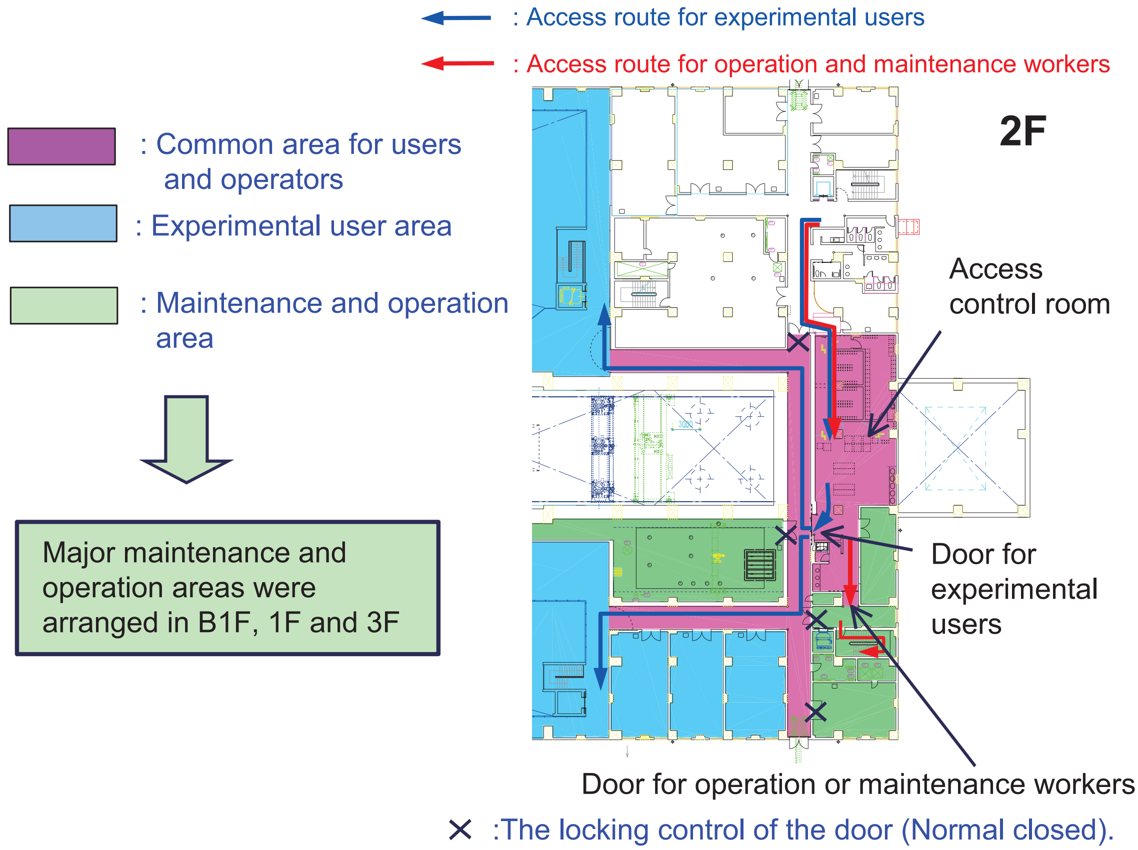

Fig. 3.5.10: Layout of the access control room. The experimental user area and the operation & maintenance area are clearly separated and classified.

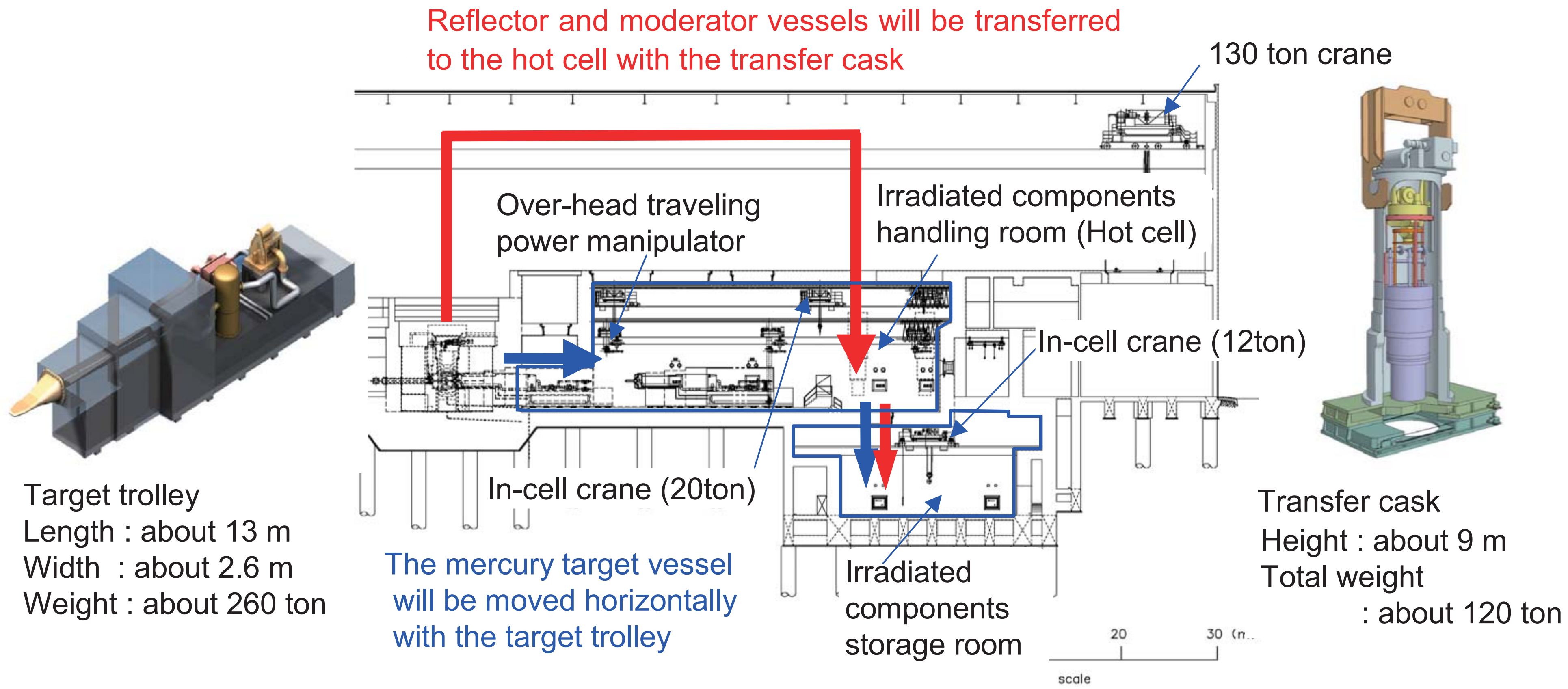

Fig. 3.5.11: Vertical cross section of the hot cell. The hot cell was designed for replacement works and storage of irradiated components as well.

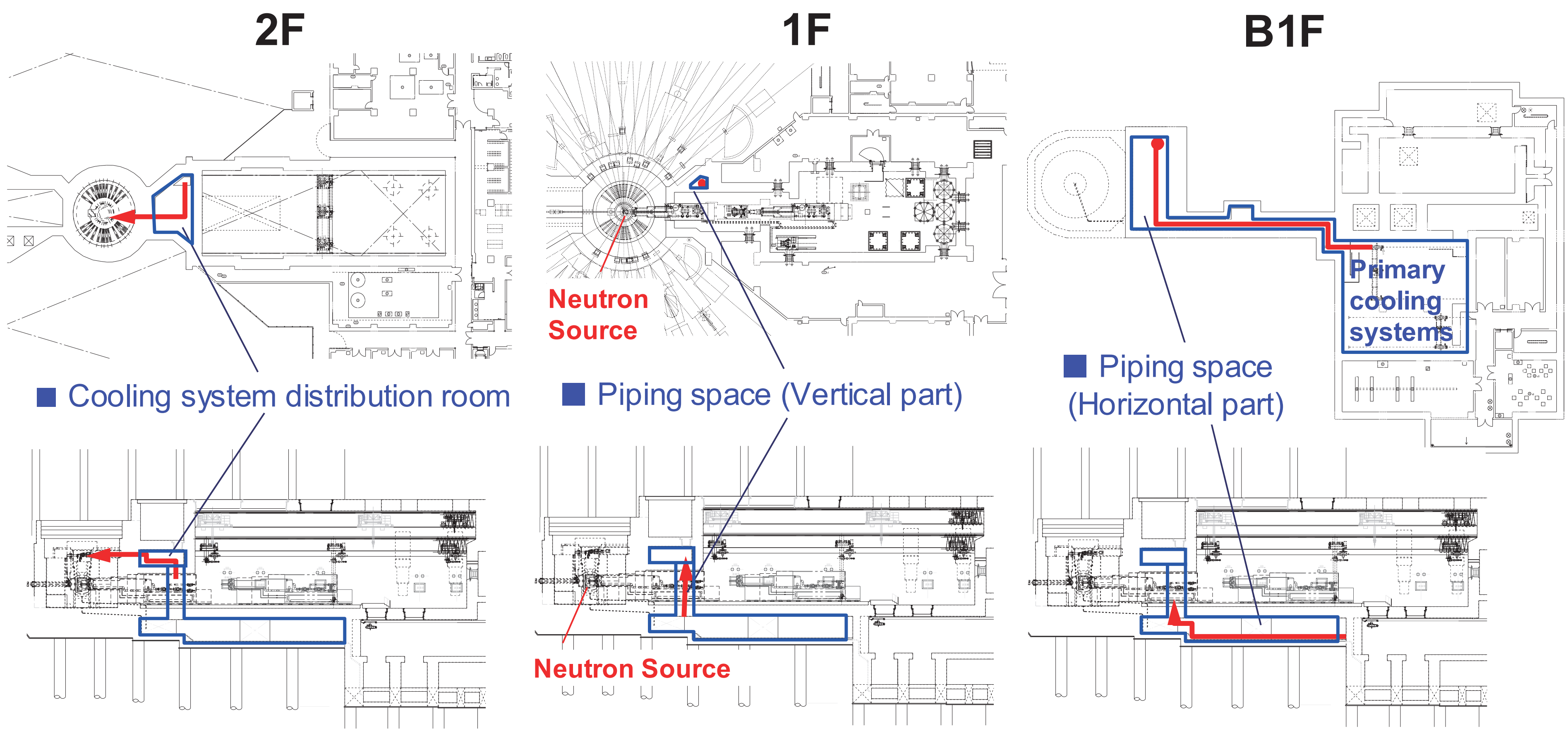

Fig. 3.5.12: Intensive arrangement of components, which include radioactive materials and hydrogen

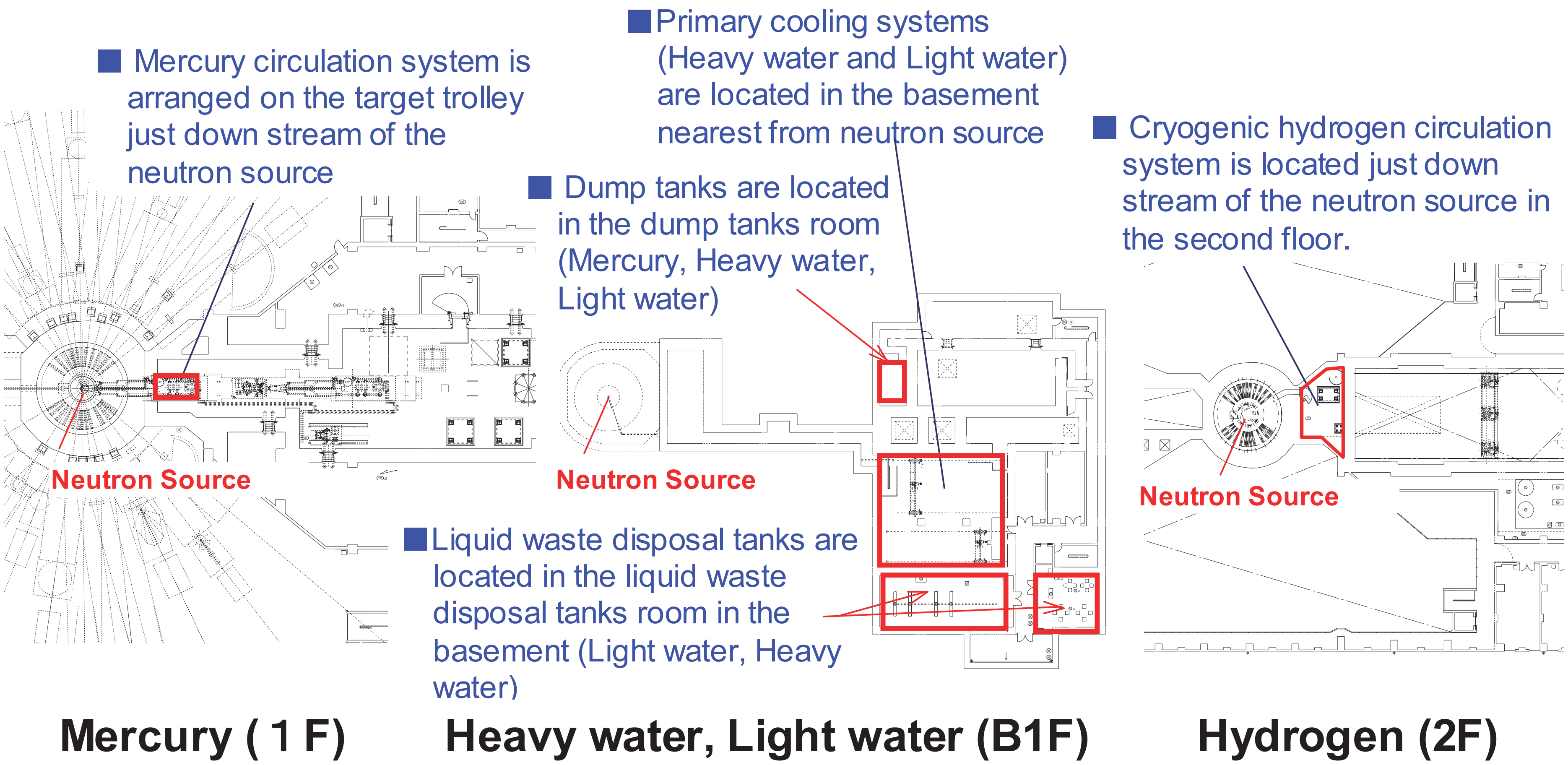

Fig. 3.5.13: Piping routes of primary cooling system

4. Commissioning and Operation

The commissioning process consists of two phases. One is called “off-beam commissioning”, which is conducted before accepting the proton beam at MLF. The other is called “on-beam commissioning”, which is carried out with injecting the proton beam on the mercury target or handling irradiated components. Once the proton beam is injected on the mercury target, many components installed at the neutron source station are activated so that the accessibility to the components is limited. At the off-beam commissioning, therefore, it is important to confirm the specifications of components at normal operation mode. Also, it is quite important to demonstrate both remote-handling and hands-on maintenance procedures as planned. The items to be completed before the beam acceptance are tabulated as “Readiness”. After completing a series of the off-beam commissioning, we will review the readiness of those readiness items.

Some components or systems are unable to be examined without proton beam. There are items to be examined step by step on way of ramping up the power level of the proton beam. Taking account of those conditions for each component, strategic planning is required for conducting the on-beam commissioning effectively. In this section, the commissioning, maintenance and readiness are described.

4.1 Off-beam Commissioning

Off-beam commissioning consists of the subsystem test and the integration test. Number of the test items is summarized in Table 4.1.1. Subsystem tests include the inspection of the dimension and material and the functional test of each component, and most of them are conducted at the vendor’s factory. For shielding components, for example, the composition of material, the dimension, and density are carefully examined. In some cases, we insisted to perform on-site tests. Most of the functional tests were repeated on site, but the cryogenic system was examined only on-site since circulation of liquid hydrogen was unable at vendor’s factory.

The role of the integration test is quite important in the present JSNS, since the total systems of the neutron source components were segmented into several units at ordering stage in view of cost-down and awarded by the different vendors. Although the boundary conditions to assemble a component with the opponent were given in the specification document, it is a key issue in this project to verify that the integrated system functions as designed.

The items of the integration test are summarized in Table 4.1.2. Fig. 4.1.1 shows the sequence of the integration test for each component. The relationship among examinations of each component was taken into account in the sequence. Major factors to determine the sequence are the tests of the cryogenic system and the remote handling of the reflector because the cryogenic hydrogen circulates in the reflector assembly and the circulation pipes must be disassembled when the reflector is pulled out from the helium vessel by a remote handling device.

We have estimated the total duration of the off-beam commissioning process as 12 months. Because of the time consumption by unexpected troubles, one-month delay takes place from the original plan. Fortunately, however, the delay of schedule was handled in the contingency duration which was pointed out to be longer by the Neutron Source Technical Advisory Committee (N-TAC).

It took long duration to conduct the remote handing test. According to the comment of the N-TAC, operators of the remote handling device should take part in the integration test. It is important for the operators to accumulate the experience to use the remote handling device. Since there are no alternative remote handling devices, it is necessary to prepare them to maintain and improve the operation technique.

Table 4.1.1: Summary of off-beam test items

Items	Number of subsystem tests	Number of integration tests
Mercury target system	49	11
Moderator and cryogenic system	32	6
Reflector plug	8	2
Vessel system	39	7
Shielding	9	2
Utility system	26	8
Remote handling system	59	13
Control system	20	5
Neutron beam line	16	12
Source system	61	11
Total	319	77

Table 4.1.2: Integration test for each component in each step

	Off beam test										On beam test
	Step1	Step2	Step3	Step4	Step5	Step6	Step7	Step8	Step9	Step10	Step11
Cryogenic system	Integrated test coupled with moderator (Power on and off with normal status) 10days	Data analysis, adjustments for control	Assembling			Integrated test coupled with moderator (For pressure fluctuation, emergency stop and emergency vent) 20days				Interlock test for integrated system	
Moderator and reflector	Pressure test, Leak test, Water flow test	Remote handling 3month	Assembling	Pressure test, Leak test	Water flow test						
Proton beam window	Water flow test	（Wait for fineished R.H.）	Remote handling	Installation	Water flow test	He vessel leak test					
Hg target	Hg and H2O flow test	Remote handling	Installation			He vessel leak test					
Target trolley		（Wait for fineished R.H.）	Remote handling	Installation		He vessel leak test					
Muon Target and monitor	Installation	Remote handling	Remote control	（Wait for Installed PBW）	Leak test for vacuum	Ultimate vacuum					
Remote cut off device			Cut off test								
Liner vessel and support	Dried air flow test					He vessel leak test	Water circulation test				
Target station shielding						（Wait for He vessel leak test）	Operation test for replacement	Installation	Confinement test for target station		
Neutron beam shutter system	Vacuum system test	Shutter drive test	Cask installation test for shutter								
Vessel window remote handling	Vacuum system test		Remote handling			He vessel leak test					
Plug and shield				Pressure test, Leak test	Water flow test						
Gas waste processing system	Leak test at intersection	Interlock test	Control test								
Device for radiation safety	Interlock test	Integrated system test									
MLF control system	Transfer test Integrated test										
MLF network for control	Network integrated test	Integrated system test									
M1 line vacuum system	Installation	Leak test for vacuum	Ultimate vacuum test								
M2 line vacuum system and pillow seal	Remote installation test by upper tunnel operation	Installation		（Wait for installation of PBW）	Leak test for vacuum	Ultimate vacuum test					
Magnets in M2 line	Remote installation test by upper tunnel operation	Installation	Excitation magnet test	Remote control test							
Shielding block for NM tunnel					（Wait for leak test in M2 tunnel）	Operation test for replacement	Install		Confinement test in NM tunnel		
Air cooler for NM tunnel							Wait for installation of shielding block for NM tunne)	Adjustment of air flow			
Water cooling system for proton beam transport	Control test	（Wait for installtion of magnet in M2 tunnel）	Excitation magnet test								
Control system for proton beam transport	Remote control and measuremen t test	Interlock test									
Measurement equipments for neutron source characteristics		（Wait for vacuum operation system）	Shutter operation test	Interlock test	Remote control test						Test for neutron source

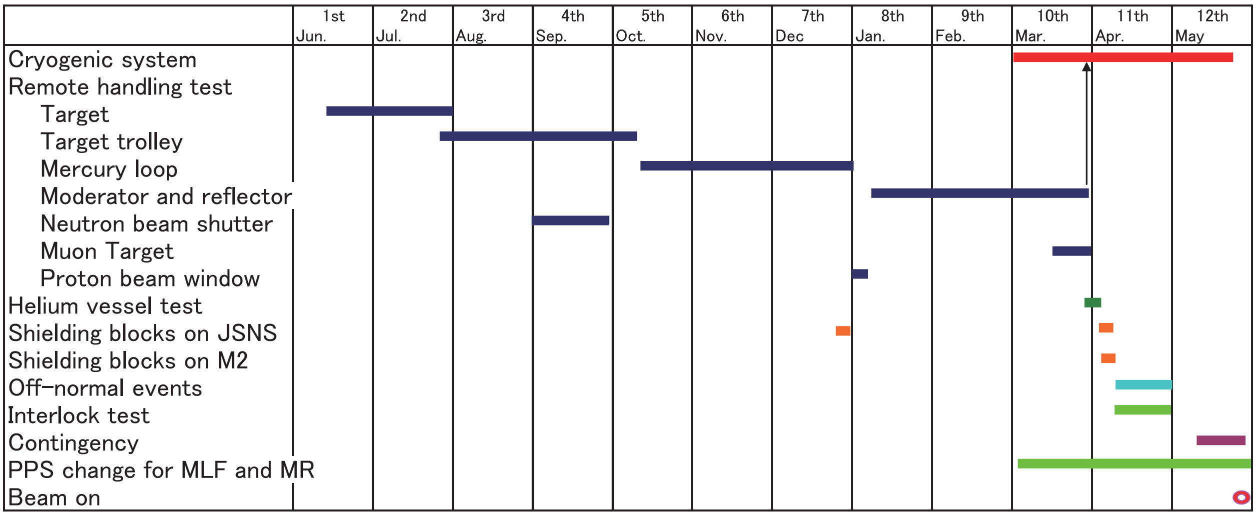

Fig. 4.1.1: Plan of off-beam commissioning examination

4.2 Maintenance

4.2.1 Preconditions and the Evaluated Maintenance Period

The system components at the center of the spallation neutron source, which are exposed to severe radiation field, become highly radioactive and the maintenance operation has to be carried out by remote handling. This was one of the most important issues for the target system design. In this chapter the basic concept of the overall maintenance scenario for the system components which have to be remote-handled will be shown. The detail procedures of the remote handling operation for each component are mentioned in other sections.

The system components which were taken into consideration in making the maintenance scenario are as follows;

a) Neutron target vessel
b) Muon target
c) Neutron shutter insert
d) Proton beam window
e) Proton beam profile monitor (Beam profile monitor)
f) Moderator/Reflector assembly (M/R assembly)
g) Helium vessel insert of the neutron beam line

In the maintenance scenario, the preconditions shown below were assumed.

a) Shutdown periods for system maintenance operation are held twice a year.
b) Spare shielding plugs of the muon target, the beam profile monitor, the proton beam window and the M/R assembly are prepared in advance.
c) Parallel maintenance operation both in the hot cell and in the large component handling room can be carried out.
d) Working time is 8 hours per day and 5 days per week.

Table 4.2.1 shows the maintenance periods for the primary large components for remote handling with their replacing cycle and maintenance period both in off-beam and on-beam state. The maintenance operations of off-beam state are carried out during the long or semi-long shutdown period, and principally the used components fixed to the shielding plugs such as the muon target, the beam profile monitor, the proton beam window and the M/R assembly are replaced to new one while the target system is running. After the proton beam shutdown, some of the system components need to be cooled down before starting the maintenance operation. For example, the radioactive gas generated in the mercury loop and the air in the NM line tunnel need 2 days to cool down. So, the off-beam maintenance period includes cooling time of 2 days in Table 4.2.1.

The components which require the most frequent replacement is the mercury target vessel and the muon target, which need 20 days and 14 days, repectively, during the off-beam period. The muon target maintenance requires additional 13 days operation during the on-beam state. The dry up means the dry up operation of cooling water remaining in the coolant channel of the components. Replacement means the installation of new components to the spare shielding plugs. The shutter insert replacement is assumed to be carried out every year in average and it needs 12 days operation. The replacing cycle put in the parenthesis is the temporal assumption. The proton beam window, the beam profile monitor and the M/R assembly needs 14 days for off-beam operation. The most time consuming process is the dry up operation of the M/R assembly, which is 50 days, but it will not affect the total scenario badly because enough time can be secured for the dry up operation during on-beam period.

4.2.2 Maintenance Scenarios

The outline scenarios to replace these primary components are shown from Figs. 4.2.1 to 4.2.4. First of all, Fig. 4.2.1 shows the scenario to replace the mercury target vessel and muon target which need to be replaced every half a year. The procedures during the off-beam period are as follows.

1. The muon target plug is replaced by the spare plug prepared in the store pit.
2. The old mercury target stored on the basement floor is moved to the storing facility outside of MLF.
3. The mercury target vessel is replaced by the new one and the used one is moved to the basement floor for cooling down

The procedures during the on-beam period are as follows.

4. The muon target plug is moved to the dry up room. Dry up needs 4 days.
5. The plug is moved to the hot cell.
6. The used muon target is replaced by the new one and the plug is moved to the store pit.
7. The used muon target is chopped for volume reduction and stored on the basement floor.

Fig. 4.2.2 shows the scenario to replace the neutron shutter insert. The procedures are done only during the off-beam period as follows.

1. The beam shutter is pulled up into the shutter cask and moved to the maintenance area.
2. The shutter insert is installed and the used insert is stored in a container.
3. The beam shutter is moved back to the target system.

Fig. 4.2.3 shows the scenario to replace the proton beam window which needs to be replaced every 2 years. The procedures during the off-beam period are as follows.

1. The proton beam window plug is moved to the dry up room.
2. The spare plug stored on the basement floor is moved to the target system

The procedures during the on-beam period are as follows.

3. After the dry up operation, the plug is moved to the hot cell.
4. The used proton beam window is replaced by the new one and the plug is moved to the basement floor.
5. The used proton beam window is chopped for volume reduction and stored on the basement floor.

Fig. 4.2.4 shows the scenario to replace the M/R assembly which needs to be replaced every 6 years. The procedures during the off-beam period are as follows.

1. The spare M/R plug stored in the dry up room is moved to the hot cell.
2. The M/R plug is moved to the dry up room.
3. The spare plug in the hot cell is moved to the target system.

The procedures during the on-beam period are as follows.

4. After the dry up operation, the plug is moved to the hot cell.
5. The used moderator vessels and reflector are replaced by new ones and the plug is moved to the dry up room.
6. The used moderator vessels are chopped for volume reduction and, with reflector, moved to the storing facility outside of MLF.

4.2.3 Off-beam Maintenance Schedule

Evaluating the required off-beam maintenance period is very important, because the length of the shutdown period of one facility has much influence on the operation schedule of other J-PARC facilities. On the other hand, the on-beam maintenance is assumed to have less influence, because enough time can be allotted to the maintenance operations.

Table 4.2.2 shows the required period for off-beam maintenance operation. It shows the total working time for many combinations of the maintenance components.

The mercury target vessel and the muon target are replaced every half a year. Because both of the operations can be carried out simultaneously, the longer period of the mercury target vessel decides the total length of the maintenance period. These maintenance periods do not include holidays. As the maintenance components are added, the total maintenance period increases, and the longest period case is 30 days in which most of the major components are subject to maintenance operation.

Table 4.2.3 shows the tentative plan of off-beam maintenance schedule. In order to avoid a long shutdown, the combination of the maintenance components is arranged to make the maintenance period uniform. Thus, it is seen that the maintenance operation can be finished within 5 weeks for the summer shutdown period and within 4 weeks for the winter shutdown period.

Table 4.2.1: Maintenance period for each component

Component	Replacing cycle (year)	Maintenance period (day)			
		Off-beam	Out of place operation of spare plugs (On-beam)		
			Dry up	Replace-ment	Volume reduction
Mercury target vessel	1/2	20	---	---	---
Muon target	1/2	14	4	6	3
Shutter insert	(1)	12	---	---	---
Proton beam window	2	14	4	6	3
Beam profile monitor	5	14	---	6	3
Moderator Reflector	6	14	50	12	7
Vessel window insert	(6)	16	---	---	---

Table 4.2.2: Required period for off-beam maintenance operation

Component	Combination of maintenance components												
Mercury target vessel	○	○	○	○	○	○	○	○	○	○	○	○	○
Muon target	○	○	○	○	○	○	○	○	○	○	○	○	○
Shutter insert		○					○	○	○	○	○	○	
Proton beam window			○				○				○	○	○
Beam profile monitor				○				○			○		
Moderator vessel Reflector					○				○			○	○
Vessel window insert						○				○			
Total working time (days)	20	20	25	26	20	23	26	26	23	27	26	30	26
Required period (weeks)	4	4	5	5	4	4	5	5	5	5	5	6	5

Table 4.2.3: Tentative plan of off-beam maintenance schedule

Operation cycle (year)	1/2		1		2		5		6		10	
Component	S	W	S	W	S	W	S	W	S	W	S	W
Mercury target vessel	○	○	○	○	○	○	○	○	○	○	○	○
Muon target	○	○	○	○	○	○	○	○	○	○	○	○
Shutter insert			○		○		○		○		○	
Proton beam window					○				○		○	
Beam profile monitor							○				○	
Moderator vessel Reflector										○		
Vessel window insert								○				
Total working time (day)	20	20	20	20	26	20	26	22	26	20	26	20
Required period (week)	4	4	4	4	5	4	5	4	5	4	5	4

S : Summer shutdown period, W : Winter shutdown period

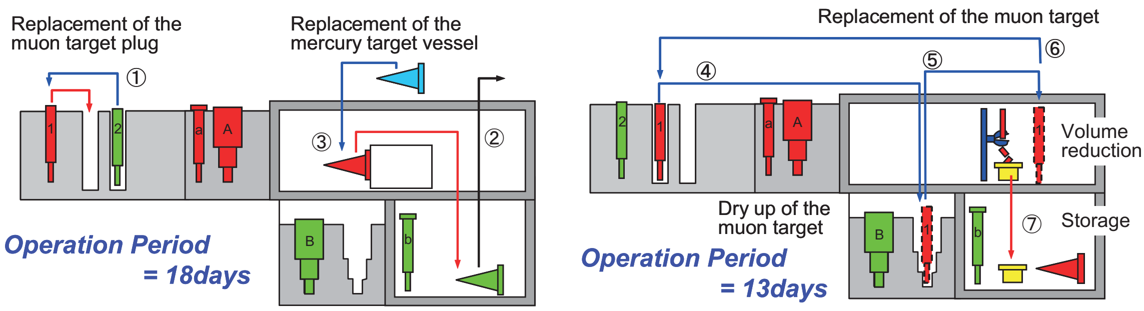

a) Off-beam operation b) On-beam operation

Fig. 4.2.1: Scenario to replace the mercury target vessel and muon target

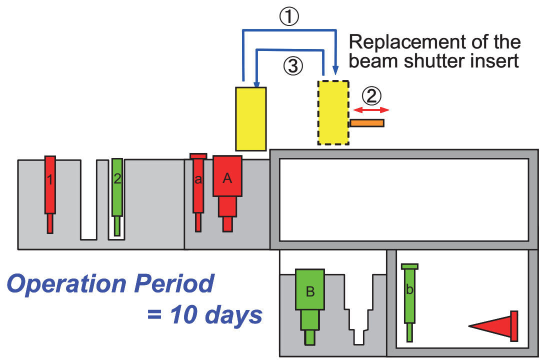

Fig. 4.2.2: Scenario to replace the neutron shutter insert

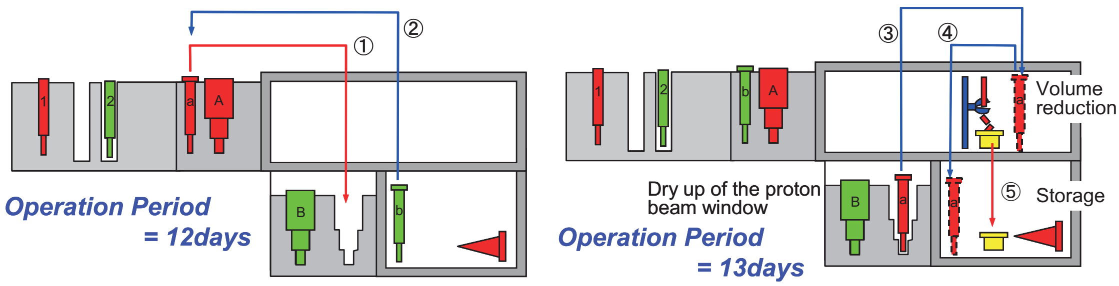

a) Off-beam operation b) On-beam operation

Fig. 4.2.3: Scenario to replace the proton beam window

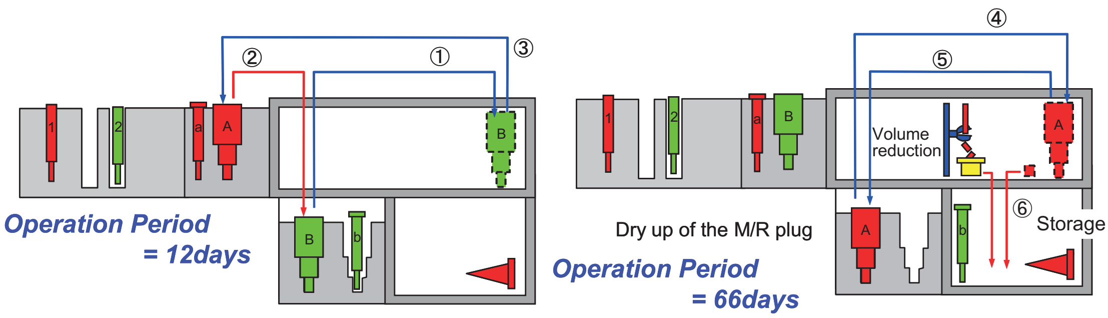

a) Off-beam operation b) On-beam operation

Fig. 4.2.4: Scenario to replace the M/R assembly

4.3 Readiness

To check *"readiness"* for all the JSNS components to accept an initial proton beam on Day-one has started in October 2007. Objectives to check *readiness* are to list all necessary conditions which are needed to be completed before the beam acceptance, and to share the lists among those who are in charge of JSNS operation for mutual confirmation. This procedure is effective to avoid forgetting to do something important before the beam acceptance, and to make acceptance criteria clear.

Table 4.3.1 is an example of a *readiness* checklist for moderators as of January 4, 2008, although it has not been completed. Four general items are defined in the first column: functions, process operation, maintainability and measures for off-normal events. Each general item is broken down in the second column, and the third column defines acceptance criteria for each detailed item. Only major acceptance criteria are described in this checklist while detailed and many other acceptance criteria are dropped for simplification. Other documents such as completion documents prepared by manufacturer and technical reports can be referred in the checklist if needed. The fourth column describes how to confirm satisfaction of the acceptance criteria. The confirmation should in principle rely on documents that are accessible by any interested persons of JSNS in order to be checked by third parties from their objective point of view. Examples of the documents are completion documents prepared by manufacturer, technical reports, presentation files for the N-TAC meeting, papers, lists on file servers, operation manual under preparation and so on. The fifth column classifies necessity to satisfy the acceptance criteria. Items that are indispensable to be completed by the Day-one are indicated by a mark "A", while those preferable to be completed by the Day-one by a mark "B". The sixth column shows current status whether each detailed item is completed or not: "A" means completed, "B" conditionally completed, and "C" not yet completed. For all the items for which the necessity A is given, status must be A or B on the Day-one.

Checklists of *"readiness"* for all the JSNS components are under preparation by the persons responsible for each component as of January 2008. They are to be reviewed in sixth N-TAC meeting (N-TAC6), and to be completed by the Day-one.

Table 4.3.1: An example of readiness checklist

Component: Moderator — Last modified: Jan. 04, 2008

General item	Detailed item	Criteria	Confirmation methods (Name of document)	Necessity A: Indispensable by Day-1 B: Preferable by Day-1	Status A: Completed B: Conditionally Completed C: Not yet Completed
1.1 Functions	Moderators have been installed at the right positions. Pressure proof and leak tests have been passed after connecting to the hydrogen circulation system.	Hydrogen region Pressure proof test: 1.5 MPa Leak rate: not detectable by He-leak test Vacuum region Leak rate: not detectable by He-leak test He-blanket region Leak rate: not detectable by He-leak test Cooling water region Pressure proof test: 0.6 MPa (CM) 0.2 MPa (DM&PM)	Off-beam commissioning report	A	C
	Stable operations of hydrogen, vacuum, He-blanket and cooling water systems at the nominal conditions have been confirmed.	Hydrogen system: OK Vacuum system: OK He-blanlet system: OK Cooling water system: OK	Off-beam commissioning report	A	C
	Integrity of cryogenic temperature region has been confirmed.	Unexpected contact between cold and room temperature regions: No	Off-beam commissioning report	A	C
	Arrangement with the process control system has been completed.	NA	NETH transmission list Console display pages	A	C
	Levels for PPS, TPS, MPS, alarm and warning have been determined.	Hydrogen Temperature: Pressure: Flow rate: Vacuume Degree of vacuum: He-blanket Pressure: Cooling water region Pressure: Flow rate:	NETH transmission list Operation parameter list	A	C
1.2 Process operation	Nominal values and ranges for operation parameters have been determined.	Hydrogen Temperature: 20K Pressure: 1.5 MPa Flow rate: Vacuum Degree of vacuum: < 1e-4 Pa He-blanket Pressure: Cooling water region Pressure:	Operation parameter list	A	C
	Operation manuals have been prepared.	NA	Operation manual	A	C
1.3 Maintainability	Criteria when the moderators are to be replaced have been established.	6 MW*years	Technical report	B	C
	A procedure to replace the moderators has been established.	NA	Maintenance manual	A	C
	Smooth remote-handling replacement of the moderators has been demonstrated.	NA	Off-beam commissioning report	A	C
	Working time, manpower and necessary tools have been estimated, and prepared.	NA	Off-beam commissioning report	A	C
	Templates to manufacture spare moderators have been prepared.	NA	Off-beam commissioning report	B	C
	A disposal method (cooling, drying, cutting and retaining) has been established.	NA	Technical report	B	C
1.4 Measures for off-normal events	Kinds, detection methods and counter-measures against off-normal events have been arranged.	NA	Off-normal event list	B	C
	A scenario for preparing a spare moderator in case of unexpected failure has been established.	NA	Technical report	B	C

4.4 On-beam Commissioning

The flow of the on-beam commissioning is shown in Fig. 4.4.1. The on-beam commissioning starts with the tuning of the proton beam transport line. First of all the beam monitors and their data acquisition (DAQ) system are set up using proton beam. Then the excitations of the beam line magnets are adjusted to make the beam orbit in the center of the beam line. More certain evidence that the proton beam arrives at the mercury target is proved by observing neutron beam generation.

From the view point of maintenance work, the residual radiation in the hot cell has to be kept as low as possible. The distribution of residual radiation is measured while the beam power is low. After very short duration of irradiation and cooling time, the distribution of radiation in the hot cell is planned to be measured. After the radiation mapping is completed, the on-beam commissioning moves to the tuning of the neutron beam line by delivering the proton beam continuously. After long irradiation, the radiation mapping is again planned.

For the future power ramping, target study is quite important. A devise to measure the pressure wave in the mercury target with a Laser Doppler method was adopted to obtain the characteristics on the target vessel. The study is done intensively by changing the proton beam properties.

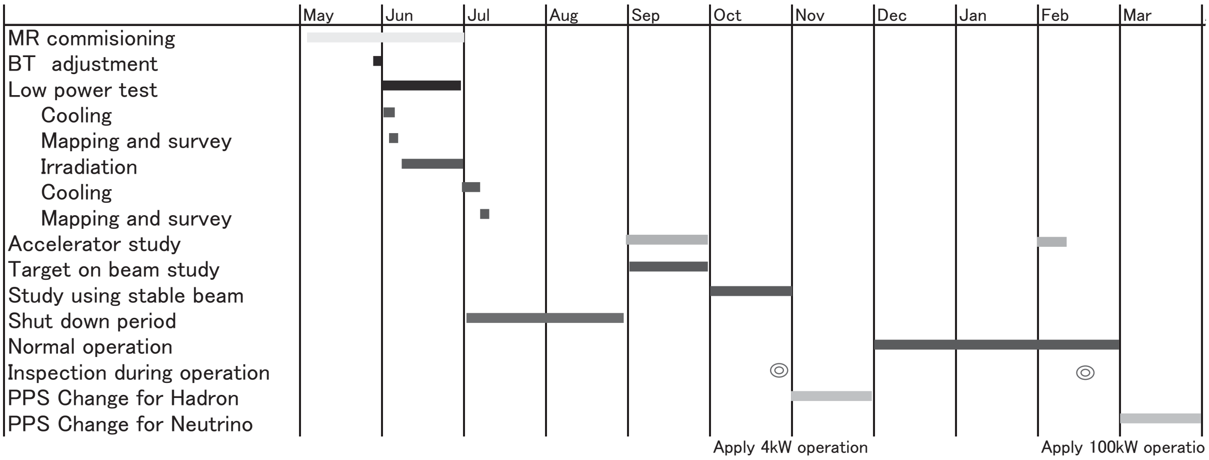

Fig. 4.4.1: Flow of on-beam commissioning

5. Issues, R&D and Future Direction

5.1 Mercury Target

5.1.1 Target Design Revised

The mercury target vessel is a large component and has to be exchanged twice a year in the case of 1 MW beam operation. The separate target structure will be applied taking into account of the following concepts:

- to reduce the waste volume of mercury target vessel,
- to conserve the flange of mercury pipe in target trolley by reducing the frequency of exchange,
- to simplify the structure,
- to reduce the cost of mercury target vessel.

The 3D image of the separate mercury target vessel is shown in Fig. 5.1.1. The separate mercury vessel consists of two parts (front and rear parts) and two parts are connected by flanges with 18 bolts and four connectors for heavy water lines using a power manipulator and master slave manipulators. The power manipulator accesses upper and lower bolts from front side and bolts on the both side from rear side. The front part will be exchanged twice a year in the case of 1-MW beam operation. On the other hand, it is predicted that the frequency of exchanging the rear parts is very low.

The schematic drawing of the separate mercury target vessel is shown in Fig. 5.1.2. The size of the front part is 0.4 m × 0.6 m × 1.4 m. The volume of the separate mercury target vessel (1.2 × 1.2 × 2.5 m^3) is one tenth as small as that of whole mercury target vessel. The storage container used in irradiated components storage room (MLF) and the transport cask with shielding performance to transport it to other facility can be small and light. As a result, the waste volume of the mercury target vessel is reduced, as well as the handling performance improves and the storage space is used effectively. The safety hull is not set in the rear part composed of the mercury pipes, because there is little possibility that the mercury spilt from the mercury pipes.

The schematic drawing of the flange is shown in Fig. 5.1.3. There are two mercury lines, helium gas lines for babbling and monitoring the mercury leakage from the mercury vessel of the front part, pins for positioning and hanging the iron seal gasket and tray to preventing the mercury spilt in the exchange process. The mercury lines and helium gas line for babbling are sealed by double knife edge type seal system. The mercury that leaks outside of an inner knife edge also can be detected immediately by passing the monitoring helium lines through the space between knife edges and it is possible to cope before the mercury spilt from the seal part.

5.1.2 Pressure Wave

5.1.2.1 Introduction

Liquid mercury was suggested to be used as a high-power pulsed spallation neutron source, taking account of the benefits of the neutron yield, coolant and a damageless spallation material. At the moment the proton beams bombard the target, a stress wave will be imposed on a beam window and the pressure wave will be generated in the mercury resulting from high heat deposition rates.[5.1-1, 2)] In the JSNS, the proton beams with 1 μs pulse duration are injected into the mercury through the beam window at a repetition rate of 25 Hz. The structure of JSNS mercury target was designed to allow the stress imposed by the pressure wave not to beyond the fatigue limitation.

Additional concern related with the pressure wave was brought about through the off-beam tests, which had been carried out without the proton beams to evaluate the dynamic response of mercury, by using Split Hopkinson Pressure Bar (SHPB) impact machine, namely the so-called pitting damage that was found on the interface between solid metal and mercury.[5.1-3, 4)] Following the SHPB tests, the pitting damage which was observed in the off-beam tests were confirmed through the on-beam tests using an actual proton beam.[5.1-5)] After both of the experiments, the pitting damage becomes a critical issue to determine the lifetime of the target vessels and realize the high power spallation neutron sources. The lifetime of target vessels is estimated to be remarkably reduced by the pitting damage which degrades the fatigue limit.[5.1-6)] The failure probability analysis on the target vessel was carried out taking the radiation and pitting damages into account. After 30-h operation under MW-class condition, the failure probability was estimated to be about 10%.[5.1-7)]

Therefore, the mitigation technique for pressure waves and pitting damage is essential to realize the high power target. We carried out R&D on the mitigation technology under international and domestic collaborations. Microbubble injection into mercury is one of prospective technologies to mitigate the pressure wave. Then, the microbubble effect was experimentally investigated from the viewpoint of pitting damage in the mercury loop with a device which can apply the pressure pulse to the mercury and induce the pitting damage, and the result was numerically examined from the viewpoint of bubble dynamics which has been carried out so far in JSNS with collaborators.

5.1.2.2 Experiment

(1) Off-beam test

To investigate the effect of bubble on the mitigation of the pressure wave, mercury test loop was developed. The test loop can be connected to an electro-Magnetic IMpact Testing Machine (MIMTM), which has a pulse generator driven by electromagnetic force.[5.1-8)] The MIMTM is able to impose the impulsive pressure into the mercury through an electromagnetically driven striker. Fig. 5.1.4 shows a schematic diagram and components of the mercury loop with the MIMTM. A pump with rotated permanent magnet was newly developed. The inventory of mercury is about 5 litters.

In the present experiment, the mean flow velocity of a rectangular channel (33 mm of width and 12 mm of height) was kept constant at 0.3 m/s (7100 cc/min), and the void fraction of injected helium gas bubble, V_f, was defined to be the ratio of the gas flow rate to the mercury flow rate, was set to 10^{-3} constant. Micro-bubbles of helium gas are formed and injected into the flowing mercury by using a sintered porous tube made of tungsten which is mounted at the neck of Venturi pipe upstream the MIMTM as shown in Photo. 5.1.1. The dimension of the bubbler is a tube of 10 mm in outer diameter, 6 mm in inner diameter, 10 mm in length, and 35% of porosity. The mean velocity of the mercury in the bubbler is 4.2 m/s. Bubbles are generated in this bubbler by tearing the gas from the pores by the flowing mercury. The injected helium gas was controlled by a mass flow meter with an accuracy of 0.01 cc/min. An average diameter of the bubble at the MIMTM test section, which was measured as projection radius in contact with a glass wall, was about 100 μm.

The MIMTM has a mercury chamber (inner diameter of 100 mm and thickness of 12 mm), through which rectangular pipe passes diametrically. The plate specimen of 316L stainless steel (diameter of 70 mm and thickness of 1 mm) was installed at the lid of the mercury chamber to examine the relationship between the pitting damage and the mercury flowing condition: no flow, flowing at 0.3 m/s, and flowing at 0.3 m/s with injected gas bubbles. Hereinafter called *stagnant, flowing, bubbling*, respectively. Impulsive pressure was imposed in the mercury at the power of 560 W/pulse and a repetition rate of 1 Hz. Also, the impulsive pressure was measured at the lid of mercury chamber by a pressure transducer (Entran® EPXH).

Photo. 5.1.2 shows the micrographs of the pitting damaged surfaces of specimens after 10^2 and 10^4 impacts under each mercury flowing condition: stagnant, flowing, and bubbling, which were taken by a laser microscope. The pitting damages were formed by the microjet and/or shock wave which were caused by aggressively cavitation-bubbles collapsing. After 10^2 impacts, the difference of the pitting damaged area was difficult to distinguish by the flowing condition. On the other hand, after 10^4 impacts, it was recognized that the pitting damaged area was remarkably reduced by bubbling or even by only flowing. The fraction of damaged area, which was defined as the ratio of pitting damaged area A_e to measured area A_0, after 10^4 impacts are 0.63 for stagnant, 0.12 for flowing and 0.01 for bubbling, respectively. It was confirmed from these observations that the pitting damage was mitigated by the mercury flowing and flowing with gas-bubbles injection and that injected bubbles were decidedly effective to reduce the pitting damage.

Fig. 5.1.5 shows the time response of impulsive pressure. The triggered signal was set to the applied voltage of electromagnetic coil, and the sampling rate of the waveform was 1 MHz. In the MIMTM tests, the rapid pressure rising was not expected as the proton beam bombarding induces. The first peak of compressive pressure response was observed around 0.75 ms after impacting. The peak values of compressive pressure are hardly affected by the flowing condition. On the other hand, the negative pressure is slightly varied by the mercury condition: the absolute value of negative pressure was reduced by bubbling but not by flowing. This point will be discussed in more detail in the next section.

(2) On-beam test

The MIMTM can not apply the rapid pressure rising as the proton bombarding condition. Then, the damage test was carried out by using proton beams at Weapons Neutron Research (WNR) facility in Los Alamos National Laboratory assuming MW-class proton beams. The dynamic response of pipe wall was measured by a laser Doppler vibrometer.

The morphology of pitting damage observed by the on-beam tests in Weapons Neutron Research

(WNR) facilities at Los Alamos National Laboratory, assuming MW-class proton beam[5.1-5] was sufficiently similar to that obtained in the MIMTM at the electric power of 560 W/pulse.

The mitigation effect was observed in the 2005 WNR on-beam test by measuring the dynamic response of the mercury pipe wall, as shown in Fig. 5.1.6.[5.1-9] The amplitude of the displacement velocity was clearly reduced by bubbling. Also, the pitting damage was mitigated by flowing and bubbling. Unfortunately, we did not know the bubble condition precisely that time.

5.1.2.3 Numerical simulation

In order to understand how the microbubble injection mitigates the cavitation damage and predict what condition is the most effective to reduce the amplitude of the pressure wave, three kinds of numerical simulations are carried out: *i.e.* macro, meso, micro-scale simulations.

(1) Macro-scale simulation

In the macro-scale simulation, the interaction between the target structure and the mercury with pressure wave propagation is evaluated by a conventional FEM code: LS-DYNA and ABAQUS.[5.1-10, 11, 12] From the simulation we understand the period of negative pressure imposing on the target vessel wall, which is one of the important parameters for cavitation bubble formation.

Fig. 5.1.7 shows the pressure distribution in the mercury induced by the proton bombarding. After the bombarding, intensive compressive pressure strikes the beam window of the target vessel. The target vessel was excited by the interaction between dynamically pressurized mercury and the target vessel wall. The interaction results in the negative pressure formation in the mercury, which has potential to induce cavitation. The period of the negative pressure near the beam window was estimated to be a few ms approximately, which is similar to the period of the negative period obtained in the off-beam test as shown in Fig. 5.1.5.

(2) Meso-scale simulation

In the meso-scale simulation, we developed an original code, PAC-MT, to simulate the mitigation effect of the pressure wave by the bubbles injected into the mercury.[5.1-13]

The PAC-MT gives the relationship between the mitigation effect on the compressive pressure wave and the injected bubble conditions. The typical results are shown in Fig. 5.1.8. The peak pressure at the center of bombarding area is reduced by the absorption effect of bubbles. The mitigation effect gets to be distinguished by relatively small bubbles with less than 50 μm in radius and void fraction of more than 0.3%, as shown in Fig. 5.1.8(a). Also, as shown in Fig. 5.1.8(b), the compressive pressure near the beam window is reduced through the propagation process from the bombarding area to the window wall by the attenuation effect. The two mechanisms, absorption and attenuation, will be remarkable to mitigate the compressive pressure induced by the proton beam bombardment.

(3) Micro-scale simulation

In the micro-scale simulation, radial motion of the single bubble was analyzed by using the following equation derived by Plesset, et al.[5.1-14)]

$$R\ddot{R}+\frac{3}{2}\dot{R}^2=\frac{1}{\rho}\left[\left(P_0+\frac{2\sigma}{R_0}-P_v\right)\left(\frac{R_0}{R}\right)^{3\gamma}+P_v-\frac{2\sigma}{R}-\frac{4\eta\dot{R}}{R}-P(t)\right] \tag{5.1.1}$$

where, R is the time dependent bubble radius, ρ is the density of liquid, σ is the surface tension, P_v is the vapor pressure, η is the viscosity, γ is the specific heat ratio, *P(t)* is the external pressure, subscript 0 denotes initial state, and overdots denote time derivative, respectively. The parameters of mercury at 300 K were used for the calculation using Eq. 5.1.1: ρ = 13,528 kg/m^3, P_v = 0.28 Pa, σ = 0.47 N/m, η = 1.52×10^{-3} Pa•s, γ = 1.402 and P_0 = 0.1013 MPa. This nonlinear equation governs the radial motion of a spherical bubble in an incompressible liquid, driven by *P(t)*.

We recognized the mitigation effect of injected bubbles on pressure response in the MIMTM mercury loop test. Although the measured compressive pressure was hardly reduced by the bubbling, the amplitude of negative pressure was slightly decreased.

The experimentally measured pressure responses of Fig. 5.1.5 were used as *P(t)* for stagnant and bubbling cases. The initial radius of the bubble, R_0, was assumed to be 20 μm. The dynamics of the single bubble is shown in Fig. 5.1.9, where one can see that the bubble behavior is strongly affected by the slightly change in the negative pressure: *i.e.* under stagnant condition the bubble expands explosively and shrinks rapidly, on the other hand, in the case of bubbling the bubble oscillates gently.

To systematically understand the effects of the negative pressure amplitude, A_p, and the imposing period, T_p, on the cavitation inception, we performed an additional numerical study, in which *P(t)* was assumed to be a rectangular pressure wave. Fig. 5.1.10 shows the relationship between the maximum bubble radius, R_{max}, A_p, and T_p at R_0 =20 μm. It is quantitatively understandable from Fig. 5.1.10 that the threshold of negative pressure for cavitation inception is very dependent on A_p, and if the negative pressure amplitude exceeds the threshold, the maximum bubble size increases with T_p and A_p.

A possible answer for the negative pressure reduction due to the bubbling is that the compressive pressure waves emitted by expanding gas bubbles is superimposed on the negative pressure wave around cavitation nuclei and reduce the amplitude to a value lower than the threshold. This means that the compressive pressure emitted from gas bubbles suppresses cavitation bubble formation or inception. A more detailed explanation on this mechanism is shown by Ida, *et al*.[5.1-15)]

Therefore, we consider the third mechanism to mitigate the pitting damage as focusing on the reduction of the negative pressure related to the cavitation threshold.

The suggested mechanisms of bubbling mitigation are summarized as illustrated in Fig. 5.1.11. Three mechanisms for each region are considered; *i.e.* the absorption for compressive pressure wave induced by the proton beam bombarding in region A, the attenuation for compressive pressure wave propagation in region B, the suppression for negative pressure by compressive pressure emitted from gas bubbles in region C.

5.1.2.4 Future plan

As mentioned above, the effect of bubble injection on the mitigation of cavitation damage was recognized. Then, for the next step, we will focus on how the bubbles are formed and controlled in the mercury; *i.e.* on bubbling system, suitable target design, etc. and the dynamic response of bubbles against the pressure waves with much higher rising rate, which will be likely to be induced by proton bombarding.

5.1.2.5 Summary

The mitigation technology of pressure wave is essential to realize a pulsed high-power mercury target for spallation neutron sources. Microbubble injection into mercury is one of prospective technologies to mitigate the pressure wave and the pitting damage. The effects of injected microbubbles were experimentally and numerically examined from the viewpoint of bubble dynamics and are summarized as follows:

a) R&D on the mitigation technology was carried out by using the MIMTM mercury loop under the various mercury flowing conditions: stagnant, flowing, flowing with bubbling. The effect of injected gas bubbles into the mercury on the mitigation of pitting damage was recognized experimentally, as well as, the mercury flowing reduced the damage.
b) The above mitigation mechanisms were numerically examined. Three mechanisms are considered; *i.e.* the absorption for compressive pressure induced by the proton beam bombarding, the attenuation for compressive pressure wave propagation, and the suppression for negative pressure by compressive pressure emitted from gas bubbles.
c) The effect of bubble injection on the mitigation of the pressure wave and the pitting damage was recognized. For the next step, we will focus on how the bubbles are formed and controlled in the mercury; *i.e.* bubbling system, suitable target design, and how gas bubbles are collapsed by pressure waves with high rising rate.

5.1.3 Post Irradiation Experiment (PIE)

5.1.3.1 Objectives of PIE

Radiation damage of the mercury target vessel material becomes severe with the increase in the operation time by increase in the irradiation quantity of the neutron and the proton, and the material characteristics presumed at the time of the design are degraded. That is, the lifetime in design is brought about. In particular, there is a fear that the material degradation might be accelerated due to the simultaneous irradiation by protons and neutrons, although the sufficient data related to the mechanical strength due to the simultaneous irradiation of protons and neutrons are not obtained so far. Furthermore, the acquisition of the material data exposed to the actual environment is indispensable to evaluate material degradation quantitatively because the material is degraded by the cavitation damage and the mercury immersion in addition to the radiation damage. The rationalization of the life evaluation is also indispensable from the viewpoint to reduce the storage capacity for the spent target vessel in the facility as much as possible.

It is necessary that structural material keeps ductility in the design philosophy. In other words, when it is judged from the neutron irradiation damage of 316SS simulating a fast reactor and a fusion reactor structure though the operational temperature range is different, the necessary ductility presumed in the design is significantly kept up to the radiation damage of 5DPA. Therefore, the lifetime is set as the operation time when the radiation damage becomes 5DPA, though the material data to face in a limit environment like the practical target don't exist as mentioned above. However, if the high power and more stable operation and the reduction of storage capacity are taken into consideration, it is important to rationalize the structural integrity evaluation and the lifetime evaluation based on the material data obtained under the practical target condition. Therefore, the objectives of PIE are 1) to assemble the mechanical degradation data of the target vessel material exposed to the actual environment and to make the data useful for the rationalization of the target life evaluation and 2) for the accumulation of the experimental data of the radiation damage due to the simultaneous irradiation of the high energy proton and the spallation neutron to use the radiation damage research. The outline of the PIE schedule presumed at present is shown in Table 5.1.1. And, presumed contents of an examination are mentioned in the next section.

5.1.3.2 Contents of PIE

In PIE, the test procedure should be simple because the radiated specimen must be handled remotely. And it is important to establish the experimental technique using a small specimen because the specimens are cut from the thin-walled spent target vessel to limit the size of the specimen. The items of PIE which are carried out to rationalize the lifetime evaluation of the target vessel are shown in the following.

(1) Ductility evaluation examination

It is necessary that the ductility of the material is kept during the operation so that the structural integrity of mercury target vessel may be suitable according to the design standard. Charpy impact test is applied in the JIS standard as an evaluation technique for the ductility degradation (embrittlement). However, it is difficult to cut the standard test piece for the Charpy impact test from the beam window which is thin wall. Because of that, the development of the ductility evaluation technique is necessary, such as the small punch test in which the small specimen was used.

(2) Tensile test and bending test

A membrane stress, bending stress and thermal stress and those combined stresses are generated in the target vessel by the operational pressure, the pressure wave, the temperature gradient and so on. Fracture surface observation after the test is carried out to acquire the material data which was damaged against these stresses and to make the data useful for the material embrittlement estimation and the lifetime estimation.

(3) Indentation test

Since the size of the specimen is limited in the above-mentioned tests to restrain scale effect as much as possible, the number of the specimen cut from the beam window is limited. Moreover, the processing of the specimen should be done accurately, and the test must be carried out remotely. The indentation test can be carried out with easy procedure and it is possible to evaluate the material characteristics from the acquired data. So, the indentation test can be expected as a technique to evaluate the degradation of material.

(4) Microscope observation, SEM observation, TEM observation and He and H_2 gas analysis

Microstructure is observed to examine the influence on the change in the mechanical properties. And, an influence on the micro structure of the irradiation damage by the proton and the neutron is investigated.

5.1.3.3 Issues on the PIE

Issues to carry out the PIE are shown in the following.

(1) Establishment of the execution system

The cooperation of the various fields of majority is indispensable to the execution of PIE, such as the material researcher, the maintenance of the sample handling machine and the facility to maintenance the radiated material. It is important to establish the partnership to carry out the PIE.

(2) Issues in the preparation stage of the PIE

- Making scenario of the PIE and of waste disposal after PIE

Many specimens can't be prepared so that they are cut from the target vessel or the surveillance test pieces installed in the space around mercury target are used as the specimens. Therefore, the data must be acquired efficiently, and a plan must be considered to evaluate lifetime from the limited specimens. The specimen after the test must be discarded as a radioactive waste.

- Establishment of test procedure

Because the target vessel is thin walled structure, it is difficult to make the test piece with enough size. So, it is necessary to establish the test technique using the small specimen.

- Selection of the test apparatuses for PIE and finishing machines

It is necessary to prepare the equipment to cut the specimen from the spent target vessel exposed to the operation environment by the remote control and the PIE apparatuses which can be also handled by the remote control.

- Issues on the shipping and reception in each facility

Facilities inside Tokai establishment will be used effectively because there is no space in the hot cell to carry out PIE in MLF. Because of that, the issues on the shipping between each facility and MLF and reception in each facility are cleared and must be solved.

References

5.1-1) K. Skala, G. S. Bauer: “On the pressure wave problem in liquid metal targets," Proc. 8th Int. Collabo. on Adv. Nuron Source (ICANS-XIII), Villigen, Switzerland, Oct. 11-14 1995, 1995, pp. 559-576.

5.1-2) M. Futakawa, K. Kikuchi, H. Conrad, H. Stechemesser: “Pressure and stress waves in a spallation neutron source mercury target generated by high-power proton pulses,” Nucl. Inst. Phys. Res., A 439, 2000, pp. 1-7.

5.1-3) M. Futakawa, H. Kogawa, R. Hino: “Measurement of dynamic response of liquid metal subjected to uniaxial strain wave,” J. Phys. IV France, 10[PR9], 2000, pp. 237-242.

5.1-4) M. Futakawa, H. Kogawa, R. Hino, H. Date, H. Takeishi: “Erosion damage on solid boundaries in contact with liquid metals by impulsive pressure injection,” Int. J. Imp. Eng., 28[2], 2003, pp. 123-135.

5.1-5) J. R. Haines, K. Farrell, J. D. Hunnm, D. C. Lousteau, L. K. Mansur, T. J. McManamy, S. J. Pawel, B. W. Riemer: Summery of Mercury Target Pitting Issue, SNS-101060100-TR0004-R00, Oak Ridge National Laboratory, 2002.

5.1-6) M. Futakawa, T. Naoe, H. Kogawa, M. Teshigawara, Y. Ikeda: “Effects of pitting damage on fatigue limit and lifetime in mercury target," J. Nucl. Mater., 356, 2006, pp. 168-177.

5.1-7) M. Futakawa, T. Wakui, H. Kogawa, Y. Ikeda: “Pressure wave issues in high power mercury target,” Nucl. Inst. Meth, in Phys. Res., A 562, 2006, pp. 676-679.

5.1-8) M. Futakawa, T. Naoe, H. Kogawa, C. C. Tsai, Y. Ikeda: “Pitting damage formation up to over 10 million cycles -off line test by MIMTM,” J. Nucl. Sci. Technol., 40[11], 2003, pp. 895-904.

5.1-9) H. Kogawa, S. Hasegawa, M. Futakawa, Y. Ikeda, B. Riemer, M. Wendel, J. Hains: “Damage potential measurements in WNR proton beam tests,” Proc. 17th Int. Collaboration. on Advanced. Neutron Source (ICANS-XVII), April 25-29 2005, Santa Fe, New Mexico, 2005, pp. 572-581.

5.1-10) LS-DYNA3D Theoretical Manual, Livemore Software Technology Corporation, 1996.

5.1-11) ABAQUS Theory Manual, Ver. 5.8, Hibbitt, Karlsson & Sorensen, Inc., 1998.

5.1-12) T. Wakui, M. Futakawa, H. Kogawa, S. Ishikura: “Failure probability estimation of multi-walled vessels for mercury target,” J. Nucl. Sci. Technol., 44[4], 2007, pp. 530-536.

5.1-13) K. Okita, Y. Matsumoto, S. Takagi: “Propagation of pressure waves, caused by a thermal shock in liquid metals containing gas bubbles,” Proc. 2005 ASME Fluids Eng. Div. Summer Meeting and Exhibition, FEDSM2005-77397, June 19-23, 2005, Houston, TX, USA, 2005, [CD-ROM].

5.1-14) M. S. Plesset: “The dynamics of cavitation bubbles,” J. Appl. Mech., 16, 1949, pp. 228-231.

5.1-15) M. Ida, T. Naoe, M. Futakawa: “Suppression of cavitation inception by gas bubble injection: A numerical study focusing on bubble-bubble interaction,” Phys. Rev., E 76, 2007, pp. 046309.

Table 5.1.1: Outline of the PIE schedule

2007	2012	2013	2015	2016
5 years for operation of the 1st target				
	1 year for cooling the 1st target			
	Preliminary cutting			
	Carrying out to hot lab.			
	2 years for cooling			
			Cutting into specimen	
	PIE			
			The data would be got in 10 years	

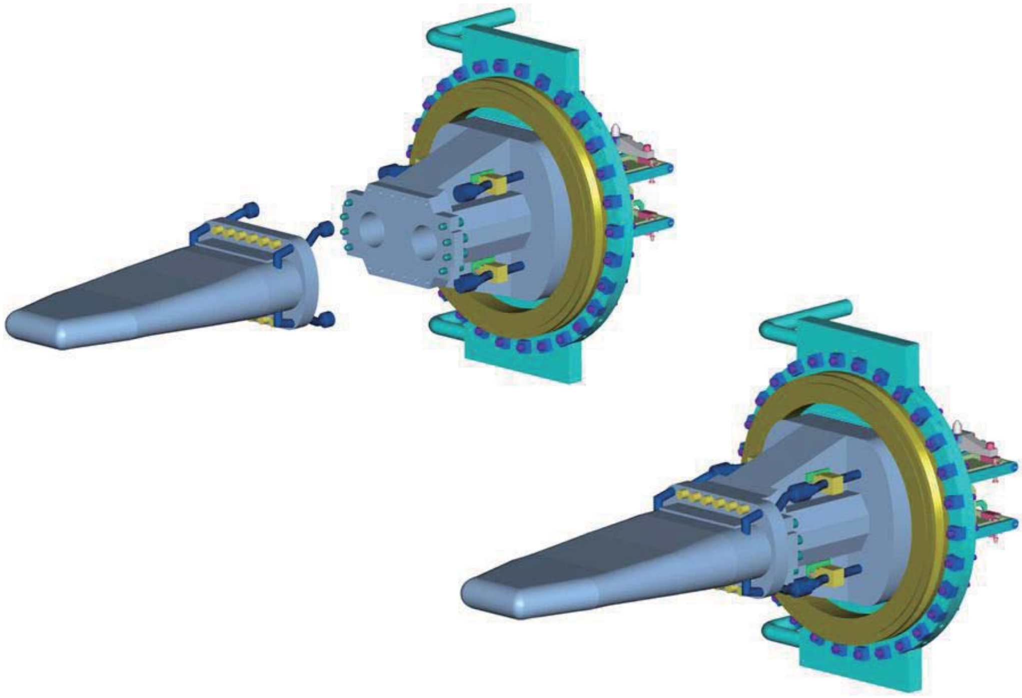

Fig. 5.1.1: 3-D image of separate mercury target vessel

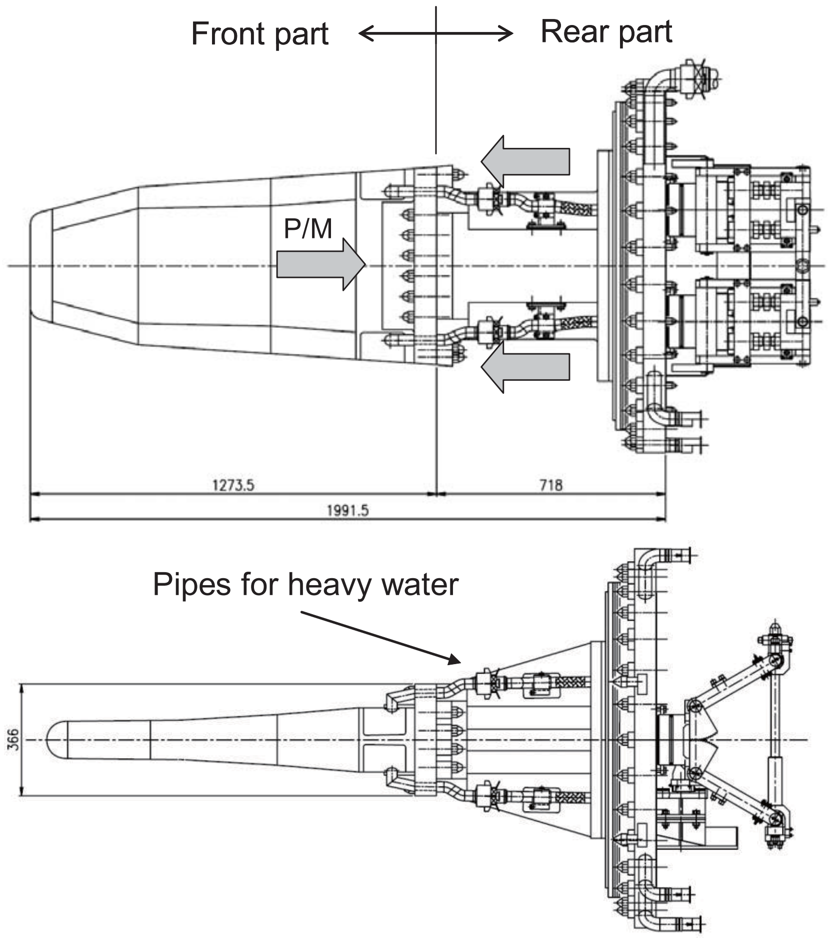

Fig. 5.1.2: Schematic drawing of separate mercury target vessel

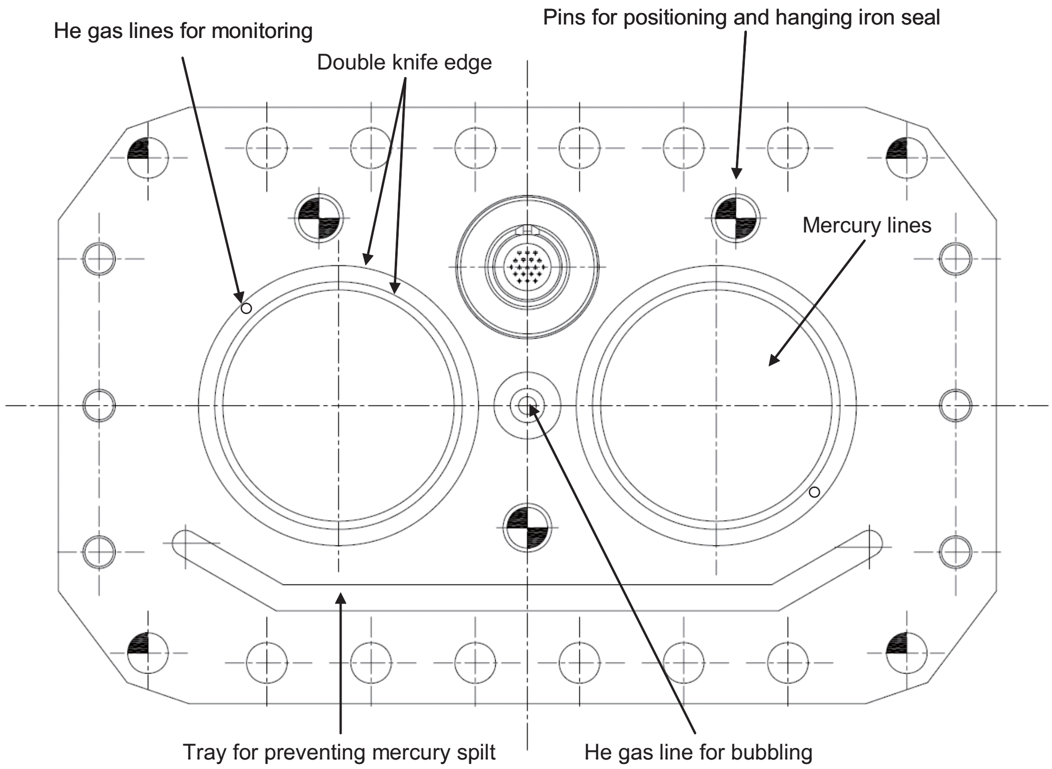

Fig. 5.1.3: Schematic drawing of flange with multi gas and fluid lines

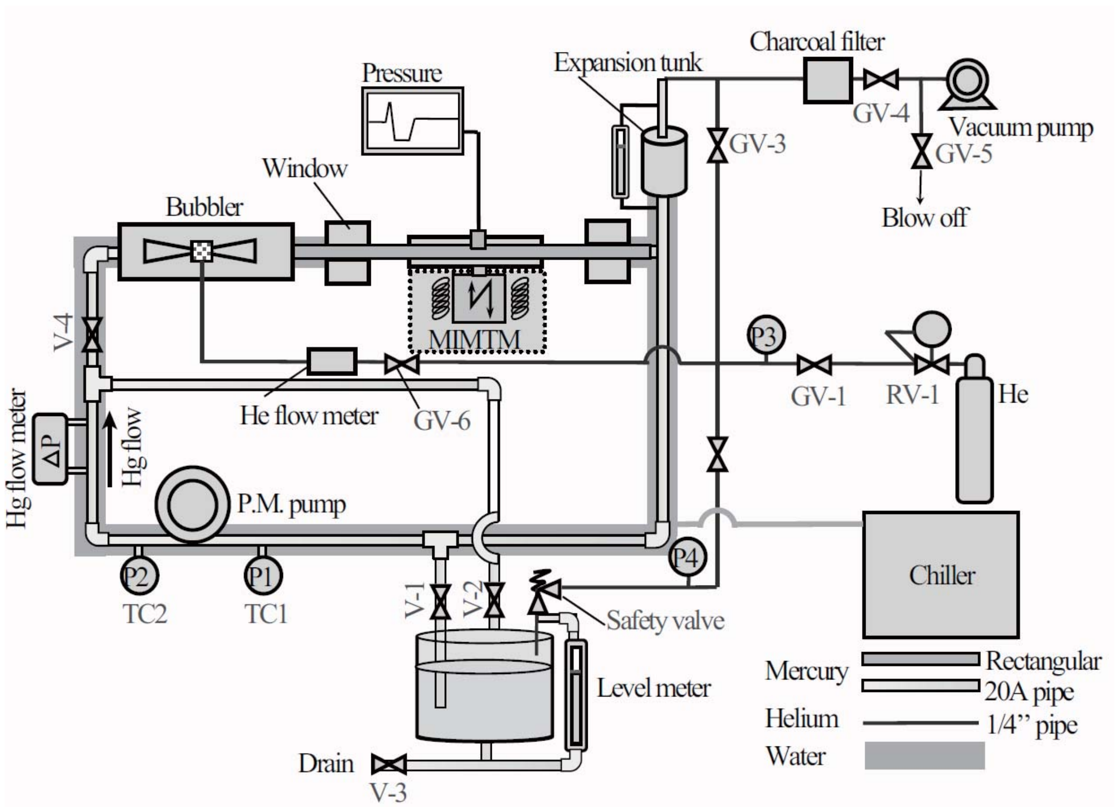

Fig. 5.1.4: Schematic diagram of MIMTM mercury loop to investigate the bubbling effect on pitting damage

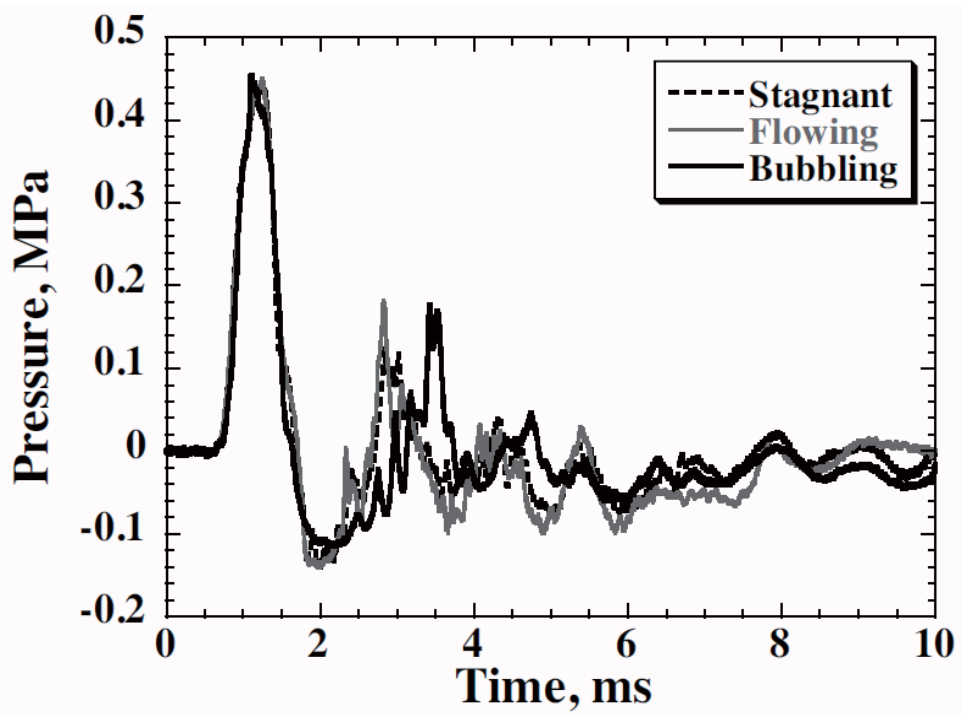

(a) Impulsive pressure response

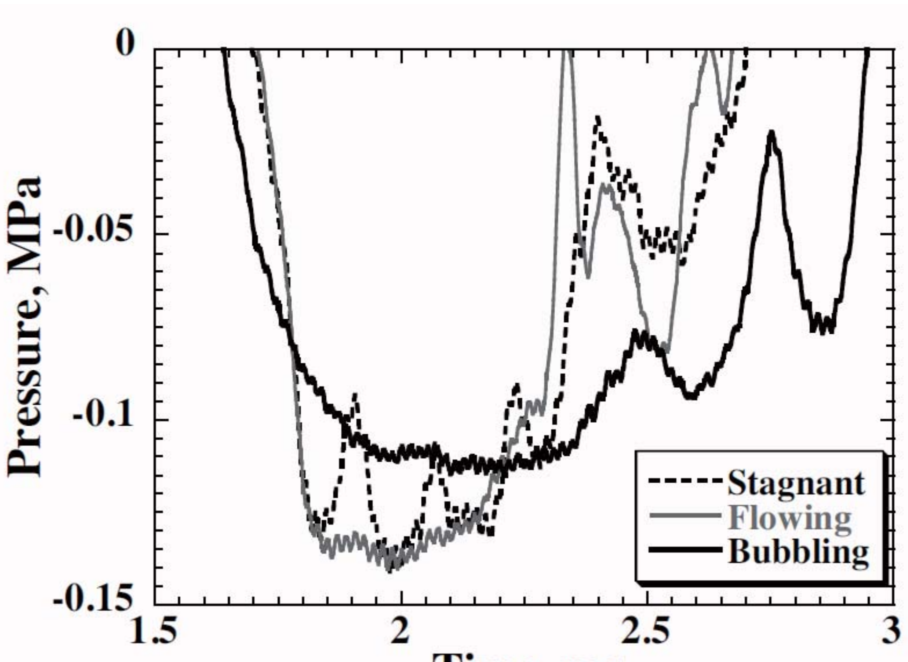

(b) Negative pressure response from 1.5 to 3 ms

Fig. 5.1.5: Time response of low-pass filtered (a) impulsive pressure and (b) magnified negative pressure from 1.5 to 3 ms. The first peak of compressive pressure response was observed around 0.75 ms after impacting. The peak values are hardly affected by the mercury flowing condition. The negative pressure was slightly varied by the mercury flowing condition: the absolute value of negative pressure was reduced by bubbling but not by flowing.

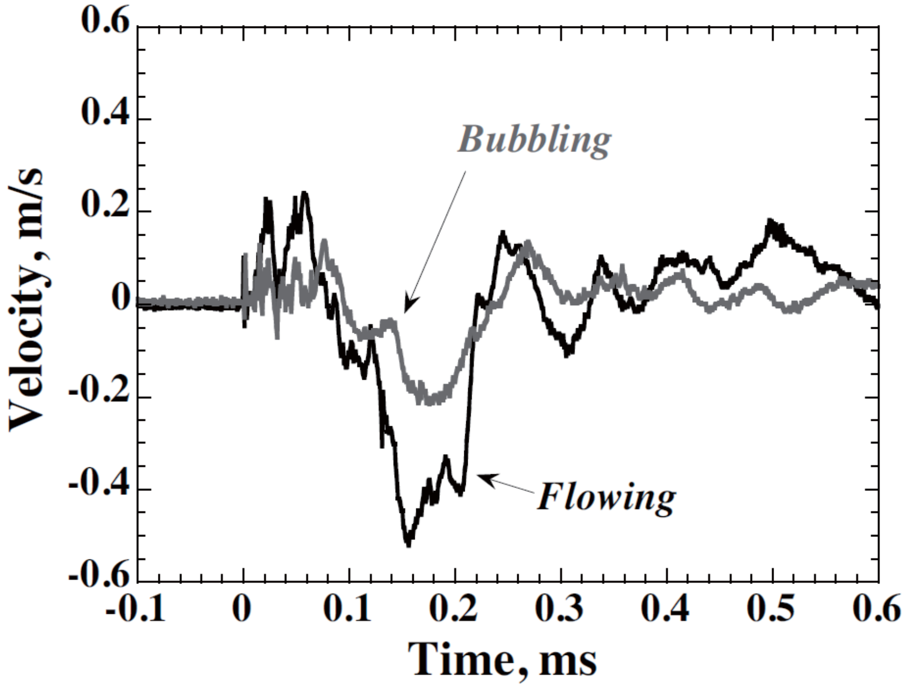

Fig. 5.1.6: The dynamic response of pipe wall measured by a laser Doppler vibrometer in 2005 WNR test. The amplitude of the displacement velocity was clearly reduced by bubbling.

Fig. 5.1.7: The pressure distribution induced by the proton bombarding mercury in the quarter model of LS-DYNA

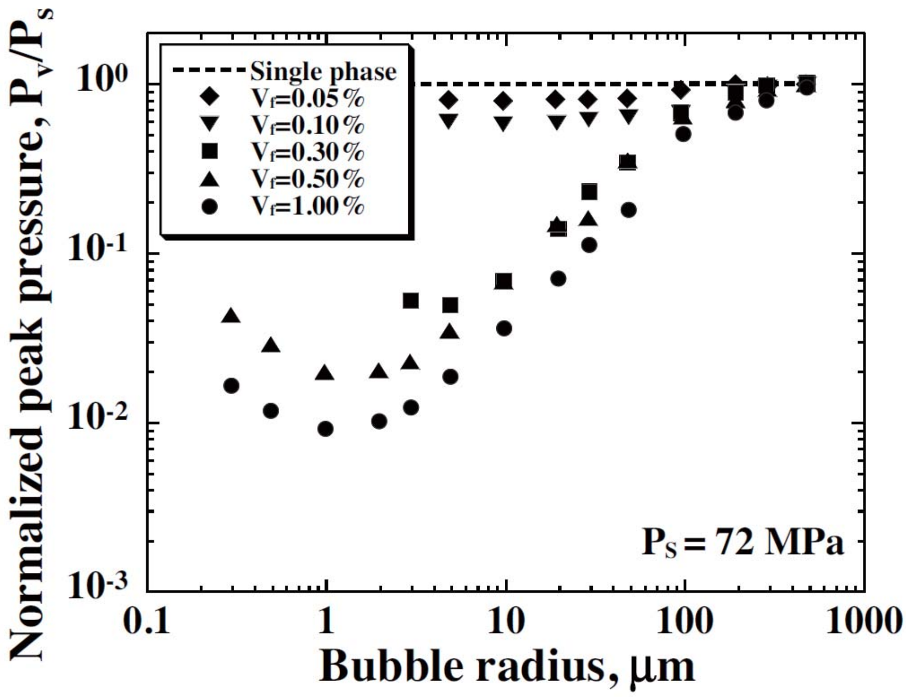

(a) Peak pressure at the center of bombarding area

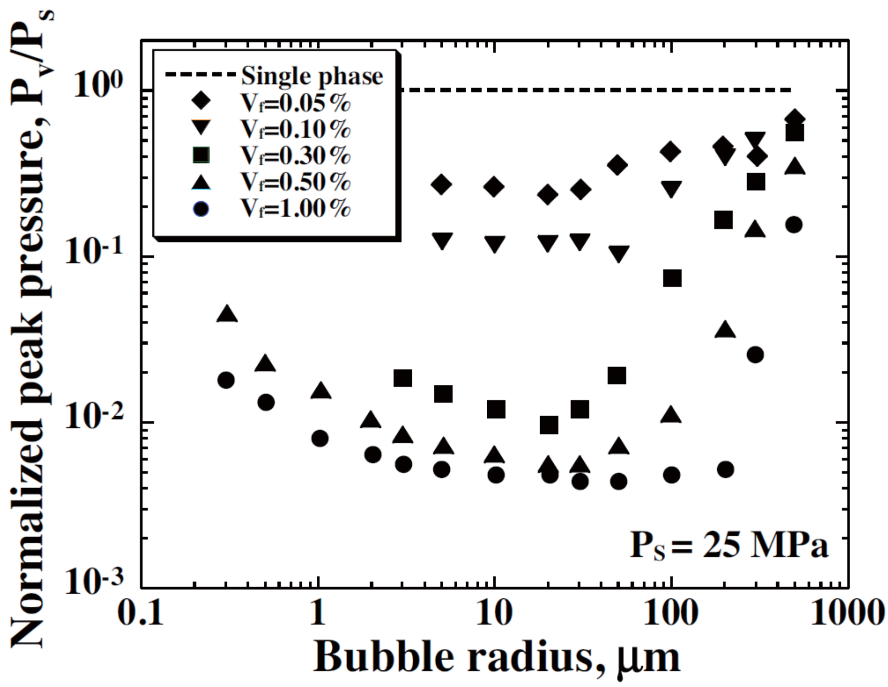

(b) Pressure nearby beam window wall

Fig. 5.1.8: Typical results given by PAC-MT. (a) The peak pressure at the center of bombarding area is reduced by the absorption effect of bubbles. (b) The compressive pressure nearby the beam window is reduced through the propagation process from the bombarding area to the window wall by the attenuation effect.

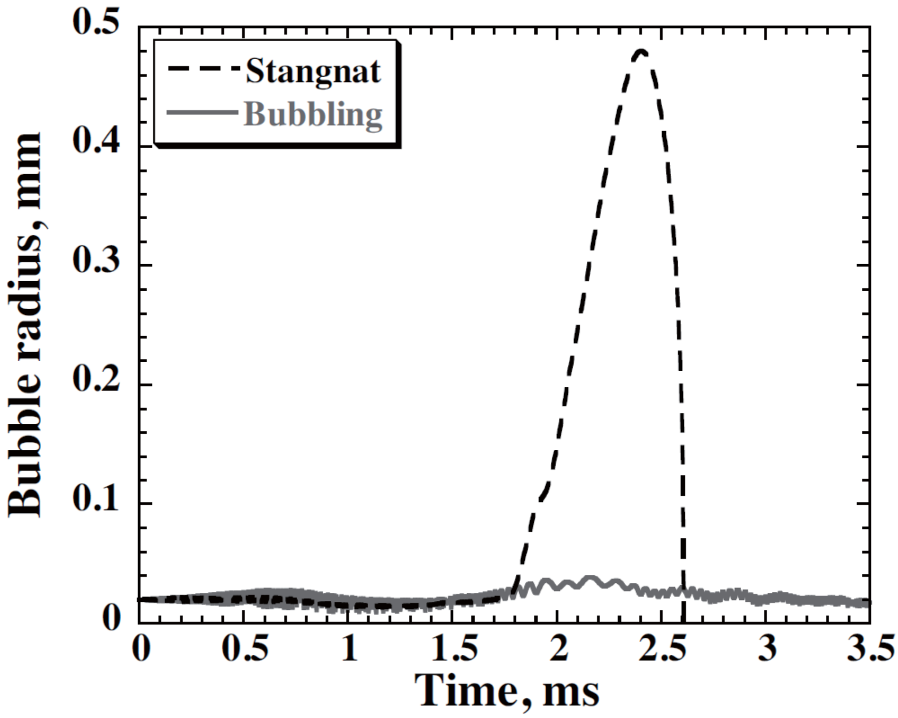

Fig. 5.1.9: Time response of bubble radius caused by the pressure change shown in Fig. 5.1.5. Bubble response is strongly affected by slightly changing negative pressure.

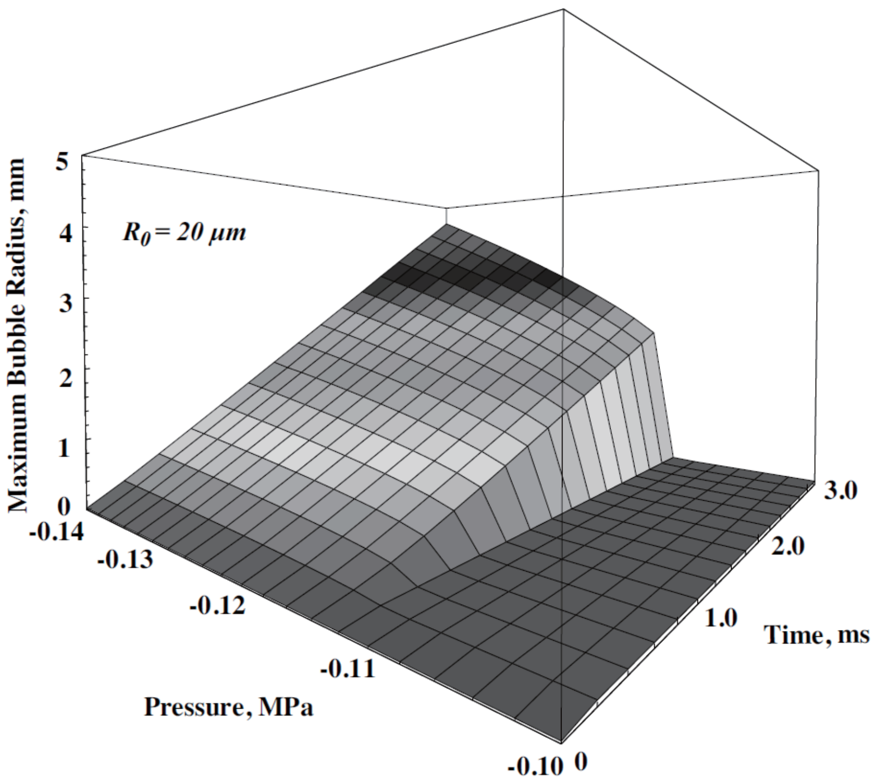

Fig. 5.1.10: Bubble growth condition on period and amplitude of negative pressure. Bubble growth is very dependent on not only the amplitude of the negative pressure but also the period of negative pressure.

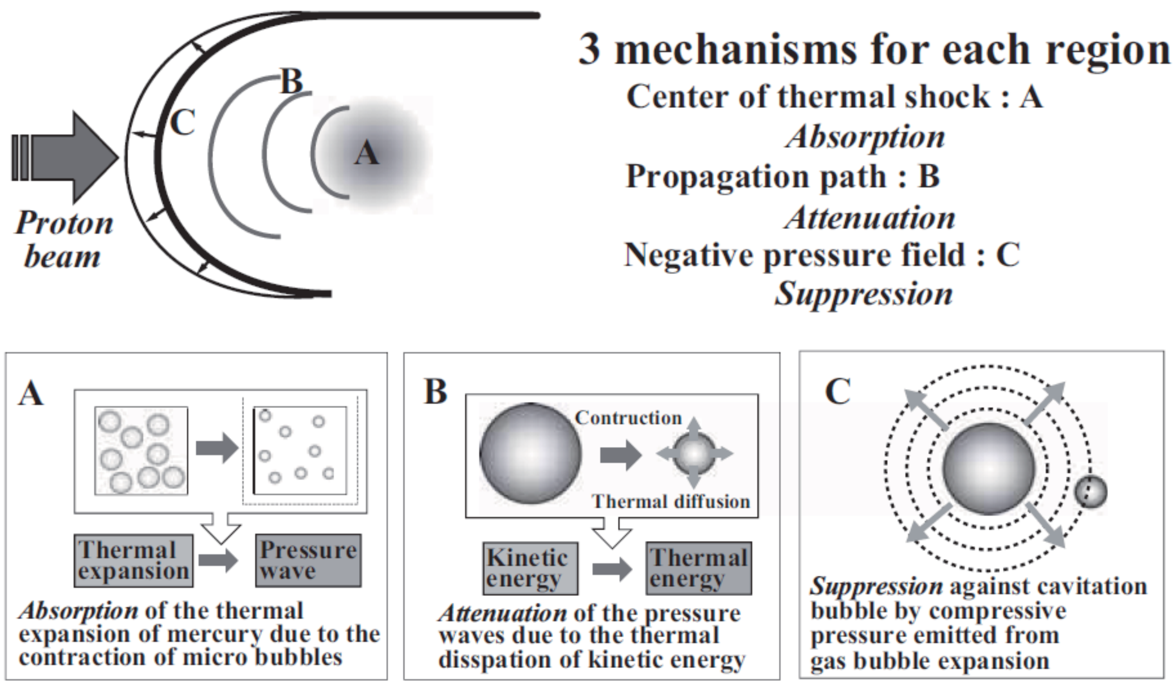

Fig. 5.1.11: Mechanism of the pressure wave mitigation by bubbling

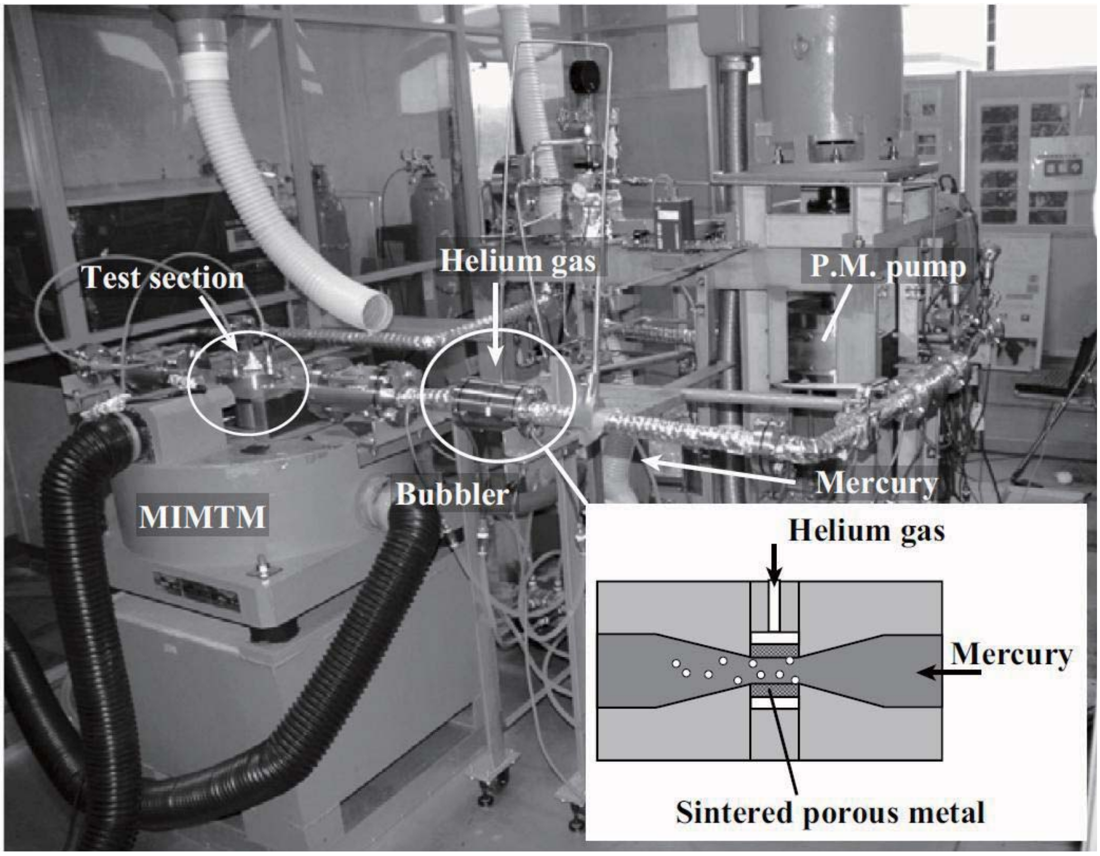

Photo. 5.1.1: Components of MIMTM loop

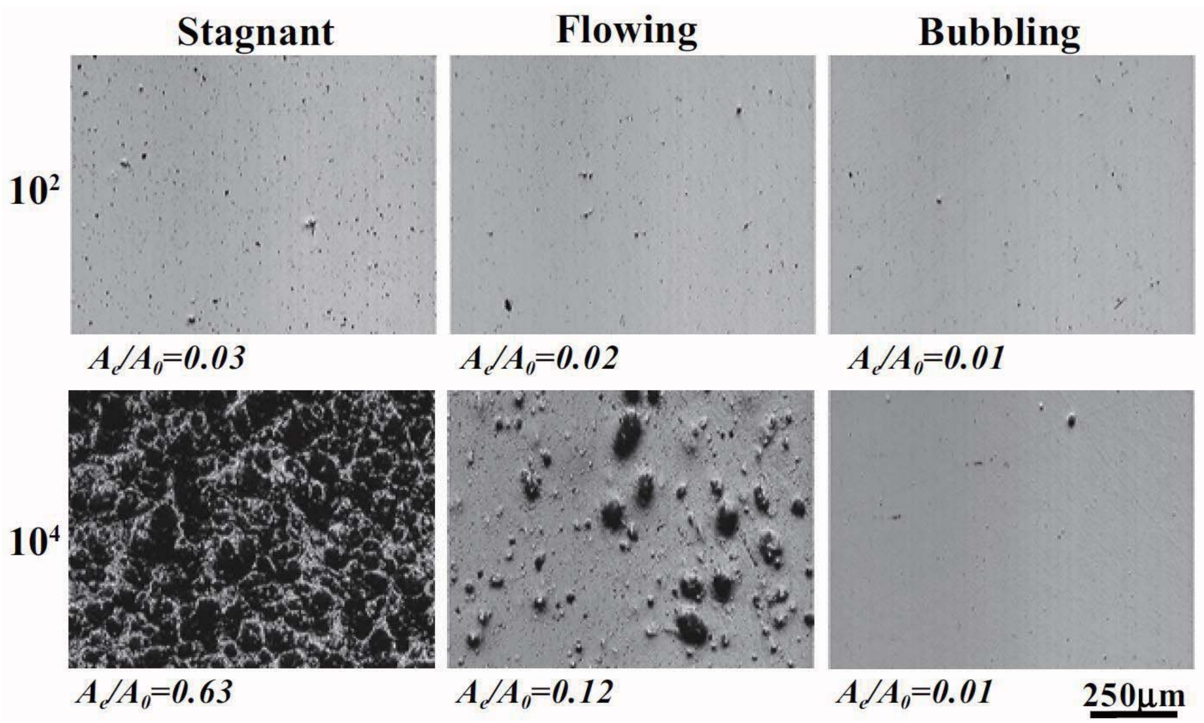

Photo. 5.1.2: Micrographs of pitting damaged surface of specimens after 10^2 and 10^4 impact cycles under each mercury condition

5.2 Moderators, Reflector and Related Components

Future R&D items on the moderators, reflector and their related components can be classified into urgent action items and long-term ones. As lessons in manufacturing the actual moderators and reflector, several issues were found in their structures, manufacturability, remote-handling capability and so on. Subsection 5.2.1 describes these issues. In case of unexpected failure of these components, the current designs of these components have to be reviewed to solve those issues found so far, and spare components have to be prepared urgently. Some ideas of the design review are described in Subsection 5.2.2.

The expected lives of moderators and reflector are all 6 MW-years that are limited by both radiation damage of their container made of aluminum-alloy and burn-out of the AIC decoupler and the Cadmium poison. When rising up of accelerator power up to 1 MW during initial years is considered, it will take at least 10 years to reach the 6 MW-years. Accordingly, we can devote about a 10 years period for the long-term R&D program. In the program, the current design concept of the moderators and the reflector can be changed drastically. Subsection 5.2.3 describes the long-term R&D program.

5.2.1 Issues Found in Manufacturing

Before manufacturing the actual moderator, a prototype coupled moderator was fabricated, and tested. The actual moderators (coupled, decoupled and poisoned ones, abbreviated as CM, DM and PM hereafter) and the reflector were fabricated and installed on-site. A series of preliminary remote-handling test was conducted by using their remote-handling devices. Although these processes have been completed successfully, several issues are found as follows.

(1) Issues in structure

1) Clearance between the moderator heads and the reflector

Nominal clearance between the PM head and the reflector, and also the DM and the reflector are 4 mm. However, the actual clearance is about 2 mm or less due to fabrication tolerance and positioning error. It is not easy to insert the PM and DM heads into the reflector by remote-handling due to the small clearance. When one of the PM, DM and reflector will be replaced with a spare one, the difficulty will increase because dimensions of the replaced components differ from those of the original components in orders of millimeters.

2) Pressure-proof capability of the moderator heads

Cooling water boundaries for CM, DM and PM are designed to withstand water pressure up to 0.5 MPa. However, both the PM and DM heads have a weak point in their cooling water boundaries that can withstand water pressure up to 0.2 MPa.

3) Retention of vacuum insulation layers

To retain vacuum insulation layers between regions at the cryogenic temperature (about 20 K) and those at room temperature (about 300 K) in the moderators their transfer lines is very important.

Although the vacuum insulation layers of the actual moderators at room temperature are confirmed to be kept adequately by X-ray photography, there are some points where clearance is smaller than that expected: corners of PM and DM heads, a central horizontal part of the CM transfer line, parallel transfer lines of all the three moderators and so on. The clearance at the cryogenic temperature has not been tested as of December 2007.

(2) Issues in manufacturability

1) Unstuck of the AIC alloy

Parts of moderators and reflector containing the AIC alloy were prepared successfully with applying the HIP-bonding method of the AIC alloy to the aluminum alloy. However, some portions of the bonding came unstuck in assembling the parts in welding process. The unstuck portions were repaired by laser welding. The repaired parts are considered not to cause any problems in use.

2) Welding distortion

Welding always introduces some distortion. Such distortion resulted in difficult problems in manufacturing the moderators in the right shape because of the multi-coaxial and complicated structure and thin-walled welding of the moderators. Very skilled hands and technical know-how were required to manufacture the moderators.

3) Reliability of dissimilar joints

Dissimilar joints of aluminum alloy and stainless steel are used in moderators. It is better to make sure reliability of the dissimilar joints although they have been pressure-proof tested. Heat load to the dissimilar joints may deteriorate their properties when the dissimilar joint is close to a welding line.

(3) Issues in remote-handling capability

1) Difficulty in introducing the PM and DM heads into the reflector

Due to the reason mentioned in (1)-1), it is not easy to introduce the PM and DM heads into the reflector by remote handling.

2) Template for spare components

Templates are needed to precisely reproduce dimensions of connection parts in relation to other components when spare moderators and reflector are produced. Dummy reflector and reflector plugs function as the templates, and dimensions of the actual moderators and reflector are to be transferred to the dummy components. Although the procedure is feasible, there is a concern if the transfer of the dimensions is accurate enough or not because allowable clearance among the components is rather small.

(4) Issues in manufacturing schedule

1) Period for material arrangements

It takes time, probably more than 1 year, to arrange beryllium and AIC alloy. This period should be considered in ordering the spare moderators and reflector.

2) Production period

It takes much time to fabricate spare moderators and reflector because of their complexity. Completion of fabrication in one-year may be difficult.

3) Availability of factory

Because manufacturer of the moderators and the reflector is limited, availability of the factory should be considered in ordering the spare components.

5.2.2 Urgent Action Items

The purpose of the urgent action is to provide quickly a spare component in case of unexpected failure. Issues found in subsection 5.2.1 have to be solved with keeping the following points of view in mind.

a) Improvement of manufacturability
b) Enhancement of reliability
c) Improvement of remote handling capability
d) Shortening of production period
e) Reduction of production cost

(1) Design study

The issues described in (1) of subsection 5.2.1 are to be solved by design studies.

(2) Demonstration test

Clearances between room temperature region and cryogenic temperature region for the three actual moderators were planed to be tested by X-ray photography in January 2008. This test gives a judgment for the issue (1)-3) in subsection 5.2.1. As for the issue (3)-2) in subsection 5.2.1, a commissioning test to transfer dimensions of actual moderators and reflector to their templates was conducted in February 2008.

(3) R&D

Some R&D activities are needed to solve urgently the issues described in (2) of subsection 5.2.1. A vendor who produces the AIC-alloy in the past does not produce it any more. Test production of the AIC-alloy by a new vendor is effective to avoid supply instability of the AIC-alloy that is related to the issue (4)-1) in subsection 5.2.1.

(4) Schedule controlling

Schedule controlling is important to provide spare moderators and reflector in time. Purchase of beryllium blocks in advance is effective. These are related to the issues described in (4) of subsection 5.2.1.

These urgent action items should be conducted in Japanese fiscal year 2008 to provide a spare moderator in case of unexpected failure.

5.2.3 Long-term R&D Program

(1) Low activation decoupler development

Although the decoupler made of the AIC-alloy improves neutronic performance significantly, it has a demerit in its high residual radioactivity. Use of the AIC-alloy imposes difficulties in handling used moderators and reflector, and future storage as retained waste. Development of a low activation decoupler material is desirable.

Since silver is the main cause of the high residual radioactivity, elimination of silver is one of the most effective ways. Fig. 5.2.1 (a) shows total residual radioactivity in the AIC-alloy contained in PM, DM and the reflector after 6 years operation at 1 MW as a function of cooling time. The ^{110m}Ag mainly produced by the ^{109}Ag(n,γ)^{110m}Ag reaction is as strong as 10^{14} Bq. Decay of the ^{110m}Ag activity is slow due to its half life ($T_{1/2}$ = 250 days), and the ^{110m}Ag emits relatively high energy gamma-rays above 1 MeV. The ^{108m}Ag activity brings another difficulty due to its long half-life ($T_{1/2}$ = 127 years) and high gamma-ray energy about 0.7 MeV. Fig. 5.2.1 (b) shows similar decay curves, but silver in the AIC-alloy is replaced by gold although feasibility of the replacement has not been studied. It is clear that decay of total radioactivity for AuIC is faster than that of AgIC. In addition, ^{109}Cd and ^{113m}Cd which are dominant after 1 year cooling emit actually no gamma-rays. Accordingly, handling of moderators and reflector with the AuIC decouper will be much easier than that with the AgIC decoupler. To realize such decoupler material, extensive R&D is needed on neutronic performance, irradiation property, compatibility with Al-alloy, HIP capability, workability, commercial availability and so on.

Another approach is to use a boron contained material such as Boral as a decoupler material. In this case, swelling due to dense helium production by the ^{10}B(n,α)^{7}Li reaction is a key concern.

(2) Design renewal

When the moderators and reflector are replaced with new ones, the reflector plug is reused in the current design concept. If the three moderators and the reflector endure up to their expected lives of 6 MW-years without any failure, they can be replaced all together. In this case, one idea is to renovate not only the moderators and reflector but also the reflector plug with an advanced design. Although the used reflector plug cannot be used any longer, this renovation brings the following advantages.

a) Compatibility between the old and new moderators in their dimension for connection parts with the old reflector plug is not required. Difficulties which may arise from template transfer can be avoided.
b) Issues described in Section 5.2.1 can be solved much easier because boundary conditions related to the old reflector plug disappear.
c) Innovative concept for moderator/reflector assembly to achieve higher neutronic performance can be introduced much easier.

Patient design efforts to improve the moderator/reflector/plug assembly are essential.

(3) Post irradiation experiment (PIE)

One of reasons to limit the lives of the moderators and reflector is irradiation damage of the structural material. Aluminum-alloy A5083 is adopted as the moderator and reflector container material with considering existing irradiation experimental data. To strengthen the experimental database, it is desirable to conduct PIE of the actually used moderator and reflector container material. The PIE will provide precious experimental data for materials irradiated in spallation neutron field, and may extend lives of those components.

Details of the PIE program covering other components are described in subsection 5.1.4.

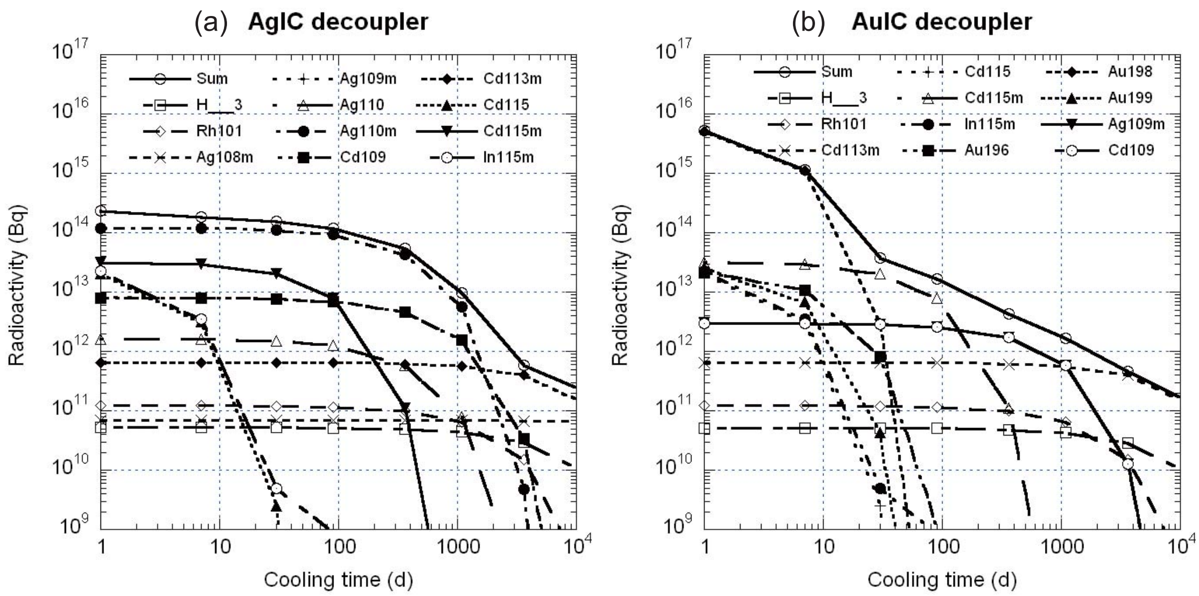

Fig. 5.2.1: Decay curves of radioactivity produced in (a) the AgIC decoupler and (b) the AuIC decoupler

5.3 Proton Beam Window

One of the important factors to determine the lifetime of the aluminum used for the proton beam window is the production rates of hydrogen gas and helium gas when one is irradiated. They were measured at PSI experimentally and the results showed some discrepancy with simulation calculations. Our replacement schedule is based on the experimental results. Since the energies of proton beam are not the same, more accurate lifetime has to be derived from the post irradiated experiment (PIE) in J-PARC. The present proton beam window is not designed to be cut out to PIE samples. The proton beam window of the next generation will be designed in terms of PIE sampling.

The present proton beam window assembly has beam profile monitors, which play an indispensable role in measuring the proton beam properties just upstream of the mercury target. Those monitors are of multi-wire type and may have shorter lifetime than the proton beam window itself due to the interaction with proton beam. Non-destructive type of profile monitors are desired for following generations of the proton beam window assembly. A profile monitor that detects secondary electrons due to the interaction of proton beam with residual gas is one of the likeliest candidates. Residual ionization profile monitor is adopted in 50-GeV synchrotron of J-PARC, as shown in Photo. 5.3.1. The intensity of the secondary electrons around the proton beam window is extremely low and provisional studies will be required for its development. This type of monitor may work also in the helium vessel side of the proton beam window. In the second proton beam window assembly, there is high possibility to develop a new type of profile monitor to prolong the lifetime.

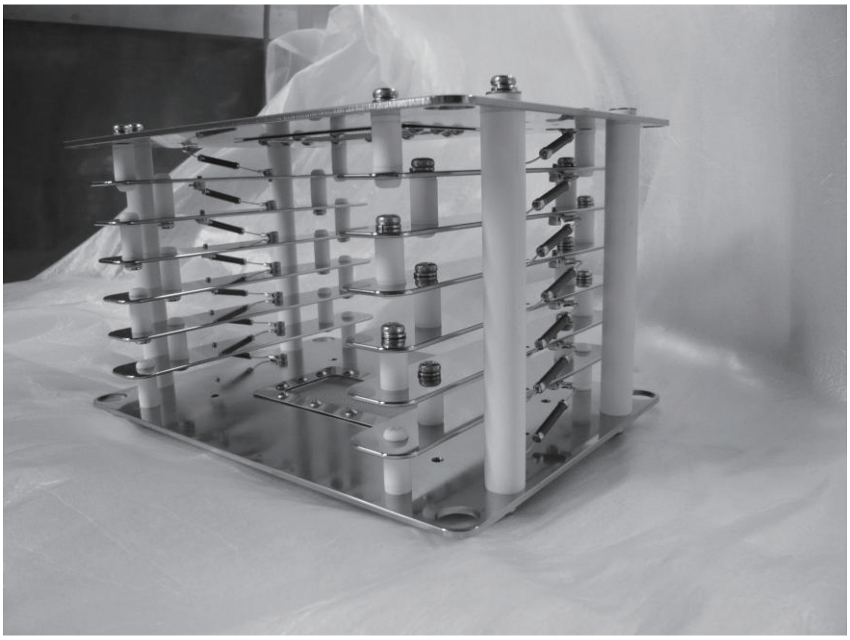

Photo. 5.3.1: View of residual gas ionization profile monitor using at MR in J-PARC

Appendix Installation Sequence of Neutron Source Station Components

Figures used in this appendix are cited from those published as JAEA-Technology 2006-060 (2007) that is entitled “Planning and Implementation on Transportation of Large and Heavy Components of 1-MW Spallation Neutron Source for Japan Proton Accelerator Research Complex”.

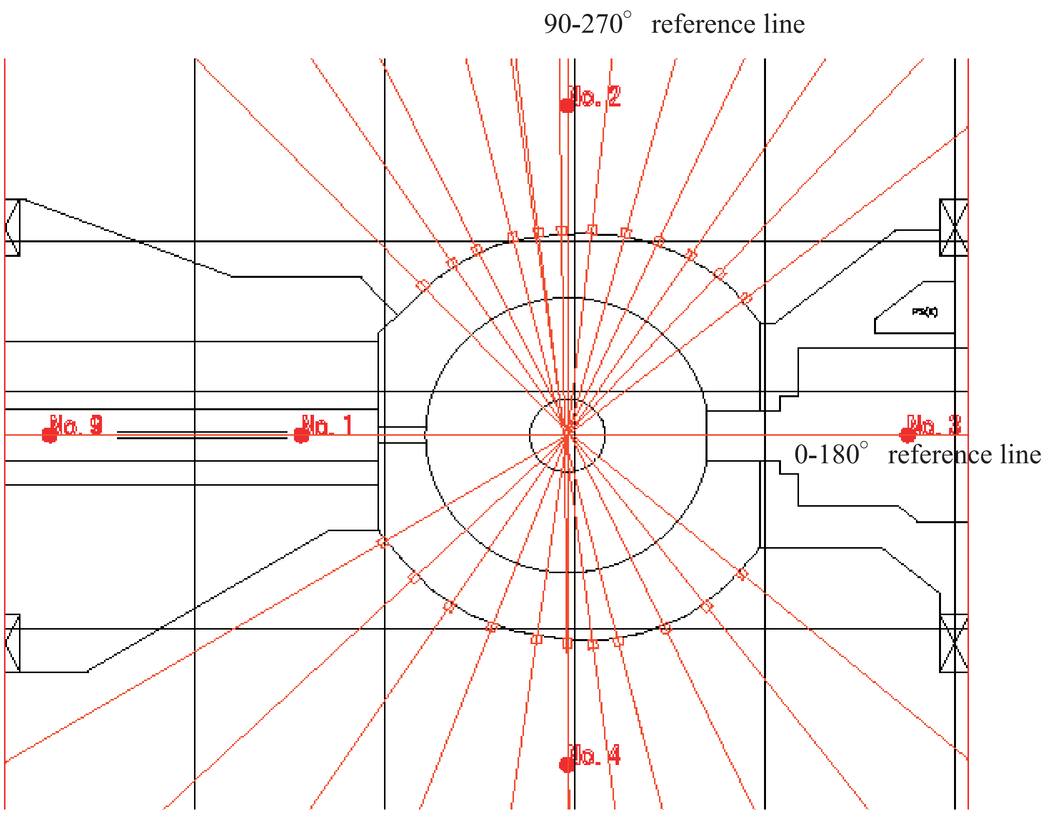

(1) Set reference markers No.1 to 4 on the basement

The center lines of the 23 neutron beam lines were determined with respect to the center of the helium vessel cylinder by means of the precise measurement when it was installed.

Fig. A.1: Installation procedure of neutron source station components

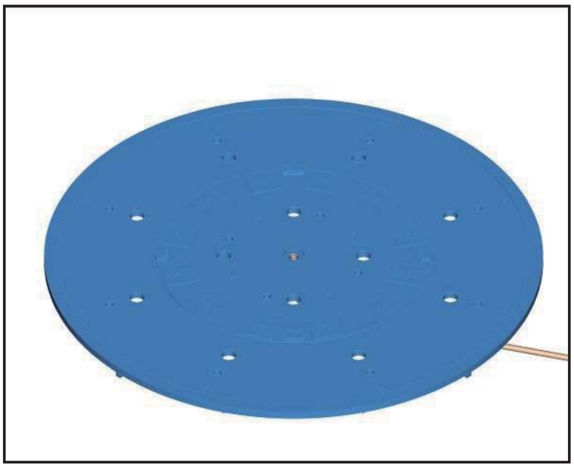

(2) Base-plate

Accuracy: within ±3 mm with respect to 0-180°, and 90-270° baselines, respectively, elevation: within (1FL−1495)±3 mm horizontal level: within 1.2mm at 2400 mm diameter

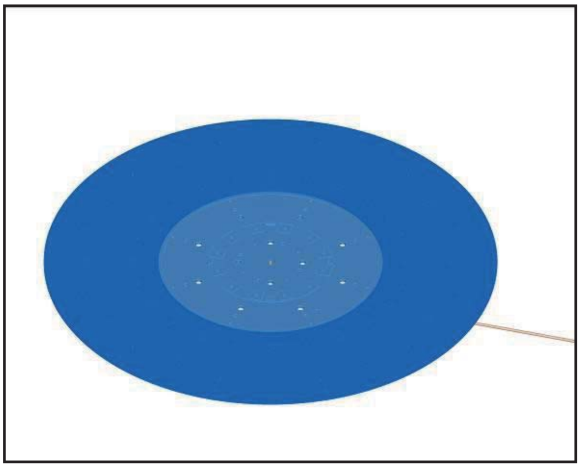

(3) Bottom liner

Accuracy: elevation within (1FL−1485)+3/−20 mm.

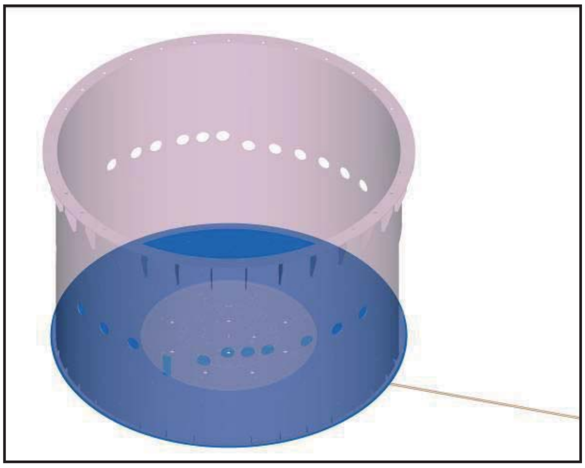

(4) Lower part of outer-liner installation

Accuracy: within ±10 mm with respect to 0-180°, and 90-270° baselines, respectively, elevation: within (1FL+5115)±15 mm, horizontal level: within 10mm at 10140mm diameter.

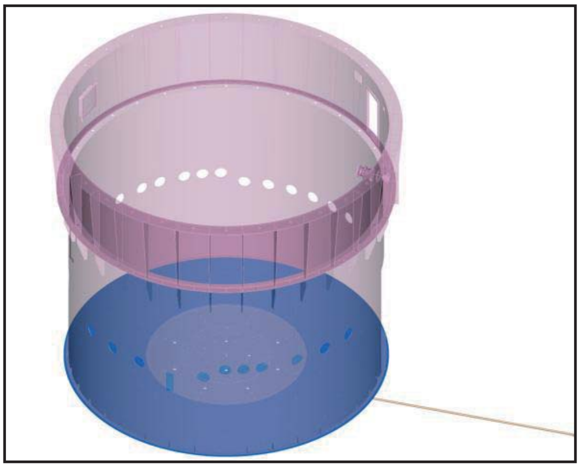

(5) Upper part of outer liner installation

Accuracy: elevation: within (1FL+7515)±20 mm horizontal level: within 10 mm at 10340 mm diameter.

Fig. A.1: Installation procedure of neutron source station components (continued)

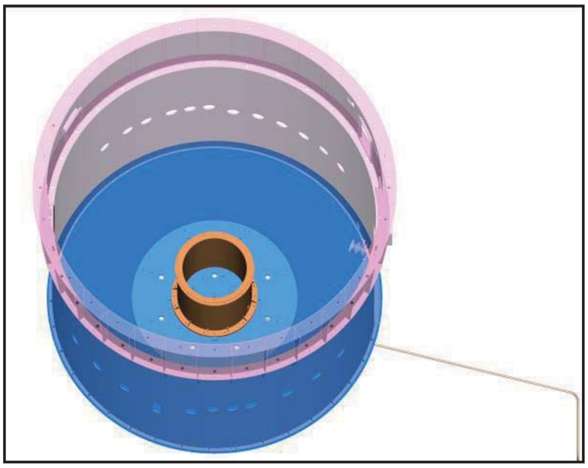

(6) Installation of vessel support cylinder support cylinder

Accuracy: within ±1 mm with respect to 0-180°, and 90-270° baselines, respectively, elevation: within (1FL+910)±0.5 mm, horizontal level: within 1.2 mm at 2400mm diameter.

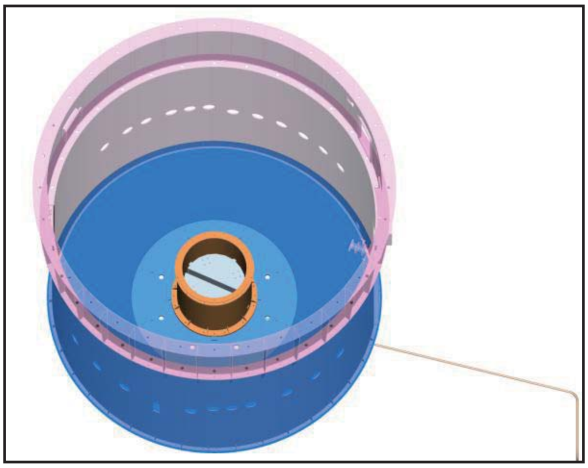

(7) Installation of shielding blocks inside the vessel

Accuracy: elevation within (1FL+1225)±25 mm at top of the block, gap between blocks and support: within 40±10 mm.

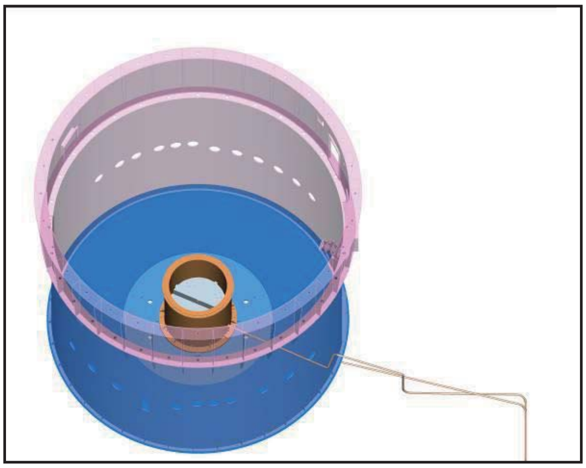

(8) Drain piping of vessel

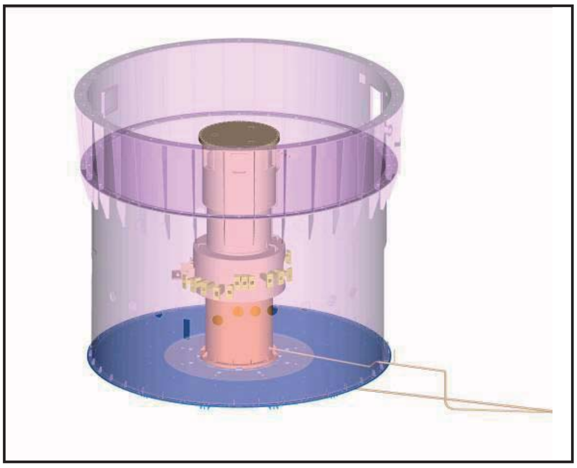

(9) Helium vessel

Extend the line connecting center of proton beam and target trolley ports outside the vessel to be 0-180° reference line and make marks on reference markers No.1, 3 and 9.

Fig. A.1: Installation procedure of neutron source station components (continued)

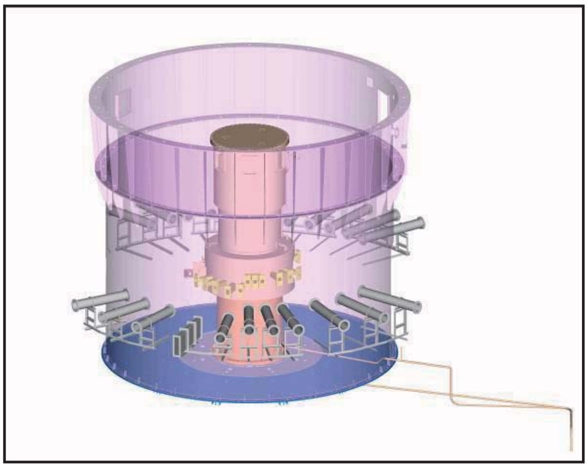

(10) Neutron beam ducts on outer liner

Distance accuracy from origin to outer edge of neutron beam port: within ±1 mm,
Accuracy on horizontal and elevation: within ±3 mm.

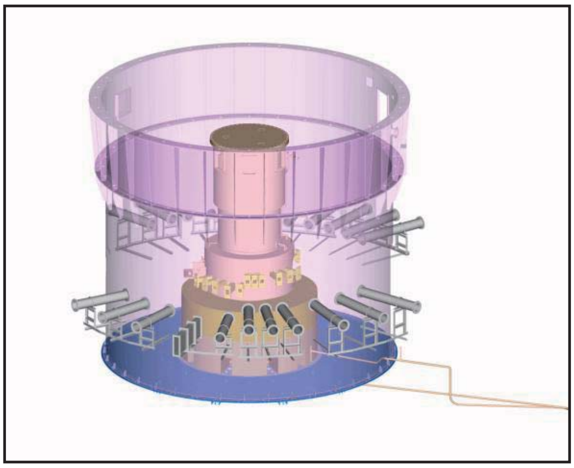

(11) Shielding blocks under neutron beam port on the middle section.

Accuracy: elevation within (1FL+2255)±4 mm,
gap between blocks and support: within 40±10 mm.

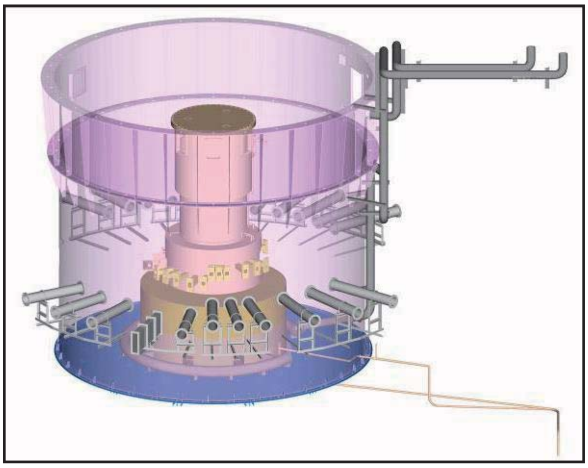

(12) Dry air ventilation pipings inside and outside of outer-liner.

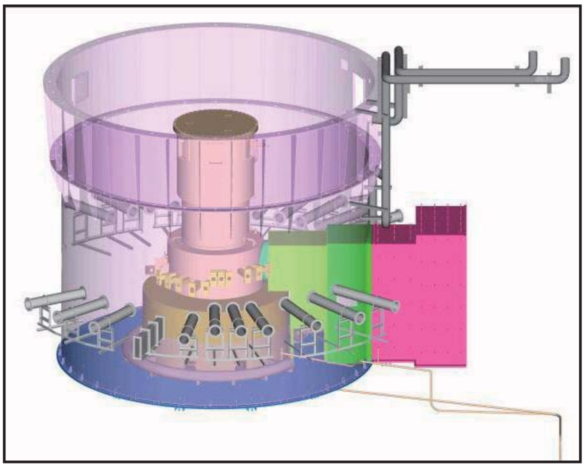

(13) Liner around target trolley insertion part

Elevation at bottom of liner:
(1FL−1315)+0/−6 mm.

Fig. A.1: Installation procedure of neutron source station components (continued)

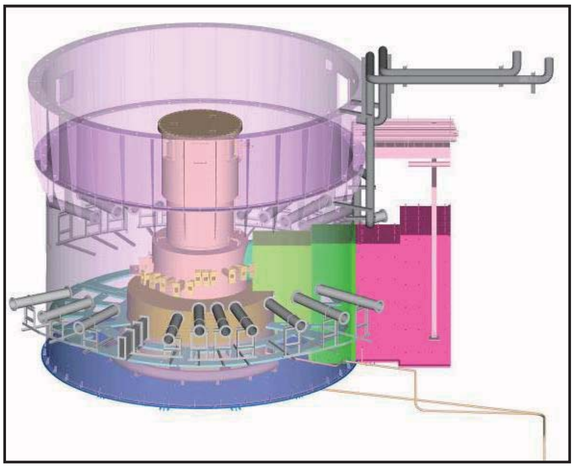

(14) Pedestals for interstitial blocks

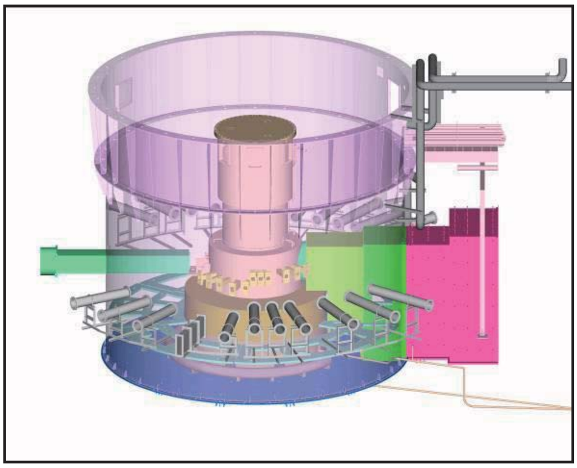

(15) Proton beam duct liner

Horizontality of upper surface: within 1/1000.

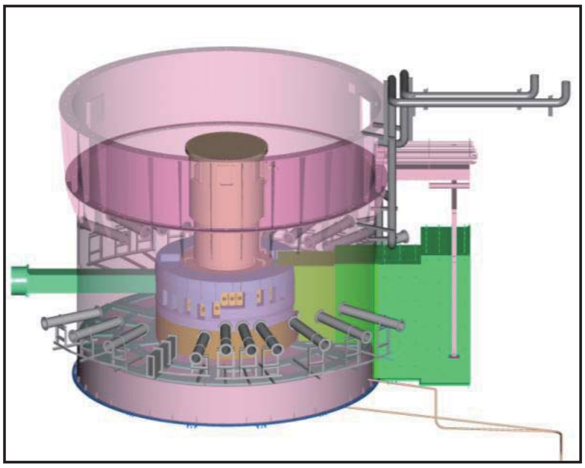

(16) Fill heavy concrete under pedestal and Shield blocks around middle section

Maximum outer radius within 2300±3mm,
gap from helium vessel: within 40±10 mm,
gap between blocks and bottom of neutron beam duct ports: within 25 to 40±10 mm,
gap from side and/or upper of neutron beam duct ports: within: 25±5 mm.

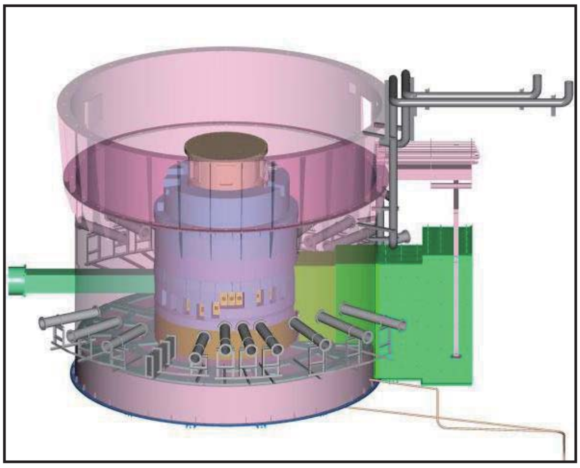

(17) Shield blocks upper middle section

Elevation: within (1FL+4115)±6 mm,
Maximum outer radius within 2300±3mm,
Displacement with upper ring-shaped shield blocks and upper vessel blocks: within 1 mm.

Fig. A.1: Installation procedure of neutron source station components (continued)

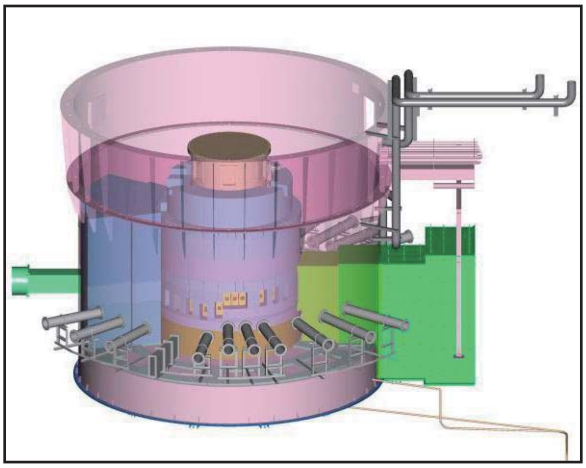

(18) Shield around proton beam duct
elevation: within (1FL+5115)±5 mm,
elevation: within 4 mm at individual layer,
gap between blocks and those under neutron beam duct ports: within 40±10 mm,
gap from outer-liner: within 40±10 mm,
Accuracy on 0-180° base-line: within ±10mm.

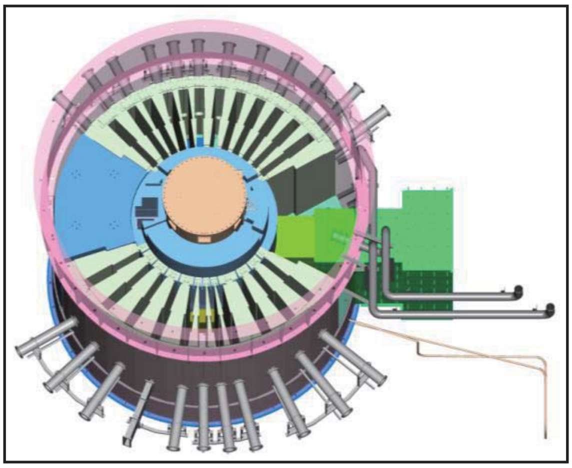

(19) 25 interstitial blocks for shutters
Horizontal position accuracy with respect to designed neutron beam line: within ±3 mm,
Verticality : within 0.5/4000.

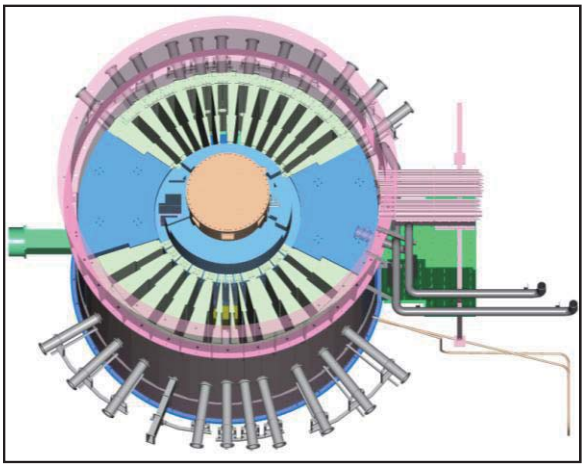

(20) Shield blocks around target trolley liner

Elevation: within (1FL+5115)±5 mm,
Elevation: within 4 mm at individual layer,
gap between blocks and those under neutron beam duct ports: within 40±10 mm,
gap from outer-liner: within 40±10 mm,
gap from interstitial block: within 10±5 mm,
Accuracy on 0-180° base-line: within ±10mm.

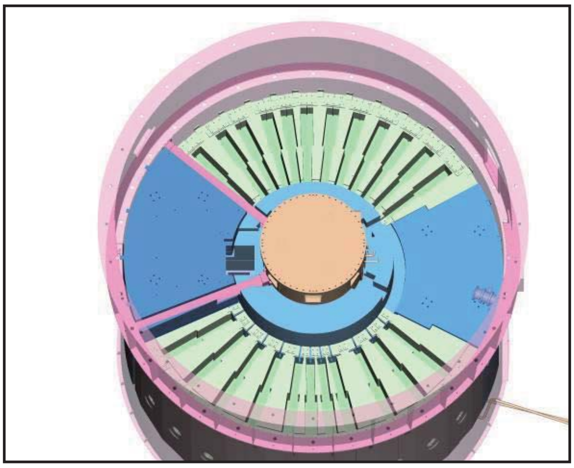

(21) Helium vessel support beams and most upper part shield around proton beam duct

Fig. A.1: Installation procedure of neutron source station components (continued)

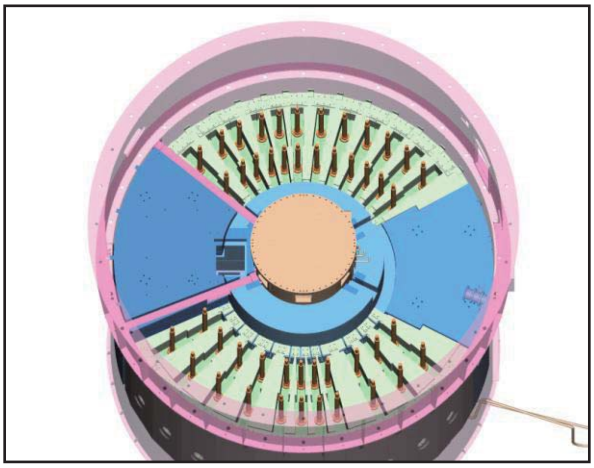

(22) Shutter gates

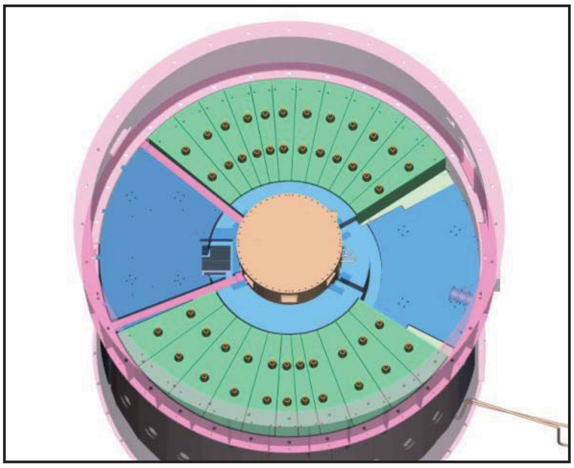

(23) Shield blocks over shutter gates
Horizontality of upper surface of knocks: within 1/1000.

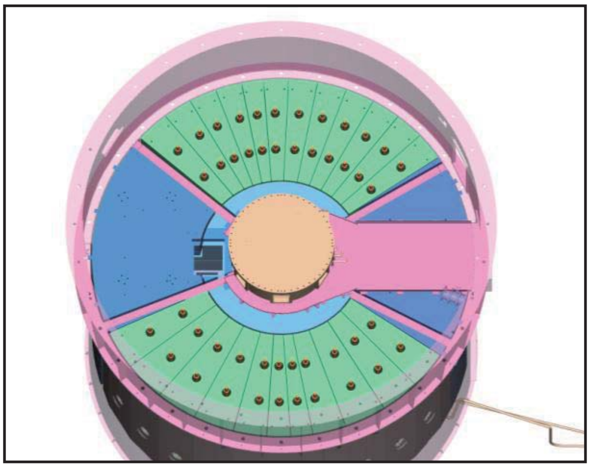

(24) Piping pan

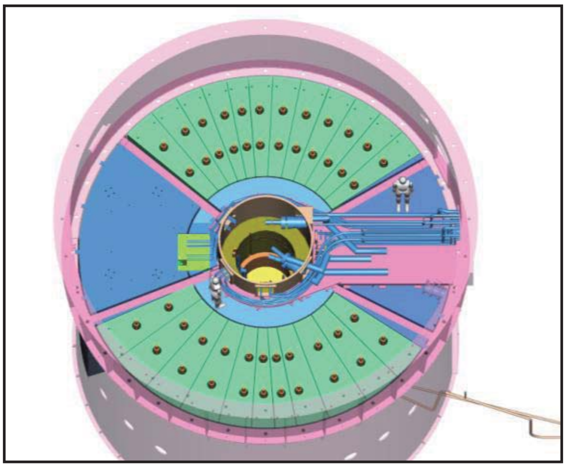

(25) In-vessel components and its piping

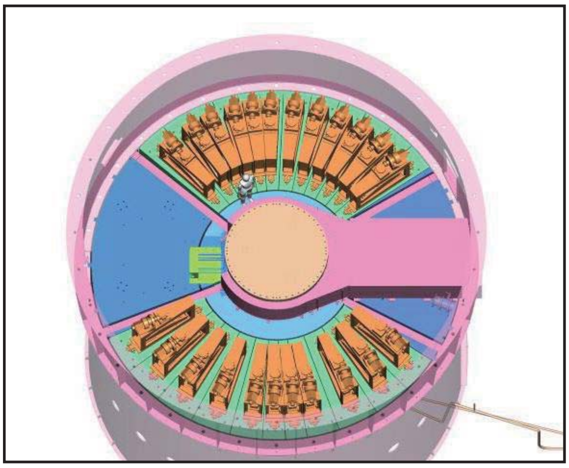

(26) Cover piping pan and set shutter drive mechanisms to sustain shutter gates

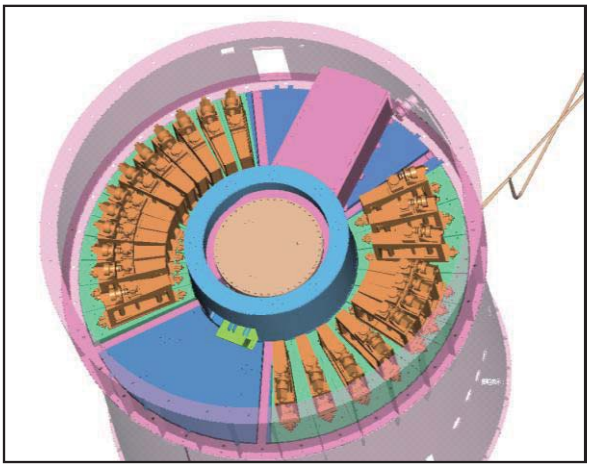

(27) Proton beam windows with shield plug, and ring-shaped shield blocks

Fig. A.1: Installation procedure of neutron source station components (continued)

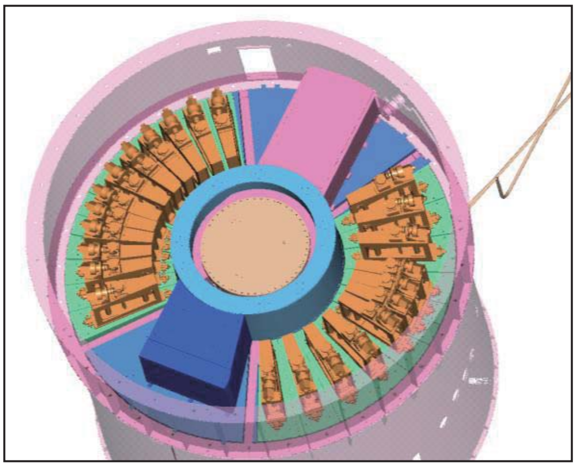

(28) Shield blocks over proton beam window

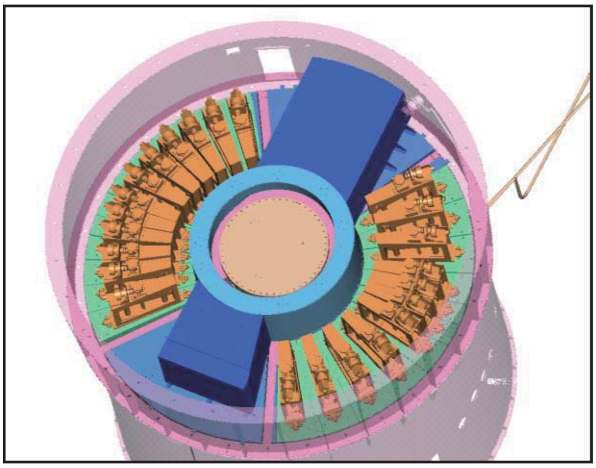

(29) Shield blocks surrounding piping pan

Elevation accuracy of reference surfaces between ring-shaped shield block and block over proton beam window: within ±2 mm.

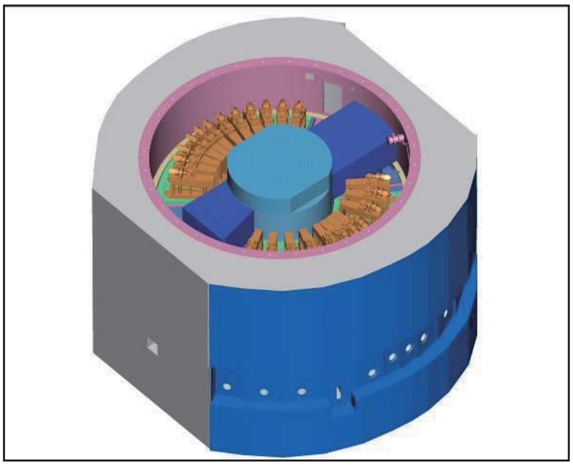

(30) Upper vessel shield block (magnetite concrete surrounding outer line is also illustrated.)

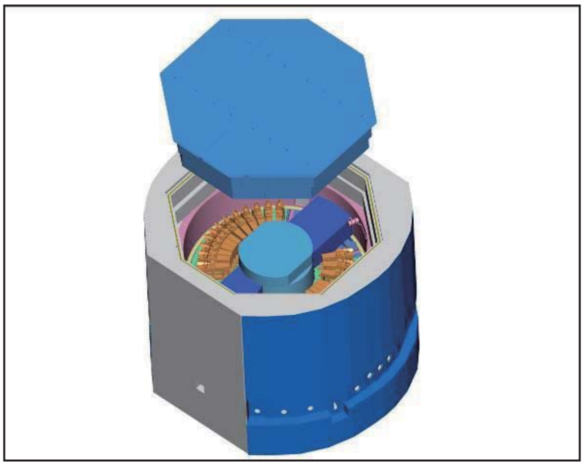

(31) Ceiling shield blocks

Fig. A.1: Installation procedure of neutron source station components (continued)

国際単位系（SI）

表１．SI 基本単位

基本量	SI 基本単位 名称	記号
長さ	メートル	m
質量	キログラム	kg
時間	秒	s
電流	アンペア	A
熱力学温度	ケルビン	K
物質量	モル	mol
光度	カンデラ	cd

表２．基本単位を用いて表されるSI組立単位の例

組立量	SI 基本単位 名称	記号
面積	平方メートル	m^2
体積	立法メートル	m^3
速さ，速度	メートル毎秒	m/s
加速度	メートル毎秒毎秒	m/s^2
波数	毎メートル	m^{-1}
密度，質量密度	キログラム毎立方メートル	kg/m^3
面積密度	キログラム毎平方メートル	kg/m^2
比体積	立方メートル毎キログラム	m^3/kg
電流密度	アンペア毎平方メートル	A/m^2
磁界の強さ	アンペア毎メートル	A/m
量濃度 (a)，濃度	モル毎立方メートル	mol/m^3
質量濃度	キログラム毎立法メートル	kg/m^3
輝度	カンデラ毎平方メートル	cd/m^2
屈折率 (b)	（数字の）１	1
比透磁率 (b)	（数字の）１	1

(a) 量濃度（amount concentration）は臨床化学の分野では物質濃度（substance concentration）ともよばれる。
(b) これらは無次元量あるいは次元１をもつ量であるが、そのことを表す単位記号である数字の１は通常は表記しない。

表３．固有の名称と記号で表されるSI組立単位

組立量	SI 組立単位 名称	記号	他のSI単位による表し方	SI基本単位による表し方
平面角	ラジアン(b)	rad	1 (b)	m/m
立体角	ステラジアン(b)	sr(c)	1 (b)	m^2/m^2
周波数	ヘルツ (d)	Hz		s^{-1}
力	ニュートン	N		$m\ kg\ s^{-2}$
圧力，応力	パスカル	Pa	N/m^2	$m^{-1}\ kg\ s^{-2}$
エネルギー，仕事，熱量	ジュール	J	N m	$m^2\ kg\ s^{-2}$
仕事率，工率，放射束	ワット	W	J/s	$m^2\ kg\ s^{-3}$
電荷，電気量	クーロン	C		s A
電位差（電圧），起電力	ボルト	V	W/A	$m^2\ kg\ s^{-3}\ A^{-1}$
静電容量	ファラド	F	C/V	$m^{-2}\ kg^{-1}\ s^4\ A^2$
電気抵抗	オーム	Ω	V/A	$m^2\ kg\ s^{-3}\ A^{-2}$
コンダクタンス	ジーメンス	S	A/V	$m^{-2}\ kg^{-1}\ s^3\ A^2$
磁束	ウエーバ	Wb	Vs	$m^2\ kg\ s^{-2}\ A^{-1}$
磁束密度	テスラ	T	Wb/m^2	$kg\ s^{-2}\ A^{-1}$
インダクタンス	ヘンリー	H	Wb/A	$m^2\ kg\ s^{-2}\ A^{-2}$
セルシウス温度	セルシウス度(e)	℃		K
光束	ルーメン	lm	cd sr(c)	cd
照度	ルクス	lx	lm/m^2	m^{-2} cd
放射性核種の放射能 (f)	ベクレル (d)	Bq		s^{-1}
吸収線量, 比エネルギー分与, カーマ	グレイ	Gy	J/kg	$m^2\ s^{-2}$
線量当量, 周辺線量当量, 方向性線量当量, 個人線量当量	シーベルト (g)	Sv	J/kg	$m^2\ s^{-2}$
酸素活性	カタール	kat		s^{-1} mol

(a)SI接頭語は固有の名称と記号を持つ組立単位と組み合わせても使用できる。しかし接頭語を付した単位はもはやコヒーレントではない。
(b)ラジアンとステラジアンは数字の１に対する単位の特別な名称で、量についての情報をつたえるために使われる。実際には、使用する時には記号rad及びsrが用いられるが、習慣として組立単位としての記号である数字の１は明示されない。
(c)測光学ではステラジアンという名称と記号srを単位の表し方の中に、そのまま維持している。
(d)ヘルツは周期現象についてのみ、ベクレルは放射性核種の統計的過程についてのみ使用される。
(e)セルシウス度はケルビンの特別な名称で、セルシウス温度を表すために使用される。セルシウス度とケルビンの単位の大きさは同一である。したがって、温度差や温度間隔を表す数値はどちらの単位で表しても同じである。
(f)放射性核種の放射能（activity referred to a radionuclide）は、しばしば誤った用語で”radioactivity”と記される。
(g)単位シーベルト（PV,2002,70,205）についてはCIPM勧告2（CI-2002）を参照。

表４．単位の中に固有の名称と記号を含むSI組立単位の例

組立量	SI 組立単位 名称	記号	SI 基本単位による表し方
粘度	パスカル秒	Pa s	$m^{-1}\ kg\ s^{-1}$
力のモーメント	ニュートンメートル	N m	$m^2\ kg\ s^{-2}$
表面張力	ニュートン毎メートル	N/m	$kg\ s^{-2}$
角速度	ラジアン毎秒	rad/s	$m\ m^{-1}\ s^{-1}=s^{-1}$
角加速度	ラジアン毎秒毎秒	rad/s^2	$m\ m^{-1}\ s^{-2}=s^{-2}$
熱流密度，放射照度	ワット毎平方メートル	W/m^2	$kg\ s^{-3}$
熱容量，エントロピー	ジュール毎ケルビン	J/K	$m^2\ kg\ s^{-2}\ K^{-1}$
比熱容量，比エントロピー	ジュール毎キログラム毎ケルビン	J/(kg K)	$m^2\ s^{-2}\ K^{-1}$
比エネルギー	ジュール毎キログラム	J/kg	$m^2\ s^{-2}$
熱伝導率	ワット毎メートル毎ケルビン	W/(m K)	$m\ kg\ s^{-3}\ K^{-1}$
体積エネルギー	ジュール毎立方メートル	J/m^3	$m^{-1}\ kg\ s^{-2}$
電界の強さ	ボルト毎メートル	V/m	$m\ kg\ s^{-3}\ A^{-1}$
電荷密度	クーロン毎立方メートル	C/m^3	m^{-3} sA
表面電荷	クーロン毎平方メートル	C/m^2	m^{-2} sA
電束密度，電気変位	クーロン毎平方メートル	C/m^2	m^{-2} sA
誘電率	ファラド毎メートル	F/m	$m^{-3}\ kg^{-1}\ s^4\ A^2$
透磁率	ヘンリー毎メートル	H/m	$m\ kg\ s^{-2}\ A^{-2}$
モルエネルギー	ジュール毎モル	J/mol	$m^2\ kg\ s^{-2}\ mol^{-1}$
モルエントロピー, モル熱容量	ジュール毎モル毎ケルビン	J/(mol K)	$m^2\ kg\ s^{-2}\ K^{-1}\ mol^{-1}$
照射線量（Ｘ線及びγ線）	クーロン毎キログラム	C/kg	kg^{-1} sA
吸収線量率	グレイ毎秒	Gy/s	$m^2\ s^{-3}$
放射強度	ワット毎ステラジアン	W/sr	$m^4\ m^{-2}\ kg\ s^{-3}=m^2\ kg\ s^{-3}$
放射輝度	ワット毎平方メートル毎ステラジアン	$W/(m^2\ sr)$	$m^2\ m^{-2}\ kg\ s^{-3}=kg\ s^{-3}$
酵素活性濃度	カタール毎立方メートル	kat/m^3	$m^{-3}\ s^{-1}$ mol

表５．SI 接頭語

乗数	接頭語	記号	乗数	接頭語	記号
10^{24}	ヨタ	Y	10^{-1}	デシ	d
10^{21}	ゼタ	Z	10^{-2}	センチ	c
10^{18}	エクサ	E	10^{-3}	ミリ	m
10^{15}	ペタ	P	10^{-6}	マイクロ	µ
10^{12}	テラ	T	10^{-9}	ナノ	n
10^9	ギガ	G	10^{-12}	ピコ	p
10^6	メガ	M	10^{-15}	フェムト	f
10^3	キロ	k	10^{-18}	アト	a
10^2	ヘクト	h	10^{-21}	ゼプト	z
10^1	デカ	da	10^{-24}	ヨクト	y

表６．SIに属さないが、SIと併用される単位

名称	記号	SI 単位による値
分	min	1 min=60s
時	h	1h =60 min=3600 s
日	d	1 d=24 h=86 400 s
度	°	1°=(π/180) rad
分	’	1’=(1/60)°=(π/10800) rad
秒	”	1”=(1/60)’=(π/648000) rad
ヘクタール	ha	$1ha=1hm^2=10^4m^2$
リットル	L，l	$1L=1l=1dm^3=10^3cm^3=10^{-3}m^3$
トン	t	$1t=10^3$ kg

表７．SIに属さないが、SIと併用される単位で、SI単位で表される数値が実験的に得られるもの

名称	記号	SI 単位で表される数値
電子ボルト	eV	$1eV=1.602\ 176\ 53(14)\times10^{-19}J$
ダルトン	Da	$1Da=1.660\ 538\ 86(28)\times10^{-27}kg$
統一原子質量単位	u	1u=1 Da
天文単位	ua	$1ua=1.495\ 978\ 706\ 91(6)\times10^{11}m$

表８．SIに属さないが、SIと併用されるその他の単位

名称	記号	SI 単位で表される数値
バール	bar	$1\ bar=0.1MPa=100kPa=10^5Pa$
水銀柱ミリメートル	mmHg	1mmHg=133.322Pa
オングストローム	Å	$1\ Å=0.1nm=100pm=10^{-10}m$
海里	M	1 M=1852m
バーン	b	$1\ b=100fm^2=(10^{-12}cm)2=10^{-28}m^2$
ノット	kn	1 kn=(1852/3600)m/s
ネーパ	Np	SI単位との数値的な関係は、対数量の定義に依存。
ベル	B	
デジベル	dB	

表９．固有の名称をもつCGS組立単位

名称	記号	SI 単位で表される数値
エルグ	erg	$1\ erg=10^{-7}$ J
ダイン	dyn	$1\ dyn=10^{-5}N$
ポアズ	P	$1\ P=1\ dyn\ s\ cm^{-2}=0.1Pa\ s$
ストークス	St	$1\ St=1cm^2\ s^{-1}=10^{-4}m^2\ s^{-1}$
スチルブ	sb	$1\ sb=1cd\ cm^{-2}=10^4cd\ m^{-2}$
フォト	ph	$1\ ph=1cd\ sr\ cm^{-2}\ 10^4lx$
ガル	Gal	$1\ Gal=1cm\ s^{-2}=10^{-2}ms^{-2}$
マクスウェル	Mx	$1\ Mx=1G\ cm^2=10^{-8}Wb$
ガウス	G	$1\ G=1Mx\ cm^{-2}=10^{-4}T$
エルステッド (c)	Oe	$1\ Oe ≙ (10^3/4π)A\ m^{-1}$

(c) ３元系のCGS単位系とSIでは直接比較できないため、等号「 ≙ 」は対応関係を示すものである。

表10．SIに属さないその他の単位の例

名称	記号	SI 単位で表される数値
キュリー	Ci	$1\ Ci=3.7\times10^{10}Bq$
レントゲン	R	$1\ R=2.58\times10^{-4}C/kg$
ラド	rad	$1\ rad=1cGy=10^{-2}Gy$
レム	rem	$1\ rem=1\ cSv=10^{-2}Sv$
ガンマ	γ	1γ=1 nT=10-9T
フェルミ		1フェルミ=1 fm=10-15m
メートル系カラット		1メートル系カラット = 200 mg = 2×10-4kg
トル	Torr	1 Torr = (101 325/760) Pa
標準大気圧	atm	1 atm = 101 325 Pa
カロリー	cal	1cal=4.1858J（「15℃」カロリー），4.1868J（「IT」カロリー）4.184J（「熱化学」カロリー）
ミクロン	µ	$1\ µ=1µm=10^{-6}m$

（第8版，2006年改訂）